

Proceedings of the 33rd Linear Accelerator Conference (LINAC2026)

Publication identifiers

ISBN: 978-3-95450-275-2
ISSN: 2226-0366
DOI: 10.18429/JACoW-LINAC2026

Copyright © 2026 by JACoW — Creative Commons Attribution 4.0 — Publishing Policies & Ethics

ISBN: 978-3-95450-275-2 ISSN: 2226-0366 doi: 10.18429/JACoW-LINAC2026-MO1A002

UPDATES ON THE WORLDWIDE EFFORTS FOR TRANSMUTATION OF SPENT NUCLEAR FUEL WITH ACCELERATOR DRIVEN SYSTEMS

B. Yee-Rendon*
Japan Atomic Energy Agency, Tokai Mura, Japan

Abstract

To address the challenge of nuclear waste storage, the international community is pursuing the use of accelerator-driven subcritical systems (ADS) to decrease both the volume and radiotoxicity of spent nuclear fuel. ADS utilizes high-intensity linacs, which must operate with high reliability to prevent thermal stress on reactor structures. This presentation provides an overview of global transmutation activities, considering both government-funded research and industry-sponsored projects.

INTRODUCTION

Global warming presents a significant threat to both human society and the planet's ecosystems. The primary driver of global warming is carbon dioxide emissions. As a result, governments around the world are prioritizing the goal of achieving net-zero emissions by 2050 [1]. The power and heat generation sectors alone account for 44 % of these emissions [2], making the transition to low-carbon energy sources, such as nuclear energy, essential. However, there are societal concerns regarding nuclear safety and the long-term waste produced by nuclear energy. The partitioning and transmutation strategy provides an effective way to reduce the challenges related to geological disposal of nuclear waste [3], Fig. 1.

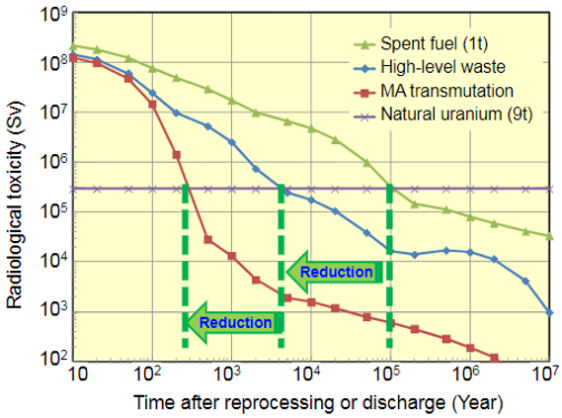


Figure 1: Reduction of radiotoxicity by applying partitioning and transmutation strategy [4].

The accelerator-driven subcritical system (ADS) is an advanced nuclear technology designed for transmutation, which reduces waste volume and its radiotoxicity, making geological disposal more affordable. Furthermore, it enables electricity generation—similar to the energy amplifier proposed by Rubbia [5]—as well as the production of fissile material through a process known as accelerator breeding [6]. In addition, the production of radioisotopes for nuclear medicine [7].

ADS consists of three main components: a high-power accelerator, a spallation target, and a subcritical reactor, as shown in Fig. 2. The accelerator directs a proton beam toward the spallation target to produce neutrons for the subcritical reactor. Since the reactor operates in a subcritical state, it requires an external neutron source to sustain nuclear fission; therefore, if the accelerator stops, the fission process also ceases. This inherent safety feature makes the ADS a more attractive option. Additionally, the ADS offers greater flexibility regarding fuel composition, such as the use of thorium.

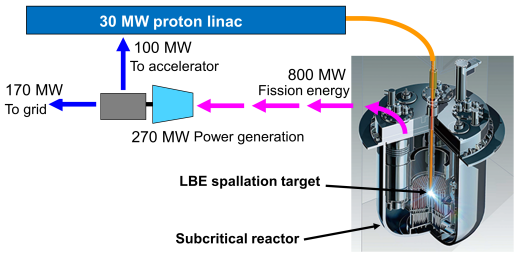


Figure 2: JAEA-ADS design.

The ongoing increase in the power of megawatt (MW)-class accelerators, combined with advancements in Superconducting Radio Frequency (SRF) technology, has opened new possibilities for ADS. Consequently, ADS will contribute to ensuring efficient and stable operation in the MW range and beyond, enhancing the reliability of current operation. This work reviews the essential characteristics of ADS accelerators and provides a summary of ADS-related activities taking place around the world.

ADS TIMELINE

Transmutation was one of the initial motivations for the use of particle accelerators. This motivation has persisted over the years to the present day. A simplified chronology of ADS systems is presented below [8, 9]:

Early Stage (1910-1950)

- 1919: The first artificial transmutation (E. Rutherford)
- 1932: Splitting the atom using an accelerator (J. Cockcroft)
- 1940s: Accelerators as neutron sources (E. O. Lawrence (USA) and W.N. Semenov (USSR))

* byee@post.j-parc.jp

Content from this work may be used under the terms of the CC BY 4.0 licence (© 2026). Any distribution of this work must maintain attribution to the author(s), title of the work, publisher, and DOI.

ISBN: 978-3-95450-275-2 ISSN: 2226-0366 doi: 10.18429/JACoW-LINAC2026-MO2A001

HIGH-DIMENSIONAL BEAM TOMOGRAPHY WITH PolariX: EXPERIMENTAL RESULTS FROM DESY AND PSI

S. Jaster-Merz[1,*], R. W. Assmann[1,†], J. Beinortaitė[1], B. Beutner[1], J. Björklund Svensson[1,‡], R. Brinkmann[1], F. Burkart[1], P. Craievich[2], R. D'Arcy[1,§], F. Demurtas[4,5], P. Dijkstal[2], H. Dinter[1], E. Ericson[2], Á. Ferran Pousa[1], P. González Caminal[1,¶], W. Hillert[3], R. Ischebeck[2], A. L. Kanekar[1], M. Kellermeier[1], W. Kuropka[1], F. Marcellini[2], D. Marx[1,‖], M. Maxton[1], F. Mayet[1], J. Osterhoff[1,**], E. Prat[2], S. Reiche[2], B. Stacey[1], M. Stanitzki[1], T. Vinatier[1], S. Wesch[1]
[1]Deutsches Elektronen-Synchrotron DESY, Germany
[2]PSI Center for Photon Science, Paul Scherrer Institute, Switzerland
[3]Department of Physics Universität Hamburg, Germany
[4]Sapienza University of Rome, Roma, Italy
[5]Istituto Nazionale di Fisica Nucleare-Laboratori Nazionali di Frascati, Frascati, Italy

Abstract

PolariX transverse deflection structures (TDS) are installed at different accelerators at DESY and PSI to enable advanced characterization of the particle beams for applications like free-electron lasers, beam-driven plasma acceleration, or advanced acceleration R&D projects. The variable streaking angle of PolariX – a differentiating capability of this TDS – allows us to apply a variety of tomographic methods for beam characterization. These methods provide insight into the behavior of particle beams by reconstructing their phase space in multiple dimensions, revealing information that would otherwise be inaccessible. In this contribution, we present an overview of the high-dimensional beam reconstructions obtained experimentally at DESY and PSI. Furthermore, we show our latest developments of the applied tomographic methods including a significant improvement in measurement speed – an important step towards regular usability.

INTRODUCTION

The polarizable X-band transverse deflection structure (PolariX TDS) [1–5] was developed by a collaboration of scientists from CERN, PSI, and DESY and driven by a common interest in longitudinal beam diagnostics with fs to sub−fs resolution. Currently, PolariX structures are installed, commissioned, and in routine operation at the FLASHForward [6], FLASH2 [7], and ARES [8] facilities at DESY, as well as at the Athos [9] beamline at SwissFEL, PSI. The PolariX TDS is operated at X-band frequency and has demonstrated single-digit femtosecond down to sub-femtosecond resolution [10]. A distinguishing feature of the PolariX TDS is the ability to vary the streaking direction, allowing for the measurement of time-resolved information in any transverse dimension. This flexibility to vary the streaking direction is enabled by the ability to change the relative phase between two RF ports of the so-called E-rotator [2,4], a device that acts as the input and output coupler of the deflection structure.

The PolariX TDSs are routinely used to measure the bunch duration and peak current [10], perform slice emittance measurements in the two transverse planes [5], or to monitor the longitudinal phase space of bunches for either free-electron laser (FEL) performance optimization and special mode characterization [11–13] or for minimizing the energy spread in beam-driven plasma acceleration [14, 15].

Phase-space Tomography

Apart from these conventional applications of the PolariX TDS, its variable streaking angle allows us to retrieve information of higher-dimensional phase spaces using tomographic reconstruction algorithms [16, 17]. These kinds of reconstructions provide a direct measurement of the particle beam's phase space and use projections of the characterized bunch under various angles which ideally cover a range of 180°. One example for such a method enabled by PolariX is the three-dimensional (3D) (x, y, t) charge density tomography [3, 16, 18, 19]. It can be applied on its own or combined with other tomography schemes to obtain higher-dimensional distributions of the beam. For example, the combination of the variable streaking with a 4D transverse phase space tomography [20] provides a reconstruction of the 5D (x, x', y, y', t) distribution, as described in detail in Refs. [17, 21]. Figure 1 shows an overview of these different phase-space tomographies. The general working principle of a 2D tomography is illustrated in Fig. 1 a). Projections of an object under various angles are combined in a sinogram and used to reconstruct a higher-dimension, in this case a 2D distribution, using a tomographic reconstruction algorithm (e.g., SART [22]). Figure 1 b) shows an example of a reconstructed 3D charge density distribution at ARES using the variable streaking of the PolariX TDS. A sketch of a transverse 4D phase space tomography using quadrupoles

* sonja.jaster-merz@desy.de
† Present address: GSI Helmholtzzentrum für Schwerionenforschung GmbH, Darmstadt, Germany
‡ Present address: Lund University, Lund, Sweden
§ Present address: Oxford University, Oxford, United Kingdom
¶ Present address: ATG Science & Technology S.L., Barcelona, Spain
‖ Present address: Brookhaven National Laboratory, Upton, NY, USA
**Present address: Lawrence Berkeley National Laboratory, Berkeley, California 94720, USA

Content from this work may be used under the terms of the CC BY 4.0 licence (© 2026). Any distribution of this work must maintain attribution to the author(s), title of the work, publisher, and DOI.

ISBN: 978-3-95450-275-2 ISSN: 2226-0366 doi: 10.18429/JACoW-LINAC2026-MO2A002

BEAM COMMISSIONING OF THE ESS ACCELERATOR: RESULTS AND CHALLENGES

S. Johannesson*, M. Eshraqi, I. Gorgisyan, N. Milas, R. Miyamoto, D. Noll, E. Salehi
European Spallation Source, Lund, Sweden

Abstract

In 2025, the beam produced by the European Spallation Source (ESS) accelerator, a 600 m-long superconducting proton machine, reached the beam dump for the first time. This presentation will give an overview over the results achieved during the commissioning rounds in 2025 and 2026, and the challenges remaining for high power and user operation.

INTRODUCTION

The European Spallation Source, ESS, is a European collaboration with thirteen member-states. The neutron source is located in southern Sweden and the ESS Data Management and Scientific Computing centre (DMSC) is located in the neighboring country Denmark.

Currently, the facility is in the midst of a series of commissioning campaigns to reach the design parameters for neutron production. When finalized, the neutron source will have an average neutron flux comparable to the continuous ILL source, while maintaining a low pulse repetition rate that enables the production of high-flux, low-energy neutrons [1].

When finalized, ESS will host fifteen specialized instruments, each optimized for a particular type of neutron experiment, with energy range determined by the moderator and the neutron beam extraction geometry [2]. The neutrons are produced through spallation when high-energy protons strike the target. The ESS target station employs a rotating tungsten target wheel designed to withstand the unprecedented average beam power of the facility.

Since construction began in 2014, significant progress has been made toward commissioning the European Spallation Source, with first spallation neutrons expected in early 2027. Of the planned fifteen instruments, five are expected to be ready for neutron operations in 2027 [3]. Below, a status update of the ESS LINAC is presented together with the objectives of the next commissioning run.

THE ESS LINAC

The high-level parameters of the proton LINAC needed to achieve the desired neutron flux are summarized in Table 1.

These parameters are reached using a 600 m high power LINAC. The general layout can be seen in Fig. 1, with intermediate energies marked in green and intermediate beamstops marked in purple. A 75 keV, 80 mA proton beam with a 6 ms pulse length is generated in the ion source (ISrc) and transported through the Low Energy Beam Transport (LEBT), where two solenoids provide transverse focusing and a slow chopper shortens the pulse before matching into the four-vane Radio-Frequency Quadrupole (RFQ). The RFQ is the first accelerating structure of the ESS LINAC and bunches, focuses, and accelerates the beam to 3.62 MeV. In the Medium Energy Beam Transport (MEBT), quadrupoles and three buncher cavities provide transverse and longitudinal focusing, while an additional chopper, collimators, and diagnostics clean and characterize the beam. The beam is then accelerated to 90 MeV in the normal-conducting Drift Tube Linac (DTL), consisting of five tanks with permanent quadrupole magnets in alternating drift tubes for transverse focusing, alongside integrated correctors and diagnostics. The accelerator components up until this point make up the Normal Conducting LINAC (NCL) [4].

Table 1: ESS Proton LINAC High-Level Proton Parameters for Neutron Production

Parameter	Unit	first neutrons	design
Beam Power	MW	2	5
Beam Energy	GeV	0.8	2
Peak Current	mA	62.5	
Pulse Length	µs	2860	
Rep. Rate	Hz	14	
Duty Cycle	%	4	
RF Frequency	MHz	352.21/704.42	

The superconducting LINAC (SCL) consists of three RF cavity families grouped into cryomodules, with LINAC Warm Units (LWUs) placed between them to house quadrupole doublets and beam diagnostics. The spoke cavity section (SPK) comprises 26 cavities operating at 352.21 MHz, arranged as two cavities per cryomodule, and accelerates the beam to 216 MeV. The medium-β section (MBL) contains 36 cavities and accelerates the beam to 571 MeV, while the high-β section (HBL) contains 84 cavities and accelerates the beam to its final energy of 2 GeV. At this time, 20 HBL cavities are ready, which puts the final beam energy to 877 MeV. Both the MBL and HBL cavities operate at 704.42 MHz, twice the SPK frequency, and are arranged as four cavities per cryomodule. In Fig. 1, each cryomodule is represented by a blue rectangle [5].

The lighter blue rectangles indicate cryomodules that have been installed but will not yet be available for commissioning in 2026, while the grey rectangles represent cryomodules planned for installation in the coming years. Downstream of the 21st HBL cryomodule is the High Energy Beam Transport (HEBT) section, which houses quadrupole doublets and beam diagnostics and also provides contingency space for future upgrades. At the end of the linac, the beam can be directed to the Tuning Beam Dump (TBD), a cylindrical

* sofia.johannesson@ess.eu

Content from this work may be used under the terms of the CC BY 4.0 licence (© 2026). Any distribution of this work must maintain attribution to the author(s), title of the work, publisher, and DOI.

ISBN: 978-3-95450-275-2 ISSN: 2226-0366 doi: 10.18429/JACoW-LINAC2026-MO2A004

COUPLED DYNAMICS AND TRANSVERSE MATCHING OF INTENSE HEAVY ION BEAMS

A. Gonzalez*, T. Maruta, K. Fukushima, P.N. Ostroumov
Facility for Rare Isotope Beams, Michigan State University, East Lansing, MI, USA

Abstract

Ion beams are extracted from the Electron Cyclotron Resonance source with an initial angular momentum. The focusing in the FRIB diver linac is provided by electric and magnetic solenoids and quadrupoles. Understanding the coupled dynamics and proper matching of the beams along the superconducting linac is critical to maintaining high-power, low-loss operation. The errors in the measured 4D rms emittances of various heavy-ion beams are highly sensitive to the quadrupole scan procedure.

INTRODUCTION

In the FRIB linac, quadrupole scans are used to reconstruct transverse beam emittances. The beam profiles are measured by wire-scanner profile monitors. The monitors contain three wires, one measuring the horizontal profile, one measuring vertical profile, and one measuring the 45-degree profile, which can be used to calculate the xy coupling term. The superconducting accelerating cryomodules contain solenoids for transverse focusing. Because the solenoids cause emittance exchange between vertical and horizontal projected 2D emittances, reliable 4D emittance reconstructions are necessary to properly track the evolution of the beam along the linac. This study documents the improvements made to the quadrupole scan procedures in the FRIB linac to produce more consistently accurate 4D emittance reconstructions.

4D Formalism

The transverse beam envelope matrix is known as the sigma matrix and is written as:

$$\Sigma = \begin{bmatrix} \langle x^2 \rangle & \langle xx' \rangle & \langle xy \rangle & \langle xy' \rangle \\ \langle xx' \rangle & \langle x'^2 \rangle & \langle x'y \rangle & \langle x'y' \rangle \\ \langle xy \rangle & \langle x'y \rangle & \langle y^2 \rangle & \langle yy' \rangle \\ \langle xy' \rangle & \langle x'y' \rangle & \langle yy' \rangle & \langle y'^2 \rangle \end{bmatrix} \tag{1}$$

It is a symmetric matrix with 10 independent elements. The 4D emittance of the beam is given by:

$$\epsilon_{4D} = \sqrt{\det(\Sigma)} \tag{2}$$

The projected 2D emittances ϵ_x and ϵ_y are calculated by:

$$\epsilon_x = \sqrt{\det \begin{bmatrix} \langle x^2 \rangle & \langle xx' \rangle \\ \langle xx' \rangle & \langle x'^2 \rangle \end{bmatrix}} \tag{3}$$

$$\epsilon_y = \sqrt{\det \begin{bmatrix} \langle y^2 \rangle & \langle y' \rangle \\ \langle y' \rangle & \langle y'^2 \rangle \end{bmatrix}} \tag{4}$$

The intrinsic emittances or eigenemittances ϵ_1 and ϵ_2 can be found by diagonalizing the sigma matrix to get:

$$\begin{bmatrix} \epsilon_1 & 0 & 0 & 0 \\ 0 & \epsilon_1 & 0 & 0 \\ 0 & 0 & \epsilon_2 & 0 \\ 0 & 0 & 0 & \epsilon_2 \end{bmatrix} \tag{5}$$

The 4D emittance is related to the eignemittances by $\epsilon_1 \epsilon_2 = \epsilon_{4D}$. If there is no transverse coupling, then $\langle xy \rangle = \langle xy' \rangle = \langle x'y \rangle = \langle x'y' \rangle = 0$ and the eigenemittances are equal to the 2D projected emittances [1]. However, if the beam is transversely coupled then the eigenemittances will be different from the projected emittances. Rivkin's inequality gives the relationship between the projected and eigenemittances as $\epsilon_x \epsilon_y \geq \epsilon_1 \epsilon_2$ [2, 3].

MEASUREMENTS AND RECONSTRUCTION

If R is the transfer matrix between the reconstruction location 0 and the measurement location 1, the sigma matrix at location 1 is calculated by:

$$\Sigma_1 = R \Sigma_0 R^T \tag{6}$$

At the profile monitor, $\langle x^2 \rangle_1$, $\langle y^2 \rangle_1$, and $\langle xy \rangle_1$ can be measured. They can also be written in terms of the elements of R as [4]:

$$\langle x^2 \rangle_1 = R_{11}^2 \langle x^2 \rangle_0 + R_{12}^2 \langle x'^2 \rangle_0 + 2R_{11}R_{12}^2 \langle xx' \rangle_0 \tag{7}$$

$$\langle y^2 \rangle_1 = R_{33}^2 \langle y^2 \rangle_0 + R_{34}^2 \langle y'^2 \rangle_0 + 2R_{33}R_{34}^2 \langle yy' \rangle_0 \tag{8}$$

$$\begin{aligned} \langle xy \rangle_1 = {} & R_{11}R_{33} \langle xy \rangle_0 + R_{12}R_{33} \langle x'y \rangle_0 \\ & + R_{11}R_{34} \langle xy' \rangle_0 + R_{12}R_{34} \langle x'y' \rangle_0 \end{aligned} \tag{9}$$

It is obvious that since each measurement produces three equations, at least four measurements are necessary to calculate the 10 independent parameters of the sigma matrix. After taking the profile measurements, a linear beam transport code called FLAME [5] is used to simulate the beam. The sigma matrix parameters are optimized using the Nelder-Mead method [6] to obtain the best least-squares fit to the measured data.

The FRIB linac can accelerate a wide range of heavy ion beams from oxygen to uranium. The beam is produced by an Electron Cyclotron Resonance (ECR) ion source [7] which contains sextupole fields and solenoid fields. The beam

* gonzalea@frib.msu.edu

Content from this work may be used under the terms of the CC BY 4.0 licence (© 2026). Any distribution of this work must maintain attribution to the author(s), title of the work, publisher, and DOI.

ISBN: 978-3-95450-275-2 ISSN: 2226-0366 doi: 10.18429/JACoW-LINAC2026-MO1P002

SIMPLE AND STABLE 3-GeV LINEAR ACCELERATOR IN HIGH BRILLIANCE SYNCHROTRON LIGHT SOURCE NanoTerasu

T. Asaka†
NanoTerasu center/National Institutes for Quantum Science and Technology, Sendai, Miyagi, Japan

Abstract

NanoTerasu is a highly brilliant synchrotron light source primarily focusing on the soft- to tender-X-ray region. The compact high-performance accelerator system at NanoTerasu consists of a storage ring with a circumference of 349 m and a 3 GeV linear accelerator with a length of 110 m. The linear accelerator is designed not only for full energy injection into the storage ring but also for future extension to soft X-ray free-electron laser (SX-FEL). A prominent feature of the injector system is a low-emittance, compact RF electron gun employing a transparent-grid scheme with a gridded thermionic cathode. The low-emittance beam from the electron gun is bunch-compressed to 5 ps using a sub-harmonic buncher and accelerated up to 40 MeV with an S-band accelerating structure. The bunched beam is accelerated up to 3 GeV using a C-band accelerator. Since beam commissioning of the linear accelerator began in April 2023, a 3 GeV electron beam with bunch charge of 0.36 nC and a normalized emittance of around 10 mm mrad has been successfully supplied to the storage ring. Despite its compact and simple configuration, this system is capable of producing a high-brightness, stable electron beam, making it a valuable model for future electron accelerators.

INTRODUCTION

The high-brightness synchrotron radiation facility NanoTerasu employs a 3 GeV low-emittance storage ring based on a multi-bend achromat lattice [1]. Synchrotron radiation generated by undulators achieves a brilliance exceeding 10^{21} photons/s/mm^2/mrad^2/0.1%b.w. in the soft- to tender-X-ray region, with coherence ratio of approximately 10%. At NanoTerasu, long-term stability of the optical system in the X-ray beamlines is maintained by top-up injection, thereby improving experimental performance and efficiency [2]. For ideal top-up injection, it is essential that the linear accelerator generate highly stable, high-performance electron beams. In addition, reducing the failure rate of accelerator components is an important issue to improve operational efficiency for user experiments, and this is reflected in the design guidelines of the NanoTerasu linear accelerator [3].

In the linear accelerator, the types of beam monitors used for beam tuning were optimized to enable rational and precise accelerator commissioning. For each component, the response of the beam parameters is compared with the results of particle tracking simulations obtained in advance, ensuring that the optimized parameters are fully realized.

† asaka.takao@qst.go.jp

3 GeV LINEAR ACCELERATOR

Design Concept

To minimize downtime during continuous operation, the accelerator was designed with a focus on improving the mean time between failures (MTBF) and the mean time to repair (MTTR). Simplification of accelerator components is essential to achieving this; it also facilitates efficient beam tunning helps minimize sources of instability.

Four design principles were established, provision for future expansion into an SX-FEL system based on the linear accelerator.

- High availability and robustness: A new DC gun with a gridded thermionic cathode was introduced to generate of high-quality, stable electron beams.
- Compact and simplified design: A simplified bunching system in the pre-injector and C-band accelerator with a high accelerating gradient were adopted to improve controllability and reduce construction costs.
- Improved MTBF and MTTR: Magnet power supplies and RF amplifiers were designed for high maintainability to enable rapid fault recovery.
- SX-FEL compatibility: Space for a bunch compression system is reserved to allow future system expansion.

Based on these guiding principles, a linear accelerator was developed as an injector for the low-emittance storage ring. Table 1 summarizes the required and measured beam parameters for the 3 GeV linear accelerator. At the injection point to the storage ring, the emittance of the injected beam is designed to be 3 nm rad, which corresponds to a normalized emittance of approximately 18 mm mrad. The beam charge of 0.3 nC or higher at 3 GeV is required per bunch.

Table 1: Design and Measured Beam Parameters

Items	Design	Measurement
Beam enegy	3 GeV	3 GeV
Energy spread	< 0.16% (FWHM)	0.04% (FWHM)
Energy stability	< 0.1 % (rms)	0.04 % (rms)
Bunch charge	0.3 nC	0.35 nC
Bunch length	< 10 ps (FWHM)	~ 5 ps (FWHM)
Emittance	3 nm rad	2.5 nm rad
Repetition rate	1 Hz	1 Hz

Content from this work may be used under the terms of the CC BY 4.0 licence (© 2026). Any distribution of this work must maintain attribution to the author(s), title of the work, publisher, and DOI.

ISBN: 978-3-95450-275-2 ISSN: 2226-0366 doi: 10.18429/JACoW-LINAC2026-MO1P003

SYSTEMATIC MITIGATION OF INTRA-BEAM STRIPPING AND DISTRIBUTED BEAM LOSS IN HIGH-INTENSITY H⁻ LINACS: EXPERIMENTAL AND OPERATIONAL EXPERIENCE AT J-PARC

Y. Liu*[1], M. Otani[1], T. Miyao[1], Y. Nakazawa[1], T. Shibata[1], K. Nanmo[1], Z. Fang[1], K. Futatsukawa[1], Y. Fukui[1], S. Mizobata[1], E. Cicek[1], K. Moriya[2], R. Kitamura[2], J. Tamura[2], K. Hirano[2], T. Itou[2], K. Okabe[2], K. Ohkoshi[2], K. Shinto[2], H. Takahashi[2], F. Kobayashi[2], Y. Kondo[2], T. Morishita[2], Y. Fuwa[2], H. Nakano[2], S. Shinozaki[2], P. Saha[2], H. Harada[2], F. Tamura[2]
[1]High Energy Accelerator Research Organization, Tsukuba, Japan
[2]Japan Atomic Energy Agency, Tokai, Japan

Content from this work may be used under the terms of the CC BY 4.0 licence (© 2026). Any distribution of this work must maintain attribution to the author(s), title of the work, publisher, and DOI.

Abstract

Charge-exchange injection with H⁻ beams enables high-intensity proton accumulation, but electron-stripping processes impose an intrinsic beam-loss challenge in high-power H⁻ linacs. In particular, intra-beam stripping (IBSt) becomes an important intensity-dependent loss mechanism that is strongly coupled to the beam phase-space distribution and focusing lattice.

At the J-PARC linac, we established a systematic approach to IBSt mitigation based on reliable beam characterization, controlled lattice manipulation, beam-dynamics simulation, and beam-loss measurements. The dependence of IBSt-induced loss on the lattice temperature ratio was quantitatively reproduced over a range of lattice settings, providing a basis for systematic optics optimization. An important further observation was that, although the relative loss levels agreed with simulations, the measured spatial loss distribution differed fundamentally from the calculated stripping distribution. Analysis of stripped H^0 transport revealed delayed and long-range loss localization governed by beamline aperture geometry, including substantial transport of H^0 to a downstream 0-degree dump.

These results led to a combined mitigation strategy using global lattice optimization and local aperture management, eliminating abnormal radiation hot spots and supporting stable high-power operation. The J-PARC experience contributes to a systematic methodology for predicting, localizing, and mitigating beam loss, from which design guidance for future high-intensity H⁻ linacs is distilled toward near-complete loss control.

INTRODUCTION

High-power proton sources have advanced substantially in both H⁻ linac-based and proton-linac approaches. For short-pulse, MW-class operation, H⁻ charge-exchange injection remains uniquely effective for accumulating high beam intensity in rapid-cycling synchrotrons and storage rings. For instance, with the J-PARC parameters, H⁻ charge-exchange injection enables approximately an order of magnitude higher accumulated beam intensity than proton multi-turn injection.

This advantage, however, comes with an intrinsic beam-loss mechanism: the weakly bound electron in H⁻ can be stripped by electromagnetic fields, collisions, or interactions within the beam itself. At the intensities required for MW-class operation, intra-beam stripping (IBSt) [1, 2] becomes particularly important, as its rate is strongly enhanced by beam density and convergence. And hence the IBSt rate can be controlled through the focusing lattice and the resulting transverse–longitudinal phase-space balance. This provides a direct handle for IBSt mitigation, as discussed in Sec. 3.

The IBSt production rate does not by itself determine where the resulting beam loss occurs, since the H^0 atoms produced can travel over extended distances before interception. Their loss locations are therefore governed by H^0 transport and the detailed beamline aperture geometry, and can differ substantially from the stripping distribution. At J-PARC, this behavior was identified experimentally through beam-loss and residual-radiation measurements and reproduced by explicit H^0 transport analysis.

The J-PARC linac provides a suitable platform for such a systematic investigation, combining beam characterization, beam-dynamics simulation for lattice manipulation to quantify and optimize IBSt, and analyze the subsequent H^0 transport to identify the mechanisms governing loss localization. This approach connects the control of H^0 production through the lattice with its subsequent localization through beamline geometry, enabling both global lattice optimization and local loss management.

J-PARC LINAC AND EXPERIMENTAL PLATFORM

The J-PARC linac is the high-current H⁻ injector for the Rapid Cycling Synchrotron (RCS) [3]. It consists of an ion source and low-energy beam transport (LEBT), radio-frequency quadrupole (RFQ), medium-energy beam transport 1 (MEBT1) for transverse and longitudinal matching and beam chopping to form the intermediate-pulse structure, drift-tube linac (DTL), separated-type drift-tube linac (SDTL), MEBT2 at 191 MeV for matching and frequency transition from 324 to 972 MHz, and annular-ring coupled structure (ACS) sections.

The linac was designed for 50 mA operation with pulse widths up to 500 μs, corresponding to 1-MW-class beam

* yong.liu@kek.jp

ISBN: 978-3-95450-275-2 ISSN: 2226-0366 doi: 10.18429/JACoW-LINAC2026-MOPO002

CONCEPT OF EMITTANCE EXCHANGE USING TWO BENDING MAGNETS AND TWO TRANSVERSE DEFLECTORS AT CLEAR (CERN LINEAR ELECTRON ACCELERATOR FOR RESEARCH)

C. Moore[1], A. Aksoy, R. Corsini, W. Farabolini, D. Gamba, A. Gilardi, J. Leygonie[2,3], S. Simonsson[4], K. Skilling[5], G. Tangari[6], T. Tus[5], S. Wang[5], A. Malyzhenkov[7]
CERN, Geneva, Switzerland
[1] also at University of Exeter, Exeter, United Kingdom
[2] also at Theryq, Rousset, France
[3] also at Gustave Roussy, Villejuif, France
[4] also at Lund University, Lund, Sweden
[5] also at University of Oxford, Oxford, United Kingdom
[6] also at Sapienza University of Rome, Rome, Italy
[7] also at Swiss International Institute Lausanne (SIIL), Prilly, Switzerland

Abstract

A second beam line has recently been installed and commissioned at CLEAR (CERN Linear Electron Accelerator for Research). The line begins with a switchyard consisting of two dipole bending magnets that offset the beam from its original path, along with quadrupoles and sextupoles placed between the bends to close the first- and second-order dispersion, respectively. In this work, based on analytical methods and numerical simulations, we present a concept for an emittance exchange scheme realized using the switchyard. We show that transverse-to-longitudinal phase space exchange can be achieved by activating a transverse deflector located upstream, together with an additional deflector downstream (the only missing element). Furthermore, we demonstrate that such a scheme enables advanced beam phase-space tailoring and expands the CLEAR beam parameters beyond its nominal operational range.

INTRODUCTION

Longitudinal-to-transverse Emittance Exchange (EEX) is an established and advanced method of phase space manipulation, allowing various bunch shaping and beam gymnastics. This concept is useful for free-electron lasers and bunch compressions with reduced coherent synchrotron radiation effects [1]. EEX beamlines are usually designed and built as a separate beam complex or beamline, utilizing double DogLeg concepts with transverse deflecting cavities (TDC) between dipoles [2–4].

Several FEL and irradiation facilities with multiple beamlines feature only a single dogleg switchyard comprised of two dipole bending magnets, making standard EEX scheme inapplicable. For instance, at CLEAR, the switchyard consists of 2 dipole magnets with a quadrupole triplet in between. The proposed EEX setup needs a TDC upstream of the switchyard, which has already been installed for longitudinal beam diagnostics [5], and also a TDC downstream of the switchyard, which has not been installed yet. Thus, this concept repurposes the current DogLeg beamline at CLEAR, with the addition of only one extra TDC.

In this paper, both thin and thick cavity models are presented, each with reproducible conditions to have ideal EEX. The linear beam dynamics based off this model is then tested through simulations and optimal parameters for the CLEAR beamline calculated.

EEX SETUP

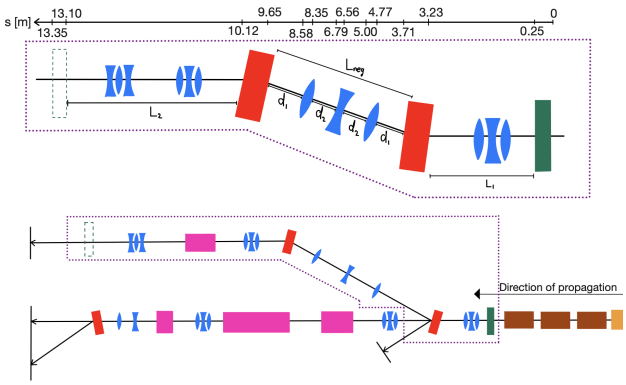


Figure 1: Simplified schematic of the CLEAR beamline with test areas (pink), quadrupoles (blue), dipoles (red), accelerating cavities (brown), gun (orange), and TDCs (green). The proposed EEX setup is circled in the purple dotted line, with a close-up view above the beamline schematic. The last TDC (left) is depicted with a dashed green box as it is the only component that has not yet been installed.

At CLEAR, a recently built DogLeg beamline comes off the mainline at 22° via a dipole magnet, as depicted in Fig. 1. The upstream TDC couples the transverse and longitudinal phase spaces, while the DogLeg provides the required horizontal dispersion, such that x depends on δ.

MATRIX FORMALISM

As previously stated, the Dogleg section consists of two dipoles, with quadrupoles and drift spaces in between. It

Content from this work may be used under the terms of the CC BY 4.0 licence (© 2026). Any distribution of this work must maintain attribution to the author(s), title of the work, publisher, and DOI.

ISBN: 978-3-95450-275-2 ISSN: 2226-0366 doi: 10.18429/JACoW-LINAC2026-MOPO006

THE HIGH-POWER GALLIUM-INDIUM LIQUID TARGET AT SARAF: DESIGN, VALIDATION, AND MULTI-DISCIPLINARY APPLICATIONS

S. Vaintraub, I. Mardor, K. Barda, S. Harosh, A. Perry, E. Reinfeld,
I. Silberman, B. Schwartzman, L. Weissman, I. Eliyahu
Soreq NRC, Yavne, Israel

Content from this work may be used under the terms of the CC BY 4.0 licence (© 2026). Any distribution of this work must maintain attribution to the author(s), title of the work, publisher, and DOI.

Abstract

The Soreq Applied Research Accelerator Facility (SARAF) is advancing to Phase II to deliver continuous wave proton and deuteron beams (5–40 MeV, ~5 mA). Handling the resulting ~200 kW beam power requires a robust dump capable of dissipating high power densities. To meet this challenge, a windowless liquid gallium-indium (Ga-In) jet target, GaLiT, was designed. It generates a stable ~5 m/s jet with a verified thickness of 5.6±0.3 mm, sufficient to stop the incident beam. Ga-In offers superior heat transfer and reduced chemical hazards compared to liquid lithium.

Beyond serving as a beam dump, this system functions as a high-intensity neutron source, designated MARZEPAN, yielding > 10^{15} n/s with energies up to ~45 MeV. This facility supports a broad spectrum of physics applications: Fusion Material Research (simulating reactor environments and radiation damage studies), Astrophysics (enabling research into stellar nucleosynthesis via tunable neutron spectra), and Fundamental Nuclear Physics (producing short-lived isotopes via systems like SARONA for weak interactions and cross-section measurements). This contribution presents the design and scientific applications of GaLiT.

INTRODUCTION

The Soreq Applied Research Accelerator Facility (SARAF) is currently undergoing its Phase II upgrade, which integrates superconducting modules to deliver continuous wave (CW) proton and deuteron beams at energies up to 35/40 MeV [1]. Transporting and utilizing this beam requires optimized quadrupole and steering magnets designed to maintain stability for up to 5 mA of current. To manage the extreme power density deposited by this beam, which can reach up to 200 kW/cm^2, a high-power infrastructure and "beam dump" are essential. This requirement led to the development of the Gallium-Indium Liquid Target (GaLiT), which utilizes a high-velocity liquid jet to prevent material evaporation into the vacuum system [2].

TARGET INFRASTRUCTURE AND SHIELDING

The layout of the facility connects the accelerator directly to the experimental target areas, culminating in the Beam Dump Room (see Fig. 1) [1]. This area houses the primary GaLiT target and is critical for fully stopping the 5 mA, 40 MeV beam.

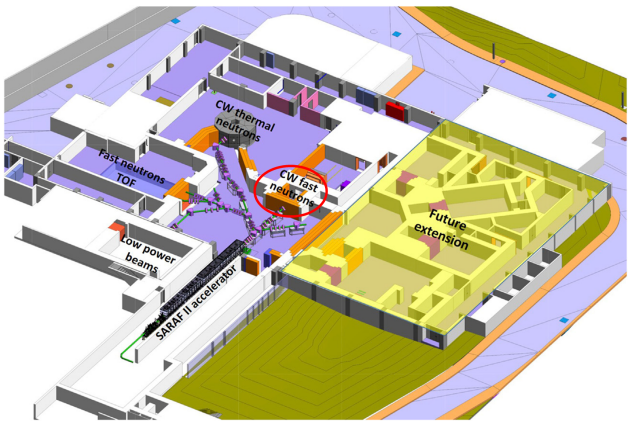


Figure 1: Layout of the SARAF Phase II facility, highlighting the accelerator, beam transport lines, and the target rooms, including the dedicated CW fast neutrons area.

Shielding Architecture

To ensure safe operation and mitigate radiation hazards, the bunker vault incorporates a heavy concrete and localized lead shielding architecture designed to contain both prompt and activation radiations. The strategic layout minimizes air activation and includes a massive concrete door to allow for safe maintenance access. Figure 2 shows a visualization of the Beam Dump Room and its related infrastructure.

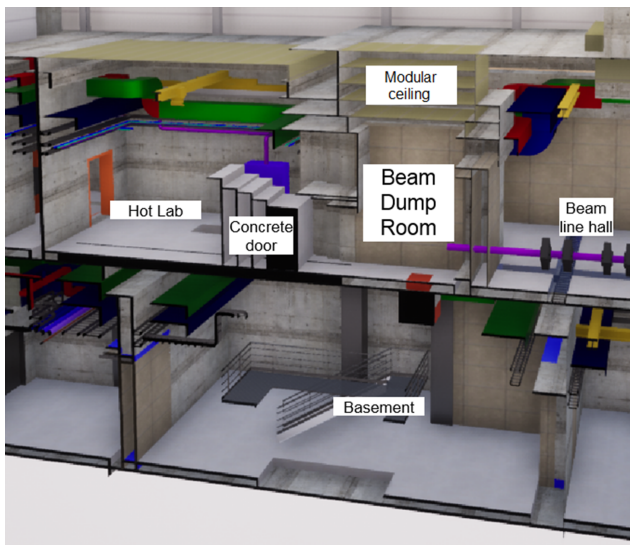


Figure 2: A 3D visualization of the Beam Dump Room and surrounding facility, highlighting the modular ceiling, basement, and concrete door for controlled access. This infrastructure is designed with strategic heavy concrete shielding to contain radiations.

ISBN: 978-3-95450-275-2 ISSN: 2226-0366 doi: 10.18429/JACoW-LINAC2026-MOPO007

L4-RFQ2 RF CONDITIONING AND BREAKDOWN LOCALIZATION STUDIES

P. Martinez-Reviriego*, A. Grudiev, W. L. Millar, S. Ramberger, L. Timeo, R. Wegner
CERN, Geneva, Switzerland

Abstract

CERN's Linac4 is a linear accelerator for H^- ions that has been in operation since 2020. At the injection into the proton synchrotron booster, the ions are converted to protons via electron stripping and sent downstream to various experiments on the CERN site. Its first accelerating structure is a 3 m long Radio-Frequency Quadrupole (RFQ), operating at 78 kV inter-vane voltage and a peak surface field of 34 MV/m. In 2025, a dedicated campaign was launched to condition and test the recently constructed spare RFQ, providing the opportunity to study vacuum breakdown behavior in this complex structure.

This work presents high-power RF conditioning results to improve the understanding of breakdown limitations in the new RFQ. It also focuses on localizing breakdown events using signals from 4×4 pick-ups distributed in the 4 quadrants along the cavity. These measurements are compared with RF simulations to correlate signal patterns with breakdown locations and provide insight into the underlying physical mechanisms.

INTRODUCTION

Since 2020, Linear accelerator 4 (Linac4), designed to accelerate negative hydrogen ions to 160 MeV, supplies proton beams to the CERN accelerator complex [1]. After the H^- source, four types of accelerating structure are used: a radio-frequency quadrupole (RFQ), drift tube linacs, coupled-cavity drift tube linacs and π-mode structures.

In the case of the RFQ [2], the high surface electric field in the vanes can induce RF breakdowns (BDs), leading to beam losses and potentially limiting the lifetime of the machine. In addition, the RFQ is exposed to low-energy hydrogen ion irradiation, leading to blistering in the copper surface [3]. After a visual inspection of the Linac4 RFQ, a decision was made to build, tune [4] and high-power condition a spare RFQ (RFQ2) for Linac4 in case of performance degradation.

This work shows the lessons learnt during the ongoing high-power conditioning campaign carried out for the spare RFQ, bringing valuable knowledge to the high-power accelerating cavities community. In addition, a method to localize BDs in the RFQ has been developed to complement existing diagnostic techniques based on the strategies used for the high-power conditioning of CLIC structures [5].

HIGH-POWER CONDITIONING

The RFQ for the Linac4 is an accelerating cavity that focuses, bunches and accelerates a continuous beam of low-energy H^- from 45 keV to 3 MeV. Its main specifications are listed in Table 1.

Table 1: RFQ Design Parameters [2]

Parameter [unit]	Value
Frequency [MHz]	352.2
Type	Standing wave
Mode	TE210
Pulse width [μs]	1000
Repetition rate [Hz]	0.833
Structure length [m]	3.06
Quality factor	6772
Coupling factor (β)	1.6
Peak input power [kW]	380
Vane voltage [kV]	78
Max E_s [MV/m]	34
Max H_s [kA/m]	5.17
Max S_c [MW/mm^2]	0.01

The RF behavior of the cavity is monitored by measuring the input and reflected signal, in combination with 16 pick-ups that are placed at different longitudinal positions in each of the quadrants of the cavity, as shown in Fig. 1.

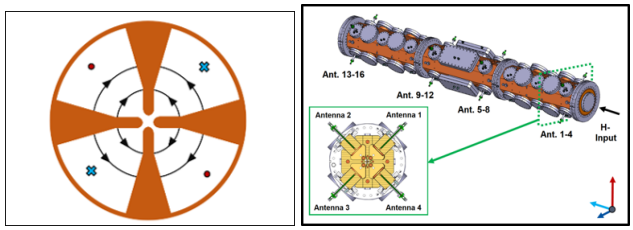


Figure 1: (a) Field distribution; (b) set-up for the RFQ measurements.

During a normal pulse, the signals correspond to square amplitudes. However, BDs events disrupt the normal behavior of the cavity, producing large reflected power and a rapid decrease in the stored cavity energy. A comparison between a typical event and a BD is shown in Fig. 3. Note that incident and reflected signals are in linear scale, while antenna data are shown on a log scale [6].

High power conditioning of the spare RFQ started around March 2025. The test stand is limited to a maximum pulse length of 660 μs and a 0.8 Hz repetition rate. The fact that the high-power conditioning improves with cumulative RF pulses, results in a slow conditioning rate for this structure [5]. To increase the speed of the conditioning, the pulse length was reduced to 50 μs, allowing the repetition rate to be doubled by introducing two short RF pulses in the same

* pablo.martinez.reviriego@cern.ch

Content from this work may be used under the terms of the CC BY 4.0 licence (© 2026). Any distribution of this work must maintain attribution to the author(s), title of the work, publisher, and DOI.

ISBN: 978-3-95450-275-2 ISSN: 2226-0366 doi: 10.18429/JACoW-LINAC2026-MOPO009

STATUS UPDATE OF PERMANENT MAGNET RADIATION RESILIENCY STUDIES AT CEBAF*

R.M. Bodenstein†, C. Decker, K.E. Deitrick, B.R. Gamage, J.F. Gubeli, D. Hamlette, M.B. Imber Safdar, M. Janak, K. Jordan, E.B. Juarez, S. Lee, M.X. Mason, J. Meyers, B. Mosbrucker, I. Neththikumara‡, E. Nissen, V. Okey-Ejiowhor, A. Ramirez, J. Samari, S. Shriner, M. Smith, D. Thomas, N. Wilson,
Thomas Jefferson National Accelerator Facility, Newport News, VA, USA
C. Matthews, Old Dominion University, Norfolk, VA, USA
S.J. Brooks, Brookhaven National Laboratory, Upton, NY, USA
S. Boogert, Cockcroft Institute, Daresbury, UK
W. Shields, Royal Holloway, University of London, Egham, UK
B. Shepherd, STFC, Daresbury, UK

Abstract

The proposed energy upgrade of the Continuous Electron Beam Accelerator Facility (CEBAF) incorporates Fixed-Field Alternating-gradient (FFA) arcs utilizing permanent magnet technology. Given the radiation environment within the CEBAF tunnel enclosure, validating the long-term magnetic stability of these materials is a critical step for the project's technical feasibility. This contribution presents an overview of the ongoing permanent magnet radiation resiliency program at Jefferson Lab, which has expanded into one of the largest and most comprehensive in-situ studies of its type ever performed in an accelerator environment. We briefly review the experimental methodology used to monitor demagnetization and summarize the operational experience from the initial data-taking campaign. Furthermore, we discuss the upgrades implemented for the second exposure campaign, currently underway, which aims to refine dose correlation and reduce systematic uncertainties. We report on the latest results from the program and the roadmap for certifying permanent magnet optics for the proposed upgrade energies.

INTRODUCTION

The FFA@CEBAF energy upgrade proposes increasing the beam energy beyond 20 GeV by replacing conventional electromagnetic arcs with permanent-magnet FFA arcs [1]; the long-term radiation stability of these magnets is critical to its technical feasibility. Radiation-induced demagnetization is well studied for undulator magnets [2], with an established damage hierarchy ranking protons above neutrons, electrons, and gammas [3, 4]. However, prior studies typically used small sample sets ($N \leq 12$), doses far exceeding the CEBAF environment, or single material families. This project addresses all three limitations, deploying 60 plates carrying 540 magnets (two NdFeB and two SmCo grades) in the operational tunnel for 12 months, with 57 further plates as unexposed laboratory controls. Co-locating radiation-sensitive NdFeB with radiation-hard SmCo on each plate enables a gain-immune intra-plate differential that cancels instrumental drift and isolates radiation-induced changes. Prior publications [5–7] detail the design, dosimetry, simulations, and apparatus.

EXPERIMENTAL OVERVIEW

Sample Design

Thirty plates, each carrying four randomized permanent magnet samples (two NdFeB grades: N42EH and N52SH; two SmCo grades: SmCo33H and SmCo35), were deployed at eight tunnel regions (four recirculating arcs, two linacs, and two labyrinths) for approximately 12 months. Nine identical plates remained in the laboratory as unexposed controls. The randomized co-location of all four materials on each plate is central to the analysis: the intra-plate differential between the radiation-sensitive NdFeB and radiation-hard SmCo cancels the dominant Helmholtz coil gain drift (± 0.124 %) by construction, enabling sub-percent detection sensitivity.

Additionally, pair assembly plates with controlled magnetic configurations (aligned, antiparallel, and perpendicular) approximate different field orientations within a Halbach array [8, 9], providing data relevant to multifunction FFA magnet design.

Measurement and Dosimetry

Magnetic moments are measured with a precision Helmholtz coil system [10] and point fields with a Senis 3MH6 Teslameter [11], both mounted on mobile carts for in-situ tunnel access during accelerator downtime [12, 13]. Each plate is tracked with co-located dosimetry: optically stimulated luminescence (OSL) area monitors for photon and neutron dose, and FWT-70 optichromic rods for high-dose gamma fields [5]. Gamma doses span five orders of

* Work supported by the U.S. Department of Energy, Office of Science, Office of Nuclear Physics under contract 89243126CSC000213. The research described in this work was conducted under the Laboratory Directed Research and Development Program at Thomas Jefferson National Accelerator Facility for the U.S. Department of Energy.

† ryanmb@jlab.org

‡ Now at Los Alamos National Lab.

Content from this work may be used under the terms of the CC BY 4.0 licence (© 2026). Any distribution of this work must maintain attribution to the author(s), title of the work, publisher, and DOI.

ISBN: 978-3-95450-275-2 ISSN: 2226-0366 doi: 10.18429/JACoW-LINAC2026-MOPO010

MACHINE LEARNING APPLICATIONS FOR BEAM DIAGNOSTICS AND AUTOMATED TUNING AT CLEAR

A. Gilardi*, M. Bergamaschi, S.Burger, R. Corsini, W. Farabolini, O. Franek[1], D. Gamba, J. P. Leygonie, A. Malyzhenkov[2], C. M. Moore[3], F. Roncarolo, S. J. Simonsson[4],G. Tangari[5], G. Trad, Q. Xu[6], S. Wang[7] CERN, Geneva, Switzerland
[1]also at Czech Technical University in Prague, Prague, Czech Republic
[2]also at Swiss International Institute Lausanne (SIIL), Prilly, Switzerland
[3]also at University of Exeter, Exeter, United Kingdom
[4]also at Lund University, Lund, Sweden
[5]also at Sapienza University of Rome, Rome, Italy
[6]also at University of Liverpool, Liverpool, United Kingdom
[7]also at University of Oxford, Oxford, United Kingdom

Abstract

Machine learning (ML) is increasingly recognized as a fundamental tool in modern accelerator physics, offering new capabilities to complement and extend traditional analytical approaches. A structured programme of ML studies has been initiated at CLEAR (CERN Linear Electron Accelerator for Research), covering three principal directions: beam diagnostics, charge forecasting, and automated tuning via reinforcement learning. Deep learning models were explored to reconstruct transverse beam profiles from indirect measurements, offering a pathway toward radiation-resistant diagnostics. Classical and deep learning approaches were benchmarked for charge prediction, demonstrating the potential for accurate real-time beam characterization. A reinforcement learning framework was interfaced with the CERN control infrastructure, enabling proof-of-principle autonomous beam steering through iterative magnet corrections. These results demonstrate the feasibility of integrating ML into routine CLEAR operations and position the facility as an attractive testbed for the development and validation of machine learning techniques for particle accelerators.

INTRODUCTION

Machine learning (ML) has emerged over the past decade as a powerful tool for data-driven accelerator physics, with applications spanning beam diagnostics, surrogate modeling, performance optimization and anomaly detection [1–3]. A persistent obstacle to deploying it on operational machines is the gap between algorithm development, typically carried out in simulation, and real accelerators, where noise, non-stationarity and hardware constraints impose stringent requirements on robustness and sample efficiency. Bridging it requires facilities where algorithms can be exercised directly on hardware without jeopardizing a high-stakes physics programme.

The CERN Linear Electron Accelerator for Research (CLEAR), a versatile 40 m-long electron linac operated as a user facility since 2017 [4, 5], is well positioned for this role: its compact scale allows rapid iteration between algorithm and experiment, its reconfigurable beamline provides several independent training and validation environments, and the CERN control middleware gives direct programmatic access to all machine parameters and diagnostics [6].

This paper reviews the main three ML research lines currently pursued at CLEAR: deep-learning reconstruction of transverse profiles for radiation-tolerant diagnostics, charge forecasting and virtual diagnostics, and reinforcement learning (RL) for autonomous tuning.

TRANSVERSE PROFILE RECONSTRUCTION

Transverse beam imaging in high-radiation areas is limited by camera degradation: irradiation tests at CHARM showed a sharp loss of visibility above 250 Gy of total integrated dose, whereas some accelerator areas are expected to exceed 400 Gy [7], and radiation-hardened VIDICON tubes are no longer produced. A promising alternative relays the light from the radiation zone to a shielded area through a large-core multi-mode fiber (MMF), where a standard CMOS camera can operate safely [8, 9]. MMF transmission, however, mixes tens of thousands of guided modes: scattering, mode coupling and inter-modal dispersion turn the input image into a speckle pattern at the fiber output. Recovering the transverse distribution from that pattern is an inverse problem well suited to deep learning.

To train and test the models without using beam time, the scintillating screen is emulated on an optical bench by a laser-illuminated digital micro-mirror device (DMD), onto which any image, synthetic or previously measured, can be loaded. A beam splitter sends part of the light to a camera recording the ground truth and part into the MMF, whose output is imaged on a second, synchronized camera. Each acquisition therefore yields a matched ground-truth/speckle pair, and tens of thousands can be collected in a few hours without exposing the reference camera to radiation.

Training samples are generated by a stochastic Gaussian mixture (SGM) simulation, each image being a superposition of K rotated two-dimensional Gaussians with ran-

* antonio.gilardi@cern.ch

Content from this work may be used under the terms of the CC BY 4.0 licence (© 2026). Any distribution of this work must maintain attribution to the author(s), title of the work, publisher, and DOI.

ISBN: 978-3-95450-275-2 ISSN: 2226-0366 doi: 10.18429/JACoW-LINAC2026-MOPO011

GENERATIVE PHASE-SPACE RECONSTRUCTION FOR LOW-INTENSITY BEAM CHARACTERIZATION IN THE J-PARC MUON LINAC MEBT LINE

E. Cosgun*[1], Y. Nakazawa[1], M. Otani[1], Y. Kondo[2]
[1]High Energy Accelerator Research Organization (KEK), Tokai, Ibaraki, Japan
[2]Japan Atomic Energy Agency (JAEA), Tokai, Ibaraki, Japan

Abstract

Generative phase-space reconstruction is investigated as a method for beam characterization in the J-PARC Muon Linac MEBT-I. For 4D reconstruction, the results show that transverse beam parameters can be reproduced with relative errors below approximately 10 % even for a limited number of particles and measurement settings. To extend the method to six-dimensional phase space, a differentiable sliced-field cavity model is implemented to represent the low-β buncher cavity in MEBT-I. The model enables the buncher phase to provide sensitivity to the longitudinal phase-space distribution. A proof-of-principle six-dimensional reconstruction demonstrates good recovery of the longitudinal beam properties, indicating the feasibility of generative model for high-dimensional characterization of low-intensity muon beams.

INTRODUCTION

The J-PARC muon linac is being developed for a precision measurement of the muon anomalous magnetic moment, $a_\mu = (g-2)_\mu/2$, and a search for the muon electric dipole moment using a re-accelerated, low-emittance ultra-slow muon (USM) beam [1]. The Medium Energy Beam Transport (MEBT-I) line, planned for commissioning in 2027, will transport and match the accelerated muon beam from the radio-frequency quadrupole (RFQ) to the Inter-digital H-mode drift tube linac (IH-DTL). Because the intensity of the accelerated USM beam is expected to be low during this commissioning stage [2], the applicability of conventional phase-space characterization methods is limited by the available particle statistics. Machine-learning-based reconstruction techniques, which can extract high-dimensional beam information from a limited set of diagnostic measurements, are therefore particularly attractive for beam characterization in the J-PARC muon linac.

In this study, we investigate the applicability of generative phase-space reconstruction (GPSR) [3] to the MEBT-I beamline. First, the accuracy of four-dimensional transverse phase-space reconstruction is evaluated under limited particle statistics and quadrupole-scan settings. The method is then extended toward six-dimensional reconstruction using the MEBT-I buncher and downstream dispersive section.

MEBT-I BEAMLINE LAYOUT

In the low-velocity section, the 324 MHz RFQ accelerates the muons to a kinetic energy of 0.34 MeV. The MEBT-I line then transports the beam and provides the transverse and longitudinal matching required for injection into the IH-DTL, which accelerates the beam to 4.26 MeV [4].

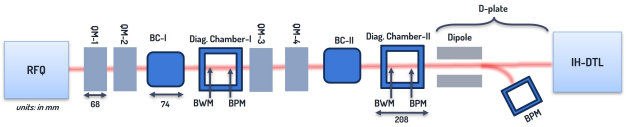


Figure 1: J-PARC Muon Linac MEBT-I line.

As shown in Fig. 1, MEBT-I contains four quadrupole magnets (QM1–QM4) arranged as two doublets, two 324 MHz single-gap buncher cavities (BC-I and BC-II), and two diagnostic chambers. Each diagnostic chamber contains a microchannel-plate (MCP)-based beam profile monitor (BPM) [5] and a bunch-width monitor (BWM) [6]. These diagnostics provide the transverse beam profile in the x–y plane from the BPMs and the longitudinal bunch time distribution from the BWMs for beam commissioning. A dipole magnet together with the downstream profile monitor forms the dispersive diagnostic system, referred to as the D-plate in Fig. 1. This D-plate measurement provides sensitivity to the longitudinal phase-space coordinates and is used for the 6D reconstruction study.

GENERATIVE MODEL IN MEBT-I

The generative model combines a neural-network representation of the unknown beam distribution with a differentiable accelerator simulation [7]. As shown in Fig. 2, fixed latent samples are transformed into macroparticle coordinates by a neural-network generator. The generated beam is then transported through a differentiable model of MEBT-I and converted into simulated diagnostic images. The generator parameters are optimized by minimizing the difference between the simulated and measured images, yielding an estimate of the initial phase-space distribution.

The MEBT-I layout is well suited to this approach because its quadrupoles, buncher cavities, and diagnostic chambers provide complementary information about the transverse and longitudinal beam distributions. The BPM and BWM can also be used to validate the reconstructed distribution by comparing predicted and measured transverse profiles and bunch widths at the diagnostic chambers.

4D Phase-Space Reconstruction

The different MEBT-I settings provide complementary projections of the initial beam distribution. In particular, a quadrupole scan changes the transverse beam transport to the diagnostic plane. By observing the beam profile over several

* ecosgun@post.kek.jp

Content from this work may be used under the terms of the CC BY 4.0 licence (© 2026). Any distribution of this work must maintain attribution to the author(s), title of the work, publisher, and DOI.

ISBN: 978-3-95450-275-2 ISSN: 2226-0366 doi: 10.18429/JACoW-LINAC2026-MOPO015

PMULTI-OBJECTIVE GENETIC ALGORITHM-BASED BEAM MATCHING OPTIMIZATION FOR CSNS-II SUPERCONDUCTING LINAC

X. Y. Feng†, J. Peng, S. Wang
Institute of High Energy Physics, Beijing, China

Abstract

This paper presents a matching optimization method based on multi-objective genetic algorithm for beam recovery of the superconducting linac in the China Spallation Neutron Source Phase II (CSNS-II). The method takes cavity voltage and synchronous phase of superconducting cavities as optimization variables, and uses multiple parameters such as output beam energy, energy spread, and emittance as objective functions. Through mutation, selection, and iteration mechanisms of the genetic algorithm, the optimal combination of RF parameters is sought. Simulation results show that the method can effectively restore beam parameters under hardware constraints, providing technical support for stable operation of the superconducting accelerator.

INTRODUCTION

The China Spallation Neutron Source (CSNS) Phase II upgrade aims to increase the target power from 100 kW to 500 kW. This requires constructing a new ~90-meter-long superconducting section after the existing 80 MeV linac to boost the beam energy to 300 MeV. The superconducting section, as shown in Figure 1, consists of 44 cavities: the first 20 are spoke cavities (324 MHz) and the remaining 24 are elliptical cavities (648 MHz)[1].

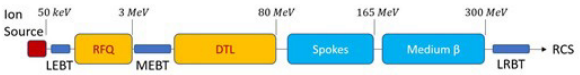


Figure 1: CSNS-II linac layout.

Superconducting accelerators face challenges such as cavity failures and RF system fluctuations, necessitating an effective beam recovery mechanism. Based on multi-objective genetic algorithm, this paper develops a beam matching optimization method for the CSNS-II superconducting linac, capable of rapidly restoring beam parameters under abnormal conditions such as cavity failure.

PROBLEM DESCRIPTION

Optimization Objectives

The requirements on injection beam of Rapid Cycling Synchrotron (RCS) in CSNS-II is show in table 1. Under the current design, the output beam parameters at the superconducting section exit are: energy 300 MeV, longitudinal RMS emittance 0.1632 π·deg·MeV, RMS energy spread 0.1908 MeV, transverse combined emittance growth ~4.1%, longitudinal emittance growth ~15.6% [2,3].

Table 1 Beam Requirements of CSNS-II RCS

	Parameter
Injection energy	300MeV
Energy deviation limit	0.1%
Energy deviation	0.3MeV
Energy spread limit	0.05%-0.15%
Energy spread	0.15-0.5 MeV

Hardware Constraints

The optimization algorithm must consider the following hardware boundaries:

- Maximum cavity gradient of spoke cavities: 9 MV/m.
- Maximum cavity gradient of elliptical cavities: 14.3 MV/m.

The nominal and Maximum cavity gradient of SC cavities are shown in Figure 2.

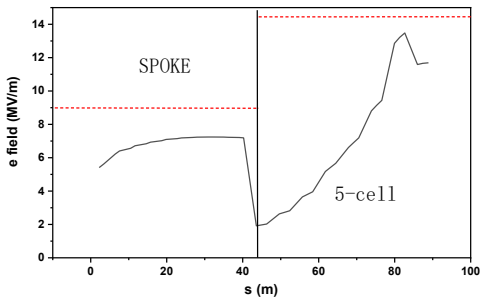


Figure 2: Superconducting cavity hardware parameter limits.

Cavities are named in the format “section-cryomodule number-cavity number", e.g., the twelfth cavity in the spoke section is designated SPOKE06-2.

GENETIC ALGORITHM DESIGN

Each chromosome represents a set of superconducting cavity parameters, containing both cavity voltage and synchronous phase for all cavities. The initial population is randomly generated, with generally low individual fitness.

Mutation introduces new parameter values by randomly altering certain loci of chromosomes. The mutation range for cavity voltage is limited by hardware constraints (spoke cavities ≤ 9 MV/m, elliptical cavities ≤ 14.3 MV/m), and for synchronous phase within -40° to -10°.

†fengxinyuan@ihelp.ac.cn

Content from this work may be used under the terms of the CC BY 4.0 licence (© 2026). Any distribution of this work must maintain attribution to the author(s), title of the work, publisher, and DOI.

ISBN: 978-3-95450-275-2 ISSN: 2226-0366 doi: 10.18429/JACoW-LINAC2026-MOPO016

STUDY OF TRANSIENT BEAM EFFECTS IN THE SARAF INJECTOR

L. Weissman†, A. Perry, I. Sabo-Napadensky, A. Shor, R. Weiss-Babai
SARAF, SNRC, Yavne, Israel

Content from this work may be used under the terms of the CC BY 4.0 licence (© 2026). Any distribution of this work must maintain attribution to the author(s), title of the work, publisher, and DOI.

Abstract

Transient processes such as build-up of space charge neutralization in the LEBT and beam loading in the RFQ and cavities influence the beam properties during pulses formation. Understanding these processes is critical for the machine commissioning and operation. In this report we describe our study to identify the relevant processes, estimate their effects on the beam dynamics in the linac and apply mitigations to minimize those effects.

INTRODUCTION

The SARAF accelerator [1] operates in a pulse mode in the broad duty cycle range. It is expected, that the initial part of the beam pulse may exhibit different properties than the stabilized part of the beam due to the so-called transient processes. This leads to an important question whether the use of short pulses in the accelerator commissioning and general tune is adequate for general operation in the whole duty cycle range. Understanding the transient phenomena is particularly important in the context of the possible beam loss in a superconducting linac, which may take place due to different beam optical conditions at the beginning of the pulse, potentially causing quenching of superconducting solenoids or damage in superconducting cavities. These considerations motivated us to perform extensive studies of the transient effects, originating in the accelerator injector.

OBSERVATION OF THE TRANSIENTS

LEBT: Charge Neutralization

The transient effect associated with the build-up of space charge neutralization in the SARAF LEBT section was studied in [2]. The dynamic space charge neutralization following the beam pulse formation by the LEBT chopper has been evaluated based on beam pulse measurements at a collimator and beam blocker at the RFQ entrance (Fig.1). This simple methodology, together with extensive beam dynamic simulations, provide insight into the transient dynamic processes taking place during beam pulse formation in LEBT. The obtained neutralization built up time is of the order of 70 μs. The final steady state neutralization, of the order of 80 %, was also obtained in this analysis.

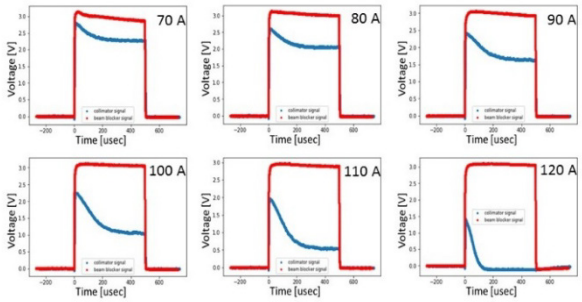


Figure 1: The collimator (blue) and beam blocker (red) beam traces collected for various excitation currents of the third solenoid. Measurements performed for 4 mA deuteron pulse.

MEBT: Overall Transmission

In the following paper [3] we studied the influence of the LEBT dynamic beam neutralization and beam loading in the SARAF RFQ on the overall beam transmission through the SARAF MEBT section. This was performed by observing the MEBT dynamic beam transmission as a function of the RFQ RF field. The signals from the ACCTs at the MEBT entrance (ACCT1) and exit (ACCT2) were used for this test. The reduction of transmission at the beginning of the pulse was clearly observed for various values of RFQ fields (Fig. 2). The main reason of this effect is temporary reduction of the RFQ electric field due to the fact that the accelerated pulse takes the energy stored in the cavity (beam loading). Reduction of the RFQ field is compensated by the LLRF system, however, this process stabilizes during the first few tens of microseconds of the pulse.

Measurement of the RFQ field trace during the beam pulse, allowed one to parametrize beam loading effect and to perform tidious beam dynamic simulations using the TRACK code [4] in order to predict the transmission through the injector as a function of time. Both the LEBT beam neutralization and the RFQ beam loading were included in the simulations. Comparison of the measurements and the simulations results for several values of the RFQ fields is presented in Fig. 3. As it is seen in the figure the transient effect in the injector transmission are qualitatively described by the simulations.

† leo.weissman@gmail.com

ISBN: 978-3-95450-275-2 ISSN: 2226-0366 doi: 10.18429/JACoW-LINAC2026-MOPO020

A STUDY ON GENERATION, PROPAGATION, AND SUPPRESSION OF DARK CURRENT IN A C-BAND PHOTOINJECTOR*

Cheng Wang[1,2], Wencheng Fang[†,1,2], Zihe Gao[1,2], Hanyu Gong[1,2] Jianhao Tan[1,2]
Shanghai Synchrotron Radiation Facility, Shanghai, China
[1]also at Shanghai Advanced Research Institute, Chinese Academy of Sciences, Shanghai China
[2]also at Shanghai Key Laboratory of Particle Accelerator Science and Technology, Shanghai China

Abstract

High-gradient RF structures, serving as main accelerators for advanced linear light sources, have been fully validated to enhance the overall performance of the system. As high gradient electron guns emerge as the future trend for ultra-compact electron sources, the extremely high electric fields within the cavity induce significantly stronger dark currents. Without additional suppression strategies, the operation status of the high-gradient acceleration structure will be affected, and the service life of downstream magnetic components will be shortened. This paper simulates this effect and proposes preliminary methods for suppressing such dark currents.

INTRODUCTION

High-gradient accelerating structures represent the most reliable technological pathway toward high-performance, compact linear accelerators. The current iteration of high-gradient acceleration technology has achieved a paradigm shift from macroscopic statistical laws to microscopic surface characterization, thereby establishing a solid technical foundation for next-generation large-scale scientific facilities such as linear colliders and free-electron lasers. Taking the linear accelerator light source of the SXFEL facility as an example, the application of high-gradient accelerating structures is primarily reflected in two aspects. First, the high gradient at the cathode surface effectively reduces the bunch emittance at the injector exit, providing room for trade-offs between transverse and longitudinal beam dynamics. Second, without altering the original layout, such structures enable an energy upgrade, further enhancing the overall performance potential of the facility.

Previously, a RF gun based on C-band high gradient acceleration technology was designed and successfully tested under high power, shown in Fig.1, achieving a stable operating gradient of 165 MV/m at the cathode [1]. On this basis, a cryogenic RF gun and an accelerating structure were also designed and subjected to preliminary high-power tests. In such standing wave structures, the high field is expected to cause significant field emission, leading to the generation of dark current. Dark current is one of the factors that degrade the performance of accelerating structures: it reduces the achievable operating gradient, and the associated radiation losses can damage electronic components [2]. In cryogenic accelerating structures, the heat load induced by dark current may also cause non uniform surface properties, thereby disrupting the operating state. Furthermore, dark current propagates along the beamline and can cause persistent and irreversible damage to downstream magnetic components such as undulators.



Figure 1: The C-band high-power test platform and the C-band gun in SXFEL.

In general, there are two approaches to suppressing dark current. The first is to minimize its generation at the source through meticulous surface treatment, including reducing surface roughness and employing dry ice cleaning. The second approach targets beam transport, using collimators or fast kicker systems to intercept dark current along the beamline [3].

This paper presents three dimensional simulations of dark current in a C band cryogenic photocathode gun operating at a higher accelerating gradient. A scheme using a deflecting structure within the photoinjector is proposed to effectively suppress the propagation of dark current. This scheme serves as a complement and refinement to the C band photocathode injector, which is a backup scheme for the SXFEL facility, and is expected to improve the overall performance of the linear accelerator.

DARK CURRENT PIC SIMULATION

Distinct from the photocurrent that serves as the primary beam in linac, dark current is fundamentally an electron flow arising from unwanted electron emission. In general, the emitted electron current depends on the material surface temperature and the local electric field strength. The thermal-emission is described by the Richardson–Schottky equation [4]:

$$J_{RS} = \lambda^T A_R T^2 \exp\left\{\frac{-1}{k_B T}\left[\phi - \left(\frac{e^3 F}{4\pi\varepsilon_0}\right)^{\frac{1}{2}}\right]\right\}$$

* Work supported by National Natural Science Foundation of China, (NSFC) No. 12405178
† fangwc@sari.ac.cn

Content from this work may be used under the terms of the CC BY 4.0 licence (© 2026). Any distribution of this work must maintain attribution to the author(s), title of the work, publisher, and DOI.

ISBN: 978-3-95450-275-2 ISSN: 2226-0366 doi: 10.18429/JACoW-LINAC2026-MOPO021

PROGRESS OF THE INTENSE URANIUM BEAM DTL PROJECT ALVAREZ 2.0 AT GSI

L. Groening[1,*], T. Dettinger[1], M. Heilmann[1], M. S. Kaiser[1], M. Maier[1], S. Mickat[1], L. Ferreira[2], S. Roupioz[2]
[1]GSI Helmholtzzentrum für Schwerionenforschung, Darmstadt, Germany
[2]CERN, Geneva, Switzerland

Content from this work may be used under the terms of the CC BY 4.0 licence (© 2026). Any distribution of this work must maintain attribution to the author(s), title of the work, publisher, and DOI.

Abstract

The Alvarez-type post-stripper DTL at GSI accelerates intense ion beams with A/q ≤ 8.5 from 1.4 to 11.4 MeV/u. After more than 45 years of operation, it suffers from ageing and its design does not meet the requirements of the upcoming FAIR project. Series production of the new DTL Alvarez 2.0 is ongoing. In 2025, the last out of 25 cavity sections, forming five cavities, underwent the site acceptance test. Nine of them have been copper plated at GSI's in-house galvanic workshop with a rate of about 2.5 month per section. All 187 drift tubes have been ordered. Production of 68 tubes is completed as well as copper plating of 50 of them at CERN's galvanic workshop. 36 drift tubes have been installed inside of the cavity sections. This year shall see the assembly of one cavity from five single sections. Production of many small parts is completed to a large extend. This contribution summarizes the actual project status.

INTRODUCTION

Like the current DTL, the new section will accelerate ions up to the injection energy of the subsequent synchrotron SIS18. All species up to the mass-to-charge ratio of A/q = 8.5 are accelerated, corresponding to FAIR's reference ion of $^{238}U^{28+}$ [1]. Five cavities with lengths of about 11 m each are operated at 108.4 MHz with peak powers of up to 1.35 MW including beam loading. Figure 1 sketches the new DTL. The normal conducting DTL covers a beam repetition rate of up to 10 Hz with flat top RF-pulse length of up to 1.0 ms corresponding to the beam pulse length. Within the cavities, transverse FDDF focusing is provided with a zero current phase advance of 65°. The large intensities cause transverse tune depressions of up to 40% along the first cavity [2]. Longitudinal focusing is from RF-phases of −30° along the first three cavities and −25° along the last two ones. Cavities are separated by four identical inter-tank sections [2] which serve for 3D beam envelope matching by three quadrupoles and one re-buncher. The inter-tank sections provide also for a beam current and phase probe, a sector valve, and a transverse beam profile measurement

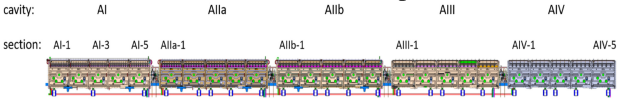


Figure 1: New post-stripper DTL Alvarez 2.0 under construction at GSI.

Although the machine is mainly designed as an injector for the synchrotron SIS18, several low-energy experiments shall be served as well. The DTL design allows for switching off the RF-power of the last cavities while the transversely focusing quadrupoles inside the drift tubes remain switched on. Accordingly, the DTL output energies correspond to the individual cavity exit energies of 3.212, 5.173, 7.142, 9.237, and 11.318 MeV/u. The quadrupoles are pulsed, such that focusing can be adapted individually to each ion species and design energy; the latter can be changed between the individual DTL pulses, i.e., within less than 100 ms. The DTL design is described in detail within the dedicated Technical Design Report [3] and the main design parameters are listed in Table 1.

Table 1: Main Design Parameters of GSI's New Post-Stripper DTL Alvarez 2.0 [3]

Parameter	Value
Ion A/q	≤ 8.5 ($^{238}U^{28+}$)
Input beam energy	1.358 MeV/u
Output beam energy	3.212 – 11.318 MeV/u
Electrical beam current	1.76 emA· A/q
Transv. tune depression	≤ 40 %
Beam pulse duration	0.2 – 1.0 ms
Beam repetition rate	≤ 10 Hz
Number of cavities	5
RF-frequency	108.408 MHz
Max. RF-power per cavity	1.35 MW
RF-sources per cavity	1
Transv. focusing scheme	FDDF
Total length	55 m

CAVITIES

After successful prototyping in 2021 [4], production of the 5×5 cavity sections as well as of the 5×2 end plates has been completed in late 2025 including the SATs. No considerable issues have been encountered. Copper plating of the sections started with section AIIa-1 in September 2024 and recently section AIIb-3 has been finished. Figure 2 shows one example of a section right after plating. For the time being, no significant problems have been met and the actual plating rate is about 2.5 months/section. The duration is dominated by proper masking, while plating inside of the basins just takes about eight hours. After finishing cavity AIIb, the workshop will be re-structured in order to plate the 10 end plates and afterwards the other three cavities will

* la.groening@gsi.de

ISBN: 978-3-95450-275-2 ISSN: 2226-0366 doi: 10.18429/JACoW-LINAC2026-MOPO022

RESEARCH ON HIGH-INTENSITY PROTON IH-DTL ACCELERATING STRUCTURE BASED ON APF*

S. Li, J. Yang†, Y. Fan
China Institute of Atomic Energy, Beijing, China

Abstract

High-intensity proton linacs are crucial in spallation neutron sources (SNS), compact accelerator-driven neutron source (CANS), proton therapy, together with other facilities that require higher beam intensity as the development of application systems. To meet the research and engineering demands of high-intensity pulsed proton linacs, a structure consisting of modular APF IH-DTLs and external quadrupole triplets has been proposed. This structure can accelerate an 80 mA pulsed proton beam from 2.5 MeV to 13 MeV in mean energy. Alternating phase sequences, tapered aperture matching and variable-diameter cavity shaping are employed to optimize the transport of high-intensity proton beams. This structure can yield a viable scheme for the core accelerating part of 13 MeV, 80 mA high-intensity proton linac and lay a technical basis for APF IH-DTLs applied to intense beams.

INTRODUCTION

To meet the requirements of high-intensity pulsed beams in proton linacs, a 13 MeV, 80 mA high-intensity pulsed proton linac has been proposed, with an interdigital H-mode drift tube linac (IH-DTL) adopted as its core accelerating structure. Compared with conventional TM-mode DTLs, the IH-DTL structure features low RF loss, high accelerating gradient and compact layout.

The alternating-phase focusing (APF) method was introduced and further developed by Iwata et al [1]. Due to its structural advantage of eliminating the need for embedded focusing magnets, APF has been implemented in various accelerator facilities, including the Advanced Proton Therapy Facility (APTRON) [2] in China, the muon linac at J-PARC [3], the Heavy Ion Medical Accelerator Center (HIMAC) [4] in Japan, and the Helmholtz linac (HELIAC) [5] at GSI in Germany. However, the li mited focusing strength of conventional APF restricts its capability to suppress space-charge effects in high-intensity beam transport. Consequently, its application in high-intensity proton acceleration remains limited.

A modular APF IH-DTL structure with external quadrupole triplets is proposed in this paper, combining the merits of IH-DTL, APF method, and modular configuration. The proposed structure enables stable and low-loss acceleration of high-intensity pulsed proton beams. It provides a promising approach to addressing the limitations of IH-DTL structures in high-intensity proton applications.

BEAM DYNAMICS

The high-intensity pulsed proton linac (Fig. 1) consists of an ECR ion source, a low-energy beam transport line (LEBT), a radio-frequency quadrupole (RFQ), a medium-energy beam transport line (MEBT), a modular APF IH-DTL structure, and a high-energy beam transport line (HEBT).

The proposed modular APF IH-DTL structure offers three key advantages:

1. The modular configuration reduces the demand for high-power RF sources and relaxes the precision requirements in design, fabrication, and testing, providing sufficient engineering tolerance.
2. The external quadrupole triplets compensate for the limited focusing strength of APF and suppress transverse space-charge effects.
3. The APF method provides in-cavity longitudinal focusing, preserves beam quality, and reduces beam loss.

The structure consists of six APF IH-DTLs and five external quadrupole triplets. Strong bunching is adopted in the first three tanks to preserve beam quality, while smooth bunching is applied in the later tanks to improve RF efficiency. A tapered aperture design is employed to optimize beam transport and reduce RF losses.

A theoretical design procedure was performed to determine the main accelerating structure parameters, including the cavity length, cell number, synchronous phase, and focusing scheme. The obtained parameters were used to

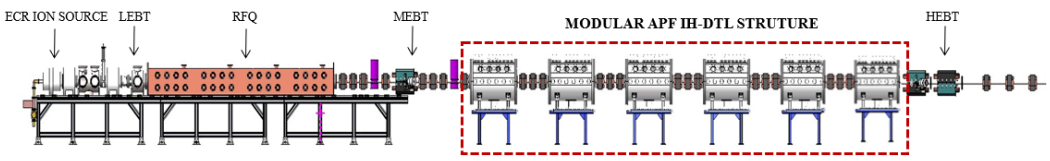


Figure 1: The layout of the high-intensity pulsed proton linear accelerator.

* Work supported by Continues-Support Basic Scientific Research Project.
† yangjinghe@ciae.ac.cn

Content from this work may be used under the terms of the CC BY 4.0 licence (© 2026). Any distribution of this work must maintain attribution to the author(s), title of the work, publisher, and DOI.

ISBN: 978-3-95450-275-2 ISSN: 2226-0366 doi: 10.18429/JACoW-LINAC2026-MOPO024

DESIGN OF BEAM TRANSPORT LINES FOR THE 200 MeV ENERGY UPGRADE AT KOMAC

S. Moon*, S. Lee, S.-B Park, H.-S Kim, H.-J Kwon
Korea Atomic Energy Research Institute, Gyeongju, Republic of Korea

Abstract

The Korea Multi-purpose Accelerator Complex (KOMAC) in Gyeongju, currently operates a 100 MeV high-current proton linear accelerator. This facility actively supports a wide range of applications, including semiconductor radiation testing and fundamental scientific research. Recently, a upgrade plan has been initiated to upgrade the maximum beam energy to 200 MeV to meet increasing user demands.

Following the energy upgrade, the implementation of new target rooms and dedicated beam transport lines is essential. The current extension plan includes two distinct target rooms: one optimized for terrestrial radiation test and the other specialized for space radiation test. This study presents the beam optics of the transport lines required to deliver the 200 MeV proton beams while satisfying the specific beam parameters requested by each target room.

ENERGY UPGRADE PLAN

The Korea Multi-purpose Accelerator Complex (KOMAC) [1], located in Gyeongju, South Korea, currently operates a 100-MeV proton linear accelerator that supports a wide range of scientific and industrial research applications. As part of its long-term development strategy, KOMAC aims to construct a GeV-scale spallation neutron source in the future.

Although the ultimate goal is to realize a GeV-scale accelerator facility, achieving this objective requires substantial financial investment, manpower, and construction time. Therefore, as an intermediate step toward the final facility, KOMAC is planning to upgrade the existing accelerator to an energy of 200 MeV [2].

One of the primary motivations for selecting 200 MeV as the intermediate upgrade energy is the increasing demand for radiation hardness testing of semiconductor devices. While 100-MeV proton beams can also be utilized for such tests, the internationally recognized standard generally recommends proton energies of 200 MeV or higher to accurately evaluate radiation effects on semiconductor components. Consequently, upgrading the accelerator to 200 MeV will significantly enhance its capability to support semiconductor radiation testing.

Another important advantage of the 200-MeV upgrade is its compatibility with future expansion to a GeV-scale spallation neutron source. If a Rapid Cycling Synchrotron (RCS) is selected as the main accelerator, the 200-MeV linear accelerator can serve directly as the injector. Alternatively, if a full linear accelerator (linac) configuration is adopted, the existing 200-MeV linac can be extended simply by adding additional accelerating structures downstream. These considerations make the 200-MeV upgrade an effective and practical intermediate stage toward the realization of a GeV-scale spallation neutron source.

The overall layout of the proposed 200-MeV accelerator upgrade is shown in Fig. 1.

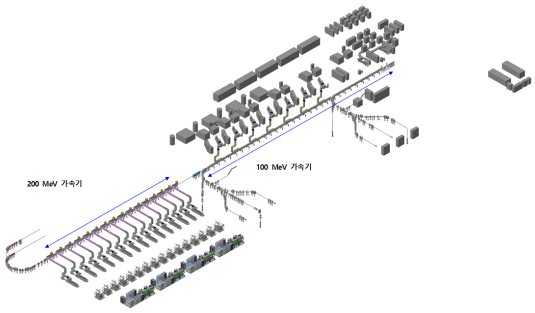


Figure 1: Layout of 200 MeV energy upgrade plan.

The 200-MeV energy upgrade is planned by extending the existing 100-MeV proton linac with Separated Drift Tube Linac (SDTL) accelerating structures [3], which are based on the design currently employed at J-PARC. According to the current design, a total of 16 SDTL accelerating tanks will be installed downstream of the existing accelerator to achieve the target beam energy of 200 MeV. The schematic view of SDTL tank is shown in Fig. 2

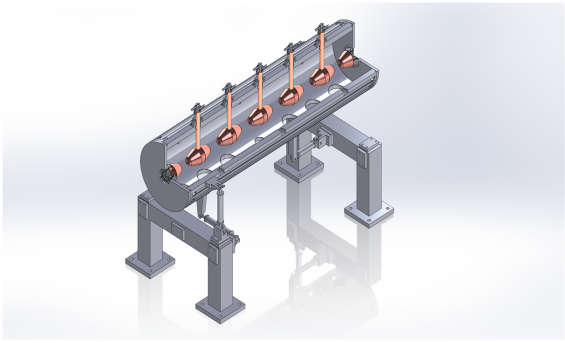


Figure 2: Layout of SDTL tank.

In addition to the accelerator upgrade, two target stations are included in the current facility plan. The number of target stations will be expanded in the future according to user demand and the operational requirements of the facility.

BEAM TRANSPORT LINE

As mentioned in the previous section, the current facility plan includes two target stations. The first is a space radiation beamline designed to provide a large-area, low-dose

* msh3069@kaeri.re.kr

Content from this work may be used under the terms of the CC BY 4.0 licence (© 2026). Any distribution of this work must maintain attribution to the author(s), title of the work, publisher, and DOI.

ISBN: 978-3-95450-275-2 ISSN: 2226-0366 doi: 10.18429/JACoW-LINAC2026-MOPO025

DEVELOPMENT OF A DIGITAL LLRF CONTROL SYSTEM FOR KAHIF RFQ*

S.-B.Lee†, S.-H. Lee, K.-H. Lee, D.-S. Chang, M.-W. Kim, S.-H. Huh, D.-W. Lee
Korea Atomic Energy Research Institute, Daejeon, South Korea

Abstract

The Heavy-ion Irradiation Facility (KAHIF) RFQ is transitioning its Low-Level RF (LLRF) infrastructure from a legacy analogue system to a modern digital architecture to enhance the stability of its 25.96 MHz pulsed operation. The existing analogue system faces limitations in precise phase regulation and compensation for the nonlinear pulse droop inherent in its vacuum tube amplifier chain. This paper presents the design and verification of a digital LLRF controller featuring electronic Auto Frequency Control (AFC) loop and a hybrid Feedforward-PID amplitude control logic. A key contribution of this work is the development of a high-fidelity RLC equivalent circuit model that serves as the physical plant in an integrated closed-loop simulation environment. Simulation results demonstrate that the digital architecture tracks resonance deviations and mitigates amplifier-induced instabilities, ensuring superior field stability.

INTRODUCTION

The Radio Frequency Quadrupole (RFQ) at the Korea Atomic Energy Research Institute Heavy-ion Irradiation Facility (KAHIF) plays a crucial role in accelerating various ion beams at an operating frequency of 25.96 MHz. Currently, the multi-stage vacuum tube RF system operates in pulsed mode with a legacy analogue controller. This configuration faces two critical hardware challenges: 1) continuous thermal frequency shifts (Δf~1.34 kHz) due to an out-of-service mechanical tuner (tuner-less condition), and 2) significant amplitude fluctuations (up to 3.7%) caused by initial transient delays and nonlinear pulse droops inherent to tube amplifiers. To achieve high-quality beam dynamics, transitioning to a fully digital LLRF system is highly demanded [1]. The quantitative specifications required for the proposed digital LLRF architecture are defined in Table 1. This paper introduces integrated closed-loop simulation environment that couples the digital LLRF control logic directly with a newly developed RLC equivalent circuit model representing the RFQ cavity.

MODELING AND RESULTS

Digital LLRF System and RFQ Modelling

The proposed digital LLRF architecture relies on electronic Auto Frequency Control (AFC) combined with a Feedforward (FF) pulse control logic. As illustrated in the system architecture, the design consists of core digital loops designed to suppress both frequency detuning and amplitude instabilities. Figure 1 shows the overall LLRF system for KAHIF RFQ cavity.

The cavity pickup signals are directly demodulated into In-phase (I) and Quadrature (Q) baseband components [2]. The phase difference is calculated in real-time, allowing the Proportional-Integral (PI) controller to dynamically adjust the Numerically Controlled Oscillator (NCO) frequency, ensuring robust resonance tracking combined with the PID feedback compensation [3].

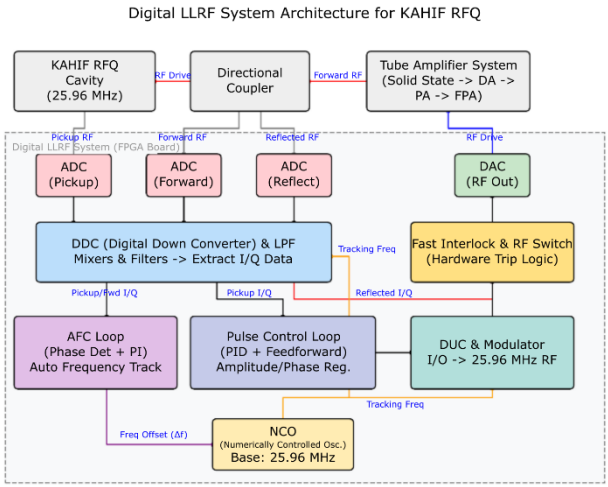


Figure 1: Overall block diagram of the proposed digital LLRF architecture combining the purely electronic AFC loop and Feedforward-PID amplitude control.

Table 1: Requirements for LLRF

Parameter	Value	Unit
Operating Frequency	25.96	MHz
Tuning Range	≥ ±10	kHz
Amplitude Stability	< 1 %	
Phase Stability	< 1°	
Operating mode	Pulsed mode	

To overcome the initial delay and nonlinear droop of high-power vacuum tubes, a hybrid FF+FB amplitude control loop is implemented. Furthermore, an RLC equivalent circuit model of the RFQ cavity is integrated as the physical plant in MATLAB/Simulink to establish a closed-loop testing platform.

* This work was supported by the National Research Council of Science and Technology (NST) grant by the Korea government (MSIT) (No. GTL25031-410) and the National Research Foundation of Korea (NRF) funded by the Korea government (Ministry of Science and ICT)(RS-2022-00156272).
† slee6306@kaeri.re.kr

Content from this work may be used under the terms of the CC BY 4.0 licence (© 2026). Any distribution of this work must maintain attribution to the author(s), title of the work, publisher, and DOI.

ISBN: 978-3-95450-275-2 ISSN: 2226-0366 doi: 10.18429/JACoW-LINAC2026-MOPO026

RESEARCH AND ANALYSIS ON A C-BAND TRAVELLING WAVE CAVITY

R. Ghazal*[1,2], J.R. Zhang†[1,2], H.J. Cao[1,2], O.Z. Xiao[1,2]
[1]Institute of High Energy Physics, Beijing, China
[2]Chinese Academy of Sciences, Beijing, China

Abstract

Researchers have been working on methods to enhance the accelerating gradient of accelerating structures in electron linear accelerators for years, as this can reduce the cost of accelerator development. The Circular Electron-Positron Collider (CEPC) is a 100-kilometer-long ring e^+e^- collider designed to produce Higgs particles. A C-band accelerating structure in the high-energy section should be considered for the CEPC injector so that the beam energy can reach 30 GeV. To develop a high-gradient C-band accelerating structure, an optimized constant-gradient structure with a specific phase advance and optimal iris thickness for the desired operating mode is required. This improves breakdown stability and enhances the overall efficiency of the high-gradient structure. This paper analyzes the C-Band accelerating cavity at four operational modes, with a primary focus on optimizing cavity parameters for a high-gradient accelerating structure.

INTRODUCTION

In modern electron linear accelerators, particularly in large-scale facilities such as the CEPC injector linac, C-band accelerating structures are widely adopted due to their ability to provide higher gradients and improved RF efficiency [1]. The performance of high-gradient accelerating structures strongly depends on the electromagnetic design of the cavity, particularly the iris region. The iris geometry governs cell-to-cell coupling and influences key RF parameters. It has been observed that the iris region is especially susceptible to high electromagnetic fields, which can lead to RF breakdown and limit the achievable gradient [2, 3]. Among these, iris thickness with varying phase advances leads to different field distributions and coupling characteristics, resulting in a mode-dependent response of key parameters. Since a single phase advance cannot satisfy all design constraints, it must be treated as an optimization parameter [4, 5]. In this work, a parametric study of phase advance with iris thicknesses from 3.5 mm to 6 mm is carried out in a C-band elliptical iris cavity.

SHORT-RANGE WAKEFIELD (SRW)

The CEPC injector adopts a one-bunch-per-pulse operation mode with a bunch charge of 3 nC, the dominant wakefield contribution is the SRW [1]. The longitudinal SRW changes the energy of trailing particles and can increase the correlated energy spread along the bunch. The transverse SRW gives transverse kicks to particles behind the driving charge and can lead to emittance growth if not properly controlled. These effects become more significant at high bunch charge; therefore, the wakefield behavior must be evaluated together with RF efficiency and high-gradient performance. For a simplified modal description, the longitudinal wake potential can be written as [6]

$$E_z(z) = q \sum_n K_n \cos(k_n z),$$

where q is the bunch charge, K_n is the loss factor which depends on a the aperture radius, σ_z is the rms bunch length, and k_n is the corresponding wave number. An approximate scaling is [6].

In the present work, the SRW are evaluated mathematically. This approach provides a comparison of the relative influence of aperture, phase advance, and iris thickness on wakefield. The longitudinal SRW and transverse SRW calculated as,

$$W_L(s) = \frac{Z_0 c}{\pi a^2} \exp\left(-\sqrt{\frac{s}{S_1}}\right),$$

$$W_T(s) = \frac{4 Z_0 c S_2}{\pi a^4} \left[1 - \left(1 + \sqrt{\frac{s}{S_2}}\right) \exp\left(-\sqrt{\frac{s}{S_2}}\right)\right].$$

Here, $Z_0 = 377\ \Omega$ is the impedance of free space, c is the speed of light, a is the aperture radius, and s is the distance behind the driving charge. The parameters S_1 and S_2 describe the geometry-dependent decay behavior of the longitudinal and transverse wakefields and are given by [1, 7, 8].

$$S_1 = \frac{g}{8}\left[\frac{a}{(1 - 0.465\sqrt{g/L} - 0.07(g/L))L}\right]^2,$$

$$S_2 = 0.169 \frac{a^{1.79} g^{0.38}}{L^{1.17}},$$

where g is the gap length and L is the cell length.

Figure 4 illustrates parameter definitions for wakefield evaluation. In Fig. 1, wakefield is evaluated for varying aperture radii at t = 4.5 mm and $4\pi/5$ mode, it shows that both longitudinal and transverse wakefields decreases with increasing a. This is consistent with the approximate $1/a^2$ and $1/a^4$ dependencies, respectively, indicating stronger suppression of transverse wakefields at larger apertures. Therefore, large aperture is effective for suppressing both longitudinal and transverse wakefield effects The influence of phase advance is then evaluated at aperture radius $a = 5$ mm and iris thickness $t = 4.5$ mm. Figure 2 shows that both longitudinal and transverse wakefields decrease with increasing phase advance, indicating that higher phase advance is favorable for wakefield suppression. Finally, the effect of iris thickness

* ghazalrao@ihep.ac.cn
† zhangjr@ihep.ac.cn

Content from this work may be used under the terms of the CC BY 4.0 licence (© 2026). Any distribution of this work must maintain attribution to the author(s), title of the work, publisher, and DOI.

ISBN: 978-3-95450-275-2 ISSN: 2226-0366 doi: 10.18429/JACoW-LINAC2026-MOPO027

A NEW 4-ROD RFQ FOR THE ION THERAPY INJECTOR AT HIT HEIDELBERG

U. Ratzinger†,[1], S. Altürk[1], R. Cee[2], E. Feldmeier[2], H. Höltermann[1], M. Hun[2], H. Hähnel[1], P. Müller[1], A. Peters[2], H. Podlech[1], J. Schreiner[2], M. Schütt[1], T. Winkelmann[2], C. Zhang[3].
[1]BEVATECH GmbH, Mörfelden-Walldorf, Germany
[2]Heidelberg Ion Beam Therapy Centre, Heidelberg, Germany
[3]J. W. Goethe University, Frankfurt, Germany

Abstract

An improved version of the 4-rod RFQ was developed to improve the mechanical precision of the rod-alignment and to achieve a higher quality factor. Design features developed during a prototyping project within the Hessian funding initiative LOEWE3 were implemented in an operational RFQ for the first time. This resulted in substantially reinforced electrode-supports and suppression of dipole-field components. The RFQ was manufactured in 2025 and was installed at the test bench of the Heidelberg Therapy Centre HIT in April 2026. Results from the successful and detailed beam measurements are reported

INTRODUCTION

The HIT therapy centre has been in operation since 2006. The 7 MeV/u synchrotron injector linac designed for C^{4+} beams consists of an RFQ that accelerates the beam from 8 to 400 keV/u and of one IH-DTL cavity up to the final energy. RFQ and IH-DTL are connected by a very compact Inter Tank section (ITS), consisting of an xy-steerer, a quadrupole doublet and a phase probe, see Figure 1 and ref. [1]. The beam transmission along RFQ and ITS remained less than half of the expected value of at least 85% during all the years. Recently higher beam currents from the injector linac became desirable to improve the facility efficiency. That motivated the development of a new RFQ with completely new beam dynamics design and a significantly improved beam matching to the compact ITS [2]. The longitudinal match is now accomplished by modified beam-dynamics along the last RFQ cells and by a single drift tube at the exit which is RF-coupled to one pair of RFQ electrodes. Moreover, the new design of the stems improved the mechanical precision and stability of the electrodes as well as the resulting field quality. The new RFQ was manufactured in 2025 by Kress GmbH, Biebergmuend, Germany, and was installed at the Heidelberg RFQ test bench in April 2026 [3]. The test bench is based on a Pantechnik Supernanogun electron-cyclotron-resonance (ECR) ion-source, Pantechnik, Bayeux, France, a 90° double-focussing analysing magnet, a quadrupole triplet and a solenoidal focusing into the RFQ. It is very similar to each of the three injector lines of the medical accelerator. The test bench is shown in Figure 2. This paper reports the RFQ beam measurements.

† email address U.Ratzinger@iap.uni-frankfurt.de

Figure 3 shows a photo of the new 1.4-m-long RFQ which accelerates C^{4+} ions from 8 to 400 keV/u. A drift tube was added to one of the quadrupole pairs at the exit to achieve the needed longitudinal match to the ITS [2].

Table 1 lists the main RFQ parameters for the design ion C^{4+}. The vacuum pressure is around $2x10^{-7}$ hPa.

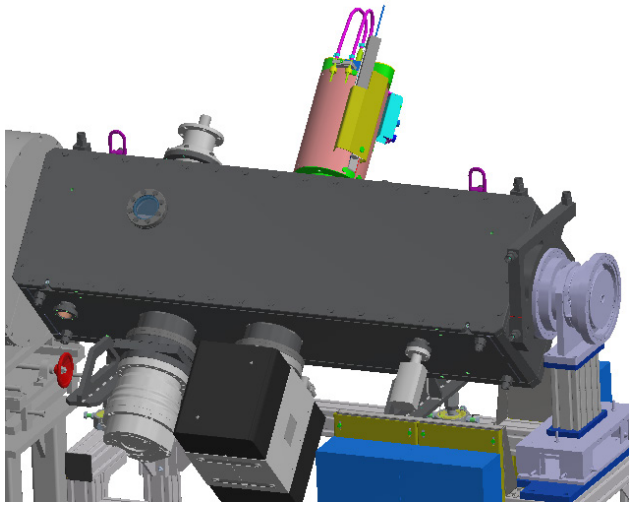


Figure 1: RFQ cavity with alignment jigs, coupler, tuner, pumps and with the complete Inter Tank Section on the right.

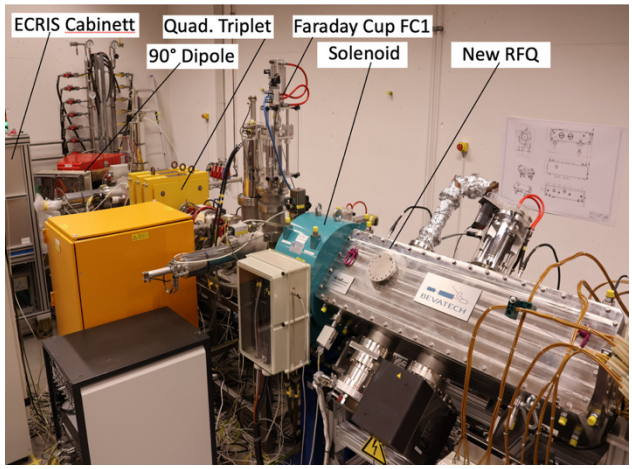


Figure 2: Photo of the HIT test bench.

BEAM MEASUREMENTS

Downstream of the RFQ and the original HIT-ITS, a diagnostic bench was installed as shown in Figure 4. It comprises three identical phase probes for TOF measurements

Content from this work may be used under the terms of the CC BY 4.0 licence (© 2026). Any distribution of this work must maintain attribution to the author(s), title of the work, publisher, and DOI.

ISBN: 978-3-95450-275-2 ISSN: 2226-0366 doi: 10.18429/JACoW-LINAC2026-MOPO028

UPDATE ON CONDITIONING THE NEW INJECTOR LINAC AT THE CANADIAN LIGHT SOURCE

T. Sové*, C. Baribeau, D. Beauregard, J. Doucette-Garr, B. Dubé, I. Kolmakov, R. S. Kotha, A. McCormick, T. McKeith, A. Nikolaichuk, E. Paulson, C.-L. Randall, A. Rosset, S. Saadat, D. Schneberger, X. Shen, B. Smith, S. Smith, J. Stampe, X. F. D. Stragier, W. A. Wurtz,
Canadian Light Source, Saskatoon, Canada
K. Dunkel, RI Research Instruments GmbH, Bergisch Gladbach, Germany
D. Kumbaro, MAX IV, Lund, Sweden
N. Shafqat, Elettra, Basovizza, Italy

Abstract

In 2024 the Canadian Light Source (CLS) retired its ~60 year old 2856 MHz, 250 MeV injector electron LINAC, and replaced it with a 3000 MHz LINAC designed and built by RI Research Instruments GmbH. The design includes a SLAC energy doubler (SLED) system to power two of the three main accelerating structures and is intended to also deliver a 250 MeV beam. Many setbacks were encountered during the initial conditioning and commissioning phases which required reconditioning the structures. Outside input and lessons learned from past conditioning attempts shaped the latest RF conditioning campaign. While not without its own setbacks, this conditioning campaign succeeded and allowed the beam commissioning phase to proceed at a lower energy. This paper is a report on this most recent RF conditioning campaign and CLS's current state of operations.

INTRODUCTION

To improve reliability, the CLS replaced its aging LINAC in 2024 with a new one shown in Fig. 1. Commissioning was expected to be done by the end of 2024, but many issues resulted in multiple accelerating structures being unable to hold appreciable power, and the project was still in the conditioning phase as of May 2025 [2].

* tylor.sove@lightsource.ca

In early 2025, we reached out to the community to understand our issues and seek guidance. While the advice varied, core themes were: previous conditioning was too aggressive, set more realistic goals with realistic timelines, and make decisions based on the data and not on timelines. We were also advised to appoint a single person to lead the conditioning efforts to improve efficiency. The advice was heeded; CLS and RI agreed upon who should lead the conditioning efforts, decided to condition towards lower power levels, and agreed upon a "less aggressive" conditioning procedure.

We conditioned RF components individually to identify power-limiting hardware, and several proved incapable of withstanding the required power levels [2]. We also reconfigured the waveguides to isolate accelerating structure #3 (ACC3), the structure with the fewest breakdowns, to assess the accelerating structure design and the less aggressive conditioning procedure. Successful conditioning validated the design, demonstrated the viability of the procedure, and justified baking the rest of the LINAC. The LINAC was reassembled without the failed components and baked, excluding the waveguides due to mechanical constraints [2].

LESS AGGRESSIVE PROCEDURE

The procedural changes implemented for this campaign were guided by five key principles. The first, data-driven decision making, is discussed in the context of the others.

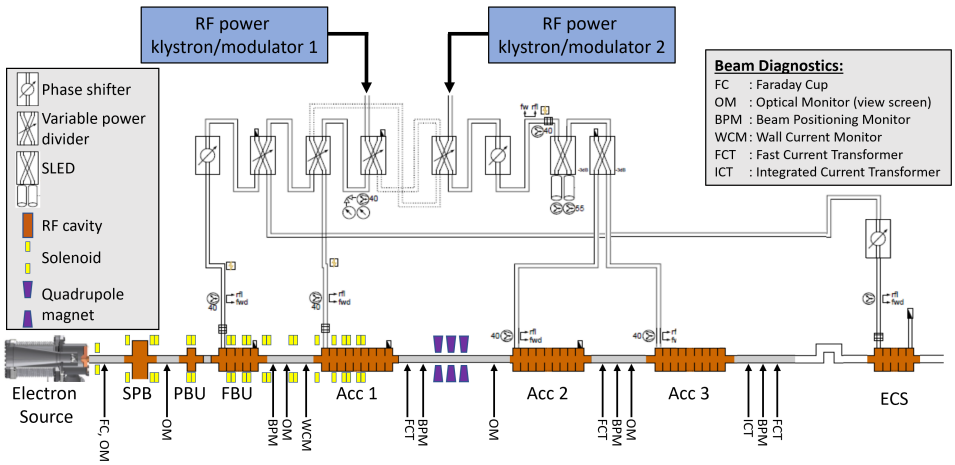


Figure 1: CLS injector LINAC layout [1]. Highlighted are the various RF structures, the waveguide network including the recovery mode waveguides shown as dotted lines, various magnets and diagnostic equipment.

Content from this work may be used under the terms of the CC BY 4.0 licence (© 2026). Any distribution of this work must maintain attribution to the author(s), title of the work, publisher, and DOI.

ISBN: 978-3-95450-275-2 ISSN: 2226-0366 doi: 10.18429/JACoW-LINAC2026-MOPO030

THE PROTON BEAM IRRADIATION FACILITY (PBIF) BEAMLINE DESIGN AT THE J-PARC LINAC

B. Yee-Rendon*, Y. Kondo, J. Tamura, Y. Yamaguchi, M. Yoshimoto,
Y. Fuwa, S. Meigo, F. Maekawa
Japan Atomic Energy Agency, Tokai Mura, Japan

Content from this work may be used under the terms of the CC BY 4.0 licence (© 2026). Any distribution of this work must maintain attribution to the author(s), title of the work, publisher, and DOI.

Abstract

In recent years, the Japan Proton Accelerator Research Complex (J-PARC) has completed the design report for a Proton Beam Irradiation Facility (PBIF). This facility will be used for material irradiation, the manufacturing of medical radioactive isotopes, testing semiconductor soft errors, and providing proton beams for space applications, utilizing the H^- beam generated by the J-PARC linac. The PBIF beamline will be in an existing tunnel within the J-PARC linac. It will extract the H^- beam from the J-PARC's linac using a pulse bending magnet and septum arrangement and transport the beam through achromatic lattices. One of the main challenges for the PBIF beamline is to efficiently transport the beam from the main line of the J-PARC linac to the testing area, while ensuring that the design fits within the existing tunnel and does not interfere with the components already installed in the J-PARC linac. This work provides a report and discussion on the optical design of the PBIF beamline.

INTRODUCTION

The Japan Proton Accelerator Research Complex (J-PARC) is a world-class research center composed of high-intensity proton accelerators, including a 400-MeV linear accelerator (linac), a 3-GeV rapid-cycling synchrotron (RCS), and a 30-MeV main ring synchrotron (MR). Additionally, J-PARC is equipped with several experimental facilities, including the Materials and Life Science Experimental Facility, the Hadron Experimental Facility, and the Neutrino Experimental Facility [1], as shown in Fig. 1.

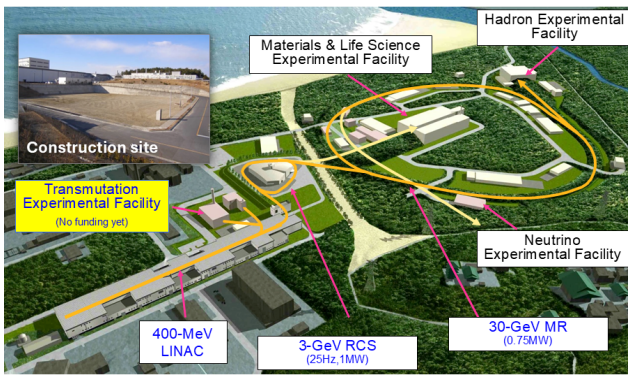


Figure 1: Overview of J-PARC.

Moreover, as part of the R&D on the Accelerator Driven System, a Transmutation Experimental Facility (TEF) [2] was proposed for the J-PARC. TEF consists of two experimental facilities: the Transmutation Physics Experimental Facility (TEF-P) and the ADS Target Test Facility (TEF-T) [3]. In recent years, J-PARC has developed the conceptual design of a Proton Beam Irradiation Facility (PBIF) for a multipurpose facility [4] based on the TEF design. Table 1 shows the main beam parameters for the PBIF facility.

Table 1: PBIF Beam Parameters [5]

Parameter	Value
Particle	H^-
Average current (mA)	62.5
Energy (MeV)	400
Beam power (kW)	250

Currently, the J-PARC linac transports a H^- beam to the RCS at a repetition frequency of 25 Hz via the 3-GeV Linac-to-Synchrotron Beam Transport (L3BT) line. For the operation of the PBIF, the J-PARC linac will increase its repetition rate to 50 Hz [6], and a new beam line will be installed in the existing branch tunnel for the TEF/PBIF within the J-PARC linac tunnel, see Fig. 2. This work presents an updated beam transport model that will transport a 250 kW H-beam from L3BT to the entrance of the PBIF facility. The optic model is based on the best practices of previous TEF-T beamlines [7–9] while ensuring that it does not interfere with already installed components and use a simpler lattice configuration.

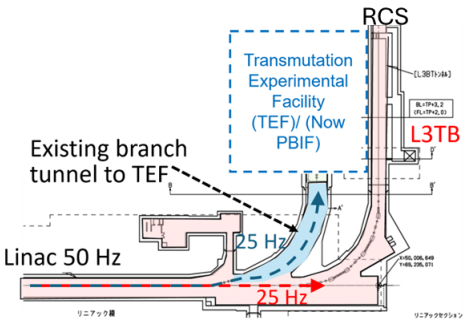


Figure 2: Drawing of the J-PARC linac tunnel.

DESIGN PHILOSOPHY

The PBIF beamline's design focuses on three points: compatibility, robust design, and pragmatism.

Compatibility

The PBIF beamline must fit in the existing branching part in the J-PARC linac's tunnel. In addition, must have minimal interference with the installed components at L3BT to minimize any beam degradation in the downstream accelerator systems of J-PARC. These impose constraint locations in the PBIF beamline elements.

* byee@post.j-parc.jp

ISBN: 978-3-95450-275-2 ISSN: 2226-0366 doi: 10.18429/JACoW-LINAC2026-MOPO031

L-BAND GUN DEVELOPMENT AND OPERATION AT DESY*

A. Oppelt†,1, N. Aftab[1], A. Aksoy[1], S. Aminzadeh Gohari[1], Z. Amirkhanyan[1], F. Brinker[2], J. Good[2], A. Grebinyk[1], M. Gross[1], Y. Komar[1], M. Krasilnikov[1], B. Li[1], X.-K. Li[1], S. Pakluea[1], C. Richard[1], F. Riemer[1], F. Stephan[1], E. Tarakci[1], G. Vashchenko[1], D. Villani[1], D. Xu[1], S. Zeeshan[1]
[1]Deutsches Elektronen-Synchrotron, Zeuthen, Germany
[2]Deutsches Elektronen-Synchrotron DESY, Hamburg, Germany

Abstract

Gun5, the new generation of normal-conducting 1.3 GHz RF guns for high-gradient and long-pulse operation at DESY's linac driven free-electron lasers is in operation at PITZ and European XFEL. The improved gun design allows for RF pulse durations of up to 1 ms at 10 Hz repetition rate, at gradients of ~60 MV/m at the cathode. Special features are two redundant RF pickups for RF regulation and a symmetric power coupler to reduce RF asymmetries. Four cavities of the Gun5 type have already been produced, and three of them have been tested at PITZ. Two guns are currently in operation at PITZ and the European XFEL. This article will give an overview on the operation experiences with these gun cavities.

INTRODUCTION

At DESY, a new generation of RF guns was developed: Gun5. The design features an improved cell geometry and cooling concept which allows for RF pulse durations of up to 1 ms at 10 Hz repetition rate, at gradients of up to 60 MV/m at the cathode, and for average power levels of more than 60 kW [1]. The cavity design also includes two redundant RF probes to measure the RF field inside the gun. A new symmetric RF power coupler reduces RF asymmetries in the gun and removes coupler kicks formerly observed when using a single-side RF input coupler [2, 3]. This new RF power coupler possesses also a laser incoupling window which allows omitting the in-vacuum laser mirror located in the path of the electron beam used so far.

The gun cavity is setup with its surrounding solenoid magnets, the symmetric RF power coupler, and two Thales windows on an interchangeable transport frame which allows for easy transportation and exchange between the facilities FALCO, PITZ, European XFEL, and FLASH. A view of this setup is shown in Fig. 1.

GUN5.1

Gun5.1, the prototype, was tested at the Photo Injector Test Facility at DESY in Zeuthen (PITZ) till 2024. As reported in [4], an improved cathode spring design [5] was developed to overcome the observed issues in the cathode area which were induced by the high average RF power operation of the gun: 6-8 MW peak RF power were applied at different RF pulse durations up to 1 ms, and average power levels up to 60 kW have been reached. The new spring design was implemented at Gun5.1 and subsequently tested at PITZ. Gradients close to 60 MV/m were reached with an RF pulse duration of 900 µs (54 kW average RF power), Fig. 2. The investigations stopped after ~1000 hours of operation due to the need to dismount Gun5.1 from the PITZ facility in order to prepare Gun5.2 for its installation at European XFEL.

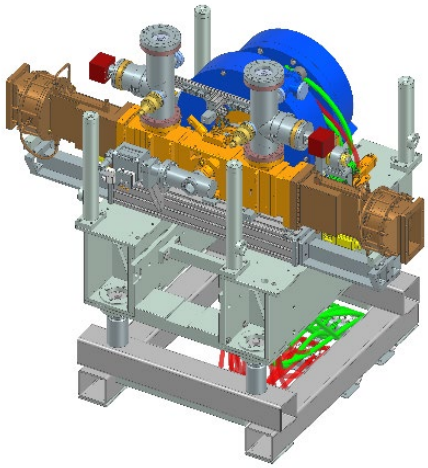


Figure 1: Gun5 setup. The gun cavity is surrounded by the solenoid magnets (main and bucking, in blue). The symmetric RF power coupler is shown in orange, and the Thales windows in brown.

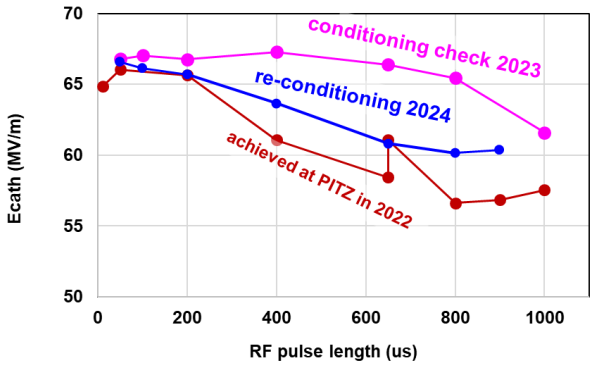


Figure 2: Results of the Gun5.1 conditioning at PITZ with the old (2022 and 2023, red and magenta) and the new spring design (2024, blue).

The setup of Gun5.1 was dismounted and components were re-used. The cavity was refurbished by polishing away the marks at the cathode hole and subsequently dry-ice cleaned. It is currently waiting for a re-tuning in order to slightly reduce the operation temperature and the field

* Work supported by the European XFEL R&D program
† anne.oppelt@desy.de

Content from this work may be used under the terms of the CC BY 4.0 licence (© 2026). Any distribution of this work must maintain attribution to the author(s), title of the work, publisher, and DOI.

ISBN: 978-3-95450-275-2 ISSN: 2226-0366 doi: 10.18429/JACoW-LINAC2026-MOPO032

DESIGN AND DEVELOPMENT STATUS OF THE SSR2 CAVITY AND CRYOMODULE*

Heetae Kim†, Giyeol Han, Eunsol Go, Seojeong Kim, Heejin Do, Jangwon Han, Yoo-Lim Cheon, Juwan Kim, Junyoung Yoon, Wookang Kim, Youngkwon Kim, Jaehyung Lee, Yong-Sub Cho
Institute for Rare Isotope Science, Institute for Basic Science, Daejeon, Republic of Korea

Abstract

The pre-production development of the SSR2 cavity and cryomodule for the RAON SCL2 superconducting linac is in progress. The 325 MHz, β_{opt} = 0.51 cavity is designed for 4.1 MV accelerating voltage and $E_{acc} \geq 8.7$ MV/m at 2.05 K. RF and mechanical analyses confirm acceptable peak fields, pressure sensitivity, and Lorentz-force detuning. The fundamental power coupler is designed for 7 kW CW operation and is planned to be tested up to 20 kW CW in travelling-wave mode. The six-cavity cryomodule incorporates thermal intercepts, a 50 K thermal shield, and multilayer insulation to reduce cryogenic heat loads. The 2 K heat-load design goal is 100 W, consisting of 20 W static and 80 W dynamic load. Fabrication of the first pre-production cavity is underway.

INTRODUCTION

RAON is a heavy-ion accelerator facility developed to provide stable and rare-isotope beams for nuclear-physics research and related applications [1, 2]. Its low-energy superconducting linac, SCL3, employs quarter-wave resonator (QWR) and half-wave resonator (HWR) cavities that were fabricated, tested, installed, and successfully operated with argon beams [2–4]. The high-energy superconducting linac SCL2 is being developed with 325 MHz SSR1 and SSR2 cryomodules [2]. The SSR2 cavity is the β_{opt} = 0.51, 325 MHz single-spoke resonator, with six cavities per cryomodule. Prototype SSR2 cavities were fabricated and vertically tested, providing RF performance, Lorentz-force-detuning, and helium-pressure-sensitivity data [5], and the RF surface-loss behavior has also been investigated [6]. The present pre-production configuration has since been revised. It integrates the updated cavity and helium vessel with a dual-stage tuner, a 7 kW CW fundamental power coupler, and a six-cavity cryomodule based on the RAON cryomodule architecture [7]. This work focuses on RF and mechanical performance, thermal management, manufacturability, and integrated assembly.

CAVITY RF AND MECHANICAL DESIGN

RF Performance

The dressed-cavity performance requirements and the principal electromagnetic results are summarized in Table 1. The reference operating point is 325 MHz at 2.05 K, with V_{acc} = 4.1 MV and $E_{acc} \geq 8.7$ MV/m. The optimized model gives R/Q = 252 Ohm and G = 123 Ohm. The calculated peak-field ratios are E_p/E_{acc} = 3.67 and B_p/E_{acc} = 8.96 mT/(MV/m). At E_{acc} = 8.7 MV/m, the corresponding peak surface electric and magnetic fields are approximately 32 MV/m and 78 mT, respectively. Figure 1 shows the surface-field distributions at the nominal gradient.

Table 1: Main SSR2 Cavity Parameters

Parameter	Value	Parameter	Value
Frequency	325 MHz	β_{opt}	0.51
V_{acc}	4.1 MV	E_{acc}	≥ 8.7 MV/m
Q_0	≥ 5 × 10^9	R/Q	252 Ohm
G	123 Ohm	E_p/E_{acc}	3.67
B_p/E_{acc}	8.96 mT/(MV/m)	df/dP target	< 10 Hz/mbar

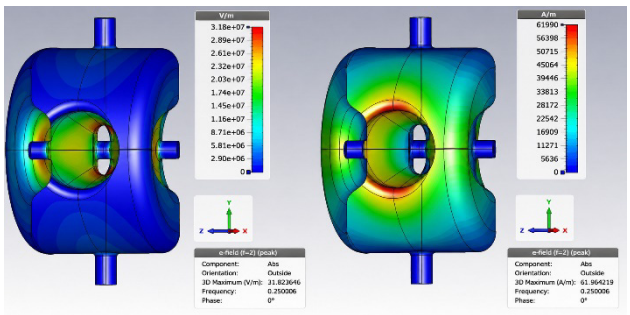


Figure 1: Calculated electric-field (left) and magnetic-field (right) surface distributions at E_{acc} = 8.7 MV/m.

The cavity RF loss is a major contribution to the 80 W dynamic heat-load allocation of the six-cavity cryomodule. Major processing-related frequency offsets were estimated as -0.1 MHz for room-temperature evacuation, +0.5 MHz for cooldown to 2 K, and +0.2 MHz for about 180 µm of buffered chemical polishing. Higher-order modes and low-gradient multipacting were also evaluated; the latter is expected to be processed through RF conditioning.

Mechanical Stability and Tuning Response

The bare cavity uses niobium and Nb-Ti alloy. The cavity shell and spoke are 3.5 mm thick, the nose is 6 mm, and the end covers are 4 mm. The dressed cavity is 470.8 mm long between beam ports and uses a 35 L liquid-helium jacket with a 610 mm outer diameter. The jacket volume is below the 40 L KGS limit, and a minimum 10 mm clearance is maintained between the niobium surface and the helium vessel. Structural analyses covered leak checking,

* This work was supported by the National Research Foundation of Korea (NRF) funded by the Ministry of Science and ICT (RS-2022-00214790).
† kimht7@ibs.re.kr

Content from this work may be used under the terms of the CC BY 4.0 licence (© 2026). Any distribution of this work must maintain attribution to the author(s), title of the work, publisher, and DOI.

ISBN: 978-3-95450-275-2 ISSN: 2226-0366 doi: 10.18429/JACoW-LINAC2026-MOPO034

DEVELOPMENT OF A HIGH-POWER TRAVELING WAVE RESONANT RING FOR SRF LINAC APPLICATIONS*

Fanyu Wang†,1,2, Zusheng Zhou[1,2], Ouzheng Xiao[1], Nan Gan[1], JinDong Liu[1]
[1]Institute of High Energy Physics, Chinese Academy of Sciences, Beijing, China
[2]University of Chinese Academy of Sciences, Beijing, China

Abstract

The reliable operation of high-power RF components, including superconducting cavity input couplers and RF windows, is critical for superconducting radio-frequency (SRF) accelerator facilities. Prior to installation into accelerator systems, these components typically require high-power conditioning to verify their RF performance and thermal stability. However, establishing megawatt-level RF test facilities is challenging due to the complexity and limited availability of high-power RF sources. To address this challenge, the Institute of High Energy Physics (IHEP) has developed a 650 MHz traveling-wave resonant ring (TWRR) system, which enables megawatt-level circulating power by accumulating RF energy in a closed-loop structure with a relatively low-power RF source. The system was tested under high-power continued-wave (CW) operation. A circulating power of approximately 1.2 MW was achieved with an injected RF power of only 42.7 kW. Stable continuous-wave operation was maintained for 8 h without interruption. These results demonstrate the feasibility of MW-level CW RF conditioning using a TWRR and provide an effective test platform for future CEPC RF components.

INTRODUCTION

Because high-power RF sources above the megawatt level are expensive and difficult to operate, resonant-ring technology provides an economical solution for high-power RF component qualification. Traveling-wave resonant ring (TWRR) has been investigated since the 1960s as an effective approach for high-power RF power accumulation [1]. Previous studies have demonstrated significant power enhancement in different frequency bands, while also investigating gain optimization, phase control, and thermal limitations under high-power operation. However, MW-level CW operation of large-aperture WR1500 waveguide-based TWRR systems for accelerator component conditioning has rarely been reported.The Institute of High Energy Physics (IHEP) has developed a 650 MHz P-band WR1500 TWRR for high-power RF components conditioning.

BASIC THEORY

The basic configuration of a traveling-wave resonant ring is illustrated in Fig. 1. The TWRR is a feedback system that uses a main directional coupler to inject RF power into a closed waveguide loop, which enables unidirectional propagation around the ring.

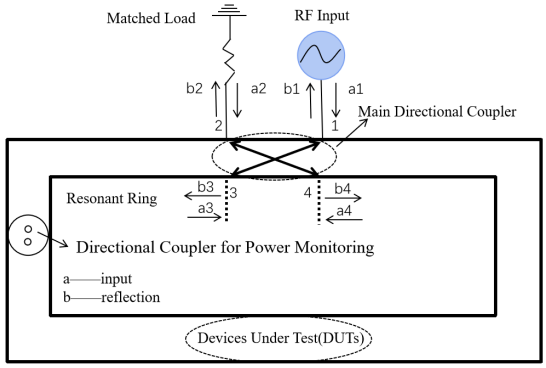


Figure 1: Schematic diagram of a TWRR.

Under the resonance condition, the theoretical power gain without reflection of the TWRR can be expressed as [2]:

$$G = |\frac{b_3}{a_1}|^2 = \frac{C^2}{(1-\sqrt{1-C^2}\cdot e^{-\alpha l_0})^2}. \quad (1)$$

where G is the circulating power gain, C is the power coupling coefficient of the main directional coupler, α is the attenuation constant of the waveguide, and l_0 is the total length of the resonant loop.

The maximum gain is achieved when the total phase shift around the loop satisfies the resonance condition, where the accumulated phase shift is an integer multiple of 2π.

MAIN COMPONENTS OF THE P-BAND TWRR SYSTEM

The 650 MHz P-band TWRR was designed based on a WR1500 waveguide structure to support high-power CW operation. The system mainly consists of a 10dB main directional coupler, a 60.73dB power-monitoring coupler, a mechanical phase shifter and other waveguide sections.

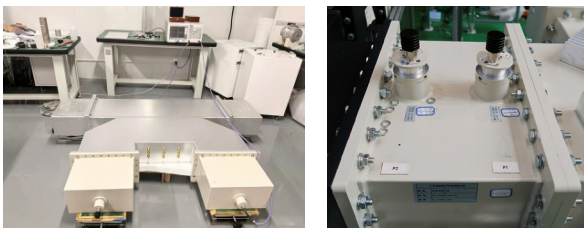


Figure 2:10 dB coupler(left) and 60.73 dB coupler(right).

A 10 dB main directional coupler (left in Fig. 2) was used to inject RF power into the resonant loop, while a 60.73 dB

* Work supported by Yifang Wang's Science Studio of the Thousand Talents Project and National Key Programme for ST Research and Development (Grant NO.: 2024YFA1610602)
†Wangfy@ihep.ac.cn

Content from this work may be used under the terms of the CC BY 4.0 licence (© 2026). Any distribution of this work must maintain attribution to the author(s), title of the work, publisher, and DOI.

ISBN: 978-3-95450-275-2 ISSN: 2226-0366 doi: 10.18429/JACoW-LINAC2026-MOPO035

DEVELOPMENT OF THIRD HARMONIC CAVITY CRYOMODULE FOR HALF

Z. Mi †,[1,2], W. Pan[1,2], R. Ge[1,2], F. He[1,2], S. Jin[1,2], X. Yang[1], B. Liu[1,2], H. Zheng[1,2], T. Liu[1], Y. Liu[1], T. Zhao[1], Y. Wei[3], Z. Huang[3], F. Xu[3], K. Zhang[3], G. Feng[3]
[1]Institute of High Energy Physics, CAS, Beijing, China
[2]University of Chinese Academy of Sciences, Beijing, China
[3]University of Science and Technology of China, Hefei, China.

Abstract

The Institute of High Energy Physics, Chinese Academy of Sciences (IHEP-CAS) developed the 1.5 GHz third harmonic cavity system for the Hefei Advanced Light Facility (HALF) project. Supported by the comprehensive infrastructure of the Platform for Advanced Photon-source Studies (PAPS), the IHEP project team has completed the full-chain workflow for the cryomodule, including overall structural design, performance characterization of key materials, high-precision welding and forming, multi-pass post-processing optimization, as well as mod-ule integration and testing. This paper primarily introduces development and test results of the 1.5 GHz cavity and cryomodule. The structure of the harmonic cavity has been simplified, and an integral welding method for the cavity with helium vessel has been adopted to enhance operational reliability. All key technical parameters are significantly superior to the acceptance indicators.

INTRODUCTION

Hefei Advanced Light Facility (HALF) [1] is a soft X-ray and Vacuum Ultra-Violet fourth-generation diffraction limited light source which is being constructed by National Synchrotron Radiation Laboratory (NSRL), University of Science and Technology of China. HALF consists of a full energy linac injector and a circular storage ring. The overall layout of HALF is shown in Figure 1.

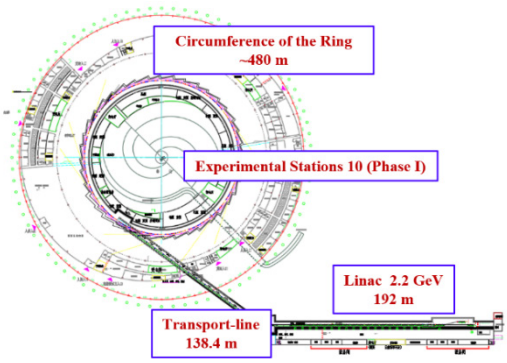


Figure 1: Layout of HALF.

The RF system consists of a main 500 MHz Superconducting (SC) cavity and a passive 3rd-harmonic 1.5 GHz SC cavity for the HALF storage ring. A 3rd harmonic superconducting cavity system is being developed by IHEP for lengthening bunch and improving beam lifetime in the Hefei Advanced Light Facility (HALF) storage ring. This SC cavity is excited by an electron beam with 350 mA current, 1 nC charge, and ~6.7 ps length [2, 3]. Refer-ring to the physical and engineering requirements of HALF, the structural and process design of the Superconducting cavity and cryomodule have been carried out. The design parameters are listed in Table 1. System-level integration and performance verification tests have also been performed.

Table 1: Main Parameters of Cryomodule

Parameters	Value	Units
Frequency	1499.4	MHz
Operating temperature	4.5±0.5	K
Operating gradient	0.6	MV/m
Q0 @ 0.6	⩾2E+8	--
Ep/Eacc	2.05	--
Bp/Eacc	4.72	mT/(MV/m)
G	291.6	Ω
R/Q	81.8	Ω
Frequency tuning range	14499.2 ~1499.9	MHz
Cavity stiffness	~20	N/um
Tuning sensitivity	1.99	MHz/mm
df/dp	83	Hz/mbar
LFD	-0.76	Hz/(MV/m)^2
Ultimate vacuum	＜ 8E-8	Pa
Static heat loss	25	W

THE SC CAVITY AND CRYOMODULE DESIGN

The 1.5 GHz harmonic SC cavity utilizes the TESLA shape with different beam pipes to simplify manufacturing complexity and efficiently extract the higher order modes. As Fig. 2 shown is There are two pickup ports on the small beam tube, one for operation and the other as standby. The liquid-helium tank is integrally welded to the

† mizh@ihep.ac.cn

Content from this work may be used under the terms of the CC BY 4.0 licence (© 2026). Any distribution of this work must maintain attribution to the author(s), title of the work, publisher, and DOI.

ISBN: 978-3-95450-275-2 ISSN: 2226-0366 doi: 10.18429/JACoW-LINAC2026-MOPO036

OPTIMIZATION OF A COOLING SYSTEM FOR THE IPHI RFQ UPGRADE

P. Hamel[1], A. Deville[1], T. Hamelin[1], O. Piquet[1]
[1]CEA-IRFU, Gif-sur-Yvette, France

Content from this work may be used under the terms of the CC BY 4.0 licence (© 2026). Any distribution of this work must maintain attribution to the author(s), title of the work, publisher, and DOI.

Abstract

The IPHI RFQ, designed at CEA in the early 2000s and commissioned in 2016, was the first RFQ developed at CEA. It accelerates a 100 mA beam up to 3 MeV at high duty cycle. Subsequent RFQ projects (SPIRAL2, LINAC4, ESS, NEWGAIN) enabled improvements in RFQ design and modeling. Based on this experience, an upgrade of the IPHI accelerator has been investigated to increase beam energy and improve efficiency. The proposed design is a 6 m long, four-vane RFQ, divided into six 1 m sections, constrained to operate with the existing RF amplifiers (352 MHz, 1.8 MW peak power, 70 % duty cycle). Under these conditions, RF power losses in the cavity walls reach about 1 MW and must be removed by a cooling system. The spatial distribution of the cooling channels impacts thermal expansion, leading to local deformations and associated cavity detuning. These effects must be controlled to ensure the electric field distribution remains consistent with beam dynamics requirements. This paper presents the method used to optimize the cooling channel layout and its impact on RF performance. The final design achieves a detuning below 20 kHz and an inter-vane voltage error below 0.1 %.

INTRODUCTION

Based on recent RFQ delivered by CEA (SPIRAL2, LINAC4, ESS [1], NEWGAIN [2]), an upgrade of the IPHI RFQ has been investigated [3]. The RF power injected into the RFQ cavity is dissipated within the copper wall due to the finite surface resistance R_S (about 5 mΩ at the nominal frequency f_0 = 352 MHz). To dissipate this heat, 20 longitudinal cooling channels are drilled through the cavity. The resulting temperature rise induces thermal expansion of the cavity, leading to a frequency detuning. This thermal expansion, and consequently the detuning, can be controlled by optimizing the position of the cooling channels. Performing such an optimization using an eigenmode solver would require a prohibitively large number of simulations. Therefore, a simplified model was developed from a selected set of channel configurations to estimate the local cavity detuning. This model was then used to optimize the channel positions with the objective of minimizing the overall cavity detuning while maintaining the same water temperature in each cooling channel.

COOLING STRATEGY

The cooling circuit layout along the RFQ is shown in Fig. 1. The water flow direction alternates from one module to the next in order to reduce the effect of water heating along each module on the overall cavity detuning. The inlet water temperature is set to 28 °C for all cooling channels.

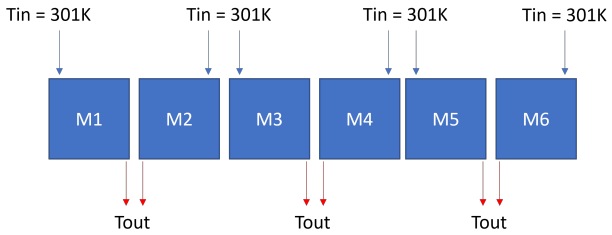


Figure 1: Cooling circuit layout along the RFQ.

The RFQ body has an octagonal cross section with a width of 280 mm. A quarter of the cross section is shown in Fig. 2. By symmetry, the 20 longitudinal cooling channels are fully defined by the positions of four channels: three channels (C1, C2 and C3) are drilled into the vane midplane, while the fourth (C4) is drilled into the RFQ body. The position of C4 is fixed because it is constrained by the tuner location, which is required to compensate for manufacturing tolerances, and by the cooling channels of the pump grids, which are not considered in this study. All cooling channels have a diameter of 8 mm.

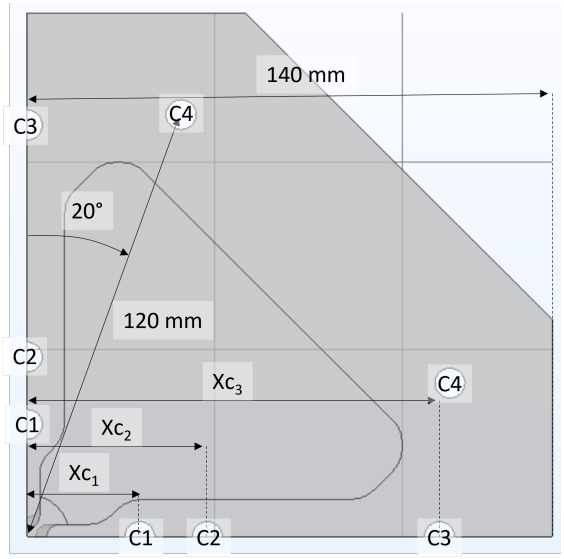


Figure 2: Geometry of the RFQ quarter cross section.

THERMOMECHANICAL SIMULATION

To reduce the computational time, the RFQ is approximated as a succession of simple cells, each corresponding to half a vane modulation period, with a length and an amplitude depending on the longitudinal position along the RFQ. For instance, shorter cell lengths and smaller vane modulation amplitudes are considered at the beginning of the cavity. The thermomechanical simulations are performed using COMSOL Multiphysics [4].

ISBN: 978-3-95450-275-2 ISSN: 2226-0366 doi: 10.18429/JACoW-LINAC2026-MOPO037

SIMULATION OF DC BIAS-BASED MULTIPACTING SUPPRESSION IN FCC-ee FUNDAMENTAL POWER COUPLERS*

A. Durdevic†, S. Gorgi Zadeh, F. Peauger, CERN, Geneva, Switzerland

Abstract

In fundamental power couplers for RF accelerators, secondary electron emission can give rise to multipacting (MP), leading to RF losses, heating, and performance degradation. A mitigation technique consists of superimposing an electrostatic DC field onto the RF field by applying a bias voltage between the inner and outer conductors of the coaxial power coupler. This approach alters electron trajectories and disrupts the resonant conditions required for MP. This work investigates the effectiveness of DC bias in suppressing MP in FPCs designed for the Future Circular Collider (FCC-ee) accelerating cavities operating at 400.79 MHz and 801.58 MHz. Two baseline coaxial FPC designs are analyzed, with nominal maximum power levels of 382 kW and 195 kW, respectively, extended to 500 kW and 250 kW to account for operational margins. Using the Spark3D MP simulation tool, the required DC bias voltage for MP suppression is systematically evaluated across the full power range. The study also examines the influence of different secondary electron yield (SEY) models for copper surfaces in the coaxial structure and ceramic materials in the RF window on the required DC bias voltage.

INTRODUCTION

Fundamental power couplers (FPCs) are essential components of superconducting RF accelerator systems, enabling efficient RF power transfer from the RF source to the accelerating cavity [1, 2]. Due to the presence of strong RF electromagnetic fields under vacuum conditions, FPCs are susceptible to multipacting (MP), which can lead to RF losses, local heating, vacuum degradation, prolonged conditioning, and operational limitations. Multipacting is a resonant electron multiplication phenomenon in which electrons synchronize with the RF electromagnetic field and repeatedly impact metallic or dielectric surfaces. Depending on the geometry and operating conditions, this process may result in exponential electron growth sustained by secondary electron emission. The occurrence and intensity of MP strongly depend on the RF field distribution, operating frequency, geometry of the structure, surface material properties, and secondary electron yield (SEY). In high-power coaxial RF structures, MP suppression is particularly important due to the large transmitted RF power and demanding operational reliability requirements.

Surface conditioning, coatings, and geometry optimization are commonly used to reduce MP susceptibility. However, these approaches may not always fully eliminate MP barriers over the complete operating power range. Previous studies [3–5] demonstrated that applying a DC bias voltage between the inner and outer conductors of coaxial structures can significantly modify MP behaviour by perturbing resonant electron trajectories. Depending on the applied voltage and geometry, DC bias may shift MP barriers or suppress them entirely [5]. The effectiveness of this technique depends strongly on the electric field distribution and surface emission properties.

Motivated by these observations, this work investigates the effect of DC bias on MP behaviour in two FCC-ee FPC designs shown in Fig. 1, operating at 400.79 MHz and 801.58 MHz [6, 7]. The couplers are hereafter denoted as the 400 MHz and 800 MHz couplers, respectively. Numerical simulations are performed using CST Studio Suite and Spark3D [8] by superimposing RF and electrostatic field solutions. Different SEY models for copper and TiN-coated ceramic surfaces are considered in order to evaluate the sensitivity of the MP behaviour to realistic surface conditions and material assumptions.

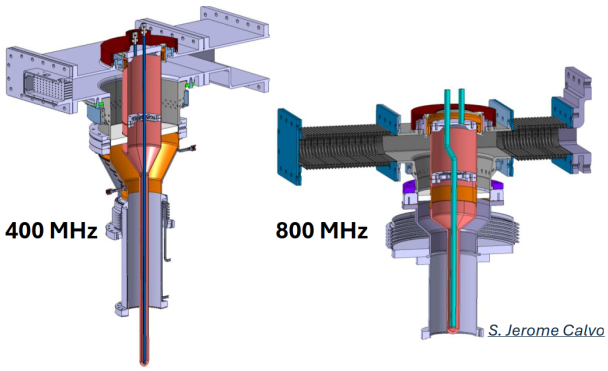


Figure 1: Mechanical models of the FCC-ee fundamental power couplers operating at 400.79 MHz (left) and 801.58 MHz (right) [7].

SIMULATION METHODOLOGY

The RF electromagnetic fields were calculated using the CST Studio Suite frequency-domain solver. Electrostatic simulations were additionally performed to generate the DC electric field distribution between the inner and outer conductors of the coaxial structures. The resulting RF and electrostatic field maps were then imported into Spark3D, scaled to the desired RF power and DC voltage levels, and superimposed for MP particle-tracking simulations. FCC-ee FPC models operating at 400.79 MHz and 801.58 MHz were investigated over their full operating power ranges, including additional operational margins up to 500 kW and 250 kW, respectively.

Figure 2 illustrates the simulation model of the 400 MHz FPC. The RF electromagnetic fields were computed in

* Work supported by CERN
† ana.djurdjevic@cern.ch

Content from this work may be used under the terms of the CC BY 4.0 licence (© 2026). Any distribution of this work must maintain attribution to the author(s), title of the work, publisher, and DOI.

ISBN: 978-3-95450-275-2 ISSN: 2226-0366 doi: 10.18429/JACoW-LINAC2026-MOPO038

EMITTANCE INVESTIGATIONS AT THE ESS LINAC

S. Johannesson*, M. Eshraqi, I. Gorgisyan, R. Kuriakose,
L. A. Martins, N. Milas, R. Miyamoto, D. Noll, E. Salehi
European Spallation Source, Lund, Sweden

Abstract

The European Spallation Source (ESS) is in the final stages of commissioning its linear accelerator (LINAC), which aims to deliver a high-power proton beam for neutron production. Understanding the dynamics in the machine and comparing measurements with the model can provide a deeper insight into the machine's performance and help avoid possible issues when we start ramping up the power. Several techniques are available for measuring both transverse and longitudinal emittance, making comparison and benchmarking important. At ESS, existing transverse emittance measurements show some variation between methods and differ from the design values. This work investigates possible sources of these discrepancies.

INTRODUCTION

The European Spallation Source (ESS) is a neutron source under construction in Lund, Sweden. The pulsed, high neutron flux source produces neutrons by shooting high-energy protons at a rotating tungsten target. A moderator, comprised of water and liquid hydrogen, cools the neutrons down to the desirable energy ranges [1].

The ESS LINAC is a high-power, high-intensity proton linear accelerator, and its high level parameters are listed in Table 1.

Table 1: ESS Proton LINAC High-level Proton Parameters for Neutron Production

Parameter	Unit	First Neutrons	Design
Beam Power	MW	2	5
Beam Energy	GeV	0.8	2
Peak Beam Current	mA	62.5	
Beam pulse length	µs	2860	
Beam pulse rep. rate	Hz	14	
Duty cycle	%	4	
RF frequency	MHz	352.21/704.42	

This paper will focus on measurements in the MEBT (Medium Energy Beam Transport) section of the machine. A schematic view of this section can be seen in Fig. 1.

The total length of this section is 4 m and the beam energy is 3.62 MeV. The design transverse envelope and emittance can be seen in Fig. 2.

The beam instrumentation devices in the MEBT used in this work include the Emittance Measurement Unit (EMU) [2, 3], a slit–grid device that samples the transverse phase space, and three wire scanners [4]. The wire scanners consist of thin wires that are moved through the beam to measure the transverse beam profile.

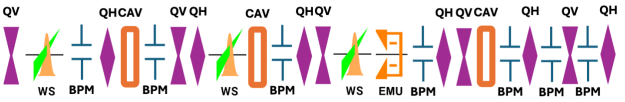


Figure 1: A schematic layout of the ESS MEBT section. QH and QV stands for horizontal and vertical quadrupoles, WS stands for wire scanner, CAV stands for buncher cavity, BPM stands for beam position monitor and EMU stands for emittance measurements unit.

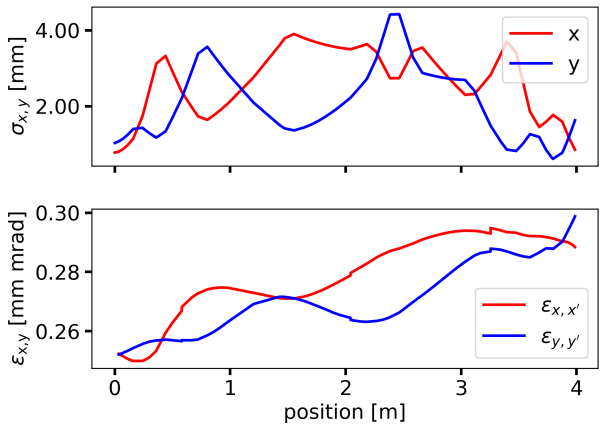


Figure 2: The normalized transverse envelope and emittance of the ESS MEBT section.

Measuring and understanding the beam emittance in both the transverse and longitudinal planes is essential for achieving the design parameters of the accelerator and for assessing the current performance of the machine. This paper examines three different methods for measuring the transverse emittance.

THREE-WIRE METHOD

One way of reconstructing the beam emittance is to measure the beam size at several locations and reconstruct the Twiss parameters. We have three wires and three Twiss parameters in each plane. An initial guess of Twiss parameters is simulated in TraceWin [5]. Further optimizations of the transverse Twiss parameters, to find the minimal difference, are then done using OpenXAL simulation [6]. The longitudinal Twiss parameters are kept constant during this process. An example of measured beam profiles from the wires for a 10 mA beam can be seen in Fig. 3. The beam size is calculated by doing a double-Gaussian fit on the profiles, and the fit to each profile is plotted as dotted lines.

For these measurements, all quadrupoles downstream of quadrupole 4, as well as the buncher cavities, were turned off.

* sofia.johannesson@ess.eu

Content from this work may be used under the terms of the CC BY 4.0 licence (© 2026). Any distribution of this work must maintain attribution to the author(s), title of the work, publisher, and DOI.

ISBN: 978-3-95450-275-2 ISSN: 2226-0366 doi: 10.18429/JACoW-LINAC2026-MOPO039

PROTOTYPE DRIFT TUBE DEVELOPMENT FOR SEPARATED DRIFT TUBE LINAC

Sungbin Park[1], Seunghyun Lee[1], Han-Sung Kim[1], Hyeok-Jung Kwon[1]
[1]Korea Atomic Energy Research Institute, Korea Multi-purpose Accelerator Complex, Gyeong-ju, Republic of Korea

Abstract

As a possible option for 200 MeV energy upgrade in Korea Multi-purpose Accelerator Complex (KOMAC), separated drift tube linac (SDTL) structure is considered. In this study, the first drift tube in the first tank is developed and tested. The design of the drift tube is characterized by independent cooling channels in the central and peripheral regions to effectively mitigate RF heat load. The feasibility of the drift tube is investigated through a combined experimental and numerical approach. A transparent acrylic-based prototype is fabricated to empirically visualize the internal flow and measure hydraulic pressure drop across the drift tube. Concurrently, a multi-physics analysis integrating electromagnetic, thermal, and structural solvers is conducted to deduce the structural integrity and frequency detuning under operational condition.

DRIFT TUBE PROTOTYPE

The cross-sectional view of the drift tube is shown in Fig. 1. The external geometry of the drift tube is optimized to maximize the acceleration efficiency while minimizing the risk of electrical breakdown [1]. Considering the long geometry and thick central section of the drift tube, separate cooling channels are configured for the central and peripheral regions. Coolant is supplied via the outer channel in the stem, flows through the central channel, enters the peripheral channels at the bottom, circulates upward through them, converges back at the top, and is finally discharged along the interior channel in the stem. Since the drift tube does not incorporate a quadrupole magnet inside, it features only these cooling channels. Furthermore, except for the internal cooling channels, the remaining sections inside the drift tube are designed to be hollow for weight reduction.

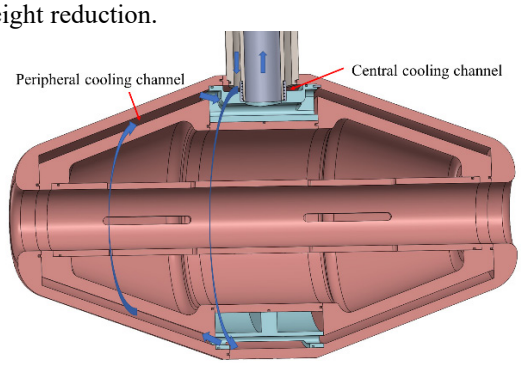


Figure 1: Cross-sectional view of the drift tube. (blue arrows describe flow of coolant inside the drift tube).



Figure 2: Acrylic drift tube prototype with a manifold for coolant flow test.

For the empirical verification of the coolant flow inside the drift tube, acrylic-based transparent prototype is manufactured as can be seen in Fig. 2. To evaluate the hydraulic performance, the pressure drop across the cooling channels is measured as a function of the flow rate. In Fig. 3, it is shown that pressure drop has linear relation with flow rate. When cooling water temperature increase is limited as 1°C under RF duty of 3%, required flow rate is 6.5 GPM. At that flow rate, required pressure drop is found to be 0.6 bar, confirming that it can be sufficiently achieved in the nominal cooling system. Additionally, a flow visualization test is subsequently performed by introducing blue tracer particles into the working fluid as seen in Fig. 4, allowing for the direct observation and qualitative assessment of the internal fluid behavior. In the central cooling channel, a relatively uniform flow distribution is observed. Conversely, in the peripheral channels, the flow is primarily concentrated in the upper and lower regions as interconnecting passages linking the central and peripheral channels are positioned at the top and bottom. Consequently, a stagnation zone characterized by recirculating flow is developed

Content from this work may be used under the terms of the CC BY 4.0 licence (© 2026). Any distribution of this work must maintain attribution to the author(s), title of the work, publisher, and DOI.

ISBN: 978-3-95450-275-2 ISSN: 2226-0366 doi: 10.18429/JACoW-LINAC2026-MOPO041

PRELIMINARY DESIGN OF AN RF-FOCUSED IH-DTL

Q. Kong[1,2,*], H. Liu[1,2,3], A. Li[1,2,3], Y. Yang[1,2,3]
[1]Spallation Neutron Source Science Center, Dongguan, China
[2]Institute of High Energy Physics, Beijing, China
[3]University of Chinese Academy of Sciences, Beijing, China

Abstract

Developing compact, high-efficiency low-energy linear accelerators is of great importance for advanced scientific research and medical applications. This paper presents the operating principle and beam dynamics study of a Radio-Frequency focused Interdigital H-mode DTL. By reshaping the drift tubes to introduce internal pole tips, the RF field itself can be used to achieve transverse quadrupole focusing, thereby meeting the requirement of stable longitudinal transport without relying on internal quadrupole for transverse focusing. In addition, full-cavity optimization was carried out, FFFDDD transverse focusing periodic lattices has been chosen, yielding an RF structure with a high accelerating gradient, high beam quality, and high transmission efficiency.

INTRODUCTION

In the low- to medium-β range ($0.05 < \beta < 0.2$), the Alvarez-type drift-tube linac (Alvarez-DTL) [1], operating in TM010 mode, has long been the standard for efficient acceleration, but its embedded quadrupole magnets lower shunt impedance. H-type linacs (TE110 interdigital, IH [2], or TE210 crossbar, CH) offer much higher impedance and compactness in this range, but face strong transverse defocusing from the RF field at the gaps. This is typically addressed via KONUS dynamics [3], operating at 0° synchronous phase, though over long multi-gap acceleration this causes beam filamentation and emittance growth, and periodic refocusing requires PMQs/EMQs inside the drift tubes, raising fabrication difficulty and cost.

To address this, this paper proposes a Radio-Frequency-focused Interdigital H-mode DTL (RFI-type DTL), which deforms the drift tubes with inward-extending electrodes to convert part of the RF power directly into a transverse quadrupole focusing field. This removes any dependence on magnetic lenses and enables operation at a negative synchronous phase (e.g., -30°), restoring longitudinal stability. This paper describes the structure's operating principle, compares focusing lattices, and presents end-to-end 3D beam-dynamics simulation results.

OPERATING PRINCIPLE OF THE RFI-TYPE DTL

The core innovation of the RFI-type DTL is its integrated, composite drift-tube geometry. Instead of a conventional cylindrical vacuum tube, the interior is reshaped into a structure with four orthogonally extended pole tips (Fig. 1). As the cavity resonates in the fundamental TE110 mode, these pole tips alternately charge and discharge, exciting a time-varying RF quadrupole field on the drift-tube axis. Since focusing now derives from the RF field itself, the structure escapes KONUS dynamics' requirement of a 0° synchronous phase, and the phase can instead sit near -30°, giving the bunch strong longitudinal confinement.

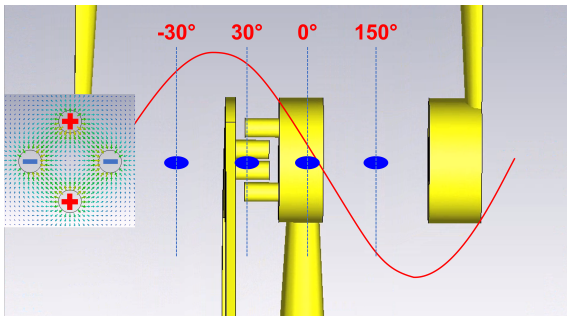


Figure 1: Schematic of the RF phase sequence experienced by particles in the RFI-type DTL.

The dynamics follow this phase-evolution sequence: at -30° the bunch center reaches the gap center for peak accelerating gradient; at +30° it reaches the pole-tip center, where transit-time effects give peak quadrupole strength and strong focusing; at 0° it drifts through the field-free tube interior; at 150°, combined with the inherent 180° phase reversal between adjacent IH gaps, the effective synchronous phase resets to -30° for the next cycle.

The F/D element arrangement sets the required field gradient and beam quality. Three periodic sequences FDFD, FFDD, and FFFDDD were compared using TraceWin [4], scanning the zero-current phase advance per period (σ_0) at 20°, 40°, 60°, and 80° to map the envelope stability boundary. As shown in Fig. 2 and Fig. 3, FDFD is nearly ideal physically, but FFFDDD is more practical due to its much lower field-strength requirement; its beam loss at intermediate phase advances can be resolved by operating in the strong-focusing region ($\sigma_0 \geq 60°$), which both compresses the envelope and eliminates loss.

SINGLE-CELL ELECTROMAGNETIC MODELING OF THE RFI-TYPE DTL

CST was used to perform three-dimensional simulations of the resonant cavity's high-frequency properties [5]. As shown in Fig. 4, the core geometric parameters that determine the resonant and focusing performance include: the

* kongqy@ihep.ac.cn

Content from this work may be used under the terms of the CC BY 4.0 licence (© 2026). Any distribution of this work must maintain attribution to the author(s), title of the work, publisher, and DOI.

ISBN: 978-3-95450-275-2 ISSN: 2226-0366 doi: 10.18429/JACoW-LINAC2026-MOPO042

OPTIMIZATION OF LOW-ENERGY-CONTRIBUTING POWER SOURCE POSITIONS DURING THE BEPCII LINAC ENERGY UPGRADE

X. He†, H. Shi, C. Meng, B. L. Deng, Y. R. Wei, L. Qian
Institute of High Energy Physics, Chinese Academy of Sciences, Beijing, China

Abstract

BEPCII Linac operated with 20 power sources before the energy upgrade in summer 2024. To support sustained 2.35 GeV electron-positron collisions and maintain at least one redundant power source for operational reliability, the Linac required an energy increase. Among these, Power sources No. 6 (K6) and No. 12 (K12) exhibited relative lower energy contribution. Phase-matching misalignment between adjacent accelerating structures was identified as the most probable cause after checking the peak power gain of pulse compressors, the input power reflection of accelerating structures, and the total transmission loss. During the energy upgrade, the microwave phase at the input of K6's accelerating structure was directly measured and adjusted—increasing K6's net energy gain significantly. However, no corresponding work was carried out on K12 due to the recovery issues after vacuum destruction. As an engineering solution, one additional pulse compressor was installed at K4, and both K6 and K12 were upgraded from single-klystron to dual-klystron configurations. This strategy ensured stable, high-luminosity operation—directly enabling BEPCII to achieve its target luminosity in April 2026.

INTRODUCTION

The Beijing Electron-Positron Collider (BEPC), located in Beijing, China, commenced routine operation in 1988. Over the past decade, increasingly large experimental datasets have underscored the scientific necessity of extending the collider's beam energy range to 2.25–2.45 GeV. This interval is pivotal for exploring exotic XYZ hadronic states and conducting high-precision studies of CP violation in charmed baryons. Delivering stable, high-brightness beams across this extended energy range imposes stringent requirements on accelerator performance—motivating a targeted upgrades of the linear accelerator's (Linac's) microwave system.

This paper presents the strategic reconfiguration of two low-energy-contribution klystron positions—K6 and K12—as a central component of the broader energy upgrade initiative, alongside a synthesis of key upgrades implemented across the microwave system [1].

SYSTEM OVERVIEW

Figure 1 illustrates the overall configuration of the BEPCII microwave system. With the exception of K1—which powers the bunching section—and K3 and K4—both situated downstream of the positron production target—all other klystrons were originally configured in a 1-to-4 topology (i.e., one klystron driving four accelerating structures). At locations labeled KnA, this topology was upgraded to a dual 1-to-2 architecture: each former 1-to-4 channel was subdivided into two independent, individually controllable 1-to-2 paths. Pulse compressors were integrated into 20 klystron channels, excluding K1 and K3. Prior to the 2024 energy upgrade, the Linac delivered electron and positron beams with peak energies of approximately 2.85 GeV and 2.55 GeV, respectively, at its output.

To meet escalating operational demands—including higher final beam energy, tighter beam quality specifications, and enhanced reliability—the upgrade program incorporated several coordinated interventions: an additional pulse compressor was installed at K4; K6 and K12 were converted to dual 1-to-2 configurations; and complementary improvements were implemented across supporting subsystems—including the microwave excitation chain, the Low-Level Radio Frequency (LLRF) control system, and the Sub-Harmonic Buncher (SHB) system—alongside full replacement of aging pulse compressors and integration of auxiliary monitoring and interlock systems [1].

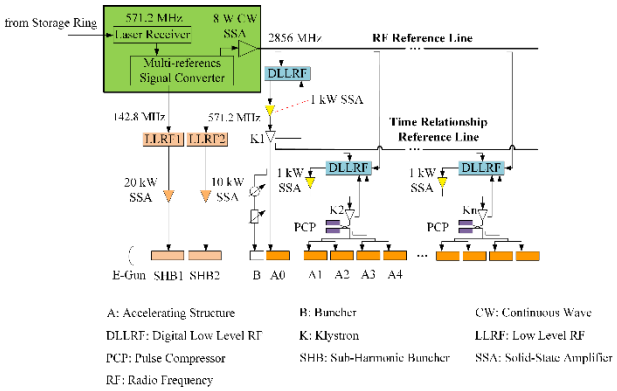


Figure 1: Configuration of the microwave system.

ENERGY UPGRADE

Although the Linac achieved a maximum positron beam energy of ~2.55 GeV as early as 2009, sustained, reliable operation at the center point of 2.35 GeV—within the scientifically critical 2.25–2.45 GeV window—requires not only sufficient total energy gain but also redundancy to ensure robustness against component failure. To close this operational gap, a dedicated energy upgrade strategy was formulated.

The first five klystrons (K1–K5) serve exclusively for longitudinal bunch compression and initial acceleration of both electron and positron beams. In contrast, K8, K9, K11,

† hexiang@ihep.ac.cn

Content from this work may be used under the terms of the CC BY 4.0 licence (© 2026). Any distribution of this work must maintain attribution to the author(s), title of the work, publisher, and DOI.

ISBN: 978-3-95450-275-2 ISSN: 2226-0366 doi: 10.18429/JACoW-LINAC2026-MOPO043

STUDY ON RF FIELD BUILD-UP AND CASCADING IMPACTS IN THE STCF INJECTOR MAIN LINAC*

Y.A. Xia[1], H. Hu[1], S.T. Teng[1], T.N. Hu[†,1], Y. Wang[1],
Y.F. Zeng[1], J. Pang[2], Y.J. Yuan[3], J.Y. Tang[2]
[1]Huazhong University of Science and Technology, Wuhan, China
[2]University of Science and Technology of China, Hefei, China
[3]University of Chinese Academy of Sciences, Beijing, China

Content from this work may be used under the terms of the CC BY 4.0 licence (© 2026). Any distribution of this work must maintain attribution to the author(s), title of the work, publisher, and DOI.

Abstract

The Main Linac (ML) of the Super Tau-Charm Facility (STCF) injector comprises 36 series-connected constant-gradient traveling-wave accelerating structures. Variations in injection timing induce complex coupling between the independent Radio Frequency (RF) transient filling and transient beam loading effects, systematically altering the beam energy spread. As a bunch traverses successive structures, these localized coupled perturbations propagate, accumulate, and superimpose. This cascading impact severely restricts the overall energy stability and beam quality. This paper systematically investigates the dual-transient coupling mechanism in a single structure, perturbation differences under varying injection timings, and the cumulative amplification characteristics across the multi-stage configuration. The findings provide a vital theoretical foundation for RF timing co-regulation and transient perturbation suppression, effectively enhancing beam quality stability for the STCF.

INTRODUCTION

STCF is a next-generation electron–positron collider designed for high-brightness beam experiments. The ML section of its injector is required to accelerate the beam to the energy needed for subsequent injection [1]. After the RF power is injected, the electromagnetic field inside the linac undergoes a transient field build-up process. Since the electromagnetic field gradually propagates and builds up along the traveling-wave structure, the beam injection timing is closely related to the RF field build-up state. Injecting the beam either too early or too late will change the accelerating voltage actually seen by the beam.

In traveling-wave accelerating structures, the transient effects also include the transient beam-loading. The beam extracts energy from the accelerating field, causing the accelerating voltage to decrease as the beam passes through the structure [2, 3]. Since the RF field build-up voltage and the beam-loading voltage can be treated and solved separately, the influence of beam injection timing on the beam energy and energy spread can be analyzed.

* This work is supported by the National Natural Science Foundation of China (No.12341501), the National Key R&D Program of China under Contract No. 2022YFA1602200, the international partnership program of the Chinese Academy of Sciences Grant No. 211134KYSB20200057 and the STCF key technology research and development project.

† TongningHu@hust.edu.cn

For cascaded linac, since the beam arrives at each linac at different times, the corresponding transient field build-up states are also different. Therefore, the beam energy gain after cascading should be regarded as the superposition of the responses of multiple linac at different times. Meanwhile, various errors exist in the practical system, so the influence of cascading on the energy spread of the first bunch needs to be comprehensively considered.

This paper focuses on the transient field build-up, beam loading, and cascade effects in the ML section of the STCF injector. After establishing the transient field build-up model of a single 3 m traveling-wave linac, the process in which RF power propagates cavity by cavity along the linac and gradually builds up the field is obtained. Then, three 36-linac cascade models are constructed, including the theoretical cascade, the without errors cascade, and the with errors cascade. Based on beam loading theory, two cases are compared: injection at the completion of RF filling and optimal early injection. The results can provide a reference for optimizing the beam injection timing and suppressing the first-bunch energy spread.

RF FIELD BUILD-UP IN LINAC AND ITS CASCADING

The ML section of the STCF injector adopts a constant-gradient accelerating structure. Since the field build-up in different cavities does not reach the steady state simultaneously, a distinct transient process exists. In this section, a circuit-equivalent model of a single linac is established, and the field build-up characteristics of the 36-linac cascade are further analyzed.

Transient Field Build-up Equation of the Linac

The traveling-wave linac consists of multiple mutually coupled resonant cavities. Each accelerating cavity can be equivalently represented as a resonant unit composed of an inductance, a capacitance, and a resistance, while electromagnetic energy is transferred between adjacent cavities through coupling terms. Let the voltage in the n-th cavity be v_n, and let its eigen angular frequency, quality factor, and coupling coefficient be ω_n, Q_n, and k_n, respectively. The beam-induced current in the linac is denoted as i_n^{ind}. Then, based on the coupled-resonator model [4], the transient voltage variation equation of the coupled-cavity chain can be written as:

ISBN: 978-3-95450-275-2 ISSN: 2226-0366 doi: 10.18429/JACoW-LINAC2026-MOPO045

OPTICS MODEL OF THE 805 MHz SECTION OF THE FERMILAB LINAC*

A. Shemyakin†, J.-P. Carneiro, E. Chen, A. Pathak, R. Sharankova
Fermi National Accelerator Laboratory, Batavia, IL, USA

Abstract

The Side-Coupled Linac (SCL) section of the FNAL Linac accelerates the 20-25 mA H- beam from 116 MeV to 400 MeV in 7 cavities referred to as Modules. Most major components of this section are re-calibrated using beam-based measurements. Module gradients and phases are determined from phase scans, while calibrations of quadrupoles and dipole correctors are improved using differential trajectories. Longitudinal bunch parameters at the entrance of the section are reconstructed using a Bunch Shape Monitor. Transverse initial beam conditions are deduced from profile measurements along the SCL. Using the developed optics model, the beam behavior in the SCL section is predicted using the TraceWin code and compared with additional measurements.

MOTIVATION

The Fermilab 400 MeV Linac [1, 2] (that will be referred here as Linac1) reliably delivers H- beam to the Booster and 400 MeV experiments. In several years, it will be replaced by the new superconducting 800 MeV Linac2 [3, 4]. A set of tools and procedures is being developed for the coming commissioning of Linac2, and the Linac1's SCL section is used to test them [5-7]. The goal of such measurements is to form an optics model of an accelerator. In terms of the work presented in this paper, predictive capability of the model validates the toolkit, providing confidence in the success of Linac2 commissioning. These efforts can help with Linac1 operational issues.

SIDE-COUPLED LINAC DESCRIPTION

Linac1 (Fig. 1) consists of a front end, preparing a bunched 0.75 MeV H- beam; 201.25 MHz Drift-Tube Linac (DTL) section accelerating the ions to 116 MeV; transition section matching the beam between DTL and SCL; and 805 MHz SCL sending a nominally 401 MeV beam to the Booster, one of two beam dumps, or test area through a transfer line.

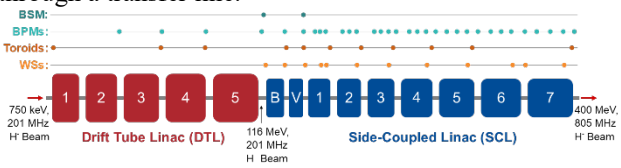


Figure 1: Schematic of Linac1 and diagnostic positions.

The SCL is composed of 7 RF Modules, preceded by 2 cavities (Buncher and Vernier) in the transition section. Each of these 9 RF components is fed by its own amplifier.

* This manuscript has been authored by Fermi Forward Discovery Group, LLC under Contract No. 89243024CSC000002 with the U.S. Department of Energy, Office of Science, Office of High Energy Physics.
†shemyakin@fnal.gov

In turn, every Module consists of 4 Sections with a quadrupole between them, and each Section has 16 identical accelerating cells. The length of these cells L_{gap} is chosen so that, at the nominal energy profile, the electric field flips polarity in the time a particle travels between the cells:

$$L_{gap} = \frac{\beta\lambda}{2} \equiv \frac{\beta c}{2f_{RF}} \quad (1)$$

where βc is the ion's average design velocity in the Section, and $f_{RF} = 805$ MHz. The distance between centers of the end cells in neighbouring Sections is $3\beta\lambda/2$. The Buncher is a copy of the first Section of Module 1, and the Vernier has 4 gaps of the same length as in the Buncher.

The 32 quadrupoles in the SCL and transition section are arranged in a FODO lattice. The trajectory is adjusted by 19 pairs of dipole correctors (trims).

The bunch centroid position (transverse X/Y and phase) is measured by 28 Beam Position Monitors (BPMs). Profile diagnostics are provided by 12 Wire Scanners (WS) [5] and 2 Bunch Shape Monitors (BSMs) [6]. The beam current is measured by 6 Beam Current Monitors (toroids), and radiation is reported by 28 ionization chambers.

TOOLKIT

Beam measurements were taken with dedicated High-Level Applications (HLAs). A Cavity Phasing HLA records readings of all BPMs while changing the phase of a cavity, typically with RF off in the downstream cavities ("cavity phase scan"). The Orbit Response Matrix (ORM) is recorded with a set of HLAs described in Ref. [7]. Quadrupole Scan HLA measures WS profiles while changing the current of a quadrupole [5].

The optics model is realized with the TraceWin code [8]. It spans 65 m from the exit of DTL to the beginning of the 400 MeV transport line. The quadrupoles are implemented as hard-edge elements, and the trims are represented by zero-length kicks. The Buncher, Vernier, and 28 SCL Sections are generated with the TraceWin NCELL command. The beam distribution at the beginning of the model is 6D Gaussian. Note that because of the available accuracy of the measurements, comparison between simulations and measurements is restricted to rms values. Therefore, the initial conditions are characterized by the rms emittance and two Twiss parameters in each plane.

Apart from the initial conditions, the simulated beam envelope is determined by the fields in the magnets and cavities. For accurate assignment of the field values, one needs a correct relationship (calibration) between settable parameters (e.g. quadrupole current) and the relevant field figure (e.g. quadrupole gradient integral). Such calibrations are established by comparing in simulations and measurements the changes in perturbed (differential) trajectories.

Content from this work may be used under the terms of the CC BY 4.0 licence (© 2026). Any distribution of this work must maintain attribution to the author(s), title of the work, publisher, and DOI.

ISBN: 978-3-95450-275-2 ISSN: 2226-0366 doi: 10.18429/JACoW-LINAC2026-MOPO047

THEORETICAL AND EXPERIMENTAL STUDY OF RESONANT FREQUENCY SHIFTING FOR VARIOUS SPARK-GAP DISTANCES IN AN ACTIVE MICROWAVE PULSE COMPRESSOR

T. H. Kim†, H. J. Lim, U. Namkoong
National Security Research Institute, Daejeon, Republic of Korea

Abstract

This paper investigates the effects of spark-gap distance on the resonant characteristics of an active Microwave Pulse Compressor (MPC). An equivalent-circuit model was developed by representing the upper electrode of the spark-gap switch as a variable height cylindrical post and corresponding shunt reactance. The model predicts changes in the optimum side arm length at a fixed operating frequency and shifts in the resonant frequency when the side arm length is fixed. These predictions were compared with full-wave electromagnetic (EM) simulations and further supported by measurements using a WR-650 waveguide prototype. The measured optimum side arm lengths for the 60 mm gap and reference configuration showed a trend consistent with the equivalent-circuit model and EM simulations.

INTRODUCTION

Microwave Pulse Compressors (MPCs) have been employed to generate peak RF power in various applications, including linear accelerators and high-level electromagnetic susceptibility testing [1-3]. In addition to conventional passive compressors, active MPCs utilizing plasma-based switches have been researched for application in linear accelerators [4]. Active MPCs release the stored energy by triggering a spark-gap switch that rapidly changes the state of MPC; thus, the structural design of the switch and cavity resonator determines the overall performance. While transmission line-based equivalent models have been used to design the resonance and coupling conditions of active MPCs [5, 6], and analyses on switching characteristics during plasma discharge have been performed [7], the effect of the switch gap distance in the energy-stored state (switch-off) on the resonance characteristics has not been sufficiently addressed in existing equivalent-circuit models. Although reducing the gap distance is advantageous for breakdown, it also increases the electromagnetic coupling between the switch and the resonator, consequently altering the design parameters.

In this study, an equivalent model was developed to analyse the resonance characteristics of active MPCs according to variations in the spark-gap distance during the energy-stored state. The resonance characteristics calculated using the equivalent-circuit were compared with full-wave EM simulations and further supported by experimental measurements using a WR-650 waveguide prototype.

† taekheon@nsr.re.kr

SPARK-GAP DISTANCE EFFECTS ON MPC PERFORMANCE

Equivalent-Circuit

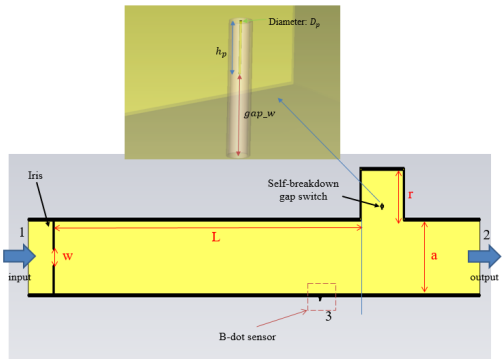


Figure 1: Active microwave pulse compressor and gap switch model.

The active MPC can be analysed using the transmission line equivalent-circuit models reported in [5, 6], which provide input impedance and the design relations for optimum gain, leakage and r, w, L. In the proposed model, the gap switch is modelled as a thin upper electrode inserted into a dielectric tube, as shown in Fig. 1. In this context, w is the iris width, r is the side arm length, L is the cavity length, h_p is the upper electrode length in the spark-gap switch, gap_w is the distance between the upper electrode tip and the bottom electrode, and D_p is diameter of the upper electrode.

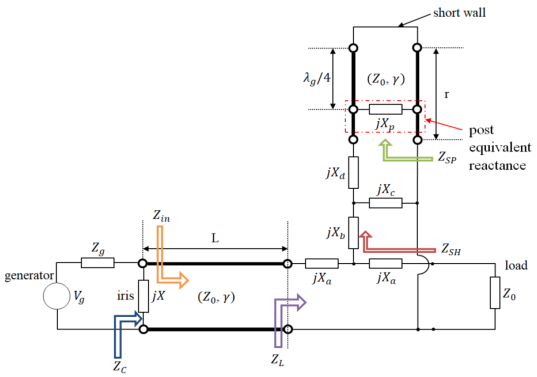


Figure 2: The equivalent-circuit of MPC with variable spark-gap distance.

Under the switch-off state, the upper electrode is approximated as a variable-height cylindrical post in the equivalent-circuit model [8]. The dielectric tube, which is not explicitly represented in the simplified model, is included in

Content from this work may be used under the terms of the CC BY 4.0 licence (© 2026). Any distribution of this work must maintain attribution to the author(s), title of the work, publisher, and DOI.

ISBN: 978-3-95450-275-2 ISSN: 2226-0366 doi: 10.18429/JACoW-LINAC2026-MOPO048

A NEW METHOD TO CHARACTERIZE SINGLE-CAVITY RF PULSE COMPRESSORS BASED ON REFLECTION MEASUREMENTS

P. Martinez-Reviriego*, P. Alonso-Arias, A. Grudiev, P. Wang
CERN, Geneva, Switzerland

Abstract

Pulsed high-power Radio Frequency (RF) systems frequently employ pulse compressors to augment peak output power, thereby reducing the required number of RF sources and enhancing cost-efficiency. A prominent class of these devices utilizes single resonant cavities supporting two degenerate modes to achieve high performance within a compact footprint. However, the inherent coupling of these modes complicates experimental characterization, a challenge exacerbated by the fact that these units are typically non-dismountable.

This work proposes a novel analytical method to disentangle the complex electromagnetic data encoded within these systems. By separately extracting the parameters of the individual degenerate modes and the characteristics of the associated waveguide network, the method provides a granular view of device performance. This approach enables a more comprehensive interpretation of measurement data, offering a pathway for the precise tuning and optimization of monolithic RF pulse compression systems.

INTRODUCTION

High-power GHz-range radio-frequency (RF) normal-conducting devices typically operate with short RF pulses (on the order of ~100 ns) and extremely high peak powers (up to ~100 MW). To reduce the number and cost of the RF power sources (i.e. klystrons), pulse compression techniques are employed. For this purpose, high-Q resonant cavities can be used to store energy and subsequently release it in a shorter time interval, thereby increasing the output peak power.

Three different cavities were designed, fabricated and tested at CERN as the prototypes for the pulse compression system of the klystron-based CLIC main linac [1]. A BOC-type was conceived for the storage cavity while two alternative approaches, based on spherical and bowl geometries, were investigated for the correction chain. Following fabrication, low-power measurement campaigns were carried out to study the RF performance and verify the design. However, disagreements between design and measurements induced questions about the performance of these cavities.

Single-cavity pulse compressors are challenging to diagnose due to the coexistence of degenerate modes and the inability to characterize them individually. This work proposes a method to characterize and disentangle the information concealed in these complex systems by using the full set of measurements. More details can be found in [2].

MATHEMATICAL MODEL

A schematic representation of a general pulse compressor system can be seen in Fig. 1.

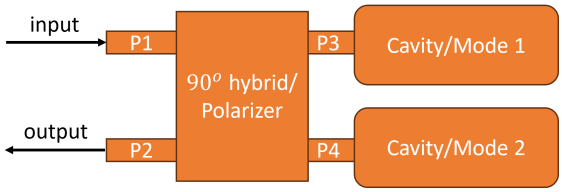


Figure 1: Schematic view of a general pulse compressor system.

A mathematical model describing the dependence of the full system on the parameters of each element (including the cavities/modes and the waveguide system) will be developed to extract information from the set of measurements of the entire system.

The reflection coefficient of a resonant cavity is given by [3],

$$\Gamma = \frac{(1/Q_{ext} - 1/Q_0) - i\xi}{(1/Q_{ext} + 1/Q_0) + i\xi}, \tag{1}$$

where $i = \sqrt{-1}$, Q_0 is the unloaded quality factor, Q_{ext} the external quality factor and $\xi = f/f_0 - f_0/f$ with f_0 and f being the resonant and measured frequency, respectively.

The full system can be characterized by a 2×2 matrix [4],

$$M_{PC} = \begin{pmatrix} s_{11}^{PC} & s_{21}^{PC} \\ s_{21}^{PC} & s_{22}^{PC} \end{pmatrix}, \tag{2}$$

which depends on two reflection coefficients, one for each cavity/mode, following Eq. (1) and a 4×4 matrix that models the waveguide network. The waveguide matrix can be generalized using the following form,

$$M_{wg} = \begin{pmatrix} s_{11} & s_{21} & s_{31} & s_{41} \\ s_{21} & s_{22} & s_{41} & s_{31} \\ s_{31} & s_{41} & s_{33} & s_{43} \\ s_{41} & s_{31} & s_{43} & s_{44} \end{pmatrix}, \tag{3}$$

where we assumed $s_{32} = s_{41}$ and $s_{42} = s_{31}$, leading to a pulse compressor system defined as [5],

$$s_{11}^{PC} = s_{11} + \frac{s_{41}^2(1/\Gamma_1 - s_{33}) + s_{31}^2(1/\Gamma_2 - s_{44}) + 2s_{41}s_{31}s_{43}}{(1/\Gamma_2 - s_{44})(1/\Gamma_1 - s_{33}) - s_{43}^2}, \tag{4}$$

$$s_{22}^{PC} = s_{22} + \frac{s_{31}^2(1/\Gamma_1 - s_{33}) + s_{41}^2(1/\Gamma_2 - s_{44}) + 2s_{41}s_{31}s_{43}}{(1/\Gamma_2 - s_{44})(1/\Gamma_1 - s_{33}) - s_{43}^2}. \tag{5}$$

* pablo.martinez.reviriego@cern.ch

Content from this work may be used under the terms of the CC BY 4.0 licence (© 2026). Any distribution of this work must maintain attribution to the author(s), title of the work, publisher, and DOI.

ISBN: 978-3-95450-275-2 ISSN: 2226-0366 doi: 10.18429/JACoW-LINAC2026-MOPO049

RF DESIGN OF THE COMPACT RF POWER COUPLER FOR FCC-ee INJECTOR LINACS

P. Martinez-Reviriego*[1], P. Craievich[2], A. Grudiev[1], A. Kurtulus[1], J.-Y. Raguin[2], R. Zennaro[2]
[1]CERN, Geneva, Switzerland
[2]PSI, Villigen, Switzerland

Abstract

The high-energy linac of the Future Circular Collider electron–positron (FCC-ee) injector requires high-performance RF accelerating structures to efficiently reach 20 GeV with stable operation. A tapered travelling-wave structure operating at 3 GHz has been designed to optimize accelerating performance and suppress wakefields.
This work focuses on the development of a full 3D model of the accelerating structure, including the RF power couplers, to ensure efficient power transfer and reliable high-power operation. Several coupling strategies were investigated to achieve a compact design while minimizing higher-order multipole components in regions lacking axial symmetry.

INTRODUCTION

The Future Circular Collider (FCC-ee) is a proposal for a high-luminosity e^-e^+ collider for high-precision studies of the electroweak sector. A key element of the system is the high-energy linac, which accelerates e^- and e^+ beams from 2.86 to 20 GeV before injection into the booster. The specifications for this linac consist of 4 bunches per RF pulse at a 100 Hz repetition rate, up to a 5 nC bunch charge, and a nominal 25 ns bunch spacing. Based on the RF technology developed for the SwissFEL [1], 3 m-long tapered travelling-wave structures were designed following the requirements given by wakefields and RF performance based on pulse compression at 3 GHz [2].

The optimization performed so far was done for the geometry of the regular cells, assuming 2D axial symmetry throughout the system. This study presents the next step in the 3D optimization process by adding the input and output couplers to the regular cell geometries, following the methodology presented in [3, 4]. Several coupler geometries based on electrical coupling were studied to create a design as compact as possible while ensuring that the transverse kicks, primarily dipole and quadrupole, induced by the couplers do not perturb the stability of the beam dynamics.

DOUBLE-FEED RF COUPLER

RF Design

Once the regular cell geometry is fixed, the RF coupler design can proceed using CST MS [5]. Travelling-wave structures require input and output power couplers, which, due to the structure's tapered geometry, will have different geometries. First, the RF design must be done independently for both couplers, assuming constant-impedance structures using the parameters of the first and last cell for the input and output coupler, respectively. In the following step, the full tapered configuration is studied to fine-tune the geometry of the couplers for the final performance.

For this study, we will focus on the design of the input coupler since the output coupler design can be done analogously. Thus, we study a constant-impedance structure with regular cells as the input cell of the full structure and symmetric input and output couplers. Then, two identical matching cells connecting the first and last regular cells to the waveguides are added to optimize the geometry. Figure 1 shows the magnitude of the electric field on a log scale in an optimized structure with double-feed couplers and 3 regular cells, along with the geometric parameters of the waveguide and the matching cells.

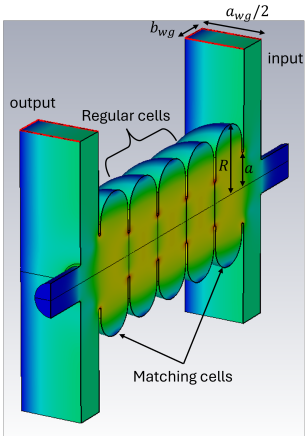


Figure 1: Magnitude of the electric field in an optimized structure with double-feed couplers.

Then, after fixing the parameters of the waveguide, the power transmission can be optimized by scanning the values of a and R of the matching cell to minimize reflection and maximize field flatness. Results for the optimum geometry can be found in Fig. 2.

Multipolar Analysis

The introduction of the RF couplers breaks the previously existing axial symmetry of the structure. Therefore, the longitudinal electric field must be represented as a multipolar expansion [6],

$$E_{acc}(r,\phi,z) = E_z(r,\phi,z)e^{j\omega z/c} = \sum_{n=0}^{\infty} E_n(z) r^n \cos(n\phi), \quad (1)$$

* pablo.martinez.reviriego@cern.ch

Content from this work may be used under the terms of the CC BY 4.0 licence (© 2026). Any distribution of this work must maintain attribution to the author(s), title of the work, publisher, and DOI.

ISBN: 978-3-95450-275-2 ISSN: 2226-0366 doi: 10.18429/JACoW-LINAC2026-MOPO050

THE PLASMA PROCESSING DEVELOPMENT IN CSNS-II*

Cong Zhang†,1,2, Huachang Liu1,2, Rui Ge1, Wenzhong Zhou1,2, Ahong Li1,2, Qiang Chen1,2, Bo Li1,2, Xiaolei Wu1,2, Mengxu Fan1,2, Peihua Qu1,2, Qiyu Kong1,2
[1]Institute of High Energy Physics, Beijing, China
[2]Spallation Neutron Source Science Center, Dongguan, China

Abstract

The 80-300 MeV accelerating section of the CSNS-II linac is a superconducting accelerator, consisting of 10 double spoke modules and 8 elliptical cavity modules. For a user facility, the downtime associated with removing the module from the linac and returning it to the cleanroom for rinsing and reconditioning is unacceptable. Therefore, it is necessary to develop on-line performance recovery techniques for superconducting cavities to eliminate field emission and restore the operating gradient within a short time. On-line plasma cleaning has been proven to be a safe and effective technique for mitigating field emission in superconducting cavities. This report presents the development of plasma cleaning technology at CSNS-II, including the construction of the plasma cleaning platform, the implementation of plasma cleaning experiments, low-temperature CH_4 adsorption tests on a 2-cell elliptical cavity, and plasma cleaning of it.

INTRODUCTION

The Phase-II superconducting linear accelerator of the China Spallation Neutron Source (CSNS-II) integrates 10 double-spoke cryomodules and 8 elliptical cavity cryomodules, accommodating a total of 44 superconducting cavities [1]. For modern superconducting accelerators, field emission stands as the dominant driver of operational performance degradation in superconducting cavities. As a dedicated user facility, CSNS-II cannot afford to disassemble and clean superconducting cavities for performance restoration without severely disrupting scheduled user experiments. Accordingly, research on in-situ plasma cleaning techniques has been conducted to mitigate performance degradation induced by field emission [2, 3].

PLASMA PROCESSING DEVELOPMENT AT CSNS-II

Plasma Processing Experiment Setup and Initial Ignition Experiments

Figure 1 illustrates the gas system layout for the CSNS-II plasma processing platform. Initial plasma ignition tests were carried out on a 648 MHz single-spoke cavity to verify applicability to both cavity types deployed in CSNS-II. The process gas was a 90% He/Ne–10% O_2 mixture: noble gas components drive physical sputtering of surface contaminants, while O_2 reacts with hydrocarbon contaminants to form volatile species readily removed by vacuum pumping. Required ignition power and peak cavity electric field are specified in Ref. [4].

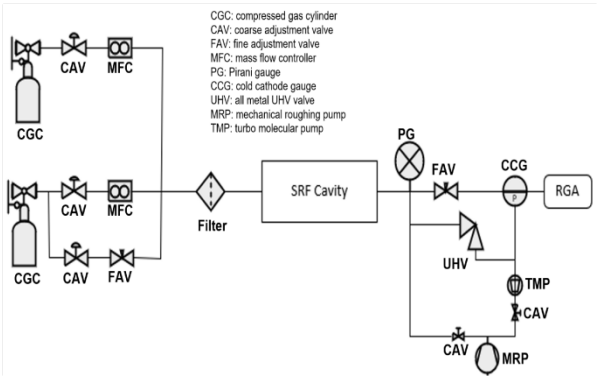


Figure 1: Schematic of gas system of plasma processing.

Plasma Coupler Breakdown Suppression

Plasma breakdown on the coupler was observed for the noble gas (helium, neon, argon) once the applied RF power exceeded a critical threshold, with a markedly higher propensity for this phenomenon at higher gas pressure[4].

Once the plasma ignites on the coupler, there is a significant risk of copper sputtering from the antenna probe or fracture of the ceramic window due to the plasma impact. To suppress plasma ignition on the coupler, a negative DC bias was applied to the inner conductor. This approach effectively elevated the power threshold for plasma breakdown on the coupler. (see Fig. 2) [5].

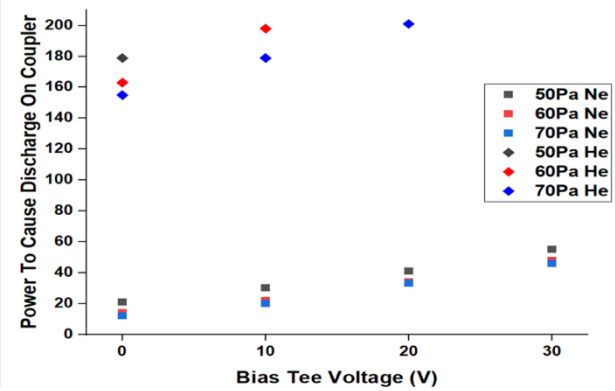


Figure 2: Negative bias tee voltage functions on improving the threshold power to trigger coupler breakdown.

* Work supported by Guangdong Basic and Applied Basic Research Foundation (Grant No.2022B1515120027) and Doctoral and Master's Joint Training Program of Songshan Lake High-Tech Industrial Development Zone, Dongguan（Grant No.DG2531351N）
† zhangcong@ihep.ac.cn

Content from this work may be used under the terms of the CC BY 4.0 licence (© 2026). Any distribution of this work must maintain attribution to the author(s), title of the work, publisher, and DOI.

ISBN: 978-3-95450-275-2 ISSN: 2226-0366 doi: 10.18429/JACoW-LINAC2026-MOPO051

BEAM DYNAMICS MATCHING DESIGN FOR THE INJECTION LINE OF A 150 MeV SEPARATED-SECTOR CYCLOTRON*

Jing Fang, Shizhong An, Luyu Ji, Jinrong Lu, Cong Wu
China Institute of Atomic Energy, Beijing, China

Content from this work may be used under the terms of the CC BY 4.0 licence (© 2026). Any distribution of this work must maintain attribution to the author(s), title of the work, publisher, and DOI.

Abstract

A beam-dynamics matching design is developed for the 11.07 m injection line of a 150 MeV separated-sector cyclotron using an Opera-3D and OPAL workflow. The adopted scheme combines two 50.85 MHz bunchers upstream of an opposite-bend vertical Z-dogleg, a conventional upstream matching channel, and independently powered inter-bend triplets. At the design beam current of 7.77 mA, two otherwise identical full-bunch OPAL simulations including space charge are compared to evaluate the effect of the bunchers. With both bunchers switched off, the output rms bunch length is 76.27 mm and the rms momentum spread is 0.718%. Operating F1 and F2 reduces these values to 24.83 mm and 0.194%, respectively. The corresponding rms output spot changes from 7.438 × 12.810 mm to 9.514 × 5.803 mm, indicating a transverse redistribution accompanying the longitudinal compression, while the transmission efficiency remains 99.99%. These results demonstrate that buncher-induced longitudinal matching must be evaluated together with space-charge effects and transverse envelope matching at the design current.

INTRODUCTION

High-energy, high-current proton beams are widely used to produce medical isotopes that are not readily accessible with low-energy accelerators, including ^{82}Sr, ^{68}Ge, ^{67}Cu, ^{88}Y, ^{173}Lu, and ^{85}Sr [1, 2]. The High Intensity Proton Accelerator facility at the Paul Scherrer Institute (PSI) employs a 590 MeV ring cyclotron and operates at a beam current of up to 2.2 mA, corresponding to a beam power of 1.3-1.4 MW [3]. The proton beam is used primarily to drive a spallation neutron source and to produce pion and muon beams.

The China Institute of Atomic Energy is developing an integrated research facility based on a high-current H_2^+ separated-sector cyclotron. The facility is intended to serve as a high-power continuous-wave neutron source with a high duty factor and favourable cost-effectiveness. To mitigate space-charge effects during injection and acceleration, the scheme employs H_2^+ acceleration, an RFQ injector, and electrostatic-deflector extraction. The design goal is to deliver an extracted beam with an equivalent proton energy of at least 150 MeV and a current of at least 10 mA, corresponding to a beam power of approximately 1.5-2 MW.

This work develops an 11.07 m, 2 MeV injection line from the RFQ exit to the cyclotron entrance. Rather than treating it as a single-particle transfer channel, the adopted scheme separates the matching tasks: two upstream fundamental-frequency bunchers control longitudinal phase-space rotation, a conventional quadrupole channel sets the entrance Twiss parameters without forcing an excessively small intermediate waist, and two independently powered quadrupole groups inside an opposite-bend vertical Z-dogleg regulate the transverse envelopes and vertical-dispersion closure. Opera-3D buncher fields are imported into 3-D OPAL full-bunch tracking [4, 5] with space charge, allowing longitudinal compression and transverse transport to be assessed in one consistent model.

LATTICE AND FIELD MODEL

Figure 1 shows the complete lattice on the reference trajectory. The 7.50 m upstream section follows T1-F1-D1-F2-T4: T1 and T4 are quadrupole triplets, D1 is a doublet, and F1/F2 are independent 50.85 MHz bunchers. These groups provide local matching freedom around both RF elements and establish moderate beam slopes at the dogleg entrance. B1P (the first bend magnet) then bends the beam vertically by +45 degrees and generates vertical dispersion. A1 and A2 are independently powered triplets in the 3.00 m inter-bend section; their six gradients are not constrained to equal-strength mirror pairs, so the betatron match and dispersion closure can be adjusted together. B2P (the second bend magnet) supplies the opposite -45-degree bend and restores an output axis parallel to the incident axis. The principal design parameters are summarized in Table 1.

Table 1: Principal Design Parameters

Parameter	Value
Transported ion	H_2^+
Beam current	7.77 mA
Kinetic energy	2.00 MeV
Transmission efficiency	99.99%
Total reference-path length	11.07 m
Output rms spot, x / y	9.51 / 5.80 mm

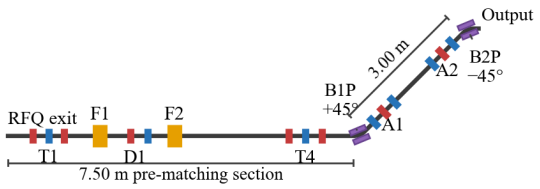


Figure 1: Complete injection-line layout. T1, D1 and T4 are the upstream triplet, doublet and final pre-bend triplet; F1/F2 are the bunchers; A1/A2 are the inter-bend triplets; B1P/B2P are the opposite 45-degree vertical dipoles.

* Work supported by the National Natural Science Foundation of China (Grant No. 12375156).

ISBN: 978-3-95450-275-2 ISSN: 2226-0366 doi: 10.18429/JACoW-LINAC2026-MOPO053

BUNCH SHAPE MONITOR RESOLUTION STUDIES IN THE FERMILAB LINAC TRANSITION SECTION *

R. Sharankova†, J. P. Carneiro, E. Chen, A. Shemyakin
Fermi National Accelerator Laboratory, Batavia, IL, USA

Abstract

The Fermilab Linac delivers 400 MeV H⁻ beam to the Booster rapid cycling synchrotron. Longitudinal dynamics in the Linac affects the beam losses in the Linac itself as well as at the Booster. To understand better the longitudinal beam properties, two bunch shape monitors (BSM) in the Linac transition section where RF frequency changes from 201 MHz to 805 MHz, were recently brought back to operation. A technique was developed to estimate the resolution of the BSMs directly from measurements by scanning the focusing/deflecting DC voltage of the deflecting plates and RF deflector phase. The estimations made for the Linac BSMs are correlated with known mechanical BSM details. The effect of finite resolution on the bunch length measurements is discussed.

THE LINAC AND TRANSITION SECTION

The Fermilab Linac consists of a drift-tube Linac (DTL) and a side-coupled Linac (SCL) separated by a transition section [1]. The DTL comprises five Alvarez RF cavities (tanks) operating at 201.49 MHz, accelerating the H⁻ beam to a design energy of 116.5 MeV. The SCL operates at 805 MHz across seven RF cavities (modules), further accelerating the beam to a final design energy of 401.5 MeV for injection into the Booster rapid cycling synchrotron. The transition section (Fig. 1), located between the DTL and SCL, matches the beam transversely and longitudinally. Longitudinal matching is accomplished using two bunching cavities called the Buncher and the Vernier. The transition section is well instrumented with beam diagnostics including two Bunch Shape Monitors (BSMs).

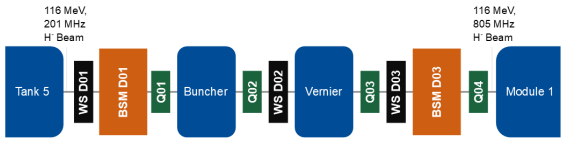


Figure 1: Schematic of the Transition section. RF cavities in blue, quadrupoles in green, wire scanners in black and BSM in orange.

The longitudinal Twiss parameters can be reconstructed by measuring the effect of Buncher RF focusing strength on the bunch length, analogous to a quadrupole scan for transverse Twiss reconstruction [2]. The reliability of this reconstruction depends critically on the correct understanding of the measurement resolution of the BSM, which is be discussed below.

BUNCH SHAPE MONITORS

The BSM [3] measures the longitudinal profile of the H⁻ bunch through the process illustrated schematically in Fig. 2 (left). A 0.1 mm thick tungsten wire held at a -10 kV potential with respect to ground is placed in the middle of the beampipe. H⁻ ions striking the wire produce secondary electrons, which are accelerated by the wire potential toward a primary slit. The electrons then enter a RF deflector cavity which also has two electrostatic deflector plates under negative high voltages $U1$ and $U2$. After the deflector cavity, the electrons drift to an exit aperture of size d and are detected by an electron multiplier tube (EMT).

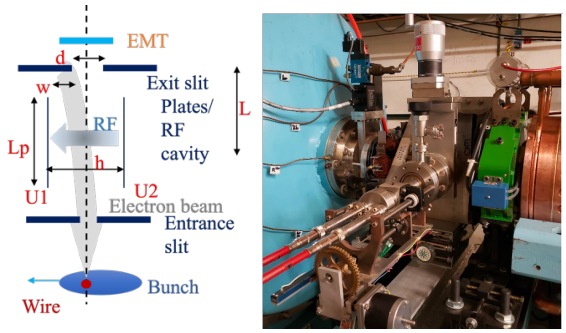


Figure 2: Left: Schematic of the BSM deflection system defining the geometric parameters L, Lp, h, d, and the plate voltages $U1$, $U2$. Right: Photograph of D01 following reinstallation in the Fermilab Linac transition section.

Position of the beam center at the exit slit is given by:

$$x = x_0 + a_{DC} + a_{RF}\cos(\omega t + \varphi_{RF}), \qquad (1)$$

where x_0 is the mechanical misalignment of the system, a_{RF} is the amplitude of the deflection by RF proportional to the BSM RF power P_{RF}, ω is the RF angular frequency, φ_{RF} is RF phase assuming that the secondary electrons produced by the H− bunch center reach the BSM RF field at $t = 0$, and a_{DC} is the shift created by potential difference between the BSM plates

$$a_{DC} = \frac{e(U_1 - U_2)}{W} \cdot \frac{L_p}{2h} L \equiv k_{DC}\Delta U \qquad (2)$$

where e is the electron charge, W is the electron kinetic energy at the plates, L_p is the deflector plate length, h is the gap between the plates, and L is the distance from the midpoint of the plates to the exit slit.

The RF sweep projects the H⁻ bunch longitudinal distribution (integrated over the wire) $j_{H^-}(\varphi)$ to the transverse spread of the secondary electrons over the surface of the exit slit. If the electron beam is DC-centered ($x_0 + a_{DC} = 0$), the electron beam is point-like, there are no chromatic

* This manuscript has been authored by Fermi Forward Discovery Group, LLC under Contract No. 89243024CSC000002 with the U.S. Department of Energy, Office of Science, Office of High Energy Physics.
† rshara01@fnal.gov

Content from this work may be used under the terms of the CC BY 4.0 licence (© 2026). Any distribution of this work must maintain attribution to the author(s), title of the work, publisher, and DOI.

ISBN: 978-3-95450-275-2 ISSN: 2226-0366 doi: 10.18429/JACoW-LINAC2026-MOPO055

A PHYSICS-MOTIVATED SURROGATE FRAMEWORK FOR BEAM TRANSPORT OPTIMIZATION IN LINEAR ACCELERATORS

H. Sargsyan[†,1,2], B. Grigoryan[1], G. Amatuni[1,2], A. Vardanyan[1], A. Grigoryan[1,2]
[1]CANDLE Synchrotron Research Institute, Yerevan, Armenia
[2]Yerevan State University, Yerevan, Armenia

Abstract

Optimization of beam transport in linear accelerators often requires computationally expensive high-fidelity particle-tracking simulations. This work develops a physics-motivated surrogate framework intended to reduce this cost while retaining high-fidelity simulation for verification. The framework is evaluated on the Advanced Research Electron Accelerator Laboratory (AREAL) electron linear accelerator with a laser-driven radio-frequency gun at CANDLE Synchrotron Research Institute, Yerevan, Armenia. AREAL operates up to 5 MeV and supports bunch charges of 30–800 pC; the present study considers 150 pC, where space-charge effects strongly influence beam evolution. A transport-completion classifier trained on 9,975 A Space Charge Tracking Algorithm (ASTRA) simulations rejected all failed-transport cases on an independent test set while retaining 94.7% of complete cases. Direct regression from machine settings was then evaluated as a baseline using 8,855 complete simulations, predicting 12 beam properties at 13 longitudinal positions. Accuracy depended strongly on both property and position. A controlled state-history comparison, with the regression algorithm fixed, showed that the best representation—combining the previous beam state with its recent change—reduced mean absolute errors by factors of 2.6–19.2 relative to direct regression. The results show that surrogate performance depends not only on model selection but also on beam-state representation, motivating sequential state-propagation models for future accelerator optimization.

INTRODUCTION

Optimization of beam transport in linear accelerators can require many high-fidelity particle-tracking simulations and therefore become computationally expensive when large machine-setting spaces are explored. Surrogate models can reduce this cost by approximating the relation between machine settings and beam properties while retaining high-fidelity simulations for verification. Such approaches have been investigated for accelerator optimization and tuning [1, 2]. Optimization frameworks such as GIOTTO [3] can require many repeated beam-dynamics simulations, further motivating methods that reduce the number of high-fidelity evaluations.

For prediction at multiple longitudinal positions, a natural baseline is to infer beam properties directly from the machine settings. However, beam evolution is sequential: acceleration, focusing, and space-charge effects act throughout the lattice, while the machine settings alone do not explicitly provide the regression model with the beam condition developed at intermediate locations. The central question of this work is whether including upstream beam-state information improves prediction at later positions. This is investigated on the AREAL electron linear accelerator by comparing direct regression with state-history representations while keeping the regression algorithm fixed.

SIMULATION SETUP AND DATASET

AREAL Linear Accelerator and Simulation Setup

The AREAL electron linear accelerator at CANDLE Synchrotron Research Institute is based on a laser-driven radio-frequency (RF) photogun and includes magnetic focusing and diagnostic elements [4–7]. A schematic of the accelerator is shown in Fig. 1. Beam transport was simulated with A Space Charge Tracking Algorithm (ASTRA) [8], with space charge enabled throughout the simulations. Four machine settings were varied: maximum on-axis RF field, RF phase, solenoid field, and quadrupole gradient. Their ranges are given in Table 1. Other components shown in Fig. 1 were not independently varied in the surrogate input space.

Each simulation used a 150 pC electron bunch with Gaussian transverse distributions of $\sigma_x = \sigma_y = 1$ mm and a Gaussian emission-time distribution $\sigma_t = 0.19$ ps. A macroparticle convergence study covering 250–20,000 particles against a 100,000-particle reference was performed, and 8,000 macroparticles were selected as a compromise between numerical stability and computational cost.

Table 1: Varied Machine Settings

Machine setting	Range
Maximum on-axis RF field, E_0	$25 - 100$ MV/m
RF phase, ϕ	$165 - 290°$
Solenoid field, B_{sol}	$0.06 - 0.27$ T
Quadrupole gradient, G_{quad}	$0 - 1.28$ T/m

† sargsyan@asls.candle.am

Content from this work may be used under the terms of the CC BY 4.0 licence (© 2026). Any distribution of this work must maintain attribution to the author(s), title of the work, publisher, and DOI.

ISBN: 978-3-95450-275-2 ISSN: 2226-0366 doi: 10.18429/JACoW-LINAC2026-MOPO056

UPGRADE OF THE CAVITY PHASE MONITOR SYSTEM FOR MULTI-CAVITY MEASUREMENTS AT J-PARC LINAC

E. Cicek*, Z. Fang, Y. Fukui, K. Futatsukawa, S. Mizobata
High Energy Accelerator Research Organization, Tsukuba, Japan
H. Nakano, Japan Proton Accelerator Research Complex, Tōkai Mura, Japan
Y. Sato, NAT Corporation, Hitachinaka, Japan
O. E. Delialioglu, The Graduate University for Advanced Studies, SOKENDAI, Hayama, Japan

Abstract

At J-PARC LINAC, cavity phase monitors (CPMs) monitor RF phase variation between neighboring cavities; existing system remains reliable but requires dedicated hardware per station and supports only two RF inputs per monitor. As LLRF DFB system has been upgraded from cPCI to MicroTCA.4, RF pickup signals are aggregated in a common rack, requiring CPM upgrade to multi-channel monitoring; as an initial step, we developed a MicroTCA.4-based CPM at MEBT1 with vector-sum capability. System acquires eight RF inputs from RFQ, Buncher 1/2 and Chopper 1/2; 324-MHz pickup signals are down-converted to 12 MHz on μRTM, digitized at 240 MHz, and converted to I/Q yielding amplitude/phase. Vector sums are formed for RFQ, Buncher 1/2, while Chopper 1/2 are single-channel; all phases referenced to RFQ. Existing LLRF firmware and EPICS IOC framework were adapted with modifications; new sequencer logic and GUI were developed. System is installed in the LLRF MicroTCA.4 environment, synchronized via shared ADC/FPGA clocks under temperature- and humidity-controlled conditions. Initial results demonstrate simultaneous multi-cavity monitoring with improved integration over the conventional distributed CPM.

INTRODUCTION

The linear accelerator (LINAC) of the Japan Proton Accelerator Research Complex (J-PARC) accelerates a 50-mA negative-hydrogen (H^-) beam to 400 MeV for injection into the 3-GeV rapid-cycling synchrotron (RCS), using a radio-frequency quadrupole (RFQ), a drift-tube linac (DTL), a separated-type DTL (SDTL) and an annular-ring coupled structure (ACS) linac, with medium-energy beam transport lines at 3 MeV (MEBT1) and 191 MeV (MEBT2). MEBT1 houses two buncher cavities (Buncher 1/2, henceforth BUN1 and BUN2) and two RF chopper cavities (Chopper 1/2, henceforth CHOP1 and CHOP2), as shown in Fig. 1 [1–3]. Cavities up to the SDTL are driven at 324 MHz and the ACS at 972 MHz.

Stable injection into the RCS requires the accelerating field to be held within $\Delta A/A < \pm 1$ % peak-to-peak (pp) in amplitude and $\Delta\theta < \pm 1$ deg (pp) in phase. The low-level RF (LLRF) system with digital feedback and feedforward (DFB&FF) provides this short-term stabilization at each station [4], while the long-term phase variation between

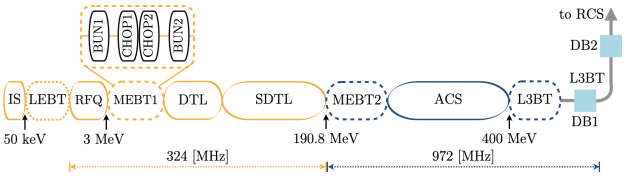


Figure 1: J-PARC LINAC layout; the monitored MEBT1 cavities are shown in the inset.

cavities is followed by cavity phase monitors (henceforth "CPM"), installed in the 19-inch LLRF racks to measure the phase difference of two neighboring cavities [5]. The phase stability between neighboring cavities was demonstrated with beam [5], and the resulting point data are used by a real-time system that compensates for long-term drift at 324 and 972 MHz.

Table 1: Comparison of the Conventional CPM and the Upgraded MEDS-CPM

Parameter	Conventional	MEDS-CPM
Platform	19-inch rack	μTCA.4 shelf
Technique	Down-conv. + IF	Down-conv. + IF
RF inputs	2	8
Frequency	324 / 972 MHz[a]	324 MHz
ADC	14 bit, 48 MS/s	16 bit, 240 MS/s
Vector sum	No	Yes

[a] Three variants; the two frequencies use separate units.

Although the conventional CPM system has proven reliable, the LLRF DFB&FF system is being updated to a Micro Telecommunications Computing Architecture (μTCA.4) platform [4, 6, 7], in which the RF pickup signals are aggregated in a common rack, requiring the CPM to be upgraded to multi-channel monitoring. Multi-channel acquisition also allows the vector sum of the two pickups of a cavity, as in the DFB&FF system. Aligned with that development, a μTCA.4-based multi-channel CPM (MEDS-CPM) has been developed and installed at MEBT1C, the μTCA rack at MEBT1, as the first step towards replacing the conventional CPM system; Table 1 compares the two. This paper presents the hardware, the FPGA firmware modifications, the EPICS-IOC implementation and the first measurements under beam operation.

* ecicek@post.kek.jp

Content from this work may be used under the terms of the CC BY 4.0 licence (© 2026). Any distribution of this work must maintain attribution to the author(s), title of the work, publisher, and DOI.

ISBN: 978-3-95450-275-2 ISSN: 2226-0366 doi: 10.18429/JACoW-LINAC2026-MOPO057

FEASIBILITY STUDY OF A LASER-PLASMA INJECTOR FOR PLS-II STORAGE RING

Soyeon Kim[1], Moses Chung[2]
[1]Department of Physics, Ulsan National Institute of Science and Technology (UNIST), Ulsan, Republic of Korea
[2]Department of Physics and Division of Advanced Nuclear Engineering, Pohang University of Science and Technology (POSTECH), Pohang, Republic of Korea

Abstract

The linear accelerator of PLS-II in Pohang has been in operation for approximately 30 years, leading to performance degradation and stability issues. To address these challenges, this study proposes a laser-plasma accelerator (LPA)-based injector for the PLS-II storage ring. An active energy compression scheme, consisting of a magnetic chicane and an RF cavity, was employed to mitigate the intrinsic limitations of LPA electron beams, including large energy spread and energy jitter. The simulation results confirm that the compressed beam satisfies the injection requirements of the 3 GeV PLS-II storage ring. Furthermore, the proposed injector significantly reduces the accelerator footprint compared with the existing PLS-II linear accelerator, demonstrating the feasibility of a compact storage-ring injector based on an LPA.

INTRODUCTION

Active Energy Compression

Laser-plasma accelerators (LPAs) are promising compact alternatives to conventional RF accelerators because of their ultrahigh accelerating gradients. However, their relatively large energy spread, energy jitter, and beam divergence limit practical applications [1]. To improve the beam quality of LPA electron beams, an active energy compression scheme has recently been demonstrated. In this approach, a magnetic chicane first stretches the electron bunch and introduces an energy–position correlation (energy chirp), which is subsequently compensated by an RF cavity (see Fig. 1). This technique reduces both the energy spread and the energy jitter by more than one order of magnitude, enabling beam qualities compatible with the energy acceptance of modern synchrotron light sources [1, 2].

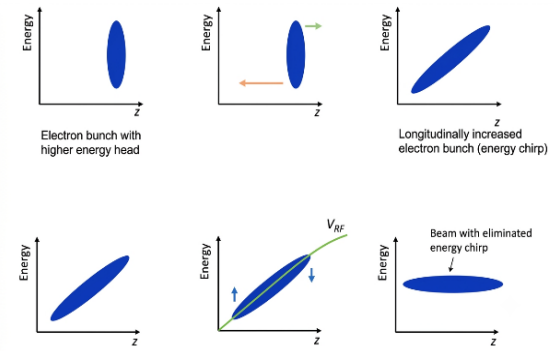


Figure 1: Schematic diagram of active energy compression.

PLS-II Linear Accelerator

The PLS-II linear accelerator consists of a thermionic DC gun, an S-band linac, and an 86-m beam transport line. The beam transport line comprises three isochronous systems, quadrupole magnets, and steering magnets that deliver the 3 GeV electron beam to the storage-ring injection system. The main parameters of the PLS-II linac are summarized in Table 1. The normalized horizontal and vertical emittances measured at the 100 MeV pre-injector are approximately 120 μm·rad, corresponding to a geometric emittance of about 20 nm·rad at 3 GeV [3].

Table 1: Major Parameters of the PLS-II Linear Accelerator

Parameter	Value
Beam energy	3 GeV
Energy jitter (rms)	<0.2%
Energy spread (rms)	<0.3%
Emittance (normalized, rms)	120 μm rad

PLS-II Storage Ring

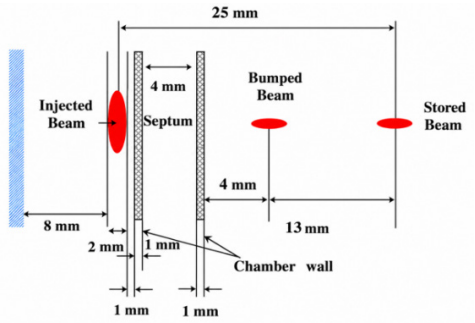


Figure 2: Horizontal space diagram of the PLS-II injection.

The PLS-II storage ring provides one 6.88-m-long and one 3.69-m-long straight section per cell. A horizontal dispersion of 0.25 m is introduced in the long straight section, where the RF cavities are installed, to reduce the beam emittance. The injection section employs four kicker magnets located in the 6.88-m-long straight section to generate a local orbit bump, as shown in Fig. 2. The injected beam is horizontally parallel to the bumped stored-beam orbit and enters the storage ring with a vertical angle of 8.234° at a horizontal offset of approximately −25 mm from the stored beam. A Lambertson magnet then bends the beam by −8.234° to place it on the same vertical level as the

Content from this work may be used under the terms of the CC BY 4.0 licence (© 2026). Any distribution of this work must maintain attribution to the author(s), title of the work, publisher, and DOI.

DESIGN STUDY OF A LARGE-APERTURE CAPACITIVE PICK-UP TYPE BUNCH SHAPE MONITOR FOR NONRELATIVISTIC ION BEAMS*

Changsun Na[1], Geunwoo Kim[1,] Donghyun Kwak[2], Moses Chung[†,1]
[1]Pohang University of Science and Technology, Pohang, Republic of Korea
[2]Korea Atomic Energy Research Institute, Jeongeup, Republic of Korea

Abstract

The longitudinal bunch shape is an important parameter for beam-dynamics studies and accelerator optimization, including the development of future beam diagnostics at the Rare Isotope Accelerator complex for ON-line experiments (RAON). A Capacitive Pick-Up type Bunch Shape Monitor (CPU-BSM) was previously developed for non-destructive measurements of non-relativistic ion beams. In this study, an enlarged aperture (from 30 to 60 mm) CPU-BSM structure was designed using CST Studio Suite. The aperture dependence of the curved pick-up-ring characteristic impedance, signal amplitude, and temporal response was evaluated, and preliminary matching-structure designs were compared in terms of S_{21}. A frequency-domain reconstruction procedure applied to the simulated large-aperture response reproduced the main input bunch profiles. Finally, we discuss the electronics and control system for the large-aperture CPU-BSM and its application to longitudinal phase-space tomography at RAON.

INTRODUCTION

Longitudinal bunch-shape measurements are important for understanding beam dynamics and verifying accelerator performance. At the Rare Isotope Accelerator complex for ON-line experiments (RAON), the Post-linac to Driver-linac Transport line (P2DT) connects SCL3 and SCL2 through a 180° transport section. In P2DT section, longitudinal diagnostics can support beam-matching studies [1].

Conventional bunch shape monitors and fast Faraday cups provide high-resolution measurements but intercept the beam [2-4]. The CPU-BSM was developed for non-destructive measurements of non-relativistic ion beams [5]. For low-β beams, longitudinal electric-field spreading broadens the induced response, requiring dedicated algorithms to reconstruct the original bunch distribution [5, 6].

This study, the CPU-BSM aperture was increased from 30 to 60 mm, and the curved pick-up-ring impedance, matching structure, signal response, and reconstruction performance were evaluated using CST Studio Suite [7].

LARGE-APERTURE CPU-BSM DESIGN

A bunched ion beam induces a time-dependent image-charge signal on the capacitive pick-up without interruption. For nonrelativistic beams, longitudinal electric-field spreading broadens this signal relative to the actual bunch-current distribution, requiring reconstruction.

* Work supported by National Grant No. RS-2022-00154676.
† moses@postech.ac.kr

Figure 1 shows the configuration and main components of the previously developed CPU-BSM.

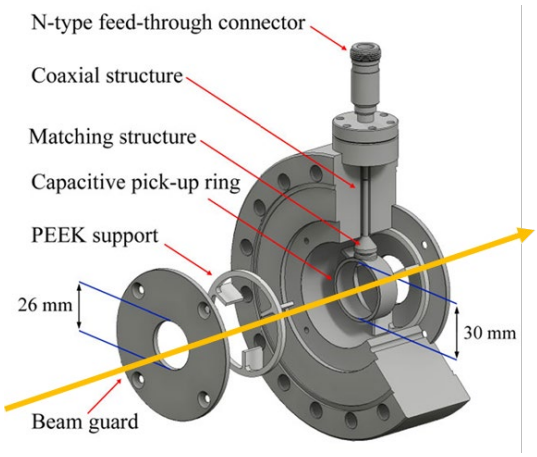


Figure 1: Configuration and main components of the previously developed CPU-BSM. The arrow indicates the beam direction. Adapted from Ref. [5].

A 30 mm reference model based on the previous CPU-BSM was constructed in CST Studio Suite. In practical beamline applications, a larger aperture may be required due to beam size, alignment tolerances, and installation constraints. Hence, in this study, the aperture was then increased to 60 mm, and the surrounding pick-up and matching structures were modified accordingly. Figure 2 compares the two models at the same scale.

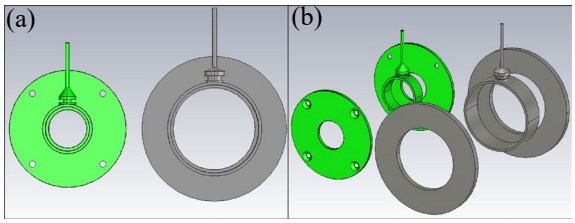


Figure 2: Comparison of the 30 mm reference (green) and 60 mm large-aperture CPU-BSM models: (a) front view and (b) exploded isometric view. Both models are shown at the same scale.

IMPEDANCE MATCHING AND SIGNAL RESPONSE

Impedance-Matching Strategy

The signal path was divided into the coaxial line, curved pick-up ring, and matching structure. Following the previous design [5], the coaxial section targeted 50 Ω and the pick-up-ring section approximately 100 Ω. The coaxial impedance was calculated from

ISBN: 978-3-95450-275-2 ISSN: 2226-0366 doi: 10.18429/JACoW-LINAC2026-MOPO059

DEVELOPMENT OF A ROBOTICS SYSTEM FOR SRF CAVITY ASSEMBLY IN A CLEANROOM AT KEK

Y. Abe*[1,2], H. Araki[1], S. Araki[1], A. Hattori[3], M. Hiraki[1,2], Y. Yamamoto[1,2]
[1]High Energy Accelerator Research Organization, KEK, Tsukuba, Japan
[2]The Graduate University for Advanced Studies, SOKENDAI, Hayama, Japan
[2]National Institute of Technology (KOSEN), Ibaraki College, Hitachinaka, Japan

Abstract

Contamination by particulate matter, such as dust, during the assembly of SRF cavities and their associated components can significantly degrade cavity performance through localized heating and field emission. Therefore, both particulate generation and intrusion must be minimized while maintaining a clean environment. Since human activity is a major source of particulate contamination in cleanrooms, robotic assembly is being developed at KEK to reduce human intervention in SRF cavity assembly. Following previous demonstrations of simple assembly motions using direct teaching, we built a simulated workcell in FANUC ROBOGUIDE, where robot motions can be developed and verified before transfer to the real cobot. A hybrid control framework has been established, combining reliable FANUC motion execution with a flexible KEK-developed control system that provides task-dependent functions, including vision-based position correction and control of cleaning and particle-monitoring devices. In addition, a tool changer and tool station were introduced to support task-specific end effectors. This paper presents the developed robotic system and ongoing developments toward its application to single-cell SRF cavity assembly.

INTRODUCTION

Superconducting radio-frequency (SRF) cavities are key components of modern high-performance accelerators because they can provide high accelerating gradients with low RF losses. Their performance, however, is highly sensitive to particulate contamination introduced during cavity preparation and assembly. Particles deposited on the inner surface can induce field emission under high surface electric fields, resulting in additional RF power loss and heating and, in severe cases, contributing to cavity quench [1]. Field emission is one of the major factors limiting SRF cavity performance. In the European XFEL cavity production, additional high-pressure rinsing reduced the occurrence of field emission between successive vertical tests, demonstrating the importance of particulate control in achieving reliable cavity performance [2]. Therefore, both the generation of particulates during assembly and their intrusion from the surrounding environment must be minimized.

Human activity is a major source of particulate contamination in cleanrooms. Reducing human intervention is therefore a promising approach to improving the cleanliness and reproducibility of SRF cavity assembly. At KEK, we are developing a robotic assembly system to perform cleaning and assembly operations in a cleanroom environment. Examples of conventional manual assembly and the robotic assembly test bench developed at KEK are shown in Fig. 1.

In previous work, basic motions relevant to cavity assembly and cleaning were demonstrated using direct teaching [3]. However, this approach requires motion programs to be prepared using the real robot, typically in the cleanroom, and makes it difficult to modify or reuse the programs for different tasks. Furthermore, collision risks and task feasibility cannot be sufficiently evaluated before execution.

To overcome these limitations, we developed a simulation-based workflow in which robot motions are generated and verified in a simulated workcell before being transferred to the real robot. A hybrid control framework has been established, combining reliable FANUC motion execution with a flexible KEK-developed control system that provides task-dependent functions, including vision-based position correction and control of cleaning and particle-monitoring devices. In addition, a tool changer and tool station were introduced to support task-specific end effectors. This paper presents the developed robotic assembly system and ongoing developments toward its application to single-cell SRF cavity assembly.

DEVELOPMENT OF THE ROBOTIC ASSEMBLY SYSTEM

Simulation-Based Motion Development

A simulated workcell reproducing the robotic assembly environment was constructed using FANUC ROBOGUIDE [4]. The simulated workcell includes the collaborative robot, cavity-related components, work tables, and peripheral equipment corresponding to those used in the actual development environment, as shown in Fig. 2.

Robot trajectories can be generated and modified in the simulated workcell without occupying the real robot or entering the cleanroom. This allows the feasibility of the robot motion and potential interference with surrounding equipment to be checked before execution. Motion programs developed and verified in ROBOGUIDE can subsequently be transferred to the real robot.

As an initial demonstration, cleaning motions were prepared in the simulated environment and transferred to the real collaborative robot. The corresponding motions were successfully executed on the actual system, confirming the

* yuki.abe@kek.jp

Content from this work may be used under the terms of the CC BY 4.0 licence (© 2026). Any distribution of this work must maintain attribution to the author(s), title of the work, publisher, and DOI.

ISBN: 978-3-95450-275-2 ISSN: 2226-0366 doi: 10.18429/JACoW-LINAC2026-MOPO061

FEATURES OF LONG PARTICLE BUNCH SELF-MODULATED IN PLASMA

V. Yarygova*, K. Lotov
BINP SB RAS, Novosibirsk, Russia

Abstract

A new analytical model for the transverse equilibrium of self-modulating beams in plasma was recently developed. The model is fairly accurate; however, its validation was limited to a single test case with a specific beam radius and a flat-top current profile. Here, we use numerical simulations with the quasistatic code LCODE to demonstrate how this theoretical framework performs under various conditions. The geometric limits of the model are determined by scanning the initial beam radius across a wide range of values. The parametric analysis shows that, for narrow beams, the conservation of the transverse adiabatic invariant, which is a cornerstone of the theory, is violated. The model is valid for short bunches with a smooth current profile. These results define the limits within which the analytical methods can serve as a reliable alternative to computationally intensive simulations of plasma wakefield accelerators.

INTRODUCTION

Plasma wakefield acceleration is a rapidly developing field that offers accelerating gradients orders of magnitude higher than conventional solid-state structures [1, 2]. One promising approach to exciting strong wakefields involves using long high-energy particle beams as wakefield drivers, which undergo self-modulation in dense plasma. As a result of self-modulation, the long beam breaks up into a train of short bunches, which can then resonantly drive plasma waves. This scheme is currently being actively investigated, particularly in the AWAKE experiment at CERN, where a long proton beam is used as the driver [3].

Under the influence of strong focusing plasma fields, the beam particles are pulled toward the axis, and the beam changes its radial profile from an initial Gaussian shape to a highly peaked equilibrium state with a density singularity on the axis. Recently, an analytical iterative model was developed to describe this transverse equilibrium state of the bunches [4]. The model comprises two distinct regimes: an adiabatic regime, based on the conservation of the transverse invariant for the main part of the bunch train, and an empirical relationship for the first bunch, where the adiabaticity is violated.

Although the model demonstrates excellent quantitative agreement with numerical simulations, it was validated on a single test problem featuring a flat-top beam current profile and a single initial beam radius $\sigma_r = 0.5k_p^{-1}$, where k_p is the plasma wavenumber corresponding to the plasma density n_0 near the injection point. In real experiments, however, the beams may initially have more complex density profiles or different radii.

In this paper, we explore the limits of applicability of the developed equilibrium model, paying particular attention to those cross-sections of the beam that efficiently drive the wave (referred to as the bunch "bodies"). First, we investigate how the model performs for various initial beam radii. Second, we verify the invariance of the model for non-uniform current profiles by examining its applicability to a cosine-shaped beam profile.

METHODS

The research process includes tracking the non-adiabatic and adiabatic regimes for various geometries, initial radii, or longitudinal density distributions of the beam. We simulate beam dynamics in plasma using the axisymmetric quasistatic code LCODE [5, 6] and compare the results with the analytical models [4]. The code computes the plasma response with periodicity $\Delta z = 10k_p^{-1}$ along the z-axis. The simulation domain of radius $R_{\max} = 8k_p^{-1}$, moving with the speed of light c, is covered with a rectangular grid of size $\Delta\xi = \Delta r = 0.01k_p^{-1}$, where $\xi = z - ct$. Plasma electrons are represented by 10 radius-weighted macro-particles per radial interval Δr. Plasma ions are immobile. There are 2500 equal beam macro-particles per interval $\Delta\xi$ in cross-sections of maximum beam current.

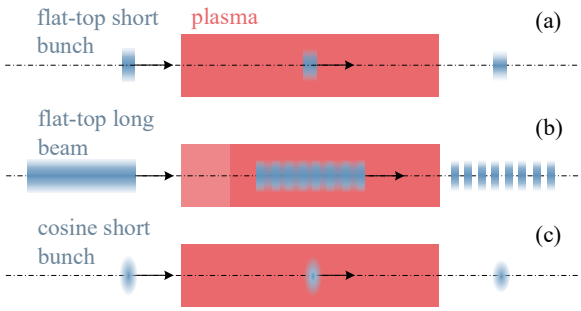


Figure 1: Beam and plasma configurations used for analyzing different interaction regimes: (a) a single short flat-top bunch in a uniform plasma, for the non-adiabatic regime; (b) a long flat-top beam propagating through plasma with a density step, for the adiabatic regime; (c) a single short bunch with a cosine-shaped longitudinal density profile in a uniform plasma, for the non-adiabatic regime with a smoothly varying beam current.

We consider three scenarios of beam-plasma interaction. In the first scenario, we focus on the non-adiabatic dynamics typical for the head of the beam by simulating a single,

* v.m.yarygova@inp.nsk.su

Content from this work may be used under the terms of the CC BY 4.0 licence (© 2026). Any distribution of this work must maintain attribution to the author(s), title of the work, publisher, and DOI.

ISBN: 978-3-95450-275-2 ISSN: 2226-0366 doi: 10.18429/JACoW-LINAC2026-MOPO062

REINFORCEMENT LEARNING-BASED ORBIT CORRECTION USING A CALIBRATED SURROGATE MODEL FOR THE RAON LEBT

C. S. Park*
Korea University, Sejong, Republic of Korea
J.-H. Jang, D.-O. Jeon, C. Kim, and H. J. Kim
Institute for Basic Science, Daejeon, Republic of Korea

Content from this work may be used under the terms of the CC BY 4.0 licence (© 2026). Any distribution of this work must maintain attribution to the author(s), title of the work, publisher, and DOI.

Abstract

Precise orbit control in low-energy heavy-ion transport sections is required for efficient beam delivery to downstream accelerators. In the RAON low-energy beam transport (LEBT) line, steering response is coupled to electrostatic-quadrupole focusing, calibration offsets, and nonlinear beam dynamics, so repeated TRACK correction studies are computationally expensive. This work develops a calibrated simulation and machine-learning workflow for LEBT surrogate modeling and orbit-correction studies. A calibrated centroid surrogate is used for preliminary reinforcement-learning (RL) orbit correction. The workflow is then extended to a 44-output surrogate that predicts diagnostic centroids, rms beam sizes, and transverse beam-state moments at the last wire scanner and LEBT exit for a no-offset optics/orbit data set with fixed beam current. A plain multilayer perceptron trained with up to 1M TRACK samples gives the best diagnostic accuracy. A physics-regularized model trained with 900k samples gives zero invalid covariance predictions and the best covariance-safe state model within this operating family. These results define an initial injected-beam-state representation for the next MEBT surrogate and RL correction stage.

INTRODUCTION

The RAON accelerator is designed to provide high-intensity rare-isotope beams for nuclear science experiments [1]. Reliable transport from the electron-cyclotron-resonance ion source to the radio-frequency quadrupole requires controlled transverse centroids and beam sizes in the low-energy beam transport (LEBT) line. At these energies, orbit response is sensitive to focusing, space charge, alignment and calibration errors, and the injected beam distribution [2, 3]. A correction method based on a single response matrix can therefore lose accuracy when the operating point changes, even though response-matrix methods remain a standard basis for beam-based optics calibration [4].

High-fidelity TRACK simulations provide a controlled environment for developing correction algorithms, but direct use in reinforcement-learning (RL) training is impractical because policy optimization requires many repeated evaluations. Machine-learning surrogate models reduce this cost by learning nonlinear accelerator responses from simulation data [5–7]. The approach used here is implemented in `synapticTrack`, a Python workflow that connects TRACK lattice execution, calibrated accelerator settings, deterministic sample generation, PyTorch surrogate training, beam-physics metric evaluation, and Gymnasium-compatible RL environments. The calibrated TRACK LEBT model is first used to train a fast centroid surrogate for RL orbit-correction studies, and the target vector is then extended to include beam-size and beam-state quantities needed by downstream sections. The LEBT beam-state results provide the state representation required for the planned medium-energy beam transport (MEBT) surrogate.

* kuphy@korea.ac.kr

LEBT CALIBRATION

The LEBT model follows the calibrated TRACK lattice used in this work, including steering elements, electrostatic quadrupoles, drifts, and the diagnostic locations used for wire scanner (WS) and Allison scanner (AS) comparisons [8]. The beam transported in the simulation is an Ar^{8+} beam, and the transverse input distribution is represented by an uncoupled four-dimensional Gaussian in (x, x', y, y'), using the second-moment/Courant-Snyder conventions of transverse beam optics [9].

The calibration adjusts steering response, diagnostic offsets, and grouped electrostatic-quadrupole scale factors. Steering kick scales are inferred separately in the horizontal and vertical planes, and wire scanner offsets align the simulated and measured centroid references. The electrostatic quadrupoles are grouped into three calibration families to correct the focusing model without fitting each quadrupole independently. Figure 1 shows the resulting agreement with measured centroids and rms beam sizes.

CENTROID SURROGATE MODEL

The calibrated TRACK model is used to generate a Latin-hypercube-sampled data set for surrogate training [10]. The centroid-surrogate workflow uses a 13-dimensional input vector consisting of 5 horizontal steering settings, 5 vertical steering settings, and three grouped electrostatic-quadrupole scale factors. The target vector contains 12 centroid outputs: horizontal and vertical centroids at WS1, AS, WS2, WS3, WS4, and the LEBT exit. A fully connected neural network is implemented in PyTorch and trained with mean-squared-error loss [11]. The best production configuration used GELU activations, the Adam optimizer, and a learning rate of 10^{-3}.

Table 1 summarizes the current 50k-sample result. The best validation loss is 3.96×10^{-5}. The maximum diagnostic rms centroid error is 0.0274 mm, occurring at WS4 in

ISBN: 978-3-95450-275-2 ISSN: 2226-0366 doi: 10.18429/JACoW-LINAC2026-MOPO063

DESIGN OF A PRECISION CLOCK UNIT FOR THE INJECTION KICKER PULSED POWER SUPPLY IN THE BEPCII-U STORAGE RING

Peng Liu†, Jinhui Chen, Guanwen Wang, Lei Wang
Institute of High Energy Physics, Chinese Academy of Sciences, Beijing, China

Content from this work may be used under the terms of the CC BY 4.0 licence (© 2026). Any distribution of this work must maintain attribution to the author(s), title of the work, publisher, and DOI.

Abstract

The upgrade of Beijing Electron–Positron Collider (BEPCII) is a double-ring machine used for both high-energy physics experiments and synchrotron radiation research. In order to further improve the performance of the machine, BEPCII has upgraded the luminosity in the high-energy region (BEPCII-U). As a critical subsystem of BEPCII-U, the kicker pulser for storage ring injection is crucial. Its performance directly determines the injection efficiency of the machine. In the pulser system, the local clock unit plays an important role in triggering and pulse blocking protection. The kicker pulser requires low output time jitter(<5 ns), which places high demands on the local clock unit. The designed clock unit uses FPGA as the main controller. The system includes a clock adjustment section, an output clock output section, and a display section. A prototype is built. Offline testing and joint debugging between systems were conducted on the prototype, and its performance meets the design specifications.

INTRODUCTION

BEPCII serves both high energy physics and synchrotron radiation research [1]. The BEPCII-U luminosity upgrade requires digital modernization of storage ring injection systems. A slot-pipe kicker is used for storage ring injection system. The slot-pipe kicker depends critically on precise triggering and robust protection. The slot-pipe kicker is a compact in-vacuum magnet for tight beam pipe geometries. BEPCII-U injection sections each have two units driven by the thyratron-based 25 kV pulser, it delivering 450 ns half-sine pulses. The kicker pulser diagram is shown in Fig. 1.

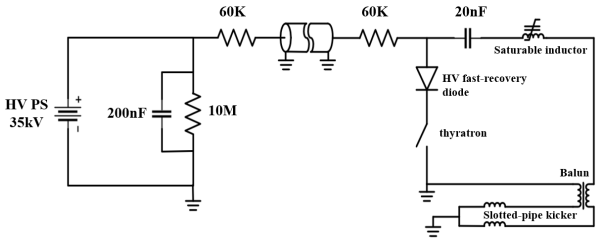


Figure 1: Thyratron-based 25kV pulser diagram.

Machine protection is equally critical: high-voltage pulsed operation risks vacuum degradation, detector faults, and power supply anomalies. A fast hardware clock-gating mechanism serves as the first defense layer, complementing slower PLC (kicker pulser's local control station) shutdown sequences.

This paper presents an FPGA-based clock unit for the BEPCII-U storage ring injection system. Sections cover system design requirements, hardware architecture, firmware design, and experimental results.

DESIGN REQUIREMENTS

The key operational parameters of the proposed clock unit are summarized in Table 1. These specifications characterize the system's operational envelope and timing performance, tailored for low-repetition-rate pulsed trigger and synchronization applications.

The system accepts input trigger pulses with a maximum repetition frequency of 50 Hz. The output pulse features a fixed bottom width of 10 μs and maintains the same 50 Hz maximum repetition rate as the input. For timing fidelity, the output pulse exhibits a clock jitter of 1 ns. The design parameters is shown in Table 1.

Table 1 System Design Parameters

Parameters	Value
Maximum Input pulse repetition frequency (Hz)	50
Output pulse bottom width (us)	10
Maximum Output pulse repetition frequency (Hz)	50
Output pulse clock jitter (ns)	1

HARDWARE DESIGN

The local clock unit receives the reference trigger signal from the timing system to implement precise trigger control for the kicker pulser. It interfaces with the local control station of the kicker pulser, and performs interlock control of the kicker pulser as well as fault blocking for the high-voltage charging power supply (HVPS). The overall hardware diagram is shown in Fig. 2.

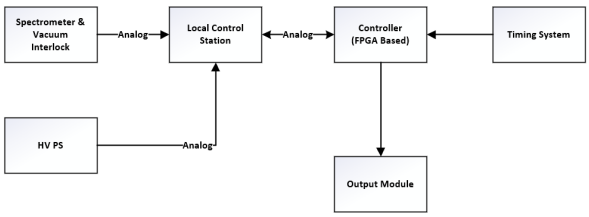


Figure 2: Overall hardware architecture diagram.

The local clock unit consist two parts: controller module and clock output module.

The controller module consists of two functional parts: the FPGA-based precision timing control section and the interlock and fault protection section.

†liupeng@ihep.ac.cn

ISBN: 978-3-95450-275-2 ISSN: 2226-0366 doi: 10.18429/JACoW-LINAC2026-MOPO064

BEAM DYNAMICS DESIGN OF A 17 GHz COMPACT X-BAND SW ACCELERATING STRUCTURE BASED ON GENETIC ALGORITHM*

Z.H. Gao, P. Wang†, J.H. Tan‡, C. Wang, D.H. Su, Y.F. Lan, X.X. Huang, H.Y. Gong
Y.X. Lu, Y.S. Guo, C. Xia, C.C. Xiao, R.C. Qin, H.L. Wan, X.Y. Sun, W.C. Fang, Z.T. Zhao
Shanghai Advanced Research Institute, Chinese Academy of Sciences, Shanghai, China
Shanghai Key Laboratory of Particle Accelerator Science and Technology, Shanghai, China

Abstract

A fully automated beam dynamics design method based on genetic algorithm is proposed for a 17 GHz X-band three-cell standing wave accelerating structure to meet the miniaturization requirements of X-ray based intraoperative radiotherapy(IORT) devices. The genetic algorithm simultaneously optimizes the field distribution of the three cavities, achieving both electron beam bunching and acceleration within a single framework without manual intervention. The design results demonstrate that the 8 keV electron bunch is accelerated to a target energy of 50 keV, satisfying the constraints of IORT equipment. The six-dimensional design space, comprising the peak field (E_1, E_2, E_3) and the axial length (L_1, L_2, L_3) of the three cells, is searched with a genetic algorithm (GA) coupled to the RF-Track particle-in-cell tracking engine. The fitness function integrates multiple parameters including the target energy to ensure the optimization results meet the requirements. After 100 generations, the GA reaches a best fitness of 123.73, with 76.57 % of the particles inside the 48-51keV acceptance band, and a transmission of 93.89 %.

INTRODUCTION

In the research and development of intraoperative X-ray radiotherapy equipment, one of the key parts is the design and development of the electron linear accelerator. Compact X-band standing-wave(SW) accelerating structures in the 8 - 20 GHz range are attracting renewed interest for the application. At 17.136 GHz the RF wavelength is 17.5 mm, allowing millimetre-scale accelerating cells and total structure lengths below 30 mm for sub-100-keV beams. This compactness is essential for next-generation intraoperative radiotherapy (IORT) devices and other footprint-limited systems. In addition, accelerating electrons by microwaves reduces the high voltage of the equipment to below 10 kV, much lower than the 50 kV of conventional equipment. Accordingly, it features a small size, high gradient and light weight, offering prominent advantages [1].

For such low-energy injectors the SW bi-periodic disk-loaded structure is a particularly attractive topology. Accelerating cavities are separated by coupling cavities that, in the $\pi/2$-mode, carry negligible on-axis field and merely provide the inter-cell coupling required [2, 3]. The entire accelerating chain therefore behaves as a sequence of independent π-mode cells. A key advantage of this geometry is that the effective peak field and the equivalent axial length of every accelerating cell can be adjusted independently by changing the coupling strength and the accelerating-cavity geometry, giving the designer a large degree of freedom to shape the longitudinal field profile for simultaneous bunching and acceleration.

The 8 keV electron bunch considered here has a velocity far below the speed of light, so the transit-time factor changes rapidly with bunch accelerated. A purely analytical phase-matching approach is inaccurate, and the cavity parameters must be determined by direct particle tracking. Genetic algorithms (GAs) are well suited to this task because they require only black-box evaluations of the objective function and can explore the strongly multi-modal design landscape globally [4]. Coupling a GA to the RF-Track toolkit [5] allows an automated, hands-off search of the cavity field distribution.

In this paper we report a beam dynamics design of a 17 GHz compact X-band SW accelerating structure optimized by a GA. The design target is to accelerate an 8 keV electron bunch to approximately 50 keV with a strict 51 keV upper energy bound, motivated by intraoperative X-ray radiotherapy equipment.

DESIGN SPECIFICATIONS AND METHODOLOGY

This chapter introduces the requirements for beam parameters, the generation of fields, and construction of the fitness function.

Structure and Beam Specifications

The accelerating structure is modeled as three cells operating in a $\pi/2$-mode without coupling cells, which means the phase advance between adjacent accelerating cells is 180°. The same 17 GHz RF source drives all three cells. The input beam is an 8 keV electron bunch, modeled as a 10 000-macro-particle RF-Track `Bunch6d` distribution with transverse Gaussian r.m.s. sizes of 0.003 mm and 0.003 mrad and a uniform longitudinal extent covering ten RF periods. The target output energy is 50 keV, with a hard upper limit of 51 keV imposed to prevent downstream over-acceleration. The design space is summarised in Table 1.

* Work was supported by the National Natural Science Foundation of China (No. 12405178) and (No. 12505171).
† wangping@sari.ac.cn
‡ tanjh@sari.ac.cn

Content from this work may be used under the terms of the CC BY 4.0 licence (© 2026). Any distribution of this work must maintain attribution to the author(s), title of the work, publisher, and DOI.

ISBN: 978-3-95450-275-2 ISSN: 2226-0366 doi: 10.18429/JACoW-LINAC2026-MOPO065

INTRODUCTION TO A THREE-DIMENSIONAL MULTI-PARTICLE SIMULATION CODE FOR LINEAR ACCELERATORS

J. Y. Du, Y. S. Yuan*
Institute of High Energy Physics, Chinese Academy of Sciences, Beijing, China
Spallation Neutron Source Science Center, Dongguan, China

Abstract

With the rapid advancement of high-intensity linear accelerators, achieving efficient and accurate design has become a critical challenge in modern accelerator physics. As beam intensity increases, the space charge effect — arising from the mutual repulsion among charged particles within the beam — becomes increasingly significant and must be incorporated into realistic simulations. In this paper, we develop a comprehensive multi-particle simulation program specifically tailored for linear accelerators. The program employs a novel three-dimensional space charge solver based on the tensor decomposition method, which offers both high computational efficiency and numerical accuracy. To validate the proposed program, we apply it to simulate the linear section of the China Spallation Neutron Source (CSNS). The simulation results are systematically compared with those obtained from Tracewin, a well-established beam dynamics code. Good agreement between the two sets of results demonstrates the effectiveness and reliability of our developed simulation program.

INTRODUCTION

The China Spallation Neutron Source (CSNS) is an accelerator-driven neutron facility in which a high-power pulsed proton beam is delivered to a spallation target to produce neutrons for scientific instruments [1]. Its proton accelerator is consequently more than a transport system: it must preserve beam quality, minimize beam loss and deliver stable longitudinal and transverse distributions to the downstream accelerator chain. The front end and linac provide the initial acceleration, while the subsequent rapid-cycling synchrotron raises the beam energy before extraction to the target. The drift-tube-linac (DTL) section is a particularly important part of this process because it accelerates the still non-relativistic beam while establishing strong transverse focusing.

A DTL accelerates non-relativistic charged particles through a sequence of RF gaps, while quadrupoles installed in the drift-tube structure provide alternating-gradient focusing [2]. The individual elements are well understood, but their combined effect is strongly coupled: the RF phase determines longitudinal capture and energy gain, the increasing particle velocity changes the magnetic rigidity and focusing strength, and space-charge forces can modify the envelope and phase-space density. The development of linac simulation tools has followed the increasing demand for both speed and physical fidelity. Early lattice-design calculations were commonly based on envelope equations and first- or second-order transfer matrices [3,4]. These methods remain efficient for optical matching and rapid parameter scans, but they represent a beam mainly through its moments and cannot fully describe distribution distortions, tails or particle loss. The expansion of computing resources made macro-particle tracking practical: a beam can be represented by many particles in six-dimensional phase space and transported through a detailed sequence of beam-line elements. For intense proton beams, the most important research is self-consistent or model-based treatment of space charge. Grid-based Poisson solvers, particle-in-cell methods and transverse or quasi-three-dimensional approximations make it possible to estimate the collective electric field while retaining practical run times [5]. Modern multi-particle codes consequently combine element maps, RF models, diagnostics and several space-charge solvers in modular workflows.

The Python program presented here follows this multi-particle approach in a transparent, dictionary-based lattice format. This article documents a focused comparison with TraceWin [6] using the supplied kinetic-energy, rms-envelope and final phase-space results at different beam intensity. Meanwhile, for the space-charge solver, we adopt the three-dimensional algorithm based on tensor decomposition proposed in [7].

THE SIMULATION CODE

The code (TEST-Linac) is organized around a Bunch object, an element library and the TransMap tracker. A bunch is represented by macro-particles in the coordinates $(x, x', y, y', z, \delta)$. TransMap converts the dictionary-based lattice into an ordered beam line, assigns longitudinal positions and tracks the bunch element by element. Drifts and quadrupoles use transfer maps, while the RF-gap model applies phase-dependent acceleration and transverse RF focusing. Marker elements record beam statistics and particle snapshots, allowing direct comparison of energy, rms quantities and phase-space projections. The code base also contains interchangeable space-charge solvers, including TDM solver. The structure of code is shown as Fig. 1.

Dynamics Equations

In this section, we will introduce the dynamic equations of RFGap element. We treat RFGap as a thin element, so it can only change the momentum of the particles which known as kicker. The energy gain is

$$\Delta W = qV_{\mathrm{eff}} \cos(\phi_{\mathrm{s}}), \tag{1}$$

* ysyuan@ihep.ac.cn

Content from this work may be used under the terms of the CC BY 4.0 licence (© 2026). Any distribution of this work must maintain attribution to the author(s), title of the work, publisher, and DOI.

ISBN: 978-3-95450-275-2 ISSN: 2226-0366 doi: 10.18429/JACoW-LINAC2026-MOPO066

BEAM LOSS MEASUREMENTS WITH NEUTRON AND IONIZATION CHAMBER MONITORS DURING ESS BEAM COMMISSIONING TO THE TUNING BEAM DUMP

H. Hassanzadegan†, A. Gorzawski, A. Jansson, A. Persson, I. Dolenc Kittelmann, J. Norin, L. Alves Martins, M. Eshraqi, T. J. Shea, V. Grishin
European Spallation Source, Lund, Sweden

Content from this work may be used under the terms of the CC BY 4.0 licence (© 2026). Any distribution of this work must maintain attribution to the author(s), title of the work, publisher, and DOI.

Abstract

The European Spallation Source (ESS) employs 266 ionization chamber beam loss monitors (icBLMs) and 82 neutron beam loss monitors (nBLMs). These detectors provide detailed information on beam loss distribution along the ~600 m ESS linac and play a critical role in machine protection. During the second round of beam commissioning to the Tuning Beam Dump in spring 2026, systematic tests were performed with both BLM systems to evaluate their performance, including operational challenges and limitations. The stability of the systems and the readout signals was checked in low- and high-loss scenarios and under different environmental conditions. This paper provides a brief overview of the BLM system design and machine protection functions, followed by recent beam loss measurement results obtained with beam.

INTRODUCTION

The second ESS Beam on Dump (BOD2) commissioning campaign began in February 2026. During this campaign, the proton beam was accelerated up to 860 MeV through both the normal-conducting and superconducting sections of the ESS linac and transported to the Tuning Beam Dump (TBD) located at the end of the accelerator. The beam current and pulse length were progressively increased to 20 mA and 1.5 ms, respectively. For comparison, during the first BOD campaign, the beam parameters were limited to 6 mA and 50 µs.

The beam properties were then measured by more than 500 beam diagnostics devices distributed along the ESS linac, including Beam Current Monitors (BCMs), Beam Position Monitors (BPMs), BLMs, Wire Scanners (WSs) and an imaging system measuring the beam footprint on the TBD.

The ESS BLM system consists of ionization chamber and neutron-based detectors distributed along the accelerator to provide both machine protection and beam-loss diagnostics. Commissioning and performance evaluation of these systems were among the objectives of the BOD2 campaign. Their performance was then assessed under beam operation in terms of beam-loss measurement quality and susceptibility to external disturbances. A first validation of machine-protection functions was also carried out.

The following sections summarize the BLM results obtained during the BOD2 activities, the issues encountered during testing and the corrective actions.

† hooman.hassanzadegan@ess.eu

BLM SYSTEM DESIGN

The design and architecture of the icBLM and nBLM systems are presented in [1] and [2] respectively. The main specifications are summarized in Table 1.

Table 1: IcBLM and nBLM Specifications Summary

	icBLM	nBLM
No. of detectors	266	82 (41 Fast, 41 Slow)
Detector type	LHC/IHEP	Micromegas
Concentration	SPK, MBL, HBL, HEBT, A2T	DTL, SPK
Gas type	N_2	He-Ethane
Gas system	Detector filled with gas	Gas storage cage, distribution rack
Power Supply	1-CH ISEG	48-CH CAEN, 8-CH CAEN
Detector HV (typ.)	1500 V	950 V (Drift) 450 V (Mesh)
Detector LV	N/A	±8 V
ADC card	PICO FMC 1M4	IOxOS FMC ADC3111
A-to-D conversion	20 bit, 1 MSPS, 300 kHz BW	16 bit, 250 MSPS
ADC full-scale	±500 µA, ±2.5 µA	±500 mV
AMC	IOxOS IFC1410	IOxOS IFC1410
FPGA processing	ABW subtract	Pedestal comp., single N, pile-up

ICBLM TESTS WITH BEAM

With the start of the BOD2 activities, the overall performance of the icBLMs was assessed with an Xray source [3] and beam. The later was done through dedicated tests generating localized beam losses and during routine machine studies, including RF amplitude and phase scans, beam interception on insertable beam stops, and other activities resulting in measurable beam losses.

The secondary particles from cavity field emissions resulted in a step on the raw signal of some icBLM detectors. Figure 1 shows the RF background on a High Beta Linac (HBL) icBLM signal in time domain. A digital filter is

ISBN: 978-3-95450-275-2 ISSN: 2226-0366 doi: 10.18429/JACoW-LINAC2026-MOPO068

UPGRADE OF THE LLRF SYSTEM FOR THE X-BAND LINEARIZER IN SXFEL

Chengcheng Xiao[1,2,3],Ping Wang[2,3], Jianhao Tan[2,3], Yixing Lu[2,3], Zihe Gao[2,3], Cheng Wang[2,3], Chenyu Wei[2,3], Wencheng Fang[†,2,3], Yiming Xu[‡,2,3]
[1]University of Chinese Academy of Sciences, Beijing, China
[2]Shanghai Advanced Research Institute, Chinese Academy of Sciences, Shanghai, China
[3]Shanghai Key Laboratory of Particle Accelerator Science and Technology, Shanghai, China

Abstract

The X-band linearizer is an important component of the Shanghai Soft X-ray Free-Electron Laser (SXFEL), and its RF stability has a direct impact on downstream beam quality. To further improve the operational stability of the linearizer, the X-band clock and local oscillator electronics were upgraded, together with the development of a high-stability solid-state power amplifier. These improvements reduced the RF amplitude, phase, and timing fluctuations of the X-band system and enhanced its overall stability. Beam measurements were performed using a downstream stripline beam position monitor (SBPM). After the upgrade, the RMS horizontal beam position fluctuation decreased from 0.01348 to 0.004714, corresponding to an improvement of approximately 65%. The results demonstrate that the upgraded X-band RF system can effectively improve the beam stability of SXFEL and provide more reliable operation for user experiments.

INTRODUCTION

The Shanghai Soft X-ray Free-Electron Laser (SXFEL) is an X-ray free-electron laser facility providing high-brightness and coherent soft X-ray radiation for scientific experiments[1]. Stable electron beam transport and acceleration are essential for maintaining the output performance of the facility. In particular, fluctuations in the RF systems can introduce variations in beam energy, arrival time, and transverse orbit, and may finally affect the stability of the FEL output. The overall layout of SXFEL is shown in Fig. 1, including the injector, main accelerating sections, X-band linearizer, undulator sections, and associated beam transport systems [2].

An X-band linearizer is installed at the front section of the SXFEL linac to compensate for the nonlinear longitudinal phase-space distortion introduced by the main accelerating sections. Since the linearizer acts on a relatively low-energy electron beam, fluctuations in its RF amplitude, phase, and timing can be transferred to the downstream beam and influence the overall machine stability. Therefore, improving the stability of the X-band RF system is important for reliable and reproducible operation of SXFEL.

To improve the overall stability of the X-band linearizer system, the clock and local oscillator electronics were upgraded to reduce timing jitter and long-term phase drift. Meanwhile, a new high-stability X-band solid-state power amplifier was developed to improve the pulse-to-pulse stability of the RF drive signal. The upgraded system was installed and tested at SXFEL, and its performance was evaluated through beam measurements. After the upgrade, the RMS horizontal beam position fluctuation measured by a downstream stripline beam position monitor (SBPM) decreased from 0.01348 to 0.004714, demonstrating a significant improvement in beam stability. This work provides a practical approach for improving the operational stability of the X-band linearizer and supports more stable operation of SXFEL.

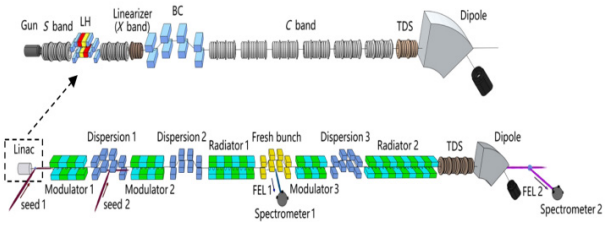


Figure 1: Layout diagram of the SXFEL.

DESIGN OF A 1200W X BAND AMPLIFIER

To improve the RF stability of the X-band linearizer, a new 1200 W solid-state power amplifier was developed for operation at 11.424 GHz. As shown in Fig. 2, the amplifier adopts a six-channel parallel architecture. The input RF signal is first modulated and amplified, then divided into six channels and recombined after high-power amplification. This configuration provides the required output power while allowing the individual amplification stages to operate with sufficient power margin [3].

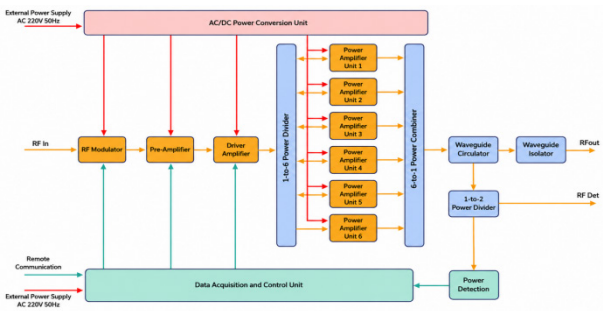


Figure 2: Schematic of 1200W SSA.

For a multi-channel amplifier, the stability of the combined output depends not only on the performance of each

† fangwencheng@sinap.ac.cn
‡ xuyiming19@mails.ucas.ac.cn

Content from this work may be used under the terms of the CC BY 4.0 licence (© 2026). Any distribution of this work must maintain attribution to the author(s), title of the work, publisher, and DOI.

ISBN: 978-3-95450-275-2 ISSN: 2226-0366 doi: 10.18429/JACoW-LINAC2026-MOPO069

STATUS OF A C-BAND TEST PLATFORM FOR PROOF-OF-PRINCIPLE ULTRA-SHORT BUNCH GENERATION

X. Liu*, W. Liu, S. Jiang, S. Liu, X. Cao, Z. Lu, R. Liu, H. Zhang, Z. Xie,
W. Huang, R. Yang, A. Li, C. Deng, J. Wei, G. Zhao, M. Li, Y. Wang, P. Wang,
N. Ma, T. Wang, S. Chen, L. Wang, K. Xue, Y. Ma, W. Qin, X. Li, S. Wang
Institute of High Energy Physics, Beijing, China

Abstract

A C-band test platform at IHEP-Dongguan is being prepared for proof-of-principle ultra-short bunch generation based on angular dispersion modulation (ADM). The RF photocathode gun, travelling-wave accelerating structures, and pulse-compression system were developed and tested in earlier stages. Installation of the ADM beamline is complete, and RF conditioning is in progress ahead of the beam test planned for August 2026. This paper presents the platform status, installed layout, and a start-to-end simulation for a 10 pC working point. A 50,000-macroparticle ASTRA–Elegant calculation predicts transport from the cathode to the coherent-transition-radiation station without particle loss. The RMS bunch duration is 560 fs at the ASTRA–Elegant hand-off and 41 fs at the observation station, corresponding to an expected compression factor larger than 13. A modulation-voltage scan indicates tunable compression around the selected 3.2074 MV setting. These results provide initial machine settings and expected performance for the forthcoming beam experiment.

INTRODUCTION

A C-band test platform has been developed at IHEP-Dongguan to study high-gradient RF technology and advanced beam manipulation for future light sources. The platform employs a 3.6-cell C-band RF photocathode gun, C-band travelling-wave structures (TWSs), a high-power RF pulse compressor, and a configurable low-energy beamline. The original platform configuration was reported in Ref. [1]. The spherical pulse compressor was subsequently designed, fabricated, and tested [2]. Two TWSs were also tested, and the design of the 44-cell TWS (TWS-44) is reported in another contribution to this conference [3]. Initial beam extraction from the gun was presented at HG2025 [4] and reported in the SAP2025 proceedings [5]; related dark-current beam-loading studies were presented at IPAC2026 [6]. The gun was conditioned close to a cavity gradient of 150 MV/m, and electron-beam extraction was demonstrated at a cathode gradient of approximately 137 MV/m. The accelerating structures and associated RF system were also tested in 2025.

The platform has since been reconfigured for a proof-of-principle angular dispersion modulation (ADM) experiment. In the ADM process, the first bend introduces transverse dispersion, after which a longitudinal energy correlation can be generated using either a laser pulse or an RF structure. The following bends then convert this correlation into bunch compression. This two-dimensional compression principle and its application to sub-femtosecond bunch generation are described in another contribution [7]. As a compact proof-of-principle experiment with limited available space, the platform uses an 18-cell C-band TWS (TWS-18). The present paper focuses on the installed platform and expected beam performance. At the time of writing, installation is complete and RF conditioning is under way; first beam operation with the upgraded line is planned for August 2026.

PLATFORM AND PRESENT LAYOUT

Figure 1 shows the installed platform from the C-band gun to the Faraday Cup (FC), which also serves as a beam dump, and Fig. 2 gives an upstream view of the assembled injector. The injector consists of the photocathode gun, solenoids, and a 44-cell accelerating TWS (TWS-44). Screens (SCRs) and current transformer CT1 provide transverse-profile and charge diagnostics before the downstream ADM section. Four quadrupoles (Q1–Q4) prepare the beam before the first bend (B1). TWS-18 provides the modulation required for bunch compression. Beam-position monitors between the bends support orbit commissioning, while a coherent-transition-radiation (CTR) station will be used to infer the compressed bunch length.

Only two klystrons are available for this platform. One powers the gun exclusively, while the other powers both TWS-44 and TWS-18. To compensate for transmission losses in the long waveguides and the limited output of the second klystron, a pulse compressor increases the peak RF power, and a tunable power divider distributes it between the two accelerating structures.

The gun and accelerating TWS were high-power tested during 2025. The cathode surface was replaced for the new layout because the previous one had suffered damage from RF breakdown and discharge. The present activity is integrated RF conditioning after installation in the upgraded beamline. This stage establishes the operating gradients, interlocks, and RF timing required for beam commissioning. The simulated working point below defines the initial RF and magnet settings for the beam compression test.

* liuxg@ihep.ac.cn

Content from this work may be used under the terms of the CC BY 4.0 licence (© 2026). Any distribution of this work must maintain attribution to the author(s), title of the work, publisher, and DOI.

ISBN: 978-3-95450-275-2 ISSN: 2226-0366 doi: 10.18429/JACoW-LINAC2026-MOPO074

LEVERAGING AI TOOLS IN RF AND SRF OPERATIONS AT FRIB*

S. Kunjir†, W. Chang, S. Kim, S. Zhao
Facility for Rare Isotope Beams, Michigan State University, East Lansing, MI, USA

Abstract

Radio-frequency (RF) and superconducting radio-frequency (SRF) operations at the Facility for Rare Isotope Beams (FRIB) require rapid, high-consequence decision-making across low-level RF controls, cryomodules, tuners, interlocks, diagnostics, cryogenics, and machine-protection interfaces. In many troubleshooting scenarios the bottleneck is not diagnostic-signal availability, but is the time required to locate relevant context, reconstruct event timelines, interpret heterogeneous data, and transfer institutional knowledge across shifts and teams. This paper proposes a responsible generative artificial intelligence (AI) framework for RF/SRF operations that combines retrieval-augmented generation, multimodal interpretation, and structured workflow acceleration. Three use cases are emphasized: faster RF trip triage, high-efficiency raw-data collection and visualization, and documentation support. A four-level architecture is introduced for an RF/SRF operational brain: event and raw-data acquisition, data cleaning and visualization, document-grounded assistance, and expert-reviewed knowledge generation. AI outputs are treated as draft decision-support artifacts that must be verified by personnel, measurements, and approved procedures.

INTRODUCTION

Modern accelerator facilities operate at the intersection of RF engineering, superconducting cavity physics, cryogenics, controls, beam dynamics, and machine protection. FRIB's driver linac contains 324 superconducting resonators housed in 46 cryomodules and supports heavy-ion beam delivery above 200 MeV/u for rare-isotope production [1, 2]. RF/SRF operation therefore requires operators and system experts to reason over live process variables, low-level RF (LLRF) waveforms, alarm histories, electronic logbook entries, maintenance records, procedures, and hardware configuration details.

The central operational challenge addressed here is information latency. During an RF trip, field-emission study, tuner problem, or cavity turn-on, relevant evidence may exist but be distributed across archived process variables, waveform files, screenshots, shift summaries, and institutional knowledge. The time required to assemble this context can dominate the time required to make a technically sound decision. Generative AI provides a practical mechanism to reduce this latency, provided that the system is grounded in facility data and procedures, bounded by safety constraints, and used as decision support rather than as an authority.

Recent work in accelerator and scientific-facility AI motivates this direction. Deep-learning methods have been used to classify SRF cavity faults from RF waveform captures at Jefferson Lab [3]. Machine-learning optimization has been used to reduce field-emission-induced radiation while preserving required linac energy gain [4]. Retrieval- and tool-augmented language-model systems have been proposed for scientific facilities [5], and language-model-driven accelerator assistants have demonstrated archive retrieval, process-variable resolution, script generation, and auditable workflow execution in accelerator environments [6, 7]. This paper adapts these ideas to the specific needs of RF and SRF operation at FRIB.

OPERATIONAL MOTIVATION

FRIB's SRF linac cavities include quarter-wave resonators (QWRs) and half-wave resonators (HWRs) operated under different cryogenic and RF conditions. The QWR cryomodules in the first linac segment are operated at 4 K, while HWR cryomodules downstream are operated at 2 K [2]. Stable cavity amplitude and phase control have been demonstrated with slow tuner systems, but practical operation remains constrained by field emission, multipacting, tuner limits, cryogenic stability, interlock thresholds, and evolving beam-power requirements [1, 2]. Figure 1 shows the layout of the FRIB driver linac.

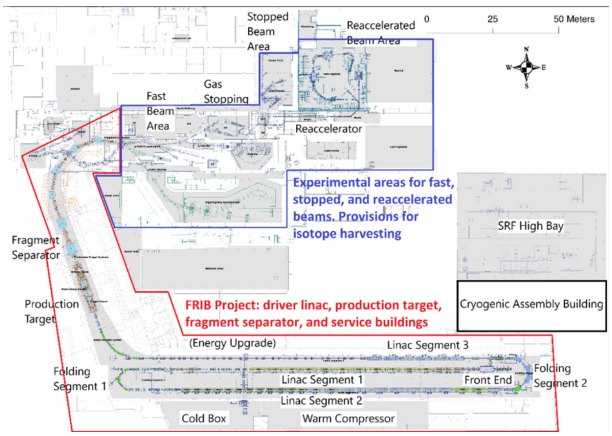


Figure 1: Layout of the FRIB driver linac, target, fragment separator and experimental areas.

Field emission is a representative example of an operationally important SRF problem. RF pulse conditioning has been used at FRIB to reduce field emission in cryomodules, with recent work reporting conditioning and analysis for roughly 50 cavities and distinguishing rapid electrical breakdown events from slower thermal breakdown or quench-like events [8]. Such events generate large volumes of waveforms, X-ray trends, cavity-gradient information,

* Work supported by the U.S. Department of Energy, Office of Science under Cooperative Agreement DE-SC0023633, the State of Michigan, and Michigan State University.
† kunjir@frib.msu.edu

Content from this work may be used under the terms of the CC BY 4.0 licence (© 2026). Any distribution of this work must maintain attribution to the author(s), title of the work, publisher, and DOI.

ISBN: 978-3-95450-275-2 ISSN: 2226-0366 doi: 10.18429/JACoW-LINAC2026-MOPO076

DESIGN OF THE POSITRON LINAC FOR THE FCC-ee INJECTOR COMPLEX

Y. Zhao*, S. Doebert, A. Grudiev, B. Humann, A. Kurtulus[1], A. Latina,
A. Lechner, P. Desire Valdor[2], CERN, Geneva, Switzerland
F. Alharthi, I. Chaikovska, R. Chehab, V. Mytrochenko, Y. Wang, CNRS/IJCLab, Orsay, France
Y. Enomoto, KEK, Tsukuba, Japan
O. Etisken, Kirikkale University, Kirikkale, Turkiye
A. De Santis, C. Milardi, S. Spampinati, LNF-INFN, Frascati, Italy
B. Auchmann, P. Craievich, M. Duda, J. Kosse, J.-Y. Raguin, M. Schaer, N. Vallis,
R. Zennaro, PSI, Villigen, Switzerland
[1]also at Institute of Electromagnetic Fields, Zurich, Switzerland
[2]also at University of Groningen, Groningen, Netherlands

Content from this work may be used under the terms of the CC BY 4.0 licence (© 2026). Any distribution of this work must maintain attribution to the author(s), title of the work, publisher, and DOI.

Abstract

The FCC-ee injector complex is mainly composed of an electron source, a positron source, a damping ring, and a high-energy linac. The positron linac, which is part of the positron source, accelerates the positron beams from about 200 MeV to 2.86 GeV before their injection to the damping ring. It is designed, simulated and optimized for the best positron beam performance at the end of the linac with a maximized positron yield for positrons accepted by the damping ring. In the latest baseline design of the FCC-ee injector, 4 bunches per pulse is assumed, with a bunch separation of 25 ns and a repetition rate of 100 Hz. The required bunch charge at the end of the Positron Linac is 13.5 nC, assuming a 50 % loss in the damping ring and an additional loss of 20 % positrons from the target exit to the damping ring entrance. A chicane collimator is used to dump electrons and photons from the upstream Capture Linac. The Positron Linac is composed of two sections, where NC solenoids surrounding the accelerating structures with 0.5 T magnetic field and FODO cells with quadrupoles placed between the structures are used for beam focusing. A 3 m long RF accelerating structure working at 2 GHz is used. RF gradients and phases are optimized for a maximum positron yield. Imperfections are studied and the impact is found to be small.

INTRODUCTION

The Future Circular e^-e^+ Collider (FCC-ee) [1,2] is a proposed large circular, high-luminosity, high-precision e^-e^+ collider, hosted by the European Organization for Nuclear Research (CERN). It is designed to be operated in a ~ 91 km long tunnel at center-of-mass energies ranging from the Z pole (~ 91 GeV) to the $t\bar{t}$ threshold (~ 365 GeV). It will later be upgraded to a proton-proton collider (FCC-hh) with a center-of-mass energy of 100 TeV. This study is mainly focused on the Z pole operation mode which has the highest beam intensity, and is the most challenging mode for positron source.

* yongke.zhao@cern.ch

The FCC-ee positron source is part of the injector complex and provides high-intensity and high-energy positron beams, that are injected into the damping ring (DR) operating at 2.86 GeV. The schematic layout of the current baseline design of the FCC-ee positron source, from the target to the damping ring, is presented in Fig. 1. Positrons are generated with a 2.86 GeV electron driver beam from an electron driver linac impinging on an amorphous tungsten target. The simulation of the electron driver linac is not included in this study and is therefore not discussed. The parameters of the electron driver beam at the target assumed in the simulation are summarized in Table 1. The RMS spot size is optimized to 1 mm, as a good compromise between a high positron yield and low peak energy deposition density (PEDD) and total deposited power in the target, which is critical for effective target cooling. The PEDD and the total deposited power in the target are ~ 7.7 J/g and ~ 1.3 kW, respectively, for the given parameters in Table 1. A much larger normalized transverse emittance of the driver electron beam is also acceptable and will not affect the final positron yield significantly, if the spot size is the same. The target is placed inside a High-Temperature Superconducting (HTS) solenoid [3] and has a cylindrical shape with a radius of 15 mm and an optimized axial thickness of 15 mm for a maximum positron production rate. A HTS solenoid is used as the adiabatic matching device (AMD), providing an adiabatically decreasing magnetic fringe field for capturing positrons. The PSI Positron Production (P^3) experiment [4],

Table 1: Parameters of the Electron Driver Beam at the Target Assumed in the Simulation

Parameter	Unit	Value
Energy	GeV	2.86
Energy spread (σ_E/E)	%	0.5
Bunch length (σ_z)	mm	1
Normalized transverse emittance ($\epsilon^n_{x,y}$)	mm·mrad	4
Spot size ($\sigma_{x,y}$)	mm	1
Bunch charge	nC	5
Bunches per train		4
Bunch spacing	ns	25
Repetition rate	Hz	100

ISBN: 978-3-95450-275-2 ISSN: 2226-0366 doi: 10.18429/JACoW-LINAC2026-MOPO078

A COMPACT ELECTRON ACCELERATOR FOR MUON PRODUCTION

Z. J. Liptak*, M. Kuriki, L. Guo, Hiroshima University, Higashihiroshima, Japan

Abstract

Because muons possess high material penetration capabilities, they are an extremely effective tool for non-destructive testing of large-scale structures. While cosmic-ray muons have traditionally been used for imaging infrastructure such as bridges and tunnels, as well as the interiors of buildings, challenges have included long measurement times and limitations on installation locations. In this study we propose the design of a portable muon source and accelerator utilizing a superconducting microtron that can be mounted on a standard highway truck. In this presentation, we will detail the muon generation process, potential applications, key technologies required for implementation, and the technical challenges encountered during development. Through these discussions, we will present a novel concept for a compact accelerator with a view toward societal implementation.

INTRODUCTION

Muons are leptons which carry the same electric charge as electrons, but with approximately 200 times more mass and a short (2.2 μs) lifetime. They are well-known to have a high penetrating ability, making them ideal candidates for non-destructive imaging of large structures such as buildings [1].

While cosmic-ray muons are generated relatively consistently, the low rate ($\approx 1\,\mathrm{cm}^{-2}\,\mathrm{s}^{-1}$ at sea level) and fixed angular range of these muons makes them difficult to use outside of a narrow range of applications. To make more structures available to muon imaging, it would be desirable to have a source which can produce muons on demand and on location, and with controlled energies across a range of several GeVs to accommodate varying sizes of structures.

Accelerator-produced muons have been in use at several facilities around the globe [cite g-2, J-PARC muons] for several years. However, they have thus far made use of pre-existing accelerator facilities which generate muons by colliding a proton beam with a fixed carbon target. Such facilities are typically on the order of several hundred meters and notably stationary, rendering them unsuitable for imaging of building and infrastructure.

We have therefore begun to investigate the possiblity of creating a portable muon source which can be transported by a highway truck to locations of interest. The fixed maximum size of a highway truck provides limitations on the size of both the accelerator itself as well as the associated cryogenic equipment. To meet this challenge, we consider a compact electron racetrack microtron (RTM) with superconducting linear acclerators in both straight sections capable of accelerating electrons to a final energy sufficient to generate muons via the Δ resonance when incident on a fixed target.

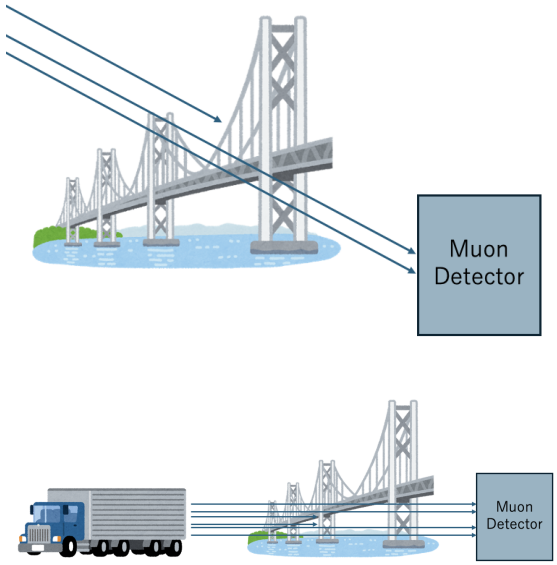


Figure 1: Top: An illustration of cosmic ray muon tomography. Cosmic ray muons passing through the structure to be examined are detected on the opposite side to form an image of the interior. The rate and angle of incoming muons cannot be controlled. Bottom: Accelerator-based muon tomography. The same principle is used to form an image, but the muon flux is greatly increased and the angle can be controlled by placement of the vehicle.

Figure 1 shows an illustration of cosmic ray-based versus portable accelerator-based muon tomography.

Usefulness to Society

The ability to non-destructively examine large structures has a great number of practical uses in society. In particular, we consider that much infrastructure, particularly in Japan, the United States, and Europe, was built in the post-WWII decades and is now approaching 70 years old, or in some cases more, as discussed in Ref. [2]. Bridges, tunnels, and other large civil engineering structures often hide signs of decay with no visible signs deterioration. If this decay progresses far enough, it can result in sudden and unexpected catastrophic collapse. However, checking for internal decay is time-consuming and costly. A portable muon beam capable of detecting signs of deterioration before they progress to catastrophic failure could thus potentially make non-invasive safety checks with minimal disruption to use, saving human lives as well as money and time.

MUON PRODUCTION

We consider the production of muons from the electron-proton Δ resonance. The threshold for the Δ resonance is

* zjl@hiroshima-u.ac.jp

Content from this work may be used under the terms of the CC BY 4.0 licence (© 2026). Any distribution of this work must maintain attribution to the author(s), title of the work, publisher, and DOI.

ISBN: 978-3-95450-275-2 ISSN: 2226-0366 doi: 10.18429/JACoW-LINAC2026-MOPO080

DEVELOPMENT OF PROTOTYPE RF ABSORBING LOAD FOR HIGH-POWER ACCELERATOR APPLICATIONS

KwangHoon Kim, Chang Ki Min, Dong-hyun Na, Yong-jung Park
Pohang Accelerator Laboratory (PAL), POSTECH, Pohang, Republic of Korea

Content from this work may be used under the terms of the CC BY 4.0 licence (© 2026). Any distribution of this work must maintain attribution to the author(s), title of the work, publisher, and DOI.

Abstract

A prototype RF absorbing load was developed at Pohang Accelerator Laboratory (PAL) to absorb multi-megawatt peak power and kilowatt-level average power in S-band accelerator systems. Conventional RF loads commonly employ silicon carbide (SiC) absorbers; however, this work adopts a Kanthal spray-coated aluminum structure to achieve effective RF absorption with improved thermal conduction and reduced fabrication cost. The load was designed for operation at 2.856 GHz with a peak power of 30 MW, pulse width of 1 μs, repetition rate of 120 Hz, and input VSWR below 1.1. The structure has an overall length of 1.1 m and consists of six wedge absorbers and two taper sections for efficient impedance matching and RF attenuation. Low-power RF measurements yielded a return loss of −46.53 dB and a transmission coefficient of −24.16 dB at 2856 MHz, demonstrating excellent impedance matching and RF attenuation performance. High-power tests were subsequently performed up to 32 MW at a repetition rate of 60 Hz. The experimental results demonstrate that the proposed load is a reliable and cost-effective alternative to conventional SiC RF loads for high-power S-band accelerator applications.

INTRODUCTION

High-power radio-frequency (RF) loads are key components in linear accelerator (LINAC) systems, where they absorb transmitted RF power and suppress reflections from accelerating structures, waveguide networks, and RF test stations. In facilities such as PAL-XFEL, RF loads must operate reliably under high peak power, repetitive pulsed operation, and ultra-high vacuum conditions while maintaining low reflection and stable thermal performance.

Conventional RF loads typically employ silicon carbide (SiC) absorbers because of their excellent microwave absorption and thermal properties [1]. However, their fabrication process is relatively complex and expensive. In the PAL-XFEL RF system, the cost of a SiC load is approximately four times higher than that of a Kanthal spray-coated load, motivating the development of a more economical alternative.

Kanthal, an Fe-Cr-Al alloy widely used in high-temperature applications, offers favorable electrical resistivity, oxidation resistance, and thermal durability. Combined with thermal spray technology, it can provide a practical and cost-effective RF absorbing surface.

In this study, a high-power S-band RF load based on a Kanthal spray-coated absorber was developed for the PAL-XFEL RF system. A two-step wedge taper structure was adopted to minimize RF reflections and distribute absorbed power along the load. The RF characteristics were evaluated through electromagnetic simulations, low-power RF measurements, and high-power testing at the PAL-XFEL Soft X-ray Modulator Test Facility (MTF).

RF LOAD DESIGN

A high-power RF load based on a Kanthal spray-coated absorber was developed for the PAL-XFEL S-band LINAC RF system. The load was designed to operate at 2856 MHz with a peak power of 30 MW, a pulse width of 1 μs, a repetition rate of 120 Hz, and an input VSWR below 1.1. The structure consists of an aluminum waveguide body coated with a 100 μm Kanthal layer and integrated cooling channels for efficient heat removal. Compared with conventional SiC absorbers, the proposed structure offers a simpler fabrication process and significantly reduced manufacturing cost. The overall mechanical configuration of the developed RF load is shown in Fig. 1.

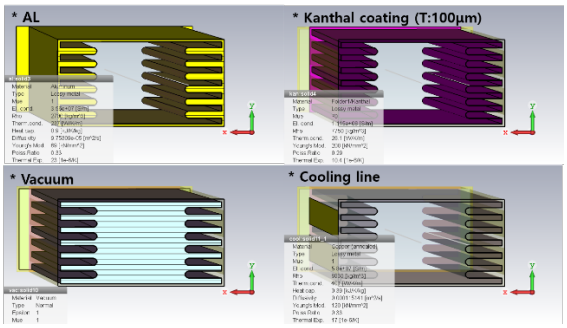


Figure 1: Mechanical configuration of the Kanthal spray-coated RF load.

To minimize RF reflections and distribute absorbed power along the propagation direction, a two-step wedge taper configuration was adopted. The absorber consists of two taper sections with lengths of 119.92 mm and 222.88 mm and six wedge absorbers with a thickness of 2.79 mm. The gradual impedance transition improves power absorption while suppressing localized field enhancement. The optimized two-step wedge taper geometry is illustrated in Fig. 2.

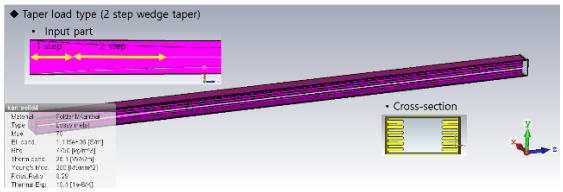


Figure 2: Cross-sectional view of the optimized two-step wedge taper absorber.

ISBN: 978-3-95450-275-2 ISSN: 2226-0366 doi: 10.18429/JACoW-LINAC2026-MOPO081

CONSIDERATION ON THE ASSEMBLY PROCESS OF PROTOTYPE ILC CRYOMODULE USING 3D CAD

T. Hara[1,*], K. Umemori[1], Y. Yamamoto[1,2], T. Dohmae[1,2], T. Yamada[1,2]
[1]High Energy accelerator Research Organization (KEK), Tsukuba, Japan
[2]The graduate University for Advanced Studies (SOKENDAI), Hayama, Japan

Abstract

A prototype ILC cryomodule (CM) is being manufactured at KEK. The CM consists of eight 9-cell superconducting cavities, magnetic shields, power couplers, frequency tuners, a single-layer thermal shield, cooling pipes and a superconducting magnet. The CM assembly procedure is complex due to the large number of components and strict spatial constraints. Therefore, careful assembly planning is essential before actual assembly work. A 3D CAD study was performed to visualize the assembly procedure and identify interference risks during assembly. The study revealed interference involving the gas return pipe (GRP) leg during cold mass assembly. To eliminate the interference, the dimensions of the GRP leg were modified in advance. In addition, a fit check was performed using mock-ups to evaluate assembly feasibility and tool accessibility. The results of fit check were fed back into the magnetic shield design, and the identified issues were resolved. These results contribute to reliable assembly planning of the prototype ILC CM.

INTRODUCTION

Under the MEXT Advanced Accelerator Element Technology Development (ATD) program, a prototype ILC cryomodule (CM) is being manufactured at KEK [1, 2]. The prototype ILC CM consists of the cold mass and the vacuum vessel covering the cold mass [3]. The cold mass consists of eight 9-cell cavities, a superconducting quadropole magnet (SCQ), a single-layer thermal shield, power couplers, a gas return pipe (GRP) and cooling pipes (Fig. 1), single-layer magnetic shield and a frequency tuner are installed on each cavity (Fig. 2).

The entire CM assembly process is carried out in the COI building at KEK. The assembly process is divided into several workstations, each dedicated to a specific assembly task.

Due to the large number of CM components and strict spatial constraints, the assembly process is complex and there is potential for component interference during assembly. In addition, assembly work is performed in a limited space. Therefore, careful assembly planning is essential.

To support assembly planning, a 3D CAD analysis was performed to visualize each assembly process, identify interference risks and develop an efficient assembly procedure. This paper reports the results of the assembly study and the measures taken to mitigate identified assembly issues.

* thara@post.kek.jp

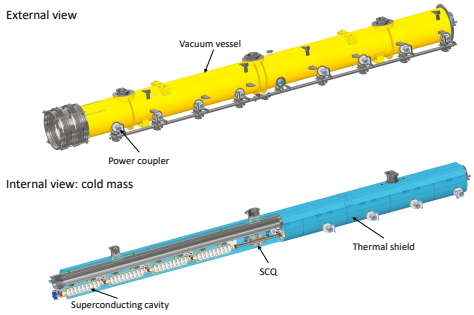


Figure 1: Overview of the prototype ILC cryomodule.

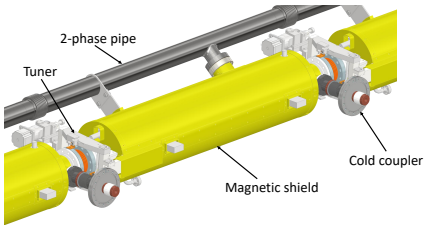


Figure 2: Cavity with a magnetic shield, cold coupler, tuner and 2-pahse pipe.

VISUALIZATION OF THE ASSEMBLY PROCEDURE USING 3D CAD

The assembly procedure was visualized and evaluated using 3D CAD.

Assembly Environment

The COI building contains workstations for each assembly step of the CM. The assembly process is divided into six workstations (WS1-WS6) (Fig. 3). Each workstation is assigned to a specific task.

WS1: Cavity String assembly

The cavity string is assembled in an ISO Class 4 cleanroom. At WS1, the cryogenic parts of the coupler (cold coupler) are attached to the cavities. Two gate valves are attached to both ends of the cavity string to seal and protect the cavity interior. In this CM, the SCQ magnet is installed at the center of the cavity string so a beam pipe is located at the center of the cavity string. After completion of the cavity string assembly, the cavity string is rolled out of the cleanroom and transferred to WS2.

Content from this work may be used under the terms of the CC BY 4.0 licence (© 2026). Any distribution of this work must maintain attribution to the author(s), title of the work, publisher, and DOI.

ISBN: 978-3-95450-275-2 ISSN: 2226-0366 doi: 10.18429/JACoW-LINAC2026-MOPO082

PERFORMANCE COMPARISON OF LaTeX PREPROCESSING METHODS AND EMBEDDING MODELS FOR RAG ON RAON CONTROL SYSTEM TECHNICAL NOTES*

Won Hee Min† [1,2], Jong-Ryul Lee[2], Hyun Man Jang[1]
[1] Institute for Rare Isotope Science, Institute for Basic Science (IBS), Daejeon, South Korea
[2]Chungnam National University, Daejeon, South Korea

Content from this work may be used under the terms of the CC BY 4.0 licence (© 2026). Any distribution of this work must maintain attribution to the author(s), title of the work, publisher, and DOI.

Abstract

RAON uses EPICS as the primary framework for integrating local control systems into the central control system. Technical notes for control system installation and management are documented in LaTeX format and managed with relevant code and files in a Git-based configuration management environment on an isolated internal network. As part of efforts to introduce AI technologies into the control infrastructure, this study examines the applicability of Retrieval-Augmented Generation (RAG) to control system technical documents.

LaTeX documents were converted into formats such as Markdown under multiple preprocessing scenarios with different document representations and chunk segmentation conditions. Different embedding models were ap-plied to construct vector databases. Relevant queries were designed, and performance was compared in terms of retrieval accuracy and contextual relevance. This study aims to evaluate the feasibility of applying RAG to EPICS technical documents and to suggest directions for building a retrieval framework for LaTeX-based docu-mentation. BGE-M3 with Structured LaTeX and heading-based chunking achieved the best retrieval performance, with an MRR of 0.647 and Hit@5 of 0.777.

INTRODUCTION

Technical documents for the RAON control system are managed in LaTeX format. LaTeX documents contain structural information such as sections, labels, and environments in addition to their textual content. How this structural information is preserved or transformed during preprocessing and chunking may affect the retrieval of relevant information. When applying Retrieval-Augmented Generation (RAG) [1], preprocessing methods, chunking strategies, and embedding model selection may affect retrieval performance. This study compares these factors to identify an appropriate retrieval configuration for LaTeX-based EPICS technical documents To examine the feasibility of applying RAG, retrieval effectiveness was evaluated based on the accuracy and relevance of the retrieved information.

* This work was supported by the Institute for Basic Science (IBS-I001-D1)
† alsdnjsgml@gmail.com

RAG RETRIEVAL CONFIGURATION AND EVALUATION

Experimental Environment

All evaluations were conducted in a Python-based environment, and Chroma was used as the vector database for storing and retrieving embedded document chunks. The dataset consisted of 129 LaTeX-based technical documents with a total size of approximately 3.09 MB.

Embedding Models

Three embedding models were selected to compare lightweight, English-oriented, and multilingual retrieval characteristics. MiniLM-L6-v2 [2] was used as a lightweight baseline, while BGE-base-en-v1.5 [3] was selected as an English-oriented retrieval model. BGE-M3 [4] was included as a multilingual model with a longer input length to examine retrieval performance for both English and Korean queries. The main characteristics of the models are summarized in Table 1.

Table 1: Characteristics of the Embedding Models Used in the Experiments

Model	Dim.	Input length (tokens)
all-MiniLM-L6-v2	384	256
BGE-base-en-v1.5	768	512
BGE-M3	1024	8192

Document Preprocessing and Chunking Strategies

Table 2 summarizes the document representation methods, while Table 3 presents the chunking strategies

Fixed-size chunking was applied to Original LaTeX, cleaned LaTeX, and plain text, while both fixed-size and heading-based chunking were applied to Markdown, HTML, and structured LaTeX. This resulted in nine pre-processing and chunking configurations, each of which was combined with three embedding models to compare retrieval performance across a total of 27 experimental configurations

Question Dataset

A total of 300 queries (150 English and 150 Korean) were constructed based on the contents of the technical documents for retrieval performance evaluation. The English and Korean queries were organized as semantically equivalent query pairs, enabling the observation of how retrieval performance changes with the query language for the same information

ISBN: 978-3-95450-275-2 ISSN: 2226-0366 doi: 10.18429/JACoW-LINAC2026-MOPO087

A COMPACT ELECTRON LINAC FOR THE X-RAY BASED INTRAOPERATIVE RADIOTHERAPY

Hanlin Wan, Yixing Lu*, Ping Wang†, Zihe Gao, Cheng Wang,
Jianhao Tan, Wencheng Fang, Zhentang Zhao
Shanghai Synchrotron Radiation Facility, Shanghai, China

Abstract

Intraoperative radiotherapy(IORT) is one of the important treatment modalities for cancer. To advance the development of X-ray IORT equipment technology, this paper presents a design study of a dedicated electron linear accelerating tube for X-ray IORT equipment. The accelerator adopts an X-band standing-wave accelerating structure with an operating frequency of 9.3 GHz, and consists of two cavities. There is no direct coupling between the two cavities. The RF power for each cavity is fed separately through a power divider and two input couplers. The total RF power required by the two cavities is within 20 kW, and the operating voltage is within 10 kV, which increases the safety and stability of the equipment. The electromagnetic simulation software CST was used for modeling, and the RF_Track software was employed for beam dynamics simulation. The final results show that the most probable energy of the electron beam at the accelerating tube exit is 50 keV, and the electron capture efficiency is 39.19%. This design achieves electron beam parameters that meet the requirements of X-ray IORT equipment under low-power and low-voltage conditions, verifying the feasibility of a compact X-band standing-wave accelerating tube scheme.

INTRODUCTION

Statistics released by the International Agency for Research on Cancer (IARC) and the American Cancer Society (ACS) indicate that in 2022, there were an estimated 20 million new cancer cases and 9.7 million cancer deaths worldwide [1, 2]. These data show that cancer has become one of the major global health challenges facing humanity. In clinical treatment principles, surgery holds the highest priority. However, during surgical procedures, incomplete local tumor resection or residual cancer cells in the tumor bed may lead to tumor recurrence [3]. To reduce the recurrence rate, the concept of IORT was introduced. IORT is defined as radiotherapy delivered during surgery, typically administered as a single high-dose irradiation to the tumor bed or unresectable residual lesions after tumor removal [4, 5]. IORT can be divided into electron-beam and X-ray types based on the type of radiation. X-ray IORT devices are compact, highly movable, and impose relatively lower requirements for radiation protection. To address the lack of X-ray IORT technology and considering equipment safety and stability, this paper proposes applying microwave method to the design of the accelerating tube in X-ray IORT devices. This approach can reduce the high voltage required by typical foreign devices from 50 kV to below 10 kV, thereby enhancing the overall safety and stability of the equipment.

* luyx@sari.ac.cn
† wangping@sari.ac.cn

LAYOUT

The output energy of the accelerating tube described in this paper is 50 keV. Given that there are many mature RF power source operating around 9.3 GHz, which facilitates selection, the X-band frequency of 9.3 GHz is adopted. The specific design targets of the electron linear accelerating tube for the X-ray IORT device are shown in Table 1.

Table 1: Design Targets

Parameter	Value
Frequency	9.3 GHz
Input Energy	8 keV
Output Energy	50 keV
Capture Efficiency	>30 %
Peak Current	40 μA
Pulse Length	4 μs
Repetition	100Hz

Figure 1 shows the overall 3D structure of the accelerating structure, which operates at 9.3 GHz. The entire accelerating structure consists of two cavities. The first cavity is used to accelerate electrons, and the second cavity is used to optimize the energy spectrum of the electron beam. RF power is supplied by a microwave power source and is fed into two cavities through a power divider and two input couplers. There is no direct coupling between the two cavities.

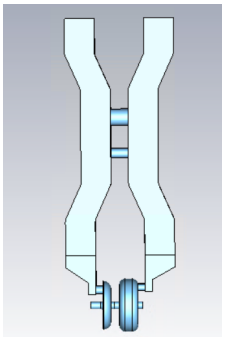


Figure 1: 3D structure of the accelerating structure.

RF DESIGN

The accelerating cavity adopts a nose-cone structure, which can reduce cavity losses [6]. CST software was used

Content from this work may be used under the terms of the CC BY 4.0 licence (© 2026). Any distribution of this work must maintain attribution to the author(s), title of the work, publisher, and DOI.

ISBN: 978-3-95450-275-2 ISSN: 2226-0366 doi: 10.18429/JACoW-LINAC2026-MOPO089

DESIGN STUDY OF A DUAL-MODE HIGH-POWER COAXIAL CAVITY

Jiayi Zhu[1,2,3,4], Yusen Guo[1,2,4*], Yixing Lu[1,2,4], Zongyang He[1,2,4], Chaopeng Wang[1,2,4]
Cheng Wang[1,2,4],Ping Wang[1,2,4†], Xiaobin Tang[3],Wencheng Fang[1,2,4], Zhentang Zhao[1,2,4]
[1]Shanghai Advanced Research Institute, Shanghai, China
[2]Shanghai Synchrotron Radiation Facility, Shanghai, China
[3]Nanjing University of Aeronautics and Astronautics, Nanjing, China
[4]Shanghai Key Laboratory of Particle Accelerator Science and Technology, Shanghai, China

Abstract

Accelerator technology has become increasingly essential in medical applications, particularly in particle therapy and radioisotope production. To address the growing demands for medical accelerators, the Shanghai Advanced Research Institute (SARI) is planning to construct two new facilities operating at 425 MHz and 714 MHz, respectively. This work presents a dual-mode coaxial cavity designed for power source acceptance testing of these two accelerators. The cavity operates at 425 MHz in the TEM mode and at 714 MHz in the TE_{110} mode. The design offers a compact and reliable solution for dual-frequency high-power load applications.

INTRODUCTION

In recent years, accelerator technology has become increasingly essential in the medical field, particularly for particle therapy and the production of medical radioisotopes. To address these growing demands, the Shanghai Advanced Research Institute (SARI) is planning to construct two new medical accelerators operating at 425 MHz and 714 MHz, respectively [1, 2]. This initiative aims to strengthen domestic capabilities in high-end medical equipment and to promote further advances in particle therapy and isotope production.

For a new accelerator, the RF power source must be qualified before the accelerating cavity is fabricated, since the cavity typically has a complex structure and a long manufacturing lead time. This qualification process requires a high-power load capable of emulating the impedance characteristics of the actual cavity. The acceptance specifications include a peak power of 1 MW and a duty factor of 0.1 %, corresponding to an average power of 1 kW.

Conventional high-power loads [3], nevertheless, present two major drawbacks in such applications. First, single-frequency loads are typically bulky, which increases system complexity and space requirements. Second, and more importantly, a single load supports only one operating frequency. When multiple frequencies are involved, multiple loads must be used, which complicates the test configuration and reduces overall system reliability. Broadband loads, while capable of covering a wide frequency range, generally suffer from degraded matching performance at specific frequencies and more complex thermal management, making them less suitable for high-power operation at discrete frequency points.

To overcome these limitations, this work proposes a compact dual-mode high-power coaxial cavity capable of working both at 425 MHz and 714 MHz simultaneously. The design features a shared resonant structure, a mode-separation tuner, a dual-frequency matching coupler, and an integrated cooling channel. The cavity supports TEM mode at 425 MHz and TE_{110} mode at 714 MHz. Simulation results indicate that the proposed coaxial cavity meets the requirements for high-power load applications in power source acceptance testing.

RF DESIGN

A coaxial cavity can be essentially treated as a transmission line resonator. For a coaxial line short-circuited at both ends, resonance occurs when the cavity length equals an integer multiple of half the guided wavelength, i.e., $L = n\lambda/2$ ($n = 1, 2, 3, \ldots$), where L is the cavity length, λ is the wavelength in the cavity, and n is the mode index. The resonant frequency is inversely proportional to L for a given mode. In this work, the cavity is defined by three geometric parameters: the inner conductor radius r_1, the outer conductor radius r_2, and the cavity length L. The design procedure begins by adjusting L to tune the fundamental TEM mode to 425 MHz (Fig. 1a). With the fundamental mode fixed, the higher-order TE_{110} mode is then tuned to 714 MHz by varying r_1 and r_2, with its two degenerate polarizations shown in Figs. 1b and 1c. Regarding material selection, initial electric field calculations using the E-solver indicate that copper would result in excessively high field strengths, making it unsuitable. In contrast, stainless steel and aluminum show acceptable field levels, and further analysis of these two candidates is presented later.

To feed microwave power into both modes, a coaxial coupler with three degrees of freedom — axial position, azimuthal angle, and probe insertion depth — is employed. Through iterative full-wave optimization, critical coupling is achieved at both frequencies simultaneously. The simulated return loss S_{11} reaches −30.69 dB at 425 MHz and −27.82 dB at 714 MHz, corresponding to VSWR of 1.06 and 1.08, respectively. However, the two degenerate TE_{110} modes couple with each other due to their close frequencies, causing one polarization to become overcoupled when the other is critically matched. A mode separation mechanism is therefore required.

* guoyusen@sari.ac.cn
† wangping@sari.ac.cn

Content from this work may be used under the terms of the CC BY 4.0 licence (© 2026). Any distribution of this work must maintain attribution to the author(s), title of the work, publisher, and DOI.

ISBN: 978-3-95450-275-2 ISSN: 2226-0366 doi: 10.18429/JACoW-LINAC2026-MOPO090

A VERSATILE LOW LEVEL RF CONTROLLER DESIGN FOR FRIB AND EXTENDED PROJECTS*

S. Zhao†, S. Kunjir, D. Morris
Facility for Rare Isotope Beams, Michigan State University, East Lansing, MI, USA

Abstract

The FRIB LLRF controller was developed as a flexible hardware platform for multiple cavity types operating at six RF frequencies from 40.25 to 322 MHz. Key choices—direct RF sampling, compatible footprints for frequency-dependent RF components, common PCB form factors, and spare RF, analog, and digital I/O—enabled reuse across diverse systems. The platform supports several tuner technologies, including stepper motor, piezoelectric, and pneumatic tuners. Integrated pneumatic valve control and monitoring proved valuable during commissioning and operations. As FRIB needs evolved, the controller accommodated unforeseen requirements, including bias-tee high-voltage supply control, serial links to tuner servo controllers, and cold cathode gauge monitoring for faster interlock response. More recently, it supported SLAC LCLS-II e-gun testing with piezo tuner control and is being evaluated for the K500 cyclotron RF control upgrade, which requires continuous coverage from 10 to 27 MHz. This paper shows how modular design, hardware margin, and tuner-control flexibility transformed a project-specific LLRF controller into a versatile platform for future accelerator RF applications.

INTRODUCTION

The low level radio frequency (LLRF) controller for the Facility for Rare Isotope Beams (FRIB) project was first designed in 2014. Nine prototypes were built in early 2015 which were used for firmware development and supported vertical test of the superconducting cavities, fundamental power coupler conditioning and cryomodule bunker tests. A second version design with some improvements was finalized in 2016 and became the production version of the FRIB LLRF controllers [1]. Mass production started in 2017 and close to 400 units were built.

The FRIB cavity types include multi-harmonic buncher (MHB), radio frequency quadrupole (RFQ), medium energy beam transport (MEBT) buncher, quarter wave resonator (QWR) and half wave resonator (HWR). The re-accelerator (ReA) multi-harmonic buncher (MHB) has three harmonic frequencies (F1, F2 and F3).

The detailed design was well documented in [1] and will not be repeated too much in this paper. In this paper we focus on how those design choices helped us navigate through some unforeseen requirements and how the LLRF was used for some other projects with minimum or no hardware modifications.

THE DESIGN

To accommodate the various FRIB cavity types with a common hardware platform, we considered minor variation of parts on the printed circuit board (PCB) with compatible footprints, modular PCBs with same electrical interfaces and mechanic form factors as well as spare analog and digital input/output (I/O) channels.

The RF Board

For the RF front end, the choice of direct sampling and synthesis of RF signals allowed us to eliminate the analog mixer, hence no temperature control is needed for the chassis to achieve high accuracy. Undersampling relaxes the requirement for the analog-to-digital converter (ADC).

The six supported RF frequencies are in harmonic relationships and can be sampled with the same ADC sampling rate. By simply changing the frequency of the digital mixing signal, the in-phase and quadrature (I/Q) components can be obtained. Note that non-IQ sampling is used to minimize the effect of waveform distortion.

For the RF output chain, an RF switch is used to select between two band-pass filter paths so that one RF board can support two frequencies (see Fig. 1), minimizing the number of RF board variations to three. The first variation (S01xxx) supports 80.5 MHz (HQ1157) and 322 MHz (HF1139); the second variation (S02xxx) supports 40.25 MHz (HF1139) and 120.75 MHz (HQ1157); the third variation (S03xxx) supports 161 MHz (HQ1157) and 240.5 MHz (HF1139). Commissioning therefore required a controller architecture that could preserve a common digital core while adapting the analog RF path and tuner interface to each application [2].

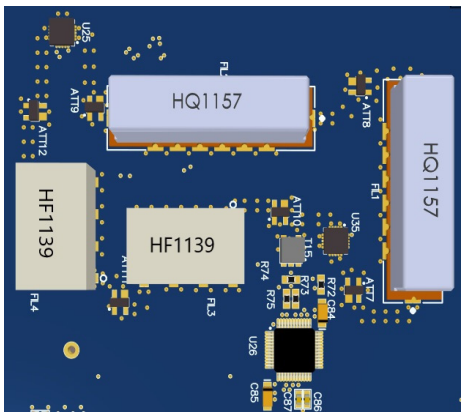


Figure 1: RF board output chain layout.

* Work supported by the U.S. Department of Energy Office of Science under Cooperative Agreement DE-SC0023633, the State of Michigan, and Michigan State University.
† zhaos@frib.msu.edu

Content from this work may be used under the terms of the CC BY 4.0 licence (© 2026). Any distribution of this work must maintain attribution to the author(s), title of the work, publisher, and DOI.

ISBN: 978-3-95450-275-2 ISSN: 2226-0366 doi: 10.18429/JACoW-LINAC2026-MOPO091

INTEGRATED MAGNET–CAVITY CO-DESIGN OF A COMPACT 2.45 GHz PERMANENT-MAGNET ECR SOURCE

Z. He[1], X. Huang[1], P. Wang[1], Y. Guo[1], Y. Lu[1], Z. Gao[1], W. Fang[1], Z. Zhao[2]
[1]Shanghai Synchrotron Radiation Facility, Shanghai, China
[2]Shanghai Advanced Research Institute, Shanghai, China

Content from this work may be used under the terms of the CC BY 4.0 licence (© 2026). Any distribution of this work must maintain attribution to the author(s), title of the work, publisher, and DOI.

Abstract

Permanent magnets can reduce the size and continuous electrical load of a compact electron cyclotron resonance (ECR) source, but their fixed field makes the magnetic topology inseparable from the microwave mode. We investigate a 2.45 GHz axial-mirror source by combining three-dimensional magnetostatic, driven-cavity, prescribed-plasma, and full-orbit electron calculations. Magnet–cavity coupling is quantified by the overlap between the ECR surface and the co-rotating microwave field and further assessed with the loaded RF field and paired electron trajectories. A two-solenoid field is calibrated to the same centre field and axial ECR crossings. Under a common driven field, the permanent-magnet case gives an ECR-surface mean co-rotating intensity of 1.526×10^{8} V^2 m^{-2} W^{-1}, 3.19 times the solenoid value. With the same stored loaded field, 8 W accepted power, and 200 paired electrons tracked for 50 ns, the wall-loss fractions are 7.0 % and 25.0 %, and the fractions ever exceeding the argon ionization threshold are 47.0 % and 44.5 %. The solenoid gives the larger median energy gain, whereas the permanent-magnet field gives the larger 90th percentile, revealing a heating–retention trade-off. The corresponding room-temperature solenoid winding estimate is 15.56 kW. The results show that matching only the axial ECR crossings is insufficient and support integrated magnet–cavity co-design for compact ECR source development.

INTRODUCTION

Electron cyclotron resonance ion sources (ECRISs) combine magnetic confinement with resonant microwave heating to maintain an ionizing electron population [1–3]. Their performance depends not only on the nominal resonance field but also on the magnetic topology, microwave-mode structure, and the trajectories by which electrons repeatedly cross the resonance region [4–6]. These dependencies become especially important when the source is made compact.

Permanent magnets remove coil supplies and cooling systems and have enabled small 2.45 GHz sources [7, 8]. Their field is fixed, however, and cannot compensate an unsuitable cavity mode during operation. Conversely, a microwave cavity designed independently of the magnets can place a strong field away from the electron cyclotron resonance (ECR) surface. Selected-mode cavities and frequency-tuning studies have shown that the plasma response is sensitive to field structure and coupling [9–11]. A compact permanent-magnet source should therefore be treated as a coupled magnet–cavity system rather than as a magnet placed around a pre-defined chamber.

This work combines vacuum overlap, loaded-field response, and electron dynamics in an axial-mirror geometry. A matched-crossing solenoid comparison isolates the effect of static-field topology and evaluates resonant heating, short-time retention, and magnetic-system power.

PHYSICAL AND NUMERICAL MODEL

Magnetic Configuration and Solenoid Comparison

The copper cavity has a radius of 90 mm and a length of 109.4 mm (Fig. 1(a)). Two axially magnetized N42SH annular magnets have outer and inner radii of 90 and 30 mm, a thickness of 19 mm, and an axial gap of 5 mm. These dimensions define the proposed permanent-magnet configuration.

For non-relativistic electrons, the resonance field is

$$B_{\mathrm{ECR}} = \frac{2\pi m_e f}{|e|} \simeq 87.523\,\mathrm{mT} \quad \text{at} \quad f = 2.45\,\mathrm{GHz}. \quad (1)$$

The three-dimensional permanent-magnet solution gives $B_0(0) = 80.432$ mT and axial ECR crossings near $z = \pm 49.2$ mm. The comparison uses two identical rectangular-section solenoid packs with inner and outer radii of 95 and 115 mm, an axial thickness of 20 mm, and centres at $z = \pm 73.697$ mm. Their current is calibrated in the three-dimensional finite-air-domain model, not by an on-axis thin-coil formula. Each coil requires 12.813 kA turn; the resulting centre field is 79.785 mT, and the axial ECR crossings are −49.314 and +49.200 mm.

Microwave Field and Overlap Metric

The cavity is fed through an alumina window by a 10 mm × 10 mm U-loop. For a cylindrical cavity, the ideal TE_{011} frequency is

$$f_{011} = \frac{c}{2\pi}\left[\left(\frac{x'_{01}}{R}\right)^2 + \left(\frac{\pi}{L}\right)^2\right]^{1/2}, \quad x'_{01} = 3.8317, \quad (2)$$

which gives 2.450 275 GHz for the present radius and length. Eigenfrequency and driven frequency-domain models use perfect-electric or copper-impedance boundaries as appropriate. With the engineering feed, the eigenfrequency becomes 2.450 630 GHz, with an azimuthal electric-field energy fraction of 0.966. The driven solution has its best match at 2.450 610 GHz, where $S_{11} = -25.679$ dB and 99.7295 W is accepted for 100 W incident power. The power closure is 99.9968 %; the resulting meridional vacuum field is shown in Fig. 1(c).

ISBN: 978-3-95450-275-2 ISSN: 2226-0366 doi: 10.18429/JACoW-LINAC2026-TU1A001

OPERATIONAL STATUS OF THE KOMAC 100 MeV PROTON LINAC AND PILOT R&D FOR THE 200 MeV UPGRADE*

Han-Sung Kim†
Korea Atomic Energy Research Institute, Gyeong-ju, Republic of Korea

Abstract

The Korea Multipurpose Accelerator Complex (KOMAC) has operated a 100-MeV proton linear accelerator (linac) since 2013, delivering proton beams to a wide range of research and industrial users through four beamlines. To further expand its capabilities, an energy upgrade of the existing linac to 200 MeV is under consideration. The proposed upgrade includes the construction of an additional 200-MeV linac section, two new beamlines with dedicated target rooms, expansion of the accelerator facility, and associated utility upgrades. The extended linac is designed based on a normal-conducting separated drift tube linac (SDTL) structure. Two beamlines downstream of the SDTL are planned to support applications such as space radiation effects and terrestrial radiation environment testing. In parallel with the conceptual design, pilot R&D activities are currently in progress to validate key technologies for the upgrade, including RF system performance, cavity fabrication, and beam dynamics optimization. This paper presents the current operational status of the KOMAC linac and outlines the upgrade plan together with the ongoing R&D efforts toward the 200-MeV extension.

INTRODUCTION

Korea Multi-purpose Accelerator Complex (KOMAC) is one of branches of Korea Atomic Energy Research Institute (KAERI). It was developed as part of the 21st century Frontier Project, and the facility was constructed between 2002 and 2012. The 100-MeV proton beam user service started in 2013. A 100-MeV proton linac is installed in the accelerator building. In addition to the linac, several low energy ion beam facilities, including a 250-kV gas ion implanter, a 150-kV metal ion implanter, 1.7 MV tandem accelerator, 1 MeV/u RFQ accelerator, are installed in the ion beam building for user service. Therefore, KOMAC can supply proton beams with energies from several tens keV up to 100 MeV to users.

Since its commissioning in 2013, the 100-MeV high-power proton linear accelerator (linac) at the Korea Multipurpose Accelerator Complex (KOMAC) has been operated continuously for more than a decade and has become an important user facility for accelerator-based research in Korea. The layout of the 100-MeV linac and beamlines is shown in Fig. 1. The linac consists of a 50-keV ion source, a 3-MeV radio-frequency quadrupole (RFQ), and a 100-MeV drift tube linac (DTL). It began operation in 2013 with two general-purpose beamlines (TR23 and TR103), providing beams up to 10 kW for applications in material, biological, and nuclear sciences. The RI production beamline (TR104), which started operation in 2016, is the highest-power beamline at KOMAC, with an approved beam power of 30 kW, and is primarily used for the production of radioisotopes such as ^{67}Cu and ^{82}Sr.

The low-flux beamline (TR102) has been in operation since 2018 and provides proton fluxes of 10^6–10^8 protons/cm^2·s over a 100 mm × 100 mm irradiation area with a uniformity of ≤10%. It is mainly used for space-radiation testing of spacecraft components, particularly semiconductor devices, and currently serves more than 60% of KOMAC users [1]. A neutron beamline began pilot operation in 2025, providing neutrons generated from the beam dump for terrestrial radiation testing of semiconductor memory devices. Based on its beam services for space and semiconductor applications, KOMAC is listed as a proton facility in JEDEC JESD89B [2]. Two additional beamlines, TR105 and TR104, are used for internal research. TR105 supports accelerator testing, while TR104 is also used to investigate RI beam production, including ^{8}Li RI beams using a target ion source.

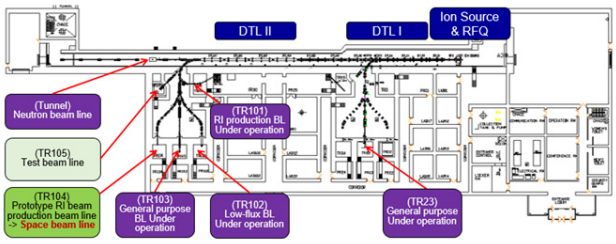


Figure 1: Layout of KOMAC 100 MeV linac facility.

OPERATIONAL STATUS

The KOMAC linac has accumulated more than 40,000 operating hours as of May 2026, as shown in Fig. 2. This is an important milestone because the machine has now been operating continuously for more than a decade. Another major change in KOMAC operation is the introduction of 24-hour beam service, which started in August 2024. This change was mainly driven by the increasing demand for beam time from users. However, this is not simply an extension of the operating time. During one day, we may need to change the proton beam energy, target room, beam condition, and user requirements several times (Fig. 3). This has increased the operational complexity and placed additional requirements on accelerator reliability and control.

* This work has been supported through KOMAC operation fund of Korea Atomic Energy Research Institute (No. 524320-26) and Pilot R&D for proton linac upgrade (NRF RS-2026-25583624) by the Ministry of Science and ICT (MSIT).
† kimhs@kaeri.re.kr

Content from this work may be used under the terms of the CC BY 4.0 licence (© 2026). Any distribution of this work must maintain attribution to the author(s), title of the work, publisher, and DOI.

ISBN: 978-3-95450-275-2 ISSN: 2226-0366 doi: 10.18429/JACoW-LINAC2026-TU1A002

PIP-II PROJECT PROGRESS AND CHALLENGES*

O. Napoly†
Fermi National Accelerator Laboratory, Batavia, IL, USA

Abstract

The Proton Improvement Plan-II (PIP-II) project is under construction to provide the Fermilab Accelerator Complex with a new H- superconducting radiofrequency (SRF) linac and beam transfer line delivering 800 MeV protons at Booster injection at double energy and double intensity (6.7×10^{12} protons per 20 Hz pulse) in comparison with the present Linac. The design goals of PIP-II Linac are described, including delivering 1.2 kW beam power on Long Baseline Neutrino Facility (LBNF) target, continuous wave (CW) operation compatibility and future upgrades. The progress of the Linac construction. Finally, the challenges of operating the SRF Linac to drive the Fermilab Booster are addressed.

PIP-II DESIGN GOALS

The Proton Improvement Plan-II (PIP-II) project [1] is an upgrade of the Fermilab accelerator complex whose main goals are to deliver 1.2 MW power on target from a beam of 120 GeV protons and to support the current 8 GeV program at Fermilab including the Mu2e and short baseline neutrinos experiments [2]. The LBNF beam line will extract protons from the Main Injector (MI) rapid cycling synchrotron (RCS) at 1.2 s cycle period which includes accumulation and storage of 12 8-GeV proton batches from Booster RCS cycled at 20 Hz in the Recycler Ring (RR) followed by transfer to MI and acceleration to 120 GeV. In parallel with the MI acceleration, another 12 Booster batches are distributed to various 8 GeV neutrino and muon experiments. Hence the total beam power delivered by the Booster will be in excess of 160 kW corresponding to 6.5×10^{12} protons per 20 Hz pulse. Reducing the MI acceleration time will provide a path to LBNF power up to 2 MW with the identical Booster batch input and dropping the proton yield to the 8 GeV physics program.

The main elements of this upgrade (Fig. 1) are an 800 MeV superconducting radiofrequency (SRF) linac, named Linac2, accelerating 6.7×10^{12} H- at 20 Hz repetition rate and a beam transfer line (BTL) delivering the H- beam to a new Booster injection region including an H- foil stripping system. The main parameters of the Linac2 are listed in Table 1. The maximum beam power at 800 MeV is 17.6 kW. This new facility will double the proton energy and intensity in comparison with the present 400 MeV H- Booster room-temperature injector, aiming at a yield of 3.3×10^{21} protons/year assuming 76% uptime (44 weeks at 90% reliability).

Table 1: Linac2 Main Parameters

Linac parameters	
Beam energy	800 MeV
Beam pulse length	550 µs
Repetition rate	20 Hz
Pulse average current	2 mA
Fundamental RF frequency	162.5 MHz
Cryogenic power	2.5 kW @ 2 K
Beam duty factor	1.1 %
RF duty factor	100 %
Linac/BTL length	267/308 m

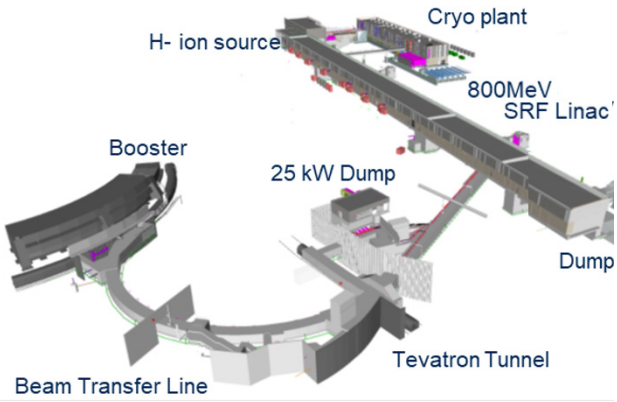


Figure 1: Schematic layout of PIP-II facility.

THE PIP-II FACILITY

The Warm Font End

The WFE starts with two 30 kV H- ion sources generating up to 15 mA current, followed by (Fig. 2):

- the low-energy beam transport (LEBT) section including a DC chopping system and a ±30° dipole which selects the beam from either of the two H- sources,
- a 4.43 m long radio-frequency quadrupole (RFQ) of 162.5 MHz RF frequency that brings the kinetic energy to 2.1 MeV, and
- a medium-energy beam transport (MEBT) section including 4 RF buncher cavities, a travelling-wave chopping system and a 21 kW-rated beam absorber.

The WFE is located in the injection high bay building (HBB) which includes all the WFE power supplies and utilities. However, the last WFE girder supporting two focusing triplets and the 4th RF buncher is in the linac tunnel with the upstream beam line traversing the HBB to tunnel concrete wall.

* This manuscript has been authored by Fermi Forward Discovery Group, LLC under Contract No. 89243024CSC000002 with the U.S. Department of Energy, Office of Science, Office of High Energy Physics.
†napoly@fnal.gov

Content from this work may be used under the terms of the CC BY 4.0 licence (© 2026). Any distribution of this work must maintain attribution to the author(s), title of the work, publisher, and DOI.

ISBN: 978-3-95450-275-2 ISSN: 2226-0366 doi: 10.18429/JACoW-LINAC2026-TU1A005

FIRST COBOTIC-ASSISTED STRING ASSEMBLY OF PIP-II SSR2 CAVITIES AT FERMILAB*

M. Parise†, T. Aiazzi, C. Narug
Fermi National Accelerator Laboratory, Batavia, IL, USA

Abstract

Achieving robotic-assisted string assembly has been a longstanding objective in superconducting cavity production to improve precision, repeatability, and throughput while reducing operator-dependent variability. At Fermilab, robotic systems have been successfully deployed for the installation of individual components on SSR2 cavities inside a cleanroom environment. The single-cavity installations validated the feasibility of robotic techniques and provided confidence to extend automation to the assembly of a full prototype cavity string. Leveraging lessons learned from earlier operations, the robotic system was adapted for the string assembly. This work describes the robotic-assisted assembly process in detail, including alignment strategies for coupler flanges, torque control for bellows connections, and mitigation of particulate generation in cleanroom conditions. Performance metrics of the cryomodule are presented, together with an analysis of improvements needed for robotic assembly. The effort also represents a broader R&D initiative at Fermilab to the long-term goal of scalable SRF cryomodule production.

INTRODUCTION

The Proton Improvement Plan-II (PIP-II [1]) project at Fermilab entails the procurement and assembly of a large number of superconducting radio-frequency (SRF) cryomodules. The spoke cavities section alone comprises of sixteen Single Spoke Resonator type 1 (SSR1) [2] and thirty-five Single Spoke Resonator type 2 (SSR2) [3-6] jacketed cavities, distributed over the two SSR1 [7] and seven SSR2 [8] cryomodules. Every cavity to be integrated into a cavity string along with superconducting magnets, Beam Position Monitors (BPMs), bellows and gate valves and each string shall be assembled without contaminating the beam volume.

SRF cavity strings are assembled in cleanrooms, generally of ISO class 4 or 5 according to ISO 14644-1 [9]. Microscopic particulate contamination on the interior surfaces of a cavity may trigger field emission, may cause local quenching and may degrade both the quality factor and the accelerating gradient. Each individual component is therefore wet-cleaned with specialized detergents in ultrasonic baths, the cavities receive high-pressure rinsing (HPR), the quality and the effectiveness of which can now be predicted by simulation before the process is executed in the cleanroom [10], and filtered air is pushed continuously from the ceiling towards the floor or the sides of the room, so that any particulate generated during the operations is swept away from the assembly area.

Since all parts are thoroughly cleaned before they enter the room, the operator becomes the predominant source of contamination during any cleanroom assembly. The skills and the experience of the cleanroom operators, along with the design of the tooling, are paramount for a successful string assembly [11, 12].

Manual tooling for cleanroom assembly is a double-edged sword. A typical device requires six degrees of freedoms (DOFs) to regulate the position of the component being installed and the operator is not the one holding the weight, as shown in Fig. 1. It must be flexible and generate the least possible amount of particulate and comply with cleanroom design principles, with sliding connections and threaded features placed at the bottom whenever possible, away from the assembly area. A six DOFs machine, however, is never truly particle-free, nor easy to use: it requires training, dry fits and mock-ups. Finally, as soon as the component is revised, slightly changed, or the next project starts, custom tooling machined from stainless steel and anodized aluminium becomes obsolete, and it is expensive.



Figure 1: Manual, tooling-assisted installation of a component onto an SRF cavity in the cleanroom.

THE ROAD TO THE FIRST ASSEMBLY

In late 2023 Fermilab procured its first collaborative robot, a Universal Robots UR16e [13], with the goal of developing cobotic applications for the cleanroom assembly of SRF components, specifically for PIP-II. The main characteristics of the arm are summarized in Table 1. Two additional cobots, one UR16e and one UR5e, have been procured since.

* This manuscript has been authored by Fermi Forward Discovery Group, LLC under Contract No. 89243024CSC000002 with the U.S. Department of Energy, Office of Science, Office of High Energy Physics.
† mparise@fnal.gov

Content from this work may be used under the terms of the CC BY 4.0 licence (© 2026). Any distribution of this work must maintain attribution to the author(s), title of the work, publisher, and DOI.

ISBN: 978-3-95450-275-2 ISSN: 2226-0366 doi: 10.18429/JACoW-LINAC2026-TU2A001

CHARGE SELECTOR CHALLENGES IN HIGH POWER HEAVY ION LINACS*

A. S. Plastun†, B. Abdelmegied, N. Bultman, S. Carter, S. Chrenka, F. Pereira de Figueiredo, E. Fletcher, T. Ginter, N. Jockheck, T. Kanemura, M. Larmann, M. LaVere, F. Marti, S. Miller, I. Nesterenko, P. N. Ostroumov, M. Patil, R. Quispe-Abad, D. Simon, E. Wakai, X. Wang, J. Wei, J. C. Zamora, L. Zampieri, Q. Zhao, Q. Zhong
Facility for Rare Isotope Beams, Michigan State University, East Lansing, MI, USA

Content from this work may be used under the terms of the CC BY 4.0 licence (© 2026). Any distribution of this work must maintain attribution to the author(s), title of the work, publisher, and DOI.

Abstract

Heavy ion linacs use charge stripping to increase accelerating efficiency. At FRIB, the charge selector intercepts unwanted charge states from their broad distribution produced by stripping at the energies of 17–20 MeV/u. The design of a movable collimator for high-power heavy ion beams is challenging due to high volumetric power deposition, radiation damage, radioactivation, and mechanical constraints. A uranium beam, for instance, produces an average power density on the charge selector that is orders of magnitude higher than that produced by proton beams, and the radiation damage rates that heavy ions produce reach several dpa/hour. This paper presents the design challenges and our experience in the development of the FRIB charge selector.

INTRODUCTION

The Facility for Rare Isotope Beams (FRIB) at Michigan State University is a U.S. Department of Energy Office of Science User Facility dedicated to studying the properties and fundamental interactions of rare isotopes, advancing nuclear astrophysics, and exploring applications in medicine, homeland security, and industry. FRIB produces radioactive isotopes in-flight through the fragmentation and fission of accelerated heavy ions on a graphite target.

Since the beginning of user operations in May 2022, the FRIB linac has successfully accelerated 20 different beam species, from oxygen through uranium, delivering more than 4000 operations hours annually with an availability exceeding 90%.

The FRIB driver accelerator is currently the world's highest-power heavy-ion linac, operating at 20 kW of continuous beam power on the production target. In October 2025, a 30-kW ^{238}U beam was delivered to the target. In the next several years the beam power is planned to further ramp up to 400 kW.

As a superconducting radio-frequency linac, FRIB can accelerate a broad range of heavy-ion species to energies above 200 MeV/u [1]. To utilize the accelerating voltage more efficiently and reduce construction and operation costs, heavy ion accelerators commonly employ charge stripping [2]. To strip high-power heavy-ion beams at the optimum energy of 17–20 MeV/u, FRIB designed and built a unique liquid-lithium charge stripper [3–5]. It addresses two major limitations of solid strippers, such as carbon foils: sublimation and radiation damage, while retaining the capability to produce high equilibrium charge states [2].

Stripping in a 1 mg/cm^2 liquid-lithium film increases the charge state of heavy ions by approximately a factor of two. However, regardless of the stripping medium, the stripped heavy-ion beams generally consist of more than one charge state, except for the low-Z species such as oxygen and neon.

Charge stripping is a complex charge-exchange process. The competition between electron-loss and electron-capture cross sections determines the mean charge state and the width of the distribution [6]. For high-Z beams, the envelope of the distribution is approximately Gaussian, with the highest fraction of one charge state of around 20 –- 30% (see Fig. 1).

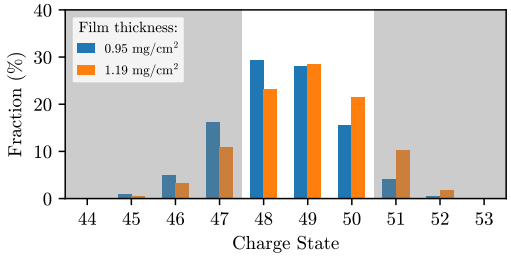


Figure 1: Measured charge state distributions in a stripped ^{124}Xe beam for two stripping film thicknesses. The gray area represents the charge selector jaws. Both distributions contain 73% of the incoming beam intensity.

Unlike cyclotrons, which are also widely used for isotope production, linear accelerators can accept and accelerate several charge states of stripped heavy-ion beams. At FRIB, the linac is designed to simultaneously accelerate multiple charge states [7].

The acceptable range of charge states, $\Delta Q/Q$, in the FRIB linac is about $\pm$3%. This range can accommodate, for example, five charge states of a ^{238}U beam, or three charge states of a ^{124}Xe beam. Multiple-charge-state acceleration enables more than 70% of the incoming beam intensity to be delivered to the target. We refer to this as the *stripping efficiency*. However, the remaining fraction, up to 30%, must be intercepted, in one or several charge states. The exact charge state distribution varies with the atomic number and kinetic energy of the ions, as well as with the stripper thickness. Figure 1 shows importance of selecting the appropriate thickness of the stripper. Although both cases provide a strip-

* This work is supported by the U.S. Department of Energy Office of Science under Cooperative Agreement No. DE-SC0023633, the State of Michigan, and Michigan State University.
† plastun@frib.msu.edu

ISBN: 978-3-95450-275-2 ISSN: 2226-0366 doi: 10.18429/JACoW-LINAC2026-TUPO001

BEAM COMMISSIONING OF THE LINEAR ACCELERATOR OF THE SKIF SYNCHROTRON RADIATION FACILITY*

M. V. Arsentyeva[1,2,3,†], D. A. Nikiforov,[1,2,3], A. E. Levichev[1,2,3], V. V. Fedorov[1,2,3], S. V. Reva[1,2], S. V. Sinyatkin[1], N. Abed[1,2], K. I. Smirnov[1], A. M. Barnyakov[1,2], A. M. Batrakov[1], D. I. Chekmenev[1], V. L. Dorokhov[1,2], L. B. Fomin[1], A. A. Kondakov[1], O. I. Meshkov[1,3], A. V. Pavlenko[1], O. A. Pavlov[1], I. L. Pivovarov[1], S. L. Samoilov[1], A. M. Semenov[1], K. A. Sibiryakova[1,2], A. V. Sudnik[2], A. V. Tur[1], I. V. Vizitiu[2], V. N. Volkov[1]
[1]Budker Institute of Nuclear Physics, Novosibirsk, Russia
[2]Synchrotron Radiation Facility "SKIF," Koltsovo, Russia
[3]Novosibirsk State University, Novosibirsk, Russia

Abstract

The linear accelerator (linac) for the injector of the synchrotron radiation facility SKIF (SRF SKIF) was successfully assembled and commissioned in Koltsovo. The linac consists of an electron source based on a thermionic radiofrequency (RF) gun, a bunching section, and five regular disk-loaded waveguide accelerating structures. Three 50 MW klystrons operating at 2856 MHz supply the RF power. During initial commissioning, the design beam energy of 200 MeV was successfully achieved. Transverse beam dynamics tuning using 14 dipole correctors reduced the orbit deviations to an RMS value of 0.5 mm. Measured normalized emittances and an energy spread of less than 1% satisfy the requirements for efficient injection into the booster synchrotron.

INTRODUCTION

The Siberian Circular Photon Source (SRF SKIF) is a flagship fourth-generation synchrotron radiation facility [1]. The general layout of the accelerator complex, comprising the linear accelerator, the booster synchrotron, and the main storage ring, is presented in Fig. 1.

The 200 MeV linear accelerator [2] serves as the initial stage of the injection complex, shaping the foundational electron beam quality. Precise optimization of both longitudinal and transverse beam parameters is a prerequisite for effective injection into the 3 GeV booster synchrotron, which was successfully commissioned and put into routine operation more than a year ago. Initial concepts and hardware configurations were validated at the Budker Institute of Nuclear Physics (BINP SB RAS) on the Linac-20 test facility [3].

At the end of 2024, the equipment was relocated to the permanent injector building in Koltsovo, where full assembly to the Linac-200 configuration was completed. This paper presents the launching workflow of the SKIF injector linac, including RF system parameters, beam dynamics tuning, and the final parameter configuration that enabled successful booster integration.

* Work partially supported by the Ministry of Science and Higher Education of the Russian Federation within the governmental order for SRF SKIF Boreskov Institute of Catalysis (project FWUR-2025-0004).
† M.V.Arsentyeva@inp.nsk.su

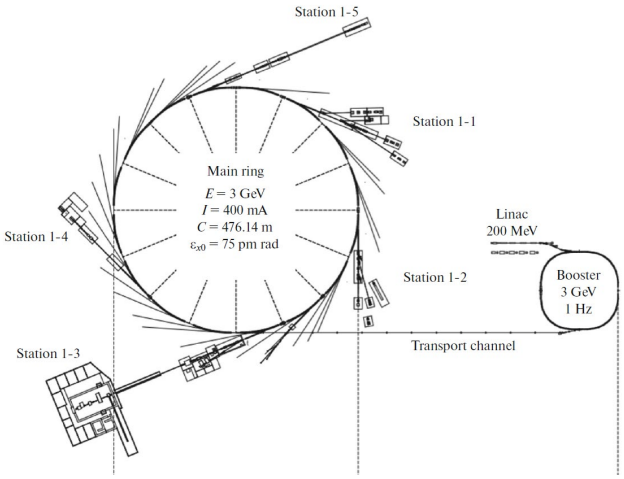


Figure 1: General layout and scheme of the SRF SKIF accelerator complex.

LINAC PARAMETERS

The injection system layout (Fig. 2) includes an RF gun operating at 178.5 MHz with a thermionic gridded cathode. Longitudinal bunching is achieved via a third-harmonic cavity operating at 535.5 MHz [4,5]. Main acceleration happens in five constant-impedance disk-loaded waveguide (DLW) structures operating at 2856 MHz [6], featuring 85 cells per structure and an individual length of 2.93 m.

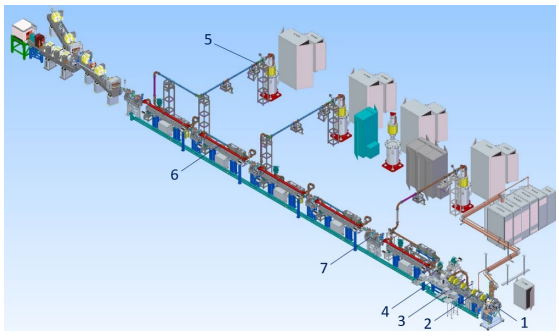


Figure 2: 3D model of the linear accelerator with the transport channel to the booster synchrotron: 1 – RF gun, 2 – third harmonic buncher, 3 – solenoids, 4 – preaccelerator, 5 – klystron, 6 – regular accelerating structures, 7 – quadrupole lenses.

Content from this work may be used under the terms of the CC BY 4.0 licence (© 2026). Any distribution of this work must maintain attribution to the author(s), title of the work, publisher, and DOI.

ISBN: 978-3-95450-275-2 ISSN: 2226-0366 doi: 10.18429/JACoW-LINAC2026-TUPO005

INTRABEAM SCATTERING STUDIES IN FREE ELECTRON LASERS WITH RF-TRACK

P. Desiré*,[1,2], A. Latina[1], A. Malyzhenkov[1,3], A. Gerbershagen[2]
[1]CERN, Geneva, Switzerland
[2]University of Groningen, Groningen, Netherlands
[3]Swiss International Institute, Lausanne, Switzerland

Abstract

Intrabeam Scattering (IBS) has recently been recognized as a limiting factor for free electron laser (FEL) performance, making it a critical concern for the linear accelerator community. There is a growing need for accurate numerical tools to compute IBS and integrate it with other collective effects, as most previous studies assumed Gaussian beams, which are not representative of FEL conditions. In response, the tracking code RF-Track has been enhanced with a novel kinetic-hybrid Monte Carlo algorithm for IBS calculations. This contribution reports on IBS studies for several FELs, including SwissFEL at PSI and FERMI at Elettra. For SwissFEL, simulation results are benchmarked against experimental measurements.

INTRODUCTION

Recent studies have established Intrabeam Scattering (IBS) as a significant source of Slice Energy Spread (SES) growth in high-brightness free-electron laser (FEL) beams. Since the SES directly affects FEL gain and performance, accurately predicting IBS has become increasingly important for the design and optimization of modern FEL facilities.

The first direct evidence of IBS in a LINAC was reported at the FERMI FEL, where the measured energy spread could only be reproduced by extending the microbunching instability model to include IBS [1]. Later studies at SwissFEL [2, 3], the European XFEL [4], DESY Zeuthen [5], and more recently SHINE [6] have confirmed that IBS is a major contributor to the SES observed in modern FEL injectors and LINACs. More recently, semi-analytical studies benchmarked against FERMI measurements have refined the theoretical description of IBS in microbunching instability [7, 8]. In parallel, independent analytical and Monte Carlo approaches have successfully reproduced SES measurements at SwissFEL [9].

In FEL injectors, beam quality is determined by the interplay of IBS with other collective effects, particularly Space-Charge (SC) at low energies, as well as wakefields and beam loading. Therefore, accurate start-to-end simulations require a self-consistent framework capable of treating these effects simultaneously.

RF-Track [10] is a freely available tracking code for accelerator simulations, including SC, wakefields, beam loading, and photocathode emission. A hybrid Monte Carlo implementation of IBS, was recently developed within RF-Track [11] and subsequently benchmarked against semi-analytical and kinetic IBS models [12]. This model is particularly well suited to the strongly non-Gaussian beam distributions encountered in FEL injectors as it does not rely on Gaussian beam assumptions. The implementation has since been used for IBS studies of the SHINE injector and superconducting LINAC [6], and has also been employed to investigate the combined effects of IBS and SC in the Muon Collider cooling channel [13].

In this contribution, the RF-Track IBS model is applied to SwissFEL and benchmarked against recent numerical simulations and experimental measurements. Simulations including both IBS and SC are presented, together with a parameter scan of the SwissFEL injector to assess the sensitivity of the SES to selected beam and machine parameters. Finally, a preliminary study of the FERMI photogun investigates the dependence of IBS-induced SES growth on the initial beam parameters.

SwissFEL INJECTOR

The SwissFEL injector provides one of the most comprehensive benchmarks currently available for IBS in high-brightness electron injectors. The study reported in Ref. [9] combines experimental measurements with predictions from the Monte Carlo tracking code REPTIL and a dedicated analytical formulation, providing a strong validation dataset for numerical IBS implementations.

Experimental Setup

The experimental setup is shown in Fig. 1, with more information available in the cited references. The initial beam distribution is defined by the parameters listed in Table 1. The beam is initialized with a uniform radial distribution in the transverse plane, a Gaussian longitudinal profile, and an isotropic longitudinal momentum distribution.

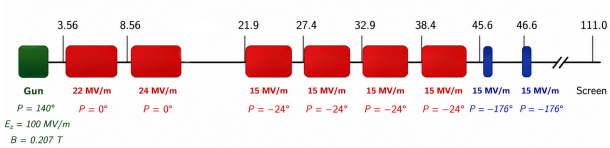


Figure 1: Experimental layout of SwissFEL, composed of a gun (green), six Sband structures (red) and two Xband structures (blue), further described in Refs. [2, 9, 14].

In Ref. [9], a charge scan was performed considering bunch charges of 1, 10, 28, 97, and 198 pC. All of the cases

* pdesirev@cern.ch

Content from this work may be used under the terms of the CC BY 4.0 licence (© 2026). Any distribution of this work must maintain attribution to the author(s), title of the work, publisher, and DOI.

ISBN: 978-3-95450-275-2 ISSN: 2226-0366 doi: 10.18429/JACoW-LINAC2026-TUPO007

THE HIGH BRILLIANCE NEUTRON SOURCE (HBS-I)

H. Podlech*[,1,2], M. Droba[1], T. Gutberlet[3], M. Händler[1], K. Kümpel[1], S. Lamprecht[1], A. Lehrach[3], O. Meusel[1], U. Rücker[3], J. Storch[1], J. Voigt[3], S. Wagner-Rossel[1], P. Zakalek[3], C. Zhang[1,2,4]
[1]Institute of Applied Physics (IAP), Frankfurt, Germany
[2]Helmholtz Research Academy Hesse for Fair (HFHF), GSI Helmholtzzentrum für Schwerionenforschung, Campus Frankfurt, Frankfurt, Germany
[3]Forschungszentrum Jülich, Jülich, Germany
[4]GSI Helmholtzzentrum für Schwerionenforschung, Darmstadt, Germany

Abstract

Neutrons are an essential tool for studying the structure and dynamics of matter. The High Brilliance Neutron Source (HBS) project aims to develop a scalable Compact Accelerator-driven Neutron Source that will enable neutron fluxes at the corresponding instruments comparable to existing fission-based or spallation neutron sources. After positive project evaluation in 2025, the German Science Council recommends strongly the construction of the first project stage (HBS-I). HBS-I uses pulsed 100 mA high-current proton beams to generate neutrons through a low-energy nuclear reaction at 20 MeV. The HBS-I Linac consists of a proton source, a 4-solenoid LEBT with chopper, two 4-Rod RFQ accelerators and a chain of room temperature CH-cavities operated at 176 MHz. The maximum RF duty factor is 25 %, resulting in a thermal load of up to 30 kW/m. The technology of this Linac is derived from the cw operated MYRRHA injector. The paper describes the status of the HBS-I proton Linac.

INTRODUCTION

Due to the shutdown of research reactors, there has been a severe shortage of neutrons for some time. Compact accelerator-based neutron sources offer the possibility of filling this gap using high-current proton beams and flexible pulse schemes. In this process, protons with energies of up to several tens of MeV hit specific target materials such as beryllium, vanadium, or tantalum, depending on energy. With a beam current of 100 mA, the High Brilliance Neutron Source first project stage (HBS-I) Linac clearly belongs to the new class of compact High Current Accelerator-based Neutron Sources (HiCANS) [1].

The design philosophy behind the HBS linac was driven by the goals of achieving the highest possible efficiency, high reliability and availability, and risk minimization. To meet these criteria while ensuring rapid implementation, proven state-of-the-art technology was utilized in the selection of components. For this reason, the HBS-I linac was derived from the cw operated 17 MeV MYRRHA injector [2]. An important aspect regarding reliability is the RF system. At HBS, only solid-state power amplifiers with sufficient power reserve are used. A total of 20 amplifiers with power ratings ranging from 50 to 600 kW are planned. The HBS-I

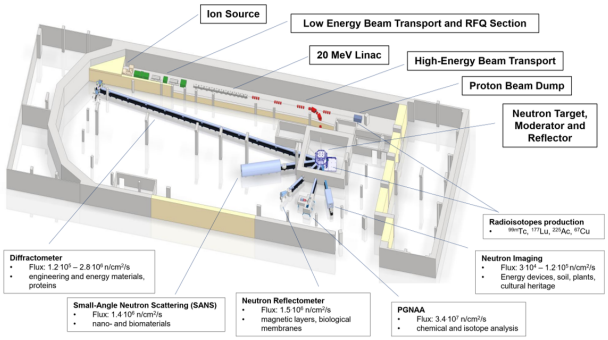


Figure 1: Planned layout of the HBS-I facility inside the former COSY hall, showing the 20 MeV Linac, the HEBT system, proton beam dump, neutron target–moderator–reflector assembly, neutron instruments, and medical radioisotope production stations. The figure also indicates the expected neutron fluxes at the instruments and their corresponding application areas [3].

Linac can provide a flexible pulse scheme depending on the requirements of the experiments. Using the maximum pulse length of 2 ms, it is also possible to produce radio-isotopes. Table 1 summarizes the parameters of the Linac and Fig. 1 shows the planned layout of the HBS-I facility at Research Center Jülich.

Table 1: Parameters of the HBS-I Linac

Parameter	Value	Unit
Accelerator type	RF Linac	–
Particles	Protons	–
Energy	20(30)	MeV
Beam current	100	mA
Frequency	176.1	MHz
Peak beam power	2(3)	MW
Maximum duty factor	25	%
Maximum average beam power	500 (750)	kW
Pulse length	208 & 833	µs

DESIGN OF THE HBS-I LINAC

Early in the development of the HBS linac, the decision was made to use normal-conducting rather than superconducting technology. The high beam current dominates the RF power, and no additional infrastructure—such as cryogenic systems, cryogenic modules, or a clean room—is re-

* h.podlech@iap.uni-frankfurt.de

Content from this work may be used under the terms of the CC BY 4.0 licence (© 2026). Any distribution of this work must maintain attribution to the author(s), title of the work, publisher, and DOI.

ISBN: 978-3-95450-275-2 ISSN: 2226-0366 doi: 10.18429/JACoW-LINAC2026-TUPO008

GENERATION AND APPLICATION OF STRIPPED PROTON BEAMS AT THE CSNS LINAC

Z. P. Li*, Y. Yuan, Y. L. Han, J. Peng
Institute of High Energy Physics, Chinese Academy of Sciences, Beijing, China
Spallation Neutron Source Science Center, Dongguan, China

Abstract

The CSNS linac delivers a primary H^- beam to the rapid cycling synchrotron (RCS), while stripped proton beams are also produced during beam transport. Protons generated naturally by residual-gas stripping are extracted to the Associated Proton beam Experiment Platform (APEP) and used for low-intensity irradiation of devices and materials. Controlled carbon-foil stripping in the LRBT removes peripheral high-emittance particles, reducing transport and RCS injection losses and enlarging the available painting range. The separated foil-stripped proton beam can reach much higher intensity and is being developed for applications including medical-isotope production. In addition, a preliminary study of intra-beam stripping (IBSt) is presented specifically for the higher-current, higher-energy CSNS-II linac. These studies illustrate how stripping processes can be treated not only as beam-loss sources, but also as tools for beam optimization and secondary-proton-beam applications.

INTRODUCTION

H^- stripping is usually considered an unwanted loss mechanism in high-power linacs, but at CSNS the stripped particles can also provide useful secondary proton beams. The present linac accelerates H^- to 80 MeV for injection into the RCS. In CSNS-II, a superconducting linac will extend the energy to about 300 MeV, while the design peak current is increased to 50 mA [1, 2]. The higher intensity and energy make both peripheral-particle control and stripping-related beam loss more important.

Three stripping processes play different roles. Residual-gas stripping naturally produces a low-current associated proton beam that can be extracted for applications. Intentional foil stripping converts selected peripheral H^- particles into a controllable proton beam while improving the phase-space distribution delivered to the RCS. Intra-beam stripping (IBSt), in contrast, is an unavoidable intensity-dependent process and is considered here as a potential beam-loss source for CSNS-II. The following sections discuss the generation and application of these three stripped-proton components, with emphasis on the foil-stripping system developed and tested in the LRBT [2].

RESIDUAL-GAS STRIPPING AND APEP

During H^- transport, collisions with residual gas produce H^0 and H^+. At CSNS, part of the associated H^+ beam is captured by the RFQ and DTL and accelerated to the linac output. Because H^+ and H^- have opposite charge, the switching magnet (LRSW) at the linac end separates the charge states: H^- is directed toward the RCS, H^0 continues toward a dump, and H^+ can be transported to APEP [3], as illustrated in Fig. 1.

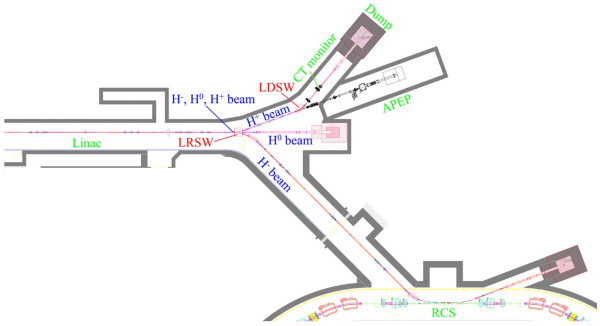


Figure 1: Layout at the end of the CSNS linac showing separation of H^-, H^0, and naturally stripped H^+ toward the RCS, dump, and APEP, respectively.

The naturally associated proton current is of order 10^{-3} of the primary H^- beam. At 100 kW CSNS operation, the APEP design value is about 10 μA peak current, with the same macropulse structure as the linac beam [3]. Although the conversion fraction is small, this beam is produced parasitically during normal H^- acceleration and therefore provides proton pulses without an independent proton injector.

APEP was developed to use this otherwise unwanted charge-state component for irradiation applications. Its 80 MeV proton beam has been used for device and material irradiation and radiation-effect studies, for which a stable and well-characterized proton fluence is required [3]. The microampere-level current therefore also motivated the development of a dedicated low-intensity current transformer; beam measurements showed good agreement with a Faraday cup [4]. In this sense, residual-gas stripping provides the first practical example at CSNS of converting a parasitic stripping product into a useful secondary beam.

FOIL STRIPPING FOR TRANSVERSE COLLIMATION AND PROTON APPLICATIONS

Operational beam-loss studies at the CSNS linac identified mismatch-generated transverse halo as an important source of beam loss [5]. Large-amplitude particles are especially vulnerable in the LRBT and RCS injection region, where the available aperture becomes more restrictive. The foil collimation system was therefore originally introduced for halo control. In practical operation, however, the foil positions

* lizp@ihep.ac.cn

Content from this work may be used under the terms of the CC BY 4.0 licence (© 2026). Any distribution of this work must maintain attribution to the author(s), title of the work, publisher, and DOI.

ISBN: 978-3-95450-275-2 ISSN: 2226-0366 doi: 10.18429/JACoW-LINAC2026-TUPO010

RF DESIGN OF A SPHERICAL-CAVITY-TYPE PULSE COMPRESSOR FOR MUON LINAC

Y. Nakazawa*[1], H. Ego[1], Y. Kondo[2], M. Otani[1], K. Sumi[1], Y. Takeuchi[3]
[1]High Energy Accelerator Research Organization (KEK), Tsukuba, Japan
[2]Japan Atomic Energy Agency (JAEA), Tokai, Japan
[3]Nagoya University, Nagoya, Japan

Abstract

The development of a muon-dedicated traveling-wave disk-loaded structure (DLS) is in progress at the Japan Proton Accelerator Research Complex (J-PARC). Cooling and subsequently accelerating ultraslow muons to relativistic energies enables a low-emittance beam with enhanced penetration capability, opening new opportunities in precision particle physics experiments and muon imaging. However, unlike electrons, muons undergo substantial velocity changes during acceleration, requiring precise phase synchronization between the beam and radio-frequency (RF) fields. This requirement becomes more critical when using pulse-compressed RF power with temporal variation. In this work, we present the RF design of a spherical-cavity-type pulse compressor (SCPC) for a DLS. Two degenerate TE_{112} modes with a 90-degree phase difference are utilized at 2592 MHz. The RF performance was optimized using 3D electromagnetic simulations to achieve the target frequency characteristics and controlled mode degeneracy.

INTRODUCTION

The muon linac for the muon g−2/electric dipole moment (EDM) experiment at the Japan Proton Accelerator Research Complex (J-PARC) [1] employs a 2592 MHz disk-loaded structure (DLS) in its high-β section. To obtain the required peak power with a single klystron, a radio-frequency (RF) pulse compressor provides a practical solution, and we are developing a spherical-cavity-type pulse compressor (SCPC) [2, 3] at 2592 MHz. The SCPC consists of only a single spherical cavity and a polarizer acting as a mode converter, far more compact than the conventional two-cavity SLED [4]. At KEK, a 2856 MHz SCPC was designed and fabricated for the SuperKEKB injector and has been demonstrated up to high-power operation [5–9].

The SCPC stores RF energy in the two degenerate, mutually orthogonal TE_{112} modes of the spherical cavity, excited in quadrature to form a circularly polarized field. The wave emitted back from the cavity returns with the opposite handedness with respect to its propagation direction, and the polarizer routes it to the opposite rectangular port: input and output are separated without a circulator. The target parameters are an operating frequency of 2592 MHz defined at 30 °C in vacuum, an input of 40 MW with a pulse width of 4 µs at 25 Hz, and a coupling coefficient β of 6.4, the proven value of the KEK 2856 MHz SCPC [5], which corresponds to a peak power gain of about 6 and an average gain of about 4 over the useful interval of about 0.5 µs, set by the filling time of the DLS [1]. The average gain of 4 is required because the high-β section contains four DLS tanks [1] which are to be driven by a single klystron. The transient analysis related to the phase synchronization between the beam and the pulse-compressed RF field is studied in Ref. [10].

To our knowledge, no 2592 MHz SCPC has been reported. We therefore built a fully parametric CST model of the entire structure, validated the analysis procedure by reproducing the KEK 2856 MHz SCPC design, and then fixed the 2592 MHz design reported here.

RF DESIGN

The analysis uses the frequency-domain solver of CST Studio Suite [11]. Figure 1 shows the three-dimensional model in CST. The SCPC consists of two components, the polarizer and the spherical cavity. Each component is first designed stand-alone, and their combination is verified in the RESULTS section.

The polarizer geometry and its main dimensions are shown in Fig. 2. The rectangular waveguide is standard WR284. The design proceeds in two steps. First, all dimensions of the 2856 MHz design are scaled by 2856/2592; by scale invariance the matching is preserved exactly, with an S11 of −103 dB at 2592 MHz. Second, the rectangular waveguide is restored to the standard WR284 size, which shifts the frequency of the matching minimum by about +30 MHz and degrades S11/S21 to the −20 dB level because of the modified guide wavelength.

The detuning is recovered by re-optimizing the polarizer around the scaled geometry. The S-parameter minima are

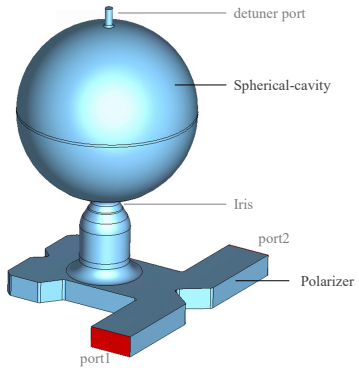


Figure 1: CST model of the spherical-cavity-type pulse compressor. The blue blocks define the vacuum region.

* yuga.nakazawa@kek.jp

Content from this work may be used under the terms of the CC BY 4.0 licence (© 2026). Any distribution of this work must maintain attribution to the author(s), title of the work, publisher, and DOI.

ISBN: 978-3-95450-275-2 ISSN: 2226-0366 doi: 10.18429/JACoW-LINAC2026-TUPO011

COMPARATIVE STUDY OF VIRTUAL PEPPER-POT AND DIFFERENTIAL VIRTUAL PEPPER-POT METHODS FOR 4D TRANSVERSE PHASE SPACE RECONSTRUCTION OF SMALL BEAMS

J. Choi[1], B. Shin[2], C.-K. Sung[2], E. Cosgun[3], M. Chung*[1]
[1]Pohang University of Science and Technology, Pohang, South Korea
[2]Pohang Accelerator Laboratory, Pohang, South Korea
[3]High Energy Accelerator Research Organization, Tsukuba, Japan

Abstract

Precise 4-dimensional (4D) transverse phase space characterization is essential for fully understanding and controlling coupled beam dynamics and beam quality. The Virtual Pepper-Pot (VPP) method has been proposed to reconstruct the 4D transverse beam phase space, including transverse coupling information, from slit-based measurements. However, the finite slit width imposes intrinsic limitations on reconstruction accuracy by introducing geometric angular spread and limiting the ability to resolve small beam sizes. To overcome these limitations, a differential slit method named the Differential Virtual Pepper-Pot (DVPP) has been proposed. In this study, we investigate the performance of the DVPP method in comparison with the conventional VPP under identical conditions for the small electron beam expected at PAL-eLABs. Their ability to recover transverse coupling information is evaluated for cases ranging from weak to strong coupling.

INTRODUCTION

Accurate characterization of the four-dimensional (4D) transverse phase space is important for understanding coupled beam dynamics. Conventional slit-scan measurements provide the projected transverse phase spaces, but do not directly resolve the interplane correlations required for a complete 4D characterization. The Virtual Pepper-Pot (VPP) method was proposed at PITZ to reconstruct the 4D transverse phase space from horizontal and vertical slit-scan measurements and was demonstrated using experimental data [1]. The VPP method has also been experimentally applied to proton-beam diagnostics at the KOMAC Beam Test Stand [2].

To apply the VPP method at PAL-eLABs, an L-shaped slit scanner was developed to acquire horizontal and vertical slit-scan images with a single-axis motion. As a slit-based technique, however, the spatial resolution of VPP is inherently limited by the finite slit width. Differential slit image processing was introduced to generate virtually narrower slit images and reduce this finite-slit-width limitation. A previous simulation study demonstrated improved emittance reconstruction accuracy using this approach for a 70-MeV electron beam at PAL-eLABs [3].

In this work, we compare the VPP and Differential Virtual Pepper-Pot (DVPP) methods for application to the low-energy Gun1 beam used for Ultrafast Electron Diffraction (UED) at PAL-eLABs. Their 4D reconstruction performance is evaluated using beam distributions with different transverse coupling strengths.

PAL-ELABS AND VPP/DVPP METHODS

The PAL-eLABs facility consists of two sections, Gun1 and Gun2. The 70-MeV beam condition considered in the previous DVPP study corresponds to the Gun2 section [3]. The present study focuses on the low-energy Gun1 section, which is used for UED experiments and provides 3–5 MeV electron beams with bunch charges below 1 pC.

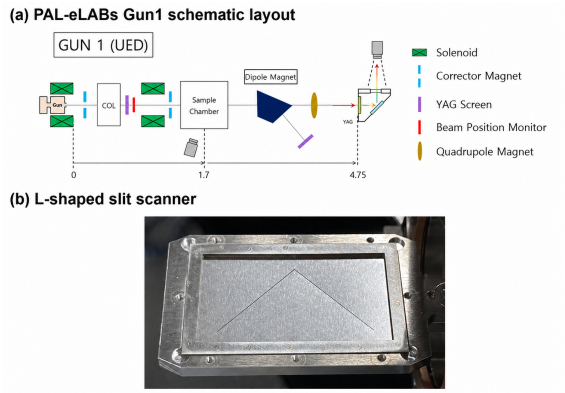


Figure 1: Schematic layout of the PAL-eLABs Gun1 section and the L-shaped slit scanner. (a) Gun1 for UED experiments. (b) L-shaped slit scanner for horizontal and vertical slit-scan measurements.

As shown in Fig. 1(b), the orthogonal slits allow horizontal and vertical slit scans with a single-axis motion.

The VPP and DVPP methods employ a pixel-wise minimum operation. For two input images, the operation is expressed as

$$Q_{\min} = \min(Q_i, Q_j), \tag{1}$$

where Q_i and Q_j denote the corresponding pixel values of the two input images. In the VPP method, the minimum operation is applied to the horizontal and vertical slit images to generate virtual beamlet distributions [1, 2]. In the DVPP method, the same operation is first applied to two slit images acquired at positions separated by one slit width to generate differential slit images. The horizontal and vertical differential images are subsequently combined by applying the same operation to obtain virtual beamlet distributions [3].

* moses@postech.ac.kr

Content from this work may be used under the terms of the CC BY 4.0 licence (© 2026). Any distribution of this work must maintain attribution to the author(s), title of the work, publisher, and DOI.

ISBN: 978-3-95450-275-2 ISSN: 2226-0366 doi: 10.18429/JACoW-LINAC2026-TUPO012

RESEARCH ON VERY HIGH INTENSITY LASER ION SOURCE WITH AN INNER-ASSEMBLED SOLENOID*

L. Lu†, J. Kuang, Z. Guo
Sino-French Institute of Nuclear Engineering and Technology,
Sun Yat-Sen University, Zhuhai, China

Abstract

Laser ion sources offer a compact configuration, straightforward operation, and convenient maintenance, with particular advantages in producing pulsed ion beams from solid metallic targets. However, free expansion of laser-produced plasma in conventional LISs leads to substantial ion loss, limiting the extracted beam intensity. To mitigate this loss, a compact solenoid was integrated directly into the target chamber of the Laser Ion Source-based Facility (LIFA) at Sun Yat-sen University. A high-purity Cu target was irradiated by a Nd:YAG laser. The peak current, pulse duration (full width at half maximum) and total charge of the Cu ion signal were investigated under different laser energies and solenoid fields. Application of the solenoid field produced pronounced enhancements in both peak current and total charge. At a laser energy of 350 mJ, the peak current increased from 15.0 to 49.3 mA, while the total charge increased from 35.5 to 154.3 nC. At 1450 mJ, the maximum measured peak current reached 108.4 mA. At a transport distance of 900 mm, the peak current increased from 8.52 to 33.50 mA when the solenoid was positioned 164 mm from the target and operated at 468.96 G. These results demonstrate that an inner-assembled solenoid can improve the delivery of laser-produced Cu plasma over both intermediate and extended drift distances.

INTRODUCTION

Laser ion sources (LIS) produce pulsed metal-ion plasmas by focusing a high-power laser onto a solid target [1]. The application of laser-produced plasmas in accelerators dates back to 1969, when Peacock and Pease first proposed using laser plasma as an ion source for accelerators [2]. After decades of development, laser ion sources have emerged as a candidate ion source capable of meeting the demand for intense, highly charged heavy-ion beams in accelerator facilities [3, 4]. However, the current available at a downstream extraction plane is often substantially lower than the current generated near the target because of rapid plasma expansion.

The confinement of laser-produced plasma during its expansion in vacuum using external solenoid magnetic fields has been extensively studied [5, 6]. A substantial body of experimental evidence demonstrates that external static solenoids can enhance the peak beam current, while multi-stage solenoid focusing mitigates current attenuation over long-distance transport. Studies by M. Okamura et al [7, 8]. have found that the solenoid field could change the beam current shape and the emittance of the LIS. However, comparatively limited attention has been paid to compact solenoids installed directly inside the target chamber. To address this critical issue, we designed a compact solenoid within the constrained inner-target-chamber space of the laser ion source. Its purpose is to mitigate the severe ion loss resulting from the free expansion of the laser-produced plasma, and a systematic experimental study was conducted based on this design.

In the present work, a compact solenoid was mounted directly inside the target chamber so that magnetic manipulation starts during the early stage of plasma expansion. Copper was selected as a representative medium-mass metallic species. The effects of laser pulse energy and solenoid field strength on the measured Cu ion current were investigated using Faraday cup (FC). The objective was to determine whether near-source magnetic transport can increase the usable Cu ion current without requiring a further increase in laser energy.

EXPERIMENTAL DESIGN AND METHODS

Figure 1 shows the layout of LIS, which mainly includes two parts: Laser ion source target chamber (inner target chamber, Inner-assembled solenoid, outer target chamber and vacuum system); Vacuum drift transmission section: beam diagnostic device (FC).

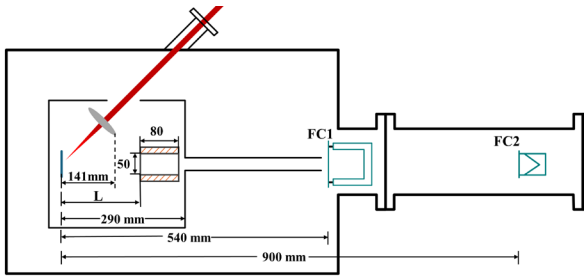


Figure 1: Schematics of the experimental setup.

A high-purity Cu target with dimension of 110×60×2 mm^3 was irradiated using an Nd:YAG laser, the pulse energy was varied from 350 to 1450 mJ, Table 1 shows the laser parameters. The focused spot diameter was approximately 1 mm, corresponding to an estimated laser power density of 4.45×10^9 to 1.83×10^{10} W/cm^2. The target was translated after each laser shot to avoid repeated irradiation of the same crater and to reduce variations caused by target-surface degradation.

* Work supported by the National Natural Science Foundation of China (Grant No. 12575170), Guangdong Basic and Applied Basic Research Foundation (Grant No. 2024B1515120028).

† luliang3@mail.sysu.edu.cn

Content from this work may be used under the terms of the CC BY 4.0 licence (© 2026). Any distribution of this work must maintain attribution to the author(s), title of the work, publisher, and DOI.

ISBN: 978-3-95450-275-2 ISSN: 2226-0366 doi: 10.18429/JACoW-LINAC2026-TUPO013

NEW COMPACT COAXIAL HOM DAMPER FOR SRF CAVITIES*

A. Lunin†, S. Belomestnykh, I. Gonin, T. Khabiboulline, K. McGee, Y. Orlov, V. Yakovlev
Fermi National Accelerator Laboratory, Batavia, IL, USA

Abstract

SRF technology enables particle accelerators to operate with greater average beam currents and higher duty cycles. In these regimes parasitic excitation of the cavity High Order Mode (HOM) spectrum becomes the limiting factor due to extra RF losses and instabilities appearing in the beam. We discussed the practical limitations imposed by HOMs for large accelerator projects, such as the Large Hadron Collider (LHC) and the KEK-B factory. A new compact HOM damper concept is proposed providing good HOM suppression. The idea is based on an oversized coaxial line with radial sections, which is directly connected to the axial region of the SRF cavity. Such radially sectioned coaxial works as a filter for the operating mode, while being transparent for the HOMs. Implementations of this design for the accelerating and crab cavities developed for the upgrade of the Main Injector (MI) at Fermilab and the Electron Ion Collider (EIC) at Brookhaven, respectively, are presented in detail.

INTRODUCTION

To fully exploit the potential of SRF technology in particle accelerators, the machine shall operate at high beam current and high duty factor. When a high-intensity beam passes through a low-loss superconducting cavity, possible resonant excitation of the high-Q HOM by harmonics of the beam current can lead to a significant parasitic heat load on the cryogenic environment, degrade the beam quality, and, under extreme conditions, cause instability of the beam operation. Thus, it is necessary to damp the HOMs by reducing their quality factors below the limits defined by the cryogenic system specification and machine beam optics requirements.

The conventional scheme of the HOM damping implies multiple HOM coupler ports with antenna or loop type feedthroughs [1-3]. To suppress arbitrary polarization of dipole and quadrupole modes, HOM couplers must be placed orthogonally in pairs which require space around the cavity. The complexity is further increased by the need to have rejection (notch) filters integrated into each HOM port to filter the operating mode signal. Assembling such HOM couplers with the cavities is often difficult and may fail to meet overall dimensional requirements.

To address the shortcomings of conventional HOM couplers, this paper proposes a novel compact HOM damper based on an oversized coaxial line around the beam pipe, which is strongly coupled to the SRF cavity. This design can function as a high-pass filter that preserves the operating mode while remaining transparent to the HOMs and taking advantage of the coaxial gap for strong coupling. Unlike traditional approaches, it also offers compact and straightforward antenna feedthrough for HOM ports without a notch filter, simplifying manufacturing and avoiding difficulties in tuning the notch frequency. Furthermore, it is possible to integrate a ceramic-based HOM absorber directly into a larger coaxial structure and thus design a broadband damper suitable for absorbing high average HOM power.

Finally, we present practical implementations of the proposed concept, tailored to 53 MHz SRF accelerating cavities for the Fermilab Main Injector (MI) upgrade and 394 MHz SRF crab cavities for the EIC project.

GENERAL CONCIDERATIONS

The idea of the HOM coaxial damper is based on the direct coupling of a radial coaxial gap to an RF cavity. The transverse size of the cavity is of the order of the wavelength of the operating mode, and if the cavity operates at a relatively low frequency (below gigahertz), its size is much larger than the aperture of a typical vacuum chamber used to transport the beam. In this case, one can introduce a low-impedance coaxial line running around the beam pipe and strongly coupled to the cavity. Figure 1 shows the simplest coaxial HOM coupler used to dampen HOM in the pillbox cavity.

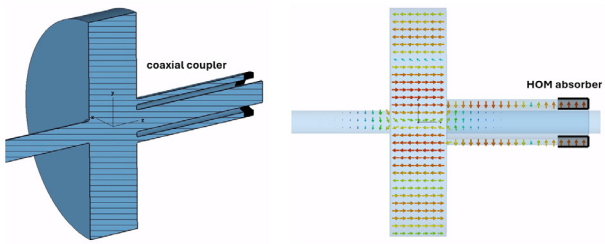


Figure 1: The idea of a coaxial coupler in the pillbox cavity (left) and an example of HOM damping (right).

In fact, the narrow-gap coaxial line is a multimode transmission line, capable of transmitting multiple modes depending on their cutoff frequencies. The first three propagating modes are the coaxial TEM mode without a cutoff frequency and two polarizations of the diploe TE_{11} mode with a cutoff wavelength of about half the average coaxial circumference: $\lambda c_{11} \approx \pi\ (R_1+R_2)$, where R_1 and R_2 are the inner and outer radii of the coaxial line.

The combination of symmetry planes and cutoff frequencies of propagating modes allows selective coupling of the coaxial line to the cavity eigenmodes. For example, the coaxial HOM damper rejects dipole modes below the cutoff frequency of the coaxial TE_{11} mode, while HOMs above the cutoff are effectively damped due to the

* This work was supported by the U.S. Department of Energy, Office of Science. This manuscript has been authored by Fermi Forward Discovery Group, LLC under Contract No. DE-AC02-07CH11359 with the U.S. Department of Energy.
† lunin@fnal.gov

Content from this work may be used under the terms of the CC BY 4.0 licence (© 2026). Any distribution of this work must maintain attribution to the author(s), title of the work, publisher, and DOI.

ISBN: 978-3-95450-275-2 ISSN: 2226-0366 doi: 10.18429/JACoW-LINAC2026-TUPO016

THE SARAF-LINAC CRYOMODULE STATUS

J. Dumas[1], A. Chance[1], G. Ferrand[1], A. Gaget[1], F. Gougnaud[1], A. Kreisel[2], J. Luner[2], A. Perry[2], N. Pichoff[1], T. Plaisant[1], E. Reinfeld[2], F. Senée[1], I. Shmuely[2], D. Simon[1], D. Uriot[1]
[1]CEA, IRFU, DACM, Université Paris-Saclay, Gif-sur-Yvette, France
[2]Soreq NRC (SNRC), Yavne, Israel

Abstract

SNRC and CEA are collaborating on developing SARAF Phase II to deliver 5 mA CW proton and deuteron beams up to 40 MeV. CEA is responsible for the design, fabrication and commissioning of the linac downstream of the RFQ. The linac includes four superconducting cryomodules (CM), comprising two low-β (β = 0.09) and two high-β (β = 0.18) units. All four cryomodules were successfully assembled and tested at Saclay, including cryogenic, vacuum, RF cavity and solenoid characterization. All four CMs have been delivered to SNRC. CM1 and CM4 are already installed in the tunnel and their integration is ongoing. This contribution presents the integration and qualification results of the cryomodules at Saclay as well as the current status of their installation at SNRC.

INTRODUCTION

The qualification of the SARAF Phase II cryomodules represented the final validation step before beam commissioning. This paper provides an overview of the qualification campaign carried out at the Cryomodule Test Stand (CMTS) at CEA Saclay and summarizes the performance achieved by the four production cryomodules before their installation at the SNRC facility. In total, 27 superconducting cavities and 20 superconducting solenoid packages (1 solenoid + 2 steerers) were qualified in four cryomodules over a one-year test campaign, as illustrated in Fig. 1.

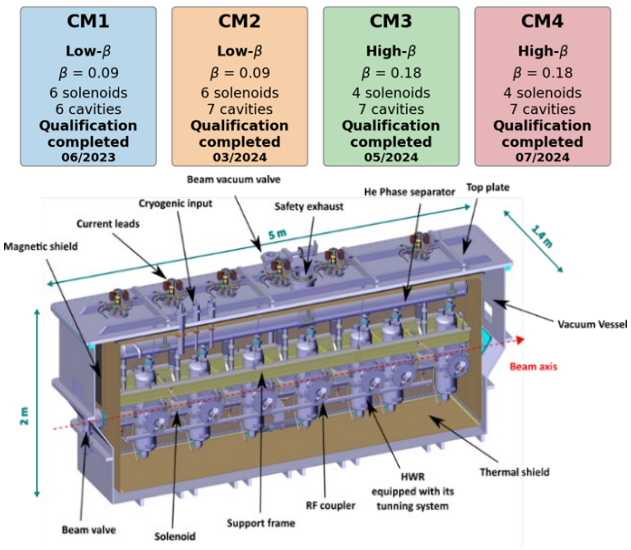


Figure 1: Cryomodule characteristics and CM2 3D model.

The qualification campaign validated the cryogenic design and the performance of all cryomodule subsystems prior to shipment. The main objectives included:

- First controlled cooldown,
- Verification of cryogenic instrumentation,
- Static and dynamic heat load measurements,
- Superconducting magnet qualification,
- Cavity RF conditioning,
- Cavity frequency tuning,
- Vacuum qualification under operating conditions.

Overall, 636 of the 653 qualification criteria (97.4%) were successfully validated across the four cryomodules. The remaining non-conformities were minor, well understood, and either resolved during the qualification campaign or scheduled for correction during installation and commissioning at SNRC.

CRYOMODULE ASSEMBLY

Each cryomodule was assembled at CEA Saclay following a dedicated integration procedure. The cavity and solenoid string was first assembled in a clean room (Fig. 2a), mounted on the top plate (Fig. 2b), and inserted into the vacuum vessel (Fig. 2c). After completion of the mechanical integration, the cryomodule was connected to the Cryomodule Test Stand (CMTS), which provides cryogenic distribution from the SUPRATECH platform, RF power, vacuum, instrumentation, and control systems required for qualification (Fig. 2d). A detailed description of the assembly facilities and procedures is given in [1].



Figure 2: Cryomodule assembly process. (a) Cavity string assembly in the clean room. (b) Top loading of the cavity string into the vacuum vessel. (c) Installation of the top plate with the cavity string, magnetic shielding, and thermal shielding assembled with the vacuum vessel. (d) Cryomodule Test Stand (CMTS).

Content from this work may be used under the terms of the CC BY 4.0 licence (© 2026). Any distribution of this work must maintain attribution to the author(s), title of the work, publisher, and DOI.

ISBN: 978-3-95450-275-2 ISSN: 2226-0366 doi: 10.18429/JACoW-LINAC2026-TUPO017

DEVELOPMENT OF A NOVEL ADAPTIVE BEAM-LOADING COMPENSATION SYSTEM FOR A HIGH CURRENT PULSED PROTON LINAC

K. Futatsukawa*[,1], E. Cicek[1], Z. Fang[1], Y. Fukui[1], H. Nakano[2], S. Mizobata[1], Y. Sato[3]
[1]High Energy Accelerator Research Organization (KEK), Ibaraki, Japan
[2]Japan Atomic Energy Agency (JAEA), Ibaraki, Japan
[3]NAT Company, Ibaraki, Japan

Abstract

Beam-loading compensation is essential for stable cavity fields in high-current pulsed linacs. At the J-PARC LINAC, a new method was developed using measured transfer functions to calculate beam-loading compensation tables. The method simplifies the calculation of compensation parameters and provides stable operation without error accumulation. Furthermore, the method can be adapted to thinned-beam operation, enabling stable cavity fields for different beam patterns.

INTRODUCTION

For high-current pulsed beams, such as the 50-mA beam in the J-PARC LINAC [1, 2], beam-loading compensation is a key factor in achieving stable cavity fields within the RF pulse. A beam-loading compensation system requiring parameter tuning for multiple cavities during beam operation must provide not only stable performance but also quick and easy adjustment.

At the J-PARC LINAC, digital control systems for the low-level RF (LLRF) system are being upgraded, enabling beam-loading compensation parameters to be configured as digital tables. Taking advantage of this flexibility, we developed a beam-loading compensation system that calculates the compensation parameters in the frequency domain and updates the compensation tables for thinned-beam operation.

OBTAINED TRANSFER FUNCTION

Figure 1 shows the relationship between the input signals ($x(t)$ and $X(\omega)$) and output signals ($y(t)$ and $Y(\omega)$) in the time and frequency domains, respectively. Once the transfer function ($H(\omega)$) is known, the input signal can be reconstructed from the output signal through calculations in the frequency domain. Therefore, accurately determining the transfer function is essential.

However, performing a frequency sweep is difficult in practice. When a rectangular pulse with a finite width is used as the input, its frequency spectrum consists of discrete frequency components. Therefore, the transfer function $H(\omega)$ was determined by analyzing the input $X^i(\omega)$ and output $Y^i(\omega)$ obtained from rectangular pulses with various pulse

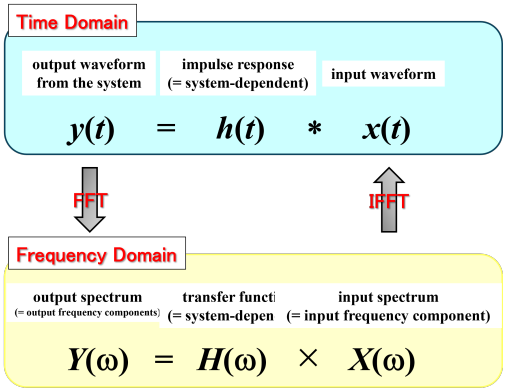


Figure 1: Relationship between the input (x, X) and output (y, Y) signals in the time and frequency domains.

widths. The transfer function was calculated using

$$H(\omega) = \frac{\sum_i X^i(\omega)[Y^i(\omega)/X^i(\omega)]}{\sum_i X^i(\omega)}, \quad (1)$$

where $X^i(\omega)$ represents the weight assigned to the i-th input signal. Figure 2 shows the transfer function obtained using the proposed method.

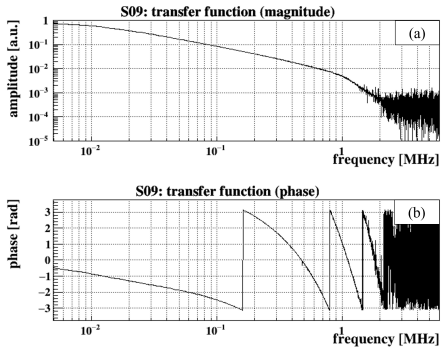


Figure 2: Obtained transfer functioncalculated using Eq. (1): (a) magnitude and (b) phase.

BEAM-LOADING COMPENSATION

The beam-loading compensation table (FF_BEAM) is schematically illustrated in Fig. 3 and calculated as follows:

$$\text{FF\_BEAM}^{\text{new}}(t) = x'(t) + fb\_out(t) + \text{FF\_BEAM}^{\text{previous}}(t), \quad (2)$$

where x denotes the time-domain representation of $X = Y/H$, and the prime symbol ($'$) denotes frequency filtering.

* kenta.futatsukawa@kek.jp

Content from this work may be used under the terms of the CC BY 4.0 licence (© 2026). Any distribution of this work must maintain attribution to the author(s), title of the work, publisher, and DOI.

ISBN: 978-3-95450-275-2 ISSN: 2226-0366 doi: 10.18429/JACoW-LINAC2026-TUPO018

STATUS OF THE FAIR PROTON LINAC

M. Schuett*, R. Hettinger, C. Kleffner, K. Knie, S. Puetz,
A. Schnase, G. Schreiber, A. Seibel, C. Will
GSI Helmholtzzentrum für Schwerionenforschung, Darmstadt, Germany

Abstract

The proton linear accelerator (p-LINAC) is the injector under construction for the antiproton physics program at the Facility for Antiproton and Ion Research (FAIR) in Darmstadt, Germany. It is designed to deliver a beam current of 70 mA at an energy of 68 MeV with a repetition rate of 2.7 Hz. The 2.45 GHz electron cyclotron resonance (ECR) ion source is developed in collaboration with CEA Saclay, France. The ladder radio-frequency quadrupole (RFQ) and the normal-conducting coupled crossbar H-type (CCH) cavities were designed by the Institute for Applied Physics (IAP), Goethe University Frankfurt. Construction, carried out with our industrial partners, has been completed for the ladder RFQ, while fabrication of the first CCH cavity is ongoing. The proton driver, together with the antiproton production chain at FAIR, has been postponed following a re-prioritization of the FAIR project and is currently in a frozen state. This paper reports on the ongoing and planned high-power radio-frequency (RF) tests of the ladder RFQ and the CCH cavities and presents the status of the associated RF systems, including the klystrons and the modulator. Maintaining and preparing the test setup will ensure a smooth transition once the p-LINAC project resumes.

INTRODUCTION

The p-LINAC is envisaged as the injector for the antiproton physics program at FAIR [1, 2]. As illustrated in Fig. 1 and summarized in Table 1, the injector consists of a 2.45 GHz ECR ion source delivering 100 mA of 95 keV protons, a low-energy beam transport (LEBT) line, a 4-rod ladder RFQ, and six normal-conducting CCH/CH cavities arranged in two sections. The proton beam can be delivered either directly to a beam dump or, via two 45° dipoles, to the injection line of the SIS18 synchrotron. The general design of the p-LINAC facility is shown in Fig. 2.

Following a re-prioritization within the FAIR project, the p-LINAC and the associated antiproton production chain have been postponed and the project is currently in a frozen state [3]. All delivered components are being maintained and prepared so that they can quickly be brought back into a state consistent with the project objectives once a new budget decision allows the project to resume. This paper summarizes the activities carried out in this context since the last status report [3], with emphasis on the ongoing and planned high-power RF tests of the ladder RFQ and CCH cavities, and on the status of the associated RF systems, including the klystrons and the modulator.

Table 1: Proton Linac Main Parameters

Parameter	Value
Particle	Proton (H^+)
RFQ input energy	95 keV
RFQ output energy	3 MeV
CCH section energy	33 MeV
Final energy	68 MeV
Pulse current	70 mA
RF frequency	325.224 MHz
Rep. rate	2.7 Hz

LADDER RFQ AND CCH CAVITY STATUS

The ladder RFQ [4] and a beam catcher were assembled at IAP Frankfurt and shipped to the storage facility on the FAIR site [5]. The connection of the RFQ coupling loop to the power feeder is designed with a geometry that allows 50 Ω matching close to the loop; the field flatness of the electrodes reaches ±1 % and the measured Q-value is about 2800 [5]. Construction of the ladder RFQ (Fig. 3) is complete [6], and high-power RF tests on the RF test bench are planned once the test-bench modulator is available.

The first of the six CCH cavities, CCH1, was manufactured by our industrial partner and delivered to GSI in a version with clamped drift-tube connectors. Low-level bead-pull measurements were performed at GSI on the RF test bench using more than 120 different tuner positions out of the 17 possible tuner locations. The design frequency is reached with the tuners close to their mid-range positions, the field flatness and the inter-segment tilt can be adjusted accordingly, and the influence of a ±3 K cooling-water temperature variation on frequency and flatness was shown to be negligible, in agreement with earlier measurements on a full-scale CCH prototype [7].

* m.schuett@gsi.de

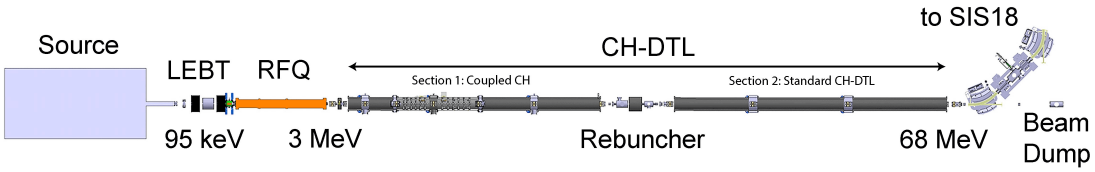


Figure 1: Layout of the FAIR proton linac.

Content from this work may be used under the terms of the CC BY 4.0 licence (© 2026). Any distribution of this work must maintain attribution to the author(s), title of the work, publisher, and DOI.

ISBN: 978-3-95450-275-2 ISSN: 2226-0366 doi: 10.18429/JACoW-LINAC2026-TUPO019

S-BAND HIGH-GRADIENT LOW β SINGLE-PERIODIC MAGNETICALLY COUPLED STANDING-WAVE ACCELERATING STRUCTURE

W. Qin, Y. L. Huang, Y. He†, W. P. Dou, Z. J. Wang, Z. L. Zhang
Institute of Modern Physics, Chinese Academy of Science, Lanzhou, China

Abstract

A novel 3 GHz single-periodic magnetically coupled standing-wave accelerating structure for $\beta = 0.26$ particles with an optimized nose cone and six coupling holes was proposed for the compact proton therapy linac under development at the Institute of Modern Physics, Chinese Academy of Sciences (IMP, CAS). High-power tests demonstrated that the accelerating structure could operate stably at an effective input power of approximately 5.7 MW, achieving an accelerating gradient of 38 MV/m at the pulse length of 5 μs and the repetition rate of 70 Hz. Further increasing the duty factor to 0.1%, the accelerating gradient decreased to 24 MV/m due to the uneven cooling of each single cell. Cavity design, optimization, manufacture, rf measurement, and high-power test are discussed in this paper.

INTRODUCTION

Compact linacs with high operating frequencies and high accelerating gradients have been widely studied and developed worldwide. In the proposed designs, most linacs consist of four sections, P-band RFQ and IH-DTL that cover the first 10 MeV/u energy range well, followed by a S-band side coupled drift tube linac (SCDTL) that accelerates protons from 10 to 70 MeV. Protons with energy above 70 MeV are accelerated by different high-gradient S-band structures, depending on the specific application.

High-gradient S-band accelerating structure is the most critical part of the proton and heavy ion accelerator, which determines the final length of the accelerator. Several structures were studied, constructed, and tested for different projects over the years, including the coupled-cavity linacs (CCL) [1], backward travelling wave (BTW) structures [2] and high gradient standing wave structures [3].

A compact linac is now under development at IMP, which comprises a 3 MeV 750 MHz RFQ, a 3–10 MeV 750 MHz IH-DTL, two 3 GHz SCDTLs that further accelerate the proton bunches to 30 MeV, following with 3GHz single-periodic magnetically coupled standing-wave accelerating structure to boost the energy to 230 MeV.

The magnetically coupled SW structure comprises of 10 regular cells and a coupling cell, which includes a single-feed coupler waveguide and a matching cell. The matching cell is in the middle of the cavity to improve mode separation. The phase advance per rf cell is π to get the highest effective shunt impedance.

RF DESIGN AND OPTIMIZATION

The RF properties of the 3 GHz single-periodic magnetically coupled SW structure with $\beta = 0.26$ were optimized using CST Microwave Studio.

Optimization of the single accelerating cell included the optimization of the nose cone, coupling holes, and the disk. The aim is to increase the shunt impedance of the structure and cell-to-cell coupling while reducing the peak electric fields and S_c, also with considerations of structural stability.

The optimized shape and its dimensions are shown in Fig. 1. Table 1 summarizes the main geometric and rf parameters of the accelerating cell.

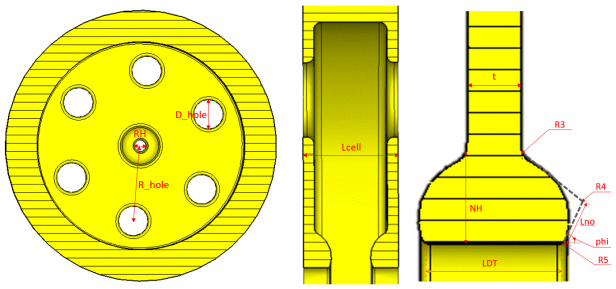


Figure 1: Profile of the $\beta = 0.26$ single-periodic magnetically coupled cells with the optimized parameters.

Table 1: Main Geometric and RF Parameters of the RF Cell

Parameter	Value
Operating frequency [GHz]	3
Lcell [mm]	12.986
D_hole [mm]	10.2
NH [mm]	7
LDT [mm]	7
t [mm]	3
Average accelerating gradient [MV/m]	30
Q factor	5967
Shunt impedance [MΩ/m]	37.5
Cell to cell coupling [%]	1.71
Peak electric field [MV/m]	112
Modified Poynting vector, S_c [MW/mm^2]	0.876

Optimizing the full cavity aims to tune the electric field distribution along the z axis and minimize the power reflection in the matching cell. The electric field distribution along the z axis could be adjusted by changing the radius

† hey@impcas.ac.cn

Content from this work may be used under the terms of the CC BY 4.0 licence (© 2026). Any distribution of this work must maintain attribution to the author(s), title of the work, publisher, and DOI.

650 MHz CW MODE RF-GRIDED GUN DESIGN FOR SRF LINAC APPLICATIONS

Z. H. Liang[1,2,†], Z. J. Wang[1,2,3,‡], Y. M. Chu[1,2], Y. Du[1,2], T. Zhang[1,2], T. L. Wang[1,2], Y. He[1]
[1]Institute of Modern Physics, Chinese Academy of Sciences, Lanzhou, China
[2]University of Chinese Academy of Sciences, Beijing, China
[3]Advanced Energy Science and Technology Guangdong Laboratory, Huizhou, China

Abstract

To address the growing demand for high-power commercial electron irradiation, the Institute of Modern Physics (IMP) has developed a 100 mA, 4.6 MeV superconducting linac prototype. This compact facility features a conduction-cooled Nb3Sn SRF cavity (650 MHz, 5-cell, βopt=0.82) to drive high-intensity beams. However, the existing conventional DC gridded thermionic gun cannot provide the requisite temporal structure or injection velocity to match the SRF cavity acceptance. This severe longitudinal mismatch induces excessive beam loss and low transmission efficiency, inherently preventing continuous-wave (CW) operation. To overcome this critical bottleneck, IMP is developing a novel RF-modulated gridded thermionic gun designed to generate 650 MHz CW bunches. By superimposing an RF electric field directly onto the cathode surface, the emitted DC beam is effectively pre-modulated and bunched, enabling seamless, lossless transmission through the downstream cavity. This paper details the systematic electromagnetic design and comprehensive beam dynamics simulations of this RF-gridded gun, concluding with an outlook on its upcoming fabrication and integration.

INTRODUCTION

Superconducting radio frequency (SRF) technology is fundamental to modern particle accelerators. However, conventional pure niobium SRF cavities require complex and costly 2 K liquid helium (LHe) refrigeration systems, which confines their application primarily to large-scale research facilities.

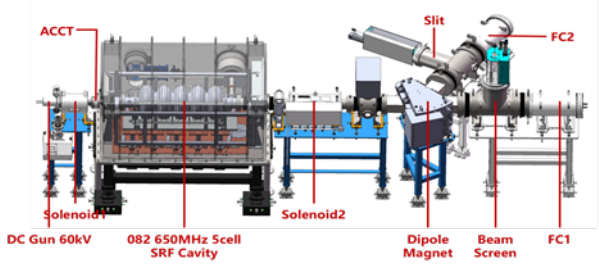


Figure 1: Currently layout of IMP LHe-free SRF e-linac.

To overcome these limitations and enable widespread industrial applications such as wastewater treatment, material modification, medical sterilization, and food preservation the Institute of Modern Physics has pioneered the development of a liquid helium-free (LHe-free) Nb3Sn demo SRF electron linac (e-linac) [1]. By utilizing Nb3Sn thin films grown via the tin vapor diffusion method, the cavity's operating temperature is significantly raised, allowing for conduction cooling driven directly by commercial Gifford-McMahon (GM) cryocoolers. The layout of this linac is presented in Fig. 1.

While this LHe-free SRF architecture presents immense industrial promise, it simultaneously imposes stringent constraints on beam dynamics and thermal management. The cooling capacity of cryocoolers is strictly bounded. Consequently, injecting an un-bunched or poorly matched DC beam into the superconducting section results in substantial particle losses. Such beam halo bombardment deposits excessive heat loads onto the cavity walls, which rapidly overwhelms the conduction-cooling network. This thermal instability inherently prevents the accelerator from sustaining CW operation, forcibly limiting it to low-duty-cycle pulsed modes. Therefore, achieving near-100% transmission efficiency by precisely tailoring the longitudinal phase space of the injected beam before it enters the SRF cavity is absolutely imperative. Figure 2 illustrates the evolution of electron beams output from a DC gun and an RF-gridded gun within the superconducting cavity, simulated using the CST PIC solver, which further demonstrates the necessity of developing this new type of electron gun.

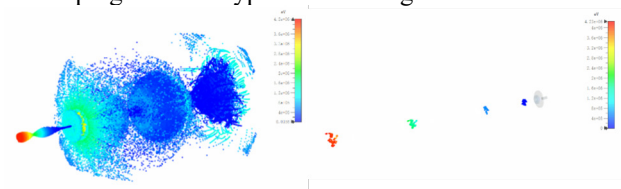


Figure 2: Simulation results by CST Studio: 082 cavity with DC gun (left); 082 cavity with RF-grided gun (right).

To circumvent this cryogenic bottleneck, an advanced injector capable of providing high-quality, pre-bunched beams is essential. In this paper, we present the comprehensive design of a 650 MHz RF-gridded thermionic gun. Unlike conventional DC thermionic sources, this design superimposes an alternating radio frequency potential across the cathode-grid gap, naturally bunching the electron beam directly at the emission surface [2-5]. We detail the conceptual design, cathode material selection, electrode geometry optimization, and the specialized RF impedance matching strategies required for the high-voltage environment. This RF-gridded gun provides a definitive pathway to establishing

† liangzehua@impcas.ac.cn
‡ Corresponding author: wangzj@impcas.ac.cn

Content from this work may be used under the terms of the CC BY 4.0 licence (© 2026). Any distribution of this work must maintain attribution to the author(s), title of the work, publisher, and DOI.

ISBN: 978-3-95450-275-2 ISSN: 2226-0366 doi: 10.18429/JACoW-LINAC2026-TUPO022

DESIGN, FABRICATION, AND TESTING OF A PLATE ELECTRODE CH-MODE CAVITY*

Fu Ma†[1], Xuejun Yin[1], Guangxian Li[1,2], Zhongshan Li[1], Guoxin Chen[2,3], Mengxue Li[2,3]
[1]Institute of Modern Physics, Chinese Academy of Sciences, Lanzhou, China
[2]University of Chinese Academy of Sciences, Beijing, China
[3]Sino-French Institute of Nuclear Engineering and Technology, Sun Yat-Sen University, Zhuhai, China

Abstract

The normal temperature drift tube linac, serving as an injector for medical synchrotrons, is typically based on APF and KONUS beam dynamics within IH-mode cavities to achieve cost-effectiveness and operational stability. While the APF structure combines acceleration and focusing through phase adjustment, its relatively low accelerating gradient results in a lengthy cavity. Conversely, the KONUS scheme offers a high accelerating gradient and compact design by operating near a zero-degree synchronous phase. However, it requires internal quadrupole triplets for transverse focusing, increasing both cost and mechanical complexity. To address these limitations, this paper proposes a novel acceleration structure that employs plate electrodes instead of conventional cylindrical drift tubes. Integrated into a CH-mode cavity with vanes to optimize the electric field and RF performance, this design is combined with KONUS dynamics to enable transverse focusing during near-zero-degree acceleration, leading to a more compact and efficient system. This paper presents the design, fabrication, and preliminary test results of this innovative structure.

INTRODUCTION

Heavy-ion therapy employs high-energy carbon-ion beams to precisely destroy tumors, offering high therapeutic efficacy and low side effects. Since the United States pioneered clinical trials in the 1970s, the technology has advanced rapidly. In 1994, Japan's National Institute of Radiological Sciences (NIRS) built the world's first dedicated clinical heavy-ion therapy center, using an injector composed of a radiofrequency quadrupole (RFQ) and an Alvarez drift-tube linac (DTL) [1]. This configuration, however, suffered from low acceleration efficiency and large cavity size. In 2011, NIRS upgraded the HIMAC injector to an RFQ combined with an interdigital H type DTL (IH DTL) based on alternating-phase focusing (APF) dynamics [2,3], which improved efficiency and reduced cost, but the weak transverse focusing limited the beam current capability. In contrast, the Heidelberg Ion Beam Therapy Center (HIT) and the Italian National Center for Oncological Hadrontherapy (CNAO) adopted a combined zero degree structure (KONUS) dynamics scheme with an IH DTL in the post injector section [4–6], achieving high acceleration gradients and a more compact footprint.

China's first independently developed medical heavy-ion accelerator, the Heavy Ion Medical Machine (HIMM), uses a "cyclotron injector + synchrotron" architecture [7]. The cyclotron injector is compact and cost-effective, directly accelerating $^{12}C^{5+}$ to the synchrotron injection energy 7 MeV/u, greatly reducing system size and cost. However, the extracted beam has inferior phase-space quality (emittance and momentum spread) compared with linear injectors, and the beam current is only about 10 euA, severely limiting the synchrotron's accumulation and extracted intensity. To overcome these limitations, the Secondary Heavy Ion Medical Machine (SIMM) adopts an RFQ and plate electrode linac (PEL) configuration. The PEL replaces conventional cylindrical drift tubes with plate electrodes arranged in a cross-bar H type (CH-DTL), where horizontal and vertical plates alternate along the beam axis to provide periodic transverse focusing and longitudinal acceleration. The overall design follows KONUS dynamics, resulting in a compact structure, high gradient, small beam envelope, and high transmission efficiency. The prototype has been commissioned and achieved an output current of 1 emA. A detailed description is provided below.

DYNAMIC DESIGN

This linac is primarily composed of a cryogen-free hybrid superconducting electron cyclotron resonance (HECRAL-C) ion source [8], a radio-frequency quadrupole (RFQ), and a plate-electrode linac (PEL). It operates at a frequency of 162.5 MHz. The beam duty cycle is 0.1 %. Between the RFQ and the PEL, only one set of triplet magnets is installed, and no buncher is employed, which results in a simple and compact overall layout. The RFQ accelerates $^{12}C^{4+}$ ions to 0.8 MeV/u, while the PEL provides an output energy of 4.0 MeV/u. The general arrangement is depicted in Fig. 1.

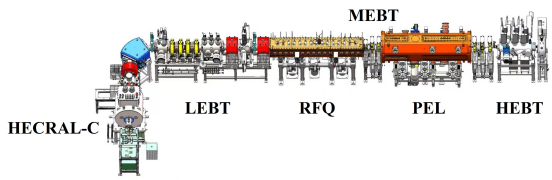


Figure 1: General layout of the linear injector.

As the primary accelerating section of the injector, the PEL adopts the KONUS dynamic, comprising two KONUS

* Work supported by NSFC No.12305159.
† mafu121@impcas.ac.cn

Content from this work may be used under the terms of the CC BY 4.0 licence (© 2026). Any distribution of this work must maintain attribution to the author(s), title of the work, publisher, and DOI.

ISBN: 978-3-95450-275-2 ISSN: 2226-0366 doi: 10.18429/JACoW-LINAC2026-TUPO024

STATUS UPDATE ON ESS icBLM DETECTOR XRAY TESTS

V. Grishin*, E. Bergman, A. Gorzawski, L. A. Martins,
A. Persson, J. Norin, H. Hassanzadegan, P. van Velze
European Spallation Source ERIC, Lund, Sweden

Abstract

The European Spallation Source (ESS) in Lund, Sweden, is a pulsed neutron source based on a proton linac. While the first Beam on Dump (BOD) campaign in 2025 demonstrated that the beam could successfully reach the tuning dump, BOD in 2026 focused on operating the accelerator at much higher performance levels. The beam operation was achieved at 860 MeV with a beam current of 62.5 mA, a pulse length of 1.5 ms, and a repetition rate of 14 Hz, towards producing the first neutrons at the rotating tungsten target. This paper focuses on the end-to-end tests of the Beam Loss Monitor (BLM) system carried out since October 2025 using an industrial X-ray gun. These tests allowed us to verify the entire signal chain of the BLM system from the detector to the top-level control system in the control room using an easily accessible, commercially available method.

INTRODUCTION

One of the most critical beam diagnostic systems for accelerator protection is the BLM system. The system is designed to protect the accelerator from beam-induced damage and unnecessary activation of components. The main detector of the ESS BLM system is an ionization chamber (icBLM) [1]. All 266 icBLM detectors have been installed, connected, powered, and tested throughout the ESS linac [2] (Fig. 1).

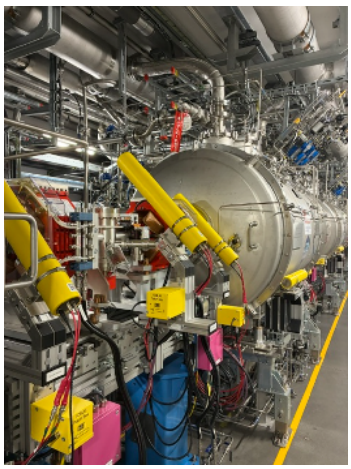


Figure 1: icBLM installation in the ESS linac.

Out of the 5,080 ionization chambers produced between 2005 and 2017, 830 modified icBLM detectors are currently in use at ESS, Gesellschaft fur Schwerionenforschung (GSI), and CERN. The ESS icBLM detector is a Large Hadron Collider (LHC) type of ionization chamber with some modifications, mostly concerning the active volume gap between the electrodes [3]. Each chamber has been tested with multiple steps during production and installation [4]. To compare the original LHC detectors with the modified detectors, the teams from CERN, ESS, and GSI tested and calibrated the detectors at the HiRadMat facility at CERN [5]. CERN BLM experts made a significant effort to verify the icBLM installation and connections. During the 2026 HiRadMat beam tests, the calibration curve was measured, and the performance of the detectors was evaluated in mixed particle fields. The detectors setup was swapped at the dump location to avoid the nonuniformity in beam dump showers. Figure 2 represents the total charge measured per proton extraction pulse for two ESS icBLM detectors for both configurations of the installation related to the dump. The performance of the ESS detector shows the expected behavior and is like that of the original LHC-type BLM.

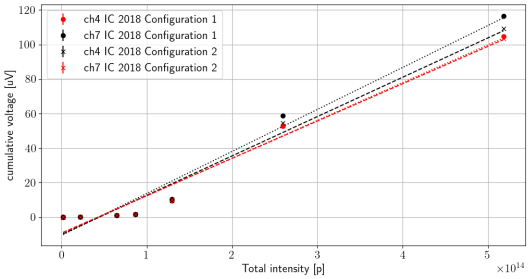


Figure 2: Total charge measured per proton extraction pulse as a function of the number of protons per pulse for two ESS icBLM (IC 2018) detectors in both configurations.

After the installation of the detectors in the accelerator tunnel, the final test with the radiation source was envisaged for the entire BLM system. At CERN, for the testing and calibration of the LHC BLM system, a trolley carrying a lead housing with a 380 MBq ^{137}Cs gamma source was utilized. At ESS, during 2025 and 2026, due to the complexity of performing gamma source tests on the detectors and following a request for urgent verification of the BLM system for the Beam on Dump campaign, we searched for an alternative to the ^{137}Cs and ^{60}Co source tests. The ESS Radiation Protection Group proposed the use of a commercial X-ray gun from DEKRA [6].

ON-SITE TESTS OF DETECTORS

The following ESS set of tests was executed after complete icBLM system installation on-site and are a prerequisite for the X-ray tests:

* slava.grishin@esss.se

Content from this work may be used under the terms of the CC BY 4.0 licence (© 2026). Any distribution of this work must maintain attribution to the author(s), title of the work, publisher, and DOI.

ISBN: 978-3-95450-275-2 ISSN: 2226-0366 doi: 10.18429/JACoW-LINAC2026-TUPO025

DEVELOPMENT OF NORMAL CONDUCTING HEAVY ION LINAC IN CHINA*

X.J. Yin†,1, Z.S. Li[1], Y.Q. Yang[1], F. Ma[1], G.X. Li[1], Y. Cong[1], X.W. Xu[1], C.C. Li[1], L. Jing[1], H.N. Wang[1], P. Jin[1], X.J. Liu[1], C. Qian[1], W.Q. Yang[1], L.J. Mao[1], D.Q. Gao[1], J.X. Wu[1], J. Meng[1], L.T. Sun[1], Q.G. Yao[1], W. Zhang[1], Z. Xu[1], J.C. Yang[1], Y.J. Yuan[1], Y. He[1], H.W. Zhao[1], J.W. Xia[1], W.L. Zhan[1], Y.R. Lu[2], K. Zhu[2], X.Q. Yan[2]
[1]Institute of Modern Physics, CAS, Lanzhou, China
[2]State Key Laboratory of Nuclear Physics and Technology, Peking University, Beijing, China

Abstract

The research on heavy ion linac was began more than ten years ago initially aim to improve the HIRFL operation at IMP. In China, a continuous wave (CW) heavy ion linac, SSC Linac, working at 53.667 MHz was developed as the SSC injector. The ion particle can be accelerated to 1.48 MeV/u with the designed A/q≤ 5.17. At present stage, this CW linac has been put into operation and the Uranium has been accelerated to 1.48 MeV/u successfully. To satisfy the continue requirements, a compact 162.5 MHz heavy ion linac operating in pulse mode was developed. The "KONUS" beam dynamics design was adopted and the heavy ions can be accelerated to 4 MeV/u with A/q≤ 3. The SESRI linac was another pulse machine which was built at Harbin. In this linac, both of the heavy ions and proton beam can be accelerated by this linac to 2 MeV/u and 5.6 MeV, respectively. In this paper, the status of these three heavy ion linacs and their beam commissioning results were presented.

SSC LINAC

The SSC Linac is a CW heavy ion linac designed as the new injector for the Separated Sector Cyclotron (SSC) at IMP-HIRFL to improve the performance efficiency [1, 2].

The SSC Linac mainly consists of a super-conducting electron-cyclotron-resonance ion source (SC-ECR), a 4-rod RFQ, four IH-DTLs and four bunches, as shown in Fig. 1. This linac was specifically designed to make use of 53.667 MHz which is four times of the SSC working frequency. For increasing the capture efficiency and longitudinal matching between linac and SSC, a pre-bunch working at 13.417 MHz was designed before the RFQ. The ion particle with the ratio of mass-to-charge A/q≤5.17 can be accelerated to 1.48 MeV/u. After then the particle can be further accelerate to 15.53 MeV/u by SSC. The beam transmission of the linac is as high as 85%.

Key Components

Super-conducting Electron Cyclotron Resonance ion source (SECRAL-I) is designed to operate at multiple microwave frequencies with 28 GHz & 18 GHz. It was upgraded from the existing magnet body of SECRAL and a new designed cryostat in 2019. In September 2023, SECRAL-I was moved to SSC-Linac front-end replacing the existing normal conducting ECR ion source to provide highly charged ion beams, such as Uranium.



Figure 1: Photo of the SSC linac.

The CW 4-rod RFQ was designed and fabricated under the collaboration between IMP and Peking University [3, 4]. Particles with mass-to-charge ratios of ≤ 5.17 can be accelerated from 3.728 keV/u to 143 keV/u.

We adopt the IH-DTL as main accelerating section. The Inter-digital H mode (IH-DTL) has a higher accelerating efficiency because this structure has higher shunt effective impedance and compact structure [5]. For our 53.667 MHz heavy ion linac, the effective shunt impedance is about 300–180 MΩ/m for the relativity factor β between 0.02–0.05 especially. All measured Q_0 values of DTL cavities are above 85% of the simulation results by CST-MWS [6].

The SSC Linac was initiated to accelerate ion particles to two inject energies using different operation modes. The first mode is that 0.58 MeV/u can be implemented using DTL1&2. The second mode can be performed using DTL3 to 1.025 MeV/u. Then 5.97 MeV/u and 10.2 MeV/u can be obtained from SSC for various experiments, respectively. Based on the successful experience, the SSC linac was upgraded by adding DTL4 in 2022. Then the extracted energy of heavy ion form linac increase to 1.48 MeV/u. The HEBT was also modified to match this upgraded.

Operation Status

In the September of 2019, the SSC Linac including DTL1&2 was installed in the SSC hall and put into operation. The heavy ion particles, such as $^{78}Kr^{13+}$, $^{129}Xe^{22+}$, $^{209}Bi^{32+}$, etc., with 0.58 MeV/u were successfully injected into SSC. With the operation of the SSC Linac, the beam

* Work supported by NSF11375243.
† yinxj@impcas.ac.cn

Content from this work may be used under the terms of the CC BY 4.0 licence (© 2026). Any distribution of this work must maintain attribution to the author(s), title of the work, publisher, and DOI.

ISBN: 978-3-95450-275-2 ISSN: 2226-0366 doi: 10.18429/JACoW-LINAC2026-TUPO028

BEAM DYNAMICS AND OPTICS MATCHING FOR THE 270-MeV INJECTOR LINAC AND TRANSPORT LINE OF SPS-II

P. Boonpornprasert*, T. Chanwattana, S. Jummunt, S. Chunjarean
Synchrotron Light Research Institute, Nakhon Ratchasima, Thailand

Abstract

The Siam Photon Source II (SPS-II) project at the Synchrotron Light Research Institute (SLRI) is developing a 270-MeV injector linac based on the proven technology of the NanoTerasu facility. This paper presents the beam dynamics simulations and optics matching for the injector linac and the subsequent Low-Energy Beam Transport line (LBT). Particle tracking through the thermionic electron gun, sub-harmonic cavities, and S-band accelerating structures was modeled using PARMELA. Following the linac, the LBT optics were optimized using MAD-X to transport the beam and match the Twiss parameters required at the booster synchrotron injection point. The combined simulation results confirm that the injector linac and LBT provide a well-matched electron beam for injection into the SPS-II booster synchrotron.

INTRODUCTION

The Siam Photon Source II (SPS-II) is a 4th-generation synchrotron radiation light source currently under development at the Synchrotron Light Research Institute (SLRI) in Thailand [1]. To provide a high-quality electron beam for the accelerator complex, the project includes the construction of a dedicated injector linac and a Low-Energy Beam Transport line (LBT). While the original project plan proposed a 150 MeV linac system [2], the baseline injection energy was subsequently increased to at least 250 MeV as it is highly beneficial for overall machine performance. This higher energy narrows the dynamic ramping range of the booster synchrotron by bypassing the low-field operating region. Consequently, this relaxes the stringent tracking specifications for the magnet power supplies, improving their stability and reproducibility.

To ensure long-term operational reliability and build local maintenance expertise, the 270 MeV injector linac is being implemented by SLRI, under the guidance of H. Tanaka (RIKEN/SPring-8) and his team. To mitigate technical risks, the system architecture was closely modeled after the proven technology of the NewSUBARU [3] and NanoTerasu [4, 5] facilities in Japan. As a starting point for this framework, T. Asaka (QST/NanoTerasu) established the initial lattice arrangement, defined the electromagnetic field and component profiles, and performed the preliminary beam dynamics simulations. The SLRI team has subsequently adopted this accelerator baseline to proceed with the overall facility integration and engineering.

A schematic layout of the injector linac and the LBT is presented in Fig. 1. The electron beam is initially generated by a gridded thermionic cathode DC gun. It is then accelerated by a 238 MHz cavity and bunched by a 476 MHz cavity. The main acceleration to 270 MeV is performed utilizing four 3-m S-band (2856 MHz) traveling-wave accelerating structures.

Following the linac, the beam enters the LBT for on-axis injection into the booster synchrotron ring. Due to the spatial constraints of the existing SPS-II facility, the positions and bending angles of the dipole magnets are strictly fixed. Consequently, the quadrupole magnets serve as the primary degrees of freedom to control and optimize the beam optics.

By focusing on the injector linac and the LBT, this study presents the particle tracking and optics optimization processes necessary to match the required Twiss parameters at the booster injection point.

INJECTOR LINAC

This section details the beam dynamics simulations modeling the electron beam transport from the exit of the DC electron gun to the exit of the final S-band accelerating structure.

Simulation Setup

Beam dynamics simulations were performed using the PARMELA code [6]. The simulation begins at the exit of the DC gun (LIN-EG-GUN) using an initial particle distribution of 22 843 macro-particles imported from the baseline CST Studio Suite [7] models. The initial beam has a bunch charge of 500 pC, a mean energy of 50 keV, an RMS bunch duration of 70.6 ps (FWHM 225.3 ps), a transverse RMS size of 1.28 mm, and a transverse RMS emittance of 2.2 nm · rad. Based on a fundamental frequency of 2856 MHz, the input beam current for PARMELA was calculated as 1.428 A, and space charge forces were evaluated on a 40×400 cylindrical mesh.

The simulated lattice begins with a drift space, followed by two active sub-harmonic cavities: LIN-RF-SHC-01 (238 MHz, 368.5 mm length, 1.20 MV/m peak field) and LIN-RF-SHC-02 (476 MHz, 300 mm length, 0.65 MV/m peak field). These are followed by four 2856 MHz traveling-wave accelerating structures (LIN-RF-ACC-01 to 04), each 2929.1 mm long. The first structure operates at a peak field of 21.00 MV/m, while the subsequent three operate at 26.00 MV/m. Note that while future transverse matching quadrupole magnets (LIN-MG-QM-01 and 02) are present in the overall design layout, they were inactive in this simulation.

To mitigate emittance growth induced by space charge, the beam is immediately accelerated to 500 keV by the first cav-

* prach.b@slri.or.th

Content from this work may be used under the terms of the CC BY 4.0 licence (© 2026). Any distribution of this work must maintain attribution to the author(s), title of the work, publisher, and DOI.

ISBN: 978-3-95450-275-2 ISSN: 2226-0366 doi: 10.18429/JACoW-LINAC2026-TUPO029

DRIVING THE SIBAF PROJECT: PHYSICS DESIGN OF A 108.408 MHz HEAVY-ION RFQ INJECTOR WITH A/Q UP TO 8.5 FOR FUSION MATERIAL IRRADIATION

Chuan Zhang[†,1,2,3], Holger Podlech[2,3]
[1]GSI Helmholtzzentrum für Schwerionenforschung, Darmstadt, Germany
[2]Institute for Applied Physics, Goethe-University Frankfurt, Germany
[3]Helmholtz Research Academy Hesse for FAIR (HFHF), Frankfurt, Germany

Abstract

A dedicated heavy-ion Radio Frequency Quadrupole (RFQ) accelerator is currently under development at GSI Darmstadt and IAP Frankfurt for the SIBAF (Superconducting Ion accelerator as BAsis technology for Fusion research) project. From an injection energy of 4 keV/u to a final energy of 300 keV/u, the SIBAF RFQ is designed to accelerate heavy ions with a mass-to-charge ratio of up to 8.5 at 108.408 MHz. Given that the subsequent main linac utilizes superconducting structures, the RFQ must deliver exceptionally high beam quality to minimize losses and ensure stable operation. This paper presents the physics design concepts, beam dynamics optimizations, and comprehensive simulation results for the SIBAF RFQ.

INTRODUCTION

Developing materials capable of withstanding extreme radiation is a critical bottleneck for commercial D-T fusion reactors. In a fusion environment, first-wall and divertor components face an intense 14 MeV neutron flux, which induces severe displacement damage and high levels of helium and hydrogen transmutations. While neutron sources generate a realistic 14 MeV-peaked spectrum, they often suffer from high operational costs, multi-year irradiation cycles to reach high displacement doses (dpa), and significant induced radioactivity that hampers rapid post-irradiation examination (PIE).

To complement neutron-based testing, the SIBAF (Superconducting Ion accelerator as BAsis technology for Fusion research) project serves as a targeted demonstration initiative based on the HELIAC (HElmholtz LInear ACcelerator) [1] infrastructure at GSI, leveraging the existing High Charge State Injector (HLI) and the first superconducting cryomodule of the HELIAC platform to construct a dedicated fusion materials irradiation test station. By utilizing this advanced continuous-wave (CW) heavy-ion acceleration technology, heavy ions simulate neutron radiation by transferring kinetic energy to lattice atoms via nuclear and electronic stopping, generating Primary Knock-on Atoms (PKAs) and displacement cascades.

The primary advantage of this heavy-ion approach is an extraordinarily high damage rate—achieving tens to hundreds of dpa within days rather than years—and negligible or minimal induced radioactivity (depending on ion species and energy), which drastically simplifies handling and enables safe PIE with minimal cooling time. However, heavy ions have a very short penetration depth (a few micrometers), leading to steep damage gradients and near-surface sink effects. Furthermore, because single heavy-ion beams do not inherently produce transmutation gases at fusion-relevant levels, simultaneous multi-beam co-injection (such as He/H implantation) is required to accurately simulate gas-driven bubble nucleation, embrittlement, and swelling. Consequently, SIBAF operates as a vital complementary tool: advancing HELIAC's technical capabilities while bridging the gap by allowing rapid screening and mechanistic studies of radiation damage before final validation in scarce neutron facilities.

Serving as the initial acceleration stage, the Radio Frequency Quadrupole (RFQ) accelerator is a key component for the SIBAF facility, responsible for bunching and pre-accelerating low energy injected ions with a mass to charge ratio A/Q up to 8.5, using U^{28+} as the design reference particle, to prepare them for subsequent drift tube structures. For this RFQ, CW operation is required for A/Q up to 6, while pulsed operation with a duty cycle of up to 25% is specified for higher A/Q ratios.

The existing HLI RFQ [2, 3] is limited to a maximum A/Q of 6, falling short of the requirement up to 8.5 necessary for comprehensive fusion radiation damage research. Furthermore, although measurements have demonstrated favorable beam dynamics performance [4], the existing HLI RFQ, originally designed for CW operation, suffers from severe mechanical vibrations under high duty cycle conditions. For the SIBAF project, therefore, a new RFQ featuring enhanced thermal and mechanical stability is required. Additionally, beam dynamics parameters should be optimized for higher A/Q ratios to achieve optimal beam quality and ensure proper matching to downstream drift tube structures, preventing beam loss especially inside the superconducting cavities.

The main requirements for the preliminary design of the SIBAF RFQ are listed in Table 1 together with those of the existing HLI RFQ for comparison.

†c.zhang@gsi.de

Content from this work may be used under the terms of the CC BY 4.0 licence (© 2026). Any distribution of this work must maintain attribution to the author(s), title of the work, publisher, and DOI.

ISBN: 978-3-95450-275-2 ISSN: 2226-0366 doi: 10.18429/JACoW-LINAC2026-TUPO030

ATTOSECOND-RESOLUTION ULTRAFAST ELECTRON DIFFRACTION ENABLED BY THz STREAKING*

Jiapeng Li, Qiao Luo, Yaodan Hu, Changda Peng, Zhengquan Wang, Cheng-Ying Tsai, Zhengyan Li, Zhengzheng Liu, Kuanjun Fan†
Huazhong University of Science and Technology, Wuhan, China
Jinfeng Yang, SANKEN, Osaka University, Ibaraki, Osaka, Japan

Abstract

A 300 GHz split-ring resonator (SRR) streaks a 3 MeV, 25 fs bunch at 97 µm/fs and resolves arrival time to 0.18 fs with no loss of charge. Arrival time written onto a transverse detector coordinate turns ultrafast electron diffraction into a single-shot measurement that is insensitive to the jitter between pump and probe and needs no sub-femtosecond bunch. We take the gap field from CST and track the beam in ASTRA, at a zero crossing of the deflecting field and a 1.0 m detector distance. Separating the contributions shows that the resonator sets a floor of 0.17 fs, which this working point already reaches; what must be kept below it is the flight time spread between sample and streaker, scaling as $L(\delta p/p)/\gamma^2$ and taking over a few millimeters further out. The diffracted orders must also fit through the 20 µm gap, which by itself calls for the same short distance. At L = 2 mm, a complete Au(001) pattern passes the structure with its diffraction information preserved, and space charge sets the usable bunch charge at a few fC.

INTRODUCTION

Ultrafast electron diffraction (UED) follows structural dynamics with atomic-scale sensitivity. In a conventional delay scan, its time resolution is bounded by the bunch duration together with the jitter between pump and probe [1]. Both bounds disappear if the arrival time of each electron is written onto a transverse coordinate of the detector: a single shot then carries the whole time axis, the sample need not recover between shots, and a timing drift displaces the pattern instead of blurring it. RF deflecting cavities demonstrated this at MeV energy and reached a few hundred femtoseconds [2, 3].

The streak speed at the detector scales with the product of deflecting voltage and drive frequency, so moving from a few GHz to a few hundred GHz gains two orders of magnitude at the same voltage. A split-ring resonator (SRR) driven by a single-cycle THz pulse concentrates the field into a gap a few tens of micrometers wide, where it reaches values of order 1 GV/m [4–6]. Resonators of this kind have already compressed MeV bunches and suppressed timing jitter, so the drive and its synchronization with the beam are established [7].

* Work supported by the National Key Research and Development Program of China (2022YFA1602202, 2024YFB4607900), the Fundamental Research Funds for the Central Universities (HUST) under Project No. 2021GCRC006, and the National Natural Science Foundation of China under Projects No. 12275094 and No. 12235005.

† kjfan@hust.edu.cn

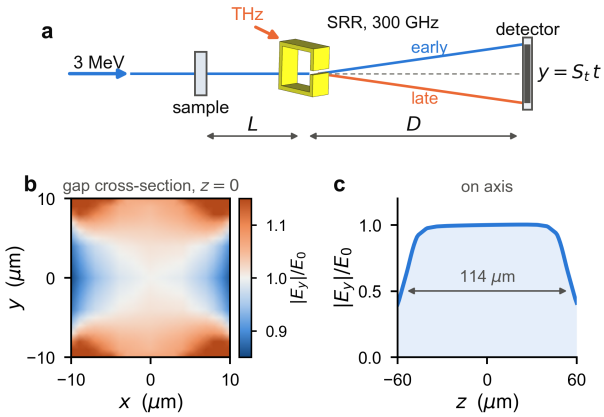


Figure 1: (a) Layout: the electrons cross the SRR a distance L after the sample and drift D to the detector, where arrival time appears as vertical position. (b) CST deflecting field over the gap cross section, normalized to the axis value E_0. (c) The same field along the beam axis.

A fast sweep does not by itself give a fine resolution. The sweep only fixes the conversion between arrival time and vertical position, whereas the resolution is the width of the image formed by electrons that left the sample at the same instant, divided by that conversion. This paper combines CST field maps with ASTRA tracking for a 300 GHz SRR, extracts both quantities from the tracked distribution, and separates the terms that contribute to the width. The resolution is 0.18 fs with the sample 2 mm away, 0.17 fs of it a floor set by the resonator.

MODEL AND SIMULATION SETUP

The near field of the SRR was solved in CST and exported as real and imaginary maps on a 1 µm grid, covering the full gap, ±10 µm transversely and ±60 µm along the beam axis. ASTRA [8] applies the two as one coupled 300 GHz module, reproducing the drive phase as the bunch crosses. The bunch is represented by 20 000 macroparticles, a sampling number and not the electron content (6.2×10^3 at 1 fC); one macroparticle per electron instead changes σ_t by 0.5 %. Figure 1 defines the geometry and shows the gap field, uniform to ±7 % across the deflecting direction; Table 1 lists the parameters.

Close to a zero crossing of the deflecting field, the vertical kick is linear in arrival time, so after the drift D the detector coordinate is $y = y_0 + S_t t$. The resolution follows from the vertical width that survives once this linear part is removed,

$$\sigma_t = \sigma_{y,\mathrm{res}}/|S_t|, \quad (1)$$

Content from this work may be used under the terms of the CC BY 4.0 licence (© 2026). Any distribution of this work must maintain attribution to the author(s), title of the work, publisher, and DOI.

ISBN: 978-3-95450-275-2 ISSN: 2226-0366 doi: 10.18429/JACoW-LINAC2026-TUPO031

A ONE-DIMENSIONAL CODE FOR WAVEGUIDED SUPERRADIANT THz FEL*

R. Y. Luo, C. Y. Ji, C. Liu, Q. S. Chen†
Huazhong University of Science and Technology, Wuhan, China

Content from this work may be used under the terms of the CC BY 4.0 licence (© 2026). Any distribution of this work must maintain attribution to the author(s), title of the work, publisher, and DOI.

Abstract

In THz regime, superradiance with zero-slippage by introducing a waveguide can greatly enhance the energy conversion efficiency of electron beam. In this paper, a one dimensional numerical code named CRABE-1D (Coherent Radiation Amplification from Bunched Electrons), is developed for waveguide-based superradiant THz-FEL simulations. The code solves the beam–radiation interaction equations based on a frequency-domain method without employing the slowly varying envelope approximation (SVEA) or undulator-period averaging. By incorporating waveguide dispersion, the model is capable of simulating the synchronism between the radiation group velocity and the electron beam. For the free space case, the developed code was benchmarked against PUFFIN 1D, showing a deviation of less than 1%. Upon incorporating waveguide effects, a comparative study was conducted between a single bunch and a bunch train under the zero-slippage condition. The results demonstrate that the bunch train not only enhances the average energy conversion efficiency but also effectively suppresses the FEL spectral broadening induced by the waveguide.

INTRODUCTION

Free-electron lasers (FELs) offer several distinct advantages, including high peak power, high coherence, broad tunability, and ultrashort pulse duration [1]. With recent advances in high-brightness electron guns and longitudinal beam modulation, superradiant terahertz free-electron lasers (THz-FELs) have attracted considerable attention [2, 3]. In this operating regime, coherent radiation can grow rapidly within a relatively short single-pass undulator, providing an effective approach to compact, high-power THz radiation sources. In superradiant THz-FELs, pronounced longitudinal slippage shortens the effective beam–radiation interaction length and limits further growth of the radiation power and pulse energy. By exploiting waveguide dispersion to reduce the radiation group velocity, zero-slippage operation can be achieved, thereby enhancing the beam–radiation interaction [4, 5]. However, existing FEL codes, such as GENESIS [6] and PUFFIN [7], are primarily designed for free-space propagation and generally do not incorporate dispersive waveguide models.

To investigate the longitudinal beam–radiation dynamics in a zero-slippage superradiant THz-FEL, we developed a one-dimensional frequency-domain simulation code CRABE-1D (Coherent Radiation Amplification from Bunched Electrons). The code solves the coupled evolution equations of the electron beam and radiation field in the frequency domain without applying either undulator-period averaging or the slowly varying envelope approximation. The incorporation of waveguide-mode dispersion enables the code to describe group-velocity variation and the beam–radiation interaction under zero-slippage conditions. A free-space benchmark against PUFFIN 1D showed agreement in radiation pulse energy within a relative difference of 1%, thereby validating the accuracy of CRABE-1D. The code was subsequently applied to the study of the longitudinal dynamics of zero-slippage superradiant THz-FELs. A comparison between a single electron bunch and an electron-bunch train under zero-slippage conditions shows that the bunch-train configuration not only further enhances the radiated energy but also significantly reduces the spectral bandwidth of the output radiation.

ONE-DIMENSIONAL CODE MODEL

To describe the longitudinal interaction between the electron beam and the radiation field in a waveguide-based superradiant THz-FEL, a one-dimensional frequency-domain model is developed. Starting from Maxwell's equations, the vector potential $\mathbf{A}$ satisfies the inhomogeneous wave equation under the Lorenz gauge [8, 9],

$$\left(\nabla^2 - \frac{1}{c^2}\frac{\partial^2}{\partial t^2}\right)\mathbf{A} = -\mu_0 \mathbf{J}. \tag{1}$$

The vector potential is represented as a superposition of frequency components,

$$A_x(x,y,z,t) = -\int \frac{\mathrm{d}\omega}{2\pi}\zeta_{q\perp}(x,y)\frac{\mathrm{i}c_q(z,\omega)}{\omega}\mathrm{e}^{\mathrm{i}[k_z(\omega)z-\omega t]}, \tag{2}$$

where $c_q(z,\omega)$ is the complex spectral amplitude, $\zeta_{q\perp}(x,y)$ represents the transverse distribution of the waveguide mode, and $k_z(\omega)$ is the corresponding longitudinal propagation constant.

For a curved parallel-plate waveguide (CPPWG) with a plate curvature radius R and a plate separation b, the transverse wavenumber is given by

$$k_{mn} = \frac{1}{b}\left[n\pi + (2m+1)\tan^{-1}\left(\frac{b}{\sqrt{2Rb-b^2}}\right)\right]. \tag{3}$$

After introducing the CPPWG, the longitudinal propagation constant of each frequency component is determined by the waveguide dispersion relation,

* Work supported by National Natural Science Foundation of China (No.12175077) and Nuclear Technology R&D Program (No.HJSYF2025(25))

† chenqushan@hust.edu.cn

ISBN: 978-3-95450-275-2 ISSN: 2226-0366 doi: 10.18429/JACoW-LINAC2026-TUPO032

RESEARCH ON LOCALLY FOCUSING ATMOSPHERIC MUON SOURCER*

L. Lu, X. Cheng, A. S. Yu, W. Ma
Sino-French Institute of Nuclear Engineering and Technology,
Sun Yat-sen University, Zhuhai, China

Abstract

Atmospheric muon imaging suffers from low efficiency due to the inherently low flux of atmospheric muons, requiring long data acquisition times. To address this limitation, this paper proposes two magnetic focusing systems to enhance atmospheric muon flux: a three-section superconducting solenoid and triplet quadrupole magnet lenses (short-range and long-range focusing configurations). For horizontally incident muons, the proposed solenoid and quadrupole lens designs both more than double the normalized muon flux for muons in the 0.6-1.2 GeV/c and 1.4-3.0 GeV/c ranges, respectively. All data are calculated based on sea-level atmospheric muon flux distribution. The long-range quadrupole design is particularly suitable for enhancing localized muon imaging within large-scale facilities. This work establishes focusing methods for atmospheric muons, enhancing efficiency in large-scale imaging applications such as archaeology, volcanology, and nuclear security.

MANUSCRIPTS

Muons are mostly produced via decay of pions generated by high-energy proton interactions [1]. Currently, muons are sourced from cosmic rays and accelerators [2]. Due to their high energy and strong penetration capabilities, atmospheric muons serve as effective non-destructive probes for rapid imaging, eliminating the need for additional radiation sources [3]. Atmospheric muon imaging has been widely applied across archaeology, volcanology, and nuclear security [4].

Despite its potential, the low flux of atmospheric muons, averaging 70 $m^{-2}\cdot s^{-1}\cdot sr^{-1}$ at zenith angle 0° , requires extended data collection periods [5]. For instance, the investigation of Xi'an City Wall required over three months of data collection [6]. Current muon focusing techniques remain confined to MeV-level energy focusing [7], rendering them incompatible with the broad energy spectrum of atmospheric muon sources. Therefore, this paper proposes methods to enhance GeV-level muon flux through two focusing schemes: a superconducting three-section solenoid and quadrupole magnets.

Characteristics of Atmospheric Muon Flux

The atmospheric muon flux data are referenced from BESS-TeV measurements [8]. Figure 1 shows sea-level atmospheric muon flux from 0.6 to 98 GeV/c. Our focusing device targets 0.5-4 GeV/c muons (approximately 68% of total flux) to enhance scattering signals for high-Z materials [9]. The focusing effect is expressed by flux magnification φ as shown in Eq. (1) and normalized flux magnification φ_N.

$$\varphi = \frac{N_{out}/\pi r_{out}^2}{N_{in}/\pi r_{in}^2}. \quad (1)$$

N_{out} and N_{in} represent particle counts through detection surfaces. Normalized flux magnification φ_N is calculated by weighting with momentum spectrum ratios.

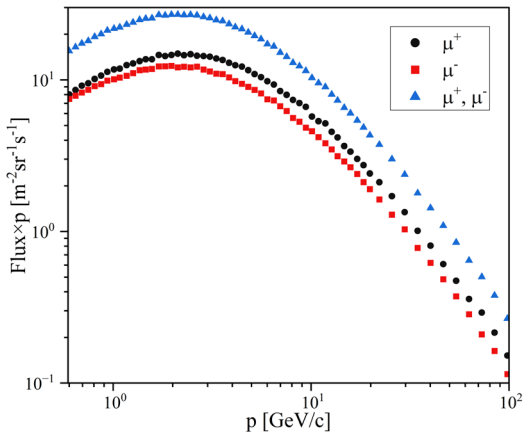


Figure 1: Sea-level atmospheric muon flux distribution [8].

Superconducting Solenoid Design

The three-section solenoid features inlet/middle/outlet diameters of 1 m, 0.75 m, and 0.5 m, with lengths optimized to 500 mm, 1000 mm, and 500 mm respectively. Magnetic field strengths are 5.5 T, 3.5 T, and 5.5 T. Figure 2 shows the solenoid dimensions with coil turns and current intensities. The superconducting solenoid utilizes niobium-titanium monolithic rectangular wire (insulated size: 1.28×0.83 mm^2) produced by Hefei Kuafu Superconducting Technology Co., Ltd [10]. The solenoid model was established using Microwave Studio [11] to obtain the simulated magnetic field, which was then imported into TraceWin [12] for beam dynamics simulations of 0.6, 0.8, 1.0, and 1.2 GeV/c muons. The results were compared with those from ideal-field simulations performed natively in TraceWin. Table 1 summarizes the comparison between the ideal and imported-field results at different detection distances. At 0.5 m from outlet, imported field simulation yields 2.17, achieving 91.17% of ideal value, reducing collection time by nearly half.

* Work supported by the National Natural Science Foundation of China (Grant No. 12575170), Guangdong Basic and Applied Basic Research Foundation (Grant No. 2024B1515120028).
† email address: luliang3@mail.sysu.edu.cn

Content from this work may be used under the terms of the CC BY 4.0 licence (© 2026). Any distribution of this work must maintain attribution to the author(s), title of the work, publisher, and DOI.

ISBN: 978-3-95450-275-2 ISSN: 2226-0366 doi: 10.18429/JACoW-LINAC2026-TUPO034

CRYOGENIC TESTING OF 650, 704, AND 1300 MHz SRF CAVITIES AT THE UKRI-STFC DARESBURY LABORATORY'S VERTICAL TEST FACILITY

A. E. T. Akintola†, A. Baig, Z. Bilques, A. Blackett-May, R. Hall, B. Harrison, J. Hassall, P. Hornickel, C. Jenkins, G. Jones, M. Jones, M. Lowe, O. B. Malyshev, D. Mason, P. McIntosh, G. Miller, J. Mutch, S. Pattalwar, M. Pendleton, D. Seal, A. Shabalina, T. Sian, I. Skachko, L. Smith, P. Smith, R. Valizadeh, A. Vick, A. Wheelhouse, S. Wilde
UKRI-STFC Daresbury Laboratory, Keckwick Lane, Daresbury, UK

Abstract

The UKRI-STFC Daresbury Laboratory operates a flexible vertical test facility (VTF) for testing superconducting radio-frequency (SRF) cavities. Thanks to a series of expansion and upgrade activities, including a new cavity test insert, improved magnetic hygiene, and increased cooldown rate (principally to facilitate residual magnetic flux expulsion), the facility is now capable of testing a single high-beta 650 MHz PIP-II cavity (with fast cooldown), up to three high-beta 704 MHz ESS cavities, or a single 1300 MHz cavity (either bulk Nb or thin film) per test cycle. The team can switch between 650, 704, and 1300 MHz cavity-testing configurations with minimal downtime between test runs. This contribution details the expanded capabilities resulting from the various upgrades, different modes of operation, and operational practices that enable cryogenic cavity testing at Daresbury.

INTRODUCTION

UKRI-STFC's Daresbury Laboratory is home to the Superconducting RF (SuRF) Laboratory, which houses the Vertical Test Facility (VTF), an ALAT Hélial ML cryoplant, a 3000 L Wessington dewar, a 2 K valve box, an ISO 4 cleanroom with a high-pressure rinse (HPR) system, and cryomodule integration workstations [1-3].

In 2019, UKRI-STFC commissioned the VTF for the qualification of SRF high-beta 704 MHz dressed bulk niobium cavities, as part of the UK's in-kind contribution to the European Spallation Source (ESS), a 5 MW spallation neutron source under construction in Lund, Sweden [4]. UKRI-STFC, with partners, qualified 84 dressed 704 MHz high-beta cavities at 2 K and delivered them to the Commissariat à l'Énergie Atomique et aux Énergies Alternatives (CEA) Saclay, France, for integration into 21 high-beta cryomodules with four spare cavities.

UKRI-STFC is also an in-kind contributor to the Proton Improvement Plan II (PIP-II) at the Fermi National Accelerator Laboratory, an upgrade to the existing proton accelerator complex that will provide the beam for the Long-Baseline Neutrino Facility Deep Underground Neutrino Experiment (LBNF-DUNE), whose far detector is located in South Dakota [5]. The scope extends to qualifying 20 dressed high-beta 650 MHz (HB650) bulk niobium cavities and integrating 18 of them into three HB650 cryomodules.

Although bulk niobium remains the established SRF cavity material of choice [6], a programme is underway at Daresbury to develop superconducting thin films and deposition processes onto bulk cavities. Coated cavities offer the prospect of reduced cavity manufacturing costs through reduced total superconducting material requirements and reduced operating costs through a higher critical temperature. This results in increased Q_0, reduced dynamic heat loading, and reduced RF input power for a given temperature, or allows a higher operating temperature, improving the cryogenic efficiency. Candidate materials include NbTiN, Nb_3Sn, V_3Si, other A15 compounds, and MgB_2, deposited onto niobium or copper substrates by physical or chemical vapour deposition [7]. Experiments and VTF upgrades [8] have been developed to enable SRF characterisation at cryogenic temperatures, from planar samples [9] through to coated cavities [10,11].

Vertical testing is performed using interchangeable cavity support inserts (CSIs): CSI-A for up to three dressed 704 MHz cavities, CSI-B for a single dressed 650 MHz cavity, and CSI-Mini for a single bare 1300 MHz cavity. All three share common cryogenic, vacuum, RF, and control interfaces, so the facility can be reconfigured between frequencies as part of the routine insert exchange.

ESS 704 MHZ DRESSED CAVITY TESTING – CSI-A

Testing of 704 MHz high-beta cavities for ESS began in 2019; CSI-A, shown in Fig. 1, accommodates up to three dressed cavities per test cycle, mounted horizontally and suspended below a header tank. Each cavity is cooled by filling its helium jacket directly rather than by immersing the cavity in a bath [12]. The insert is equipped with 12 CU-packaged Cernox thermometers, four thermometers for each cavity jacket. The cavities are five-cell elliptical structures with a geometrical $\beta = 0.86$, qualified against a nominal accelerating gradient of 19.9 MV/m at $Q_0 \geq 5 \times 10^9$ [13, 14]. Cooling, filling and testing a full insert requires ~1500 L of liquid helium per fill. Two identical CSI-A inserts were in use during the ESS testing campaign.

Content from this work may be used under the terms of the CC BY 4.0 licence (© 2026). Any distribution of this work must maintain attribution to the author(s), title of the work, publisher, and DOI.

† ayo.akintola@stfc.ac.uk

ISBN: 978-3-95450-275-2 ISSN: 2226-0366 doi: 10.18429/JACoW-LINAC2026-TUPO035

STATUS OF THE VACUUM SYSTEM FOR THE HIGH-ENERGY LINEAR ACCELERATOR SECTION OF RAON

M. O. Hyun†, H. Son, S. Choi
Institute for Rare Isotope Science, Institute for Basic Science (IBS), Daejeon, South Korea

Abstract

The Rare Isotope Accelerator complex for ON-line experiments (RAON) at the Institute for Basic Science (IBS) is currently operating the low-energy linear accelerator section successfully, and is preparing for the construction of the high-energy linear accelerator section. The fabrication of superconducting (SC) cryomodule prototypes is under way. In conjunction, the cryogenic, RF, magnet and vacuum systems are being prepared for integration and operation in alignment with the construction schedule. This paper describes the current status of the vacuum system for the high-energy linear accelerator section and details its auxiliary components, specifically the non-evaporable getter (NEG) and the cold cathode gauge (CCG).

INTRODUCTION

RAON, the rare isotope accelerator complex for ON-line experiments of the Institute for Basic Science (IBS), is being brought into operation in stages. The low-energy linear accelerator section is already operating successfully, and preparation for the construction of the high-energy section (SCL2) is now under way, with superconducting (SC) cryomodule prototypes in fabrication. The cryogenic, RF, magnet and vacuum systems are being prepared in parallel so that they can be integrated in line with the construction schedule. This paper reports the status of the beam line vacuum system for the high-energy section: the configuration of the chambers, the assembly and inspection sequence applied to the 36 units produced so far, and the treatment of the non-evaporable getter (NEG) and the cold cathode gauge (CCG).

VACUUM SYSTEM FOR THE HIGH-ENERGY LINAC

The vacuum system for the high-energy accelerator section has a configuration very similar to that of the low-energy accelerator section [1]. Figure 1 shows the layout of the vacuum system for the high-energy accelerator section.

As can be seen in Fig. 2, the vacuum system consists of the following parts arranged around the chamber: a support, a non-evaporable getter (NEG), a beam position monitor (BPM), a 10-inch CF flange, a beam pipe, an instrumentation tee, a cold cathode gauge (CCG), an all-metal angle valve (AMV) and the remaining connecting parts. With the exception of the NEG combined with a sputter ion pump (SIP), supplied as a single NEXTorr unit, the CCG and the metal valve, all of the other components were fabricated in house. This paper describes the work carried out from the post-fabrication assembly preparation onwards.

† atikus43@ibs.re.kr

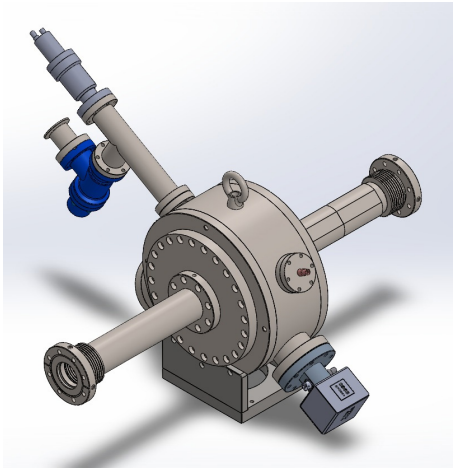


Figure 1: Layout of the SCL2 vacuum system.

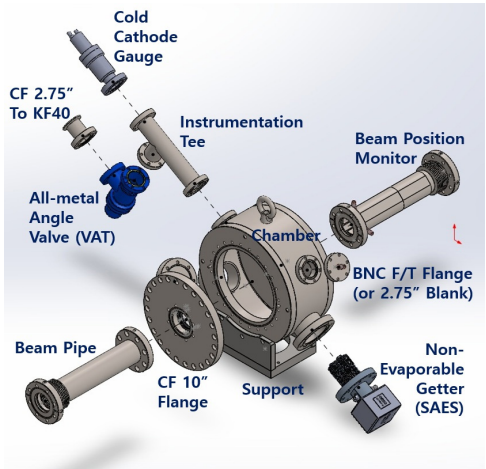


Figure 2: Exploded view and sub-components.

ASSEMBLY PROCESS

Fabrication and procurement of all components of the vacuum system for the high-energy accelerator section were completed in 2024, and assembly began in September 2025. The assembly process is shown in Fig. 3.

Figures 4 to 8 illustrate each step of the process. Every chamber and every part that forms part of the vacuum envelope is first ultrasonically cleaned at 35 kHz for 3 h at 38 °C and then blown dry with nitrogen (Fig. 4). The cleaned parts are subsequently dried in a Class 1000 clean room for more than 72 h (Fig. 5). Assembly is carried out in a Class 100 environment (Figs. 6 and 7) and covers, in sequence, the 10-inch CF flange holding the collimator, the BNC feedthrough (or a blank flange in its place), the BPM and the beam pipe, the 4.5-inch blank and the instrumentation tee, and finally the CCG, the AMV and the NEG, after which the vacuum seal is completed. Each assembled unit then passes through an inspection sequence comprising a

Content from this work may be used under the terms of the CC BY 4.0 licence (© 2026). Any distribution of this work must maintain attribution to the author(s), title of the work, publisher, and DOI.

ISBN: 978-3-95450-275-2 ISSN: 2226-0366 doi: 10.18429/JACoW-LINAC2026-TUPO036

ESS BEAM CURRENT MONITOR SYSTEM: TECHNICAL CHALLENGES AND IMPROVEMENTS FROM SEVEN YEARS OF OPERATION

H. Hassanzadegan, M. Mohammadnezhad, J. Murari
European Spallation Source, Lund, Sweden

Content from this work may be used under the terms of the CC BY 4.0 licence (© 2026). Any distribution of this work must maintain attribution to the author(s), title of the work, publisher, and DOI.

Abstract

With the restart of beam commissioning activities at the European Spallation Source (ESS) in January 2026, the Beam Current Monitor (BCM) system has been in operation for more than seven years. During this period, several beam monitoring and machine protection functions have been added to the system, including beam mode and destination consistency checks, as well as differential beam loss measurements. The overall system accuracy is about 0.1%, requiring reliable analog signal transmission over long cables, low-noise electronics and fast digital signal processing. These aspects are particularly important to minimize the impact of electromagnetic interference (EMI) from RF and other high-power pulsed equipment, thereby improving beam availability. This paper presents an overview of the ESS BCM functions, the technical challenges encountered during beam commissioning, and the solutions implemented to improve system performance and availability.

INTRODUCTION

The ESS Beam Current Monitor (BCM) system comprises a total of 19 AC current transformer (ACCT) sensors distributed along the approximately ~600 m long ESS linac [1]. In general, one ACCT is installed at the interface between successive linac sections to measure, among other parameters, the beam transmission efficiency through each section. Additional ACCTs are installed for specific diagnostic purposes, including one on the high-voltage cable of the Ion Source High-Voltage Power Supply (ISrc HVPS) to measure the current supplied to the ISrc platform, one downstream of the Medium Energy Beam Transport (MEBT) chopper beam dump to assess the chopper performance, and three ACCTs around the dipole magnets near the end of the linac to verify that the beam follows the intended path either toward the Tuning Beam Dump (TBD) or the Target. Further ACCTs are installed in the Dump Line (DmpL) and Accelerator-to-Target (A2T) sections for beam characterization and transmission measurements.

These detectors have played a key role in supporting ESS linac commissioning and operation and providing machine protection, including the achievement of several important milestones:

- First proton beam measured on the ESS site (from the ISrc to the Low Energy Beam Transport (LEBT)): September 2018
- First beam on the MEBT Faraday Cup (FC): November 2021
- First beam on the TBD: April 2025
- First 50 µs on the TBD: June 2025
- First 1.5 ms / 20 mA beam on the TBD: June 2026

Figure 1 shows a 50 µs beam pulse delivered to the TBD, as measured by 11 ACCTs distributed along the accelerator from the ISrc to the TBD itself. The change in the pulse length originates from the operation of the MEBT chopper and results in an approximately 20 µs longer pulse measured by the LEBT and Radio Frequency Quadrupole (RFQ) BCMs. A small residual beam component passing through the chopper is also visible in the signals of downstream BCMs.



Figure 1: A 50 µs beam on the TBD.

Although the BCM measurement functions proved to operate reliably, the machine-protection functions occasionally generated an excessive number of beam trips during the initial stages of beam commissioning in the abovementioned phases. Subsequent investigations showed that most of these trips were caused either by ElectroMagnetic Interference (EMI) from high-power switching equipment or by RF-related disturbances. In some cases, these perturbations generated transient signals on the BCM readout channels that exceeded the machine-protection thresholds, resulting in unwanted beam interruptions. These issues were subsequently mitigated through a combination of improvements to the BCM system and modifications to the machine-protection configuration.

In addition, operational experience gained during commissioning, together with evolving requirements, led to the implementation of several new features and enhancements to improve system performance, reliability, and operational flexibility. The following sections summarize the main issues encountered during commissioning, the corrective actions that were implemented, and the major BCM system improvements introduced since the start of beam operations.

ISBN: 978-3-95450-275-2 ISSN: 2226-0366 doi: 10.18429/JACoW-LINAC2026-TUPO037

AUTOMATED CONDITIONING UTILIZING MACHINE LEARNING: NETWORK OPTIMIZATION AND REINFORCEMENT LEARNING

S. Wagner-Rossel*,[1], H. Podlech[1,2], K. Kuempel[2]
[1]Institute of Applied Physics (IAP), Frankfurt, Germany
[2]Helmholtz Research Academy Hesse for Fair (HFHF), GSI Helmholtzzentrum für Schwerionenforschung, Campus Frankfurt, Frankfurt, Germany

Abstract

RF-conditioning is an essential pre-processing step of normal conducting cavities. This time-intensive work can pose great risks to equipment and cavity if conditioning-effects such as multipacting, discharges or degassing aren't taken seriously. To reduce the workload for human personnel, it was proposed to develop a deep-learning based algorithm to conduct conditionings on its own. This algorithm is trained on experimental data recorded from various conditionings performed by several experimenters. During initial training, the algorithm is tasked to predict the experimenters' action based on the power-levels, pressure and frequencies recorded over the last seconds. So far developed networks have been able to perform this task with average errors of few hundred Hertz and few tenths of dBm respectively. To teach the network to not only reproduce human behaviors, but identify the optimal course during conditioning, pre-trained networks are planned to be combined with reinforcement learning to enable continued learning during experiments. The results of experiments using optimized, pre-trained networks in two different *modus operandi* are being presented.

INTRODUCTION

Conditioning is a necessary but slow process, which every built cavity has to go through at least once. During a conditioning, the power injected into the cavity is slowly increased until the power levels required by the beam dynamics are reached. Since unwanted and potentially dangerous effects, such as outgassing, discharges or multipacting, can occur during this process, the standard procedure at IAP Frankfurt is to conduct a conditioning under the constant supervision of an experienced experimenter.

The process itself can take from several days to several weeks. In order to reduce the time and surveillance effort needed to perform a successful conditioning, supporting programs were developed and are further improved. As a first step, a LabView program was designed by IAP, as described in [1]. To achieve the long-term goal of fully automated conditioning, it was decided to develop a trainable machine learning algorithm, as was presented in [2]. Since a first experimental test in 2025 showed great potential [3], the network was reworked, optimized and tested again.

* s.wagner@iap.uni-frankfurt.de, ORCiD 0000-0002-3810-4820

NETWORK ARCHITECTURE

Several different architectures have been trained and tested. Even though the type of network used differs, the general layout follows the same principle: After a shared body, the network splits into two dedicated heads, one for the prediction of the right dBm (power) setting, one for the prediction of the right frequency setting. This proved more fruitful than single-headed network with two outputs. The following networks have been tested excessively: Multi-layered-perceptrons (MLP), convolutional neural networks (CNNs), long short term memory recurrent neural networks (LSTM RNNs) and a mixture of CNN and LSTM architecture (CNN-LSTMs). The latter yielded so far the best results during training and experiment. A simplified depiction of the data flow in such a CNN-LSTM is presented in Fig. 1. The CNN layers provide a sense for the importance of different features, while the LSTM layers provides a timely context.

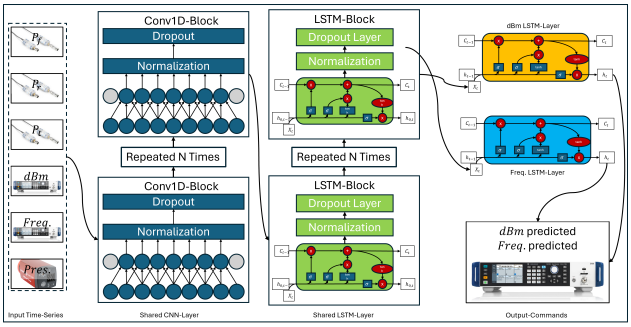


Figure 1: Simplified depiction of the architecture of a CNN-LSTM. The input time-series is processed by several shared CNN layers, before it is further analyzed using stacked LSTM layers. The final prediction is done by specialized LSTM heads, which predict the needed settings for the signal generator. Pictures adapted from [4–6].

BAYESIAN OPTIMIZATION

The performance of neural networks highly depends on their hyper parameters. Those are values predefined and not adjustable during training. They include for example the number of layers, the learning rate, the dropout rate as well as parameters important for the data pre-processing, here mainly the length of time series given as input to the network. Since all of those affect the training speed, stability and final performance, the choice of a good set of hyper parameters is crucial. Optimizers are widely used for this task due to time constraints and efficiency reasons. Many of those utilize Bayesian optimization.

Content from this work may be used under the terms of the CC BY 4.0 licence (© 2026). Any distribution of this work must maintain attribution to the author(s), title of the work, publisher, and DOI.

ISBN: 978-3-95450-275-2 ISSN: 2226-0366 doi: 10.18429/JACoW-LINAC2026-TUPO038

STATUS OF THE LOEWE-3 RFQ AT IAP FRANKFURT *

K. Kuempel[1,†], S. Altuerk[2], P. Braun[1], H. Hoeltermann[2], P. Müller[1,2], H. Podlech[1,3]
U. Ratzinger[1,2], J. Storch[1], S. Wagner-Rossel[1]
[1]Institute of Applied Physics (IAP), Frankfurt, Germany
[2]Bevatech GmbH, Mörfelden-Walldorf, Germany
[3]Helmholtz Research Academy Hesse for Fair (HFHF), GSI Helmholtzzentrum für Schwerionenforschung, Campus Frankfurt, Frankfurt, Germany

Abstract

The Institute of Applied Physics (IAP) at Goethe University Frankfurt has a long experience in the development of 4-rod RFQs. Within the LOEWE funding programme, funded by the Hessen Agentur under funding line 3, the conventional 4-rod RFQ design has been further developed. By implementing a series of improvements to the RF design and introducing metallic sealing technology, a demonstrator has been designed and constructed with the aim of achieving improved vacuum performance and a higher quality factor compared to conventional 4-rod RFQ designs. This paper presents the low-level RF (LLRF) measurements performed on the completed LOEWE-3 RFQ demonstrator, followed by the results of the subsequent high-power RF tests.

THE LOEWE-3 RFQ PROJECT

RFQs (Radio Frequency Quadrupoles) are usually used directly after the ion source or LEBT (Low Energy Beam Transport), especially in the low energy range, to accelerate, focus and bunch the ion beam before its further acceleration in the following structures.

RFQs can be realized in various configurations. The 4-rod RFQ discussed in this proceeding is a transmission-line resonator. The resonant structure consists of a series of stems, each connected to two of the four quadrupole electrodes. Between each pair of stems, a tuning plate is installed, whose height can be adjusted to tune the resonant frequency.

Although this design has proven to be highly reliable and continues to be used in modern projects, such as FRANZ [1] and MYRRHA [2], there is still potential for further development and optimization.

For the LOEWE-3 RFQ, the design effort focused on two key aspects.

Increase of the Q-Value

Usually there is a discrepancy between the simulated and the measured Q-value of a resonator. For cavity resonators, such as CH or IH-Cavities, the measured Q-value can achieve more than 90 % of the simulated Q-value. For 4-rod RFQs typically only 70–80 % of the simulated Q-value are measured. For example, measured Q-values of approximately 77 % and 75 % of the respective simulated values have been reported for the MYRRHA RFQ [3] and a 108 MHz 4-rod RFQ prototype developed for the GSI-HLI [4], respectively.

The different parts of the resonating structure of 4-rod RFQ (e.G. the stems, the tuning plates and the electrodes) are built separately and screwed together inside the tank, whereas the structure in the simulation model consists of one piece. Therefore, contact resistances between the different elements are not taken into account in the simulation.

To reduce these contact resistances that lower the Q-value the tuning plates of the previous 4-rod RFQ design will be replaced with tuning blocks that can be screwed to the stems with much higher pressure by three pull rods [5].

Improvement of the Vacuum Performance

To improve the vacuum performance in the LOEWE-3 RFQ the rubber O-rings used to seal the tank are replaced with metal seals with much higher properties in terms of leakage rate and service life. Three of these new seals are used per stem. Two for the access to the cooling channels of the electrodes and one for the connection between the steam and the bottom of the tank. [6]

The Simulation Model

As described in [6] the stems needed to be adjusted in the simulation model to create enough mounting surface for the metal sealings between the lower electrode and the stem. Also the stem had to be widened to have enough space for the metal sealing between the stem and the tank. A comparison between a conventional 4-rod RFQ simulation Model and the LOEWE-3 RFQ model is shown in Fig. 1.

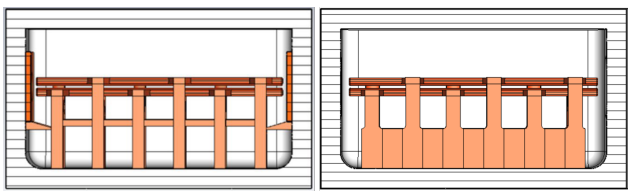


Figure 1: Comparison between a conventional 4-rod RFQ simulation model on the left side and the LOEWE-3 RFQ simulation model with tuning blocks and widened stems are needed for the metal sealings on the right side. Both models are designed for the same frequency.

* Work supported by LOEWE No. HA1575/23-128
† kuempel@iap.uni-frankfurt.de

Content from this work may be used under the terms of the CC BY 4.0 licence (© 2026). Any distribution of this work must maintain attribution to the author(s), title of the work, publisher, and DOI.

ISBN: 978-3-95450-275-2 ISSN: 2226-0366 doi: 10.18429/JACoW-LINAC2026-TUPO039

INTRA-PULSE FEEDBACK FOR SHORT RF PULSES IN LLRF SYSTEMS

B. Baričević[†,1], D. Teytelman[*,2], M. Cargnelutti[1],
L. Piersanti[3], M. Bellaveglia[3], B. Serenellini[3], A. Gallo[3]
[1]Instrumentation Technologies, Solkan, Slovenia
[2]Dimtel, Inc., San Jose, CA, United States
[3]INFN - Laboratori Nazionali di Frascati, Frascati, Italy

Content from this work may be used under the terms of the CC BY 4.0 licence (© 2026). Any distribution of this work must maintain attribution to the author(s), title of the work, publisher, and DOI.

Abstract

Low-Level Radio Frequency (LLRF) control of accelerating cavities with microsecond-scale pulses is challenging because short pulses limit the effectiveness of Field-Programmable Gate Array (FPGA)-based intra-pulse feedback, restricting control to pulse-to-pulse corrections. This is often insufficient to compensate RF-chain-induced jitter and achieve the required field stability. We propose a novel intra-pulse feedback scheme for short pulses, featuring autoconfiguration and support for advanced pulse shaping, including SLAC Energy Doubler (SLED) systems.

An implementation of this novel feedback concept was developed and deployed at the Istituto Nazionale di Fisica Nucleare (INFN) SPARC_LAB facility, representing the first realization of its kind. It is now routinely operated with state-of-the-art performance, demonstrating significantly improved phase stability compared with conventional pulse-to-pulse control.

We present here a new implementation for short-pulse operation, based on a different architecture that simplifies system integration. This paper describes its design and experimental validation, including measurements at INFN SPARC_LAB. The proposed solution extends the Libera LLRF platform and has strong potential for short-pulse accelerator applications.

INTRODUCTION

Linear accelerators (linacs) are widely used in scientific research, medical applications, and industrial systems to accelerate charged particles using RF electromagnetic fields. Many modern normal-conducting linacs operate with RF pulses of only a few microseconds, requiring the accelerating field to maintain high amplitude and phase stability in the presence of disturbances such as klystron variations, modulator ripple, cavity detuning, and beam loading.

Conventional field stabilization is achieved using digital Low-Level RF (LLRF) systems implementing pulse-to-pulse feedback and adaptive feedforward algorithms. During each RF pulse, the cavity field is measured, digitized, and processed to determine corrections that are applied to subsequent pulses. This approach is dictated by the inherent latency of digital signal acquisition, processing, and output generation, which is typically a few hundred nanoseconds. While adequate for pulse-to-pulse regulation, such latency represents a significant fraction of the RF pulse duration and prevents the implementation of effective feedback within the same pulse. Consequently, disturbances occurring during an RF pulse cannot be corrected in real time and instead affect the accelerating field until the next pulse.

As accelerator facilities demand increasingly stringent field stability requirements, particularly for short-pulse, high-gradient linacs, there is growing interest in techniques capable of compensating disturbances on an intra-pulse timescale. Such approaches can significantly improve field regulation by correcting perturbations while the RF pulse is still in progress, extending the capabilities of conventional digital LLRF systems.

One of the dominant factors limiting phase stability in high-gradient pulsed linacs is the phase modulation introduced by the RF power source. In klystron-based systems, fluctuations of the modulator high-voltage waveform, combined with the intrinsic phase-pushing characteristics of the klystron, introduce a time-dependent phase error throughout the RF pulse. Additional sources of instability contribute to stochastic phase perturbations, resulting in both deterministic and random phase errors that directly degrade beam quality. While the deterministic component can be effectively compensated using adaptive feedforward techniques, the residual pulse-to-pulse jitter cannot be predicted in advance and therefore requires feedback operating on the same timescale as the disturbance

INTRA-PULSE FEEDBACK CONCEPT

To overcome the limitations of conventional pulse-to-pulse LLRF control, several approaches have been proposed to implement feedback correction within the RF pulse. These techniques typically extract a portion of the klystron forward RF signal, measure its phase deviation relative to the RF drive signal, and apply a fast correction to the RF drive path to compensate for the phase error. In previously reported implementations [1, 2], the reference signal for the feedback loop is commonly obtained by splitting the RF drive signal and generating the required phase relationship using dedicated phase shifters. Although effective, this approach requires manual adjustment of the phase and gain settings of the correction path according to the specific RF setup and operating conditions.

The approach proposed in this work introduces a different configuration in which the phase reference required for the intra-pulse feedback loop is directly provided by the digital LLRF system as a separate signal. The proposed architecture is shown in Fig. 1. The LLRF generates the RF drive signal and provides a coherent phase reference to the feedback system. A directional coupler at the klystron output extracts a sample of the forward RF signal, which

† borut.baricevic@i-tech.si
* dim@dimtel.com

ISBN: 978-3-95450-275-2 ISSN: 2226-0366 doi: 10.18429/JACoW-LINAC2026-TUPO041

PHYSICS DESIGN AND BEAM DYNAMICS OPTIMIZATION FOR A FULLY CRYOGENIC INJECTOR TEST PLATFORM AT IHEP

Z. T. Liu[1,2], C. Meng*[1,2], O. Z. Xiao[1], N. Gan[1,2], J. R. Zhang[1,2], W. Li[1,2], Z. Ming[1,2], Y. H. Li[1,2], J. Y. Li[1,2]
[1]Institute of High Energy Physics, Chinese Academy of Sciences, Beijing, China
[2]University of Chinese Academy of Sciences, Beijing, China

Content from this work may be used under the terms of the CC BY 4.0 licence (© 2026). Any distribution of this work must maintain attribution to the author(s), title of the work, publisher, and DOI.

Abstract

High-brightness electron beams with ultra-low emittance are essential for X-ray free-electron lasers (XFELs), ultrafast electron diffraction (UED) and ultrafast electron microscopy (UEM). Radio-frequency (RF) copper structures operated at cryogenic temperatures sustain markedly higher breakdown thresholds, enabling the accelerating gradients required by ultra-bright electron sources. This paper presents the physics design of a compact test platform that integrates a C-band 5712 MHz cryogenic RF gun with a matching cryogenic accelerating structure, both operating at 77 K. A two-stage optimization contrasting an idealized model with an engineering-constrained model was carried out using the ASTRA code coupled to the non-dominated sorting genetic algorithm II (NSGA-II). Under the constrained model, longitudinal flattop and Gaussian laser profiles reach comparable normalized transverse emittances of about 0.125 mm mrad for a 100 pC bunch, indicating that the choice between them is governed by bunch-length and laser-system considerations rather than by an emittance advantage. The gradient dependence of the emittance and a tuning hierarchy for experimental operation are also quantified.

INTRODUCTION

The generation of high-brightness electron beams underpins X-ray free-electron lasers (XFELs) [1, 2] as well as ultrafast electron diffraction (UED) and ultrafast electron microscopy (UEM) [3]. Further improvements in the performance of these facilities require electron beams of still higher brightness and lower emittance in order to enhance photon flux and spatiotemporal resolution [4].

Normal-conducting radio-frequency (RF) photoinjectors are attractive for this purpose, but further gains in brightness demand higher accelerating gradients, which are fundamentally limited by RF breakdown in conventional copper structures. Cryogenically cooled copper offers a route around this limit: operation near 45 K has been shown to improve the quality factor and to sustain surface fields approaching 500 MV/m before breakdown in X-band structures [5]. Building on this, the UCLA–SLAC–LNF collaboration studied a cryogenic S-band photogun predicting a normalized emittance of 40 nm at 200 pC with a peak cathode field near 240 MV/m [6], and subsequently a cryogenic C-band photogun reaching 55 nm at 100 pC at comparable gradients [7, 8].

Extending this line of work, a compact test platform is proposed that integrates a 5712 MHz C-band cryogenic RF gun with a matching cryogenic accelerating structure (AS), with the entire machine held at 77 K. The platform is intended to explore the limits of high-gradient operation under cryogenic conditions and to serve as a proof of concept for an all-cryogenic injector architecture. Because many interdependent parameters influence the final emittance, the multi-objective genetic algorithm NSGA-II [9, 10] is used to explore the design space efficiently.

PLATFORM LAYOUT

The layout of the platform is shown in Fig. 1. It comprises a copper photocathode RF gun, a drive-laser system, focusing solenoids, an accelerating structure, quadrupoles, dipoles and beam diagnostics, with the RF structures maintained at 77 K by liquid-nitrogen cooling.

Electron beams are produced by photoemission from a copper photocathode driven by a 257.5 nm ultraviolet laser pulse. The drive-laser system is based on the high-power picosecond system reported in Ref. [11], which demonstrated 40 W green output at 515 nm. The present design extends the system to ultraviolet operation by an additional frequency-conversion stage and adds longitudinal pulse shaping. It is designed to support both unshaped Gaussian pulses of a few hundred femtoseconds to a few picoseconds and longitudinal flattop pulses of approximately 0.8 ps to 20 ps generated by a birefringent-crystal pulse-stacking module.

The 2.5-cell C-band photocathode gun resonates at 5712 MHz, with the accelerating gradient set at 180 MV/m, chosen as an experimentally achievable operating point for stable cryogenic operation. A 0.54 m long solenoid with a maximum on-axis field of 3000 Gs is placed downstream of the gun to compensate the emittance growth driven by space charge at low energy [12]. A bucking solenoid, identical to the main solenoid but operated with opposing current, is placed symmetrically upstream of the gun to cancel the residual field at the cathode and suppress emittance growth from beam magnetization [13]. At the beam waist downstream of the gun solenoid, a 1 m standing-wave accelerating structure of 40 cells raises the beam energy to 70 MeV. A large-aperture (30 mm) gun accommodates the high geometric emittance at low energy, while a smaller-aperture (11 mm) structure supports efficient downstream acceleration.

Several practical constraints prevent a free choice of layout. The main solenoid centre is fixed at 140 mm from the

* mengc@ihep.ac.cn

ISBN: 978-3-95450-275-2 ISSN: 2226-0366 doi: 10.18429/JACoW-LINAC2026-TUPO043

MAINTENANCE STRATEGIES AND HIGH-POWER RF TESTING OF ESS RFQ POWER COUPLERS AND DTL RF WINDOWS

A. Passarelli*, W. Borg, S. Ekström, A. Krawczyk, R. Montano,
D. Nicosia, P. Pierini, H. Przybilski, A. Zwozniak
European Spallation Source (ESS), Lund, Sweden

Abstract

Following the Beam on Dump (BOD) and BOD2 campaigns, the European Spallation Source (ESS) is preparing for the subsequent BOD3 and Beam on Target (BOT) phases, which require higher levels of accelerator reliability, availability, and stability. Ensuring continuous operation demands not only effective maintenance but also advanced strategies for managing critical components. This work focuses on RFQ power couplers and DTL RF windows, key elements for RF power transmission and vacuum integrity, exposed to significant electromagnetic, thermal, and vacuum stresses. Beyond maintenance, the study presents dedicated test stands for high-power RF testing and conditioning in a controlled environment. Main issues encountered during testing, such as multipacting, RF arcing, and contamination, are analyzed. These efforts aim to reduce risks, improve reproducibility, and ensure the availability of ready-to-use spare components, minimizing machine downtime. This work shows that integrating maintenance with dedicated testing infrastructure is essential to enhance RF system reliability and support future high-power ESS operation.

INTRODUCTION

The reliability and availability of high-power RF components are essential for the current commissioning and future operation of the ESS. Among these components, DTL RF windows and RFQ power couplers are subjected to high electromagnetic, thermal, and vacuum stresses, making dedicated qualification procedures necessary before installation in the accelerator.

During the Beam-on-Dump commissioning campaign, persistent multipacting was observed on one of the operational DTL RF windows, motivating its replacement and refurbishment [1]. The underlying multipacting mechanisms were subsequently investigated through dedicated numerical studies [2], supporting the development of a systematic high-power qualification procedure. In parallel, ESS is commissioning a dedicated high-power test stand for the qualification of RFQ power couplers, building upon the concepts previously developed for the RFQ [3, 4].

This paper presents the high-power qualification of refurbished DTL RF windows together with the current status of the RFQ power coupler test stand and the preliminary validation of its waveguide-to-coaxial transitions.

DTL RF WINDOW HIGH-POWER TEST

High-power RF testing of the DTL RF windows at ESS is performed using the 352 MHz test stand. A schematic overview of the experimental setup is shown in Fig. 1.

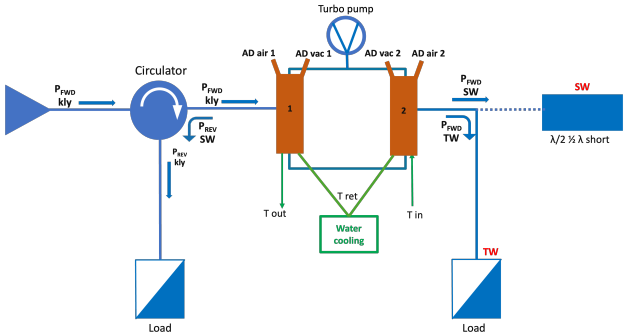


Figure 1: Schematic overview of the RF test configuration.

The RF power is generated by a klystron and first passes through a circulator, whose purpose is to protect the RF source from reflected power, particularly during standing-wave operation. Any reflected power is diverted to a matched load, preventing excessive power from returning to the klystron. The forward RF power is then delivered to the test assembly, consisting of two RF windows and a vacuum vessel. The vacuum vessel is connected to a turbomolecular pump, providing the vacuum environment required for the vacuum side of both RF windows. Before the test, both RF windows are cleaned and installed on the vacuum vessel inside a portable clean-room environment. After installation, vacuum pump-down and leak tests are performed to confirm the integrity of the vacuum envelope.

The downstream termination depends on the test configuration. During travelling-wave measurements, the RF power is absorbed by a matched load, thereby minimizing reflections. During standing-wave measurements, the load is replaced by a movable short circuit. The electrical distance between the RF window and the short is varied in discrete steps corresponding to fractions of the guide wavelength, producing different reflection phases and, consequently, different standing-wave field distributions at the window location. The test stand is equipped with a dedicated diagnostic system for continuous monitoring of the RF window performance. Six thermocouples are mounted on the external surfaces of the windows to monitor their temperature during operation. In addition, AFT photodiodes are installed on both the air and vacuum sides of each RF window to detect light emission associated with RF breakdown or multipacting activity.

* andrea.passarelli@ess.eu

Content from this work may be used under the terms of the CC BY 4.0 licence (© 2026). Any distribution of this work must maintain attribution to the author(s), title of the work, publisher, and DOI.

ISBN: 978-3-95450-275-2 ISSN: 2226-0366 doi: 10.18429/JACoW-LINAC2026-TUPO044

ANALYTICAL OPTIMIZATION OF LONGITUDINAL PHASE SPACE AND WAKEFIELDS COMPENSATION FOR THE MAIN LINAC OF STCF*

H. Hu[1], S. T. Teng[1], T. N. Hu†[1], Y. F. Zeng[1], Y. Wang[1], D. Gu[2], Y. J. Yuan[3], J. Y. Tang[4]
[1]Huazhong University of Science and Technology, Wuhan, China
[2]Shanghai Advanced Research Institute, Shanghai, China
[3]University of Chinese Academy of Sciences, Beijing, China
[4]University of Science and Technology of China, Hefei, China

Content from this work may be used under the terms of the CC BY 4.0 licence (© 2026). Any distribution of this work must maintain attribution to the author(s), title of the work, publisher, and DOI.

Abstract

In the Super Tau-Charm Facility (STCF) Main Linac, intense short-range longitudinal wakefields from high-charge bunches cause severe energy spread degradation and nonlinear longitudinal phase space (LPS) distortions. We present an analytical model describing LPS evolution under RF acceleration, wakefields, and longitudinal space charge. By utilizing an equivalent truncated-Gaussian distribution, we derived closed-form analytical expressions for the high-order moments of the LPS. Based on this, an analytical optimization method is proposed to determine the optimal RF phase that minimizes the root-mean-square (RMS) energy spread. Theoretical predictions show good agreement with Elegant macro-particle tracking simulations, particularly in the core bunch region. With this optimized configuration, wakefield-induced degradation is effectively compensated, fulfilling the stringent beam requirements of the STCF.

INTRODUCTION

The Super Tau-Charm Facility (STCF) is a next-generation high-luminosity e^+e^- collider in the τ-charm energy region [1]. Its main linac must deliver high-charge electron bunches with sub-percent-level RMS energy spread. Intense short-range geometric wakefields, together with longitudinal space charge (LSC), distort the longitudinal phase space (LPS) and degrade beam quality. Particle tracking simulations are the standard tool for RF parameter optimization, but they provide limited physical insight and become computationally expensive for multi-dimensional scans.

This paper presents an analytical framework that captures the essential beam dynamics in closed form. A unified expansion of the wake potential yields wake-induced LPS coefficients of arbitrary order as linear combinations of $I(\nu)$ integrals. The RMS energy spread is a quadratic function of the exit chirp δ_1', whose minimum and optimal RF phase are obtained analytically. Predictions are benchmarked against ***Elegant*** tracking simulations with good agreement, providing a computationally efficient tool for linac optimization.

* This work is supported by the National Natural Science Foundation of China (No.12341501), the National Key R&D Program of China under Contract No. 2022YFA1602200, the international partnership program of the Chinese Academy of Sciences Grant No. 211134KYSB20200057 and the STCF key technology research and development project.
† TongningHu@hust.edu.cn

LONGITUDINAL PHASE SPACE ANALYSIS

We describe the longitudinal phase space of a bunch in terms of the relative energy deviation $\delta(s)$ as a function of the longitudinal position s relative to the bunch center ($s = 0$). The LPS is parameterized by a third-order Taylor expansion:

$$\delta(s) = \delta_0' s + \frac{1}{2}\delta_0'' s^2 + \frac{1}{6}\delta_0''' s^3, \tag{1}$$

where the constant term vanishes by definition of the reference particle. The coefficients $\delta_0^{(n)}$ characterize the linear chirp ($n = 1$), curvature ($n = 2$), and cubic distortion ($n = 3$) of the LPS.

RF Acceleration

For an RF accelerating structure operating at voltage V_{rf} and phase ϕ, the energy gain of a particle at position s is:

$$\Delta E_{rf}(s) = eV_{rf}\cos(\phi + ks), \tag{2}$$

where $k = 2\pi/\lambda$ is the RF wave number. Since $|ks| \ll |\phi|$ for typical bunch lengths, we expand Eq. (2) to third order:

$$\Delta E_{rf}(s) \simeq \Delta E_{rf}(0) + \Delta E_{rf}'(0)s + \frac{1}{2}\Delta E_{rf}''(0)s^2 + \frac{1}{6}\Delta E_{rf}'''(0)s^3, \tag{3}$$

where the coefficients are:

$$\begin{aligned} \Delta E_{rf}(0) &= eV_{rf}\cos\phi, \\ \Delta E_{rf}'(0) &= -keV_{rf}\sin\phi, \\ \Delta E_{rf}''(0) &= -k^2 eV_{rf}\cos\phi = k^2\Delta E_{rf}(0), \\ \Delta E_{rf}'''(0) &= k^3 eV_{rf}\sin\phi = -k^2\Delta E_{rf}'(0). \end{aligned} \tag{4}$$

A critical observation from Eq. (4) is that a single-frequency RF cavity cannot independently control all LPS coefficients: the second-order coefficient is locked to the energy gain $\Delta E_{rf}(0) = E_1 - E_0$, and the third-order coefficient is proportional to the first-order one .

Longitudinal Geometric Wakefields

The short-range geometric wakefield in a periodic accelerating structure can be modeled by the Karl Bane wake function [2, 3]. For short bunches, we expand it to third order:

$$\begin{aligned} W(z) &= W_m \exp\left(-\sqrt{z/s_0}\right) \\ &\approx W_m\left[1 - \left(\frac{z}{s_0}\right)^{1/2} + \frac{1}{2}\left(\frac{z}{s_0}\right) - \frac{1}{6}\left(\frac{z}{s_0}\right)^{3/2}\right], \end{aligned} \tag{5}$$

ISBN: 978-3-95450-275-2 ISSN: 2226-0366 doi: 10.18429/JACoW-LINAC2026-TUPO045

PLASMA PROCESSING DEVELOPMENTS FOR MEDIUM- AND HIGH-BETA CAVITIES IN THE ESS LINAC

E. Del Core*[1], A. Passarelli†[2], A. Bignami[2], A. Bosotti[1], E. Cenni[3], A. Gevorgyan[2], C. Maiano[2], P. Pierini[2], H. Przybilski[2], D. Sertore[1]
[1]Istituto Nazionale di Fisica Nucleare (INFN), LASA, Segrate, Italy
[2]European Spallation Source (ESS), Lund, Sweden
[3]Commissariat à l'Énergie Atomique et aux Énergies Alternatives (CEA), Paris-Saclay, France

Content from this work may be used under the terms of the CC BY 4.0 licence (© 2026). Any distribution of this work must maintain attribution to the author(s), title of the work, publisher, and DOI.

Abstract

Plasma processing is increasingly recognized as an effective technique for mitigating field emission and restoring the performance of SRF cavities. A collaboration between CEA, ESS and INFN is currently working to adapt and optimize this method for the medium- and high-beta elliptical cavities installed in the ESS linac. This contribution summarizes ongoing efforts to implement plasma processing both in cavities assembled in cryomodules and in cavities prepared for vertical testing. The work presents electromagnetic analyses performed to identify the modes that best allow processing of the cavities, together with the conceptual design of the vacuum system for the experimental setup. Results obtained on a 704 MHz medium-beta cavity equipped with different couplers are also reported, along with preliminary investigations carried out on the 704 MHz high-beta cavity.

INTRODUCTION

Superconducting radiofrequency (SRF) cavities provide high accelerating gradients with low RF power dissipation and are key components of modern particle accelerators. Nevertheless, their performance is often limited by field emission caused by hydrocarbon contaminants deposited on the niobium surface. Early studies at the Spallation Neutron Source (SNS) demonstrated the potential of plasma processing to mitigate field emission in SRF cavities [1, 2], through the removal of hydrocarbon contaminants and improvement of the niobium work function [3]. The technique was subsequently implemented at other facilities, including in-cryomodule processing of LCLS-II cavities [4, 5] and in-tunnel activities at CEBAF [6, 7]. These studies confirmed the effectiveness of low-pressure discharges, typically using a noble gas with a small oxygen admixture, in removing surface contaminants and reducing field emission.

CEA, ESS and INFN are jointly developing a plasma processing procedure for the ESS 704.42 MHz medium-beta (MB, $\beta = 0.67$) six-cell and high-beta (HB, $\beta = 0.86$) five-cell elliptical cavities. Two scenarios are being investigated: plasma processing in a vertical test stand before cold RF testing and in-situ treatment of cavities installed in the cryomodule, the latter reducing downtime, manpower and operational costs while mitigating field emission.

* elisa.delcore@mi.infn.it
† andrea.passarelli@ess.eu

As part of this collaboration, previous activities on the MB cavities demonstrated the feasibility of plasma processing through the development of the RF and vacuum systems, electromagnetic simulations, bead-pull measurements, and controlled plasma ignition and transfer through all cavity cells [8–10]. Starting from these results, the first part of this work is dedicated to the optical emission spectroscopy (OES) analysis of the plasma produced in the MB cavity. This analysis provides an initial characterization of the discharge and allows the emitting species present during plasma operation to be identified. The activity is then extended to the HB cavities. Electromagnetic simulations are presented to identify suitable HOMs for plasma ignition and cell-to-cell propagation. Finally, the conceptual design of the HB vacuum system is described.

SPECTROSCOPY ANALYSIS ON MEDIUM BETA CAVITY

Optical emission spectroscopy was employed to analyze the characteristic emission lines of plasma. The analysis served two main purposes. First, it allowed us to verify the gas composition by identifying the characteristic emission lines associated with each gas species. Second, it provided information on the atomic and molecular species present in the plasma, as well as on their excitation state, thereby offering insights into the plasma characteristics and its underlying physical processes. Emission spectra were acquired using an Ocean FX spectrometer operating over the wavelength range from 200 to 850 nm and under different operating conditions to investigate the evolution of the plasma as a function of the process parameters. This spectrometer was mounted on the beam tube, in correspondence with the viewport.

Since the ignition gas used was nitrogen, particular attention was devoted to the identification of the characteristic molecular nitrogen and ionized nitrogen band systems, together with atomic nitrogen lines when present. The spectra were also inspected for the presence of oxygen-related emission features, which could originate from residual air in the cavity.

As OES is a non-invasive diagnostic technique, spectra could be acquired in real time without perturbing the discharge. The relative intensity of the emission lines was used to qualitatively assess variations in the concentration of the emitting species, particularly during plasma tuning, as this process leads to an increase in the plasma density.

ISBN: 978-3-95450-275-2 ISSN: 2226-0366 doi: 10.18429/JACoW-LINAC2026-TUPO046

DEVELOPMENT OF A C-BAND HIGH-GRADIENT TRAVELING WAVE ACCELERATING TUBE FOR THE SOUTHERN ADVANCED PHOTON SOURCE (SAPS)

Ahong Li*[1,2], Huachang Liu[1,2], MengXu Fan[1,2], Xiaolei Wu[1,2], Qi Yu Kong[1,2], Xingguang Liu[1,2], Xiao Li[1,2], Jibran Latif[1,2], Qiang Chen[1,2]
[1]Spallation Neutron Source Science Center, Dongguan, China
[2]Institute of High Energy Physics, Beijing, China

Abstract

A C-band high-gradient traveling-wave accelerating tube is developed for the Southern Advanced Photon Source (SAPS) injector linac. The tube operates in the 2π/3 constant-gradient mode with a target average gradient of 40 MV/m over a 2 m structure. An arched cavity geometry is adopted to improve shunt impedance, achieving an 11.6 % increase in Q value and a 10.3 % increase in shunt impedance compared with the conventional rectangular cavity. An iterative optimization method based on shunt impedance correction is established for constant-gradient cavity chain design, achieving axial field uniformity better than ±2 %. A 44-cell prototype was fabricated, tuned, and high-power tested. Low-power measurements using the non-resonant perturbation method demonstrate S11 better than -50 dB and field uniformity within ±2 %. High-power conditioning achieves a maximum gradient of 42 MV/m with a breakdown rate meeting the design requirements.

INTRODUCTION

The Southern Advanced Photon Source (SAPS) is a planned 3.5 GeV fourth-generation diffraction-limited storage ring designed to provide ultra-high-brightness synchrotron radiation beams [1]. To achieve extremely low emittance, the storage ring possesses a small dynamic aperture. Therefore, a "linac + booster" scheme is adopted as the injector route for the project. Compared with S-band accelerating structures, C-band cavities offer smaller dimensions and higher shunt impedance, which can achieve higher-gradient. In contrast to X-band structures, C-band cavities allow more relaxed machining tolerances, offer superior suppression of short-range wakefields, and reduce manufacturing costs [2-3]. In recent years, C-band technology has been successfully applied at facilities including SACLA, SwissFEL and the Shanghai Soft X-ray FEL (SXFEL) [4-6]. This paper describes the design, fabrication and experimental verification of a C-band high-gradient travelling-wave accelerating tube developed for the SAPS injector. Aiming to develop a 2 m-long accelerating tube with an average accelerating gradient of 40 MV/m. The structure parameters are optimized to reduce breakdown probability and improve shunt impedance. The design of a 113-cell cavity is accomplished, and a 44-cell prototype cavity is fully designed, fabricated, tuned and experimentally validated, furthermore it can serve for beam experiments on the electron gun test platform (in Fig. 1).

* Email: liah@ihep.ac.cn

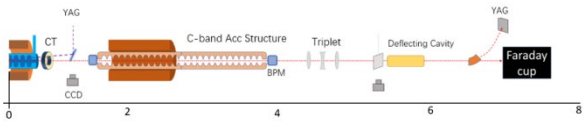


Figure 1: Schematic layout for the C-band test platform (Phase-II).

PHYSICAL DESIGN AND STRUCTURE OPTIMIZATION

Cell Structure Optimization

The C-band travelling-wave accelerating tube operates in the 2π/3 mode with a constant-gradient configuration. Superfish is employed for cavity modelling and rapid iteration to optimize the quality factor and effective shunt impedance. Afterwards, three-dimensional electromagnetic simulations are carried out for analysis of the couplers and full cavity structure [7].

In this design, arched cavities are adopted to replace conventional rectangular cavities for higher shunt impedance. The key geometric parameters for arched cavity optimization include the elliptical edge semi-axes A and B, disk thickness t, average iris aperture a, and arch curvature radius R_0. The optimization objective is to reduce the ratio of peak electric field to accelerating gradient E_{peak}/E_0, while maintaining a high shunt impedance, as shown in Fig. 2.

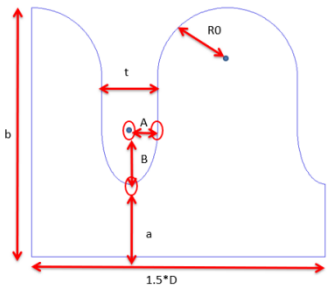


Figure 2: 1.5Cell structure model.

Superfish is used to compare the two cavity types. Simulation results show that under the same average iris radius and disk edge shape, the arched cavity achieves an 11.6 % increase in Q value and a 10.3 % increase in shunt impedance R_s compared with the rectangular cavity. The effects of different A and B values on E_{peak}/E_0 and shunt impedance were analyzed. After comprehensive consideration, $A = 2$ mm and $B = 4$ mm were selected as the optimal structural parameters.

Content from this work may be used under the terms of the CC BY 4.0 licence (© 2026). Any distribution of this work must maintain attribution to the author(s), title of the work, publisher, and DOI.

ISBN: 978-3-95450-275-2 ISSN: 2226-0366 doi: 10.18429/JACoW-LINAC2026-TUPO047

MULTIPHYSICS-BASED OPTIMIZATION OF COOLING STRUCTURE FOR DRIFT TUBES IN A HIGH-INTENSITY PROTON LINAC

Ahong Li†[1,2], Huachang Liu[1,2], Xiaolei Wu[1,2], Peihua Qu[1,2], Bo Li[1,2], MengXu Fan[1,2], Qiyu Kong[1,2], Cong Zhang[1,2], Wenzhong Zhou[1,2], Qiang Chen[1,2], Jibran Latif[1,2]
[1]Spallation Neutron Source Science Center, Dongguan, China
[2]Institute of High Energy Physics, Beijing, China

Abstract

A multiphysics simulation model is established using COMSOL to analyse drift-tube water-cooling structures in the DTL for the CSNS-II upgrade. Whole-cavity temperature rise and frequency shift are evaluated, and some cooling schemes are systematically compared. Results show the water pipe cross-section is the primary limiting factor: increasing the inner diameter from 4 mm to 6 mm reduces the maximum temperature by ~28%. An improved structure with coaxial nested pipes and a double-layer water jacket is proposed. Two partition strategies are compared; the axial U-shaped baffle achieves better cooling performance and temperature uniformity.

INTRODUCTION

The Drift Tube Linac (DTL) is the core accelerating structure of room-temperature high-intensity proton linacs. The China Spallation Neutron Source (CSNS) upgrade project will increase the beam power from 100 kW to 500 kW, raising the H- linac energy from 80 MeV to 300 MeV [1-2], and increasing RF repetition frequency from 25 Hz to 50 Hz. The higher RF duty factor increases the drift tube heat load, requiring improved water-cooling capacity.

Higher RF duty factors impose severe cooling demands on drift tubes (DTs). However, DTs embedded with electromagnetic quadrupoles (EMQs) have extremely limited space for water channels due to complex fabrication. This problem is more critical in higher-energy DTL sections, where the heat flux density at the DT nose cone is substantially higher and harder to dissipate. a multi-physics coupling calculation can be performed.

Thermal stability analysis of RF cavities typically employs multiphysics methods combining electromagnetic fields, solid heat transfer, and structural mechanics [3-4]. However, systematic studies on cooling optimization of individual drift-tube structures in Alvarez-type DTLs remain limited [5-6]. This paper uses COMSOL Multiphysics to compare some water-cooling improvement schemes through temperature and flow field analysis, and proposes an optimized cooling structure for the DTL with high RF duty.

WHOLE-CAVITY TEMPERATURE RISE AND FREQUENCY SHIFT

First, the temperature rise and frequency shift of the four DTL cavities under increased RF duty factor in CSNS-II are evaluated through simulation. The computational model is shown in Fig. 1.

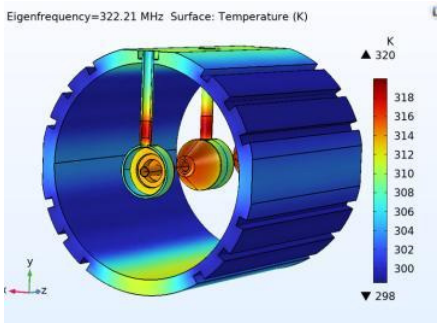


Figure 1: DTL cavity temperature rise distribution simulation model.

Table 1: Temperature Rise and Frequency Shift of Each DTL Cavity in CSNS-II

Cavity	Freq. shift [kHz]	Temp. change [°C]	Relative to DTL1
DTL1	68.64	16	1.00
DTL2	79.69	17	1.16
DTL3	87.72	19	1.28
DTL4	100.67	22	1.47

As shown in Table 1, the temperature rise and frequency shift increase monotonically from DTL1 to DTL4, with DTL4 reaching 1.47 times the shift of DTL1 [7]. Along the beam direction, drift tube dimensions increase, leading to higher RF power loss for each DT, while the cooling tube cross-section remains fixed due to same stem size. Since DTL4 shows the largest shift, detailed simulations for single-drift-tube in the Tank4 are conducted below.

SIMULATION MODEL AND IMPROVEMENT SCHEMES

The CSNS DTL comprises four cavities (DTL1-DTL4) with drift tubes of increasing dimensions. Each drift tube connects to the cavity via a support stem housing the cooling pipes and quadrupole magnet conduit. The conduit limits the pipe inner diameter to 4 mm (12.56 mm²), constraining water supply. The structure is shown in Fig. 2.

The simulation uses the COMSOL "Non-Isothermal Flow" multiphysics interface, retaining only the drift tube copper body and water-cooling channels. A uniform heat flux (1000 W total) is applied to the drift tube surface, with a cooling water inlet at 25 °C and an outlet pressure boundary.

† liah@ihep.ac.cn

Content from this work may be used under the terms of the CC BY 4.0 licence (© 2026). Any distribution of this work must maintain attribution to the author(s), title of the work, publisher, and DOI.

ISBN: 978-3-95450-275-2 ISSN: 2226-0366 doi: 10.18429/JACoW-LINAC2026-TUPO048

BEAM DYNAMICS DESIGN OF RFI BASED ON REALISTIC THREE-DIMENSIONAL RF FIELDS

Y. Yang[1,2,3], H. Liu*[1,2,3], Q. Kong[1,2], A. Li[1,2,3]
[1]Spallation Neutron Source Science Center, Dongguan, China
[2]Institute of High Energy Physics, Chinese Academy of Sciences, Beijing, China
[3]University of Chinese Academy of Sciences, Beijing, China

Abstract

The RF-focused interdigital (RFI) linac combines longitudinal acceleration and transverse RF quadrupole focusing in a compact IH-type cavity without embedded magnets. In a multicell RFI cavity, fringe fields and phase dependent focusing make simplified beam dynamics models difficult to map reliably onto the final three-dimensional geometry. A staged electromagnetic beam dynamics optimization framework is therefore established by integrating Python reference particle calculations, CST three-dimensional electromagnetic simulations, and TraceWin multiparticle tracking. The longitudinal stage corrects the axial gap and drift tube layout through phase feedback in the recalculated field, whereas the transverse stage varies the focusing geometry under transmission, aperture, mismatch, and emittance criteria. For the 200 MHz model, the present longitudinal candidate reaches 3.3038 MeV, while the transverse candidate gives 97.48 % transmission. Common geometry verification remains in progress.

INTRODUCTION

Compact low energy ion linacs require a balance among accelerating efficiency, transverse confinement, and limited footprint. IH drift tube linacs (IH-DTLs) provide high shunt impedance at low β and can use embedded quadrupoles, alternating-phase focusing (APF), or KONUS-type beam dynamics for transverse confinement [1–4]. The RFI structure instead introduces four inward-pointing electrodes into the drift tubes. Their RF potential produces a near-axis quadrupole field, enabling acceleration and alternating-gradient focusing without internal magnetic lenses [5, 6]. Previous studies have examined CW and integrated RFQ/RFI implementations [7, 8]; earlier work by the present group selected an FFFDDD focusing sequence and established usable ranges of the transverse geometry parameters [9].

For a complete multicell cavity, geometry changes simultaneously affect the eigenfrequency, axial field, RF quadrupole field, particle arrival phase, and effective focusing strength. This work therefore adopts staged longitudinal and transverse optimization followed by re-evaluation on a common three-dimensional geometry, so that beam-dynamics feedback acts directly on the electromagnetic model.

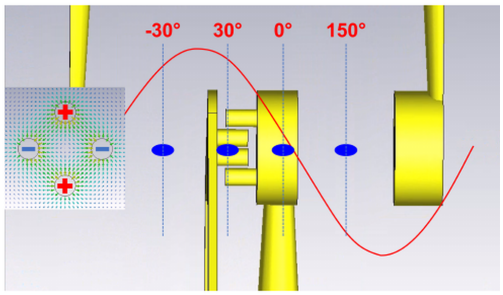


Figure 1: RFI principle. Four inward pointing electrodes generate the transverse RF quadrupole field, while the particle samples the accelerating, focusing, and drift regions at different RF phases.

BEAM DYNAMICS DESIGN

The model operates at 200 MHz with 1 MeV injection energy, 13 accelerating cells, two FFFDDD transverse focusing periods, and 12 focusing sections. The explored minor stem opening angle is 55°–75°, and the stem-to-cavity distance is 65 mm to 85 mm. Neglecting higher-order components, the local transverse field in a focusing section (Fig. 1) is represented by

$$E_x \simeq -G_{\mathrm{eff}}(z,\psi)x, \qquad E_y \simeq G_{\mathrm{eff}}(z,\psi)y, \tag{1}$$

where G_{eff} depends on the focusing geometry and on the RF phase ψ at section entry. Geometry therefore modifies the RF quadrupole field, while particle phase and energy determine the effective focusing sampled along the channel.

For the longitudinal stage, the ideal π-mode center to center length, $L_i^{(0)} \simeq \beta_i\lambda/2$, is used only as an initial value. For each candidate geometry, the working eigenmode is recalculated in CST and the signed on-axis field $E_z(z)$ is extracted with a common axial field normalization. A reference particle is then integrated from the cavity entrance according to

$$\frac{dW}{dz} = qE_z(z)\cos\phi, \qquad \frac{dt}{dz} = \frac{1}{\beta(W)c}, \qquad \phi = \omega t + \phi_0. \tag{2}$$

Finite gap fields, fringe fields, and continuous velocity increase are retained. With $\Delta\phi_i = \phi_i^{\mathrm{tar}} - \phi_i^{\mathrm{cal}}$, the upstream cell length correction is

$$\Delta L_i = \alpha\frac{\beta_i\lambda}{360^\circ}\Delta\phi_i, \tag{3}$$

where α is a feedback coefficient. Step limiting and relaxation suppress downstream overshoot, while the cell length

* liuhc@ihep.ac.cn

Content from this work may be used under the terms of the CC BY 4.0 licence (© 2026). Any distribution of this work must maintain attribution to the author(s), title of the work, publisher, and DOI.

ISBN: 978-3-95450-275-2 ISSN: 2226-0366 doi: 10.18429/JACoW-LINAC2026-TUPO049

CORRELATING LONGITUDINAL ELECTRON BEAM STRUCTURES WITH XFEL PULSE DURATION AND PEAK POWER USING AN X-BAND TRANSVERSE DEFLECTOR SYSTEM

K. Yasutome*,[1], T. Inagaki[1, 2], H. Maesaka[1, 2], E. Iwai[2, 1], T. Ohshima[2, 1], C. Kondo[2, 1], S. Matsubara[2]
[1]RIKEN SPring-8 Center, Kouto, Sayo, Hyogo, Japan
[2]Japan Synchrotron Radiation Research Institute (JASRI), Kouto, Sayo, Hyogo, Japan

Abstract

We have been developing an X-band transverse deflector system (X-TDS) at the X-ray free-electron laser facility SACLA to diagnose longitudinal electron beam structures for both SASE and sub-femtosecond XFEL operations. The full system targets a time resolution of 1 fs at a deflecting voltage of 80 MV for 8 GeV electrons. This summer, an initial single-cavity configuration was installed downstream of the undulator section, with first beam operation planned for this autumn. In this paper, we report the high-power test results of the RF components, including the conditioning history of the deflecting cavity, and propose a data-driven analysis framework based on Gaussian process regression and phase space reconstruction for XFEL performance optimization.

INTRODUCTION

Applications of XFEL light sources are becoming increasingly diverse, demanding precise accelerator control to satisfy their respective requirements. Attosecond XFEL generation has attracted particular attention within the XFEL community over the past decade. A longitudinal diagnostic plays a role in efficient tuning of such extremely short XFEL pulses, as well as in electron beam characterization during normal SASE operation. We employ X-band technology to develop the transverse deflector system (TDS) to be located downstream of the undulators at SACLA as shown in Fig. 1. The target RMS time resolution is sub-femtosecond, which is sufficiently short compared with the typical SASE pulse duration at SACLA (10 fs). The development of X-band technology also serves the R&D objectives for the planned SACLA upgrade, which targets a tenfold increase in repetition rate within the current power budget [1]. In this paper, we describe the X-band TDS and the measured performance of the high-power radio frequency (RF) components — including the deflecting cavity, pulse compressor, and dummy load — along with the conditioning history of the cavity. We also introduce an analysis framework for applying the TDS to longitudinal electron beam characterization.

SUB-FS TRANSVERSE DIAGNOSTIC SYSTEM

System Overview

The developed X-band TDS consists of a modulator-energized klystron (CANON E37116), pulse compressor, deflecting cavity, high-power dummy load, screen monitor, and an RFSoC-based low-level RF control system [2]. The property of the RF source is shown in Table 1. The operating frequency is 11.424 GHz; the klystron, driven by 40 W from the drive amplifier, delivers an output power of 20 MW. In the full TDS configuration, we plan to use 4 one-meter cavities in total. The 20 MW pulse with a duration of 1.5 µs is compressed to 80 MW with a duration of 0.15 µs by the pulse compressor. The compressed power is then divided among 4 cavities to drive the deflecting mode. This summer, we installed the TDS with only 1 cavity as shown in Fig. 2; the remaining 3 cavities are scheduled to be installed in subsequent years through 2028.

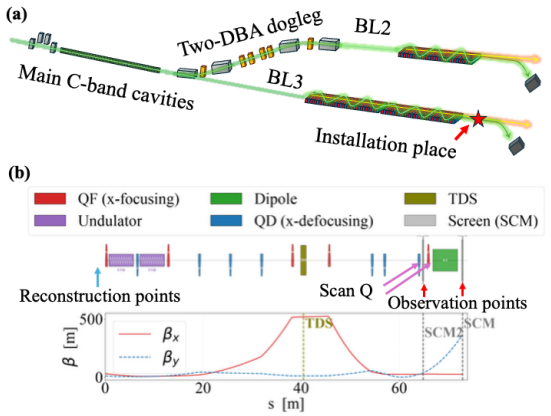


Figure 1: The accelerator transport line in the downstream part of SACLA, featuring the X-band TDS location at BL3 (a) and beam optics design for the TDS (b).

Table 1: Basic Property of X-band RF Source

Item	Value	Unit
Frequency	11.424	GHz
Drive power	40	W
Kly. output	20	MW
Kly. voltage	250	kV
Kly. current	160	A
Kly. pulse len.	1.5	µs

Cavity Performance and Conditioning

The basic structure of the deflecting cavity is based on that of the conventional C-band deflector [3] installed after the final bunch compression. The distinctive feature is the horizontally split structure. Thanks to this structure, the one-meter cavity consists of six half copper blocks (three per half:

* yasutome@spring8.or.jp

Content from this work may be used under the terms of the CC BY 4.0 licence (© 2026). Any distribution of this work must maintain attribution to the author(s), title of the work, publisher, and DOI.

ISBN: 978-3-95450-275-2 ISSN: 2226-0366 doi: 10.18429/JACoW-LINAC2026-TUPO051

DESIGN & SIMULATION OF A PARALLEL COUPLED ACCELERATING STRUCTURE IN C-BAND

J. Latif[1,2], Q. Kong[1,2], A. Li[1,2], X. Liu[1,2,3], Y. Wang[4], X. Wu[1,2], H. Liu*[1,2,3]
[1]Spallation Neutron Source Science Center, Dongguan, China
[2]Institute of High Energy Physics, Chinese Academy of Sciences (CAS), Beijing, China
[3]University of Chinese Academy of Sciences, Beijing, China
[4]Institute of Advanced Light Source Facilities, Shenzhen, China

Content from this work may be used under the terms of the CC BY 4.0 licence (© 2026). Any distribution of this work must maintain attribution to the author(s), title of the work, publisher, and DOI.

Abstract

A C-band accelerating structure that utilizes a parallel-coupled configuration to achieve high gradient performance under short-pulse operation is presented. Unlike conventional traveling-wave designs, where power propagates sequentially through each cell, the proposed architecture employs a parallel feed network that delivers RF power to every cavity cell simultaneously. This approach effectively eliminates the power transit time between cells, resulting in a substantial reduction in the overall structure filling time. The cavity geometry has been systematically optimized to maximize the shunt impedance, ensuring efficient RF-to-beam energy conversion. To realize uniform excitation, a dedicated RF distribution system comprising coupling irises, waveguide feed lines, and a power divider has been designed to supply each cell with equal amplitude and the prescribed phase progression. The structure is deliberately operated in an overcoupled regime to further minimize the filling time, thereby taking full advantage of the short input pulse duration. Electromagnetic simulations indicate that the proposed design supports an accelerating gradient of 80 MV/m when driven by a 150 MW input pulse of 50 ns duration, confirming its suitability for compact accelerator applications requiring high peak fields and fast rise times.

INTRODUCTION

The pursuit of higher accelerating gradients is a central driver in the development of compact and cost-effective linear accelerators for advanced light sources, including free-electron lasers (FELs) [1–7]. Operating in the C-band frequency range (5–6 GHz) offers a distinct advantage over conventional S-band systems, as the higher frequency enables substantially greater accelerating fields, thereby reducing both the physical footprint and the overall capital cost of the accelerator [8]. However, the primary physical limitation to achieving these elevated gradients is RF breakdown, which follows an empirical scaling law of the form Breakdown Rate $\propto E^{30}t^5$. This relationship implies that even a modest reduction in the RF pulse duration t allows for a significant increase in the sustainable electric field E.

To exploit this pulse-length dependence, it is essential that the structure filling time be commensurately short. In traditional traveling-wave designs, power propagates sequentially from cell to cell, resulting in a cumulative filling time that often exceeds the available pulse width. Attempts to shorten the filling time by enlarging the beam aperture prove counterproductive, as this approach lowers the shunt impedance and exacerbates surface electric fields, thereby increasing breakdown risk. Consequently, a fundamentally different feeding strategy is required one that decouples the filling time from the number of accelerating cells.

In this work, the concept of parallel-coupled accelerating structures is studied by presenting a C-band design that incorporates a distributed RF power feed network [9]. This architecture delivers power to each cavity cell concurrently, drastically minimizing the overall filling time while maintaining localized control over the field amplitude and phase in each cell. By synergizing the high-gradient potential of C-band operation with the transient response benefits of parallel feeding, the proposed design offers a viable pathway to operate at breakdown-limited gradients without compromising structural efficiency or beam quality.

ACCELERATING STRUCTURE DESIGN

Single Cavity Design

A fundamental requirement in the RF design of a multi-cell linac is the delivery of equal power to each accelerating cavity while maintaining precise phase synchronization across the entire structure. For a relativistic particle beam, the required phase advance per cell is given by $2P\pi/\lambda$, where λ is the free-space wavelength corresponding to the operating frequency. However, this condition is complicated by the difference between the free-space wavelength and the guided wavelength λ_g within the feeding network, which introduces phase distortions if not carefully managed. To address this challenge, a practical and effective solution employs a parallel feed configuration consisting of multiple distribution waveguides, each coupled to the accelerating cells at periodic intervals. Specifically, the coupling points are spaced by integer multiples of $m\lambda_g/2$, ensuring that the power tapped from each branch arrives at the corresponding cell with the correct phase relationship. This periodic coupling scheme, illustrated in Fig. 1, not only guarantees uniform power distribution but also maintains the prescribed inter-cell phase advance, thereby preserving beam synchronization and optimizing acceleration efficiency across the entire linac section.

The cavity geometry has been designed to resonate at 5.712 GHz, with the resonant frequency chosen to match

* liuhc@ihep.ac.cn

ISBN: 978-3-95450-275-2 ISSN: 2226-0366 doi: 10.18429/JACoW-LINAC2026-TUPO053

THE DESIGN OF THE FERROELECTRIC BASED FAST TUNER*

Cong Zhang†,1,2, Tianyi Sun2,3, Huachang Liu1,2, Rui Ge1, Wenzhong Zhou1,2, Ahong Li1,2, Qiang Chen1,2, Bo Li1,2, Xiaolei Wu1,2, Mengxu Fan1,2, Peihua Qu1,2, Qiyu Kong1,2
[1]Institute of High Energy Physics, Beijing, China
[2]Spallation Neutron Source Science Center, Dongguan, China
[3]Lanzhou University, Lanzhou, China

Abstract

The CSNS-II accelerator adopts 648 MHz superconducting elliptical cavities as core RF components. Conventional mechanical tuners cannot adequately compensate fast frequency drifts induced by microphonics, Lorentz-force detuning, and transient beam loading under cryogenic conditions. A ferroelectric fast tuner employing ferroelectric ceramics is proposed as an alternative. A model was established in CST, and several key geometric parameters were systematically optimized through layered parametric sweeps. The optimized tuner achieves a resonant frequency of 648 MHz. This work provides a feasible technical route for high-frequency dynamic compensation of CSNS-II superconducting cavities.

INTRODUCTION

The China Spallation Neutron Source phase II (CSNS-II) upgrade design will increase the total beam power from 100 kW to 500 kW and boost the beam energy from 80 MeV to 300 MeV in the linac by adding a superconducting linear accelerator to the existing accelerator complex. The 648 MHz elliptical cavity is employed for the beam energy range from 165 MeV to 300 MeV. Main operational parameters of the CSNS-II 648 MHz elliptical cavity are listed in Table 1. During high-power operation, these cavities experience rapid frequency drifts caused by microphonics and Lorentz-force detuning. Traditional tuning methods for superconducting cavities, such as mechanical tuning and piezoelectric tuning, suffer from drawbacks including slow tuning response, low tuning accuracy, susceptibility to mechanical-stress introduction, and degraded stability of superconducting cavities [1, 2]. Ferroelectric materials offer purely electrical control of permittivity via DC bias voltage [3]. This paper presents the electromagnetic design of a ferroelectric fast tuner for the CSNS-II 648 MHz superconducting elliptical cavities, using a coaxial geometry with an annular BST ceramic element.

Table 1. Main Parameters of the CSNS-II 648 MHz Superconducting Elliptical Cavity

Parameters	Value	Units
Frequency	648	MHz
bandwidth of cavity	668	Hz
operation mode	pulse	--
pulse frequency	25	Hz
Operating gradient	14	MV/m
KL	1.5	Hz·m2·MV−
pressure sensitivity	0.15	Hz·Pa−1
field flatness	>90%	--
R/Q	310	Ω
beam current	40	mA
operation temperature	2	K
operation pressure	3100	Pa
cavity axial stiffness	2225	N·mm^{-1}

STRUCTURAL DESIGN

The ferroelectric fast tuner adopts a coaxial transmission line geometry, chosen because coaxial lines support modes, enable compact designs, confine fields well between conductors to minimize radiation losses [4, 5]. The tuner is designed as an external module coupled to the superconducting cavity via a coaxial power coupler. The principal element is an annular BST ceramic sheet positioned coaxially between inner and outer conductors. The tunability originates from the characteristic that the dielectric constant of ferroelectric materials varies with the bias voltage.

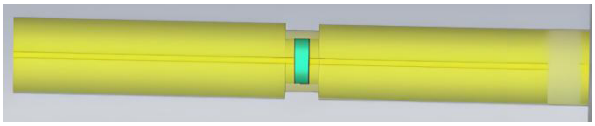


Figure 1: Ferroelectric fast tuner structure (CST model). The annular BST ceramic (green) is embedded between the inner and outer conductors.

* Work supported by Guangdong Basic and Applied Basic Research Foundation (Grant No.2022B1515120027) and Doctoral and Master's Joint Training Program of Songshan Lake High-Tech Industrial Development Zone, Dongguan（Grant No. DG2531351N）
† zhangcong@ihep.ac.cn

Content from this work may be used under the terms of the CC BY 4.0 licence (© 2026). Any distribution of this work must maintain attribution to the author(s), title of the work, publisher, and DOI.

ISBN: 978-3-95450-275-2 ISSN: 2226-0366 doi: 10.18429/JACoW-LINAC2026-TUPO054

RECONSTRUCTION OF BEAM TRANSVERSE PARAMETERS IN THE FERMILAB SIDE-COUPLED LINAC USING A NORMALIZED COORDINATE FRAMEWORK*

E. V. Chen†, J-P. Carneiro, R. V. Sharankova, A. V. Shemyakin
Fermi National Accelerator Laboratory, Batavia, IL, USA

Abstract

Quadrupole scans are a commonly used tool for beam second moment reconstruction. Limitations in the strength of the magnets and layout of the beamline elements frequently preclude simple quadrupole-drift-detector scans from collecting sufficient data for reconstruction. Using a normalized coordinate framework, we characterize the prerequisites for a robust simple quadrupole scan and expand these prerequisites to reconstruction from more complex optics. The beam second moments are investigated at two locations in the Fermilab Side-Coupled Linac under simple and complex optics, using this framework to maximize information gained from wire scanner profile measurements.

INTRODUCTION

In the transverse planes, the quadrupole scan is the classical method for measuring beam second moments [1]. The simplest form of the quadrupole scan varies the current in a quadrupole and measures the beam size at a downstream detector, with only a drift between the two elements. Reconstruction of beam second moments occurs at the upstream quadrupole position. However, limitations in the quadrupole strengths, element layout, or permissible beam losses frequently prohibit successful 'simple' quadrupole scan measurements.

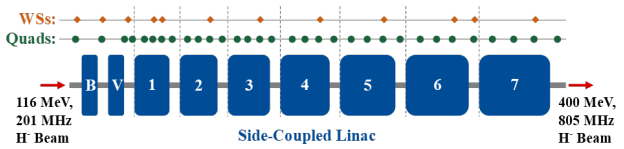


Figure 1: Side-Coupled Linac schematic.

The 'simple' quadrupole scan can be generalized to be compatible with any transfer matrix between the reconstruction point and detector(s). This freedom allows for mitigation of the 'simple' quadrupole scan limitations; however, more complex beam transport precludes simple, visual assessment of the quality of the reconstruction.

Here we use the Fermilab Side-Coupled Linac (SCL) [2], Fig. 1, to conduct three measurements of beam second moments at different locations with the simple and generalized quadrupole scan techniques. We compare results from the reconstructions, assess the robustness of these setups via a normalized coordinate framework, and use this information to develop suggestions for more efficient measurements. Note that the space charge is mostly neglected in this work. Although beam second moment reconstruction only informs on rms properties of the beam, these principles similarly underly reconstruction techniques beyond the first order, such as in phase space tomography.

Quadrupole Scan Formulae

The beam second moments, $\boldsymbol{\Sigma}$, are directly related to the Twiss parameters and emittance and are propagated via the transfer matrix, $\boldsymbol{M}$, from the initial upstream location, i, to the final downstream location, f, as shown in Eq. (1).

$$\boldsymbol{\Sigma}_f = \boldsymbol{M}\boldsymbol{\Sigma}_i\boldsymbol{M}^T = \begin{pmatrix}\sigma_{11,f} & \sigma_{12,f}\\ \sigma_{21,f} & \sigma_{22,f}\end{pmatrix} = \epsilon_f \begin{pmatrix}\beta_f & -\alpha_f\\ -\alpha_f & \gamma_f\end{pmatrix} \quad (1)$$

The σ_{11} term of $\boldsymbol{\Sigma}$ is equal to the rms beam size squared, σ_{rms}^2. In the simple quadrupole scan with a thin lens approximation and ignoring space charge, the relationship between $\sigma_{11,f}$ and quadrupole strength, kl, is parabolic.

To generalize, the beam size $\sqrt{\sigma_{11,f}}$ is measured under varying transfer matrices between the upstream reconstruction point and downstream detector. The three unique second moments, $\sigma_{11,i}$, $\sigma_{12,i}$, and $\sigma_{22,i}$, can thus be solved for via Eq. (2) and (3), which reshape the relationship in Eq. (1) to isolate the collected beam sizes in $\boldsymbol{\eta}$ and leave the transfer matrix terms generalized but reshaped in $\boldsymbol{A}$ [3].

$$\begin{pmatrix}\sigma_{11,f}\\ \vdots\end{pmatrix} = \begin{pmatrix}m_{11}^2 & 2m_{11}m_{12} & m_{12}^2\\ \vdots & \vdots & \vdots\end{pmatrix}\begin{pmatrix}\sigma_{11,i}\\ \sigma_{12,i}\\ \sigma_{22,i}\end{pmatrix} \quad (2)$$

$$\boldsymbol{\eta} = \boldsymbol{A}\boldsymbol{\sigma} \quad (3)$$

The pseudoinverse of $\boldsymbol{A}$, $\boldsymbol{A}^+$, can be used to solve this simple minimization problem for $\boldsymbol{\sigma}$.

Normalized Coordinates

In (x, x') phase space, shear and expansion during beam transport complicates visualizing the optimal set of downstream projections for reconstruction of beam second moments. This visualization is simpler in normalized coordinates (x_n, x_n') where the beam transport is rotation of a rigid body.

The transfer matrix can be decomposed into the betatron amplitude matrix, $\boldsymbol{\beta}$, and rotational matrix, $\boldsymbol{R}$, Eq. (4) [4].

$$\boldsymbol{M} = \boldsymbol{\beta}_f\boldsymbol{R}\boldsymbol{\beta}_i^{-1} \quad (4)$$

The transition to normalized coordinates (x_n, x_n') occurs via incorporating the betatron amplitude matrices into the coordinates (x, x'), leaving behind only the rotational matrix, Eq. (5) and (6). The rotational angle is the betatron phase advance, ψ, and units are $\mathrm{m}^{-1/2}$ for both x_n and x_n'.

$$\begin{pmatrix}x_{n,f}\\ x_{n,f}'\end{pmatrix} = \begin{pmatrix}\cos\psi & \sin\psi\\ -\sin\psi & \cos\psi\end{pmatrix}\begin{pmatrix}x_{n,i}\\ x_{n,i}'\end{pmatrix} \quad (5)$$

* This manuscript has been authored by Fermi Forward Discovery Group, LLC under Contract No. 89243024CSC000002 with the U.S. Department of Energy, Office of Science, Office of High Energy Physics.
† erinchen@fnal.gov

Content from this work may be used under the terms of the CC BY 4.0 licence (© 2026). Any distribution of this work must maintain attribution to the author(s), title of the work, publisher, and DOI.

ISBN: 978-3-95450-275-2 ISSN: 2226-0366 doi: 10.18429/JACoW-LINAC2026-TUPO055

FULL 4D RECONSTRUCTION OF PHASE SPACE VIA MAXIMUM ENTROPY THEORY FOR SLIT-BASED BEAM DIAGNOSTICS *

D. Lee[1], J. Choi[2], L.W. Liu[3], B.H. Ma[3], Y. Du[3], J.C. Wong[†3], M. Chung[‡2]
[1]Kangwon National University, Gangneung, South Korea
[2]Pohang University of Science and Technology, Pohang, South Korea
[3]Institude of modern Physics, Chinese Academy of Sciences, Lanzhou, China

Content from this work may be used under the terms of the CC BY 4.0 licence (© 2026). Any distribution of this work must maintain attribution to the author(s), title of the work, publisher, and DOI.

Abstract

Emittance is a key parameter that characterizes beam quality and its behavior under given optics. Conventional emittance measurement methods reconstruct the beam phase-space based on Twiss parameters calculated from beam profiles, and are therefore based on Gaussian beam optics. To overcome this limitation, tomography techniques have been introduced to reconstruct the phase-space distribution using projection data measured at various phase-space angles. In this study, we reconstruct the phase-space distribution using the Maximum Entropy Theory (MENT) with data from the slit-based Virtual Pepper-Pot (VPP) diagnostics at the Beam Test Stand (BTS) of the Korea Multipurpose Accelerator Complex (KOMAC). To avoid nonlinear effects such as space charge, which can occur in conventional multi-optics tomography when the measurement point and the reconstruction point are different, a single-optics configuration is established using a fixed quadrupole setting. In this configuration, angular projection data are obtained by introducing Additional Diagonal Scan (ADS) and Multi-Screen Scan (MSS). Using X-suite simulations, the two methods are quantitatively compared in terms of total variation distance (TVD) and emittance error.

INTRODUCTION

To operate accelerators and to maintain beam performance, it is necessary to accurately determine the beam emittance, which is related to beam quality. In particular, it is important to know the transverse emittance in order to produce the beam desired by users or to maintain beam stability. Many diagnostic devices and methods have been developed to measure transverse emittance in linear accelerators, such as the slit-grid and pepper-pot methods. Both methods are destructive diagnostics. In these methods, particle positions are selected by masking the beam with an upstream slit or pepper-pot plate, and the downstream positions are measured using a grid or screen. Then, by applying the linear transfer matrix for the drift section between the slit or plate and the detector, the position and momentum components at the upstream location can be reconstructed. From measurements covering the entire beam, the beam emittance and the corresponding Twiss parameters can be obtained.

The pepper-pot method, which is widely used in linear proton accelerators, has the advantage of measuring emittance in a single shot. However, to achieve higher spatial resolution, the density of holes in the pepper-pot plate needs to be increased, which can cause beamlet overlap. In addition, reducing the hole diameter to improve spatial resolution decreases the number of transmitted particles, resulting in a lower signal intensity.

To overcome these limitations, a diagnostic technique called the Virtual Pepper-Pot (VPP) has been developed [1]. Unlike the conventional pepper-pot method, which uses a plate with a matrix of holes, the VPP method employs sequential slit scans to obtain beamlets in the x and y directions. During data processing, a VPP image is generated using the minimum-bit principle, in which the lower intensity of the horizontal and vertical beamlets is assigned to each virtual intersection. The emittance is then reconstructed from the second-order moments of the VPP image. Although the VPP method requires multi-shot measurements, it overcomes mechanical limitations of the conventional pepper-pot method, such as the requirement for a specific beam size, and its slit assembly is much simpler to fabricate. However, many conventional phase space reconstruction methods rely on second-order beam moments and a Gaussian approximation, which limits their ability to accurately reproduce detailed phase space structures of non-Gaussian beams.

In this study, MENT is applied to reconstruct the beam phase space from VPP measurement data instead of using the conventional VPP data analysis method. This approach satisfies the single-optics condition, in which the measurement point and the reconstruction point coincide, and it enables reconstruction not only of the emittance but also of the phase space distribution. In addition, by incorporating additional data, the coupling terms are more accurately estimated, allowing a full 4D reconstruction. To obtain these additional data, two novel diagnostic methods, the ADS and MSS, are introduced. To evaluate how accurately the two methods reconstruct a coupled beam, a coupling factor t is used to quantify the degree of transverse coupling [1].

MAXIMUM ENTROPY THEORY

First, it starts with one question. How can probability density functions (pdfs) be assigned?

When testable information(same as constraints) is available, Jaynes has suggested that we should make the assignment by using the principle of maximum entropy [2]. That is, we should choose the pdf that has the information entropy

* This work was supported by the National Research Foundation of Korea (NRF), funded by the Ministry of Science and ICT (MSIT) of the Republic of Korea (No. RS-2022-00154676 and No. RS-2025-00563391).
† wong@impcas.ac.cn
‡ moses@postech.ac.kr

ISBN: 978-3-95450-275-2 ISSN: 2226-0366 doi: 10.18429/JACoW-LINAC2026-TUPO056

LOW-LEVEL RF AND TIMING SYSTEMS OF THE LASER-DRIVEN RF GUN TEST BENCH AT JINR DLNP

K. Popov[1,2,*], A. S. Dyatlov[1,3], E. I. Gacheva[4], A. K. Poteomkin[4], V. V. Kobets[1], P. P. Zhuravlev[1], M. A. Nozdrin[1], D. V. Karlovets[3]
[1]Joint Institute for Nuclear Research, Dubna, Russia
[2]Institute of Nuclear Physics, Almaty, Kazakhstan
[3]School of Physics and Engineering, ITMO University, Saints-Petersburg, Russia
[4]Institute of Applied Physics of the Russian Academy of Sciences, Nizhny Novgorod, Russia

Content from this work may be used under the terms of the CC BY 4.0 licence (© 2026). Any distribution of this work must maintain attribution to the author(s), title of the work, publisher, and DOI.

Abstract

Low-Level RF and timing systems are of primary importance to operate a laser-driven RF-Gun. The laser oscillator piezo feedback synchronizes the phase between a laser pulse and an accelerating field. The laser pulse picking is conducted by the acousto-optic modulator in order to generate from a single shot to tens pulses per facility machine cycle. The acousto-optic modulator operation is synchronized by the trigger pulses arrival time. The trigger pulses generation and delay are controlled by the digital time delay modules, which are locked to the accelerating field clock signal. Both systems are being commissioned at the laser-driven RF-Gun test-bench at the Dzhelepov Laboratory of Nuclear Problems (DLNP), Joint Institute for Nuclear Research (JINR). The test-bench Low-Level RF and timing systems commissioning current status is presented in this report.

INTRODUCTION

A stable synchronization between the photocathode drive laser and the accelerating RF field is one of the key requirements for a laser-driven RF gun reliable operation. In addition to laser-to-RF synchronization, trigger signals deterministic generation and distribution are required for the operation of the laser pulse-picking system and the facility other pulsed components. These functions are provided by the Low-Level RF (LLRF) and timing systems.

These systems of the laser-driven RF-gun test bench at JINR DLNP are currently under commissioning. Particular attention is devoted to the implementation of laser-to-RF synchronization, for which different system architectures are considered. Their principles and applicability to the test bench are discussed in the following sections.

LASER-TO-RF SYNCRHONIZATION ARCHITECTURE APPROACHES

Two principal approaches can be used to synchronize the laser pulse arrival time with the accelerating RF phase in a normal-conducting linear accelerator. The first approach is based on using an RF signal generator (SG) as the master oscillator (MO) of the LLRF system [1]. The MO generates the S-band reference signal, which is then split into several branches and distributed to the RF drive amplifiers of the klystrons. One branch is additionally fed to a frequency divider to generate the reference signal for the laser-oscillator piezo feedback [2]. The reference frequency is selected to match the laser oscillator micropulse repetition frequency. The piezo feedback then phase-locks the laser micropulse train to the accelerating RF field. The achievable synchronization performance is primarily limited by the piezo-feedback loop bandwidth and latency, as well as by the ADC and DAC performance of the feedback controller.

The second approach follows the opposite principle and does not require a separate SG as the facility MO. Instead, the laser oscillator itself serves as the MO [3]. An electrical signal corresponding to the laser micropulse repetition frequency, which is a subharmonic of the accelerating RF frequency, is used as the facility reference clock. This signal is referred to here as the laser clock. The laser clock frequency is subsequently up-converted to the accelerating RF frequency, after which the resulting RF signal is split and distributed throughout the accelerator facility. At the final stage, the up-converted signal is supplied to the klystron drive amplifier. This configuration is referred to as the laser-clock-based synchronization architecture. It does not require a piezo-feedback system for laser-to-RF synchronization. However, its synchronization performance is affected by the number of frequency up conversion stages, the phase and amplitude noise of the RF components, and AM-to-PM conversion within the LLRF signal-processing chain. Nevertheless, this architecture provides a practical solution for the initial accelerator commissioning stage [4].

SYNCHRONIZATION ARCHITECTURES AT THE TEST-BENCH

Both synchronization approaches are currently being developed and tested at the RF-gun test bench. During the commissioning first phase, priority is given to operation based on the laser oscillator as the facility MO. However, the laser-clock-based configuration is not intended as the final solution for long-term facility operation. Therefore, development of the RF-master-oscillator-based architecture with laser piezo feedback is required for the commissioning phase 2 [4].

* popovkon@jinr.ru

ISBN: 978-3-95450-275-2 ISSN: 2226-0366 doi: 10.18429/JACoW-LINAC2026-TUPO058

CSR-RESILIENT ISOCHRONOUS TRANSPORT LINE DESIGN FOR MULTI-NC BEAM MERGING*

W. Li[1,2], Z. Liu[1,2], Z. Ming[1,2], C. Meng[1,†], Y. Jiao[1,2]
[1]Institute of High Energy Physics, CAS, Beijing, China
[2]University of Chinese Academy of Sciences, Beijing, China

Abstract

Beam-driven plasma wakefield acceleration (PWFA) for future TeV-scale colliders requires driver–witness bunch pairs with multi-nC charge, kiloampere peak currents, femtosecond timing stability and micrometre-level transverse alignment. Merging two independently optimised bunches through twin isochronous beamlines that share a common dipole avoids the charge loss of mask- or emittance-exchange approaches, but coherent synchrotron radiation (CSR) at kA peak current breaks the standard achromaticity and isochronicity conditions of the transport lattice. We extend the second-order transport-matrix formalism to include the CSR-induced energy variation, showing that the quadratic longitudinal term T_{566} feeds down into an effective linear $R_{56,\mathrm{eff}}$ that must be nulled at design time. Guided by this criterion, a symmetric quadruple-bend achromat (QBA) merger with sextupole compensation is obtained by multi-objective optimisation and validates the framework: emittance growth is limited to ~ 0.1 mm mrad in both bunches, and the analytical $R_{56,\mathrm{eff}}$ reproduces the CSR-on simulated time-of-flight response.

INTRODUCTION

Beam-driven plasma wakefield accelerators are candidates for future TeV-scale colliders such as the CEPC Plasma Injector [1] and HALHF [2] because gradients well beyond conventional RF cavities are accessible in plasma. Efficient wakefield excitation demands a driver–witness bunch pair with multi-nC driver charge, kA peak current, sub-100 fs longitudinal spacing and micrometre-level transverse overlap [3]. Existing approaches generate the two bunches from a single source: transverse masks in dispersive sections lose charge [4]; transverse-to-longitudinal emittance-exchange techniques can tailor bunch profiles but become ineffective at high charge; double-laser photocathodes avoid charge loss yet suffer from strong space-charge forces that make high-charge bunches difficult to compress and manipulate.

An alternative is to generate the two bunches in independent injectors, optimised separately, and merge them without any collimation using twin isochronous beamlines that share a common dipole (Fig. 1). The scheme preserves all charge but faces two challenges: femtosecond inter-bunch timing stability, and CSR at kA peak current that both degrades emittance and—as shown below—modifies the effective transport matrices of the merger. This work develops the CSR-corrected transport framework, uses it to guide a QBA-based lattice design, and validates the theory against `ELEGANT` [5] simulations including CSR and longitudinal space charge.

CSR-MODIFIED TRANSPORT FRAMEWORK

In the standard second-order matrix formalism, the particle coordinates $X_{i,f} = \sum_j R_{ij}X_j + \sum_{jk} T_{ijk}X_jX_k + \ldots$ transport through the beamline; first-order isochronicity of an achromat requires $R_{56} = 0$. CSR breaks this cleanly separable picture. Along a dipole, a Gaussian bunch emits CSR that induces a relative-energy change per unit arc length [6]

$$\frac{d\delta_{\mathrm{CSR}}}{ds}(z) = \frac{2\,r_e N}{3^{1/3}\rho^{2/3}\gamma_c}\int_z^{\infty}\frac{d\lambda(z')}{dz'}\,\frac{dz'}{(z'-z)^{1/3}}\,, \quad (1)$$

where ρ is the bending radius, N the bunch population and $\lambda(z)$ the longitudinal charge density.

Expanding the longitudinal coordinate to second order in the total energy deviation $\delta = \delta_0 + \delta_{\mathrm{CSR}}$ and treating δ_{CSR} as independent of the initial deviation δ_0 (valid for $|\delta_0| \lesssim 0.1\%$) leaves two contributions proportional to δ_0: the usual $R_{56}\delta_0$ plus a term that arises from the composition of the quadratic term T_{566} with the CSR-driven $\delta_{\mathrm{CSR}}(s)$ accumulated along the beamline. The linear response is therefore governed by an effective R_{56},

$$R_{56}^{\mathrm{eff}} = R_{56} + 2\int_{s_i}^{s_f} T_{566}^{s\to s_f}\,\frac{d\delta_{\mathrm{CSR}}}{ds}\,ds\,. \quad (2)$$

The additional term is a feed-down of the second-order longitudinal dispersion driven by the CSR energy chirp, analogous to the quadrupole kick produced by an off-axis sextupole. The same reasoning applies to the transverse dispersion, yielding CSR-modified effective coefficients

$$\begin{aligned} R_{16}^{\mathrm{eff}} &= R_{16} + 2\int_{s_i}^{s_f} T_{166}^{s\to s_f}\,\frac{d\delta_{\mathrm{CSR}}}{ds}\,ds\,, \\ R_{26}^{\mathrm{eff}} &= R_{26} + 2\int_{s_i}^{s_f} T_{266}^{s\to s_f}\,\frac{d\delta_{\mathrm{CSR}}}{ds}\,ds\,. \end{aligned} \quad (3)$$

Achieving true isochronicity and achromaticity in the presence of CSR therefore requires nulling *both* the standard matrix elements and the CSR feed-down integrals. CSR-induced emittance growth is separately suppressed by satisfying $\int R_{i6}^{s\to s_f}\,ds = 0$ $(i = 1, 2)$ [6–8], which constrains the betatron phase advance and ensures that the CSR kick at each dipole is optically compensated downstream.

* Work supported by the Strategic Priority Research Program of the Chinese Academy of Sciences (Grant No. XDB0530000).
† mengc@ihep.ac.cn

Content from this work may be used under the terms of the CC BY 4.0 licence (© 2026). Any distribution of this work must maintain attribution to the author(s), title of the work, publisher, and DOI.

ISBN: 978-3-95450-275-2 ISSN: 2226-0366 doi: 10.18429/JACoW-LINAC2026-TUPO059

MACHINE LEARNING-BASED CALIBRATION AND SURROGATE MODELING OF THE PHOTOINJECTOR AT PAL-XFEL

Won Jang[1], Seongyeol Kim*[,2], Haeryong Yang[2], Moses Chung†[,1]
[1]Pohang University of Science and Technology (POSTECH), Pohang, South Korea
[2]Pohang Accelerator Laboratory (PAL), Pohang, South Korea

Abstract

To achieve a high-brightness X-ray free-electron laser (FEL), it is essential to perform precise tuning of electron beam parameters at the photoinjector section, where the intrinsic emittance is determined. At PAL-XFEL, injector tuning is typically performed via manual, parameter-scan-based emittance optimization, which can be time-consuming. In addition, simulation-based beam matching often shows discrepancies with measured data, making beam prediction more challenging. To address this issue, we have developed a machine learning-based surrogate model to calibrate the simulation model and represent injector beam dynamics. The resulting surrogate model enables fast prediction of beam parameters and can be used to guide beam tuning. This approach is expected to reduce tuning time and support more efficient accelerator optimization.

INTRODUCTION

Accurate control of the photoinjector beam parameters is one of the essential tasks for high-brightness X-ray Free Electron Laser (XFEL) operation [1]. Typically, conventional tuning of the beam generated from the photoinjector involves repeated adjustments of accelerator settings followed by multiple beam measurements, which require considerable machine time. To overcome this issue, it has been actively investigated recently to train the surrogate model with both simulated data and experimental measurements to predict the beam parameters in a robust way [2, 3].

Nevertheless, a type of predicted beam parameters through the surrogate model, such as scalar values and phase space information, directly depends on the type of experimental measurements. Accordingly, it still requires a number of beam measurements to increase the diversity of the predictable beam parameters, leading to the dedicated beam time. In this study, we therefore carry out the calibration of the tracking simulation model [4] with experimental measurements. Once the calibrated simulation reproduces the overall trends observed in the experimental measurements, then it is expected that we can use the calibrated simulation to efficiently generate a number of dataset including scalar beam parameters and phase spaces at different beamline positions, thereby maximizing the diversity of observables of the surrogate model.

For the demonstration of the model calibration, we considered the photoinjector installed at the Pohang Accelerator Laboratory XFEL (PAL-XFEL) facility [5]. The schematic layout of the PAL-XFEL injector is shown in Fig. 1. It consists of an S-band RF gun, a solenoid magnet, and two accelerating cavities with the typical beam energy after the injector section reaching approximately 140 MeV. Using the Impact-T particle tracking code [6, 7], we conduct the calibration of the photoinjector using Bayesian optimization (BO) [8]. Since the BO constructs a probabilistic surrogate model of the objective function and uses previous evaluations to select the next input point, its high sample efficiency makes it well suited to problems in which each evaluation requires substantial computational resources or accelerator operation time. To improve search efficiency, we utilize Trust-Region Bayesian Optimization (TuRBO) to restrict the optimization to adaptively updated local regions [9]. A similar study using the BO for the model calibration has been reported [10].

In the first simulated demonstration, the objective function is mainly related with scalar parameters such as the RMS beam-size and transverse emittance curves from the solenoid scans and beam energy; target is thus to discuss whether our calibration approach is feasible. The BO input parameters are the solenoid-current offset and the RF gun phase. Since the initial transverse electron distribution is largely determined by the UV laser profile on the photocathode, parameters describing its horizontal and vertical widths and cutoff ranges are also included. BO is used to determine the simulation input parameters that best reproduced the reference solenoid-scan responses.

In this paper, we present demonstration results of the model calibration using simulated data. Then, we show the future plan of the experimental demonstration and deployment of the model during the user service.

BAYESIAN OPTIMIZATION (BO)

Bayesian Optimization Framework

Solenoid scans are performed at two diagnostic locations. At Screen 1, eight uniformly spaced solenoid-current settings ranging from 135.0 A to 137.0 A are used, while eight settings ranging from 123.5 A to 126.5 A are used at Screen 2. The calibration outputs consist of the horizontal and vertical RMS beam sizes and the mean kinetic energy at Screen 1, together with the horizontal and vertical rms beam sizes and projected emittances at Screen 2. At Screen 1, the beam energy can be measured using the BASG, and the projected emittances at Screen 2 can be measured using quadrupole scans.

* sykim12@postech.ac.kr
† moses@postech.ac.kr

Content from this work may be used under the terms of the CC BY 4.0 licence (© 2026). Any distribution of this work must maintain attribution to the author(s), title of the work, publisher, and DOI.

ISBN: 978-3-95450-275-2 ISSN: 2226-0366 doi: 10.18429/JACoW-LINAC2026-TUPO060

ELECTROMAGNETIC DESIGN STUDY OF A 500 MHz SUBHARMONIC BUNCHER FOR THE PLS-II LINAC

Geunwoo Kim[1], Changbum Kim[†,2], Moses Chung[*,1]
[1]Pohang University of Science and Technology (POSTECH), Pohang, South Korea
[2]Pohang Accelerator Laboratory (PAL), Pohang, South Korea

Abstract

The PLS-II is considering nonlinear kicker (NLK) injection to reduce stored beam perturbations. However, the present S-band pre-buncher and buncher produce several microbunches, motivating an examination of a single dominant bunch for NLK injection. Five axisymmetric 500 MHz subharmonic buncher geometries were compared in terms of RF parameters, power efficiency, axial field profiles, and longitudinal bunching. Preliminary PARMELA particle tracking showed that the bunching factor evolved differently within each SHB and the following drift, although all geometries gave similar values at the S-band buncher entrance. At the sampled setting selected for each geometry, all five geometries produced a dominant main bunch, with the elliptical case giving the highest sampled main bucket capture. At the SSRF reference setting, the CCL and SSRF rounded shapes showed favorable RF power efficiency and nearly identical main bucket capture at the injector exit. A joint MOGA of the SHB and downstream RF settings is planned before engineering selection.

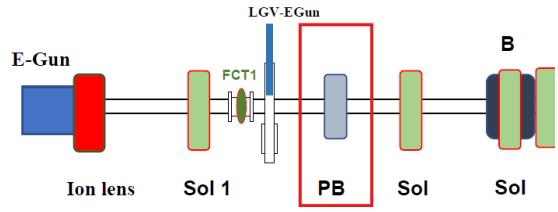
INTRODUCTION

The PLS-II linac uses a 2856 MHz pre-buncher and buncher to capture the 1 ns thermionic gun pulse into several S-band RF buckets [1, 2]. For the proposed nonlinear kicker (NLK) injection, this multibunch output motivates an examination of a single dominant bunch synchronized with the selected storage ring RF bucket. Previous PLS-II beam dynamics simulations used MOGA to optimize the phases of a 500 MHz subharmonic buncher (SHB) and the downstream RF cavities, producing a dominant bunch at the injector exit [2]. Figure 1 shows the existing pre-buncher location, where the 500 MHz SHB would be installed.

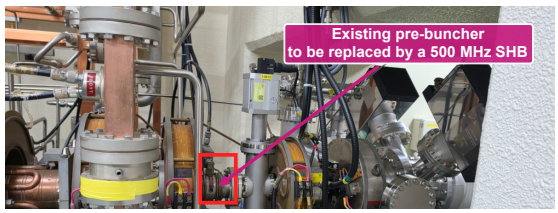
The present work compares five 500 MHz SHB geometries in terms of RF properties, power efficiency, and longitudinal bunching under common simulation conditions. Particle tracking simulations with PARMELA [3] used the same input beam and downstream injector settings to compare 500 MHz bunching within each SHB and in the following drift. Each geometry was evaluated at the sampled voltage and RF phase that gave its highest capture.

SHB GEOMETRIES AND RF PROPERTIES

The present comparison evaluates five 500 MHz SHB geometries for the pre-buncher location shown in Fig. 1. A



(a) PLS-II low energy injector section



(b) Existing pre-buncher at the proposed SHB location

Figure 1: Proposed 500 MHz SHB location in the PLS-II injector. The beamline layout in (a) is adapted from Ref. [2].

previous 500 MHz SHB study compared elliptical and coupled cavity linac (CCL) geometries. The elliptical cavity had a higher unloaded quality factor, Q_0, whereas the CCL had a higher transit time factor (TTF) and shunt impedance. Both produced a bunch length of ~ 0.32 ns under their respective field settings, and the elliptical cavity was retained because its contour was simpler [4]. The ALS quarter wave resonator (QWR) provides a practical cavity length at low frequency, the Elettra pillbox provides a simple TM_{010} implementation, and the SSRF rounded contour was developed to suppress multipacting [5–8]. Figure 2 compares the initial contours with the contours selected from the RF study. Both sets were tuned to 500 MHz and are shown on a common scale, where $\Delta z = z - z_c$ is measured from the center of each cavity.

For the present comparison, the five cavities were modeled as axisymmetric 500 MHz structures in SUPERFISH [9]. All models used copper surface resistance evaluated at 20 °C, a 20 mm beam radius, and an incident beam energy of 80 keV ($\beta \sim 0.5$). The unloaded eigenmode was calculated for each geometry.

For the elliptical shape, the iris and equator ellipse axes were varied; for the CCL, the nose radius, cone angle, and gap face width; for the ALS QWR, the ratio of nose radius to body radius, cone angle, and nose fillet; for the Elettra pillbox, the inner and outer corner radii; and for the SSRF rounded shape, the tip radius, shoulder radius, and axial shoulder position. The equator or body radius was then adjusted to restore the resonant frequency to 500 MHz.

The RF figures of merit were evaluated from the axial voltage including the transit phase,

† chbkim@postech.ac.kr
* moses@postech.ac.kr

Content from this work may be used under the terms of the CC BY 4.0 licence (© 2026). Any distribution of this work must maintain attribution to the author(s), title of the work, publisher, and DOI.

ISBN: 978-3-95450-275-2 ISSN: 2226-0366 doi: 10.18429/JACoW-LINAC2026-TUPO061

DESIGN PROGRESS OF L-BAND 10 MW HIGH EFFICIENCY MULTIBEAM KLYSTRON

N. Habib[†,1,2], Z. Zhou[††1], M. Iqbal[1], O. Xiao[1], Y. Liu[1,2], A. Aleem[1,2], Y.-A. Wang[1,2], H. Xiao[1,2], F.-Y. Wang[1,2]
[1]Institute of High Energy Physics, Chinese Academy of Sciences, Beijing, China
[2]University of Chinese Academy of Sciences, Beijing, China

Content from this work may be used under the terms of the CC BY 4.0 licence (© 2026). Any distribution of this work must maintain attribution to the author(s), title of the work, publisher, and DOI.

Abstract

This article introduces the design and simulation of a high-efficiency 10-megawatt RF power source, including a complete electron gun, magnetic focusing system, RF interaction structure, output window, and collector design. At an acceleration voltage of 115.1 kV, the designed electron gun generates a space-charge-limited beam current of 134.8 A and maintains an average cathode loading below 2.0 A/cm², making it suitable for safe and efficient operation. The maximum electric field calculated in the beam optics region remains below 5.8 kV/mm, while the high-voltage ceramic seal is limited to 0.65 kV/mm. These values indicate that the structure is operating within acceptable electrical stress limits; this reduces the risk of breakdown and improves the long-term reliability of the device in both 2D and 3D simulation. Static beam analysis showed that the electron beam has an average diameter of 5.1 mm, and is successfully focused and transported to the interaction cavity. The beam ripple remains below 5%. Beam dynamics analysis using 1D AJDISK, 1.5D KlyC, and 2D KlyC simulation tools predicted efficiencies of 73.98%, 69.35%, and 67.72%, respectively.

MOTIVATION

Central to the present work is the design of high-power RF sources for the Circular Electron Positron Collider (CEPC) injector, spanning the C-band and UHF bands; this in turn motivates the present advance: an indigenous 10-megawatt multi-beam klystron (MBK) for superconducting radio frequency (SRF) linear accelerator applications, a power class supported by only three manufacturers worldwide: Thales (TH1801) [1], Toshiba (E3736) [2], and CPI (VKL-8301) [3]. This article reports the first design iteration toward this goal.

INTRODUCTION

The Superconducting Radio Frequency (SRF) linear accelerator is an enabling technology for modern X-ray free-electron lasers and the proposed lepton collider. DESY's European XFEL is powered by 27 radio frequency stations, each centred around a 10-megawatt MBK operating at 1.3 GHz [4,5]; the same type of tube serves as the baseline RF source for the International Linear Collider [6]. The MBK divides the total beam current among several low-perveance beamlets that interact with common RF cavities; this reduces the high-voltage insulation requirement and increases the achievable efficiency relative to a single-beam klystron of the same power [7]. This article reports the design results for the electron gun, magnetic focusing system, RF interaction structure, and output window of an L-band 10-megawatt MBK, together with a preliminary collector design.

ELECTRON GUN AND BEAM OPTICS

The electron gun delivers six low-perveance beamlets (0.57 μP per beam, 3.44 μP total) at a cathode voltage of 115.1 kV, producing a total beam current of 134.8 A (22.49 A per beam), resulting in a total beam power of 15.6 megawatts. The peak and average cathode loading are 2.05 A/cm² and 2.0 A/cm², respectively, chosen to ensure long cathode lifetime. The maximum electric field in the beam optics region is 5.8 kV/mm, while the electric field at the high-voltage ceramic seal is 0.65 kV/mm; both values are within the scaling-law breakdown limit of 7.9 kV/mm at the 1.5 millisecond pulse length used in this design, with a margin of approximately 27% at the focusing electrode. The beam optics were designed using the 2D DGUN and 2.5D EGUN codes and verified in 3D CST Studio Suite; the electrode geometry was optimized to enlarge the radius of curvature on the external side of the focusing electrode and thereby minimize the surface electric field. Figure 1 shows the resulting electric field strength at the beam optics and high-voltage ceramic seal.

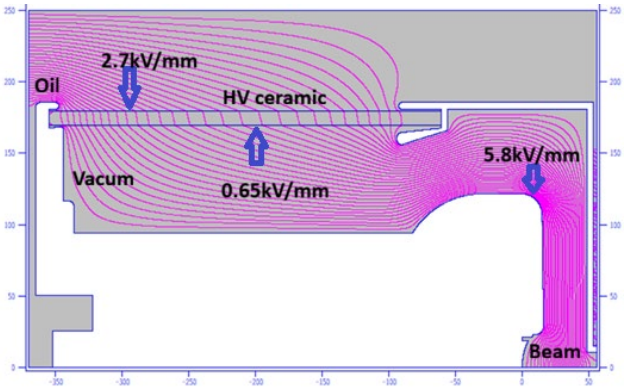


Figure 1: Beam optics design with HV ceramic and electric field strength.

Downstream of the gun, each beamlet is transported through the drift tube with an average beam diameter of 5.1 mm, a ripple rate of approximately 5.0%, and a fill factor of 0.566 relative to the drift tube radius. Figure 2 shows the current density and radial current distribution of the six beamlets at the injection plane, confirming beamlet-to-

† nomanhabib98@gmail.com
†† zhouzs@ihep.ac.cn

ISBN: 978-3-95450-275-2 ISSN: 2226-0366 doi: 10.18429/JACoW-LINAC2026-TUPO062

DEVELOPMENT AND TESTING OF TOOLS FOR ORM MEASUREMENTS AND QUADRUPOLE CENTERING*

A. Pathak†, E. Chen, A. Shemyakin
Fermi National Accelerator Laboratory, Batavia, IL, USA

Abstract

In preparation for the commissioning of Linac2 (formerly referred to as the PIP-II linac) at Fermilab, we are developing high-level applications that automate Orbit Response Matrix (ORM) measurement and beam-based localization of quadrupole magnetic centers. Both procedures are designed to run in a low-amplitude mode compatible with otherwise regular operation. The ORM is measured by exciting multiple dipole correctors simultaneously at low amplitude, each at a distinct frequency, and applying a Discrete Fourier Transform to the recorded BPM signals to extract per-element transfer functions with quantified noise. One application of the measured ORM is to predict the corrector coefficients that form local orbit perturbations (bumps). To center the trajectory in a quadrupole, such a bump is created around it, the quadrupole current is oscillated, and the responses of the downstream BPMs are recorded and analyzed. Repeating this at several beam positions inside the quadrupole – each set by the bump – the dependence of the BPM signal on beam position provides information about the quadrupole center. The applications are being tested at the Fermilab 400 MeV Linac during regular production runs, and the lessons learned are fed back into their improvement.

INTRODUCTION

Commissioning of Linac2 [1, 2] will require rapid and repeatable beam-based optics diagnostics, including orbit response matrix (ORM) [3] measurements, orbit correction, and trajectory centering through quadrupoles. During commissioning, these measurements can be performed during dedicated machine time. For the present development and testing at the Fermilab 400 MeV Linac, however, we seek to perform the measurements parasitically during routine production operation, avoiding disruption to beam delivery. We therefore apply low-amplitude multi-frequency ac excitation [4–7], which allows multiple correctors to be excited simultaneously while the resulting beam response is extracted from the BPM signals. Two high-level applications were tested in this mode. FORMA drives all selected dipole correctors simultaneously, each at its own frequency, and demodulates the BPM signals to measure the ORM. AutoCenter uses the measured ORM to form local trajectory bumps and locate quadrupole centers from the downstream response. We also study orbit correction under ORM mismatch by comparing singular-value-decomposition (SVD) correction based on the measured ORM with Bayesian optimization (BO), which does not use the supplied global ORM.

ORM MEASUREMENT METHOD

Each of the 22 horizontal (or 22 vertical) corrector channels is driven simultaneously with a sinusoidal excitation added to its operating setpoint:

$$x_j[n] = x_j^0 + A_j \sin\left(2\pi P_j \frac{n \bmod S}{S}\right), \tag{1}$$

where n is the sequence index and each corrector j carries a distinct integer harmonic number $P_j = 10, 11, \ldots, 31$. The S-sample pattern is repeated ten times, so that over the full record of $N = 10S$ samples each corrector completes $10P_j$ cycles and occupies the distinct DFT bin $k_j = 10P_j$. Because the number of samples in one period, $S = 293$, is prime, every P_j is coprime with S; each drive waveform therefore has a period of exactly S samples and repeats exactly ten times over the record, as assumed above. All correctors are driven simultaneously, and all 70 BPM channels are recorded synchronously on a common 5 Hz beam pulse, with $A_j = 0.1$ A and $N = 2930$. Although fewer samples were sufficient to reach the required noise level, the longer acquisition was retained deliberately to demonstrate the expected statistical reduction of the noise floor with record length. Because the beam-pulse-locked scan contains timing gaps, spectra are shown versus the number of periods completed over the record rather than frequency. For mean timestamp spacing T, elapsed duration $T_{\mathrm{rec}} \simeq NT$, and $f_k = k/(NT)$, the plotted coordinate is $q_k = f_k T_{\mathrm{rec}} = kT_{\mathrm{rec}}/(NT) \simeq k$. Thus the peaks occur at $q_j \simeq k_j = 10P_j = 100, 110, \ldots, 310$. At drive bin k_j, let $\tilde{b}_i$ and $\tilde{c}_j$ be the complex one-sided DFT coefficients of the mean-subtracted BPM i and corrector-readback j signals. The signed in-phase transfer coefficient is $R_{ij} = \mathrm{Re}(\tilde{b}_i/\tilde{c}_j)$ in mm/A; division by $\tilde{c}_j$ normalizes the BPM response to the measured corrector amplitude and phase. Its statistical uncertainty is propagated from the off-peak spectral RMS of both signals:

$$\Delta R_{ij} = \sqrt{\frac{\sigma_b^2}{2A_c^2} + \frac{A_b^2\sigma_c^2}{2A_c^4}}, \tag{2}$$

where $A_b = |\tilde{b}_i|$ and $A_c = |\tilde{c}_j|$ are the measured amplitudes, and σ_b and σ_c are the corresponding off-peak noise floors. Equation (2) assumes independent, isotropic complex noise, with each quadrature carrying $\sigma^2/2$; therefore, ΔR represents statistical uncertainty only. Figure 1 shows

* This work was produced by FermiForward Discovery Group, LLC under Contract No. 89243024CSC000002 with the U.S. Department of Energy, Office of Science, Office of High Energy Physics.

† abhishek@fnal.gov

Content from this work may be used under the terms of the CC BY 4.0 licence (© 2026). Any distribution of this work must maintain attribution to the author(s), title of the work, publisher, and DOI.

ISBN: 978-3-95450-275-2 ISSN: 2226-0366 doi: 10.18429/JACoW-LINAC2026-TUPO063

SPATIOTEMPORAL ELECTRO-OPTIC MEASUREMENT OF RELATIVISTIC ELECTRON BUNCHES WITH A PROPOSED HOOCS READOUT

Y. Hu[1], J. Li[1], J. Yang[2], K. Fan[1]
[1]School of Electrical and Electronic Engineering, Huazhong University of Science and Technology, Wuhan, China
[2]SANKEN, The University of Osaka, Osaka, Japan

Abstract

Spatiotemporally resolved characterization of relativistic electron bunches is essential for ultrafast accelerator diagnostics because the bunch-induced Coulomb field can vary simultaneously across the transverse plane and in time. Here we experimentally characterize this coupled response using delay-resolved multi-shot electro-optic sampling (EOS). Fifteen transverse measurements acquired from 1.12 to 16.80 ps reveal pronounced position-dependent changes in arrival time, temporal width, and waveform shape. Based on the information contained in these measurements, we further propose a high-dimensional EOS readout concept using high-dimensional one-shot optical field compressive sensing (HOOCS) to reduce sequential spatial-spectral sampling in a future implementation. The HOOCS scheme is not used to acquire the electron-bunch data reported here. A separate THz experiment is used only to demonstrate the feasibility of the underlying optical encoding and reconstruction chain. The electron-bunch measurements therefore define the spatiotemporal information that a future high-dimensional diagnostic should preserve.

INTRODUCTION

Precise characterization of relativistic electron bunches is a central requirement in ultrafast beam physics and accelerator optimization. Electro-optic sampling (EOS) transduces the transient Coulomb field of a bunch into measurable optical birefringence and therefore provides a non-invasive route to femtosecond-scale beam diagnostics [1, 2]. However, a local or spatially integrated EOS waveform cannot fully describe a bunch when the field arrival time, duration, and amplitude vary across the transverse plane.

Spatially resolved EOS measurements have already revealed substantial transverse-temporal structure in relativistic electron-bunch fields [3-6]. In this work, we focus on the experimental characterization of the electron-bunch-induced electro-optic response using delay-resolved imaging. The transverse evolution of the response is measured at successive probe delays, from which position-dependent temporal profiles are extracted to reveal the coupled spatial and temporal characteristics of the bunch-associated field. Based on these measurements, we further propose a high-dimensional EOS-HOOCS (high-dimensional one-shot optical field compressive sensing) scheme as a potential approach for acquiring such spatiotemporal information with reduced sequential sampling. In the proposed scheme, the spatial-spectral information carried by the chirped probe would be compressively encoded and reconstructed using HOOCS. A separate THz experiment is used only to demonstrate the feasibility of the underlying HOOCS reconstruction principle.

PROPOSED HIGH-DIMENSIONAL ELECTRO-OPTIC READOUT

Figure 1 schematically illustrates the proposed EOS-HOOCS concept for future electron-bunch diagnostics. In this configuration, the transient Coulomb field accompanying a relativistic electron bunch would induce Pockels birefringence in an electro-optic crystal and imprint a field-dependent polarization modulation on a linearly pre-chirped probe pulse with calibrated group-delay dispersion. Spectral dispersion and polarization analysis would convert this modulation into a wavelength-dependent probe intensity, so that the probe spectrum carries temporal information while the imaging system retains the transverse distribution.

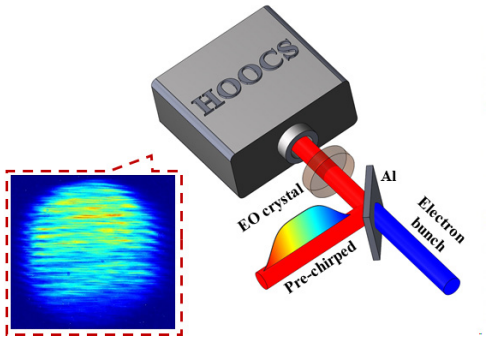


Figure 1: Proposed EOS-HOOCS readout concept for high-dimensional electron-bunch diagnostics. The bunch-induced modulation of a pre-chirped probe would be spatially and spectrally encoded for reconstruction of the coupled transverse-temporal response.

The proposed optical readout would use coded-aperture snapshot spectral imaging (CASSI) to compressively encode the probe joint spatial-spectral information into a two-dimensional detector measurement. Reconstruction would produce a high-dimensional spatiospectral data cube, and the calibrated probe chirp would provide the wavelength-to-time mapping required to convert the spectral coordinate

Content from this work may be used under the terms of the CC BY 4.0 licence (© 2026). Any distribution of this work must maintain attribution to the author(s), title of the work, publisher, and DOI.

ISBN: 978-3-95450-275-2 ISSN: 2226-0366 doi: 10.18429/JACoW-LINAC2026-TUPO064

POLE SHAPE OPTIMIZATION OF A TUNABLE PERMANENT MAGNET QUADRUPOLE FOR FUTURE ACCELERATOR BEAMLINES

J. Choi[1], J.-G. Hwang*[1], G. Hahn[2]
[1]Department of Physics, Kangwon National University, Gangneung, Republic of Korea
[2]Pohang Accelerator Laboratory, Pohang, Republic of Korea

Abstract

A permanent magnet quadrupole (PMQ) that generates its magnetic field without an external power supply and allows the gradient to be varied mechanically was designed. The two-dimensional pole shape was obtained using Non-dominated Sorting Genetic Algorithm II (NSGA-II) with objective functions of $1/|B_2|$ and $|B_6/B_2|$, and an end-edge chamfer angle was selected to minimize the integrated harmonic content. This geometry was extended to a three-dimensional model that accounted for a 2 mm longitudinal pole extrusion at each end, introduced to fabricate a clamping structure for the poles to the aluminum end plates. Although the earlier study defined the fundamental magnetic design, it did not include the 2 mm extrusion required for the mechanical support structures. The structural changes made to incorporate these supports modified the fringe-field distribution, making an additional optimization necessary to restore the correct longitudinal integrated field. Accordingly, a parametric sweep of the chamfer angle was performed over the machinable range, and the angle was re-selected to minimize the integrated harmonic content within the strength and flat-field constraints. The outcome meets the field quality requirements, with allowed multipole components remaining well below the 5×10^{-4} limit and forbidden components below 10^{-5}, and achieves a field uniformity of 0.1 % at $r_{\mathrm{ref}} = 3$ mm.

INTRODUCTION

Next-generation storage rings are designed to achieve ultra-low emittance and high brilliance, which in turn requires quadrupole magnets with higher magnetic gradients and stringently suppressed multipole field errors [1, 2]. To achieve the high gradients, conventional electromagnets consume substantial electrical power, and they also need extra energy for cooling systems to mitigate Joule heating. By comparison, a permanent magnet quadrupole (PMQ) sustains its magnetic field in steady-state operation without any power supply or active cooling. This makes the PMQ an attractive alternative [3, 4].

A hybrid Halbach structure [5], composed of an inner ring of permanent magnet blocks and iron poles, is widely utilized to achieve high magnetic field gradients. To provide tunability to the field gradient, several configurations have been proposed in previous studies. These include the mechanical translation of external magnets (e.g., DLS PMQ [6]), the rotation of an additional outer Halbach ring to modulate the magnetic flux (e.g., ILC PMQ [7]), and the rotation of additionally installed outer magnets to alter their magnetization alignment (e.g., QUAPEVA [8]). In this study, we adopted the tuning mechanism demonstrated in the QUAPEVA design; specifically, the inner hybrid ring is surrounded by four rotatable outer cylindrical magnets to adjust the quadrupole gradient (Fig. 1). The magnet material is Sm_2Co_{17} (YXG-30) and the poles are low-carbon steel (AISI 1010); the bore radius is 12.5 mm, and the iron length is 100 mm. Multipole components are evaluated at the reference radius $r_{\mathrm{ref}} = 3$ mm, and the design requirements are $|B_n/B_2| \leq 5 \times 10^{-4}$ for the allowed harmonics, $\leq 10^{-5}$ for the forbidden harmonics, and a good-field-region (GFR) uniformity of 0.1 % [9, 10].

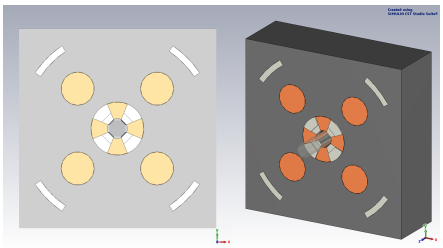


Figure 1: Schematic layout of the tunable permanent magnet quadrupole (PMQ) based on a hybrid Halbach structure. The orange components represent the Sm_2Co_{17} permanent magnets. The adjacent gray regions indicate the iron poles made of AISI 1010 low-carbon steel. The dark black parts correspond to the aluminum housing.

In a previous study, the pole profile was determined by numerical optimization, and the end chamfer angle of 41° was selected through a parameter sweep. The original design was reported to satisfy the requirements, with $\int B_6 / \int B_2 = 1.34 \times 10^{-5}$, $\int B_{10} / \int B_2 = 4.38 \times 10^{-6}$, and an effective length of 112.54 mm [11]. Due to the strong magnetic forces acting on the components, additional protruding structures were introduced alongside the poles to firmly clamp the permanent magnets and iron poles, acting as a rigid housing. Because these extrusions altered the fringe-field distribution, the validity of the previously selected 41° chamfer had to be re-examined.

POLE EXTRUSION

In the hybrid Halbach configuration, strong magnetic forces act between the permanent magnet blocks and the iron poles. The pole positions must therefore be mechanically constrained to prevent displacement and preserve the designed field quality. For prototype assembly, each iron

* hwang@kangwon.ac.kr

Content from this work may be used under the terms of the CC BY 4.0 licence (© 2026). Any distribution of this work must maintain attribution to the author(s), title of the work, publisher, and DOI.

ISBN: 978-3-95450-275-2 ISSN: 2226-0366 doi: 10.18429/JACoW-LINAC2026-TUPO065

GAIN AND BEAM QUALITY DEGRADATION IN A TRANSVERSE GRADIENT UNDULATOR IN THE LARGE-SIGNAL REGIME*

Weilun Qin†, Weihang Liu, Xingguang Liu, Yu Zhao,
Institute of High Energy Physics, Chinese Academy of Sciences, Beijing, China
Spallation Neutron Source Science Center, Dongguan, China

Abstract

The transverse gradient undulator (TGU) is a key component for realizing diffraction-limited storage-ring-based X-ray free-electron laser oscillators (XFELOs), as it can compensate for the large energy spread in storage ring electron beams. Previous studies have mainly focused on the small-signal gain of the TGU in such a setup. However, the gain can deviate significantly from the small-signal gain with the growth of intracavity power. In this contribution, we investigate the TGU gain and beam quality degradation in the large-signal regime using three-dimensional simulations. The beam emittance and energy spread degradation is understood via phase space evolution. An empirical fit model is developed for the single-pass behavior of gain and beam quality at fixed photon energy and can be used in a multipass XFELO model.

INTRODUCTION

Synchrotron light sources offer x-ray pulses with high repetition rate and average brightness. The start-of-the-art generation of synchrotron light sources now provides transverse coherent pulses with diffraction-limited storage rings (DLSR). In recent years, further development toward fully-coherent storage ring light sources is attracting increasing interest. DLSR-based x-ray free-electron laser oscillator (XFELO) is a promising way to achieve narrow-band, fully coherent hard x-ray pulses. Due to the relatively large energy spread in storage rings ($\sim 10^{-3}$), a transverse gradient undulator (TGU) combined with local dispersion is proposed to fulfill the resonant condition for off-energy electrons and recover usable single-pass gain [1]. Analytical forms of the small-signal gain were given by Li et al. for the fundamental wavelength [1–3] and Yu et al. for the harmonics [4, 5].

Together with cavity loss, the small-signal formulas give a good description of the start-up and exponential gain process, while saturation of the oscillator due to the growth of the intracavity power usually relies on numerical simulations. In conventional XFELOs, main focus has been the gain degradation due to nonlinear motion in the longitudinal phase space [6]. While in a DLSR-based XFELO, the high intracavity power not only induces nonlinear phase space motion to lower the gain, but also affects the beam quality of the next round trip. Besides, the degradation of beam quality is not limited to energy spread as in usual ring-based FEL oscillators, but also coupled to transverse emittance due to the use of transverse gradient undulator.

In this paper, we investigate the gain and beam quality degradation in a DLSR-based XFELO, which is the key process of power saturation in such a system. With the help of 3D steady-state simulation using GENESIS [7], we first validate the small-signal gain formulas at multiple photon energies, then show dependency of single-pass gain, energy spread, emittance, and mean energy on the input seed power. Beam phase spaces are shown for high power case to illustrate the mechanism of coupled beam quality degradation. Finally, we present an empirical fit model to describe the power and beam quality changes, which could be further used in a simplified multipass model for fast evaluation and optimization of the DLSR-based XFELO.

SMALL-SIGNAL GAIN

We study the small-signal gain assuming a short straight section in a typical high energy DLSR. The undulator length is 5 m and gain is obtained through higher beam current and TGU gradient. In this study, we fixed the beam and undulator parameters as: peak current $I = 150$ A, relative energy spread $\sigma_{\delta 0} = 0.2$ %, beam emittance $(\varepsilon_x + \varepsilon_y)/\gamma = 34$ pm, undulator period $\lambda_u = 15$ mm and number of periods $N_u = 333$. We use a single-objective genetic algorithm to optimize electron beam (Twiss parameters, emittance coupling ratio, vertical dispersion), radiation (waist size), and undulator (detuning, TGU gradient) parameters for optimal gain. The optimization was performed for multiple photon energies using the theoretical gain formulas and steady-state GENESIS simulation. For the GENESIS simulation, an input power of 100 W is used.

Figure 1 compares the optimized gains from GENESIS simulation with the Li and Yu integral formulas evaluated at the same photon energy. It is found that, compared with theoretical predictions, GENESIS simulations tend to give a higher single-pass gain at lower photon energies. This is because the theoretical formulas are obtained based on a perturbative analysis, while certain non-perturbative contributions could affect the gain when the theoretical gain is higher. The Li and Yu formulas agreed well and converged on optimized parameters, except for the detuning. In the following, we take the 8.51 keV working point for gain and beam quality degradation study. The optimal parameters for 8.51 keV are listed in Table 1.

* This work was supported by Guangdong Basic and Applied Basic Research Foundation (No.2026A1515030037), the Department of Science and Technology of Guangdong Province (No.2024QN11X220).

† qinwl@ihep.ac.cn

Content from this work may be used under the terms of the CC BY 4.0 licence (© 2026). Any distribution of this work must maintain attribution to the author(s), title of the work, publisher, and DOI.

ISBN: 978-3-95450-275-2 ISSN: 2226-0366 doi: 10.18429/JACoW-LINAC2026-TUPO066

BEAM PHYSICS DESIGN OF THE LINAC FOR THE CSNS POWER UPGRADE PROJECT*

J. Peng†,1,2, Y. L. Han1,2, Z. P. Li1,2, Y. Yuan1,2, B. Z. Chen1,2, F. X. Yuan1,2, M. Y. Huang1,2, H. C. Liu1,2, S. Wang1,2, S. N. Fu1,2
[1]Institute of High Energy Physics, Chinese Academy of Sciences, Beijing, China
[2]Spallation Neutron Source Science Center, Dongguan, China

Abstract

The China Spallation Neutron Source (CSNS) officially launched its power upgrade project (CSNS-II) in 2024, with the goal of increasing the accelerator beam power from 100 kW to 500 kW. The CSNS accelerator consists of an 80 MeV linear accelerator and a 1.6 GeV rapid-cycling synchrotron. To raise the peak beam intensity from 15 mA to 40 mA, the front-end system of the linear accelerator will be replaced. In addition, a superconducting linear accelerator will be installed to increase the beam energy from 80 MeV to 300 MeV. This paper presents the upgraded linac lattice design and corresponding commissioning results developed for high intensity beam operation.

INTRODUCTION

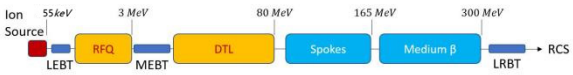


Figure 1: Overview of the CSNS-II linac layout.

The CSNS is a short-pulse neutron scattering facility dedicated to energy and materials research. The facility was designed to deliver a 100kW proton beam to the target at a pulse repetition rate of 25 Hz. CSNS officially opened to users in September 2018 with an initial beam power of 20kW. Less than two years later, in February 2020, it reached its design power of 100kW, primarily through increases in both pulse length and beam current. By this year, the accelerator's target beam power has been further increased to 185 kW, with beam availability exceeding 90%. To meet rapidly growing user demand, CSNS officially launched its Phase II power upgrade project in 2024. The main objectives of this upgrade are to increase the proton beam power on target from the Phase-I design value of 100 kW to 500 kW, and to con-struct 11 additional neutron spectrometers and experimental stations, thereby expanding the total number of beamlines to 20 [1].

The accelerator of the CSNS consists of an 80 MeV normal-conducting linear accelerator (linac) and a 1.6 GeV Rapid Cycling Synchrotron (RCS). The existing 80 MeV linac comprises a 50 keV Penning surface plasma ion source, a Low Energy Beam Transport (LEBT) line equipped with three solenoids, a 3 MeV four-vane Radio Frequency Quadrupole (RFQ), and a conventional drift tube linac (DTL). Since the output energy of the accelerator is fixed at 1.6 GeV, the beam power upgrade will be achieved by increasing the average beam current. Specifically, the peak beam current will be increased from 15 mA to 40 mA. To meet the current requirement of power upgrade, an external antenna RF-driven negative hydrogen ion source was developed and installed to replace the Penning source during the summer of 2021 [2]. As the existing RFQ has shown performance degradation, a new RFQ is scheduled to be installed during the forthcoming summer maintenance period. Meanwhile, the DTL has maintained stable operation, and beam experiments have confirmed that the existing DTL is capable of transporting the required high intensity beam. At the exit of the DTL, a new superconducting linac (SCL) will be added to increase the beam energy to 300 MeV, thereby mitigating space charge effects during beam injection into the RCS. The layout of the upgraded linac is shown in Fig. 1, and the main beam parameters are summarized in Table 1.

Table 1: Main Parameters of the Accelerator

Parameter	Units	CSNS	CSNS-II
Average beam power	kW	100	500
Proton energy	MeV	1.6	1.6
Average pulse current	μA	62.5	312.5
Linac beam energy	MeV	80	300
Linac beam peak current	mA	15	40
Macro-pulse length	μs	500	650
Repetition rate	Hz	25	25+25

LATTICE DESCRIPTION

MEBT

The Medium Energy Beam Transport (MEBT) line connects the RFQ and DTL, and performs three primary functions:

- Achieve transverse and longitudinal beam matching conditions.
- Characterize beam parameters output from the RFQ.
- Collimate partial beam halo particles to mitigate beam loss in the downstream accelerator sections.

To enable beam matching and diagnostics for high intensity beams, the MEBT was redesigned. The new MEBT preserves nearly the same overall length as the original layout-approximately 3 m-and consists of 10 quadrupole

* Work supported by the Open Fund of the China Spallation Neutron Source Songshan Lake Science City (No. KFKT2023A01) and the National Key Research and Development Project (No. 2023YFA1606802).
† pengjun@ihep.ac.cn

Content from this work may be used under the terms of the CC BY 4.0 licence (© 2026). Any distribution of this work must maintain attribution to the author(s), title of the work, publisher, and DOI.

ISBN: 978-3-95450-275-2 ISSN: 2226-0366 doi: 10.18429/JACoW-LINAC2026-TUPO070

DEVELOPMENT OF A RESONATOR FOR THE MEASUREMENT OF THE BEAM QUADRUPOLE MOMENT IN A HIGH-INTENSITY HEAVY-ION LINAC*

A. S. Plastun†, A. Al-Homoud, S. Cogan, M. Hu, S. Lidia,
P. N. Ostroumov, X. Rao, K. Saini, S. Zhao
Facility for Rare Isotope Beams, Michigan State University, East Lansing, MI, USA

Abstract

Non-invasive measurements of the beam quadrupole moment provide information for the evaluation of the beam emittance and Courant-Snyder parameters for transverse matching. Such a procedure is required for each charge state of heavy ion beams at multiple locations along the FRIB linac. We are developing a quadrupole mode resonant cavity, enabling us to extract the information about the beam quadrupole moment with much greater accuracy than non-resonant devices such as Beam Position Monitors. We have built a full-scale prototype resonator in which the quadrupole mode is excited by the 33rd harmonic of the beam frequency of 40.25 MHz The results of RF measurements and quadrupole signal acquisition with monopole and dipole mode suppression are reported. These studies are a necessary step towards the design and construction of the vacuum-tight resonator and its use for beam measurements.

INTRODUCTION

The driver linac of the Facility for Rare Isotope Beams (FRIB) at Michigan State University is the first accelerator capable of accelerating multiple charge states of stripped heavy-ion beams and delivering up to 400 kW to the isotope production target. Setting up the linac involves transverse beam matching at several locations [1,2]. Currently, a single wire scan takes about 3 min, which adds up to 25 min for a single-charge-state scan, or 2 h for the five-charge-state uranium beam. Matching at several locations along the linac therefore requires about 6 h. Since FRIB produces rare isotopes via fragmentation of the primary beam ions, the linac is tuned for each experiment every couple of weeks. Fast and non-invasive instrumentation is therefore in high demand at FRIB. This paper presents a prototype resonant cavity currently under development at FRIB for beam quadrupole-moment measurements [3].

RESONANT CAVITY

Resonant beam position monitors are well-known instruments for measuring beam position [4–6] and second moments [7]. The resonant monitors accumulate the electromagnetic energy that carries the necessary information about the beam distribution. For the quadrupole moment monitor, the cavity's quadrupole mode is set to resonate with a beam harmonic. Short bunches have wide spectra, allowing the use of higher harmonics and making the cavities relatively compact. For the monitor prototype, we selected the 33rd beam harmonic at 1328.25 MHz to be resonant with the quadrupole mode of the cavity, as a compromise between the dimensions and the strength of the beam harmonics. Figure 1 shows several fundamental cavity modes and the cavity geometry. The cavity features four quadrupole rods to enhance the quadrupole mode shunt impedance at the beam velocity $\beta = 0.566$ (200 MeV/u) and fine-tune the modes' frequencies. The main RF parameters of the modes are listed in Table 1 (x is the offset from the cavity's longitudinal axis, in meters). The cavity is equipped with four antenna pickups, which are critically coupled to the quadrupole mode.

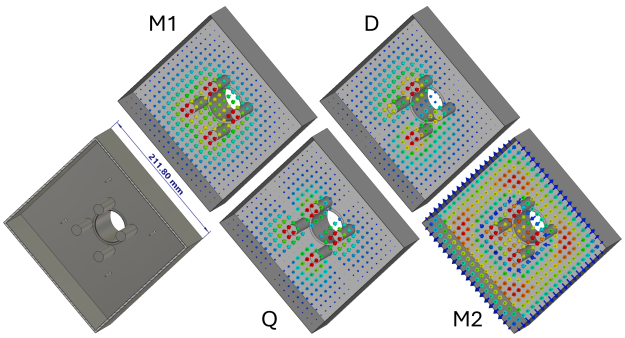


Figure 1: The cavity model (half is shown) and electric field patterns of its modes: (M1) monopole, (D) dipole, (Q) quadrupole, (M2) higher-order monopole mode.

Table 1: Modes of the Resonant Cavity Monitor

	M1	D	Q	M2
f_0 (MHz)	711	1110	1328.25	2057
R/Q (Ω)	130	$7.6e4x^2$	$7.8e7x^4$	1.3
Q_0	15500	12640	10530	12500
Coupl. β	4×0.23	2×0.68	4×0.25	4×11.5

The cavity modes that interfere with the measurement of the quadrupole moment are also known as *common modes* [4]. There are several ways to suppress the effect of the common modes on the measurements.

CAVITY PROTOTYPE

The purpose of building the prototype is to validate the simulations and calculations of the cavity response, develop a tuning strategy of the common-mode rejection circuit,

* Work supported by the U.S. Department of Energy, Office of Science, Office of Nuclear Physics under award number DE-SC0025531
† plastun@frib.msu.edu

Content from this work may be used under the terms of the CC BY 4.0 licence (© 2026). Any distribution of this work must maintain attribution to the author(s), title of the work, publisher, and DOI.

ISBN: 978-3-95450-275-2 ISSN: 2226-0366 doi: 10.18429/JACoW-LINAC2026-TUPO071

STUDY OF BEAM MISMATCH EFFECTS IN A 2.5-MeV 200-MHz 4-VANE RFQ FOR NEUTRON GENERATION*

S. Ikeda[1], H. Shuai[2], T. Kanesue[1], M. Okamura†,[1], G. Anda[3], F. Mezei[2]
[1]Collider-Accelerator Department, Brookhaven National Laboratory, Upton, NY, USA
[2]Eötvös Loránd University, Budapest, Hungary
[3]HUN-REN Centre for Energy Research, Budapest, Hungary

Content from this work may be used under the terms of the CC BY 4.0 licence (© 2026). Any distribution of this work must maintain attribution to the author(s), title of the work, publisher, and DOI.

Abstract

Four-vane radio-frequency quadrupoles (RFQs) operating around 200 MHz are a common front end for compact accelerator-driven neutron sources, where the practical performance limit is usually set by how much injection mismatch and machine error the structure can absorb rather than by the design beam dynamics. A systematic error and mismatch study has therefore been carried out for a representative 2.5 MeV, 200 MHz four-vane RFQ, taking as a concrete example the structure procured by Hungary for its first compact neutron source. Starting from the as-machined vane geometry, the acceptable injected current and emittance range was mapped, and transmission, emittance growth and output trajectory were evaluated against transverse injection offset, injection angle error and inter-vane voltage error. The resulting tolerance budget is given, and it is shown that an offset injected into an RFQ of this length completes several betatron periods before extraction, so that the exit trajectory is uncorrelated with the injected one and steering elements are required on both sides of the structure. The direction of the exit error is set by the betatron phase at extraction and hence by the vane voltage, so it follows the RF operating point and the beam loading.

INTRODUCTION

Compact accelerator-driven neutron sources (CANS) are increasingly used for neutron scattering, imaging and boron neutron capture therapy [1], and most of them are driven by a proton linac whose first accelerating structure is a four-vane RFQ operating in the 200 MHz range. Such an RFQ typically accepts a few tens of milliamperes at 30–40 keV from a single ion source and accelerates the beam to 2–3 MeV over a few metres. Because the injector chain of a compact machine is kept simple — one source, one or two solenoids, a small number of correctors — the tolerance of the RFQ to imperfect injection largely determines both the current that can be delivered and the effort required during commissioning.

The present work quantifies that tolerance for a machine of this class. The structure used as a concrete example is the 2.5 MeV, 200 MHz four-vane RFQ procured by Hungary for the 'LvB' compact neutron source at Martonvásár [2]; its main parameters are summarized in Table 1. It is injected at about 35 keV from an electron-cyclotron-resonance (ECR) proton source through a double-solenoid low-energy beam transport line. These parameters are representative of the class rather than specific to this machine.

Three questions are addressed: what injected current and emittance the structure accepts, how much injection offset dx and angle error dx′ it tolerates, and how an inter-vane voltage error, expressed through a scaling factor V_{fac}, propagates to the output beam.

RFQ MODEL AND INJECTION CONDITIONS

The beam dynamics were computed with TOUTATIS, part of the TraceWin code suite [3, 4]. The vane modulation profile was taken from the as-machined electrode data rather than the design values, and a voltage scaling factor V_{fac} = 1.02 was set by matching the simulated transmission curve to the measured cold-model response of the fabricated vanes. Unless stated otherwise the injected beam is 20 mA at 0.5 π mm mrad normalized 6-rms emittance, a condition typical of an ECR source with a 5 mm extraction aperture at 35 kV followed by a solenoid transport line. This emittance, and every Twiss parameter quoted below, refers to the entrance of the vanes; β follows the PARMTEQ convention and is given in cm/rad.

Table 1: Parameters of the Example RFQ

Parameter	Value
RF frequency	200 MHz
Vane type	4-vane
Input / output energy	35 keV / 2.5 MeV
Number of cells	167
Zero-current phase adv. σ_0	≈22.5°/cell (3760° total)
Voltage factor V_{fac}	1.02
Design / peak current	20 / up to 40 mA

Matched Injection Condition

The transmission depends strongly on the injected Twiss parameters, and the error scans below must start from a genuinely matched condition. Figure 1 maps the transmission over the (α, β) plane at 20 mA. A converging injection is clearly preferred over a waist at the last focusing element: the transmission reaches 96.2 % at α = 3.55 against 91.6 % at α = 0, at the cost of a larger envelope upstream. The operating point α = 3.55, β = 10.9 cm/rad, marked by the red cross and lying well inside the high-transmission region, was adopted for all the scans below; the

* Work supported by Brookhaven Science Associates, LLC, under Contract No. DE-SC0012704 with the U.S. Department of Energy, and by HUN-REN Centre for Energy Research, Hungary.
† okamura@bnl.gov

ISBN: 978-3-95450-275-2 ISSN: 2226-0366 doi: 10.18429/JACoW-LINAC2026-TUPO072

GENERATION OF LOCAL VERTICAL DISPERSION IN A LONG STRAIGHT SECTION OF SAPS STORAGE RING*

Y. Zhao[1,2], W. H. Liu[1,2], W. L. Qin[1,2], X. Li[1,2], Y. Jiao[1,†]
[1]Institute of High Energy Physics, Chinese Academy of Sciences, Beijing, China
[2]Spallation Neutron Source Science Center, Dongguan, China

Abstract

A promising direction for fourth-generation light sources is the integration of a free-electron laser (FEL) oscillator to achieve higher spectral brightness. This approach imposes stringent requirements not only on the FEL oscillator parameters but also on the storage ring's performance. Preliminary studies at the Southern Advanced Photon Source (SAPS) indicate that the optimal gain for an oscillator occurs when the vertical dispersion in a long straight section is approximately 1 cm. To realize this condition, we introduce local vertical dispersion in the SAPS storage ring lattice by adding skew quadrupole components to four sextupole magnets placed on both sides of a dispersion-free long straight section. These components generate the desired local vertical dispersion. This paper describes the underlying principles of this generation scheme and evaluates its impact on the overall ring performance.

INTRODUCTION

A promising direction for fourth-generation light sources is the integration of a free-electron laser (FEL) oscillator, which offers the potential to achieve significantly higher spectral brightness and improved temporal coherence compared to conventional undulator radiation or self-amplified spontaneous emission schemes [1–4]. The oscillator configuration provides distinct advantages, such as narrow-bandwidth output, high peak power, and enhanced longitudinal coherence, making it particularly attractive for advanced experiments in spectroscopy, scattering, and ultrafast dynamics. However, realizing such a system in a storage-ring environment imposes stringent requirements not only on the FEL oscillator itself—including precise cavity alignment, high-reflectivity mirrors, and sufficient single-pass gain—but also on the performance of the storage ring. The ring must deliver an electron beam with ultra-low emittance, high peak current, and exceptional orbit and energy stability, while maintaining bunch length and energy spread within tight tolerances.

This work builds on the conceptual design of the Southern Advanced Photon Source (SAPS) [5–8], a 3.5 GeV medium-energy diffraction-limited storage ring planned for Guangdong, China, adjacent to the China Spallation Neutron Source. The baseline design of SAPS has been completed, with a natural emittance of 26.3 pm·rad. Preliminary studies carried out at SAPS have identified a critical parameter for optimizing the FEL oscillator gain: the vertical dispersion in the long straight section dedicated to the oscillator. Through systematic simulations, it has been found that the optimal gain is achieved when the vertical dispersion in that section reaches approximately 1 cm. This value arises from the trade-off between the electron-beam overlap with the optical mode and the degradation of emittance caused by dispersion; too little dispersion reduces the gain, while too much leads to excessive beam size growth and loss of transverse overlap. The finding provides a concrete design target for the SAPS lattice, but it also poses a significant challenge, as the baseline lattice of SAPS is naturally dispersion-free in all straight sections, and thus no vertical dispersion is present there by default.

Therefore, to exploit the full potential of the FEL oscillator at SAPS, it becomes necessary to intentionally generate a controlled local vertical dispersion in the designated long straight section, while preserving the overall ring performance in terms of emittance, dynamic aperture, and beam stability. This paper presents our approach to introducing such local vertical dispersion and evaluates its impact on the ring optics and beam dynamics. The rest of the paper is organized as follows: Section 2 describes the lattice modification scheme, Section 3 evaluates its impact on the overall ring performance, Section 4 describes the first attempt to restore the ring performance and Section 5 summarizes the conclusions and outlines future work.

VERTICAL DISPERSION

Currently, two typical approaches are commonly adopted in the international community to generate vertical dispersion in storage rings. The first approach employs skew quadrupole coils to couple horizontal and vertical dispersions, thereby creating local vertical dispersion. In the MAX-IV storage ring [9], for instance, additional coils are installed on sextupole and octupole magnets to introduce skew quadrupole components, producing vertical dispersion in every cell. The ALS [10, 11] also implemented skew quadrupoles to generate local vertical dispersion; however, as a third-generation light source, the nonlinear effects were less pronounced. The second approach introduces dedicated vertical bending magnets to produce vertical dispersion, as exemplified by the method described in Ref. [12], which combines angular dispersion induced micro-bunching with a damping ring. In that scheme, vertical bending magnets are placed in the dispersion-free long straight section to generate the required vertical dispersion. Nevertheless, this approach consumes a significant portion of the long straight section and involves more complex operational procedures.

* Work supported by National Natural Science Foundation of China (No.12505165)
† jiaoyi@ihep.ac.cn

Content from this work may be used under the terms of the CC BY 4.0 licence (© 2026). Any distribution of this work must maintain attribution to the author(s), title of the work, publisher, and DOI.

ISBN: 978-3-95450-275-2 ISSN: 2226-0366 doi: 10.18429/JACoW-LINAC2026-TUPO073

SUB-FEMTOSECOND ELECTRON-BUNCH GENERATION VIA TWO-DIMENSIONAL BEAM COMPRESSION*

W. Liu[1,2,†], S. Jiang[1,2,†], X. Li[1,2], X. Liu[1,2], Y. Jiao[1], S. Wang[1,2]
[1]Institute of High Energy Physics, Chinese Academy of Sciences, Beijing, China
[2]Spallation Neutron Source Science Center, Dongguan, China

Abstract

Sub-femtosecond electron beams would provide a powerful probe of ultrafast electronic and nuclear dynamics, but their generation with both high beam energy and pC-level charge remains challenging. Conventional longitudinal compression requires a large energy chirp and becomes increasingly impractical for hundred-MeV beams, whereas low-energy approaches are strongly limited by space-charge effects and typically operate at very low charge. Here, we propose a two-dimensional beam-compression scheme based on transverse–longitudinal coupling. In this scheme, the compressed bunch length is governed by the beam geometric emittance, allowing the small transverse emittance of modern electron beams to be exploited for ultrashort bunch generation. Start-to-end simulations show that sub-femtosecond bunches with hundred-MeV beam energy and pC-level charge can be produced. This approach offers a potential route toward compact, high-energy attosecond electron beams and may enable sub-femtosecond radiation sources based on undulator radiation or inverse Compton scattering.

INTRODUCTION

Short electron bunches improve temporal resolution in ultrafast electron scattering and provide drivers for ultrashort radiation sources [1, 2]. Approaching the attosecond regime is difficult at hundred-MeV energies because conventional longitudinal compression couples the minimum duration to the initial energy spread. For a relative energy spread of order 10^{-4}, the required RF chirp can correspond to hundreds of megavolts of C-band voltage. Low-energy sub-femtosecond sources alleviate the RF-voltage requirement, but they are more sensitive to space charge and typically operate at very low bunch charge.

Transverse–longitudinal coupling (TLC) provides an alternative compression route by exploiting the transverse beam quality. Angular-dispersion-induced microbunching (ADM) is one class of TLC-based beam manipulation. Previous TLC theory showed that the compressed duration can be governed by the transverse beam size or angular divergence rather than by the initial energy spread [4,5]. More recently, Cheng *et al.* proposed an ADM-based two-dimensional compressor that produced an 810 as, 3.18 MeV bunch with a final charge of 6 fC in simulation [3]. This result demonstrated the feasibility of TLC-based attosecond compression at MeV energies, but did not address the high-energy, pC-level regime.

The present work turns the TLC concept into a realistic high-energy compressor, includes nonlinear transport and collective effects, and validates the method with start-to-end distributions. The main question is not simply whether an attosecond bunch can be formed, but over what range of bunch charge and beam energy it remains achievable. A more comprehensive version of this work is available as arXiv:2606.11799 [6]. It has been submitted to *New Journal of Physics*.

TWO-DIMENSIONAL COMPRESSION

The beamline is shown in Fig. 1. In the bending plane, the particle coordinates are written as $\mathbf{X} = (x, x', z, \delta)^{\mathrm{T}}$. The first rectangular dipole creates the correlations $z(x, x')$, and an off-crest C-band cavity applies $\delta \rightarrow \delta + hz$. The subsequent three-dipole section (TDS) is adjusted so that the dominant contributions from the initial longitudinal coordinate and energy spread cancel:

$$R_{31} = 0, \qquad hR_{34} + 1 = 0, \qquad R_{32}\sin\theta + R_{34} = 0. \quad (1)$$

Here R_{3j} denotes the first-order map of the TDS, h is the RF chirp, and θ is the angle of the first dipole. Under these conditions, the final rms bunch length becomes

$$\sigma_{z,f} = \left|\frac{1}{h\tan\theta}\right|\sigma_{x_0'} = \left|\frac{1}{h\tan\theta}\right|\sqrt{\frac{\gamma_{x,0}\epsilon_n}{\gamma}}. \quad (2)$$

The ideal duration therefore scales as $\gamma^{-1/2}$ and is governed by the transverse geometric emittance. Compared with an ADM dogleg, the TDS removes the direct constraint between h and the first bending angle, enlarging the feasible parameter space and allowing a substantially stronger compression.

At the large bending angles required for extreme compression, second-order transport becomes important. Expanding the RF waveform shows that its quadratic term can be independently controlled by adding a K-band cavity. The linear and second-order correlations can then be optimized separately. Tracking with zero current shows that the linearizer restores the final duration close to the ideal value of Eq. (2).

COLLECTIVE-EFFECT OPERATING WINDOW

Finite bunch charge introduces space-charge and coherent synchrotron radiation (CSR) effects. Comparisons between one- and two-dimensional CSR calculations, and between longitudinal and three-dimensional space-charge models,

* Work supported by the National Natural Science Foundation of China (Grant No. 12405176).
† These authors contributed equally to this work.

Content from this work may be used under the terms of the CC BY 4.0 licence (© 2026). Any distribution of this work must maintain attribution to the author(s), title of the work, publisher, and DOI.

ISBN: 978-3-95450-275-2 ISSN: 2226-0366 doi: 10.18429/JACoW-LINAC2026-TUPO076

DEVELOPMENT OF AN AUTOMATED LORENTZ FORCE DETUNING COMPENSATION SYSTEM FOR THE ITN CRYOMODULE AT KEK*

R. Bajpai†, M. Omet
High Energy Accelerator Research Organization (KEK), Tsukuba, Japan

Abstract

At KEK, an International Linear Collider prototype cryomodule with eight TESLA-type cavities is under development. The cryomodule will operate in pulsed mode at 5 Hz. During RF operation, electromagnetic forces mechanically deform the cavity structure, shifting the resonance frequency through Lorentz Force Detuning (LFD).

A common method for LFD compensation is feedforward control using a piezo actuator driven by a half-sine waveform to restore resonance during the flat-top. Effective compensation requires optimization of waveform amplitude, frequency, DC offset, and phase relative to the RF pulse. Manual tuning is feasible for a small number of cavities but is time-consuming and difficult to scale. To address this, an automated LFD compensation algorithm is being developed on a Red Pitaya FPGA platform using Vivado. The system automatically optimizes the piezo drive parameters for cavity tuning. This contribution presents the current progress of the automated compensation algorithm and the cavity simulator developed for testing and evaluation.

MOTIVATION

The LLRF system (Fig. 1) of ITN cryomodule [1] will have an independent hardware to control the piezo for LFD compensation. The LLRF system will provide Cavity and Forward Voltages via EPICS and the piezo controller will calculate and compensate for the detuning by driving the piezo with half-sine wave. The amplitude, frequency, phase and DC offset of the half-sine wave must be adjusted. Manually adjusting these parameters is time-consuming and not scalable, making automation necessary. Thus, a cavity simulator was developed and is now being used to develop an automation LFD compensation system.

APPROACH

The issue with timely development of tuner piezo controller with automated LFD compensation is the lack of a horizontal cryostat compatible with the prototype cavity at KEK. Therefore, a cavity simulator to substitute a real cavity was developed instead. Figure 2 shows the schematic layout for automation development. The development of the cavity simulator was carried out in several stages. First, a cavity simulator was developed in Simulink, an appropriate FPGA hardware (Red Pitaya) was selected, and the electromagnetic model of the cavity was successfully implemented on the FPGA. These initial results were reported

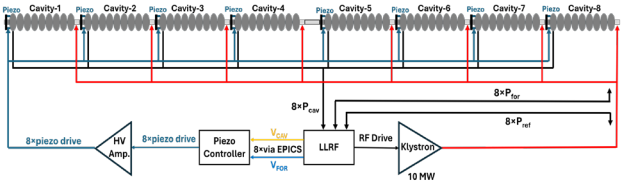


Figure 1: Simplified schematic of ITN RF System.



Figure 2: Schematic of Automation Development.

in a previous poster presentation at SRF 2025; for further details, see Ref. [2]. Subsequently, the mechanical model was implemented and integrated with the electromagnetic model to realize a real-time cavity simulator on the Red Pitaya (FPGA-1). Next, LFD compensation was verified with a half-sine wave signal from an external signal generator. Following this verification, the compensation system was implemented directly on FPGA-1 through a half-sine generator, and an automated parameter tuning algorithm was developed and demonstrated.

CAVITY SIMULATOR AND MANUAL LFD COMPENSATION

The cavity simulator was implemented on the Red Pitaya platform using Vivado. The EM model of the cavity was realized using combination of standard IP cores to implement the cavity difference equation. Whereas the mechanical model of the cavity was realized by writing a custom Verilog module.

Figure 3 shows the experimental setup used to test the cavity simulator. In this configuration, the Red Pitaya generates the cavity voltage, detuning, and trigger signals. The cavity voltage, detuning and trigger are plotted on the oscilloscope in red, yellow and green, respectively. The trigger is generated for 2 ms at start of each pulse. The trigger output is used to synchronize an external signal generator, which produces a half-sine waveform. This half-sine signal

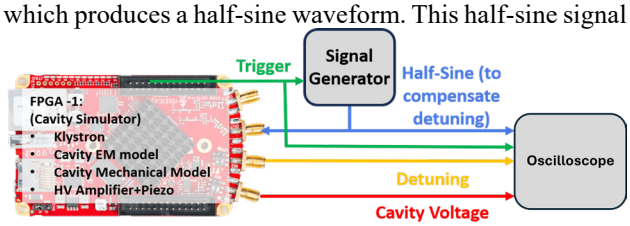


Figure 3: Setup to test cavity simulator and manual LFD compensation.

*This work was supported by the MEXT Development of key element technologies to improve the performance of future accelerators Program Japan Grant Number JPMXP1423812204.
† bajpai@post.kek.jp

Content from this work may be used under the terms of the CC BY 4.0 licence (© 2026). Any distribution of this work must maintain attribution to the author(s), title of the work, publisher, and DOI.

ISBN: 978-3-95450-275-2 ISSN: 2226-0366 doi: 10.18429/JACoW-LINAC2026-TUPO077

PSEUDO SIX-DIMENSIONAL + 1 PHASE SPACE RECONSTRUCTION WITH A CONVOLUTIONAL NEURAL NETWORK

Z. J. Liptak*[1], H. Hayano[2], M. Kurata[3], M. Kuriki[1], S. Mukherjee[1], T. Okugi[3], N. Terunuma[3], Y. Yamamoto[3]
[1]Hiroshima University, Higashihiroshima, Japan
[2]NovAccel Co. Ltd., Tsuchiura, Japan
[3]High Energy Accelerator Research Organization (KEK), Tsukuba, Japan

Abstract

In particle accelerators, full knowledge of the six-dimensional (6D) beam phase space is crucial but difficult to obtain with conventional beam diagnostics. We have developed a two-stage convolutional neural network (CNN) that reconstructs the 6D phase space from only sixteen transverse $(x - y)$ screen images taken at a place with dispersion by different phase space rotation angles. With these images, we reconstruct the 6D phase space distribution at the cathode surface and visualize it as 15 two-dimensional images covering all pairwise coordinate combinations. Compared to existing 6D beam imaging measurement techniques such as tomography, it significantly reduces measurement time and required computational resources, enabling the provision of a more practical 6D phase space measurement method.

INTRODUCTION

Successful operation of accelerator facilities depends critically upon measurement and control of beam quality, but a full representation of the the six-dimensional phase space is difficult to obtain. As current- and next-generation facilities require increasingly precise control over beam emittances to achieve their design goals, the ability to reconstruct the 6-D phase space parameters quickly and accurately is becoming increasingly important.

Conventional beam diagnostic equipment and techniques individually provide only a subset of observables, and measurement is often time-consuming and cumbersome, e.g. [1, 2], rendering them impractical for use in operation.

Here was develop a Convolutional Neural Network (CNN)-based algorithm to reconstruct the 6D phase space with minimal disruption to beam operation and requiring only modest computing hardware [3]. Once the initial CNN training has been completed, only 16 beam images with a varying beamline settings are required for the algorithm to reconstruct the 6D beam state, minimizing loss of valuable beam time, and feedback takes only minimal processing time. Beam charge is included as an additional element, giving a total of 6D+1 variables to be reconstructed. Higher-dimensional-order correlations are not explicitly included in the reconstruction, hence the nomenclature as a pseudo-6D model.

* zjl@hiroshima-u.ac.jp

PHASE-SPACE ROTATIONS

The CNN-based reconstruction technique depends upon the ability to rotate the beam in both transverse and longitudinal space, and then to measure the observable $(x - y)$ beam profile in a region with transverse dispersion. In this study, we make use of common beamline injector elements: transverse rotation is introduced by varying the solenoid field, and longitudinal rotation is effected by varying the RF phase inside the RF gun. Measurement is conducted at the center of a chicane, satisfying the horizontal dispersion condition.

An example of horizontal (longitudinal) rotation effected by varying the solenoid field (RF phase) is shown in the top (bottom) of Fig. 1.

TWO-STAGE CONVOLUTIONAL CNN METHOD

The CNN developed here operates in two distinct phases, with learning carried out in opposite directions to establish the relationship between measured 2D distribution and initial (upstream) phase state. Stage 1 fixes a particular RF phase and solenoid field and trains the network on the mapping from the chicane image to the corresponding initial state. With Stage 1 completed, Stage 2 trains the network in the opposite direction: for a given cathode (upstream) state, the model trains on all measured solenoid and RF states. Once both stages of training have been completed, the model then produces phase space distributions consistent with all projected images. Both phases of the network training are necessary to accurately establish the relationship between upstream and downstream states, preventing overtraining and allowing the model to learn appropriately. The output result of the CNN algorithm is 15 images representing each 2D phase space combination for the six beam variables, i.e. $x - y, x - x', y - y'$, etc. Charge information is extracted by integrating the total data contained in the images.

TRAINING SAMPLE CREATION

Effective training of predictive ML models is predicated on providing training sets that provide broad coverage of the phase space to be considered, allowing the model to recognize and predict not only common or good states, but also those that may arise when beam conditions are poor or out of the ordinary. To avoid the pitfall of the algorithm reconstructing common beam shapes even when exposed

Content from this work may be used under the terms of the CC BY 4.0 licence (© 2026). Any distribution of this work must maintain attribution to the author(s), title of the work, publisher, and DOI.

ISBN: 978-3-95450-275-2 ISSN: 2226-0366 doi: 10.18429/JACoW-LINAC2026-TUPO078

OPERATION STATUS OF SCINTILLATOR-BASED BEAM LOSS MONITORS FOR KOMAC DTL TANKS*

Gyuhaeng Jo, Sang-Pil Yun, Jae-Ha Kim, Young-Gi Song, HanSung Kim, Hyeok-Jung Kwon†
Korea Multi-purpose Accelerator Complex, Korea Atomic Energy Research Institute,
Gyeongju, Republic of Korea

Abstract

The Beam loss monitor (BLM) is a key device for protecting accelerator systems, as it measures secondary radiation produced by a particle beam colliding with the inner wall of the accelerator. Therefore, in the KOMAC 100 MeV proton accelerator, BLMs were installed on the 20 MeV DTL (Drift Tube Linac) and 100 MeV DTL tanks for the purpose of machine protection. These BLMs are scintillator-based radiation detectors capable of operating in high-radiation environments, with two or more devices installed on each DTL tank. In this study, BLM signals under unstable beam conditions were analyzed to verify that BLMs could not only measure proton beam loss but also detect RF instabilities.

METHODS AND RESULTS

Specifications of BLM at KOMAC

In this study, two types of scintillator detectors were utilized, and both detectors have the same electrical systematic structure, as described in Fig. 1 [1]. The first old scintillator detector type for BLMs is a hand-made type developed at KOMAC, while the other new type is a full-packaged Libera BLM [2]. Detailed BLM specifications are summarized in Table 1.

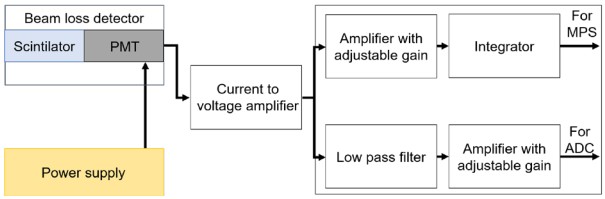


Figure 1: Typical beam loss monitor structure.

BLMs at the KOMAC 100 MeV proton accelerator are installed as shown in Figure. 2. The two old, hand-made BLMs are installed in one DTL tank [3], located from DTL 24 to 107. Proton energy passing through DTL24 is 20 MeV while that after DTL 107 is 100 MeV. Additionally, the eight new BLMs are mounted from DTL 21 to 24 BLM placed at the center of each DTL tank is defined as 'Ch1', and that at the high energy end of the tank is denoted as 'Ch2'. Under these conditions, the preliminary beam loss monitor calibration experiments were conducted by varying beam duty.

Table 1: BLM Specifications at KOMAC [2]

	Old BLMs	New BLMs
Scintillator type	BC-408 plastic (Saint-Gobain)	EJ-200 plastic (Scionix)
Scintillator size	ϕ25.4 × 30 mm	ϕ22 × 100 mm
PMT type	R1924A (Hamamatsu)	H10721-110 (Hamamatsu)
Applied voltage	-500 V	PoE
Sampling rate [kHz]	800	976.6

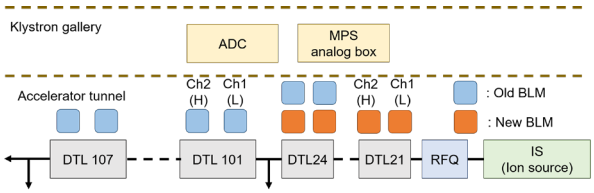


Figure 2: Scintillator BLM spots at KOMAC 100 MeV accelerator.

BLM Signal Acquisition Results

Figures 3 and 4 illustrate the signals generated at both old and new BLMs when a 100 MeV proton beam is extracted for 100 μs. Unlike the old BLMs, background radiation signals whose width is 400 μs are reduced at the new BLMs due to the thin cover around them. Since the main component of the cover is aluminium, it can be deduced that the main flat background is the cavity x-ray induced by the klystron radiofrequency.

Figure 5 demonstrates BLM signal stabilization after maintenance and repair for DTL 105 tank and the detailed values are listed on Table 2. Due to the momentum conservation, secondary radiation is detected at the BLMs behind the actual proton beam collision point. Therefore, it was certified in this study with BLMs under the DTL tanks that the tuner seals at the DTL105 which are worn out is the main cause of the RF instabilities. Additionally, due to the fast response of the plastic scintillator, the detection of sudden RF instabilities is achievable with BLMs at KOMAC.

* This work was supported through KOMAC operation fund of KAERI (KAERI ID no.524320-26) funded by MSIT (Ministry of Science and ICT).
† hjkwon@kaeri.re.kr

Content from this work may be used under the terms of the CC BY 4.0 licence (© 2026). Any distribution of this work must maintain attribution to the author(s), title of the work, publisher, and DOI.

ISBN: 978-3-95450-275-2 ISSN: 2226-0366 doi: 10.18429/JACoW-LINAC2026-TUPO079

PRELIMINARY LINAC DESIGN OPTIONS FOR THE CSNS PHASE-III UPGRADE

Y. Yuan†,[1,2], J. Peng[1,2], M. Y. Huang[1,2], W. Z. Zhou[1,2], Z. P. Li[1,2]
[1]Institute of High Energy Physics Chines Academy Sciences, Beijing, China
[2] Spallation Neutron Source Science Center, Dongguan, China

Abstract

Following the formal national acceptance of the China Spallation Neutron Source (CSNS) in 2018, the Phase II upgrade project (CSNS-II) commenced construction in 2024. CSNS-II aims to increase the beam power on target to 500 kW and elevate the linac output energy from 80 MeV to 300 MeV. The project is scheduled to pass national acceptance in October 2029. Concurrently, the planning for a future Phase III upgrade is underway, with the ultimate goal of delivering 10 MW of beam power and upgrading associated facilities, including the accelerator and target stations. For Phase III, the linac energy will be further increased to 1 GeV, with a peak beam current of 100 mA. This paper presents the preliminary technical routes for achieving the 10 MW linac, comparing two primary options: a hybrid scheme consisting of normal-conducting Drift Tube Linac (DTL) followed by a superconducting section, and an all-superconducting linac configuration starting immediately after the RFQ.

INTRODUCTION

Globally, major spallation neutron sources currently in operation or under construction—including ISIS (UK), SNS (USA), J-PARC (Japan), and the European Spallation Source (ESS)—have all targeted multi-megawatt (multi-MW) beam powers for their upgrades or initial designs. Among these, the ESS, which is currently in the construction and commissioning phase, features the highest design beam power of 5 MW [1-4].

As an established facility, the China Spallation Neutron Source (CSNS) completed its Phase I project in 2018. Its accelerator complex primarily comprises an 80 MeV H- Drift Tube Linac (DTL) and a 1.6 GeV Rapid Cycling Synchrotron (RCS) [5]. The Phase II upgrade (CSNS-II), which commenced in 2024 and is scheduled for completion in 2029, focuses on installing a superconducting (SC) linac section downstream of the DTL. This will increase the injection energy into the ring to 300 MeV and boost the beam power on target to 500 kW.

Leveraging the operational experience from Phase I and the construction insights from Phase II, the long-term vision for the CSNS Phase III upgrade aims to increase the linac energy to 1 GeV and the beam power to 10 MW. This phase will also involve the construction of a new dedicated target station, while the existing RCS will be repurposed as a storage ring.

† yuanyue@ihep.ac.cn

Status of CSNS and the Phase II Upgrade

The schematic layout of the China Spallation Neutron Source Phase I (CSNS-I) is illustrated in Fig. 1. The facility consists of a linac, a RCS, a target station, and three initial spectrometers [6]. Since passing national acceptance in 2018, the facility has been in official operation. Currently, CSNS is in a stage of concurrent operation and construction. The beam power on target has reached 185 kW, significantly exceeding the Phase I design specification of 100 kW. The facility maintains high reliability, with an annual beam delivery time exceeding 5,000 hours and a beam availability of over 95% [7].

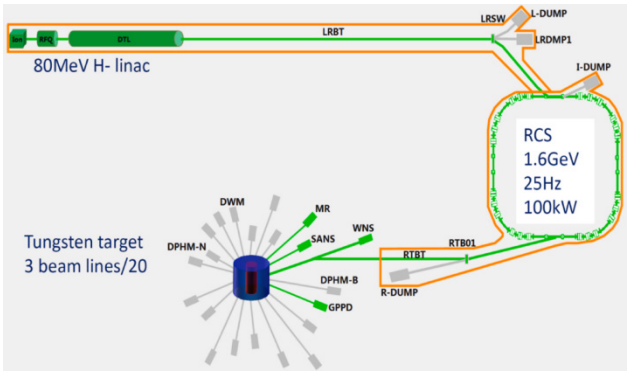


Figure 1: Schematic layout of CSNS.

The primary upgrade of the linac in Phase II involves the installation of a SC section downstream of the DTL. This addition aims to elevate the beam energy from 80 MeV to 300 MeV and increase the pulsed beam current to 50 mA before the beam is injected into the RCS ring. The layout of the CSNS Phase II linac is shown in Fig. 2 [8].

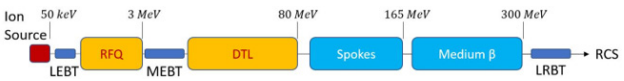


Figure 2: Layout of the CSNS Phase II linac.

Hybrid NC/SC Configuration in Phase III

To attain a 10 MW beam power on target for the planned CSNS Phase III, a newly constructed target station at the end of the linac and a beam energy upgrade to at least 1 GeV are essential. The most straightforward approach is to preserve the existing configuration and extend the superconducting (SC) section by installing additional cavities downstream of the Phase II upgrade to reach 1 GeV. High-beta elliptical cavities with a geometric beta of 0.82 are a candidate option, with specific parameters requiring further optimization and research. In this scenario, the

Content from this work may be used under the terms of the CC BY 4.0 licence (© 2026). Any distribution of this work must maintain attribution to the author(s), title of the work, publisher, and DOI.

ISBN: 978-3-95450-275-2 ISSN: 2226-0366 doi: 10.18429/JACoW-LINAC2026-TUPO081

A COMPLEXITY-NATIVE FRAMEWORK FOR INTELLIGENT PARTICLE ACCELERATORS

X. Huang[1], R. Zeng[†,1], Y. He[2,3], W. Li[4], Z. He[4], Q. Sun[4]
[1]Advanced Energy Science and Technology Guangdong Laboratory, Huizhou, China
[2]Institute of Modern Physics, Chinese Academy of Sciences, Lanzhou, China
[3]University of Chinese Academy of Sciences, Beijing, China
[4]North China University of Technology, Beijing, China

Content from this work may be used under the terms of the CC BY 4.0 licence (© 2026). Any distribution of this work must maintain attribution to the author(s), title of the work, publisher, and DOI.

Abstract

Next-generation particle accelerators are strongly coupled, multiscale, and nonlinear systems in which local optimization alone cannot guarantee global stability. This paper proposes a complexity-native framework that treats the accelerator as a complex adaptive system rather than a set of independently optimized subsystems. This framework integrates three coupled layers—physical complexity, information-flow network, and system cognition—to interpret three core operational challenges: hidden coupling, delayed feedback, and anomaly propagation, while enabling stability-first intelligent operation. A concise superconducting accelerator case illustrates how helium-pressure fluctuation may propagate through cavity detuning, tuner lag, RF compensation, power-module imbalance, and protection shutdown, supporting integrated diagnosis and early warning.

INTRODUCTION

Particle accelerators are becoming increasingly complex cyber-physical systems with growing numbers of devices, diagnostics, control channels, and operational constraints [1]. Their behavior is determined not only by isolated components, but also by nonlinear, history-dependent, and multiscale interactions across the entire system.

Conventional operation strategies based on deterministic modeling, hierarchical control, and expert-guided tuning remain effective for well-isolated subsystems. However, as subsystem coupling becomes stronger, local disturbances may propagate across boundaries, delayed feedback may accumulate into unstable behavior, and locally beneficial actions may reduce global robustness [1–3].

Recent AI-based approaches have shown value in optimization, diagnostics, surrogate modeling, anomaly detection, and operational assistance [1, 4–8]. Yet many applications still act as external enhancements to legacy control frameworks. This paper therefore reformulates intelligent particle accelerators as complex adaptive systems and develops a three-layer complexity-native framework with a representative fault-propagation use case.

MOTIVATION: COMPLEXITY IN NEXT-GENERATION ACCELERATORS

Traditional engineering methods often follow a "simplify first, process later" logic: the system is divided into independent subsystems, nonlinear behavior is approximated as linear response, and dynamic operation is reduced to a finite set of typical scenarios. This logic is useful for local parameter adjustment, but it exposes fundamental limitations for next-generation accelerators that require global dynamic stability.

The core regularity missed by such methods is that an anomaly observed at a given time and location is often not the true source. It may be the visible result of risks accumulated over time, or of disturbances originating from other coupled devices and propagating across space, subsystems, and information pathways.

A key inherent difficulty of accelerator systems is the coexistence of fast and slow physical processes within the same facility [2, 9]. Fast feedback loops operate on microsecond to millisecond timescales, while thermal drift, mechanical deformation, environmental perturbations, component aging, and operating mode transitions evolve far more slowly. A small deviation in one layer can accumulate via delayed feedback or hidden dependency chains, and eventually manifest as degraded beam quality or unexpected repeated trips in another layer.

AI is well suited to address these challenges: high-precision spatiotemporal, historical, and cross-system data enable the mining of hidden information-flow regularities and underlying causal relations. In this sense, AI-based methods provide a promising way to go beyond simplified engineering paradigms by mapping local observations to global system evolution.

These observations motivate an operational framework that connects physical-state evolution, information propagation, and higher-level decision processes. The key question is not only how to make accelerator control more accurate, but how to make intelligent operation intrinsically compatible with the complexity of the machine itself.

A COMPLEXITY-NATIVE FRAMEWORK

To address the limitations outlined above, we propose a complexity-native framework for intelligent particle accelerators. The accelerator is treated as a complex adaptive system rather than as a collection of independently optimized devices or subsystems [1, 10, 11]. In this view, intelligent operation emerges from coordinated interaction among physical processes, information propagation, and system-level cognition.

As shown in Fig. 1, the proposed framework is organized into three coupled layers: the physical complexity layer,

† rihuazeng@galhz.ac.cn

ISBN: 978-3-95450-275-2 ISSN: 2226-0366 doi: 10.18429/JACoW-LINAC2026-TUPO083

STATUS OF COMMISSIONING OF THE FRANKFURT NEUTRON SOURCE FRANZ

H. Hähnel[1,2,*], A. Ateş[1], L. Bauer[1,2], B. Dedić[1], J. Gröbel[1], J. Kaiser[1], K. Kuempel[1], P. Müller[1], H. Podlech[1,2], U. Ratzinger[1,2], A. Schall[1], R. Tiede[1], J. Traios[1], C. Wagner[1], R. Assmann[1,3], C. Zhang[2,3]

[1]Institute of Applied Physics (IAP), Goethe University Frankfurt, Frankfurt am Main, Germany

[2]Helmholtz Research Academy Hesse for FAIR (HFHF), GSI Helmholtzzentrum für Schwerionenforschung, Campus Frankfurt, Frankfurt am Main, Germany

[3]GSI Helmholtz Centre for Heavy Ion Research, Darmstadt, Germany

Abstract

The Frankfurt Neutron Source FRANZ is a compact-accelerator driven neutron source based on the $^7Li(p,n)^7Be$ reaction using a 2 MeV proton beam. Following successful stand-alone RF conditioning of the IH-DTL up to 10 kW cw, the coupled RFQ-IH-DTL cavity was assembled, tuned and conditioned up to 200 kW. First beam experiments have been performed, demonstrating proton acceleration to 2 MeV. We report on the high-power conditioning, coupling and LLRF tuning procedure, as well as initial beam commissioning results.

INTRODUCTION

The Frankfurt Neutron Source (FRANZ) is a compact accelerator driven facility originally initiated in the early 2000s [1–6]. It is designed to provide a 2 MeV proton beam for neutron production via the ^{7}Li$(p,n)^7$Be reaction [7]. The produced neutrons with a kinetic energy around 30 keV can be used for a number of experiments in the fields of applied physics and experimental astrophysics [8].

Beam Commissioning Progress

Significant progress on the driver linac was made in recent years. The commissioning of the new CHORDIS ion source [9, 10] in late 2020 was a first milestone. Since the CHORDIS ion source only provides a 35 keV proton beam, an electrostatic post-accelerator was developed and commissioned at IAP to reach the desired beam energy of 60 keV [11]. After stable operation was confirmed, the Low Energy Beam Transport line (LEBT) was commissioned and the 60 keV beam was transported up to the point of injection into the RFQ in late 2021. Following a redesign of the RFQ electrodes for 60 keV [12,13], new electrodes were delivered and mounted in the RFQ in summer 2023. The RFQ was then tuned, conditioned and commissioned with a 10 mA proton beam until the end of 2023. Emittance measurements and bunch shape measurements of the 700 keV proton beam behind the RFQ followed in 2024, reporting a RFQ transmission of 92.7 % [14, 15]. In 2025, the RFQ and IH-DTL were combined to form a coupled RFQ-IH-DTL cavity. The cavity was commissioned with beam in late 2025 with a measured beam energy of 1.9 MeV. The results of the cavity tuning and beam commissioning are reported here.

The Coupled RFQ-IH-DTL

To reduce space requirements and save the need for a second high power amplifier, the FRANZ main accelerator cavity was designed as a coupled RFQ-IH-DTL which consists of a 700 keV four-rod RFQ and a short 1.3 MV IH-DTL with an internal triplet lens [6]. The cavities are coupled inductively by a large coupling flange at the meeting point of the two cavities (see Fig. 1). Due to this fixed coupling, the RF phase between RFQ and IH-DTL is locked and had to be carefully considered during the RFQ beam dynamics design to ensure the correct phase relation between the last cell in the RFQ and the first gap in the IH-DTL. Due to this setup,

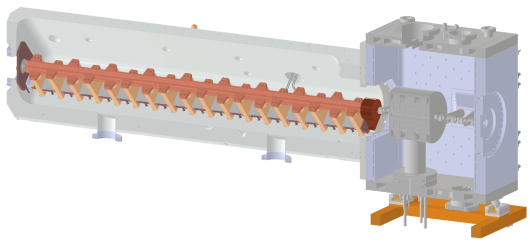


Figure 1: CAD cross-section of the coupled RFQ-IH-DTL cavity. The RFQ is on the left side and the IH-DTL with an internal quadrupole triplet lens is coupled to it on the right.

the voltage ratio between the IH-DTL and the vane-vane voltage of the RFQ is directly dependent on the coupling strength between the two cavities. After the redesign of the RFQ for 60 keV, the ideal ratio was calculated to be

$$\frac{U_{0,IH}}{U_{RFQ}} = \frac{2.06\,\mathrm{MV}}{60\,\mathrm{kV}} = 34.34 \qquad (1)$$

to match the beam dynamics simulated. To reach this ratio, both cavities have to be tuned to a frequency close to the common frequency of 175 MHz so that the correct coupling is achieved [6]. In practice, this tuning was only possible with an extensive bead pull measurement campaign.

BEAD PULL MEASUREMENTS

In contrast to typical bead pull measurements for single cavities, where usually only the relative voltage distribution

* haehnel@iap.uni-frankfurt.de

Content from this work may be used under the terms of the CC BY 4.0 licence (© 2026). Any distribution of this work must maintain attribution to the author(s), title of the work, publisher, and DOI.

ISBN: 978-3-95450-275-2 ISSN: 2226-0366 doi: 10.18429/JACoW-LINAC2026-TUPO085

IMPLEMENTATION OF AN EPICS AND EtherCAT-BASED PLC REPLACEMENT SYSTEM IN PAL-XFEL

Geonyeong Mun, Gyujin Kim, Soung Youl Baek, YoungJin Suh,
DongCheol Shin, Haeryong Yang, Hoon Heo
Pohang Accelerator Laboratory, Pohang, Republic of Korea

Abstract

PAL-XFEL is a fourth-generation X-ray free-electron laser facility in Pohang, Korea. Its operation-mode programmable logic controller (PLC) exchanges operating states with the Personnel Safety Interlock System (PSI) through dry-contact signals. The legacy embedded PLC platform had reached end-of-life status. A replacement based on a Raspberry Pi 5, Beckhoff EtherCAT input/output modules, and an Experimental Physics and Industrial Control System (EPICS) input/output controller (IOC) was developed while preserving the field interface, PSI ladder logic, process variable names, and operator displays. The EPICS IOC directly uses the EtherLab application interface for cyclic process-data handling. PREEMPT_RT, CPU isolation, interrupt affinity, FIFO scheduling, and memory locking were applied, and a 24-hour cyclictest run recorded a maximum scheduling latency of 11 µs on an isolated real-time core. The system was installed, verified with the PSI, and placed into routine PAL-XFEL operation.

INTRODUCTION

PAL-XFEL is an X-ray free-electron laser facility that requires coordinated control of the accelerator, beam transport, experimental areas, and the Personnel Safety Interlock System (PSI) [1]. The operation-mode controller sends the repetition rate, accelerator operating mode, and hard- and soft-X-ray beam destinations to the PSI through dry-contact outputs. In the reverse direction, it receives the electron-beam permission and PSI shutter status from the PSI. Each receiving PLC applies 24 V to the dry-contact circuit and detects the resulting state.

The original controller used a Yokogawa FA-M3 F3RP61 embedded Linux CPU. It executed both the PLC I/O control and an EPICS IOC, which provided a compact interface to the accelerator control system. The CPU, however, reached end-of-life. Its nominal successor uses a different processor architecture and would require rebuilding the boot loader, Linux image, root filesystem, development toolchain, and EPICS application. The replacement was therefore treated as a complete redesign rather than a CPU substitution.

The principal requirement was a drop-in migration. The PSI ladder program, field cabling, relay interface, EPICS PV names, and operator screens had to remain unchanged. In addition, the new platform had to support centralized network boot, remote maintenance, deterministic I/O processing, and future expansion.

SYSTEM ARCHITECTURE

Figure 1 summarizes the migration concept. A Raspberry Pi 5 (RPi5) replaces the embedded PLC CPU, while Beckhoff EtherCAT terminals replace the proprietary I/O modules [2, 3]. The replacement panel contains an EK1100 EtherCAT coupler, EL1809 digital input and EL2809 digital output terminals, external 24 V relays, a serial-to-Ethernet device server, and the RPi5. A PCIe Ethernet adapter provides a dedicated interface for the EtherCAT network.

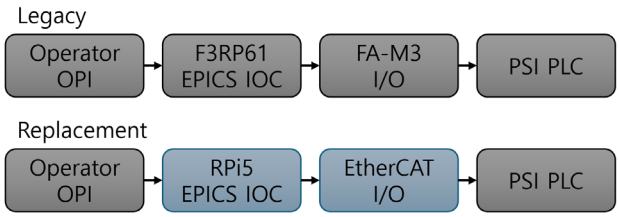


Figure 1: Migration concept preserving the EPICS and PSI interfaces.

The replacement retains the existing dry-contact field interface and preserves the legacy EPICS PV names using aliases. Therefore, the PSI ladder logic, field cabling, and operator displays require no modification.

The new hardware was arranged in a DIN-rail panel with the same external dimensions and cable entry locations as the legacy unit. The existing PSI cables were divided into input and output sides and connected without remapping. The smaller modules also left spare DIN-rail space for additional terminals.

HARDWARE INSTALLATION

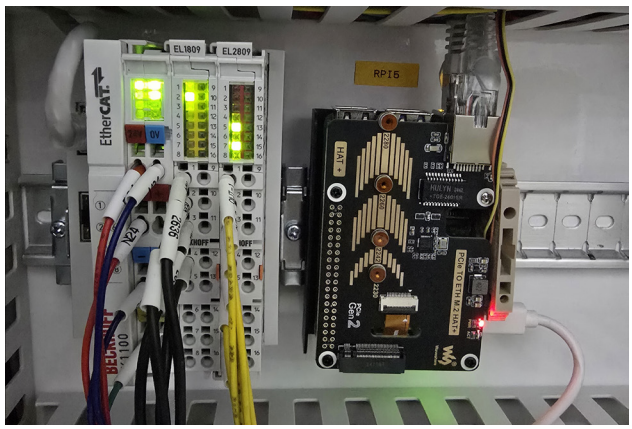


Figure 2: Installed EtherCAT I/O and RPi5 controller assembly.

Content from this work may be used under the terms of the CC BY 4.0 licence (© 2026). Any distribution of this work must maintain attribution to the author(s), title of the work, publisher, and DOI.

ISBN: 978-3-95450-275-2 ISSN: 2226-0366 doi: 10.18429/JACoW-LINAC2026-TUPO086

A COMPREHENSIVE REDESIGN OF THE MAIN BEAM INJECTOR FOR THE COMPACT LINEAR COLLIDER AT 380 GeV

Y. Zhao*[1], S. Doebert[1], A. Grudiev[1], A. Kurtulus[1,2], A. Latina[1], P. Desire Valdor[1,3]
[1]CERN, Geneva, Switzerland
[2]Institute of Electromagnetic Fields, Zurich, Switzerland
[3]University of Groningen, Groningen, Netherlands

Abstract

In this report, we present a comprehensive redesign of the CLIC main beam injector complex for the 380 GeV energy stage. The main beam injector complex generates and accelerates electrons and positrons to 9 GeV at the end of the booster linac. Benefiting from the improved positron yield, the electron drive beam energy for positron production is reduced from 5 GeV to 2.86 GeV, and the electron and positron injector linacs are redesigned to achieve a more compact layout of the injector complex, with the total length reduced by a factor of two. Jitter amplification due to short-range and long-range wakefields are studied for the injector and booster linacs.

INTRODUCTION

In the previous design, the main beam injector complex of the CLIC collider [1, 2], as presented in Fig. 1, is mainly composed of the following subsystems:

- Electron source (e^- source): generates and accelerates the electron beam to 200 MeV.
- Positron source (e^+ source): generates and accelerates the positron beam to 200 MeV. A dedicated electron linac is used to provide a 5 GeV drive beam for positron production.
- Injector linac (IL): a common linac that accelerates both electrons and positrons from 200 MeV to 2.86 GeV.
- Damping rings (DRs): includes an electron damping ring (e^- DR), a positron pre-damping ring (PDR) and a positron damping ring (e^+ DR).
- Spin rotators (SRs): includes two spin rotators for the electron beam (SR1 and SR2).
- Bunch compressors (BCs): includes an electron bunch compressor (e^- BC1) and a positron bunch compressor (e^+ BC1).
- Booster linac (BL): a common linac that accelerates both electrons and positrons to 9 GeV.

In the new design [3], as presented in Fig. 2, several changes have been made. Common electron linacs are used to accelerate two electron beams to 2.86 GeV. One beam is injected directly into the e^- DR, and the other beam is used as a drive beam to produce positrons. The common linacs include an electron pre-injector linac (e^- PIL) and an electron injector linac (e^- IL). The e^+ source drive beam energy is reduced from 5 GeV to 2.86 GeV, benefiting from a significant improvement in the positron yield optimization [4]. A dedicated positron injector linac (e^+ IL) is used to accelerates positrons to 2.86 GeV, replacing the common IL in the previous design. The three DRs are now accommodated in the same building to achieve a more compact layout. The electron and positron bunch compressors (e^- BC1 and e^+ BC1) are combined to be a common bunch compressor (BC1).

LINAC DESIGNS

FODO cells are used for focusing in the design of the e^- IL, the BC1 linac (BC1L) and the BL. Each FODO cell is 8.3 m long, consisting of two quadrupoles and two 3 m long accelerating structures. The phase advance per FODO cell is 76.345°. The accelerating structures are redesigned [5] to reduce the long-range wakefield effects and the structure parameters are summarized in Table 1. Two types of 3 m long structures of different apertures are used. The "A18 L-band" is mainly used for electron beams, and the "A22 L-band" is mainly used in the e^+ source for the positron beam which has a large beam size. The e^+ IL is therefore also redesigned, as presented in Fig. 3, to accommodate the new accelerating structure. The beam parameters for the linacs are summarized in Table 2.

Table 1: Accelerating structure parameters in the new design of the CLIC main beam injector complex.

Parameter	Unit	"A18 L-band"	"A22 L-band"
RF frequency	GHz	2	
Structure length	m	3	
Number of cells		60	
Phase advance per cell	deg	120	
First iris radius	mm	21	24
Last iris radius	mm	15	20
First iris thickness	mm	3.26	8.46
Last iris thickness	mm	4.06	8.46

JITTER AMPLIFICATIONS

Single-bunch jitter amplifications are mainly caused by short-range wakefields in the accelerating structures. To estimate the single-bunch jitter amplification, bunches with different offsets in the position and angle ellipse are simulated. The jitter amplification is defined as the ratio of the final to initial ellipse areas (also known as actions).

* yongke.zhao@cern.ch

Content from this work may be used under the terms of the CC BY 4.0 licence (© 2026). Any distribution of this work must maintain attribution to the author(s), title of the work, publisher, and DOI.

ISBN: 978-3-95450-275-2 ISSN: 2226-0366 doi: 10.18429/JACoW-LINAC2026-TUPO087

CBXFEL: DESIGN, CONSTRUCTION, AND FIRST COMMISSIONING RESULTS*

M. White†[1], J. Anton[1], L. Assoufid[1], A. Bernhard[1], D. Bianculli[1], T. Clute[1], M. Golebiowski[1], X. Huang[1], W. Jansma[1], A. Karales[1], K. Kauchha[1], S. Kearney[1], K.-J. Kim[1], K. Lang[1], R. Lindberg[1], R. Margraf-O'Neal[1], M. Martens[1], S. Mashrafi, A. Miceli[1], J-W Park[1], P. Pradhan[1], M. Rivers[1], X. Shi[1], D. Shu[1], Y. Shvyd'ko[1], J. Stevens[1], J. Sullivan[1], J. Tijerina[1], D.A. Walko[1], M. Bai[2], N. Balakrishnan[2], M. Balcazar[2], C. Curtis[2], F.-J. Decker[2], G. Gassner[2], A. Halavanau[2], Z. Huang[2], B. Jocson[2], E. Kraft[2], G. Lanza[2], P. Liu[2], A. Lutman[2], J. Mock[2], M.A. Montironi[2], H.D. Nuhn[2], X. Permanyer[2], S. Saraf[2], T. Sato[2], J. Tang[2], H. Wang[2], D. Zhu[2], T. Osaka[3], K. Tamasaku[3], W. Lewis[4], S.J. Stein[4], M. Camarena[5], B. Freemire[5], E. Gomez[5], C. Jing[5], T. Miller[5], B. Wyderski[5]
[1]Argonne National Laboratory, Lemont, IL, USA
[2]SLAC National Accelerator Laboratory, Menlo Park, CA, USA
[3]RIKEN SPring-8 Center, Saitama, Japan
[4]OspreyDCS, Ocean City, MD, USA
[5]Euclid Techlabs LLC, Bolingbrook, IL, USA

Abstract

Cavity-based X-ray free-electron lasers (CBXFELs) have the potential to dramatically improve the stability and coherence of FELs [1-3]. The CBXFEL project is an Argonne, SLAC, RIKEN collaboration to build a 65-m-long rectangular X-ray cavity at the LCLS, to demonstrate low-loss cavity ringdown and two-pass FEL gain. Argonne was responsible for design and construction of the X-ray cavity and SLAC was responsible for CBXFEL installation and preparation of the appropriate linac beam and chicane magnets, as well as additional diagnostics. Controls, physics simulations, and commissioning are joint efforts. RIKEN/Sumitomo supplied the high-quality diamond crystal plates that Argonne subsequently laser-machined, thermally treated, and characterized to produce high-reflectivity diamond crystal mirrors for the cavity. Design, fabrication, assembly, and testing of X-ray optics, X-ray diagnostics, and their precision mechanical support and motion systems are complete. Final components were installed in the LCLS tunnel in April of 2026. Commissioning with X-rays has begun, including the measurement of the first cavity ringdown. This paper provides an update on the status of the experiment. The next stage, fine tuning of the x-ray orbits in the cavity, increasing ringdown lifetime, and demonstration of amplification, will begin following the LCLS summer shutdown.

INTRODUCTION

Ideal operation of a cavity FEL would employ a high-repetition rate linac to supply many bunches whose spacing matches the cavity round trip time. Unfortunately, the 4 GeV electron beam energy of the present LCLS-II is not sufficient for FEL gain at hard X-rays. On the other hand, the repetition rate of the copper linac repetition is limited, but nevertheless it is possible to create a second bunch with the right properties and timing to test cavity functionality and verify FEL gain. Physics simulations show that a two-pass gain of 50-100 can be achieved within the expected narrow crystal bandwidth. Figure 1a shows the spectrum after the first pass, and Fig.1b shows the spectrum after pass 2. Figures 1c and 1d show the beam profile.

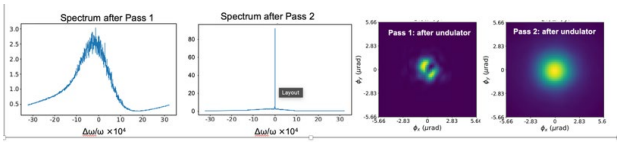


Figure 1: 1a shows the spectrum after the first pass, 1b shows the narrowed spectrum after the 2nd pass. 1c and 1d show the beam profile.

The goal of the CBXFEL project is to demonstrate these concepts experimentally.

X-RAY OPTICS

Six nearly-perfect diamond crystals were provided by our RIKEN/Sumitomo colleagues. Figure 2 shows some of the measurements that were performed to qualify the crystals. Details of the optics and diagnostic designs are provided in references [4-6].

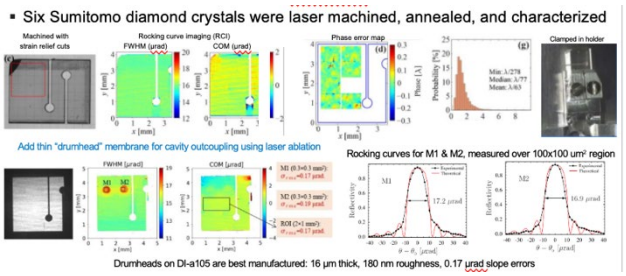


Figure 2: Some of the measurements performed to qualify and select the best diamonds for CBXFEL.

* Work supported by U.S. DOE, Office of Science, Office of BES, under Contracts No. DE-AC02-06CH11357 (ANL) and DE-AC02-76SF00515 (SLAC).
† mwhite@anl.gov

Content from this work may be used under the terms of the CC BY 4.0 licence (© 2026). Any distribution of this work must maintain attribution to the author(s), title of the work, publisher, and DOI.

ISBN: 978-3-95450-275-2 ISSN: 2226-0366 doi: 10.18429/JACoW-LINAC2026-TUPO091

ACCELERATING STRUCTURE DEVELOPMENT AND PROTOTYPING FOR THE SYLA INJECTOR LINAC

A. A. Batov†,1, T. V. Bondarenko[1], M. A. Gusarova[1], M. V. Lalayan[1],
V. V. Paramonov[2], I. V. Rybakov[2], R. A. Zbruev[1], M. V. Vladimirov[1], S. M. Polozov[1]
[1]National Research Nuclear University MEPhI, Moscow, Russia
[2]INR RAS, Moscow, Russia

Abstract

The fourth-generation synchrotron radiation facility SYLA (Synchrotron&Linac) is now under development. SYLA will be driven by a 6 GeV electron linear accelerator that will operate both as the injector for the synchrotron and as the driver for free electron lasers. A team from the National Research Nuclear University MEPhI and the Institute for Nuclear Research of the Russian Academy of Sciences is playing a leading role in the development of this linac.

The prototyping of the accelerating structure for the linac has been completed. The geometry for an accelerating cell operating on 2800 MHz has been optimized, the thermal load has been calculated, and the risk of multipactor discharge has been evaluated. Optimization of the structure yielded a coupling coefficient of 10.6 %, together with an effective shunt impedance of 84 MΩ/m and an over-voltage factor of 2.65. The axial field asymmetry was reduced by a factor of two. The final structure geometry was obtained, four cell prototypes were fabricated, and their principal electrodynamic parameters were measured. The measured characteristics are in agreement with the simulations.

INTRODUCTION

In the previous work, the superiority of the four-slot biperiodic accelerating structure over the conventional two-slot design for the SYLA (Synchrotron-Laser) [1-2] injector linac was established. That study demonstrates that the four-slot geometry reduces azimuthal field asymmetry by two orders of magnitude, mitigates transverse emittance growth in long multi-section linacs, and achieves a coupling coefficient of 8.4 % with an effective shunt impedance of 80 MΩ/m. This paper reports the next phase: further geometry optimisation, experimental validation through full-scale prototyping, manufacturing process refinement, and the final design optimization based on extensive multipactor and thermal-structural analyses.

FINAL GEOMETRY OPTIMIZATION

The optimized geometry provides an excellent balance: a 10.6 % coupling coefficient, an 84 MΩ/m shunt impedance, 15200 unloaded quality factor, and a low overvoltage factor of 2.65. It was achieved by both reducing the aperture from 10 to 9 mm and thorough adjustment of the coupling slots geometry [3-4]. Wakefield analysis showed a negligible energy loss of 200 keV per section at high energies, which is more than compensated by improved power transfer efficiency. Beam-dynamics simulations confirmed that this modification increases the energy gain by 2 MeV per section without changing the overall section dimensions.

The optimized topology also shifts the electric-field maximum closer to the nose cones while reducing magnetic-field concentrations at the coupling-slot fillets, thereby improving the structure's high-power robustness (See Fig. 1).

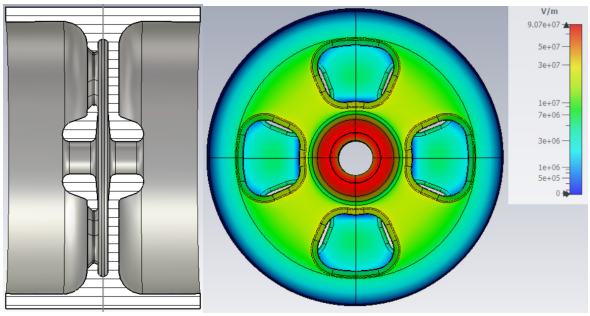


Figure 1: Sectional side view of the accelerating period and electric field topography scaled at 415 kV/cm on the beam axis.

MULTIPACTOR DISCHARGE SUPPRESSION

The final design incorporates a dedicated chamfer at the beam-aperture region of the coupling cell. This feature guides the secondary-electron cloud into the drift tube, effectively suppressing resonant multiplication. Simulations were carried out for both "manufactured" and "fully conditioned" copper surfaces using established secondary-electron-yield (SEY) models. The chamfer geometry was optimized to avoid increasing the coupling-cell diameter, which would otherwise promote discharge above the coupling slots. The resulting topology ensures that the dangerous field levels occur only in the end-cell regions, where they are mitigated by the chamfer (See Fig. 2).

Content from this work may be used under the terms of the CC BY 4.0 licence (© 2026). Any distribution of this work must maintain attribution to the author(s), title of the work, publisher, and DOI.

† AABatov@mephi.ru

ISBN: 978-3-95450-275-2 ISSN: 2226-0366 doi: 10.18429/JACoW-LINAC2026-TUPO092

DESIGN AND BEAM DYNAMICS OPTIMIZATION OF AN ELECTRON BUNCH COMPRESSOR FOR THE SYLA 4th GENERATION SYNCHROTRON LIGHT SOURCE

M. A. Gorbunov, S. M. Polozov, V. I. Rashchikov
MEPhI, Moscow, Russia

Abstract

A low-emittance magnetic bunch compressor is being developed for the injector of the SYLA 4th generation synchrotron light source. The target beam parameters are a beam energy of 250 MeV, a bunch charge of 300 pC, and an initial bunch duration of about 5 ps. Under these conditions, bunch compression is strongly affected by coherent synchrotron radiation (CSR), longitudinal space charge, and optics mismatch, which can lead to significant projected emittance growth.

We present the design and optimization of a compressor lattice aimed at maximizing compression efficiency while preserving transverse beam brightness. Several layouts were studied, with emphasis on achromatic optics, matching between dispersive sections, and minimization of the horizontal beta function in the downstream dipoles, where CSR effects are strongest. Beam dynamics simulations were performed with `ELEGANT`, including CSR and longitudinal space-charge effects. The results show that an achromat-based compressor provides a favorable compromise between compression and emittance preservation for the SYLA operating regime.

SYLA COMPRESSOR REQUIREMENTS

SYLA is a next-generation synchrotron light source designed to exceed the performance of current and planned international facilities. The electron beam is delivered from the photoinjector in several operating modes:

- Single pulses or pulse trains.
- Short bunches (up to 30 pC) or long bunches (up to 300 pC).

The photoinjector is capable of generating 1–5 ps pulses at energies up to 42 MeV across various operating modes.

Table 1: Required Beam Parameters at the Entrance of the Undulator Lines

Bunch Parameter	Short Bunches	Long Bunches
E, GeV	2–4	~6
σ_t, fs	1–3	20–40
ε_n, mm·mrad	0.4	1.2
σ_δ, MeV	0.4	1.4

To achieve the required beam parameters (Table 1), a multi-stage bunch-compression scheme is essential. Drawing on the international experience with synchrotron light sources such as MAX IV [1], SwissFEL, SLAC, and other existing or planned facilities, a classical three-stage compression layout was adopted:

- First stage at 280 MeV, where space-charge effects are minimized.
- Second stage at 1.5 GeV, the common energy level for all accelerator operating modes.
- Final stage at full energy, located within the beam switchyard feeding the undulator lines.

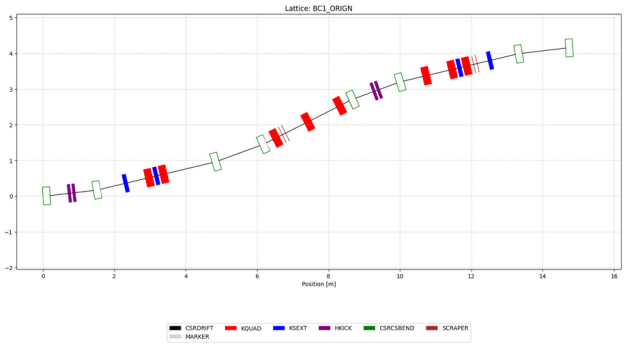


Figure 1: Design view of the bunch compressor.

High bunch compression must be combined with preservation of transverse emittance and minimal energy spread. The primary challenge in compressing short bunches is coherent synchrotron radiation (CSR). Following analysis of existing magnetic bunch compressor designs for electron bunches, an S-chicane scheme based on two symmetric double-bend achromat (DBA) cells was selected (Fig. 1). The mathematical description of compressor operation principles is well established [2]:

- Generation of a correlated energy chirp:

$$\delta_i = hz_i + \frac{1}{2}h_2 z_i^2, \tag{1}$$

where

$$h = \frac{eVk\cos\phi_s}{E_0}, \qquad h_2 = -\frac{eVk^2\sin\phi_s}{E_0}.$$

The quadratic term h_2 is generated by the RF curvature of the accelerating cavity.

- Longitudinal position shift of particles:

$$z_f = R_{56}hz_i + \left(\frac{1}{2}R_{56}h_2 + T_{566}h^2\right)z_i^2. \tag{2}$$

Content from this work may be used under the terms of the CC BY 4.0 licence (© 2026). Any distribution of this work must maintain attribution to the author(s), title of the work, publisher, and DOI.

ISBN: 978-3-95450-275-2 ISSN: 2226-0366 doi: 10.18429/JACoW-LINAC2026-WE1A001

POST-MORTEM INSIGHTS INTO THE SNS RFQ01: IMPLICATIONS AND PATHS FORWARD FOR HIGH BEAM POWER OPERATION*

Haitao Ren†, Sung-Woo Lee, John Moss, George Toby, Sang-Ho Kim
Oak Ridge National Laboratory (ORNL), Oak Ridge, TN, USA

Abstract

The first Radio-Frequency Quadrupole (RFQ01) at the Spallation Neutron Source (SNS) operated in both the main accelerator and the Beam Test Facility (BTF) for a combined period of approximately 20 years. Over this time, the performance of RFQ01 declined significantly, with beam transmission decreasing from about 90% to 70% or less. RFQ01 is currently undergoing a comprehensive post-mortem analysis. Initial visual inspections revealed substantial erosion on the low-energy side of the vane tips. To characterize the erosion profile with high precision, a 3D microstructural surface replication was produced using an in-house, 6-inch-long mold, and the measured erosion profile was applied to a full 3D CST model. Additional borescope inspections identified further vane erosion in the middle and downstream sections of the first module. The final phase of the post-mortem study will involve full disassembly of the structure to expose the entire length of each vane for complete laser scanning. The CST 3D model will then be updated to incorporate the full erosion profile. The results of these studies will help clarify the underlying degradation mechanisms and inform implications and paths forward for reliable high beam power operation.

INTRODUCTION

The SNS Front End (FE) generates and accelerates an H^- beam through an RF-driven ion source, an electrostatic low-energy beam transport line (LEBT), a 402.5 MHz radio-frequency quadrupole (RFQ), a medium-energy beam transport line (MEBT), and associated diagnostics. The RFQ bunches and accelerates the 65 keV input beam to 2.5 MeV over a 3.7 m, four-vane structure [1].

There have been three RFQs developed at SNS to support operation and beam power upgrade. RFQ01, the original unit installed in 2002 for beam commissioning, started production service in the SNS FE from 2006 until 2017, when it was replaced by RFQ02; it was then relocated to the BTF, where it remained in service for a further five years [2, 3]. Across this ~20-year history, RFQ01 exhibited several operational anomalies – resonance detuning events, difficulty sustaining closed-loop RF control at higher duty factor, and an ultimately irreversible degradation of beam transmission – whose root causes were not conclusively identified at the time [4].

RFQ01 is now the subject of a dedicated post-mortem investigation at SNS, and this paper reports on that investigation specifically: a summary of the operational issues that motivated the study, precision measurement of the vane-tip erosion by silicone surface replication and laser scanning, CST modelling with particle-in-cell (PIC) beam-dynamics of the measured erosion profile, and further borescope inspection of the full length of the first module. Together, these results begin to connect the historical operational anomalies to a concrete physical degradation mechanism and point toward the design and operational changes needed for reliable RFQ performance at the higher beam power required by the Proton Power Upgrade (PPU) project.

EXPERIENCE WITH RFQ01 OPERATION

Over its two-decade service life, RFQ01 displayed three recurring issues whose underlying causes were not fully understood at the time, and which motivated the post-mortem studies described in the following sections.

- Resonance detuning events. Two significant frequency shifts were recorded, in 2003 and 2009, coincident with cooling-system upsets – a loss of cooling-water control and an over-pressurized cooling channel, respectively. Both were corrected by re-adjusting the slug tuners, but whether the vane condition itself changed permanently was never confirmed.
- Difficulty sustaining RF control in closed-loop as the duty factor was increased, accompanied by a non-quadratic relationship between RF drive power and cavity field amplitude. Operational mitigations – a lower field setpoint, reduced ion-source hydrogen flow, upgraded cooling and vacuum systems, and improved Low-Level Radio Frequency (LLRF) pulse control – reduced the impact but did not resolve the underlying causes. With the reduced field setpoint, RFQ01 sustained 85–90% transmission during SNS's >1 MW operation from 2009 to 2010.
- A progressive and ultimately irreversible decline in beam transmission occurred over two years, from 2011 to 2013, falling from the ~90% design value to ~70% or below. No significant detuning was observed, but a field tilt was noticed. A third retuning effort in 2013 failed to restore the beam transmission, which motivated the replacement by RFQ02 and, later, the decision to dedicate RFQ01 to post-mortem study.

EROSION PRECISE MEASUREMENT

Following its removal from the BTF, visual inspection of RFQ01 revealed substantial erosion on the low-energy vane tips, concentrated near the RFQ entrance (Fig. 1).

* Work supported by the US DOE Office of Science, Basic Energy Sciences, Scientific User Facilities, and by UT-Battelle, LLC, under contract DE-AC05-00OR22725.
† renh@ornl.gov

Content from this work may be used under the terms of the CC BY 4.0 licence (© 2026). Any distribution of this work must maintain attribution to the author(s), title of the work, publisher, and DOI.

ISBN: 978-3-95450-275-2 ISSN: 2226-0366 doi: 10.18429/JACoW-LINAC2026-WE1A003

THE GLOBAL SCIENTIFIC KLYSTRON MARKET: INSIGHTS FROM THE FIRST LONG-PULSE AND CW KLYSTRON WORKSHOP

J. Moss[1], M. Champion[1], D. Horan[2], G. Aymar[3], M. Jensen[4], H. Ren[1]
[1]Oak Ridge National Laboratory, Oak Ridge, TN, USA
[2]Argonne National Laboratory, Lemont, IL, USA
[3]SLAC National Accelerator Laboratory, Menlo Park, CA, USA
[4]European Spallation Source ERIC, Lund, Sweden

Content from this work may be used under the terms of the CC BY 4.0 licence (© 2026). Any distribution of this work must maintain attribution to the author(s), title of the work, publisher, and DOI.

Abstract

Klystrons are the workhorses of the world's high-power, high-duty particle accelerators, and the continued reliable operation of these facilities depends on a stable market of supply. That market has always been small and specialized, but its volatility increased sharply in the early 2020s as pandemic-driven supply-chain and labor disruptions compounded pre-existing structural weaknesses. To assess the health of the scientific klystron market from both the manufacturer and the end-user perspective, the Spallation Neutron Source (SNS), European Spallation Source (ESS), Argonne National Laboratory (ANL), and SLAC National Accelerator Laboratory convened the first Long-Pulse and Continuous Wave (CW) Klystron Workshop at Oak Ridge National Laboratory (ORNL) on 23–25 September 2025. This paper summarizes the workshop, the structural factors that drive the volatility of the scientific klystron market, and the concrete actions now under way to place the market on stable footing for decades to come.

INTRODUCTION

The klystron remains one of the most popular high-power RF sources available for scientific facilities and is unarguably an anchor for many high-power, high-duty accelerators worldwide. Promising advances in RF generation continue, such as those in solid-state, but there is still a clear advantage for klystrons at frequencies above 350MHz and average power output above 200kW [1].

Even as alternate RF generating technologies become more mature and displace vacuum tubes in some regimes, klystron technology continues to advance as research continues throughout the global accelerator community. The advent of large accelerators such as the ILC and the FCC are helping to drive RF source developments with a clear focus on high efficiency and high peak power. New beam topologies and bunching techniques hold the promise of theoretical efficiencies of close to 90% [2]. Recent klystron retrofit efforts at the LHC demonstrate the desire of existing facilities to improve the efficiency of their current batch of klystrons [3]. Developments at SLAC demonstrate the continued improvement of digital models that will ultimately provide the nuanced information needed to push the cutting edge of tube development [4]. These are just a few examples that show the active interest in the klystron, helping to affirm that it remains a relevant RF source choice for many facilities around the world.

The technology is healthy; the market that supplies it is not. Scientific klystrons are a small, highly specialized product served by no more than four major manufacturers worldwide. Demand arrives in large, irregular bursts tied to individual construction projects with no steady baseline to sustain production. When a supplier exits or specialized expertise retires, little slack remains in the system to absorb the loss. This fragility places future facilities at risk and motivated the community to convene the workshop described here.

CONVENING THE WORKSHOP

In late 2024, representatives from SNS, ESS, ANL, and SLAC formed a committee charged with planning a workshop to examine the present state of the scientific klystron market and to identify concrete steps to stabilize it. Explicit in the charge was that the workshop includes both suppliers and end users. The first Long-Pulse and CW Klystron Workshop was held at the ORNL SNS on 23–25 September 2025. The workshop drew 44 attendees spanning seven US Department of Energy national laboratories, three international laboratories, and eight private companies, including all four major klystron manufacturers. Participation is summarized in Table 1, and the full group is shown in Fig. 1 [5].

Table 1: Workshop Participation by Sector

Sector	Organizations	Attendees
US national laboratories	7	25
International laboratories	3	4
Klystron manufacturers	4	10
Other industry	4	5
Total	**18**	**44**

Workshop Format

The first day was devoted to individual vendor sessions. Each major manufacturer was given an hour with only the end users present, while the remaining vendors waited separately, so that proprietary content and the ensuing discussion could be shared candidly. To preserve business confidentiality, none of this material was retained in the workshop record. For the remainder of the workshop, attendees rotated through four parallel roundtables, each led by a moderator and recorded by a scribe. Vendor representatives were embedded within the roundtable groups—placing every major manufacturer and the user

ISBN: 978-3-95450-275-2 ISSN: 2226-0366 doi: 10.18429/JACoW-LINAC2026-WE1A005

TRANSFORMING THE BNL 200 MeV H⁻ LINAC: 10³ LOWER LOSSES, 2× HIGH-CURRENT TRANSMISSION, AND 2× LOWER EMITTANCE*

D. Raparia†
Brookhaven National Laboratory, Upton, NY, USA

Abstract

The Brookhaven National Laboratory (BNL) 200 MeV H⁻ Drift Tube Linac has served as the front-end injector for the BNL accelerator complex since 1970. During more than five decades of operation, the accelerator has evolved through a series of upgrades to satisfy increasingly demanding requirements for high-brightness polarized H⁻ beams for RHIC and the future Electron-Ion Collider (EIC), while simultaneously providing high-current beams for the Brookhaven Linac Isotope Producer (BLIP). The most significant improvements resulted from the redesign of the low- and medium-energy beam transport systems between 2008 and 2010, followed by more than a decade of optimization of the RF systems, diagnostics, vacuum, and operating procedures. Collectively, these developments doubled high-current transmission, reduced the normalized transverse emittance of polarized beams by approximately a factor of two, lowered uncontrolled beam losses by nearly three orders of magnitude, and doubled the average beam current delivered to BLIP.

INTRODUCTION

The Brookhaven National Laboratory (BNL) 200 MeV H⁻ Drift Tube Linac has been the front-end injector for the BNL accelerator complex since its commissioning in 1970 [1]. Originally designed as a high-current proton linac, it has continually evolved to support changing scientific programs, including the AGS, RHIC polarized proton program, Brookhaven Linac Isotope Producer (BLIP), and now the future Electron–Ion Collider (EIC). Few operating linacs have undergone such a long sequence of systematic performance improvements while remaining in routine operation.

Today the linac delivers 200 MeV H⁻ beams at 6.67 Hz for two applications with very different requirements. The collider injector chain demands low-emittance, highly stable beams that preserve brightness and polarization throughout acceleration, whereas BLIP requires reliable delivery of the highest possible average beam current with extremely low beam loss to maximize isotope production and minimize residual activation.

Over the past two decades, the most important limitation to linac performance was identified as the transition between the RFQ and the first Drift Tube Linac (DTL) tank. Although numerous improvements had been made to the injector, the original 7 m medium energy transport (MEBT) produced significant longitudinal debunching and poor matching into the DTL, resulting in emittance growth, beam loss, and reduced transmission during high-current operation.

This paper describes the evolution of the BNL 200 MeV H⁻ linac and the front-end redesign that transformed its performance for RHIC, BLIP, and the future EIC.

LINAC FRONTEND EVOLUTION

The BNL 200 MeV linac was commissioned in 1970 with a 750 keV Cockcroft–Walton pre-injector followed by an 8.5 m transport line and a Drift Tube Linac optimized for accelerating 100 mA proton beams. The original injector provided reliable operation for many years; however, beam capture in the first DTL tank was limited to approximately 60–65%, with most beam loss and emittance growth occurring during the transition from the injector into Tank 1 [2].

Over the following three decades, the front end evolved to satisfy changing requirements of the BNL accelerator complex. Conversion from proton to H⁻ operation in 1982 increased AGS intensity. Installation of the RFQ in 1989 greatly improved injector reliability but did not eliminate the fundamental RFQ-to-DTL matching problem [3,4]. In 1996, permanent-magnet quadrupoles installed at the RFQ exit significantly improved transport through the MEBT [5,6], and in 2000 the high-brightness Optically Pumped Polarized Ion Source (OPPIS) was integrated into the injector to provide polarized H⁻ beams for the RHIC spin program [7]. These upgrades established the modern injector configuration but left the basic beam-dynamics limitation unchanged [8].

The principal limitation was the original 7 m medium-energy beam transport line. Although operationally flexible, it had gradually accumulated three bunchers, beam choppers, diagnostics, collimators, spin-rotation elements, and matching optics. At the RFQ output energy this transport corresponded to approximately 120βλ. The long drift allowed substantial longitudinal debunching before the beam entered the DTL. Even with three bunchers, the beam reached the first tank poorly matched in longitudinal phase space. Simple kinematic estimates and PARMILA simulations showed that the resulting mismatch produced strong RF defocusing during capture, approximately 35% beam loss in Tank 1 [9], and substantial transverse emittance growth through longitudinal–transverse coupling [10].

These studies led to a complete redesign of the front end between 2008 and 2010. Rather than attempting incremental improvements to the existing MEBT, the injector architecture was reorganized. Most transport, steering and diagnostic functions were moved upstream into the LEBT, allowing the MEBT to be reduced from 7 m to only 0.7 m. The compact system incorporated three high-gradient

*Work supported by US Department of Energy
#raparia@bnl.gov

Content from this work may be used under the terms of the CC BY 4.0 licence (© 2026). Any distribution of this work must maintain attribution to the author(s), title of the work, publisher, and DOI.

ISBN: 978-3-95450-275-2 ISSN: 2226-0366 doi: 10.18429/JACoW-LINAC2026-WE1A006

HIGH-CURRENT HEAVY-ION ACCELERATION ABOVE 100 mA IN A FOUR-ROD RFQ*

M. Okamura†,1,2, A. Cannavò[1], M. Horana Gamage[1], T. Kanesue[1], T. Sakabe[1], Shunsuke Ikeda[1], S. Kondrashev[1], Shota Ikeda[2], C. Zhang[3], K. Takahashi[4]
[1]Brookhaven National Laboratory, Upton, NY, USA
[2]Institute of Science Tokyo, Tokyo, Japan
[3]GSI Helmholtzzentrum für Schwerionenforschung, Darmstadt, Germany
[4]Nagaoka University of Technology, Nagaoka, Japan

Content from this work may be used under the terms of the CC BY 4.0 licence (© 2026). Any distribution of this work must maintain attribution to the author(s), title of the work, publisher, and DOI.

Abstract

We report the acceleration of fully stripped heavy-ion beams at peak currents in the proton-injector class: 148 mA of Li^{3+} and 135 mA of C^{6+} at an output energy of 320 keV/u, obtained with a 100 MHz four-rod radio-frequency quadrupole (RFQ) employing a variable-aperture vane geometry and a direct plasma injection scheme (DPIS) driven by a laser ion source. To our knowledge these are the highest peak currents yet accelerated for heavy ions in an RFQ. Beam loading reached 36% of the forward RF power and is resolved directly on the cavity pickup. We also describe two practical failure modes encountered during commissioning—a magnetron discharge sustained in the coaxial vacuum gap between the high-voltage transport pipe and the grounded pipe inside the solenoid, and RF back-coupling from the RFQ to the ion-source platform through the same unintended coaxial structure—and their common remedy, a PTFE tube filling the inter-pipe gap.

INTRODUCTION

Proton and H^- injectors routinely deliver 100–150 mA of peak current into RFQ accelerators [1, 2], while highly charged heavy-ion injectors have remained orders of magnitude below this benchmark. The disadvantage is rooted in the extraction and transport physics rather than in the accelerating structures: for a fixed geometry and voltage the Child–Langmuir limit scales the extractable current density as $(q/m)^{1/2}$, and once the extracted beam leaves quasi-neutrality, space charge dominates the low-energy beam transport (LEBT). Conventional high-charge-state sources sit far below the proton class: electron cyclotron resonance (ECR) sources deliver tens of µA of C^{6+} in CW operation, and electron beam ion sources (EBIS) reach a few mA in pulsed mode [3]. Meanwhile, the facilities now under construction, such as the EIC [4] and FAIR [5], require heavy-ion injector chains with proton-class brightness.

The direct plasma injection scheme (DPIS) [6] couples a laser-produced plasma directly into an RFQ, eliminating the LEBT entirely: the plasma is transported while still quasi-neutral, and beam formation is postponed until RFQ capture. DPIS has previously delivered over 30 mA of C^{6+} [7], approximately 35 mA of Li^{3+} [8], and recently a record 58 mA of Al^{11+} [9]. In the present work, a refined understanding of the plasma-to-beam transition at the RFQ entrance, combined with a purpose-designed variable-aperture four-rod RFQ [10], has raised the achievable peak current by roughly a factor of four, into the proton-injector class. The plasma physics of the beam formation is analysed elsewhere [11]; here we concentrate on the accelerator aspects: the RFQ design and its measured performance, the beam-commissioning results, and two instructive high-voltage/RF failure modes and their remedies, which we believe are of direct practical value to the linac community.

DPIS TEST BEAMLINE

The experiments were performed at the BNL Laser Research Laboratory. A Nd:YAG laser (1064 nm, 6 ns, 0.65 J on target) is focused to a spot of ~0.1 mm diameter (~10^{12} W/cm^2) on a solid target: high-purity isotropic graphite for carbon, and a lithium plate prepared and mounted under argon to suppress nitridation. The ablation plasma expands into a transport pipe surrounded by a 500 mm long solenoid. The solenoid field confines the plasma radially while leaving the axial expansion toward the RFQ unimpeded. The plasma chamber, transport pipe and extraction nozzle are biased to a high positive potential, which sets the RFQ injection energy of 21.8 keV/u: nominally 50.9 kV for Li^{3+} and 43.6 kV for C^{6+}. The highest C^{6+} transmission was in fact obtained at a 51 kV set point, which we attribute to a droop of the platform voltage under plasma loading during extraction. Ions are extracted through a 16 mm tapered nozzle directly into the RFQ. Downstream of the RFQ, a current transformer, an analyzing dipole for mass-to-charge selection, a retractable scintillator screen and a Faraday cup complete the diagnostics; reported currents are corrected for the 72% transmission of an RF-suppression mesh. The scintillator is a 3 mm thick CsI(Tl) plate viewed by a CCD camera. Faraday-cup and current-transformer traces are smoothed over a 20 ns window (200 samples) to suppress RF pick-up.

Because the plasma is produced by ablation, every shot consumes target material, and the target is mounted on a two-axis motorised stage and stepped between shots. Figure 1 shows a crater left on the lithium surface, profiled with a laser confocal microscope. The crater measures 835 µm across the outer rim and 603 µm across the inner wall, is 427 µm deep, and is bounded by a lip standing 119 µm above the original surface. It is thus far wider than

* Work supported by the U.S. Department of Energy, Office of Science, under Contract No. DE-SC0012704.
† okamura@bnl.gov

ISBN: 978-3-95450-275-2 ISSN: 2226-0366 doi: 10.18429/JACoW-LINAC2026-WE2A002

NEWGAIN PROJECT AT GANIL: CONSTRUCTION OF THE NEW HEAVY ION INJECTOR FOR SPIRAL2*

F. Chautard[1,†], D. Ackermann[1], O. Cakir[1], O. Delahaye[1], J. Dumas[5], V. Gérard[3], M. Di Giacomo[1], F. Hanchin[1], C. Haquin[1], C. Jamet[1], G. Jevelot[2], C. Lesigne[1], M. Michel[1], G. Normand[1], A. Outreman[1], C. Peaucelle[3], O. Piquet[5], Ph. Robillard[1], D. Simon[5], I. Stephan[4], Y. Trehudic[1], Q. Tura[1]
[1]GANIL, Caen, France
[2]Université de Bordeaux, CNRS-LP2I, Bordeaux, France
[3]Université Grenoble Alpes, CNRS-LPSC, Grenoble, France
[4]Université Paris-Saclay, CNRS-IJCLAB, Orsay, France
[5]CEA/IRFU, Saclay, France

Abstract

The NEWGAIN (NEW GAnil INjector) project is now in the construction phase at GANIL. It aims to install a second injector for the SPIRAL2 facility. It is designed to accelerate heavy ions with a mass-to-charge ratio (A/q) of up to 7. With this upgrade, SPIRAL2 will provide high-intensity beams, from protons to uranium, strengthening GANIL international competitiveness, both in fundamental sciences and related applications. The paper will provide an update on the progress of the construction phase and the main milestones achieved and to come. The layout and the main technical components of the new injector, based on 2 ECR ion sources (one of them existing), two Low Energy Beam Transport (LEBT) line, one RFQ and a Medium Energy Beam Transport (MEBT) line to transport the beam into the present MEBT connected to the SPIRAL2 LINAC are presented.

INTRODUCTION

The NEWGAIN project aims to build a second injector designed for A/q = 3 to 7 ions, to produce and accelerate very intense heavy ion beams using a new RFQ (RFQ2) up to uranium, far exceeding the performance of the existing injector. Thus, a new superconducting source will be developed to complement the existing sources and achieve high-intensity uranium beams.

Thanks to this improvement, the Système de Production d'Ions Radioactifs en Ligne de 2ème génération (SPIRAL2) LINAC [1] will deliver, within the limits of its operating energy, the most intense beams in the world (Table 1) on a wide variety of ions ranging from protons to uranium, and will strengthen GANIL's international competitiveness, both in fundamental sciences and in associated applications.

The project is organized within a large technical collaboration framework, composed of the following French accelerator laboratories of CEA/DRF/IRFU and CNRS/IN2P3: GANIL, IRFU/DACM and DIS, LPSC, LPCCaen, IPHC, LP2iB, IJCLab. These different partners have already collaborated in different projects with GANIL, the latest example to date being the construction of the SPIRAL2 facility. The NEWGAIN project is coordinated by GANIL.

Table 1: Ion Beam Intensities SPIRAL2 vs NEWGAIN

Ions	Intensity [pμA]		
	SPIRAL2	NEWGAIN	
	Phoenix V3 A/Q≤3	Phoenix V3 A/Q≤6	Superconducting Ion Source A/Q≤7
18O	80*	-	375
19F	>15	>40	>40
36Ar	16*	70	45
40Ar	3.6	70	45
36S	2.3	-	-
40Ca	2.9*	10	20
48Ca	1.2	10	20
58Ni	1.1*	4	8
84Kr	0.1	10	20
139Xe	0.001	7	>10
238U	<<0.001	0.1	10

*Measured, Foreseen

GENERAL LAYOUT

This second injector is designed to be fully compatible with the existing facility (Fig. 1) and to further enhance its 'multi-user' capabilities. It is composed of the following (Fig. 2):

- A high-performance superconducting ion source (the Source 1/7) called ASTERICS [2]
- Low energy beam transport lines connecting the ion sources (superconducting ion source and existing room temperature ion source) to the RFQ (LBE3). The mass separation at the exit of the ion sources can be tuned up to 150, depending on the ion choices and the experiment needs,

*This work benefited from state aid managed by the French National Research Agency under the Future Investment Program bearing the reference ANR-21-ESRE-0018
†chautard@ganil.fr

Content from this work may be used under the terms of the CC BY 4.0 licence (© 2026). Any distribution of this work must maintain attribution to the author(s), title of the work, publisher, and DOI.

ISBN: 978-3-95450-275-2 ISSN: 2226-0366 doi: 10.18429/JACoW-LINAC2026-WE2A003

BREAKING THE CRYOPLANT BARRIER: CONDUCTION-COOLED Nb_3Sn-COATED SRF LINACS FOR INDUSTRIAL AND ENVIRONMENTAL APPLICATIONS*

J. C. T. Thangaraj†, C. Edwards, T. Thompson, J. Helsper, M. Henry, Y. Ji, V. Yakovlev, T. Khabiboulline, I. Gonin, G. Eremeev, A. Sukhanov, S. Kazakov, S. Posen, N. Tagdulang
Fermi National Accelerator Laboratory, Batavia, IL, USA

Abstract

Superconducting linacs have traditionally relied on large cryogenic infrastructures, while compact accelerators have been based on normal-conducting technology. This distinction is now narrowing. At IARC at Fermilab, a dedicated SRF development and integration environment supports advances in Nb_3Sn-coated cavities operating near 4 K, together with cryocooler-based conduction cooling and solid-state RF power, enabling compact SRF linacs capable of high-duty-factor operation outside conventional accelerator facilities. Systems currently under construction address environmental remediation and medical device sterilization at approximately 10 MeV, where efficiency, reliability, and life-cycle cost are primary design drivers. These machines employ multi-cell elliptical cavities at 650 MHz and 1.3 GHz, operating at gradients of 7–10 MV/m under conduction cooling with industrial cryocoolers. By eliminating liquid-helium plants, the accelerator transitions from a facility-scale installation to an application-oriented system architecture, extending superconducting technology into regimes that have historically not been economically accessible.

INTRODUCTION

Electron-beam processing links accelerator performance directly to material throughput. For a required absorbed dose D, the ideal mass-processing rate is

$$\dot{m} = \frac{P_{\mathrm{beam}}}{D}, \qquad P_{\mathrm{beam}} = V_{\mathrm{b}} I_{\mathrm{b}}, \tag{1}$$

with utilization, transport, and deposited-energy efficiencies applied separately. The useful figure of merit is therefore sustained beam power delivered with predictable availability, rather than accelerating gradient alone. Applications under consideration include medical-device sterilization, food and material processing, and environmental treatment, for which electron energies of approximately 1–10 MeV and average powers from tens to hundreds of kilowatts are relevant [1, 2].

Normal-conducting linacs are well established in this market, but wall losses become restrictive as the duty factor approaches unity. SRF cavities reduce the RF dissipation by orders of magnitude, although conventional SRF installations require a helium refrigerator, distribution system, pressure-rated cryogenic hardware, and trained operators. Those systems are reasonable at a laboratory complex and difficult to justify for a single industrial production line.

* Work supported by the U.S. Department of Energy, Office of Science.
† jtobin@fnal.gov

The combination of Nb_3Sn and commercial 4 K cryocoolers changes this boundary. Nb_3Sn has a critical temperature near 18 K and can retain Q_0 near 10^{10} at 4 K and useful fields [3, 4]. The remaining cavity heat may then be carried through metallic links to closed-cycle cold heads. However, a cryogen-free SRF machine is obtained not solely from the cavity. The cavity coating, thermal interfaces, coupler, electron source, RF system, controls, shielding, and recovery logic must operate as one machine.

TECHNOLOGY BASIS

The 4 K load can be separated into static and RF-dependent terms,

$$P_{4\mathrm{K}} = P_{\mathrm{static}} + P_{\mathrm{dyn}}, \qquad P_{\mathrm{dyn}} = \frac{V_{\mathrm{c}}^2}{(R/Q)Q_0}. \tag{2}$$

Here $V_{\mathrm{c}} = E_{\mathrm{acc}} L$ is the cavity voltage. The surface resistance is $R_{\mathrm{s}} = R_{\mathrm{BCS}} + R_{\mathrm{res}}$, with $Q_0 = G/R_{\mathrm{s}}$. To first order, R_{BCS} scales as

$$R_{\mathrm{BCS}} \propto \frac{f^2}{T} \exp\left(-\frac{\Delta}{kT}\right). \tag{3}$$

The larger superconducting gap of Nb_3Sn is therefore the material property that permits useful Q_0 at 4 K. This reduces the generated watts.

RF loss is distributed over the cavity surface while a cryocooler removes heat at a small number of discrete locations. The approximate temperature rise from the cavity wall to a cold head is

$$\Delta T_{\mathrm{cav}} \simeq P_{\mathrm{dyn}} R_\theta, \qquad R_\theta = R_{\mathrm{ring}} + R_{\mathrm{joint}} + R_{\mathrm{link}}. \tag{4}$$

Niobium rings electron-beam welded around the cells spread the heat azimuthally. Broad clamped joints and high-purity aluminum links provide the path to the cryocooler second stages. The design problem is thus two-dimensional: Q_0 sets the heat to be removed and R_θ sets the temperature increase produced by that heat. Conduction-cooled single-cell cavities at Fermilab, Jefferson Lab, and Cornell have established the basic heat-transfer methods [5–7].

There is also little value in maximizing Q_0 without regard to the installed static load. At low gradient the available refrigeration has already been consumed by P_{static}; at high gradient, Eq. (2) gives a quadratic increase in dynamic load. A practical operating point lies near the static–dynamic crossover with margin for coating variation, thermal contacts, microphonics, and cryocooler capacity.

Content from this work may be used under the terms of the CC BY 4.0 licence (© 2026). Any distribution of this work must maintain attribution to the author(s), title of the work, publisher, and DOI.

ISBN: 978-3-95450-275-2 ISSN: 2226-0366 doi: 10.18429/JACoW-LINAC2026-TH1A001

25 YEARS OF FEL OPERATION AT FLASH (DESY)

K. Honkavaara*†, Deutsches Elektronen-Synchrotron DESY, Hamburg, Germany

Content from this work may be used under the terms of the CC BY 4.0 licence (© 2026). Any distribution of this work must maintain attribution to the author(s), title of the work, publisher, and DOI.

Abstract

First SASE lasing at the FLASH Free-electron laser (FEL) - at that time called as TTF FEL - was in February 2000. It was the first FEL worldwide producing SASE radiation at VUV wavelengths. Since then, over more than two decades, FLASH has provided high peak and average brilliance XUV and soft X-ray FEL radiation for user experiments. In order to keep FLASH as a state-of-the-art FEL, it has been continuously refurbished and upgraded. The most recent upgrade FLASH2020+ increased the energy of the superconducting linac to 1.35 GeV and reconstructed the FLASH1 undulator beamline. The new externally seeded FLASH1 will provide fully coherent radiation at up to MHz photon pulse repetition rate (in a burst). Moreover, thanks to the new APPLE-III undulators, a full polarization control is possible. As before, FLASH1 hosts also an electron beam driven THz source. FLASH2 continues in SASE operation. This paper provides an overview of FLASH's evolution from a test facility for superconducting accelerator technology to a trailblazing and innovative FEL user facility.

INTRODUCTION

FLASH [1–5] is the XUV and soft x-ray Free-Electron Laser (FEL) user facility at DESY (Hamburg, Germany). It is based on the TESLA Test Facility (TTF) Linac [6], which was constructed at DESY in 1990's within the international TESLA collaboration to test the feasibility of the high gradient superconducting accelerator technology for the TESLA linear collider project [7]. In addition, the 250 MeV TTF Linac was used to drive the SASE [8, 9] (Self Amplified Spontaneous Emission) FEL pilot facility TTF FEL [10]. Its first lasing was in February 2000, and it was the first FEL worldwide producing SASE radiation at VUV wavelengths [11]. Now, 25 years later, FLASH is driven by a 1.35 GeV superconducting linac, and has been already two decades a full scale FEL user facilty, providing meanwhile soft x-ray radiation down to 3 nm (fundamental).

A schematic layout of the TTF FEL in the year 2000 and the present FLASH facility is shown in Fig. 1. While they vary in scale and system complexity, their basic concept is identical. A high quality, bunched electron beam is produced by a photoinjector consisting of a normal conducting RF gun with a Cs_2Te photocathode and an UV injector laser. The superconducting linac uses TESLA type 1.3 GHz accelerator modules with eight 9-cell Niobium cavities each [12]. The use of superconducting RF allows long RF pulses (up to 800 μs) and thus long electron bunch trains. The electron bunches are compressed by magnetic bunch compressors, and the FEL radiation is produced by an undulator beamline.

This paper describes the evolution of FLASH from a demonstrator of the SASE lasing in VUV range to a versatile high repetition rate FEL user facility providing simultaneously externally seeded, SASE FEL, and THz radiation.

TTF FEL

The TESLA Test Facility (TTF) Linac was constructed in the mid 1990's for beam tests of the superconducting TESLA accelerator modules. In the early years, the electron beam was produced by a thermionic gun, followed by a subharmonic buncher, and a booster (capture) cavity (one TESLA type 9-cell cavity) [13]. The first complete accelerator module (M1 as ACC1) with eight 9-cell Niobium cavities [14, 15] was installed into the beamline in spring 1997. In autumn 1998, the thermionic gun was replaced by a laser-driven RF gun equipped with an exchangeable Cs_2Te photocathode [16]. Additionally, a second accelerator module (M2 as ACC2) was installed, and a bunch compressor was positioned between the two accelerator modules.

The 250 MeV TTF Linac was also used to drive the SASE free-electron laser pilot facility TTF FEL. In 1999, three fixed-gap undulator modules [17], about 4.5 m each, were added downstream of the second accelerator module (ACC2). At the same time, the original ACC1 module was replaced with a new one. The first lasing (109 nm) was achieved in February 2000 [11]. It was the first SASE lasing in the VUV range worldwide. Over the following two years, SASE was confirmed for wavelengths from 80 nm to 120 nm [18, 19]. Furthermore, first photon experiments were performed [20, 21]. The success of TTF FEL paved the way for the funding and, a few years later, the construction of the first hard X-ray SASE FELs, like LCLS at SLAC [22] and the European XFEL from DESY (injector) to the XFEL campus in Schenefeld (experimental hall) [23].

The TTF FEL completed its operation in March 2002. After a removal of the undulators and both accelerator modules, a special TESLA type module ("Superstructure") [24] was installed in the place of ACC1, while a new standard TESLA module replaced ACC2. The beam tests of these modules continued until November 2002, at which point the TTF Linac operation was finished. Ultimately, the ACC2 module (internally called M1*), which remained in operation at FLASH until late 2021, became the TESLA module with the longest beam operation time so far.

FEL USER FACILITY FLASH

Extending the superconducting linac and undulator beamline to reach 1 GeV electron beam energy and lasing down to 6 nm was a part of the original plan ("VUV-FEL at TTF2"). The civil construction of the new tunnel and experimental hall started in 1999. The first stage of TTF2 consisted of a photoinjector [25], a superconducting linac of five TESLA

* katja.honkavaara@desy.de
† for the FLASH team

ISBN: 978-3-95450-275-2 ISSN: 2226-0366 doi: 10.18429/JACoW-LINAC2026-TH1A002

COMPACT AND EFFICIENT CW ELECTRON LINACS FOR INDUSTRIAL AND ENVIRONMENTAL APPLICATIONS*

R. A. Rimmer†,1, J. Buttles[1], A. Castilla[1], P. Carriere[1], G. Ciovati[1], J. Colley[1], M. Dion[1], F. Hannon[2], J. Gubeli[1], K. Jordan[1], U. Pudasaini[1], N. Stilin[1], J. Vennekate[1], H. Wang[1], S. Wang[1]
[1]JLab, Newport News, VA, USA
[2]Phase Space Tech, Lund, Sweden

Abstract

Compact, efficient and high-power sources of electrons are of growing interest for a wide range of applications including materials processing, medical device and food sterilization, wastewater and soil treatment. Electron energy from <1 MeV to 10 MeV and beam power from kW to MW levels are desirable. We describe a compact modular system being developed at JLab starting with a gridded thermionic electron gun and using an initial graded-beta copper CW linac to capture and form the beam, followed by one or more beta=1 CW linac sections to increase the energy. These sections may be normal conducting or conduction-cooled superconducting cavities depending on the energy and power levels required. CW operation allows for reliable high average power at modest gradient using cost-effective, highly efficient industrial magnetrons for the RF sources. We describe the design and development of these components along with plans for an integrated system to demonstrate CW beam operation.

INTRODUCTION

Electron beam treatment is an established and growing process for a variety of applications including food and medical device sterilization, bulk processing of polymers, environmental applications such as water and soil remediation, sterile insect production, etc. [1]. Many of these processes are well served by existing commercial technologies, however those applications that require high volume throughput or higher doses are often limited by available beam power. Recent advances in linac technology address this shortfall by offering high current and high efficiency in a compact footprint. Beam energy is typically less than 10 MeV to avoid activation or neutron production; however, these advances may also benefit higher energy applications such as isotope production or medical therapy or those where X-ray modality is preferred. The solutions being developed at JLab focus on CW beam delivery to achieve high average power, although pulsed operation is not precluded. In such cases RF power costs are important and the use of low cost, highly efficient commercial magnetrons at 915 MHz is proposed.

*This research was supported by the U.S. Department of Energy, National Nuclear Security Administration, Office of Defense Nuclear Nonproliferation Research and Development (DNN R&D) and by the U.S. Department of Energy, Office of Science, Office of Nuclear Physics under contract 892431-26-C-SC000213. The views and opinions of authors expressed herein do not necessarily state or reflect those of the United States Government or any agency thereof.
† rarimmer@jlab.org

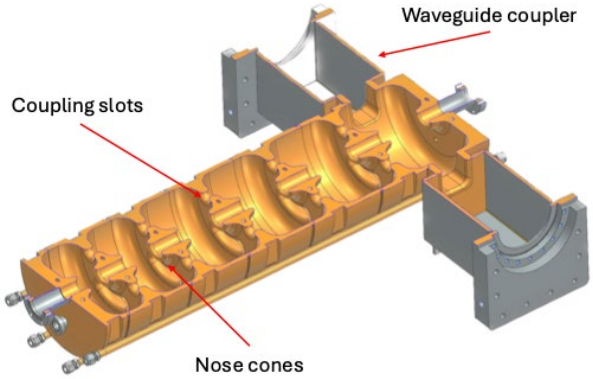


Figure 1: Graded-beta π-mode standing wave linac.

NCRF OPTION

Essentially all existing commercial linear accelerators use normal-conducting RF technology due to its proven reliability and affordability. High gradients can be achieved in pulsed operation using klystron or magnetron RF sources and pulsed modulators. At JLab a 1497 MHz CW graded-beta copper linac was designed for the capture section of the CEBAF injector [2, 3]. A version of this design scaled to 915 MHz is suitable for low energy industrial applications. In CW operation the accelerating field is limited by thermal stresses to about 3 MV/m peak on axis (~1 MV/m average). A prototype 1 MeV, 100 kW capable unit is being constructed [4], (Fig. 1). Dual pre-stressed disc-type WR975 waveguide windows from Euclid Techlabs Inc. [5] are used to allow high power transmission to the cavity. The system can be upgraded to higher power or energy by adding additional beta=1 linac sections and RF sources. Key system parameters are listed in Table 1. The electron source is a commercial gridded thermionic gun adapted to 915 MHz operation, (Fig. 2). By applying both RF and DC bias to the grid the beam is pre-bunched entering the linac leading to improved capture efficiency of >90%.

Linac Optics

The General Particle Tracer (GPT) particle tracking software [6] has been used to study the preliminary beamline layout. A bunched beam is simulated from the cathode at 30 kV, assuming both DC and RF bias on the grid. In addition to electrostatic focusing in the gun a solenoid is used to produce a waist at the cavity first cell. Figure 3 shows the graded-beta electric field profile of the cavity. Figure 4 shows the energy profile for an electron traveling down the linac. By varying the phase of the injected electrons the

Content from this work may be used under the terms of the CC BY 4.0 licence (© 2026). Any distribution of this work must maintain attribution to the author(s), title of the work, publisher, and DOI.

ISBN: 978-3-95450-275-2 ISSN: 2226-0366 doi: 10.18429/JACoW-LINAC2026-TH1A004

TECHNICAL COMMISSIONING OF THE ESS LINAC CAVITIES FOR THE BEAM ON DUMP PHASES

M. Koopmans*, A. Bhattacharyya, A. Bignami, N. Elias, F. Grespan, A. Krawczyk, E. Laface, C. Maiano, K. Mårtensson, M. Nabywaniec, D. Nicosia, A. Passarelli, P. Pierini, H. Przybilski, S. Sandilands, M. Skiba, A. Svensson, E. Trachanas, P. van Velze, M. Wang
European Spallation Source, Lund, Sweden

Abstract

The ESS linac has been commissioned in two different operation phases operation on the 12 kW commissioning beam dump. In 2025 the linac was operated at full duty cycle in the normal-conducting section (up to 90 MeV) and at reduced duty cycle in the superconducting section (up to 870 MeV), due to limitations in the cooling infrastructure and staged implementation of low-level RF (LLRF) functionalities. In the present phase the whole linac has been operated up to its full duty cycle at 14 Hz and 3.2 ms RF pulses, showing Lorentz force detuning (LFD) capabilities with long RF pulses in the superconducting RF (SRF) structures. This contribution summarizes the staged technical commissioning phases, presenting the conditioning experience and the setup for operation at nominal RF performances.

INTRODUCTION

The European Spallation Source (ESS) designated to become the world's most powerful neutron source is currently being commissioned in Lund, Sweden. The ESS Linac is designed to accelerate a 62.5 mA proton beam in 2.86 ms long pulses at repetition rate of 14 Hz to an ultimate beam energy of 2 GeV, equivalent to a beam power of 5 MW, and send it to the rotating tungsten target. A comprehensive description of the project can be found in Ref. [1].

A schematic overview of the whole Linac is shown in Fig. 1. From a technical perspective it is usually divided into two parts. The normal conducting Linac (NCL) involves the ion source, the low energy beam transport (LEBT), the radio frequency quadrupole (RFQ), the medium energy beam transport (MEBT) featuring three buncher cavities, and five drift tube Linacs (DTLs). The superconducting Linac (SCL) features 13 spoke cryo-modules (CM), which each contain two double spoke cavities, as well as nine medium-β Linac (MBL) CM and eventually 21 high-β Linac (HBL) CM, which involve four MB and HB elliptical cavities, respectively. All NCL and the spoke cavities run at an RF frequency of 352.21 MHz, while the elliptical cavities of the MBL and HBL operate at 704.42 MHz.

Of the 21 HBL CM, five are currently available for beam acceleration resulting in a maximum achievable energy of 870 MeV, equivalent to 2 MW beam power at nominal beam parameters. Six additional HBL CM have been installed in the summer of 2025 and will enable a maximum beam energy of 1.28 GeV, which is equivalent to a beam power of 3 MW at nominal beam parameters [2].

After completing the installation of the NCL [3], the magnets [4] and the SCL up to HBL-050 [5], the accelerator was prepared for the first beam on dump (BOD1) commissioning run end of 2024. The SCL was cooled down for the first time [6–8] and stable 2 K conditions were reached beginning of 2025. Further details on the preparation of the Linac for BOD1 are described in Refs. [9, 10]. During BOD1 the beam was successfully sent to the beam dump at the target energy of >800 MeV for a 5 µs long pulse of 5 mA at a repetition rate of 1 Hz [11].

Due to some unforeseen delay in the target being ready for neutron production, additional time has been allocated for two additional beam on dump commissioning runs in 2026. The preparation for the second beam on dump (BOD2) run started in October 2025, whereas the commissioning with beam started in January and concluded in July 2026. The main commissioning goals include stable RF operation at nominal RF pulse length of 3.2 ms at 14 Hz for the whole Linac and a general accelerator availability of more than 80 %. In addition, the aim of beam commissioning is to demonstrate the acceleration of beam pulses longer than 1 ms with at least 5 mA and sending pulses at the nominal current of 62.5 mA.

In this paper we will describe the NCL and SCL cavity preparation and technical commissioning for the beam on dump commissioning phases. Especially the differences in the preparation from BOD1 to BOD2 necessary to achieve nominal parameters throughout the Linac will be highlighted. The results of the beam commissioning are presented by the beam commissioning team in Refs. [12, 13].

* marten.koopmans@ess.eu

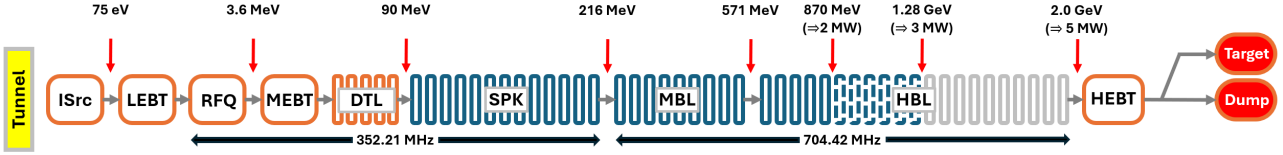


Figure 1: Schematic overview of the ESS Linac sections in the accelerator tunnel with annotated beam energy (and equivalent beam power at nominal pulse length of 3.2 ms and repetition rate of 14 Hz) after the respective section. Components with a colored outline are installed in the tunnel and everything with a solid outline is ready for beam operation (see text).

Content from this work may be used under the terms of the CC BY 4.0 licence (© 2026). Any distribution of this work must maintain attribution to the author(s), title of the work, publisher, and DOI.

ISBN: 978-3-95450-275-2 ISSN: 2226-0366 doi: 10.18429/JACoW-LINAC2026-TH1A006

PROGRESS IN THE LIPAc VALIDATION AND THE ROADMAP TOWARDS SRF LINAC BEAM COMMISSIONING

K. Kondo[†,1], J. P. Adam[4], T. Akagi[1,3], C. Arcambal[4], Y. Carin[2], J. Chambrillon[2,3], F. Cismondi[2], F. Delgado[3,7], R. Delgado[2,3], M. Dhakarwal[2,3], H. Dzitko[2,3], T. Ebisawa[1,3], J. Franco-Campos[1], D. Gex[2], F. Grespan[6], K. Hasegawa[1], K. Hirosawa[1,3], J. Hyun[1,3], H. Jenhani[4], D. Jimenez-Rey[5], N. Kaneko[1,3], A. Kasugai[1], S. Kwon[1,3], K. Kumagai[1,3], A. Madur[4], Á. Marchena[3,7], K. Masuda[1,3], L. M. Martínez[3,5], J. Merino[7], J. C. Morales[2], A. Mizuno[1], I. Moya[2,3], C. Ortiz[2,3], O. Piquet[4], A. Pisent[6], T. Plaisant[4], A. Salom[2], F. Scantamburlo[2,3], T. Vacher[4], C. Vermare[2,3]
[1]QST Rokkasho Institute for Fusion Energy, Rokkasho-mura, Aomori, Japan
[2]Fusion for Energy, Garching, Germany
[3]IFMIF/EVEDA Project Team, Rokkasho-mura, Aomori, Japan
[4]CEA Saclay, Gif-sur-Yvette, France
[5]CIEMAT, Madrid, Spain
[6]INFN Laboratori Nazionali di Legnaro, Legnaro, Italy
[7]IFMIF-DONES España, Granada, Spain

Content from this work may be used under the terms of the CC BY 4.0 licence (© 2026). Any distribution of this work must maintain attribution to the author(s), title of the work, publisher, and DOI.

Abstract

The Linear IFMIF Prototype Accelerator (LIPAc) is being commissioned to validate the low-energy accelerator section of future fusion neutron sources. Following completion of the high-duty RFQ commissioning campaign in 2024, which demonstrated acceleration of a 119 mA deuteron beam at 8.75% duty factor, the project entered the preparation phase for SRF beam commissioning. Since then, RFQ coupler qualification, SRF cryomodule assembly and installation, machine integration, and SRF warm conditioning have been carried out. By July 2026, four SRF couplers achieved CW operation at 25-32 kW. Machine integration for SRF operation is now in its final stage, with first cooldown targeted for late 2026 and subsequent proton beam commissioning planned thereafter.

INTRODUCTION

The International Fusion Materials Irradiation Facility (IFMIF) and its derivative project IFMIF-DONES and A-FNS require a high-current continuous-wave (CW) deuteron accelerator capable of delivering a 125 mA beam at 40 MeV for the generation of fusion-relevant neutrons through the D-Li reaction. To validate the most challenging low-energy section of this accelerator, the Linear IFMIF Prototype Accelerator (LIPAc) has been constructed and commissioned in Rokkasho, Japan, under the Broader Approach agreement between Europe and Japan. LIPAc aims to accelerate a 125 mA deuteron beam up to 9 MeV in CW operation and serves as the engineering validation platform for future fusion neutron sources [1].

LIPAc commissioning is organized into a series of phases, each corresponding to a specific accelerator configuration and commissioning objective, as illustrated in Figure 1. Following successful completion of injector validation (Phase-A) and RFQ beam commissioning (Phase-B and Phase-B+), the project entered the preparation stage for Phase-C, which targets the first beam acceleration through the SRF linac. Phase-D will subsequently address progressive commissioning toward nominal-current high-duty deuteron operation. Since mid-2024, activities have focused on the transition from the RFQ validation configuration to the final accelerator configuration, including cryomodule installation, machine integration, RF commissioning, and preparation for first cooldown and beam operation. This paper reviews the main achievements obtained since the completion of Phase-B+ and presents the current status and roadmap toward SRF beam commissioning.

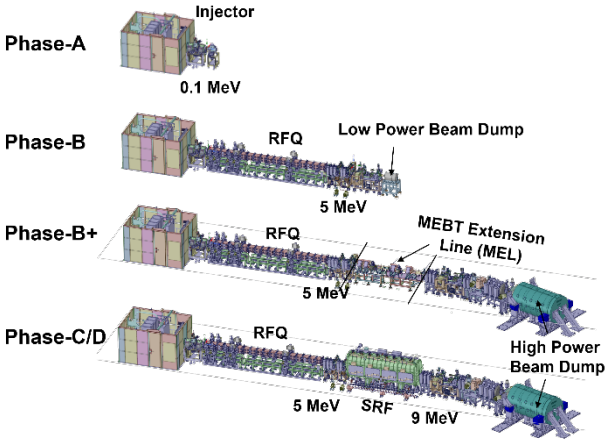


Figure 1: LIPAc accelerator configuration.

OUTCOMES OF THE PHASE B+ CAMPAIGN

The LIPAc Radio Frequency Quadrupole (RFQ) is one of the key validation elements of the IFMIF accelerator concept. The RFQ accelerates a 125-mA deuteron beam from 100 keV to 5 MeV at 175 MHz and is designed for continuous-wave (CW) operation. With a total length of 9.8 m, it is among the longest RFQs ever constructed for

[†] kondo.keitaro@qst.go.jp

ISBN: 978-3-95450-275-2 ISSN: 2226-0366 doi: 10.18429/JACoW-LINAC2026-THPO001

IDENTIFYING ANOMALIES AT CEBAF USING CROSS-PLANE COVARIANCE SVD

J. Samari, R.M. Bodenstein[1]
[1]Thomas Jefferson National Accelerator Facility, Newport News, VA, USA

Abstract

We present a method for detecting and characterizing cross-plane anomalies in a nominally decoupled, recirculating linac-type accelerator, such as the Continuous Electron Beam Accelerator Facility (CEBAF). The method computes the zero-lag cross-plane covariance $C_{xy} = \frac{1}{T} XY^\top$ from archived beam position monitor (BPM) data $X \in \mathbb{R}^{N_x \times T}$ and $Y \in \mathbb{R}^{N_y \times T}$, and analyzes its singular value decomposition (SVD) $C_{xy} = P\Sigma Q^\top$. Each singular triplet $(\boldsymbol{p}_k, \boldsymbol{q}_k, \sigma_k)$ produces paired spatial patterns and a strength that quantify where and how the two planes move together at the same instant. Projecting each array of positions at a given time onto the spatial singular vectors indicates when the coupled pattern is active. Large modes provide direct evidence of dispersion, skew optics, feedback cross-feed, scraping, or faults that introduce coupled beam motion. The construction is formalized, the differentiability is discussed, and concrete examples of anomalies such as magnet failures and known optic modulation are given.

MOTIVATION AND METHOD

The Continuous Electron Beam Accelerator Facility (CEBAF) is a recirculating superconducting linear accelerator in which multiple beam passes share portions of the transport system [1,2]. Although the horizontal and vertical optics are designed to be approximately decoupled, residual dispersion, skew fields, alignment errors, feedback cross-feed, beam loss, and equipment faults can introduce coherent motion in both planes. A model-independent diagnostic is therefore valuable for screening archived BPM data and identifying where and when such motion becomes visible [3,4].

Let $X \in \mathbb{R}^{N_x \times T}$ and $Y \in \mathbb{R}^{N_y \times T}$ contain synchronized horizontal and vertical BPM readings, with BPMs in rows and samples in columns. Each row is centered over the analysis window. The zero-lag cross-plane covariance is

$$C_{xy} = \frac{1}{T} XY^\top \in \mathbb{R}^{N_x \times N_y} . \tag{1}$$

Its thin singular value decomposition (SVD) is

$$C_{xy} = P\Sigma Q^\top, \qquad \Sigma = \mathrm{diag}(\sigma_1, \ldots, \sigma_r) , \tag{2}$$

where $\sigma_1 \geq \cdots \geq \sigma_r \geq 0$, the columns $\boldsymbol{p}_k$ of P are horizontal spatial patterns, and the columns $\boldsymbol{q}_k$ of Q are vertical spatial patterns. The leading terms give the best low-rank approximation to C_{xy} in the Frobenius norm.

Temporal activity traces are formed as

$$A = X^\top P, \qquad B = Y^\top Q , \tag{3}$$

with $a_k(t) = \boldsymbol{p}_k^\top X(:,t)$ and $b_k(t) = \boldsymbol{q}_k^\top Y(:,t)$. These projections obey the exact identity

$$\frac{1}{T} A^\top B = \Sigma , \quad \frac{1}{T} \boldsymbol{a}_k^\top \boldsymbol{b}_\ell = \sigma_k \delta_{k\ell} . \tag{4}$$

Thus, each singular value is the covariance of its paired temporal traces. The simultaneous sign ambiguity of $\boldsymbol{p}_k$ and $\boldsymbol{q}_k$ does not affect this result or the correlation of $\boldsymbol{a}_k$ and $\boldsymbol{b}_k$.

The fraction of cross-plane covariance represented by the first K modes is

$$\mathcal{E}(K) = \frac{\sum_{k=1}^{K} \sigma_k^2}{\sum_{k=1}^{r} \sigma_k^2} . \tag{5}$$

For comparisons among windows, the machine state and preprocessing must be held fixed. A robust baseline score can be defined from nominal reference windows as

$$z_k = \frac{\sigma_k - \mathrm{median}(\sigma_{k,\mathrm{ref}})}{1.4826\ \mathrm{MAD}(\sigma_{k,\mathrm{ref}})} . \tag{6}$$

Row-standardized data are useful for window-to-window screening, whereas unscaled covariance retains the physical dominance of high-response BPMs and is preferable for localization. Circularly shifting one plane in time provides a simple null test for zero-lag coherence while approximately preserving each channel's autocorrelation.

DATA HANDLING AT CEBAF

The examples use 1 Hz archived EPICS BPM readbacks. Invalid or inert channels are removed, rows are centered, and intervals without valid transported beam are excluded. Both unscaled and row-standardized analyses are retained because standardization suppresses the natural prominence of high-dispersion locations. In shared linac sections, a pulsed beam structure permits more specific pass-resolved interpretation; continuous-wave readbacks superpose multiple passes and therefore reduce spatial specificity. Small timing offsets can reduce zero-lag covariance, but lag-embedded tests did not materially change the modes in the 1 Hz data considered here.

CONTROLLED OPTICS EXCITATIONS

During a CEBAF Fast Optics (FOpt) measurement, two horizontal corrector excitations (X_1, X_2), two vertical excitations (Y_1, Y_2), and an energy excitation (E) are applied sequentially in 15 second increments. The controlled sequence provides a direct test of whether the eigenmodes separate known inputs. Figure 1 shows a steep singular spectrum and the first three relevant modes. The two leading

Content from this work may be used under the terms of the CC BY 4.0 licence (© 2026). Any distribution of this work must maintain attribution to the author(s), title of the work, publisher, and DOI.

ISBN: 978-3-95450-275-2 ISSN: 2226-0366 doi: 10.18429/JACoW-LINAC2026-THPO002

PHASE AND AMPLITUDE SETUP OF THE RF CAVITIES OF THE ESS LINEAR ACCELERATOR

D. Noll*, R. Baron, M. Eshraqi, I. Gorgisyan, S. Johannesson, N. Milas, R. Miyamoto, E. Salehi
European Spallation Source ERIC, Malmö, Sweden

Content from this work may be used under the terms of the CC BY 4.0 licence (© 2026). Any distribution of this work must maintain attribution to the author(s), title of the work, publisher, and DOI.

Abstract

The European Spallation Source (ESS) aims to be the world's brightest neutron source, designed to delivering 2 GeV protons at 5 MW to a rotating Tungsten target via a 600 m-long superconducting linear accelerator. At the present installation phase, with 81 of the total 146 cavities available in the superconducting linac, a beam of 800 MeV (2 MW) can be produced. During the first half of 2026, a second commissioning run for the full accelerator had the goal to improve the setup of the machine and to increase the beam power above the levels used during the first run in 2025.

One of the first steps required at the start of each run is to find the amplitudes and phases for each of the cavities for correct acceleration. This paper will give an update on the methods presently used for setup of both the normal conducting and the superconducting part of the machine.

THE ESS ACCELERATOR

The European Spallation Source (ESS) linac design is described in more detail in Ref. [1]. It consists of a normal conducting and a superconducting part. The Normal Conducting Linac (NCL) contains the ion source, a Low-Energy Beam Transport (LEBT) beam line, a Radio Frequency Quadrupole (RFQ), a Medium Energy Beam Transport (MEBT) line including three single-gap buncher cavities and a Drift Tube Linac (DTL) with five tanks. The Superconducting Linac (SCL) consists of 13 cryomodules containing two 3-gap Spoke cavities each, 9 cryomodules of four 6-cell medium-beta elliptical cavities (MBL) and 21 cryomodules of four 5-cell elliptical high-beta cavities (HBL). Beam energies out of the RFQ and the DTL, Spoke, MBL and HBL section are 3.6 MeV, 89.9 MeV, 216 MeV, 571 MeV and 32 GeV respectively.

During the beam commissioning period in 2026 (BOD2), only 5 HBL cryomodules were available for operation, and one of the Spoke cavities could not be powered due to issues with the motor controlling the tuning of the cavity, yielding beam energies of 210 MeV, 560 MeV and 862 MeV out of the Spoke, MBL and HBL section nominally.

In between each cryomodule, a Beam Position Monitor (BPM) is available for measurement of the phase (and position) of the beam. Only two BPM pairs, one in the Spoke section and another at the end of the HBL section, are calibrated for time-of-flight measurements and determination of the beam energy. The measurement process is however fully manual and was only used to check the beam energy once the linac was configured.

* daniel.noll@ess.eu

PHASE SCAN PROCEDURE

During the design of the linac, accelerating gradients and beam reference phases were determined for each cavity for a beam transport with low emittance growth and a large margin against beam loss. Statistical error studies were performed in [2] and [3] that determine tolerances for low-loss transport to be 1° for the RF phase and 1 % for the cavity gradients.

To determine the accelerating gradient of the cavities a pickup is used to couple out a relatively low amount of RF power, with the calibration between the two expected to be accurate to 10 %. The requested cavity field can only be expected to be accurate to that degree, an order of magnitude less certain than what is required for the beam dynamics. Without precise measurement of the phase shift between cavity pickup and Low-Level RF (LLRF) system, the correct RF phase setpoint to obtain the correct reference phase is a-priori unknown. Consequently, both of these have to be determined from beam measurements.

One available method is a phase scan: variation of the LLRF setpoint over a range of phases while recording the beam phase reading on one or multiple BPMs. Only the *relative* changes over a scan is reliable information.

For analysis, one has the option of looking at the signature of one BPM phase reading or the difference of two BPM phase readings. The latter has the benefit of being only sensitive to the energy of the beam, while the former is also influenced by the dynamics in the cavity itself e.g. the phase slip introduced by the beam being slowed down and sped up as it travels through the RF gaps. The phase signal behaviour from a single BPM over the phase scan is sensitive to the distance between BPM and cavity.

With the exception of the DTL cavities, we employ the same method based on the difference of two BPM phase readings which will be described in the following.

Phase Scan Model for the SCL Cavities

The energy gain of a particle passing through a single RF gap is known to be expressed by

$$\Delta W = qE_0T(W)\,L\cos(\varphi)\ ,$$

with the accelerating gradient E_0T including the energy dependent transit time factor $T(W)$ and the phase φ. For a multi-gap cavity, this expression only holds approximately when the synchronicity between gaps does not change significantly with φ.

To build an empirical, single-equation model that can be quickly fitted to measured data, we evaluated the energy gain of a single particle by numerical integration of field maps used in the beam dynamics model. The resulting data can

ISBN: 978-3-95450-275-2 ISSN: 2226-0366 doi: 10.18429/JACoW-LINAC2026-THPO005

RF ENERGY RECOVERY POWER CONVERSION FOR PARTICLE ACCELERATORS*

J.D. Liu†,1,2, Z.S. Zhou1,2, X. He1, F. Li1, D.Y. He1, X.P. Li1,2, J.Y. Li1,2, C. Meng1,2, Y.L. Chi†,1
[1]Institute of High Energy Physics, Chinese Academy of Sciences, Beijing, China
[2]University of Chinese Academy of Sciences, Beijing, China

Content from this work may be used under the terms of the CC BY 4.0 licence (© 2026). Any distribution of this work must maintain attribution to the author(s), title of the work, publisher, and DOI.

Abstract

With the continuously increasing energy demands in high-energy particle collider experiments, the total energy consumption of particle accelerators has risen significantly, reaching the TWh level annually. Reducing energy consumption and improving efficiency have become major challenges in the field of high-energy physics. This paper, taking the continuous-wave RF power source system as the background, addresses the various technical bottlenecks faced by conventional megawatt-level high-voltage power supplies in energy recovery applications. A multi-mode energy-recycling high-voltage power supply scheme based on modular cascaded architecture is proposed and preliminarily validated through simulation and experiment. The results demonstrate that the proposed solution can provide versatile application possibilities for future scenarios.

INTRODUCTION

Large-scale particle accelerators are essential experimental facilities for high-energy physics research, among which high-power RF power systems serve as the core energy source for particle acceleration and energy gain. In recent years, a series of new large-scale particle collider projects have been proposed, requiring increasingly higher particle beam energy. The total power consumption of such facilities reaches hundreds of megawatts, with annual power consumption climbing to the terawatt-hour (TWh) level [1]. Under the background of national "dual-carbon" strategic goals and increasingly stringent environmental energy-saving requirements, reducing accelerator energy consumption and improving energy utilization efficiency has become a key research direction and urgent challenge for advanced accelerator technology.

The RF power system accounts for the largest proportion of energy consumption in particle accelerators. In actual operation, only a small part of the RF power is used for charged particle acceleration, while most power is converted into heat through terminal devices such as collectors and accelerating tube absorbing loads, and is dissipated by the water-cooling system, causing massive energy waste. Taking the European CLIC project as an example, the total RF power demand reaches 109 MW, and klystrons, high-power RF absorbing loads and modulators contribute more than 70% of the total energy consumption. Similarly, the CEPC project in China also faces severe low energy efficiency problems. Therefore, researching energy recycling and waste energy reuse technologies to develop high-power energy recycling modes and maximize the energy conversion efficiency of RF power systems is of great practical significance for future advanced accelerator construction and national energy strategic layout.

Current research on continuous-wave RF power sources mainly focuses on efficiency improvement. Key research directions include energy-recycling klystrons with multi-stage depressed collectors (MDC), high-power RF energy-recycling microwave devices, and pulse energy-recycling power conversion equipment, as shown in Fig. 1. This paper takes the energy-recycling power conversion device as the core research object, systematically analyses the existing technical bottlenecks of traditional megawatt-class high-voltage power supplies, and proposes a novel multi-mode energy-recycling high-voltage power supply scheme with verified simulation and experimental results.

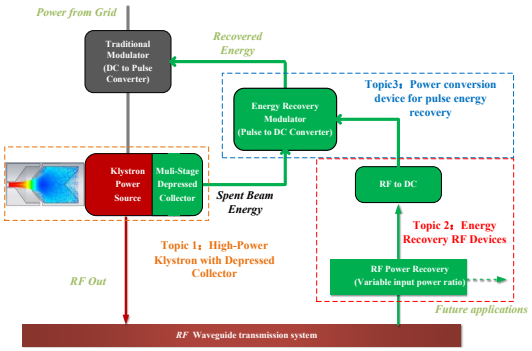


Figure 1: Schematic diagram of energy recovery verification platform.

ARCHITECTURE OF RF ENERGY-RECOVERY HIGH-VOLTAGE POWER SUPPLY

Traditional megawatt-class high-voltage power supplies for high-efficiency CW power sources face three critical technical bottlenecks that restrict the energy efficiency and operational performance of accelerator RF systems.

First, insufficient adaptability for MDC klystron multi-stage independent power supply. The multi-stage depressed collector structure of high-efficiency energy-recycling klystrons requires the power supply to provide multiple independent and adjustable high-voltage outputs [2]. The traditional single power supply architecture cannot meet the hierarchical independent power supply demand of MDC systems, limiting the efficiency improvement of klystron energy recycling.

Second, high energy consumption and insufficient test capacity in reliability verification. Megawatt-class high-

*Work supported by the National Natural Science Foundation of China under Grant 12275288
†liujd@ihep.ac.cn, chiyl@ihep.ac.cn

ISBN: 978-3-95450-275-2 ISSN: 2226-0366 doi: 10.18429/JACoW-LINAC2026-THPO006

DEVELOPMENT OF HIGH-GRADIENT BOOSTER LINAC FOR MULTI-GeV PROTON RADIOGRAPHY AT LANSCE

S. S. Kurennoy, Y. K. Batygin, J. L. Schmidt, E. I. Simakov, H. Xu
Los Alamos National Laboratory, Los Alamos, NM, USA

Abstract

Increasing energy of proton beam at the Los Alamos Neutron Science Center (LANSCE) from 800 MeV to 3-5 GeV will improve radiography resolution tenfold. This energy boost can be achieved with a compact cost-effective linac based on normal conducting high-gradient (HG) RF accelerating structures operating at liquid nitrogen temperatures (cryo-cooled). Such an HG booster is feasible for proton radiography (pRad), which requires short beam pulses at very low duty. The pRad booster starts with a short L-band section to capture and compress the 800-MeV proton beam from the existing linac. The main HG linac will be based on S- and C-band cavities. An L-band debuncher at the booster end can reduce the beam energy spread if needed for pRad experiments. We are developing proton cryo-cooled HG standing-wave structures with distributed RF coupling for the booster. Prototype cavity structures at S- and C-band are designed and will be tested cryo-cooled to measure breakdowns at high gradients. The booster linac beam dynamics design options and preliminary proton radiography simulations will also be presented.

INTRODUCTION

Proton radiography (pRad) was invented at LANL in the 1990s. It employs high-energy proton beams to image material behavior under extreme conditions. Since then, the pRad program at the Los Alamos Neutron Science Center (LANSCE) has performed hundreds of successful experiments, both static and dynamic. The LANSCE pRad now uses 800-MeV H^- beam. For dynamic experiments, multiple pulses from the linac produce movies up to a few tens of frames. Each short pRad imaging pulse consists of several successive linac bunches, which follow at the linac bunch repetition rate of 201.25 MHz, to increase the imaging pulse intensity. This is because the H^- bunch current at 800 MeV is limited to ~10 mA, mainly by the ion source but also by losses in the linac. On the other hand, the pRad pulses are restricted to 80 ns in length, i.e., contain no more than 16 linac bunches following at the 201.25-MHz frequency, to prevent image blur, e.g., see Ref. [1, 2].

Increasing the beam energy for pRad at LANSCE from present 800 MeV to 3-5 GeV would provide significant improvements: for thin objects, the radiography resolution will increase about 10 times, and much thicker objects can be also imaged [2]. We aim to develop the most efficient way to provide proton beams at energies of 3-5 GeV for enhanced proton radiography at LANSCE. A high-gradient (HG) proton booster linac after the existing LANSCE linac offers a viable cost-efficient solution [3]. Its potential location is shown in Fig. 1; the booster (red line) will be much shorter than the 800-m-long existing linac. The booster linac will be based on normal-conducting RF accelerating structures operating cryo-cooled at liquid-nitrogen (LN2) temperature, 77 K, at very low duty required for pRad.

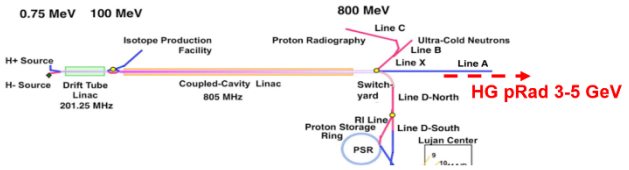


Figure 1: Location of the pRad booster linac (red dashed line) at LANSCE. The existing linac is on the left.

The Laboratory Directed Research and Development (LDRD) program at LANL supported our work on the HG pRad booster as an Exploratory Research (ER) project in 2021–2023. The ER results were presented in [3-5] and summarized in [6]. A larger LDRD Directed Research (DR) project started in Oct. 2025 with the main goal to develop accelerator technology of cryo-cooled HG structures for protons applicable to the pRad booster at LANSCE.

HIGH-GRADIENT PRAD BOOSTER

Requirements for pRad Booster

High-gradient structures for relativistic electrons with velocity $\beta = v/c = 1$ demonstrated accelerating gradients $E_{acc} = E_0 T$ up to 150 MV/m in X-band copper cavities at room temperature [7]. Here E_0 means the average on-axis electric field in the structure cell and T is transit-time factor. When such cavities are operated at cryogenic temperatures (cryo-cooled), gradients up to 250 MV/m were achieved. HG C-band cavities at room temperature provide gradients 50–60 MV/m, but at LN2 temperature one can expect gradients two times higher. 800-MeV protons at the exit of the LANSCE linac have velocity $\beta = 0.84$; at 5 GeV $\beta = 0.987$. Therefore, HG cavities must be modified for protons to cover this velocity range. HG structures for pRad booster must accept the large proton bunches out of the existing linac both longitudinally – this limits RF frequency from above – and transversely, which limits the cavity aperture from below. High accelerating gradients lead to beam defocusing by RF fields, so strong focusing is required. For good quality radiographs, it is important to control the relative momentum spread of the beam. It is $\Delta p/p = 10^{-3}$ at the exit of our 800-MeV linac, and in [3] the beam dynamics design reduced it as $1/p$, i.e., to $3.3 \cdot 10^{-4}$ at 3 GeV. However, it depends on specific pRad experiment whether such a reduction is needed [2].

Operating the HG pRad booster at 77 K makes structures more efficient and reduces the required RF power by a factor of 2-3. In addition, it is expected that the RF breakdown rates are reduced in cryo-cooled cavities, though the data

Content from this work may be used under the terms of the CC BY 4.0 licence (© 2026). Any distribution of this work must maintain attribution to the author(s), title of the work, publisher, and DOI.

ISBN: 978-3-95450-275-2 ISSN: 2226-0366 doi: 10.18429/JACoW-LINAC2026-THPO007

ADDITIVELY MANUFACTURED 4-ROD RFQ STRUCTURES WITH GYROID-BASED COOLING

J. Storch*,[1], E. Boos[2], P. Braun[1], K. Kuempel[1], H. Podlech[1,3]
[1]Institute of Applied Physics (IAP), Frankfurt, Germany
[2]GSI Helmholtz Centre for Heavy Ion Research, Darmstadt, Germany
[3]Helmholtz Research Academy Hesse for Fair (HFHF), GSI Helmholtzzentrum für Schwerionenforschung, Campus Frankfurt, Frankfurt, Germany

Abstract

Additive manufacturing (AM) offers new possibilities for the design and fabrication of radio-frequency quadrupoles (RFQs), in particular internal geometries that conventional machining cannot realize. In this work, the application of AM to 4-rod RFQ structures made from pure copper and copper alloys is investigated. A key focus is the integration of gyroid-based lattice structures within the cooling channels to enhance heat transfer and improve thermal stability under high RF load. A 4-stem RFQ prototype is designed and manufactured to evaluate the feasibility of this approach. The primary goals are to assess the potential for stable continuous-wave (CW) operation, the achievable increase in power handling capability compared to conventionally manufactured RFQs, and the reduction in manufacturing cost enabled by AM.

INTRODUCTION

The Institute of Applied Physics (IAP) at Goethe University Frankfurt has been developing 4-rod RFQs for hadron acceleration for many years. Demand has grown in particular for accelerator-driven neutron sources, which are gaining importance after the shutdown of several European research reactors. They call for high beam currents, high duty factors and, above all, long-term operational stability.

The limiting factor of the established 4-rod design is not the RF design but the removal of the dissipated power from the stems and tuning plates. The design power of the RFQs currently in operation at FRANZ and MYRRHA is below 30 kW/m. High-power tests of a shortened 4-stem 176.1 MHz prototype of this design have shown operational instabilities caused by thermal detuning above 75 kW/m, and thermal damage occurred at 150 kW/m [1]. Raising the admissible power density is the most direct way to shorten future RFQs, which offers beam dynamics advantages and reduces cost.

Conventional cooling channels are machined from the outside: deep bores need straight tool access and must be welded shut again, milled grooves have to be closed afterwards, typically by thick-film copper plating. Either way the routing is dictated by what a tool can reach rather than by where the RF losses occur, which leaves a considerable thickness of copper between the hottest surfaces and the coolant. Laser powder bed fusion (L-PBF) removes this constraint: the channel may follow the surface it is meant to cool, and its interior may be filled with a structure optimized for heat transfer rather than for manufacturability. That conventional 4-stem prototype is the baseline of this work: it is being upgraded component by component with additively manufactured parts, so the gain can be measured on one and the same machine.

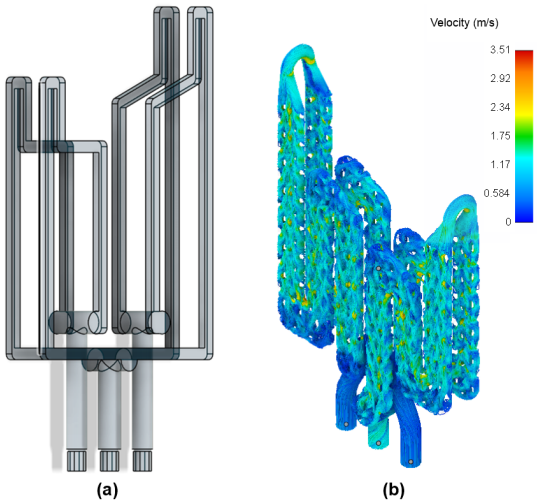


Figure 1: Coolant volume of a single stem: (a) conventional design with machined channels, (b) simulated coolant velocity in the gyroid-filled channel of the printed stem.

The material basis was established in a preceding study [2]. The conductivity of untreated, as-printed oxygen-free high-conductivity (OFHC) copper matches conventional ETP copper if the print parameters are suitable, so no plating of the RF surfaces is required. Erosion corrosion is negligible: after 3500 h of exposure the material loss stayed below 2 µm at a turbulent kinetic energy of 7.3 $m^2\,s^{-2}$, a level printed copper tolerates long-term. A CuNiCrZr alloy was characterized in the same context but is not used here.

GYROID COOLING STRUCTURE

The gyroid is a triply periodic minimal surface (TPMS) first described by Schoen [3]. It divides space into two interpenetrating, non-intersecting channel systems and has zero mean curvature everywhere. The properties exploited below are partly generic to TPMS and partly specific to the gyroid.

Printability (gyroid) The gyroid is self-supporting: its inclination never exceeds the critical overhang angle, so it

* storch@iap.uni-frankfurt.de

Content from this work may be used under the terms of the CC BY 4.0 licence (© 2026). Any distribution of this work must maintain attribution to the author(s), title of the work, publisher, and DOI.

ISBN: 978-3-95450-275-2 ISSN: 2226-0366 doi: 10.18429/JACoW-LINAC2026-THPO008

POWER EFFICIENCY ESTIMATION FOR A HIGH INTENSITY PROTON LINAC

R. E. Laxdal,
TRIUMF, Vancouver, BC, Canada

Content from this work may be used under the terms of the CC BY 4.0 licence (© 2026). Any distribution of this work must maintain attribution to the author(s), title of the work, publisher, and DOI.

Abstract

The Accelerator community needs to evolve to more efficient technologies and support R&D to reduce total energy consumption. This requires a change in culture - we need to focus on energy efficiency with the same priority as achieving higher performance. Linac installations for Accelerator Driven Systems (ADS) will be powered by the nuclear energy they produce with the surplus power going to the grid. In this case power efficiency is a key parameter in the design. Power usage can be impacted by various factors including temperature of operation and rf surface resistance. This paper presents modeling exercise to motivate future R&D towards improving power efficiency and in particular focused on linacs used to drive ADS.

INTRODUCTION

Carbon accumulation and global warming pose an existential threat. High energy physics accelerators will undergo more and more scrutiny as energy becomes a more limited commodity. New projects will be judged on their energy efficiency.

Accelerators offer a potential for producing electricity and reducing carbon accumulation through Accelerator Driven Systems (ADS). ADS (Fig. 1) allows the reactor to operate sub-critically for safer operation with a portion of the energy used to power the linac while the remainder of the power would be supplied to the grid.

The economics of such a facility requires a baseline electrical efficiency. Cyclotrons offer an efficiency of near 20% for currents up to a few mA [1]. SRF linacs offer higher intensities and higher electrical efficiencies. This paper examines the critical R&D challenges required to increase the efficiency of high intensity cw proton linacs using ADS linacs as a model.

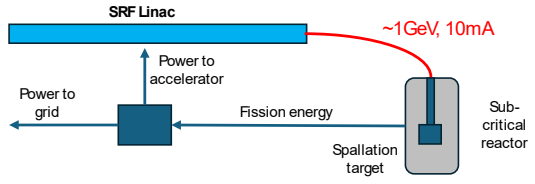


Figure 1: Schematic layout of an ADS power plant.

ELECTRICAL EFFICIENCY

The efficiency of acceleration is given by:

$$\eta_{accel} = P_{beam}/P_{wall} = P_{beam}/PW$$

with major consumption coming from RF and cryogenic dynamic loads as

$$\eta_{accel} = \frac{P_{beam}}{PW_{rf} + PW_{cr-dyn} + PW_{cr-stat} + PW_{other}}$$

The wall plug power required to produce rf power is given by

$$PW_{rf} = P_{gen}\, C_{rf}/\eta_{rf}.$$

Here, η_{rf} is the wall plug to rf power conversion efficiency and C_{rf} is a factor that allows for mismatch and performance compensation of one cavity to another. A good match for the modularity of the SRF linac is SSAs where $\eta_{rf} = 0.5$ is typically quoted and we choose $C_{rf} = 1.3$.

Wall power losses for cryogenic heat removal are calculated using

$$\mathrm{COP(T)} = \frac{1}{\eta_c(T)\eta_m(T)} = \frac{300-T}{T}\frac{1}{\eta_m(T)}.$$

Here $\eta_c(T)$ is the Carnot efficiency and $\eta_m(T)$ is a mechanical efficiency that estimates how close to Carnot we can get with a realizable machine. Table 1 gives typically quoted values for the mechanical efficiency [2] as well as the calculated Carnot efficiency. For the estimated wall plug power a further factor of C_{cryo}=1.3 is used as an overhead contingency. Note that operating at 2K requires about three times more wall power than operating at 4.4K for every 1 W removed from the system.

Table 1: Wall Power Factors for Cryogenic Loads

T (K)	η_c	η_m*	$COP(T)$	$COP(T)C_{cryo}$
2	6.71e-3	0.2	745	969
4.4	1.49e-2	0.28	240	312
5	1.69e-2	0.28	211	274
60	2.5e-2	0.17	23.5	30.6

LINAC ARCHITECTURE

A cw linac typically utilizes SRF technology starting from the RFQ exit (W_{in} from 2 MeV to 2.5 MeV) and rf frequencies of ~162 MHz to match the frequency of the first SRF cavity. Typically, five cavity types are used to accelerate the protons to ~1 GeV (Fig. 2).

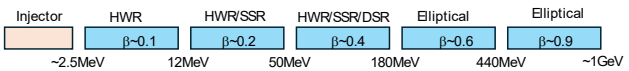


Figure 2: Typical layout of a high power 1 GeV p-linac.

TEM mode cavities of 2-3 gaps are used for β<0.5 and elliptical cavities are used for β>0.5. For the two gap structures the cavity geometry is chosen such that the entrance transit time factor is larger than 0.5 and the same cavity type is used to a velocity of ~1.1 x β_{opt}. Such an approach gives a lower average TTF but a longer cavity that increases V_c. The two gap cavities have a broad velocity acceptance such that the exit velocity of a section is ~2x the injection velocity. Three gap cavities can be used for the third variant with a range of $\beta_{out}/\beta_{in} \leq 1.67$. The last two

ISBN: 978-3-95450-275-2 ISSN: 2226-0366 doi: 10.18429/JACoW-LINAC2026-THPO009

EXPERIENCE WITH A PULSED GAS STRIPPER FROM FIRST USER BEAM TIMES AT GSI

P. Gerhard*, L. Groening, M. Maier
GSI Helmholtzzentrum für Schwerionenforschung GmbH, Darmstadt, Germany

Content from this work may be used under the terms of the CC BY 4.0 licence (© 2026). Any distribution of this work must maintain attribution to the author(s), title of the work, publisher, and DOI.

Abstract

Stripping heavy ions like ^{238}U at 1.4 MeV/u using N_2 as stripping target results in a broad charge state spectrum. This can be narrowed significantly by applying H_2, increasing the yield of the main charge state by up to ~50 %. Pulsed injection into a dedicated interaction chamber is needed to reduce the gas load of the pumping system to an acceptable level, while H_2 also introduces significant safety issues. A prototype setup was constructed, improved and has been operated at GSI UNILAC for one year in total during the user beam times 2024 and 2025. A number of ion species has been operated and a considerable amount of data on stripping efficiencies have been measured. Challenges related to establishing regular user operation with such a setup, some results obtained, and lessons learned are reported.

INTRODUCTION

The GSI accelerator facility serves as injector for the upcoming Facility for Antiproton and Ion Research (FAIR). High intensity ion beams are provided by dedicated high current sources and pre-accelerated to 1.4 MeV/u via the high current injector (HSI) at low charge states. The HSI is designed for ions with a high mass-to-charge-ratio of up to 65 [1]. Subsequently, a gas stripper is used to increase the charge state to $A/q \leq 8.5$, enabling acceleration in the subsequent Alvarez linac. Until now, a continuous N_2 gas jet was used as stripping target. Out of the charge states produced, one has to be separated for further acceleration, leading to losses of up to ~87 % for heavy ions like U.

In order to increase the yield into the desired charge state, hydrogen and other gases as stripping targets were investigated [2]. With H_2, the width of the charge state distribution of heavy ions is significantly reduced and the yield increased accordingly, e. g. by approximately 50 % for $^{238}U^{28+}$. Additionally, an increase of the mean charge state can be achieved for all ions. Since H_2 is much more difficult to pump than N_2, in order to implement operation with hydrogen the gas load had to be reduced first. Exploiting the low duty factor of the high current beams, this was achieved by delivering only short gas pulses synchronized with the beam. Pulsing of the gas target was established through commercially available, fast injection valves. This step was essential to successfully demonstrate the proof-of-principle in 2016 [3–5]. The second major challenge of H_2 in order to establish regular operation is its high combustibility. A comprehensive, protracted risk assessment had to be conducted, resulting in the requirement of several safety measures to be implemented. A complex, fully automated gas stripper facility suitable for safe regular operation, able to deliver pulses of both H_2 and N_2 at different target densities synchronized with different ion beams was devised and is being implemented [6–8].

In late 2023, it was decided to put the pulsed stripper into regular operation for the upcoming user beam time, far ahead of schedule but with N_2 only due to the still incomplete safety measures. Several improvements were quickly implemented to improve operation of the developmental setup.

SETUP AND UPGRADE FOR OPERATION

The first pulsed stripper was based on a very fast, direct high-pressure liquid fuel injection valve. It quickly turned out that these valves would break down after only a few hours of operation with gases [6]. Consequently, the valve type was changed, leading to the currently used second generation pulsed stripper [7], which was designed to contain two low-pressure gas injection valves (Fig. 1). The preliminary gas control setup allows for providing H_2 and N_2 to the valves and controlling the pressure of the gases and thereby the target density [9]. Stripping with N_2 required gas pressures well below 1 bar(a) for light and intermediate ions. To improve operation at such low pressures, two mechanical low-pressure regulators were added in preparation of the first beam time [9, Fig. 2], among other improvements. Additionally, each gas line is equipped with a safety cut-off valve controlled by a simple interlock system providing explosion safety for experimental short-term H_2 operation as well as machine safety during long-term unattended operation with N_2. Manual valves, flow meters and pressure gauges allow for gas setup, monitoring and fault detection.

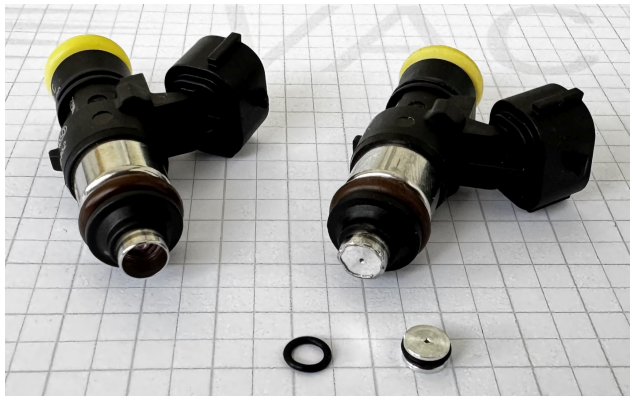


Figure 1: Low-pressure gas injection valves. Left: genuine valve. Right: modified valve with orifice of 0.6 mm diameter in the outlet tube. Front: O-ring and orifice with O-ring mounted.

The gas stripper vacuum system was improved by installing a new, explosion safe roots pump station and re-

* p.gerhard@gsi.de

ISBN: 978-3-95450-275-2 ISSN: 2226-0366 doi: 10.18429/JACoW-LINAC2026-THPO010

4D TRANSVERSE COUPLING MEASUREMENTS OF AN 18 MeV PHOTO-INJECTOR ELECTRON BEAM AT PITZ

C. Richard*, N. Aftab, Z. Amirkhanyan, A. Aksoy, J. Good, M. Gross, M. Krasilnikov, X.-K. Li, A. Oppelt, S. Pakluea, F. Stephan, G. Vashchenko, D. Xu, S. Zeeshan
Deutsches Elektronen-Synchrotron DESY, Zeuthen, Germany

Abstract

At the Photo-Injector Test facility at DESY in Zeuthen (PITZ), the horizontal and vertical phase spaces of electron beams are measured to characterize the performance of L-band photo-electron sources. These measurements are taken using the slit-screen method located 5.27 m downstream of the photo-cathode after acceleration to 18 MeV by a 14-cell booster cavity. The beamlet images from x and y plane slit scans can then be combined using a Virtual Pepper Pot (VPP) to reconstruct the full 4D transverse phase space. This technique has enabled detailed characterization of the x-y coupling originating from the electron source. Notably, the VPP analysis shows the x-y coupling is not uniform across the entire beam, instead one corner is significantly more coupled than the rest of the beam. While the cause of this effect is still under investigation, it can be reduced using a skew quadrupole near the exit of the gun.

INTRODUCTION

It is common practice in accelerator physics to separate the transverse dynamics in x and y into two uncorrelated 2D phase spaces. Beamlines are often designed with this decoupling to simplify the beam dynamics and ease transport and matching. Because of this, transverse phase space diagnostics often only measure the two planes separately. However, even in beamlines designed to have no x-y coupling, this coupling can still arise due to imperfections and asymmetries in the beamline components. This coupling increases the 2D emittances and can complicate beam transport that is not designed to handle such beams. It is therefore important to characterize the $x-y$ coupling of the transverse phase space even in beamlines that should not be coupled.

Emittance Measurements

The transverse phase spaces of a 18 MeV, 250 pC beam were measured at the Photo-Injector Test facility at DESY in Zeuthen (PITZ) as part of characterization of 1.3 GHz RF photo-guns which will be used at EuXFEL and FLASH [1,2]. These emittance were taken after the booster at the location labeled 'Slit 1' in Fig. 1 to optimize the emittance compensation scheme [3] of the booster and a solenoid around the photo-gun.

At PITZ, the transverse emittance is measured using a slit-screen method [2]. This is performed by scanning a 50 µm slit across the beam. At each slit position the passed beamlet's profile is measured on a YAG screen 3.133 m from the slit. The projection of this beamlet profile gives the angular profile of the beam at the location of the slit. With profiles measured at each slit position, the 2D phase space can be reconstructed.

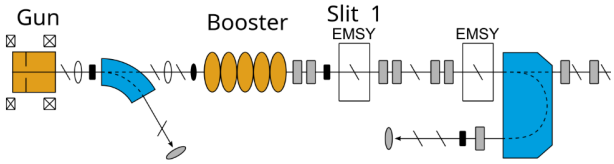


Figure 1: Layout of PITZ. 'Slit 1' is used for emittance measurements.

The 2D x and y phase spaces are measured separately as the x and y slits cannot be inserted simultaneously without collision. To reconstruct the full 4D phase space, the beamlet images of a pair of x and y scans are reprocessed using a Virtual Pepper Pot (VPP) [4]. This method virtually crosses the two slits by overlapping an x and y beamlet image and isolating the common area creating a virtual pepper pot beamlet. This is repeated for all pairs of x and y beamlet images and then the x' and y' values of each VPP beamlet can be calculated and the 4D phase space is reconstructed.

CHARACTERIZING 4D COUPLING

Visualizing Coupling

As the x and y coordinates of the 4D phase space are forced on an immutable, upright grid by the positions of the slits, it is difficult to visualize the coupling in the $x-y$ projection without analysis of the intensity profile. It is, however, easier to see the effects of coupling in the $x-x'$ and $y-y'$ phase spaces. For an uncoupled beam, the central y' at a given y is independent on x and, therefore, in the 4D phase space all y's at a given y will be the same. The resulting $y-y'$ projection must therefore be a thin line. This behavior is seen in top row of Fig. 2 where the VPP analysis is applied to a simulated, uncoupled beam. In addition, for an uncoupled beam, because the y' coordinates are linearly dependent on y and the y coordinates lay on a grid, the y' coordinates also lay on a grid. The same is also true for x' and the $x'-y'$ projection must have beamlets on a grid as seen in the top right of Fig. 2.

For beams with 4D coupling, the coupling can be easily seen by any deviation for this expected behavior of uncoupled beams. I.e. the $x-x'$ or $y-y'$ projections are not lines, but have some thickness and the $x'-y'$ projection does not have points on a upright grid.

* christopher.richard@desy.de

Content from this work may be used under the terms of the CC BY 4.0 licence (© 2026). Any distribution of this work must maintain attribution to the author(s), title of the work, publisher, and DOI.

ISBN: 978-3-95450-275-2 ISSN: 2226-0366 doi: 10.18429/JACoW-LINAC2026-THPO012

DESIGN OF SR KICKER POWER SUPPLIES FOR KICKER MAGNETS AT KLS*

S. H. Kim†,1, C. -K. Min[1], J. Lee[1], W. J. Byeon[1], S. Shin[2]
[1]Pohang Accelerator Laboratory, POSTECH, Pohang, Republic of Korea
[2]Korea Basic Science Institute, Ochang, Korea,

Content from this work may be used under the terms of the CC BY 4.0 licence (© 2026). Any distribution of this work must maintain attribution to the author(s), title of the work, publisher, and DOI.

Abstract

Prototype kicker power supplies have been designed for the storage ring beam injection of the Korea Light Source (KLS, formerly Korea-4GSR). These power supplies drive four kicker magnets to maintain field balance and synchronized beam deflection. The pulsed magnetic fields must be synchronized within a timing jitter of 5 ns and an amplitude difference of ± 0.2 %. To fulfil these requirements, a pulse-shape matching mechanism and a parallel driver configuration-where one power supply handles two kicker magnets-will be implemented to reduce kick fluctuations and trajectory offsets. The kicker power supply specifications include a pulse width of 5 μs, a 200 ns flat-top width, a half-sinusoidal waveform with a peak current of 7 kA, and a 2 Hz repetition rate. This paper discusses the circuit configuration and design methodology applied to the power supply.

INTRODUCTION

The KLS (formerly Korea-4GSR) has finalized its lattice design and established the relevant physics parameters [1]. The acceleration chain consists of a 200 MeV linac, a 2 Hz full-energy booster synchrotron, and a 4 GeV storage ring with a 799 m circumference. The storage ring (SR) kicker waveform is a half-sine pulse with a width equivalent to approximately two turns of the storage ring revolution. To achieve high injection efficiency, it is desirable for the kicker magnet current to dissipate after approximately 5 μs, given that one revolution time is 2.6 μs.

To ensure precise shape-matching of the half-sine pulses and maintain an amplitude difference within ± 0.2 %, the following design strategies were adopted:

- Parallel Driving: Controlling two kicker magnets with a single power supply.
- High Precision Charging: Utilizing a Capacitor Charging Power Supply (CCPS) with a voltage regulation accuracy of less than 50 ppm.
- Fine Tuning: Implementing a variable inductor in series with the kicker magnet for precise current pulse-shape matching.

PULSE MODULATOR FOR SR KICKER MAGNETS

Kicker Power Supply Circuit

A schematic circuit diagram of the kicker magnet power supply is shown in Fig. 1. The power supply generates half-sinusoidal pulse magnetic field to launch the bump orbit for the beam injection. Major components include a high voltage power supply, thyratrons, charging capacitors, protection devices, and pulse-shape matching mechanism. As shown in Fig. 1, one CCPS as a parallel driver is employed to charge same energy to both main charging capacitors. Using a common pulse generator as a parallel driver brings lots of benefits such as synchronized and canceled-out fluctuations of the kick [2].

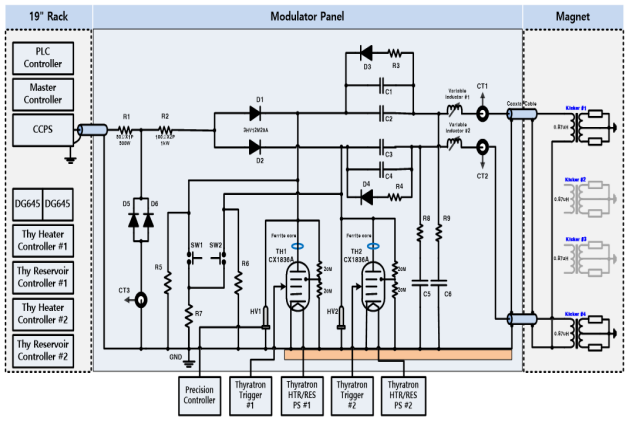


Figure 1: Circuit diagram of kicker power supply.

Major Parameters of SR Kicker Power Supply

Four kickers are used for injection into the storage ring. Kicker 1, 4 should kick 4 GeV electron beam 3.178 mrad, while kicker 2, 3 should kick the beam 2.513 mrad. Because of the requirement for an identical bump field for the 4 kickers, the pulse current difference between these 4 kickers need to be less than ±0.2%. Table 1 shows the summarized key parameters of the kicker power supply.

ENGINEERING DESIGN

The injection kicker power supply is a series resonant circuit. The current shape can be generated by using it. However, high power switches and energy storage capacitors should be carefully selected to withstand any transient and inverse voltage that could be generated during a sudden interruption of current after half period of resonance. Therefore, considering all these issues is an important part of the engineering design.

Stability of the CCPS

The factors to cause differences of field strength among the magnets due to power supplies are current stability of pulse to pulse and the switching jitters. The current stability is dependent on not only power supply but also the magnet and transmission cables. However, the current stability

* Work supported in part by the Korean Government MSIT(Multipurpose Synchrotron Radiation Construction Project).
† ksangh@postech.ac.kr

ISBN: 978-3-95450-275-2 ISSN: 2226-0366 doi: 10.18429/JACoW-LINAC2026-THPO013

USING STRETCHING-MODULATION-COMPRESSION EFFECT TO GENERATE FEMTOSECOND MeV ELECTRON BUNCHES*

Q. Luo, J. Li, C.-Y. Tsai†
Huazhong University of Science and Technology, Wuhan, China

Abstract

We propose a scheme for generating femtosecond to sub-femtosecond ultrafast electron bunches by combining undulator technology with terahertz (THz) modulation. A theoretical model has been developed to describe the transport dynamics of relativistic electrons interacting with THz modulation fields and space charge effects within the bunch. The proposed scheme successfully produces isolated ultrafast electron bunches with kinetic energy 3 MeV, bunch length about 9 fs (rms), and charge about 8 fC. By adjusting upstream and downstream longitudinal dispersion, the bunch structure and microbunch length can be effectively controlled. We provide scaling relations for key parameters with respect to initial bunch charge and analyze the influence of various physical quantities on final bunch length and arrival time. This theoretical model and scheme may offer valuable insights for generating few-femtosecond or attosecond electron bunches in accelerator-based ultrafast facilities.

INTRODUCTION

The mechanism of our proposed scheme is conceptually similar to high-gain harmonic generation (HGHG) [1]; see Fig. 1. First, the chicane 1 is optionally used to stretch the bunch, then a local portion of the bunch is modulated, finally that local portion is compressed by the second chicane. Compared with other existing schemes, this scheme mitigates space charge effects at the cost of losing some particles in the head and tail portions of the bunch. Our proposed scheme shares the common feature of using external electromagnetic field and undulator to modulate the electron beam. The key difference is that this scheme is intended for the single-MeV energy regime relevant to ultrafast electron diffraction (UED) applications. At these low electron energies, space charge effects become important during beam transport, and such dynamics have not yet been studied in detail using currently available simulation tools. In this paper, as a continuation of our recent work published in Refs. [2–4], we focus on sensitivity or tolerance studies when the chicane and THz modulation field have possible errors.

THEORETICAL MODEL

Our proposed scheme includes two chicanes and one short undulator with THz modulation. ASTRA [5] simulates beam dynamics in the two chicanes, including 3D space charge effects. In the undulator we use a period-by-period tracking algorithm that includes both the external THz modulation and the simplified longitudinal and transverse space charge effects.

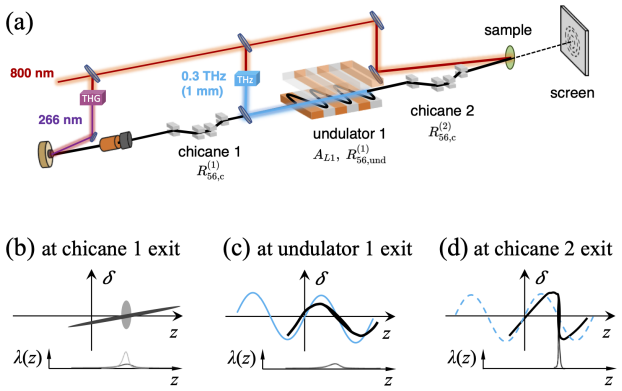


Figure 1: (a) Schematic layout of a MeV UED facility incorporating the bunch compression scheme proposed in this paper. In the figure, the 800-nm laser serves three purposes: exciting the sample, generating 266-nm UV laser through third-harmonic generation (THG) to strike the photocathode and produce photoelectrons, and generating the THz modulation wave. After acceleration by the RF cavity and focusing by the solenoid, the electron beam first passes through chicane 1 to be stretched, then modulated by the THz wave, and finally appropriately compressed in chicane 2 to achieve the possible minimum bunch length before probing the sample. (b), (c) and (d) show the bunch phase space distribution and line density at the exit of the chicane 1, the undulator 1, and the chicane 2, respectively. In the panel (b), the gray represents the initial phase space and line density distributions. The distance from the photocathode to chicane 1 is roughly 0.3 m, the length of chicane 1 itself is approximately 3.92 m, the undulator length is approximately 0.1 m and the length of chicane 2 is about 0.88 m.

Period-by-Period Tracking Equations

Assume the phase space coordinates $[x\ x'\ y\ y'\ z\ \delta]$, with x and x' the transverse horizontal position and divergence, y and y' the vertical counterparts, z the bunch coordinate ($z > 0$ for bunch head), and $\delta = (E - E_0)/E_0$ the energy deviation. To properly describe low-energy particle dynamics in the undulator, we follow the "1/2-drift-kick-1/2-drift" principle and construct the period-by-period tracking from the p-th to

* This work is supported by the Fundamental Research Funds for the Central Universities (HUST) under Project No. 2021GCRC006 and National Natural Science Foundation of China under Project No. 12275094.
† jcytsai@hust.edu.cn

Content from this work may be used under the terms of the CC BY 4.0 licence (© 2026). Any distribution of this work must maintain attribution to the author(s), title of the work, publisher, and DOI.

ISBN: 978-3-95450-275-2 ISSN: 2226-0366 doi: 10.18429/JACoW-LINAC2026-THPO015

DEVELOPMENT AND FIRST BEAM TESTS OF AN ELECTROSTATIC PRE-BUNCHER SYSTEM FOR INTENSE SHORT BEAM PULSES AT SARAF

I. Polikarpov[1,2,*], A. Shor[1], L. Weissman[1], A. Perry[1], B. Kaizer[1], R. Raz[1], T. Zchut[1], A. Nause[2]
[1]Soreq Nuclear Research Center, Yavne, Israel
[2]Department of Physics, Ariel University, Ariel, Israel

Abstract

We describe single bunch generation system based on a pre-buncher and chopper installed in the Low Energy Beam Transport section of the Soreq Applied Research Accelerator Facility. The pre-buncher is designed to longitudinally compress a relatively long segment of the DC beam to one radio frequency cycle at the entrance of the Radio Frequency Quadrupole element. In this report we describe the electrical and mechanical design and implementation of the pre-buncher unit, as well as beam dynamics simulations of the pre-buncher taking into consideration self-repulsion of the intense ion beam. Preliminary experimental results with intense proton beam is presented. These initial measurements demonstrate general validity of the system concept and highlight the importance of SC neutralization on quality of the obtained bunched beam.

INTRODUCTION

Longitudinal beam bunchers and choppers have been developed in accelerator laboratories that require intense short beam pulses for time-of-flight measurements. Large facilities such as SNS, SIS and SPIRAL II employ beam bunching and single-bunch selection techniques [1–3]. SARAF Phase II is a 176MHz superconducting LINAC, designed to deliver up to 5mA continuous-wave proton/deuteron beam at energies up to 40MeV [4]. The 4 meter long, 176 MHz, 4-rod Radio Frequency Quadrupole (RFQ) [5] is the first RF cavity of SARAF, which focuses and bunches the incoming 20keV/u DC beam, and accelerates the bunched beam to 1.3MeV/u.

The advantages of bunching and chopping in the Low Energy Beam Transport (LEBT) section are the utilization of relatively low voltages for the manipulation of low-energy beams and the use of low-power beam dump for beam interception. The main drawback is the stronger influence of the space-charge (SC) effects, which can significantly affect beam transport and bunching efficiency. The pre-buncher is designed to compress a selected section of the incident 20keV/u, 5mA proton or deuteron DC beam by applying a High-Voltage (HV) pulse of a specific time shape, so that it converges $13\beta\lambda$ onto a bunch length of $1\beta\lambda$, corresponding to a single RF cycle at the entrance of the RFQ. The RFQ will then further bunch and accelerate this $1\beta\lambda$ section [6], resulting in the emergence of a single-like RFQ bunch with enhanced bunch amplitude at 1.3MeV/u. The pre-buncher system is part of the series of technical developments in LEBT [7–9] based on fast HV switches that can be triggered on demand and thus enable the generation of intense and sharp particle pulses at an adjustable repetition rate.

In this report, we describe the electrical and mechanical design of the pre-buncher, including electrical field and beam dynamics simulations, fabrication, and optimization of the HV pulse. The results of the first online tests with 1mA proton beam are presented.

DESIGN AND IMPLEMENTATION

Pre-Buncher Concept and Design

The pre-buncher consists of two concentric cylindrical electrodes that form an electrostatic 2-gap structure (Fig. 1a). A fast negative high-voltage pulse is applied to the inner electrode while the outer electrode is held at the ground potential (Fig. 1b). The idea is to provide slight de-acceleration to the early particles and slight acceleration to the late-coming particles. This is achieved by an HV pulse with an appropriate linear rise in voltage and an equivalent linear fall, with a total pulse length equivalent to the transit time of the 20keV/u particle from the entrance to the exit HV gaps. The length of the rise-time plus fall-time determines the length of the DC beam to be compressed, in units of the RF-cycle, while the slope of the rise and fall of the HV pulse must be appropriately adjusted to provide convergence at the entrance to the RFQ.

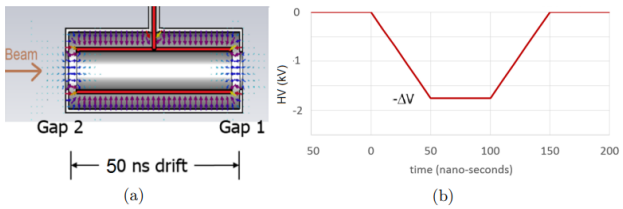


Figure 1: (**a**) Conceptual design of the pre-buncher showing E-field as calculated by the Superfish code. (**b**) A negative HV pulse shape for the optimum protons bunching.

The initial design of the configuration of the electrostatic pre-buncher was carried out using the SuperFish code [10]; it allowed us to optimize the preliminary electrode geometries by calculating the electric fields for a cylindrically symmetric system. Optimization of this design was the basis for a realistic mechanical design of the pre-buncher and the surrounding environment, which was exported to the CST program [11] for the realistic calculation of 3-dimensional electric field distributions (Fig. 2).

* ilyapo@soreq.gov.il

Content from this work may be used under the terms of the CC BY 4.0 licence (© 2026). Any distribution of this work must maintain attribution to the author(s), title of the work, publisher, and DOI.

ISBN: 978-3-95450-275-2 ISSN: 2226-0366 doi: 10.18429/JACoW-LINAC2026-THPO016

POLARIZED ION SOURCE DEVELOPMENTS FOR EIC AT BNL

D. Raparia[1], E. Beebe[1], A. Cannavo[1], C. Ianzano[2], J. Maxwell[3], R. Milner[2], A. Poblahguev[1], F. Rathmann[1], J. Ritter[1], D. Steski[1], A. Sukhanov[1], N. Wuerfel[2]
[1]Brookhaven National Laboratory, Upton, NY, USA
[2]Laboratory for Nuclear Science, Massachusetts Institute of Technology, Cambridge, MA, USA
[3]Thomas Jefferson National Accelerator Facility, Newport News, VA, USA

Abstract

The Optically Pumped Polarized H^- Ion Source (OPPIS) at Brookhaven National Laboratory has been upgraded to improve reliability and beam performance for the RHIC polarized proton program. During the final RHIC polarized proton run, the source routinely delivered a 425 μA polarized H^- beam with an average polarization of 82%, the highest average polarization achieved at this beam intensity. A redesigned rubidium (Rb) cell, together with optimized Rb injection and temperature control, improved source stability, while plasmatron and sodium (Na) jet ionizer upgrades increased component lifetime and reduced maintenance. Development of a high-intensity polarized $^3He^{++}$ source for the Electron-Ion Collider (EIC) has also progressed. The optical pumping system and polarized gas cell have been redesigned for integration with the 5 T EBIS solenoid. Polarization measurements of 65% have been achieved with the final open-cell configuration, while a sealed (closed) cell has demonstrated 77% polarization. Conceptual studies of a polarized deuterium (D^-) ion source are underway to extend the EIC polarized light-ion program.

INTRODUCTION

The Relativistic Heavy Ion Collider (RHIC) was the only collider capable of accelerating and colliding polarized proton beams, routinely delivering beam polarizations of about 60% [1]. The future Electron-Ion Collider (EIC) will extend this capability to polarized electron-ion collisions, including polarized $^3He^{++}$ beams [2]. Polarized protons for RHIC were produced using the Optically Pumped Polarized H^- Ion Source (OPPIS) [3], which routinely delivered 0.5–1.0 mA (up to 1.6 mA) in 350–400 μs pulses with 80–85% polarization. Following acceleration in the 200 MeV Linac, Booster, and AGS, Siberian Snakes preserved the beam polarization during acceleration and delivery to RHIC.

The EIC requires a polarized $^3He^{++}$ source capable of delivering approximately 2.5×10^{11} ions in a 20 μs pulse, corresponding to a peak current of about 2 mA, nearly three orders of magnitude higher than previously demonstrated. The proposed source is based on the Brookhaven Electron Beam Ion Source (EBIS) [4], where ^3He gas polarized by Metastability Exchange Optical Pumping (MEOP) in a 5 T solenoid is injected into EBIS and ionized by a 10 A electron beam. The design goal is to produce 2.5×10^{11} $^3He^{++}$ ions per pulse with about 70% polarization for acceleration by the RFQ and IH linac prior to Booster injection.

Conceptual studies of a polarized deuterium (D^-) ion source have also begun to extend the EIC polarized light-ion program. The proposed source, based on the former COSY polarized deuterium source [5], would be installed at the BNL Tandem Van de Graaff facility to provide a platform for source commissioning, polarization measurements, and future EIC injector studies.

OPPIS

The Optically Pumped Polarized H^- Ion Source (OPPIS) employs five principal subsystems: the Fast Atomic Beam Source (FABS), helium (He) cell, rubidium (Rb) cell, Sona transition region, and sodium (Na) jet ionizer/extraction system [6, 7]. The He and Rb cells operate within the 3 T field of a superconducting solenoid (Fig. 1).

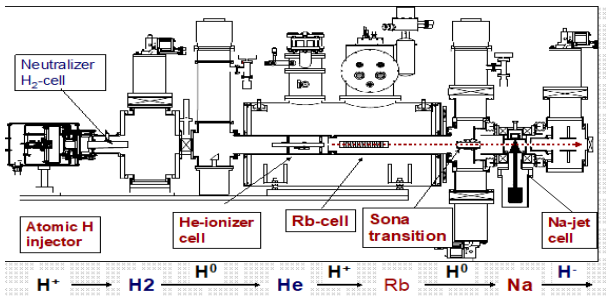


Figure 1: Layout of the OPPIS.

The FABS plasmatron cathode was redesigned by incorporating a smaller nozzle and increasing the outer rim thickness to 3.2 mm. The improved nozzle geometry provides better gas flow into the discharge channel and produces a more uniform cathode wear pattern, eliminating the blistering and clustering observed with the previous design. As a result, cathode lifetime increased from approximately 2 months to 12 months of continuous operation without failure. A new Rb cell was introduced for Run-25 to improve Rb vapor confinement and temperature uniformity. The redesigned reservoir and vapor distribution system significantly reduced Rb consumption while improving source stability. Continued optimization of Rb injection and cell temperature contributed to the improved beam polarization and operational reliability. Collectively, these upgrades significantly improved source reliability, reduced maintenance requirements, and enabled stable high-current operation throughout the final RHIC polarized proton run.

The upgraded OPPIS successfully supported the final RHIC polarized proton run. The source routinely delivered a 425 μA polarized H^- beam, fully satisfying Booster injection requirements during six months of uninterrupted

Content from this work may be used under the terms of the CC BY 4.0 licence (© 2026). Any distribution of this work must maintain attribution to the author(s), title of the work, publisher, and DOI.

ISBN: 978-3-95450-275-2 ISSN: 2226-0366 doi: 10.18429/JACoW-LINAC2026-THPO019

INVESTIGATION OF THE OPERATIONAL ASPECTS OF FERROELECTRIC FAST REACTIVE TUNERS (FE-FRTs)

M. Dissanayake[1,*], G. Burt[1], H. Jiang[1], Lancaster University, Lancaster, UK
A. Wheelhouse[1], ASTeC, STFC Daresbury Laboratory, Warrington, UK
I. Ben-Zvi, Stony Brook University, Stony Brook, NY, USA
[1]also at The Cockcroft Institute, Sci-Tech Campus Daresbury, Warrington, UK

Content from this work may be used under the terms of the CC BY 4.0 licence (© 2026). Any distribution of this work must maintain attribution to the author(s), title of the work, publisher, and DOI.

Abstract

Integrating ferroelectric fast reactive tuners (FE-FRTs) into SRF cavities offers a promising route to mitigate microphonics in LINAC cavities. This work reports the design and characterization of an FE-FRT coupled to a 1.3 GHz two-cell cavity, supported by 3D CST simulations and an extended lumped element circuit model. This extended model improves upon conventional frameworks by directly incorporating the FPC, alongside a lossy, arbitrary-length transmission line that accounts for both electric (probe) and magnetic (loop) coupling to accurately derive FPC specifications and RF power requirements, including power loss estimates to identify optimal working points. By appropriate resonant frequency choice, monopole higher-order modes (HOMs) in the tuner can be kept away from harmonics of the fundamental mode; however, the permittivity variation in the FE wafers during operation could shift a monopole HOM close to the third harmonic at 3.9 GHz, potentially affecting the stable operating range. In our example design, the two observed monopole HOMs exhibited fields mainly on the sapphire ring rather than on the FE wafers, thereby strongly reducing direct excitation by the fundamental field and mitigating associated risks for LINAC operation.

INTRODUCTION

SRF cavities, with their high intrinsic quality factors, typically suffer from resonance frequency shifts due to mechanical vibrations in the environment, known as microphonics. Traditional mechanical tuners respond too slowly to these rapid frequency shifts and apply physical stress that can damage brittle superconducting films, such as Nb_3Sn. FE-FRTs overcome these limitations by utilizing variable reactance rather than physical deformation to achieve fast frequency adjustments [1]. This approach protects fragile thin-film coatings while significantly reducing the accelerator's overall RF power demands [2, 3].

In this work, we evaluate the system's operational dynamics using an extended equivalent lumped element circuit model. This model advances standard frameworks [4] by explicitly incorporating the FPC and employing an arbitrary-length, lossy transmission line that models both probe (electric) and loop (magnetic) coupling. Applying this comprehensive model, we optimize the FPC coupling and determine the RF power requirements as the ferroelectric (FE) material's permittivity varies across its operational range. Separately, using a reduced model, we evaluate the potential operational risks posed by monopole HOMs within the FE-FRT concerning harmonic generation.

* maleesh.d.m@cockcroft.ac.uk

DESIGN

In this section, we detail the operational parameters of the studied system and its extended equivalent circuit model. We also introduce the geometry of the optimized CST model for the sample FRT.

Operational Parameters and the CST Model of the Sample FRT

Table 1 summarizes the key operational parameters, providing an overview of the values used in our study. Figure 1 shows the CST model [5] of the sample FRT used.

Table 1: Operational and other parameters selected in this study. Note: R/Q value follows the LINAC notation.

Parameter	Symbol	Value
Frequency	f_0	1.3 GHz
Max. microphonics level	Δf_{max}	$\pm$30 Hz
Max. tuning range	Δf	60 Hz
R/Q (from CST simulations)	R/Q	239 Ω
Cavity length	L_{cavity}	0.5 m
Accelerating gradient	E_{acc}	10 MV/m
Stored energy	U_c	12.80 J
Transmission line length	l	0.63 m

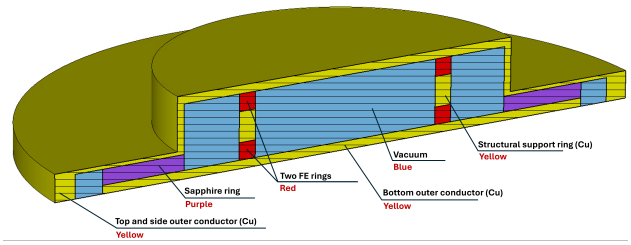


Figure 1: Cross-sectional view of the CST model of the sample FRT. The dimensions were specifically optimized to improve the Figure of Merit (FOM); the details of this optimization process are discussed in a separate study [6].

The Extended Equivalent Circuit Model of the System

Figure 2 illustrates the extended equivalent lumped element circuit model for our system. Moving from left to right,

ISBN: 978-3-95450-275-2 ISSN: 2226-0366 doi: 10.18429/JACoW-LINAC2026-THPO020

ESS ION SOURCE AND LEBT TEST STAND

E. Trachanas*, M. Koopmans† R. Baron, H. Danared, E. Donegani, A. Gevorgyan, S. Haghtalab
H. Hassanzadegan, H. Ligander, K. Mårtensson, R. Miyamoto, D. Nicosia, D. Noll, L. Page
P. Pierini, S. Sandilands, P. van Velze, European Spallation Source, Lund, Sweden

Content from this work may be used under the terms of the CC BY 4.0 licence (© 2026). Any distribution of this work must maintain attribution to the author(s), title of the work, publisher, and DOI.

Abstract

The front-end of the European Spallation Source (ESS), comprising the ion source, low energy beam transport (LEBT), radio frequency quadrupole (RFQ), and medium energy beam transport will deliver a 62.5 mA proton beam in 2.86 ms pulses at a repetition rate of 14 Hz at 3.62 MeV beam energy for further acceleration in the normal and superconducting RF structures. The ion source and LEBT parameters are critical for the parameters of the beam, which is injected into the RFQ. In addition to the beam properties itself, reliability and lifetime are key parameters of ion source performance and need to be carefully assessed. For this purpose, a dedicated ion source and LEBT test stand is installed. In general, the test stand features components for an identical setup as the configuration in the main Linac. However, the test stand is also foreseen as a testbed for dedicated ion source and LEBT studies in settings or configurations, which are not feasible in the main machine. This paper presents an overview of the test stand design, reports on the progress of the project and gives an update about the recent milestones, including first plasma in the ion source, high voltage testing, and first beam extraction.

INTRODUCTION

The European Spallation Source (ESS) Linac designated to become the world's most powerful neutron source is currently being in commissioning; a comprehensive description of the project can be found in Ref. [1]. The first part of the ESS Linac consists of a microwave discharge ion source and a Low-Energy Beam Transport (LEBT), which where delivered as an In-Kind contribution from INFN-LNS in Catania [2–4]. The present version of the ion source integrates numerous improvements and provides a substantially greater degree of flexibility to comply with the ESS requirements of at least 74 mA extracted beam current, more than 80 % proton fraction, better than 3.5 % pulse-to-pulse stability, and a 99 % transverse emittance below 1.80 mm mrad [3, 5, 6].

Following the lessons learnt from previous commissioning rounds [7–11], a key factor in system reliability is the rapid replacement of consumable components, such as the boron nitride disks of the ions source plasma chamber, magnetron filaments of the microwave generation system and the LEBT repeller, which exhibited degradation during the recent beam on dump commissioning campaigns. To enhance system reliability and performance, systematic investigations are required for both ion source and LEBT. In particular, precise characterization of the beam parameters and composition immediately after the source, combined with assessment of plasma parameters, is essential to optimize models and improve agreement between experimental data and simulations without disrupting ESS accelerator operation.

Consequently, and based on the operational experience from other facilities such as the Linac4 Test Stand at CERN [12], FNAL [13] and SNS [14] ESS initiated the design, installation, and commissioning of a dedicated test stand, Test Stand 4 (TS4), for R&D studies, system upgrades and the provision of hot spare components for the Linac ion source and LEBT. In addition, the new test stand naturally serves for evaluating novel instrumentation and components that may benefit other projects, such as ESSnuSB+ [15], as well as, for material irradiation studies [16]. Therefore, the TS4 ion source and LEBT will incorporate several developments and modifications relative to the tunnel configuration. Similar to other facilities, TS4 will establish a basis for a future ESS spare RFQ project as part of a full front end test stand.

TEST STAND DESCRIPTION

TS4 is located in the klystron gallery building of the ESS Linac, with an area of 11.7 m × 15.5 m. A schematic top view of the test stand layout and its main components is shown in Fig. 1.

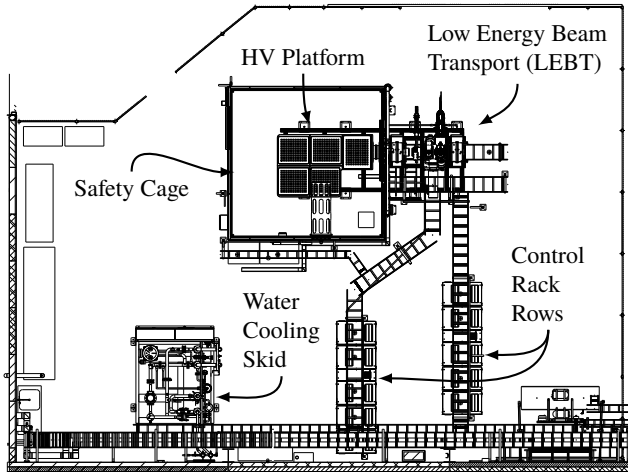


Figure 1: Schematic top view layout of TS4 at ESS.

TS4 features a full-scale copy of the Linac ion source, also supplied by INFN-LNS. However, several ion source and LEBT beamline components, along with their interfaces, were redesigned and procured by ESS, enhancing the existing design. In addition, TS4 involves a dedicated timing system and water cooling skid as well as the related racks for power supplies and controls.

* emmanouil.trachanas@ess.eu
† marten.koopmans@ess.eu

ISBN: 978-3-95450-275-2 ISSN: 2226-0366 doi: 10.18429/JACoW-LINAC2026-THPO021

DEVELOPMENT STATUS AND FIELD QUALIFICATION OF THE LATEST 80 MW S-BAND KLYSTRON FOR POHANG ACCELERATOR LABORATORY*

S. J. Park†,1, G. Y. Jang[2], H. S. Shin[2]
[1]Pohang Accelerator Laboratory, Pohang, Republic of Korea
[2]VITZRONEXTECH, Ansan, Republic of Korea

Content from this work may be used under the terms of the CC BY 4.0 licence (© 2026). Any distribution of this work must maintain attribution to the author(s), title of the work, publisher, and DOI.

Abstract

The Development status of the latest domestically produced 80 MW S-band klystron for Pohang Accelerator Laboratory (PAL) is reported, with emphasis on the VK4 tube now under field qualification at the PAL-XFEL. Earlier prototypes reached the target RF power at low repetition rate but were limited to 30 Hz by frequent gun arcing. Breakdown studies identified clump-assisted discharge in the diode region and electron multiplication from the ceramic triple point as the dominant mechanisms. Based on these findings, improved electrode polishing and cleaning and a triple-point electrostatic shield were implemented in VK4 and VK5. In laboratory processing, VK4 demonstrated stable operation at 80 MW, 4 us, and 60 Hz, while VK5 showed a further reduction of total HV arc rate by about 59% confirming the benefit of improved gun preparation. To verify accelerator readiness, site testing of VK4 has been carried out with step-wise HV and RF qualification up to 400 kV, 80 MW, 4 us, and 60 Hz. Initial field-test results and implications for routine accelerator operation will be presented.

INTRODUCTION

The Pohang Accelerator Laboratory (PAL) operates about 70 high-power S-band pulse klystrons as the radio-frequency (RF) sources of the PAL-XFEL X-ray free-electron laser and PLS-II synchrotron light source [1,2]. Long-term reliability and a stable supply of these tubes are essential for the user operation of both facilities. To secure the supply chain, PAL has carried out in-house R&Ds on S-band klystrons since 1996 and, since 2016, a national R&D program in collaboration with local industry [3,4]. During these programs, an 80 MW-class S-band pulse klystron was successfully developed [5].

The early prototype tubes reached the target RF power at low repetition rates but exhibited frequent electron-gun arcings at the 60 Hz repetition rate, and routine operation was limited to 30 Hz. Autopsies of failed guns and particle-trajectory simulations identified two dominant breakdown mechanisms: clump-assisted breakdown in the cathode–anode gap, initiated by field-emitted electrons from the focus electrode, and electron-multiplication breakdown along the ceramic-insulator surface, seeded at the metal–ceramic–vacuum triple point (TP) [6]. Two countermeasures were derived from these findings: improved surface preparation of the focus electrodes, and an electrostatic shield at the TP.

These measures were incorporated into the two latest tubes, VK4 and VK5, which were fabricated in 2024 and conditioned in the PAL klystron and modulator test laboratory through 2025 [7]. It was found fast gun arcings were dramatically reduced compared to earlier fabrications, while the slow breakdowns associated with the TP were completely eliminated [7]. VK4 reached 80 MW peak RF output with a 4 µs pulse width at 60 Hz and operated stably. VK5, whose gun electrodes received additional electro-chemical buffing (ECB), showed a further reduction of the fast arc rate by about 59 % compared to the VK4.

The necessary step toward routine accelerator service and series production was qualification of the tube in the real accelerator environment. To this end, the VK4 was installed in the PAL-XFEL linac and subjected to HV and RF qualification campaigns with target operation parameters of up to 80 MW, 4 µs, and 60 Hz from 30 March to 22 May 2026. This paper reports the field-test setup, procedures, and results.

FIELD-TEST SETUP

The test was performed at the L3-S1 modulator-klystron (MK) station of the PAL-XFEL. Figure 1 shows VK4 installed at the station. The station consists of the 200 MW modulator [5], the pulse-transformer tank on which the klystron is mounted together with its focusing solenoid, the waveguide system delivering the RF power to the S-band accelerating structures in the tunnel, and the associated cooling, vacuum, and low-level RF (LLRF) systems. The tube was transported from the test laboratory to the assembly room on 25 March 2026, mated with the pulse tank by 1 April, and installed at L3-S1 during 1–3 April, followed by heater characterization and verification of the interlock and data-acquisition (DAQ) systems.

Two complementary DAQ layers were used. Slow data—the modulator charging (inverter) voltage, the vacuum readings of the klystron, gallery, and tunnel, and the RF power measured by the LLRF system—were monitored and archived through EPICS with a CSS-based operator interface. Fast pulse waveforms of the beam voltage, the beam current, and the forward and reflected RF power were digitized by a local DAQ system based on the NI LabVIEW and the NI PCI-6110 I/O device [8], complemented by an oscilloscope for monitoring gun perveance. The RF power measurement chain was calibrated with a directional-coupler attenuation

* Work supported by the Korean Government (MSIT: Ministry of Science and ICT) and by the Pohang Accelerator Laboratory (PAL). PAL is supported by MSIT and POSTECH.

† sjpark@postech.ac.kr

ISBN: 978-3-95450-275-2 ISSN: 2226-0366 doi: 10.18429/JACoW-LINAC2026-THPO022

DEVELOPMENT OF RESONANT KICKER (RK) LLRF FOR PAL-XFEL*

Jinyul Hu†, Chang-Ki Min, Hoon Heo
Pohang Accelerator Laboratory (PAL), POSTECH, South Korea

Abstract

PAL-XFEL has been operating two beamlines simultaneously since 2021. The simultaneous operation method involves generating and accelerating single bunch of electrons at 60 Hz to provide 30 Hz beams to the hard X-ray (HX) and soft X-ray (SX) beamlines, respectively. It is intended to switch to a method developed by SwissFEL, which is capable of providing 60 Hz beams to both the HX and SX beamlines. To implement this, the two adjacent electron bunches are spaced 25 ns apart, and the operating frequency is designed so that the RK operates at 20 MHz. We chose a method of driving the RK using a combination of LLRF and SSA. Currently, the LLRF prototype is in development, and we would like to share the progress of the prototype LLRF.

INTRODUCTION TO PAL-XFEL

PAL-XFEL (Pohang Accelerator Laboratory X-ray Free Electron Laser) is a linear accelerator-based hard X-ray free-electron laser facility. Figure 1 shows a panoramic view of Pohang Accelerator Laboratory, and Fig. 2 is a schematic diagram of PAL-XFEL located within the site. It began beam commissioning in 2016 and has been operating with good stability and reliability up to date. The total length of the machine is approximately 1.1 km, with the linear accelerator section accounting for about 700 m of that. The linear accelerator is based on American S-band (2.856 GHz) traveling-wave normal-conducting accelerating structures and comprises a total of 51 RF accelerating units. Among them, one RF unit is an X-band(11.424 GHz) linearizer. The linear accelerator is designed to transport the electron bunches into each of the two beamlines at an intermediate electron beam energy of approximately 3 GeV. In the initial stage of implementation, only one beamline could be selected and operated during a shift. Years later, a system was developed to split electron bunches—generated at a 60 Hz repetition rate—into two beamlines at 30 Hz each, enabling simultaneous operation. It has been stably applied to PAL-XFEL since 2021. To further enhance accelerator operational efficiency beyond the current simultaneous operation method, a new simultaneous operation scheme utilizing a two-bunch approach is being developed. We intend to describe the progress of LLRF development associated with this method.



Figure 1: Aerial view of Pohang Accelerator Laboratory.

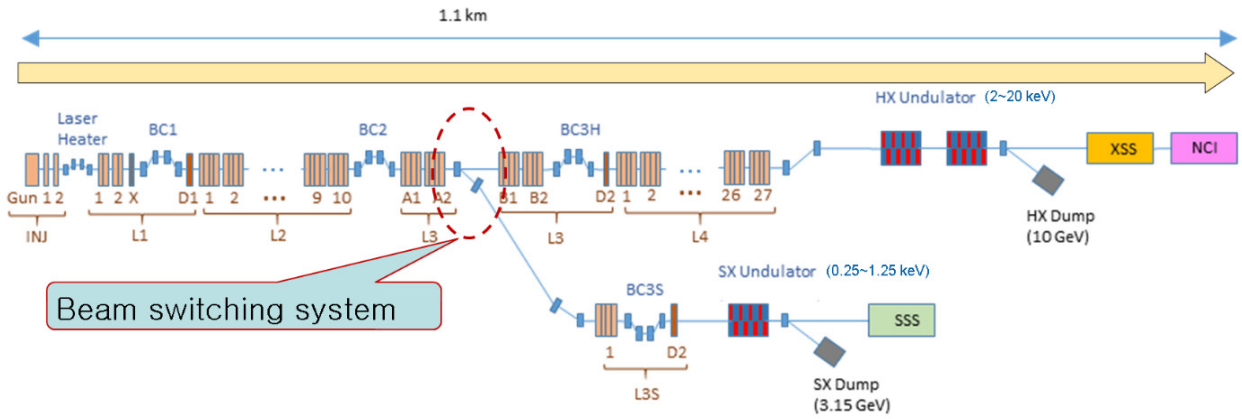


Figure 2: PAL-XFEL layout.

* Work supported by Ministry of Science and ICT (MSIT), South Korea
† hjy@postech.ac.kr

Content from this work may be used under the terms of the CC BY 4.0 licence (© 2026). Any distribution of this work must maintain attribution to the author(s), title of the work, publisher, and DOI.

ISBN: 978-3-95450-275-2 ISSN: 2226-0366 doi: 10.18429/JACoW-LINAC2026-THPO024

DESIGN OF A C-BAND ACCELERATING-UNIT RF SYSTEM AND SPHERICAL PULSE COMPRESSOR FOR CEPC

H. Cao*,[1,2], J. Zhang†,[1,2], G. Rao[1,2], O. Xiao[1]
[1]Institute of High Energy Physics, Chinese Academy of Sciences, Beijing, China
[2]University of Chinese Academy of Sciences, Beijing, China

Abstract

An 80 MW klystron-based one-to-four RF scheme is proposed for the CEPC C-band accelerating unit to reduce the number of RF sources and simplify the RF distribution system. Based on the RF power budget, a spherical pulse compressor operating at 5712 MHz is designed using a TE_{114} dual-mode spherical cavity and a 3 dB circular polarization mode converter. The optimized cavity has an unloaded quality factor of 126000 and a coupling coefficient of 5.43, achieving an energy multiplication factor of 2.0. With a 3 µs input pulse and phase reversal at 2.65 µs, a compressed pulse of approximately 350 ns is obtained with a peak power gain of 6.45.

INTRODUCTION

The Circular Electron Positron Collider (CEPC) is a proposed future electron–positron collider for precision studies in high-energy physics. Its injector linac is required to provide high-quality electron and positron beams for the collider [1]. Normal-conducting C-band accelerating structures are being developed for the CEPC linac to achieve a high accelerating gradient [2]. The overall layout of the CEPC linear accelerator is shown in Fig. 1.

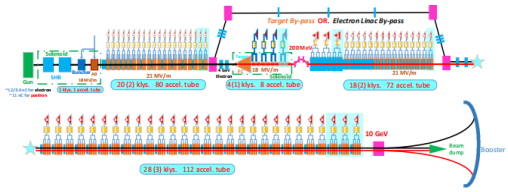


Figure 1: Layout of the CEPC linear accelerator.

To reduce the number of RF sources and simplify the RF distribution system, an 80 MW klystron-based one-to-four scheme is proposed for the C-band accelerating unit, in which one RF source feeds four accelerating structures. Compared with the previous one-to-two configuration, the one-to-four scheme requires a higher peak power gain and places more stringent requirements on the RF transmission efficiency and high-power capability of the pulse compression system.

RF pulse compression is an effective technique for increasing the peak RF power delivered to high-gradient accelerating structures. Various RF pulse compression schemes have been developed, including the conventional SLED system [3], VLEPP RF power multiplication and open-cavity pulse compression systems [4, 5], and compact spherical cavity pulse compressors [6, 7]. Among these approaches, the spherical cavity is particularly attractive because of its compact geometry, high unloaded quality factor, and large energy-storage capability. Spherical pulse compressors have been developed at both S-band [6] and C-band [7], demonstrating their potential for compact high-power RF pulse compression.

In this work, a C-band accelerating unit RF system incorporating a TE_{114} dual-mode spherical pulse compressor is designed for the CEPC one-to-four scheme. The RF power budget and waveguide transmission losses are first evaluated to determine the required pulse compressor performance. A 3 dB circular polarization mode converter and a TE_{114} spherical storage cavity operating at 5712 MHz are then designed and optimized. The pulse compression performance is evaluated in terms of the peak power gain, energy multiplication factor, and compression efficiency.

C-BAND ACCELERATING UNIT RF SYSTEM DESIGN

The C-band accelerating unit of the CEPC linac is designed to provide high-power RF to four normal-conducting accelerating structures. In the proposed one-to-four RF scheme, an 80 MW klystron is used as the RF source. To ensure stable long-term operation, the klystron is assumed to operate at 90% of its rated peak power, corresponding to an available RF power of approximately 72 MW.

The layout of the proposed C-band accelerating unit RF system is shown in Fig. 2. The RF power generated by the klystron is transmitted through the waveguide network to the spherical pulse compressor, where the RF pulse is compressed to increase the peak power. The compressed RF pulse is subsequently divided and delivered to four accelerating structures.

The waveguide transmission system is designed to minimize RF power loss. The attenuation of the main waveguide components and the calculated transmission losses before and after the pulse compressor are summarized in Table 1. In addition to the calculated waveguide attenuation, additional practical losses associated with RF connections, such as waveguide flanges, are also considered in the system power budget. Therefore, an appropriate power margin is retained when determining the required performance of the pulse compressor.

The calculated attenuation between the klystron and the pulse compressor is approximately 0.39 dB. Considering the 90% operating level of the klystron, the RF power available at the compressor input is approximately 66 MW before

* caohj@ihep.ac.cn
† zhangjr@ihep.ac.cn

Content from this work may be used under the terms of the CC BY 4.0 licence (© 2026). Any distribution of this work must maintain attribution to the author(s), title of the work, publisher, and DOI.

ISBN: 978-3-95450-275-2 ISSN: 2226-0366 doi: 10.18429/JACoW-LINAC2026-THPO025

OPERATIONAL DIAGNOSTICS AND RF MONITORING FOR THE TPS 150 MeV LINAC AND LTB TRANSFER LINE

C. Y. Wu, C. Y. Liao*, P. C. Chiu, Y. S. Cheng, J. K. Liao
National Synchrotron Radiation Research Center, Hsinchu, Taiwan

Abstract

The 150 MeV S-band electron linac is the primary injector for the Taiwan Photon Source (TPS) and supports routine top-up operation through the linac-to-booster (LTB) transfer line. The role of its diagnostic systems has gradually shifted from commissioning measurements to routine monitoring of RF conditions, charge transmission, bunch-related waveforms, beam position monitor (BPM) signals, and transverse beam profiles. The current monitoring system includes a Libera low-level RF (LLRF) platform for RF waveform and trend observation, a Libera Digit 500 for LTB integrating current transformer (ICT) readout, an oscilloscope-based wall current monitor (WCM), an ADQ7DC-based LTB BPM waveform digitizer, and calibrated screen-monitor image analysis. These GUI-based tools support routine injection checks and first-line fault diagnosis. The paper also discusses a future upgrade path based on an MTCA.4 digital LLRF (DLLRF) platform.

INTRODUCTION

The TPS injector consists of a 150 MeV S-band electron linac, an LTB transfer line, a booster synchrotron, and a booster-to-storage-ring transfer line [1]. The linac was supplied by RI Research Instruments GmbH and includes three 3 GHz accelerating structures powered by high-power pulsed klystron and modulator stations. The current RF system includes two Canon Electron Tubes & Devices E37310A klystron stations for K1 and K2 and one remaining Thales TH2100A station for K3; the K1 and K2 replacements were completed in September 2025 and February 2026, respectively, as part of the TPS linac high-power RF upgrade program [2].

The linac operates in single-bunch (SB) and multi-bunch (MB) modes, and reproducible beam delivery from the linac to the LTB transfer line is required for flexible filling-pattern operation. The original diagnostics were installed for acceptance tests and early commissioning, including charge, bunch-structure, profile, position, energy, and emittance measurements [3]. With the TPS now in long-term top-up operation, the same infrastructure is used mainly for routine injection checks and operational monitoring. This paper describes the monitoring tools currently used for routine operation and operator-level diagnosis, together with the planned RF upgrade direction.

* liao.cy@nsrrc.org.tw

MONITORING CONFIGURATION

The monitoring configuration includes RF phase and amplitude monitoring, LTB charge monitoring, longitudinal waveform observation, high-speed BPM waveform acquisition, and transverse profile analysis. Figure 1 shows the operator layout display, including the RF modulators, accelerating structures, screen-monitor locations, WCM, ICTs, vacuum gauges, and LTB connection. The display also presents RF phase and power readbacks, modulator high-voltage status, vacuum pressure, valve status, and interlock indications. It serves as the initial system overview before operators inspect the detailed RF and beam-diagnostic GUIs.

The RF signals are acquired through the installed Libera LLRF system from Instrumentation Technologies [4]. The LLRF hardware includes clock-distribution, analog front-end, and digital-processor units; the analog front-end down-converts RF signals to intermediate-frequency signals, which are digitized and processed in the FPGA. Figure 2 shows the installed hardware, including the 2998 MHz reference-distribution chassis, the analog front-end with RF and IF connections, and the digital processor used for waveform acquisition. The LTB charge monitor uses ICT1 and ICT2 waveforms acquired by a Libera Digit 500 (LD500) digitizer [5]. The WCM signal is acquired with a conventional oscilloscope. The LTB BPM waveform is acquired with a Teledyne SP Devices ADQ7DC digitizer at 10 GSPS in one-channel operation with 3 GHz analog bandwidth [6]. The screen-monitor system uses Allied Vision Manta G-032B PoE cameras and a calibrated scale of 0.038 mm/pixel for online one-dimensional profile fitting [7].

OPERATIONAL MONITORING TOOLS

RF Phase and Amplitude Monitoring

The RF monitoring GUI displays the forward amplitude and phase waveforms of RF1, RF2, and RF3, together with averaged amplitude and phase over a selected time window. The waveform panels are used to inspect individual RF pulses, while the trend panels show the corresponding averaged values. This arrangement allows operators to compare pulse-to-pulse variations with slower changes observed over the selected time window. Figure 2 shows the installed Libera LLRF hardware, and Fig. 3 shows the corresponding operator GUI.

LTB Charge, WCM, and BPM Monitoring

Charge transmission in the LTB transfer line is monitored by ICT1 and ICT2 waveforms. The ICT2/ICT1 ratio is calculated from the integrated areas of the two waveforms and is used as an operational charge-transmission indicator.

Content from this work may be used under the terms of the CC BY 4.0 licence (© 2026). Any distribution of this work must maintain attribution to the author(s), title of the work, publisher, and DOI.

ISBN: 978-3-95450-275-2 ISSN: 2226-0366 doi: 10.18429/JACoW-LINAC2026-THPO026

BEAM DYNAMICS SIMULATION AND LATTICE OPTIMIZATION FOR THE SIAM PHOTON SOURCE INJECTOR

T. Chanwattana*, P. Boonpornprasert, N. Juntong, S. Chunjarean
Synchrotron Light Research Institute, Nakhon Ratchasima, Thailand

Abstract

The Siam Photon Source (SPS) injector, comprising an injector linac and a Low-Energy Beam Transport line (LBT), delivers a 40 MeV electron beam to a booster synchrotron for acceleration to 1.2 GeV. While this system has operated in its original configuration since commissioning, prior machine studies (in 2006 and 2016) revealed that overall beam transmission efficiency had degraded to below 30 %. To address these losses without disrupting ongoing user beam services, beam dynamics simulations were developed to serve as an optimization model. By benchmarking the simulated beam parameters against both the original conceptual design and recent measurements, several discrepancies were identified. This paper details the simulation methodology and proposes machine corrections—including the optimization of RF power and phase in the bunching components, and quadrupole tuning and polarity adjustments—to control the beam envelope and increase the transmission efficiency.

INTRODUCTION

The 1.2 GeV Siam Photon Source (SPS) at the Synchrotron Light Research Institute (SLRI) has reliably supplied synchrotron radiation to a user community since 2003 [1]. While the next-generation facility, SPS-II, remains in the detailed design phase [2], ongoing upgrades of the existing SPS are vital for supporting regional scientific research.

The SPS injector consists of a linac [3] and a Low-Energy Beam Transport (LBT) line (Fig. 1). Because LBT exit parameters directly influence booster injection efficiency, beam diagnostics—primarily current and screen monitors—are deployed along the transfer line for beam characterization, including recent diagnostic upgrades [4].

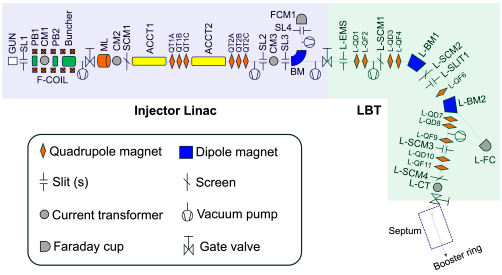


Figure 1: Layout of the SPS injector consisting of the injector linac (purple area) and LBT (green area).

Continuous operation and parameter drift have degraded transmission. Technical reports from 23.2 % in 2006 [5] and 21.0 % in 2016 [6], along with recent measurements [7], indicate overall transmission from the gun to the LBT exit remains persistently below 30 %. Improving this is essential for stable beam refills and minimizing radiation activation. Because dedicated machine development time is highly constrained, a reliable computational model is required to formulate corrective strategies offline.

Independent simulation models were developed using `ASTRA` [8] to simulate space-charge effects in the low-energy linac, and `ELEGANT` [9] for lattice optimization in the LBT.

INJECTOR LINAC

`ASTRA` simulations span from the electron gun ($Z = 0$ m) to the vacuum gate valve GV2 ($Z = 9.089$ m). The initial 0.100 MeV electron bunch features 0.0875 nC of charge, transverse RMS sizes of $\sigma_{x,y} = 2.5$ mm, and a longitudinal RMS length of $\sigma_z = 30.31$ mm (FWHM 350 ps). Initial normalized emittances and Twiss parameters are assumed zero. Distributions are modeled with 100,000 macroparticles for final tracking.

Electromagnetic fields in the linac were modeled using `CST` longitudinal RF profiles [10] for the pre-bunchers (PB1, PB2) and buncher, and standard `ASTRA` SLAC-type models for the accelerating structures (ACCT1, ACCT2). Magnetic elements (F-COIL, magnetic lens, quadrupoles) utilized scaled `ASTRA` field profiles. The RF amplitudes and phases across all cavities were then optimized to maximize energy gain while preserving the beam profile (Table 1).

Table 1: Parameters of the RF Components Selected for the Injector Linac Simulation

Component	Parameter	Value
PB1	Peak electric field [MV/m]	1.3
	Phase [degree]	48
PB2	Peak electric field [MV/m]	4.75
	Phase [degree]	124
BUNCHER	Peak electric field [MV/m]	20
	Phase [degree]	−69
ACCT1	Peak electric field [MV/m]	10.5
	Phase [degree]	35
ACCT2	Peak electric field [MV/m]	10.5
	Phase [degree]	−1

At GV2, evaluated within a $\pm 3\sigma_z$ cut, the beam reaches 39.7 MeV with an RMS energy spread of 4.2 % and a remaining charge of 47.27 % (Table 2). The evolution of these parameters is shown in Fig. 2.

The high simulated energy spread of 4.2 % correlates with recent physical beam measurements [11]. The final beam

* thakonwat@slri.or.th

Content from this work may be used under the terms of the CC BY 4.0 licence (© 2026). Any distribution of this work must maintain attribution to the author(s), title of the work, publisher, and DOI.

ISBN: 978-3-95450-275-2 ISSN: 2226-0366 doi: 10.18429/JACoW-LINAC2026-THPO027

JINR DLNP LASER-DRIVEN RF-GUN TEST BENCH COMMISSIONING STATUS

M.A. Nozdrin*[1], K. Popov†[1, 2], A.S. Dyatlov[1, 3], D.S. Shokin[1], K.E. Yunenko[1], A.A. Nozdrin[1], D.V. Karlovets[3], V.V. Kobets[1]
[1]Joint Institute for Nuclear Research, Dubna, Russia
[2]Institute of Nuclear Physics, Almaty, Kazakhstan
[3]School of Physics and Engineering, ITMO University, Saints-Petersburg, Russia

Abstract

A laser-driven RF-Gun test-bench development and commissioning is ongoing at the Dzhelepov Laboratory of Nuclear Problems at the Joint Institute for Nuclear Research. The test-bench primary purpose is to investigate the possibility of the laboratory electron linac thermionic gun replacement with the laser-driven RF-Gun. Another important task is the relativistic vortex electron beams generation study. This report shows the laser-driven RF-Gun test-bench layout, commissioning results and facility future plans.

INTRODUCTION

The 200-MeV multi-purpose electron linear accelerator for fundamental and applied studies commissioning is being finished at the Joint Institute of Nuclear Research (JINR), Dzhelepov Laboratory for Nuclear Problems (DLNP) [1]. In order to improve the beam parameters, the thermionic gun replacement to the laser-driven RF gun [2] is considered. This requires the test-bench development and commissioning to implement and test beam instrumentation technologies for the laser-driven RF-Gun successful operation and relocation to the linear accelerator. Also, the vortex electron beams generation study is ongoing at the test-bench [3, 4].

LASER-DRIVEN RF-GUN TEST-BENCH DESIGN

The laser-driven RF-Gun test-bench is a normal conducting facility (see Figs. 1 and 2). The Nd:YLF drive laser system supplies 10 ps (FWHM) duration laser pulse to the copper photocathode via a laser beamline (LBL). The LBL first part is located in air, while the second part is located in vacuum. The electron bunch is generated via the photocathode irradiation by 262 nm laser pulse. Then, the bunch is accelerated up to 5 MeV. The emittance compensation solenoid is placed over the gun cavity body. On the next step, the emittance compensated bunch passes through the focusing solenoid and steering magnet. On the final stage the bunch hits the target, which is located at the emittance measurement chamber. Table 1 presents the RF-Gun parameters.

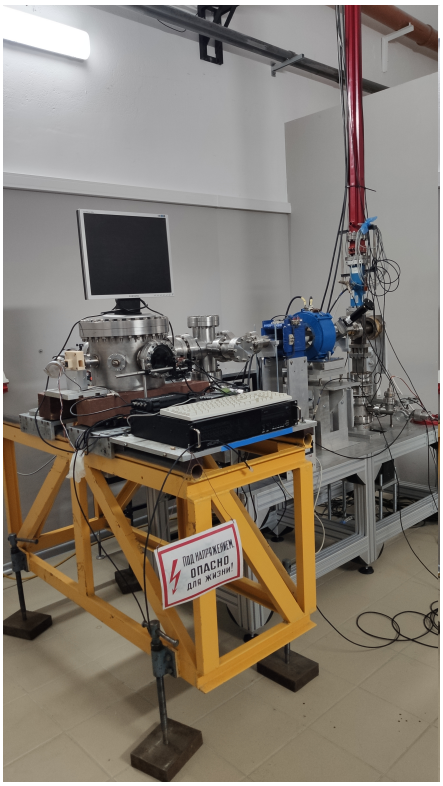


Figure 1: The laser-driven RF-Gun test-bench photo.

Table 1: RF-Gun Design Parameters

Parameter	Value
Frequency	2856 MHz
Mode	π
Cells number	1.5
Unloaded quality factor	12 000
SWR	1.1368
Accelerating gradient	120 MV/m
Energy	5 MeV

Laser Systems

The main laser system is the Nd:YLF drive laser system [5]. The system is based on a Yb-doped fiber laser oscillator, which operates in CW self-mode-locked regime without Q-switching.

There are 2 fiber preamplification cascades and 1 fiber acousto-optic modulator. The main amplifiers are 2 Nd:YLF rod amplifiers. KTP and BBO crystals are the second and

* nozdrin@jinr.ru
† popovkon@jinr.ru

Content from this work may be used under the terms of the CC BY 4.0 licence (© 2026). Any distribution of this work must maintain attribution to the author(s), title of the work, publisher, and DOI.

ISBN: 978-3-95450-275-2 ISSN: 2226-0366 doi: 10.18429/JACoW-LINAC2026-THPO028

SIMULATION-BASED ANALYSIS OF GEOMETRIC IMPERFECTIONS AND TUNING FOR A BNCT-RFQ*

Z. Q. Ren, X. M. Wan, L. Ma, X. K. Chang, Y. X. Wu, S. Q. Li, N. X. Li, B. Tang, Z. H. Li#
Institute of Nuclear Science and Technology, Sichuan University, Chengdu, China

Abstract

Boron neutron capture therapy (BNCT) is attracting increasing attention. This paper presents the structural design and error analysis of a radio frequency quadrupole (RFQ) accelerator currently being fabricated for BNCT applications. The RFQ is designed to accelerate a 15-mA proton beam to 2.5 MeV, with a total length of 4.67 m divided into four segments, each approximately 1.2 m long.

Various types of machining imperfections may inevitably exist after the final assembly of the cavity. Since these imperfections can significantly affect the RF performance and field distribution of the RFQ, tuners are provided on the cavity to compensate for such manufacturing errors. To predict the potential impact of these errors on cavity performance and to evaluate the effectiveness of the tuners, several possible structural error patterns were modelled in a CST simulation environment based on the RFQ cavity model. The simulation results reveal how these errors affect the high-frequency and electromagnetic characteristics of the RFQ and confirm the effectiveness of a proposed tuning algorithm.

INTRODUCTION

We are about to construct an RFQ-accelerator-based system for boron neutron capture therapy (BNCT) in Chengdu, China. In order to moderately reduce the length of the accelerator and thereby ensure the compactness of the entire treatment system, the operating frequency of the RFQ was chosen to be 200 MHz, considering the domestic manufacturers' accumulated expertise in RFQ cavity fabrication, as well as design and construction experience drawn from several well-established RFQ projects [1, 2]. Furthermore, to facilitate long-term reliable operation of this RFQ, which is intended to achieve a duty factor of 80% or higher, the design was implemented such that the peak surface electric field in the cavity corresponds to a Kilpatrick (KP) factor of only 1.25 [3]. Further detailed parameters of this RFQ are presented in Table 1.

Table 1: Main Results of the RFQ

Parameters	Value
Frequency (MHz)	200
Input/output energy (MeV)	0.03/2.52
Peak current (mA)	15
Inter-vane voltage (kV)	65
Duty cycle	> 80%
Peak surface field (MV/m)	18.4 (1.25 KP)
Aperture radius (mm)	4.86
Transmission efficiency (%)	99.23
Accelerator length (mm)	4666.9
Cavity power dissipation (kW, 25% margin)	147.8
Q factor (80% of simulation)	10561

EFFECTS OF GEOMETRIC ERRORS

The configuration of this BNCT RFQ is of the four-vane type with a quadrilateral cross-sectional shape, which provides favourable structural stability. During manufacturing processes such as machining and welding, various geometrical errors are introduced. Even subtle imperfections can have severe consequences for an RFQ accelerator operating at high frequency. Such errors may shift the operating frequency of the TE_{210} mode or distort its field profile away from the theoretical design, thereby degrading the quality of the output beam. Alternatively, local field enhancement due to a non-uniform field distribution can lead to RF sparking, making it difficult to feed power into the cavity. Both outcomes are unacceptable for the BNCT system. Therefore, a key objective is to understand how structural errors affect the RFQ performance and how tuners can be effectively used to correct these errors.

To address these challenges, a preliminary approach based on CST simulations provides a well-suited solution [4]. First, several representative types of vane errors were simulated to determine their influence on the RF performance of the cavity. Subsequently, based on the identified error patterns, a novel tuning algorithm was developed to correct the field distribution.

For an RFQ cavity, the four quadrants are defined counter clockwise starting from the upper right region along the direction of beam acceleration, and are designated as Quadrants 1 through 4. The typical field pattern of the operating TE_{210} mode is illustrated in Fig. 1, and the field amplitude in each quadrant is denoted by F_i, with i = 1, 2, 3, 4. On this basis, the quadrupole and dipole field components are defined as follows:

$$\begin{aligned} Q &= (F_1 + F_2 + F_3 + F_4)/4, \\ Ds &= (F_1 - F_3)/2, \\ Dt &= (F_2 - F_4)/2. \end{aligned} \tag{1}$$

* work supported by the National Natural Science Foundation of China (Grant Nos. 11375122 and 11875197)
lizhihui@scu.edu.cn

Content from this work may be used under the terms of the CC BY 4.0 licence (© 2026). Any distribution of this work must maintain attribution to the author(s), title of the work, publisher, and DOI.

ISBN: 978-3-95450-275-2 ISSN: 2226-0366 doi: 10.18429/JACoW-LINAC2026-THPO029

PRELIMINARY BEAM DYNAMICS STUDIES ON SDTL FOR 200 MeV ENERGY UPGRADE AT KOMAC

S. Lee, S. Park, S. Moon, H.-S. Kim, H.-J. Kwon
Korea Multipurpose Accelerator Complex, Korea Atomic Energy Research Institute
Gyeongju, Republic of Korea

Abstract

The proton accelerator, operational since 2013, has consistently achieved over 3,000 annual operating hours, providing 100 MeV proton beams to users. Increased demand from the semiconductor industry for testing and evaluation necessitates an energy upgrade to 200 MeV, aiming to enhance performance and support advanced materials industries. The design for this extended linac is based on a normal-conducting separated-drift tube linac (SDTL) structure, chosen for its efficiency within limited space, including some building extension. The SDTL design maintains the DTL structural configuration without quadrupole magnets, utilizing a doublet focusing structure between tanks instead. Preliminary beam dynamics studies compared 5-cell and 6-cell SDTL options, considering space constraints. This paper presents the beam dynamics results, providing insights into the feasibility of an efficient SDTL configuration for the 200 MeV upgrade shown in Fig. 1.

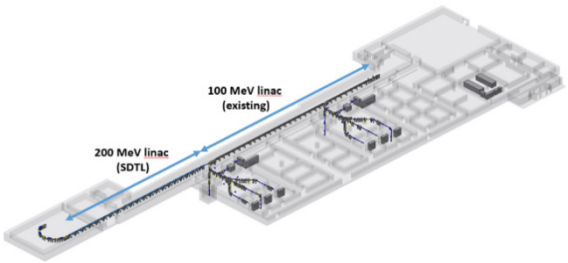


Figure 1: 200 MeV linac layout.

SDTL DT STRUCTURE

The structure of the SDTL (Superconducting Drift Tube Linac) is similar to that of the Drift Tube Linac (DTL), but unlike a typical DTL with quadrupole magnets inside the drift tube (DT), the SDTL places these magnets outside the DT. This design allows for more flexible optimization of the DT structure with increasing acceleration efficiency. Additionally, because the SDTL typically uses only 3-5 drift tubes, it does not require separate beam stabilization devices, making its construction and alignment simpler than that of a standard DTL. The acceleration structure of the SDTL was designed for beam dynamics and the linac itself, aiming to elevate the energy of the proton accelerator from 100 MeV to 200 MeV [1]. The cell structure of the SDTL, designed to accelerate protons from 100 MeV to 200 MeV, was determined. The SDTL operates at the same frequency as the 100 MeV accelerator, which is 350 MHz. Considering beam transport and DT support, the optimized parameters include tank diameter, DT diameter, face angle, flat length, inner radius, and outer radius, in addition to the predetermined bore radius, stem diameter, and corner radius. The optimized cell structure of the SDTL, and the cell parameters are summarized in [2].

To optimized the SDTL linac layout, SFDATA of the SDTL DT obtained from SUPERFISH is used with design parameters given in Table 1

Table 1: SDTL Design Parameters

Parmila Design Parameter	Value
Input energy [MeV]	102.6
RF [MHz]	350
Beam Current [mA]	20
E_0 [MV/m]	3.80
Phase [°]	-30 for 5 cell SDTL -28 for 6 cell SDTL

For a structure with 5 cells per tank (equivalent to 4 DTs per cell), a total of 20 tanks are needed to achieve acceleration up to 200 MeV. Each tank ranges in length from 187 cm to 242 cm, with a required RF power of 680 kW to 930 kW per tank for a beam current of 20 mA, resulting in a total SDTL length of 60.7 meters. In contrast, for a structure with 6 cells per tank (equivalent to 5 DTs per cell), 16 tanks are required to reach the same 200 MeV acceleration. The tanks in this configuration range from 225 cm to 289 cm in length, with an RF power requirement of 820 kW to 1110 kW per tank at a beam current of 20 mA, resulting in a total SDTL length of 55.3 meters.

We require the same number of klystron as SDTL tank number, and one modulator is going to power 4 klystron simultaneously, so 5 cell SDTL requires 20 klystrons and 5 modulators. And for 6 cell SDTL, 16 klystrons and 4 modulators are needed.

LATTICE DESIGN

A beam dynamics calculation was performed to achieve a proton beam energy of 200 MeV. The Tracewin code [3] was used for these calculations. A focusing structure with doublets between SDTL tanks was opted, and its schematic is shown for 5 and 6 cell SDTL in Fig. 2 and Fig. 3. The distance between SDTL tanks was set to 2βλ to accommodate the doublets. Matching beam parameters for one period of the doublet were calculated. One period spans from the centre of one doublet to the centre of the next.

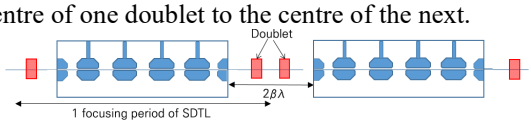


Figure 2: 5 cell SDTL doublet structure.

Content from this work may be used under the terms of the CC BY 4.0 licence (© 2026). Any distribution of this work must maintain attribution to the author(s), title of the work, publisher, and DOI.

ISBN: 978-3-95450-275-2 ISSN: 2226-0366 doi: 10.18429/JACoW-LINAC2026-THPO031

FLEXIBLE MULTI BUNCH INJECTION AT DIAMOND LIGHT SOURCE

A. Tropp, P. Hamadyk, A. Morgan
Diamond Light Source, Oxfordshire, UK

Content from this work may be used under the terms of the CC BY 4.0 licence (© 2026). Any distribution of this work must maintain attribution to the author(s), title of the work, publisher, and DOI.

Abstract

Diamond Light Source has, since the start of operation, run with both single-bunch and multi-bunch injection. Due to limitations in functionality and jitter in multi-bunch mode, Diamond has been running with an upgraded gun pulser for the past 3 years. This pulser enables flexible modulation of the gun cathode in multi-bunch mode by generating voltage waveforms from an arbitrary waveform generator (AWG). Single-bunch operation was implemented using a separate supply to replicate the old pulser, allowing simple injection while providing scope for development of the multi-bunch circuit. Leveraging the flexibility of the new pulser, fill patterns can be selected and injected with fewer shots and improved repeatability, leading to, among other things, faster fill times. Details of the functionality, design, and operation will be presented, along with results and issues related to reproducibility.

SYSTEM AND FUNCTIONALITY

Injection at Diamond Light Source has for many years run in both single-bunch (SB) and multi-bunch (MB) operation. The pulser used for this operation had quite a few limitations, one being the unevenness of the bunch-to-bunch charge, another being the charge limitation of 1 nC in SB mode. The new pulser [1] solves these limitations by the implementation of an AWG in MB mode and a complementary GaN FET pulse generator in SB mode to replicate the old SB mode.

Injection efficiency and bunch-to-bunch charge is also highly dependent on the RF power stability in the Linear accelerator (Linac). This is due to energy spread being a determinant factor in transmission efficiency through the Linac and Linac to booster (LTB) transmission lines. Energy stability has become an even more apparent reason for loss in transmission efficiency ever since Diamond implemented a pulse compressor in the RF line [2]. A lot of work has been done and is still ongoing for generating a stable RF signal where MB operation can be transmitted without too much shot-to-shot variation [3].

RF Stability

The Diamond Linac currently is experiencing RF stability issues from multiple sources. The two major sources are HV pulse to pulse stability from the modulator and pulse compressor modulation errors, which is derived from the driving Digital Low-level RF (DLLRF). Both issues can be seen contributing to injection losses and, if the stability is too low in either case, it has been seen that the AWG functionality is not enough to correct for these losses. Jitter from timing and gun output exist but is low enough that it can be corrected.

Pulser

The new pulser has increased the possible amount of charge in both single-bunch and multi-bunch operation, which is now being utilized for faster fill time in the storage ring. Higher charge will however cause a bigger energy spread of the outgoing electron beam due to space charge effects. Higher energy spread together with beam loading inside the linear accelerator structures when running multi-bunch injection, causes a big variation in beam transfer efficiency. When these electron buckets are later being accelerated in the booster to then be transferred into the storage ring the fill pattern will vary, in certain cases this bunch-to-bunch charge variation is more than 50%, see Fig. 1.

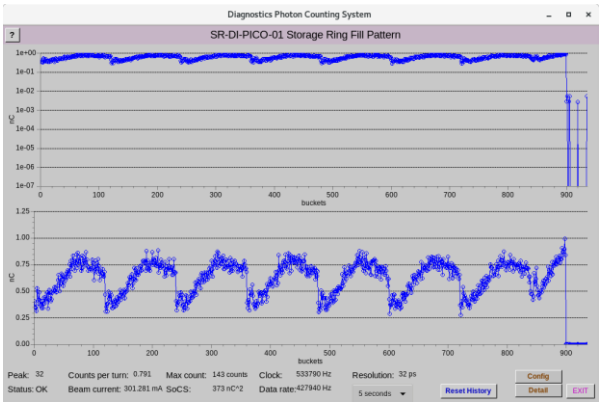


Figure 1: Non-corrected MB fill pattern as seen by the diagnostic pico-harp in the storage ring.

By using the AWG functionality of the pulser it is now possible to correct for issues that can be seen during the transfer which leads to this uneven fill pattern. This correction is implemented on the pulser records which each are long enough to fire 200 buckets, which means 8 records of 120 are required to fill the storage ring with 900 buckets of electrons. For future utilisation 5 records of 180 buckets will be used. To utilize the full memory of the pulser 10 records have been implemented leaving 2 records for development work. See Fig. 2 for the graphical interface (GUI) of the pulser information.

FEED FORWARD PROGRAM

To improve the evenness of the final fill pattern various options were considered. Due to the high update rate required for a feedback system a feedforward scheme was decided upon and implemented.

The basic operation is to inject sufficient charge into the storage ring to be able to see clear charge distribution, capture the fill pattern, calculate the percentage difference between bunch charge and mean bunch charge and apply this correction to the pulser records to then obtain a flatter fill. These new pulser records are then uploaded to the pulser

ISBN: 978-3-95450-275-2 ISSN: 2226-0366 doi: 10.18429/JACoW-LINAC2026-THPO032

ATTOSECOND STRUCTURING OF MeV ELECTRON BEAMS VIA TWO-COLOR LASER MODULATION*

Z. Wang[1], J. Li[1], C. Peng[1], Y. Hu[1], K. Fan†,[1]
[1]Huazhong University of Science and Technology, Wuhan, China

Abstract

Resolving ultrafast dynamics demands electron probes combining attosecond resolution with MeV-scale energies. Here, we demonstrate a compact, all-optical scheme to generate attosecond electron pulse trains using two-color laser modulation. By synthesizing a copropagating traveling-wave ponderomotive force, we imprint a periodic energy modulation on a relativistic electron beam, which evolves into a train of attosecond microbunches via velocity bunching.Crucially, we quantify a critical trade-off between bunch charge and temporal compression driven by space-charge effects. Benchmarked against the HUST-UED facility, our systematic parameter analysis establishes stringent tolerances for experimental realization. This work provides a viable roadmap for upgrading existing ultrafast electron diffraction systems to the attosecond regime, bridging the gap between ultrafast temporal resolution and deep material penetration.

INTRODUCTION

Mega-electron-volt ultrafast electron diffraction (MeV-UED) uniquely combines sub-picometer resolution with relativistic immunity to space-charge broadening, making it an indispensable tool for probing structural dynamics in condensed matter [1-5]. Extending this capability into the attosecond regime is the next frontier for resolving ultrafast phenomena such as electron correlation and charge migration [6-8]. However, existing demonstrations of attosecond electron pulses are largely confined to low-energy regimes, where space-charge suppression comes at the cost of beam charge and penetration depth [9, 10].

Several compression techniques, including double bend achromat compressors (DBAC), THz-driven modulation, and dielectric laser acceleration, have been proposed for relativistic electron beams [4, 5, 11-14]. While techniques like THz-driven compression offer pathways to relativistic pulse shortening , they often demand complex beamline architectures or stringent timing stability. Here, we propose a two-color laser modulation scheme that leverages a co-propagating traveling wave to imprint a precise energy modulation via the ponderomotive force [15-18]. This approach offers a compact, intrinsically synchronized route to attosecond pulse trains. Using three-dimensional ASTRA simulations, we elucidate the dynamics of velocity bunching at MeV energies, quantify the trade-offs imposed by space-charge forces, and establish robust tolerances for practical implementation at the HUST-UED facility.

THEORY

The scheme operates on the principle of converting an optical-cycle-scale energy modulation into a density modulation via ballistic phase-space evolution. The interaction is governed by the Lorentz force $F_z = e(E_z + v_x B_y)$. For a relativistic electron beam in a paraxial Gaussian field, $E_z \approx 0$, and the longitudinal force arises predominantly from the magnetic term $v_x B_y$. While this force oscillates at 2ω for a monochromatic field — averaging to zero over an optical cycle — the superposition of a second-harmonic ($\omega_2 = 2\omega_1$) introduces a non-vanishing ponderomotive force:

$$F_p \propto E_1 E_2 \cos(\phi_1 - \phi_2). \quad (1)$$

Crucially, this force manifests as a traveling wave rather than a stationary potential. Synchronism with the electron beam is achieved under the phase-matching condition $(k_1 - k_2)v_e = \omega_1 - \omega_2$, allowing electrons to experience a stationary accelerating field. This imprints a periodic energy modulation:

$$\Delta E(z) = \Delta E_m \sin(k_b z + \phi_0), \quad (2)$$

where ΔE_m denotes the energy modulation amplitude and k_b is the modulation wavenumber.

During free drift, this energy modulation induces velocity differences; faster electrons overtake slower ones via longitudinal phase-space rotation (velocity bunching). This process compresses the beam into a train of attosecond microbunches, establishing an all-optical pathway to relativistic attosecond structuring.

SIMULATION AND RESULTS

To verify the proposed scheme [Fig. 1(a)], three-dimensional particle-tracking simulations were conducted using ASTRA to investigate the modulation and subsequent bunching dynamics of a 3 MeV electron beam. The electron beam was initialized with an energy of 3 MeV, a bunch charge of 0.2 pC, an initial bunch duration of 10 fs FWHM, and an rms energy spread of 0.5 keV. As illustrated in Fig. 1(a), the electron beam first interacts with synchronized 400 nm and 800 nm laser pulses, which are introduced at incidence angles of 5.9° and 11.86°, respectively. The two laser fields form a co-propagating optical wave and induce a periodic longitudinal energy modulation through the ponderomotive force. The laser pulses have a peak intensity of approximately 10^{14} W/cm^2, a temporal duration of 100 fs FWHM, and a waist radius of 150 μm. After the laser–electron interaction, the modulated electron beam propagates through a free-space

* This work is supported by National Key Research and Development Program of China (2022YFA1602202,2024YFB4607900)
† kjfan@hust.edu.cn

Content from this work may be used under the terms of the CC BY 4.0 licence (© 2026). Any distribution of this work must maintain attribution to the author(s), title of the work, publisher, and DOI.

ISBN: 978-3-95450-275-2 ISSN: 2226-0366 doi: 10.18429/JACoW-LINAC2026-THPO036

DESIGN AND OPTIMIZATION OF A COMPACT THz-FEL OSCILLATOR WITH PLANAR UNDULATOR*

Chenyu Ji, Ruiying Luo, Cheng Liu, Qushan Chen†
Huazhong University of Science and Technology, Wuhan, China

Abstract

In a THz FEL oscillator, the undulator and optical cavity are the key components for radiation. In this paper, we present an integrated optimization of the systematic parameters under the requirement of high compactness. The joint influence of the undulator and resonator on the FEL performance introduces a multi-parameter coupling that complicates the design. Therefore, a sequential approach is used: the undulator and cavity are theoretically designed within constraints, followed by 3D simulation tuning of key parameters to maximize micropulse and macropulse energy. The joint GENESIS and OPC simulations show that, with peak currents exceeding 100 A, the output at 30 μm reaches a micropulse energy of 65 μJ and a macropulse energy of 139 mJ, while at 100 μm the output also meets the design requirements, providing a reliable basis for further implementation.

INTRODUCTION

A compact THz-FEL developed by Huazhong University of Science and Technology (HUST-FEL) [1] is undergoing an upgrade for more compactness (within 4 m) and higher output (10 μJ micropulse and 45 mJ macropulse), as shown in Fig. 1. In the new design, electron bunches are accelerated to an energy of 9-15 MeV and generate radiation with wavelengths of 30–100 μm.

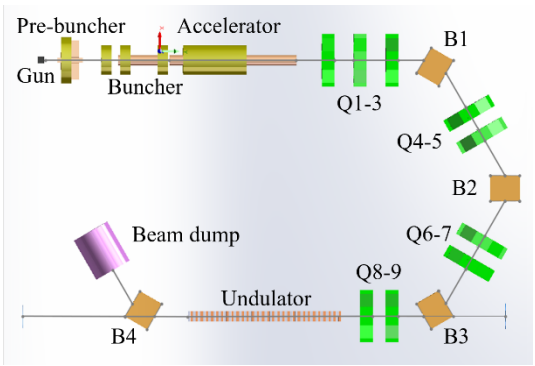


Figure 1: Layout of HUST-FEL II.

The key challenge lies in the multi-parameter coupling under compactness and output constraints. In the undulator, shortening the period λ_u increases the number of periods N_u and thus the single-pass gain, but it is technically limited by the peak field B_0 and also enhances the slippage effect, requiring a trade-off among these factors [2]. In the optical cavity, the length L_c together with the stability factor determines the Rayleigh length Z_R and spot size, directly affecting the matching between the electron beam and the radiation inside the undulator [3]. In addition, cavity detuning, outcoupling aperture, and waveguide effects introduce further complexities to parameter optimization.

This paper presents the HUST-FEL oscillator designed under stringent compactness constraints, using GENESIS [4] and OPC [5] for 3D simulations. The undulator has a period of 38 mm with 32 periods, and the optical cavity length is 3.78 m with a Rayleigh length of 0.432 m. Systematic optimizations of cavity detuning, outcoupling aperture, and waveguide are carried out. The system meets the design goals of micropulse and macropulse output for both 30 μm and 100 μm cases, validated by start-to-end simulations with upstream bunches.

OSCILLATOR DESIGN

Due to site constraints and engineering difficulties, the following requirements are proposed for the undulator and resonant cavity design:

- The undulator length should be limited to ~1.2 m.
- The optical cavity length should be kept within 4 m.
- The minimum gap of the undulator is 20 mm to provide space for the waveguide.
- The remanent field B_r = 1.2 T, and the peak magnetic field should not exceed 0.45 T.

Undulator

For planar pure permanent magnet undulators, the peak magnetic field B_{y0} at the center can be predicted using the analytical formula [6]:

$$B_{y0} = 2B_r \frac{\sin(\pi/M)}{\pi/M}\left(1 - e^{-2\pi h/\lambda_u}\right)e^{-\pi g/\lambda_u}, \quad (1)$$

where h is the height of the magnet blocks, g is the undulator gap, and M = 4 for Halbach structures. With $g_{\min}$ = 20 mm, the field distribution is shown in Fig. 2(a). For a fixed period λ_u, increasing h beyond a certain limit gains little in B_{y0}. Thus, the point where $\frac{dB_0/dh}{B_0}$ = 0.1 %/mm is selected as the maximum achievable B_{y0}, and the undulator parameter K can be calculated with the formula:

$$K = 0.934 \cdot \lambda_u[cm] \cdot B_0[T]. \quad (2)$$

For a uniform undulator, the fundamental resonant wavelength is:

$$\lambda_r = \frac{\lambda_u}{2\gamma^2}\left(1 + \frac{K^2}{2}\right). \quad (3)$$

We require that a 15 MeV beam can deliver high output power at 30 μm and also reach 40 μm by tuning K. The contours of wavelengths are shown in Fig. 2(b), and the black dashed line represents the maximum achievable K. Thus, rounding up the intersection of the dashed line and

* Work supported by:
Nuclear Technology R&D Program: HJSYF2025(25)
National Natural Science Foundation of China: 12175077
† chenqushan@hust.edu.cn

Content from this work may be used under the terms of the CC BY 4.0 licence (© 2026). Any distribution of this work must maintain attribution to the author(s), title of the work, publisher, and DOI.

ISBN: 978-3-95450-275-2 ISSN: 2226-0366 doi: 10.18429/JACoW-LINAC2026-THPO037

LORASR-DESIGNER: A GRAPHICAL INTERFACE FOR LINAC BEAM DYNAMICS DESIGN AND SIMULATION BASED ON LORASR

P. Braun*,[1], E. Boos[2], K. Kuempel[1], H. Podlech[1,3], J. Storch[1], R. Tiede[1]
[1]Institute for Applied Physics (IAP), Goethe University, Frankfurt am Main, Germany
[2]GSI Helmholtzzentrum für Schwerionenforschung, Darmstadt, Germany
[3]Helmholtz Research Academy Hesse for Fair (HFHF), GSI Helmholtzzentrum für Schwerionenforschung, Campus Frankfurt, Frankfurt, Germany

Content from this work may be used under the terms of the CC BY 4.0 licence (© 2026). Any distribution of this work must maintain attribution to the author(s), title of the work, publisher, and DOI.

Abstract

LORASR-Designer is a graphical user interface for linac beam dynamics design and simulation based on the LORASR simulation code developed at the Institute for Applied Physics. It extends existing LORASR workflows by enabling interactive configuration, parameterization, and validation of RF linac layouts. Instead of direct input-file editing, accelerator sections and design parameters are represented in a structured internal model, including section configuration, phase settings, longitudinal design modes, and aperture-related quantities. This improves consistency in model definition, supports backward-compatible handling of legacy configurations, and enables reproducible project-based workflows. LORASR-Designer is integrated into the LINAC-Multitool, where it adds design functionality while using the existing structures for visualization and evaluation of beam dynamics results.

INTRODUCTION

LORASR is a multi-particle tracking code under continuous development at the Institute for Applied Physics (IAP) [1], used for decades as a central design tool for ion linacs. It treats drift-tube structures of both $\beta\lambda/2$- and $\beta\lambda$-type, and it covers different design approaches like constant synchronous phase, equidistant gap spacing, and the KONUS (Combined Zero Degree Structure) concept, for whose definition its input format is specifically laid out. Its strength lies in a fast, space-charge-aware particle-dynamics kernel; its practical weakness is the user interface.

A LORASR run is defined by a single fixed-format text file, the deck `in`. It is composed of interdependent blocks, among them global parameters (`GRUN`), the section table, per-gap voltage (`VOLT`) and synchronous-phase (`PHIS/PHEQ`) profiles, aperture and drift-tube-length ratios (`GADI`, `DDLV`), transverse focusing elements (`RADZ`), explicit drift-tube geometry (`FIST`), and the initial phase-space distribution (`LRST`). These blocks are coupled: changing the number of gaps in a section, for example, invalidates indices referenced elsewhere in the deck.

The kernel returns its results as plain text as well, the central file being `DD`: it echoes the interpreted input, lists the synchronous particle gap by gap, and gives the `REAL DRIFT TUBE STRUCTURE` table with center distance, tube and gap length, and inner diameter of every drift tube. Together, `in` and `DD` define what the kernel is asked to do and what it made of it.

Editing such a deck by hand requires detailed knowledge of the format and offers no feedback until the simulation is run. Mistakes are easy to make and hard to spot: a stray tab character where the fixed-format deck expects spaces, a drift-tube count that no longer matches the section definition, or geometry ratios set incorrectly with nothing to show the resulting shape beforehand. The simulation then often fails to run to completion and aborts without a useful hint as to the cause. Even once a problem is noticed, it is often unclear which block or value has to be changed. Spotting the cause takes an expert.

This contribution presents the *LORASR-Designer*, a graphical front-end that replaces manual text editing with an interactive, physics-aware workflow. The tool (i) parses any existing deck into a numerical data model and re-exports it faithfully, (ii) lets the user edit each section according to its design mode while continuously assessing its consistency, (iii) visualizes the resulting drift-tube geometry to scale, (iv) guards against known crash conditions before a run is launched, and (v) automates parameter studies with parallel execution and overlaid result plots.

THE LORASR-DESIGNER

The LORASR-Designer adds a new function to the LINAC-Multitool [2], the established Python environment for the post-processing and visualization of LORASR results at IAP. Within this environment the Designer contributes the interactive design and deck-editing functionality, while the existing Multitool structures, in particular LORASR GRAPHX [3], are reused for visualizing and evaluating the beam-dynamics output. All lattice information is held in a single, strictly numerical data model that is shared between the design and the analysis side; Fig. 1 shows how the two sides are tied together through it.

Numerical Data Model

At its core the Designer parses a deck into a strictly numerical data model from which the deck is regenerated on export. Beyond the deck, the complete model (metadata, design rules and any parameter-sweep specification included) is stored as a self-contained, human-readable JSON project file, which makes a study reproducible and easy to version and share. For imported decks a byte-faithful round-trip is guaranteed: the input text is preserved and only re-serialized

* braun@physik.uni-frankfurt.de

ISBN: 978-3-95450-275-2 ISSN: 2226-0366 doi: 10.18429/JACoW-LINAC2026-THPO038

THE FUNDAMENTAL POWER COUPLER FOR CSNS-Ⅱ ELLIPTICAL CAVITIES

M. Fan†,1,2, H. Liu1,2, X. Wu1,2, A. Li 1,2, W. Zhou1,2, C. Zhang1,2, P. Qu 1,2, Q. Chen1,2, B. Li1,2, F. He2, M. Xu2, R. Ge2, S. Wang1,2
[1]Spallation Neutron Source Science Center, Dongguan, China
[2]Institute of High Energy Physics, Chinese Academy of Sciences (CAS), Beijing, China

Abstract

The China Spallation Neutron Source upgrade project (CSNS-II) uses 24 elliptical cavities in the LINAC section. Each cavity is equipped with a coaxial fundamental power coupler (FPC) featuring a characteristic impedance of 50 Ω and a fixed coupling antenna. The coupler must withstand a minimum peak power of 600 kW with 5% duty factor and an equivalent average power of at least 40 kW. This paper details the multiphysics design, which encompasses electromagnetic optimization, multipacting analysis, and thermal-stress simulations. Additionally, the high-power conditioning results for the first batch of power couplers are presented.

INTRODUCTION

The China Spallation Neutron Source project (CSNS) contains a 50-kW ion source, a 3 MeV radio frequency quadruple, an 80 MeV drift tube linac (DTL) and a 1.6 GeV rapid cycling synchrotron (RCS) has stable operated over 6 years [1]. To upgrade the beam power from 100 kW to 500 kW, the CSNS-II project entails the installation of 20 double spoke superconducting cavities (ten cryomodules) and 24 elliptical superconducting cavities (eight cryomodules) downstream of the DTL in the linear accelerator tunnel [2]. All elliptical cavities require about 10.15 MW total power to accelerate the beam energy from 165 MeV to 300 MeV. To this end, each elliptical cavity is equipped with an FPC mounted on the beam pipe.

As a critical component of the superconducting cavity system, the FPC plays an indispensable role. It serves not only as the physical and thermal transition between the ambient-temperature power source and the cryogenic cavity, but also provides essential isolation between the cavity's ultra-high vacuum (UHV) and the atmospheric environment, all while ensuring the efficient transmission of radio frequency (RF) power into the cavity. To ensure optimal performance, various coupler architectures were rigorously investigated and evaluated. A coaxial type FPC featuring a 50-ohm characteristic impedance, a single TRISTAN window and a fixed antenna was ultimately selected. Design parameters of the FPC are shown in Table 1.

This paper mainly focuses on the design and high-power conditioning results of the FPC for CSNS-II elliptical cavities. First, the electromagnetic optimization and multipacting (MP) simulations of the FPC are conducted, followed by thermal and stress analysis under various operating conditions. Finally, the high-power test results are presented to experimentally verify the design, followed by a comprehensive summary in the end.

Table 1: Design Parameters of the FPC

Parameters	Value
Frequency (f)	648 MHz
Peak power per FPC	600 kW
Repetition frequency	50 Hz
Pulse width	1 ms
Maximum average power	40 kW
External quality factor (Q_e)	9.5×10^5
FPC type	Coaxial
Impedance	50 Ω
Number of FPC per cavity	1
Coupling type	Antenna

RF DESIGN

The RF design aims to minimize reflection at the operating frequency, eliminate hard MP barriers and determine the final antenna length after the FPC and cavity are assembled. In this section, the simulations were carried out utilizing CST Studio Suite [3].

Electromagnetic Optimization

In terms of RF topology, the FPC shown in Fig. 1 can be divided into three main sections: the doorknob, the RF window, and the coaxial transition section. To minimize the probability of RF breakdown, waveguide interface dimensions of the doorknob were maintained identical to those of a standard WR1500 waveguide. For the main coaxial transmission line, the outer and inner conductor diameters were chosen to be 145 mm and 63 mm, respectively. Bridging these two distinct geometries, a knob measuring 235.2 mm in diameter and 81 mm in height was employed to ensure a smooth electromagnetic transition.

The RF window is a critical component of the FPC. At the heart of this component is a 10 mm thick planar ceramic disk fabricated from 97.6% purity Al_2O_3. To suppress MP effects, a 5-10 nm thick Titanium Nitride (TiN) film is sputtered on the vacuum side of the ceramic. Furthermore, impedance matching of the RF window was achieved by meticulously optimizing the height of the node and its vertical distance to the ceramic.

The primary function of the coaxial transition section is to smoothly taper the outer diameter of the FPC main

† fanmx@ihep.ac.cn

Content from this work may be used under the terms of the CC BY 4.0 licence (© 2026). Any distribution of this work must maintain attribution to the author(s), title of the work, publisher, and DOI.

ISBN: 978-3-95450-275-2 ISSN: 2226-0366 doi: 10.18429/JACoW-LINAC2026-THPO039

STEADY-STATE AND TRANSIENT SIMULATIONS OF AN RF CAVITY FED VIA MULTIPLE PORTS

M. Luong†, P. Hamel, T. Hamelin, O. Piquet
Université Paris-Saclay, CEA, Gif-sur-Yvette, France

Abstract

High power radiofrequency (RF) cavities such as RFQ may require multiple input couplers in order to circumvent the breakdown limitation. With advances in solid-state amplifiers, each coupler is often connected to a single source. Although all amplifiers are theoretically synchronized in amplitude and phase by an LLRF system, calibration or control errors may persist. These errors, as well as disparities in coupling factors (or external Q), affect the amplitude and phase of the voltage seen by the beam and consequently energy gain and dispersion. An imbalance between the different RF sources can also lead to excessive reflected power on one or several of the couplers. This paper presents a numerical simulation method based on the Scilab freeware with its Xcos module (equivalent to Matlab and Simulink), capable of predicting not only the steady-state but also the transient behaviour of a cavity fed in this manner. This method is applied to the ESS RFQ. As an example of the results, it appears that the reflected power is evenly distributed across the couplers, exhibiting the same transient behaviour in the event of an uneven distribution of external Q, provided that all sources deliver signals of equal amplitude and phase. This method makes it possible to consider countless failure scenarios.

INTRODUCTION

The problem of feeding an RF cavity from multiple power sources arises when a single coupler can no longer handle the required power due to its breakdown limit, or when a single RF source cannot provide that same power: the question then becomes how to balance the various sources in order to efficiently transfer power to the cavity and the beam [1]. This situation is common in RFQs [2-4]. Studies in the literature usually present analytical formulas that are difficult to derive oneself for verification purposes. Furthermore, these formulas generally apply to steady-state rather than transient conditions. The aim of our work is to present a numerical method that is easy to implement, based on the fundamental equations [5], to handle both transient and steady-state conditions in a variety of complex scenarios.

SIMULATION MODEL FOR ONE PORT

The simulation model is based on a conventional representation (Fig. 1) of an RF cavity by a LCR resonator fed through an ideal lossless transformer [5]. The required power is given by:

$$P_g = \frac{V_c^2}{4\left(\frac{r}{Q}\right)Q_L}(S1^2 + S2^2), \quad (1)$$

with:

$$S1 = 1 + \frac{\left(\frac{r}{Q}\right)Q_L I_{b0}}{V_c}\cos\phi_b,$$

$$S2 = \frac{\Delta f}{f_{1/2}} + \frac{\left(\frac{r}{Q}\right)Q_L I_{b0}}{V_c}\sin\phi_b,$$

$$\frac{1}{Q_L} = \frac{1}{Q_0} + \frac{1}{Q_e},\ \Delta f = f_0 - f_a \text{ and } f_{1/2} = \frac{1}{2Q_L},$$

where Q_L and Q_e are respectively the loaded and external quality factor. To minimize P_g, S2 can be cancelled by detuning the cavity first, then S1 can be minimized by selecting the correct coupling factor:

$$\beta_{opt} = \frac{Q_0}{(Q_e)_{opt}} = 1 + \frac{2RI_{b0}}{V_c}cos\,\phi_b, \quad (2)$$

with $Q_L = (Q_L)_{opt} = \frac{Q_0}{1+\beta_{opt}}$. Finally, the minimum required power reads:

$$\left(P_g\right)_{min} = \frac{V_c^2}{\left(\frac{r}{Q}\right)(Q_L)_{opt}}. \quad (3)$$

Note that ϕ_b is defined negatively and r/Q uses the linac definition. The model parameters used for the ESS RFQ are listed in Table 1.

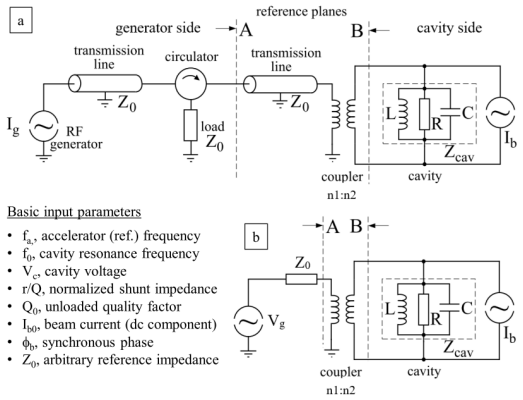


Figure 1: Conventional model for an RF cavity connected to one port: scheme (a) can be simplified to scheme (b). Amplitude and phase of V_g, ratio n2/n1, L, C and R are derived from the input parameters in Table 1.

IMPLEMENTATION IN SCILAB/XCOS AND EXTENSION TO *N* PORTS

Before discussing the transition from a single power port to *N* power ports, it is worth noting that the differential equations associated with the RLC model can be integrated over time using Scilab/Xcos [6], a freeware similar to Matlab/Simulink. This provides both transient and steady-

† Michel.luong@cea.fr

Content from this work may be used under the terms of the CC BY 4.0 licence (© 2026). Any distribution of this work must maintain attribution to the author(s), title of the work, publisher, and DOI.

ISBN: 978-3-95450-275-2 ISSN: 2226-0366 doi: 10.18429/JACoW-LINAC2026-THPO040

ONLINE BEAM ALIGNMENT STRATEGIES FOR THE STCF INJECTOR MAIN LINAC*

D.Y. Xiao[1], H. Hu[1], S.T. Teng[1], T.N. Hu[†,1], Y.F. Zeng[1], Y. Wang[1], D. Gu[2], Y.J. Yuan[3], J.Y. Tang[4]
[1]Huazhong University of Science and Technology, Wuhan, China
[2]Shanghai Advanced Research Institute, Shanghai, China
[3]University of Chinese Academy of Sciences, Beijing, China
[4]University of Science and Technology of China, Hefei, China

Abstract

The main linac of the Super Tau-Charm Facility (STCF) injector consists of 36 constant-gradient traveling-wave accelerating structures, each with a length of 3 m. Component misalignments can induce beam orbit distortions and emittance growth during long-distance transport. In this paper, an online beam alignment system for the STCF injector main linac is designed. A complete beam dynamics model is established to evaluate the effects of misalignments and determine the orbit correction requirements. A dual-direction corrector magnet is then designed through three-dimensional electromagnetic simulations to provide the required deflection capability. Finally, different BPM-corrector layouts are compared in terms of orbit correction performance and required deflection angles, and a suitable layout for high-performance beam operation is determined. The results provide a reference for the engineering design of the online beam alignment system for the STCF injector main linac.

INTRODUCTION

The STCF is a large-scale electron–positron collider dedicated to high-precision physics studies in the tau-charm energy region, for which stringent requirements are imposed on the injector beam quality and stability [1]. As a key component of the injector, the main linac is responsible for electron beam acceleration and long-distance transport, and its performance directly affects the subsequent injection process. The STCF injector main linac consists of 36 constant-gradient traveling-wave accelerating structures, each with a length of 3 m [2]. The schematic layout of the main linac and associated beamline components is shown in Fig. 1. Due to the long transport distance and numerous accelerator components, maintaining stable beam orbit transmission is a critical challenge for the STCF injector.

Under practical engineering conditions, machining and installation errors of accelerating structures and beamline components are inevitable, and initial orbit deviations may also exist in the injected beam. These errors cause the beam centroid to deviate from the reference trajectory and accumulate along the beamline. Off-axis beam transport may further induce transverse phase-space distortion and emittance growth, degrading beam quality. Therefore, mechanical alignment alone is insufficient for long-distance linacs, and an online beam alignment system is required for real-time orbit monitoring and correction [3].

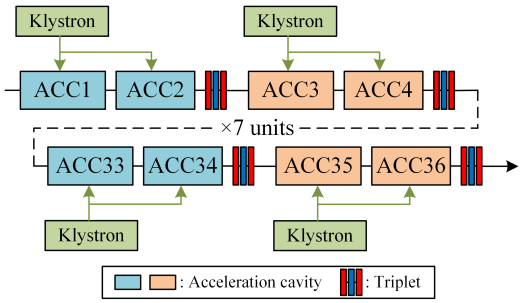


Figure 1: Layout of the STCF injector main linac.

An online beam alignment system typically consists of beam position monitors (BPMs) and orbit correctors. BPMs are used to measure transverse beam position deviations, while correctors provide corresponding transverse kicks to restore the beam orbit [4]. For long linac sections, the number and arrangement of BPMs and correctors directly influence the correction performance and system complexity, while the corrector capability determines the compensable orbit error range.

In this paper, the design of an online beam alignment system for the STCF injector main linac is investigated. The beam orbit variations induced by component misalignments without orbit correction are first analyzed. A dual-direction corrector magnet is then designed according to the correction requirements. Finally, different BPM-corrector layouts are evaluated, and an online alignment scheme suitable for high-performance beam operation is identified.

BEAM ORBIT ANALYSIS AND DUAL-DIRECTION CORRECTOR DESIGN

The STCF injector main linac consists of 36 constant-gradient traveling-wave accelerating structures, each 3 m long, together with other beamline components. Due to component misalignments, deviations between the actual mechanical centers and the reference trajectory are inevitable, causing the beam centroid to gradually deviate from the ideal orbit during transport. To investigate their effects on beam transport performance, a beam dynamics model including

* This work is supported by the National Natural Science Foundation of China (No.12341501), the National Key R&D Program of China under Contract No. 2022YFA1602200, the international partnership program of the Chinese Academy of Sciences Grant No. 211134KYSB20200057 and the STCF key technology research and development project.
† TongningHu@hust.edu.cn

Content from this work may be used under the terms of the CC BY 4.0 licence (© 2026). Any distribution of this work must maintain attribution to the author(s), title of the work, publisher, and DOI.

ISBN: 978-3-95450-275-2 ISSN: 2226-0366 doi: 10.18429/JACoW-LINAC2026-THPO041

RF DESIGN OF BROADBAND HIGH-POWER COAXIAL HOM EXTRACTORS FOR THE FCC-ee 400 MHz CAVITIES *

S. Gorgi Zadeh†, C. Barbagallo, K. Canderan , F. Peauger, CERN, Geneva, Switzerland

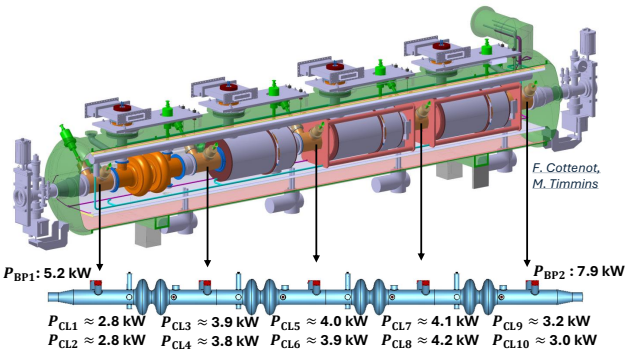
Abstract

The higher-order mode (HOM) power generated in the 2-cell 400 MHz cavities and associated auxiliary components of the FCC-ee at the Z working point, with a beam current of 1.28 A, is estimated to reach approximately 49 kW per four-cavity cryomodule. Efficient extraction of this power is essential to ensure stable operation and to limit the thermal load on the cryogenic system. In this work, the HOM damping requirements for Z operation are reviewed, and the RF design of broadband high-power coaxial HOM extractors is presented. The proposed extractors are normal-conducting devices located in the inter-cavity regions of the cryomodule, each capable of handling kilowatts of HOM power while keeping the heat load to the cryogenic system within acceptable limits. The extracted HOM energy is taken outside the cryomodule and dissipated in RF loads at room temperature. A ceramic window is used to isolate the load from the beam vacuum, with optimized RF matching to minimize reflections. The performance of the proposed design is evaluated and compared with alternative HOM damping schemes, such as beamline absorbers and waveguide dampers.

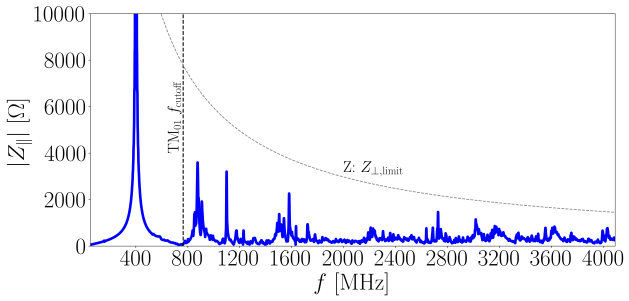
INTRODUCTION

The current baseline design of the FCC-ee RF accelerating system includes 2-cell 400 MHz cavities for the Z, W, and H collider working points [1]. Among these operating scenarios, the Z working point presents the most demanding requirements for higher-order mode (HOM) damping due to the ampere-level beam current, which leads to stringent beam stability constraints and significant HOM power deposition in the cavities. These operating conditions necessitate the development of a dedicated HOM damping scheme for the FCC-ee 400 MHz cavities.

The main HOM damping challenges for the FCC-ee 400 MHz cryomodule are achieving broadband tranmission with high-power extraction capability while maintaining a compact design and minimizing the cryogenic heat load. Conventional HOM damping approaches [2], including waveguide (WG) couplers, beam-line absorbers (BLA), superconducting coaxial HOM couplers, and beam-pipe-based coaxial transmission lines [3], each present limitations for a low-frequency, high HOM power, multi-cavity cryomodule application in terms of power handling, cryogenic heat load, or integration complexity. This paper presents the RF design of a novel high-power broadband coaxial HOM extractor for the FCC-ee 400 MHz cryomodules, developed with these constraints taken into consideration.



(a) Approximation of HOM power distribution in the 400 MHz module



(b) Longitudinal impedance of the 400 MHz module

Figure 1: Estimated HOM power distribution in the FCC-ee 400 MHz cryomodule among the coaxial lines and end beam pipes (a), and the longitudinal impedance of the cryomodule (b). The total HOM power is estimated to be 49 kW, of which approximately 0.5 kW is extracted through the eight hook-type HOM couplers.

HOM POWER IN FCC-EE CRYOMODULES

Each FCC-ee cryomodule consists of four 2-cell, 400 MHz cavities, as shown in Fig.1(a). The cavity design avoids trapping HOMs with high longitudinal impedance; however, the first dipole passband modes with large transverse impedances remain trapped and are strongly damped by two hook-type superconducting HOM couplers [4] installed near each cavity. At the Z working point, the total HOM power generated in the cryomodule is estimated to be around 49 kW. To extract this power, the current design employs two large normal-conducting coaxial HOM extractors located between cavities and outside the helium tank. Their design is therefore independent of the helium tank, but they occupy the inter-cavity space and increase the overall cryomodule length. Due to their relatively large distance from the cavities, the fundamental-mode (FM) field at the extractor locations is sufficiently low, eliminating the need for FM rejection notches.

The module longitudinal impedance spectrum (Fig. 1(b)) is broadband, with two main peaks between 800 and

* Work supported by CERN

† shahnam.gorgi.zadeh@cern.ch

Content from this work may be used under the terms of the CC BY 4.0 licence (© 2026). Any distribution of this work must maintain attribution to the author(s), title of the work, publisher, and DOI.

ISBN: 978-3-95450-275-2 ISSN: 2226-0366 doi: 10.18429/JACoW-LINAC2026-THPO042

FPGA-BASED FREQUENCY SHIFT CORRECTION FOR LINEAR ACCELERATORS

O. E. Delialioglu*, SOKENDAI, Hayama, Kanagawa, Japan
E. Cicek, K. Futatsukawa, Y. Nakazawa, M. Otani, KEK, Tsukuba, Ibaraki, Japan
Y. Fuwa, Y. Kondo, T. Takayanagi, JAEA, Tokai, Ibaraki, Japan

Abstract

The J-PARC muon $g-2$/EDM experiment features the world's first dedicated muon linac, demanding strict radio-frequency (RF) field stability. The Radio Frequency Quadrupole (RFQ), the linac's initial stage, experiences frequency shifts that cause operation outside the RFQ bandwidth. Conventional tuning methods cannot be used due to time and budget constraints. To overcome frequency shifts in the RFQ without physical tuners, this study presents a frequency-shifted operation algorithm implemented on a Field-Programmable Gate Array (FPGA). Installed for the 0.34 MeV acceleration test in June 2026, the system successfully maintained the required stability (±0.21 % amplitude, ±0.20 deg phase), demonstrating that this approach supports the precision goals of the J-PARC experiment.

INTRODUCTION

The J-PARC E34 project introduces the world's first dedicated muon linac to measure the anomalous magnetic moment of the muon $(g-2)$ and the electric dipole moment (EDM) with unprecedented precision. Accelerating ultracold muons with minimal emittance growth imposes stringent RF field stability requirements on the LLRF system: ±1 % (peak-to-peak) in amplitude and ±1 deg (peak-to-peak) in phase [1].

As shown in Fig. 1, the Muon Linac consists of four main accelerating stages over a length of approximately 40 m: a Radio-Frequency Quadrupole (RFQ-II) [2, 3], an Interdigital H-mode Drift Tube Linac (IH-DTL) [4, 5], a Disk and Washer Coupled Cavity Linac (DAW-CCL) [6], and a Disk Loaded Travelling Wave Structure (DLS) [7].

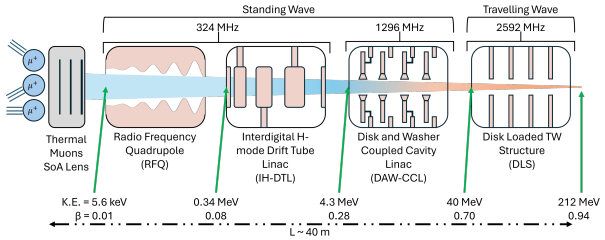


Figure 1: Overall structure of the muon linac.

Main parameters of the Muon Linac are provided in Table 1. Due to the beam current being small, a beam-loading compensation system was considered unnecessary.

The RFQ-II (Fig. 2), the initial accelerating structure, operates at 324 MHz with 4.2 kW RF power supplied by a Solid-State Amplifier (SSA). For the verification using a Vector Network Analyzer (VNA) setup (Fig. 3), the resonance of the cavity was measured under 7.10×10^{-6} Pa vacuum, 25.5 °C cavity temperature, 24.8 °C chamber temperature, and 44 % chamber humidity. As depicted in the S21 measurement result (Fig. 4), a significant shift of −153 kHz from the 324 MHz operating frequency was observed, leading to excessive power reflection that necessitates compensation.

Table 1: Main Parameters of the Muon Linac

Parameter	Value
Kinetic Energy	212 MeV
Beam Current	1×10^6 particles/s
Repetition Rate	25 Hz
Beam Pulse Width	10 ns
Cavity Type	Normal Conducting

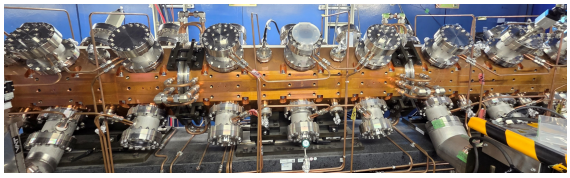


Figure 2: RFQ-II photo.

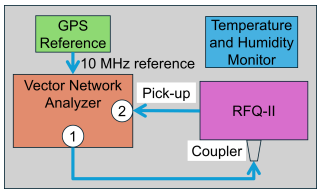


Figure 3: RFQ-II S21 measurement setup.

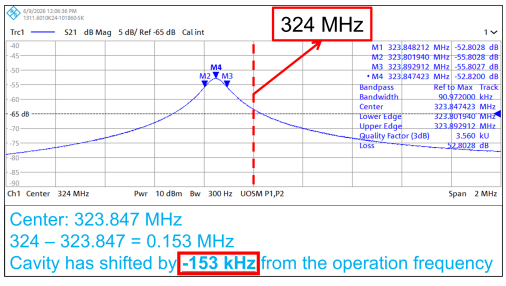


Figure 4: RFQ-II S21 measurement result.

The conventional tuning methods for RFQ-II were impractical due to budget and time constraints, considering a mechanical tuner's cost and duration of installation and adjustment. As an alternative, a real-time frequency-shifted operation algorithm was implemented on an FPGA-based digital environment.

* deliali@post.j-parc.jp

Content from this work may be used under the terms of the CC BY 4.0 licence (© 2026). Any distribution of this work must maintain attribution to the author(s), title of the work, publisher, and DOI.

ISBN: 978-3-95450-275-2 ISSN: 2226-0366 doi: 10.18429/JACoW-LINAC2026-THPO044

NEW TYPE OF HOM ABSORBER FOR CLIC ACCELERATING STRUCTURE BASED ON RESISTIVE COATING ON DIELECTRICS

P. Martinez-Reviriego*[,1], T. Flisgen[2,3], A. Grudiev[1], L. Mourier[1], S. Schmidt[1,2], W. Vollenberg[1]
[1]CERN, Geneva, Switzerland
[2]Brandenburg University of Technology, Cottbus-Senftenberg, Germany
[3]Ferdinand-Braun-Institut gGmbH, Berlin, Germany

Abstract

Accelerating cavities for multibunch operation are commonly equipped with RF loads to absorb energy deposited by the beam into higher-order modes (HOMs). These modes generate electromagnetic wakefields that can induce transverse and longitudinal kicks in the beam, potentially leading to beam instabilities.

This work investigates a novel type of HOM absorber based on resistive coatings deposited on dielectric substrates. The shape of the dielectric and the resistivity of the coating have been optimized to improve the load performance and integration in X-band accelerating cavities for the Compact Linear Collider (CLIC). The study includes experimental characterization of NEG coatings with the target surface resistance of 200 Ω/□ applied to alumina substrates, as well as low-power RF measurements.

INTRODUCTION

The first stage of the Compact Linear Collider (CLIC) is foreseen to provide electron/positron collisions at a center-of-mass energy of $\sqrt{s}$ = 380 GeV and a total luminosity of $\mathscr{L} = 1.5 \times 10^{34}$ cm^{-2}s^{-1} [1].

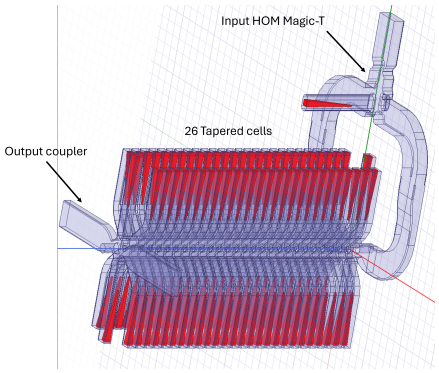


Figure 1: Schematic view of the internal volume of the CLIC-K structure with HOM damping loads [2].

Higher Order Modes (HOM) damping loads are needed to suppress long-range transverse wakefields and preserve the stability of the beam in the main linac due to the high beam current. First, the magnitude of the transverse kick at the position of the second bunch (s = 0.15 m) must be below $|W_y| < 3.4$ V/pC/m/mm [3].

Therefore, every cell of the accelerating structure is designed with 4 HOM damping waveguides with their respective RF loads to absorb the power generated by the beam, as can be seen in Fig. 1. This first stage of CLIC consists of ~ 22000 structures and a total of ~ 2.4 million RF loads. The transverse size of the accelerating structures is determined by the length of the RF loads, making the compactness and material choice of this element key factors in the total cost of the project.

RF loads for HOM mitigation are a requirement in most colliders and Energy Recovery Linacs, being lossy dielectric, such as SiC, one of the main choices for the base material. Dielectric losses follow the behavior given by the equation,

$$P_d = \frac{1}{2}\omega \tan\delta \varepsilon_0 \varepsilon' \int_V |\mathbf{E}|^2 d\tau, \quad (1)$$

where $\omega = 2\pi f$ is the angular frequency, $\tan\delta$ is the loss tangent, $\varepsilon_0\varepsilon'$ is the real permittivity and $\mathbf{E}$ is the electric vector field.

This work proposes a new type of RF absorber based on the losses of resistive coating [4] on top of a dielectric. The surface resistance of the coating is given by

$$R_s = \frac{1}{\sigma t}, \quad (2)$$

where σ is the material conductivity and t represents the coating thickness. In the case that the thickness is negligible compared with the skin depth $\delta = \sqrt{2/(\omega\sigma\mu_0)}$, coating losses are given by

$$P_c = \frac{1}{2R_s}\int |\hat{n} \times \mathbf{E}|^2 dS \quad \text{if} \quad t \ll \delta. \quad (3)$$

In addition, this loss mechanism is potentially compatible with cryogenic temperatures, while only a limited number of dielectrics can be used in this regime [5].

RF DESIGN

Given the 2D behavior of the new type of RF load, the total volume of the load does not play an important role in the absorption, allowing the design of thinner absorbers. A schematic view of the base geometry for the load can be seen in Fig. 2.

The volume is made of Alumina (Al_2O_3) 99.5%, while the red lines correspond to a thin coating (2D material) with a surface resistance R_s = 100 Ω/□. Optimization was done by calculating the wakefield induced in the CLIC cavity, and comparing with the best load obtained using SiC material [6]. A table comparing the main geometry parameters for the optimum solutions for each case is shown in Table 1.

* pablo.martinez.reviriego@cern.ch

Content from this work may be used under the terms of the CC BY 4.0 licence (© 2026). Any distribution of this work must maintain attribution to the author(s), title of the work, publisher, and DOI.

ISBN: 978-3-95450-275-2 ISSN: 2226-0366 doi: 10.18429/JACoW-LINAC2026-THPO045

TRANSIENT FIELD EVOLUTION IN TRAVELING-WAVE DISK-LOADED STRUCTURES FOR MUON ACCELERATION UNDER PULSE-COMPRESSED RF EXCITATION

Y. Takeuchi*[1], H. Ego[2], Y. Kondo[3], Y. Nakazawa[2], M. Otani[2], K. Sumi[2]
[1]Nagoya University, Nagoya, Japan
[2]KEK, Tsukuba, Japan
[2]JAEA, Tokai, Japan

Abstract

The 2.592-GHz traveling-wave disk-loaded structure for muon acceleration requires high RF power, motivating use of a spherical-cavity pulse compressor (SCPC). The quasi-constant-gradient (QCG) structure previously designed for the muon linac assumes flat-top excitation, whereas the raw compressed waveform is strongly time dependent. An equivalent-circuit model was used to calculate $E_z(z,t)$, sample it at the arrival times of a reference muon, and evaluate the mean accelerating field and RMS flatness. Under raw SCPC drive, the QCG sampled profile rises downstream. A constant impedance (CI) structure can provide a flatter sampled field profile under raw SCPC drive, but remains below the required mean field at nominal peak power. RF parameter scans were then performed for QCG flat-top duration and CI peak-power scaling. For the reference criteria adopted here, the scans indicate a 38 MW QCG flat-top interval of at least 0.65 μs and a CI peak power of 64.9 MW.

INTRODUCTION

The 2.592-GHz traveling-wave disk-loaded structure (DLS) requires high RF power for muon acceleration. A 2.592-GHz spherical-cavity pulse compressor (SCPC) is currently being designed specifically for the muon linac to provide the required high-power RF pulse [1]. Pulse-compressed RF waveforms are generally time dependent [2, 3], motivating transient analysis of the traveling-wave structure with the modeled input waveform.

The quasi-constant-gradient (QCG) structure studied here was designed assuming flat-top RF excitation, for which the intended axial field distribution is obtained [4]. Its cell lengths were chosen to maintain RF synchronism as the muon velocity increases during acceleration. The raw SCPC output, however, is strongly time dependent. Because the field at each longitudinal position depends on the delayed input waveform, the accelerating-field distribution sampled by the muon can differ from the designed profile. This changes the energy gain along the structure and can cause phase slippage relative to the designed synchronous condition.

The objective of this study is to calculate the transient field in each cell under the modeled SCPC waveform, evaluate the accelerating field sampled by a reference muon in terms of its mean value and RMS flatness, and quantify the corresponding RF conditions. In addition to the existing QCG design, a constant-impedance (CI) structure is examined as an alternative motivated by its potentially favorable response to non-flat pulse-compressed RF waveforms [5].

EQUIVALENT-CIRCUIT MODEL

The transient RF response of the DLS is calculated using a cell-by-cell equivalent-circuit model. Each cell is represented by an equivalent RLC resonator, with nearest-neighbor coupling between adjacent cells and external loading at the input and output couplers. The RF parameters of each cell used to construct the equivalent RLC resonators are obtained from SUPERFISH [6] calculations. The complex cell-voltage envelopes V_n obey

$$\frac{d^2V_n}{d\theta^2} + (2\mathrm{i} + \Gamma_n)\frac{dV_n}{d\theta} + \left[\left(\frac{\omega_n}{\omega}\right)^2 - 1 + \mathrm{i}\Gamma_n\right]V_n - \frac{k_{n-1,n}}{2A_{n-1,n}}V_{n-1} - \frac{k_{n,n+1}A_{n,n+1}}{2}V_{n+1} = \delta_{n1}F_{\mathrm{in}}(\theta),$$

with $\theta = \omega t$, where ω is the drive angular frequency, and

$$\Gamma_n = \frac{\omega_n}{\omega}\left(\frac{1}{Q_n} + \frac{\delta_{n1}}{Q_{\mathrm{ext,in}}} + \frac{\delta_{nN}}{Q_{\mathrm{ext,out}}}\right),$$

$$A_{n,n+1} = \sqrt{\frac{\omega_n R_n/Q_n}{\omega_{n+1}R_{n+1}/Q_{n+1}}}.$$

Here ω_n, Q_n, and R_n are the resonance frequency, quality factor, and shunt impedance of the equivalent RLC resonator for cell n, respectively. The parameter $k_{n,n+1}$ is the nearest-neighbor coupling coefficient, and $A_{n,n+1}$ accounts for the non-uniform voltage normalization between adjacent cells. External-Q loading is included only for the input and output coupler cells, while F_{in}, derived from the interpolated input-power waveform, drives the input cell. The coupled equations are integrated using a second-order finite-difference scheme. The cell-field envelope is evaluated as

$$E_n(t) = \frac{|V_n(t)|}{D_n},$$

where D_n is the cell length.

Figure 1(a) summarizes the analysis procedure. The time-dependent cell fields obtained from the equivalent-circuit model are sampled at the arrival times of a reference muon. For a muon injected at t_{inj}, the sampled field is defined as

$$E_{\mathrm{samp}}(z_i; t_{\mathrm{inj}}) = \left|E_z\left(z_i, t_{\mathrm{inj}} + t_{\mathrm{ref}}(z_i)\right)\right|,$$

* takeuchi@hepl.phys.nagoya-u.ac.jp

Content from this work may be used under the terms of the CC BY 4.0 licence (© 2026). Any distribution of this work must maintain attribution to the author(s), title of the work, publisher, and DOI.

ISBN: 978-3-95450-275-2 ISSN: 2226-0366 doi: 10.18429/JACoW-LINAC2026-THPO047

PARTIAL DISCHARGE-BASED CONDITION ASSESSMENT OF HIGH-VOLTAGE CAPACITORS

V. C. Kröger*, T. Weinhausen, M. Bousonville, C. Christou
Deutsches Elektronen-Synchrotron DESY, Hamburg, Germany

Abstract

High-voltage capacitors may develop localized insulation defects that remain undetected by conventional electrical diagnostics until failure occurs. This work investigates partial discharge (PD) measurements for condition assessment of pulsed-power capacitors. Fourteen capacitor units with different service histories were characterized using phase-resolved partial discharge (PRPD) patterns and the highest repeatedly occurring apparent charge, Q_{IEC}. Units with longer service histories exhibited higher Q_{IEC} values and greater deviations in PRPD patterns at elevated test voltages. The results support comparative PD assessment using reference measurements of equivalent capacitor designs rather than universal acceptance criteria.

INTRODUCTION

The reliable operation of high-voltage capacitors is essential for the availability of particle accelerator systems. Conventional diagnostic methods, including capacitance, dissipation factor ($\tan\delta$), and insulation resistance, characterize the overall electrical properties of the insulation system and may be insensitive to localized defects whose influence on these properties remains within specified tolerances. Consequently, without monitoring, progressive insulation degradation may remain undetected until failure [1].

Partial discharge (PD) measurements provide information on localized electrical activity associated with insulation defects and are widely used for condition assessment of high-voltage insulation systems. However, the product standard for power electronics capacitors does not explicitly require PD testing or provide general acceptance criteria for PD-based insulation assessment [2].

Motivated by the failure of a high-voltage capacitor unit in an RF station at the European XFEL, this work evaluates PD measurements for condition assessment of pulsed-power capacitors. Fourteen units with different service histories were investigated using PRPD analysis and Q_{IEC}. Their PD characteristics are compared to assess whether these measurements provide indications of insulation degradation not identified by conventional electrical diagnostics.

PARTIAL DISCHARGE FUNDAMENTALS

Partial discharges (PDs) are localized electrical breakdown events that remain confined to regions within or along an insulation system where the local electric field exceeds the dielectric strength of the surrounding material. Electrically, PDs appear as short-duration current pulses whose characteristics depend on the applied voltage waveform [3]. Under AC excitation, PD occurrence exhibits characteristic phase relationships to the applied voltage, whereas under pulsed excitation, corona, cavity, and surface discharges [4] as well as electrical treeing [5] still occur, but are triggered by the voltage edges rather than a fixed phase position.

PDs can be classified by their physical origin. Typical discharge sources, illustrated in Fig. 1(a–c), include corona discharges in gaseous regions, surface discharges along dielectric interfaces, and internal discharges within gas-filled voids [1]. Repeated PD activity can progressively degrade the insulation and, under suitable conditions, initiate electrical treeing, as illustrated in Fig. 1(d) [6, 7].

Under AC excitation, PRPD analysis maps the apparent charge of individual PD events to the phase of the applied voltage, providing information for comparing and classifying PD activity. The apparent charge represents the equivalent charge transferred at the terminals of the test object rather than the actual charge involved in the discharge. The highest repeatedly occurring apparent charge, Q_{IEC}, is used here as a comparative measure of PD magnitude [3].

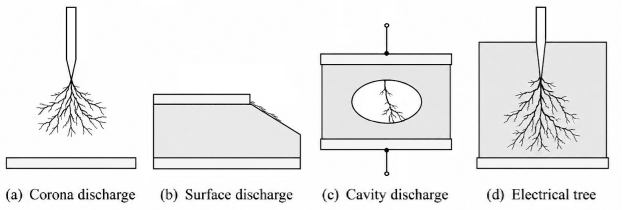


Figure 1: Different types of partial discharge sources.

TEST OBJECT

The test object is a high-voltage capacitor unit for pulsed operation manufactured by Electronicon. It consists of four capacitor elements connected in parallel, embedded in polyurethane resin and encapsulated in a polymer housing. The assembly is subsequently embedded in polyurethane resin and enclosed by a metallic outer housing. The capacitance between the HV busbar and metallic housing was approximately 850 pF. A photograph and schematic representation are shown in Fig. 2(a) and Fig. 2(b), respectively.

One capacitor unit failed after four years of operation in a pulsed-power system at approximately 9.5 kV, with a pulse width of 1.7 ms and repetition rate of 10 Hz. Post-failure inspection (Fig. 3) revealed electrical treeing between the grounded support bracket and HV busbar, indicating insulation degradation as the most probable failure mechanism. This location defines the insulation path investigated by the subsequent PD measurements.

* victor.cajus.kroeger@desy.de

Content from this work may be used under the terms of the CC BY 4.0 licence (© 2026). Any distribution of this work must maintain attribution to the author(s), title of the work, publisher, and DOI.

ISBN: 978-3-95450-275-2 ISSN: 2226-0366 doi: 10.18429/JACoW-LINAC2026-THPO048

PRELIMINARY COMMISSIONING OF THE BEPCII LINAC AS THE INJECTOR FOR PWFA ACCELERATOR

L. Du†, C. Meng, J. Li
Institute of High Energy Physics, Chinese Academy of Sciences, Beijing, China

Abstract

The Beijing Electron Positron Collider II (BEPCII) is a key large scientific installation for high-energy physics research in China, with its linear accelerator (linac) serving as the core injector system responsible for generating and accelerating high-quality electron/positron beams to the designed energy for collider operation. Recently, this linac has been updated to serve as a high-performance electron injector for the Plasma Wakefield Acceleration (PWFA) experiment. This paper presents a complete set of beam commissioning, optimization, and performance validation for the BEPCII linac to meet the strict beam requirements of PWFA. The preliminary commissioning focuses on beam energy stability, orbit quality and emittance control, aiming to provide a high-stability, low-emittance electron beam for PWFA-driven acceleration.

INTRODUCTION

Plasma Wakefield Acceleration (PWFA) has become one of the most promising advanced acceleration technologies owing to its ultra-high acceleration gradient (typically 1–100 GeV/m), which can greatly miniaturize the scale of future accelerators [1]. A high-quality electron injector is critical for PWFA: it must provide stable, low-emittance, precisely timed electron bunches.

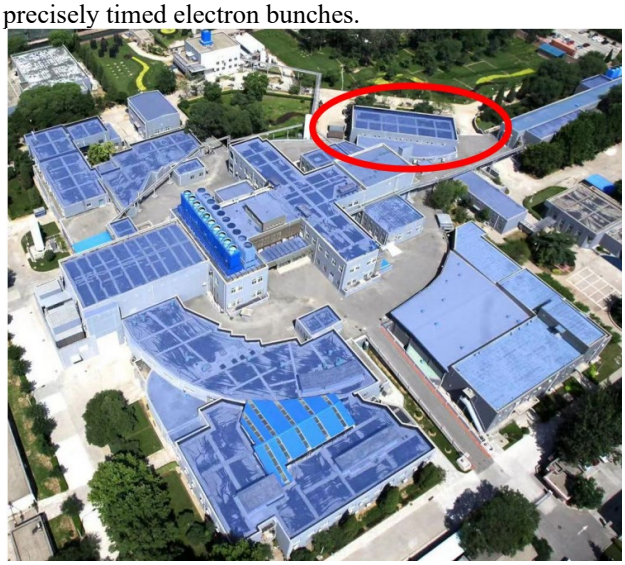


Figure 1: Aerial view of BEPCII with an annotation for the PWFA test facility.

The Beijing Electron Positron Collider II (BEPCII) is an upgraded version of the Beijing Electron Positron Collider (BEPC), built to meet the research needs of high-energy physics and synchrotron radiation applications [2], with its design goal of achieving higher collision luminosity and better beam quality [3], as shown in Fig. 1, and it has been in operation for more than ten years.

The linear accelerator is the front-end core injector of the BEPCII system, which undertakes the tasks of electron/positron generation, pre-acceleration and main acceleration. In the recent plan, the BEPCII linac will be configured as the primary electron injector both for the double-ring collider and for the PWFA acceleration, as shown in Fig. 1 and Fig. 2.

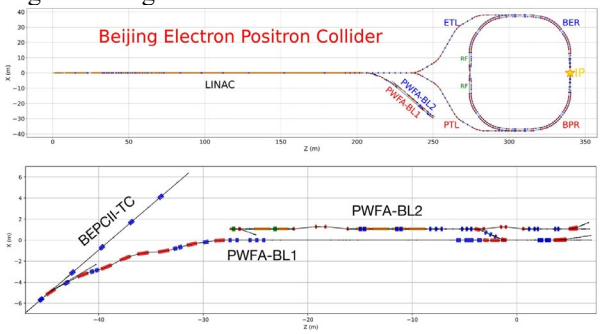


Figure 2: The layout of BEPCII beamline and the PWFA test facility.

However, the standard collider operation parameters cannot meet the strict beam demands of PWFA, including: ultra-high beam energy stability, extremely low beam orbit jitter and low normalized transverse emittance. The required beam parameters at the entrance of the PWFA beamline are shown in Table 1.

Table 1: Required Beam Parameters at the Entrance of the PWFA Beamline

Parameters	Positron	Electron
Energy [GeV]	2.0	2.0
Charge [nC]	>0.05	>2.0
Bunch length [ps]	~4	~4
Geo. Emittance x/y [mm • mrad]	<0.4/0.4	<0.1/0.1
Energy spread [%]	<0.86	<0.86
Slice energy spread [%]	<0.2	<0.2
α_x/α_y	1.5-5.5 /0-3.5	1.5-5.5 /0-3.5
β_x/β_y [m]	4-13 /2.5-14	4-13 /2.5-14

What's more, after long-term operation, the BEPCII linac has experienced large deviations in the working parameters of key components such as RF cavities, magnet power supplies and beam position monitors due to factors such as environmental temperature changes, component

† dulei@ihep.ac.cn

Content from this work may be used under the terms of the CC BY 4.0 licence (© 2026). Any distribution of this work must maintain attribution to the author(s), title of the work, publisher, and DOI.

ISBN: 978-3-95450-275-2 ISSN: 2226-0366 doi: 10.18429/JACoW-LINAC2026-THPO049

ENVELOPE OPTICS FOR A BEAM IN A TRAVELING-WAVE LINAC

E. Ghelfi*[1,2], Y. S. Sigari[1], D. Kaltchev[1], O. Shelbaya[1,2]
[1]TRIUMF, Vancouver, BC, Canada
[2]Department of Physics and Astronomy, University of Victoria, Victoria, BC, Canada

Content from this work may be used under the terms of the CC BY 4.0 licence (© 2026). Any distribution of this work must maintain attribution to the author(s), title of the work, publisher, and DOI.

Abstract

We present a first-order Hamiltonian model describing a beam in a traveling-wave RF structure given the on-axis electric field. Using the infinitesimal transfer matrix formalism, the linear optics about the accelerating reference particle are computed. The spatial phase advance is obtained from electromagnetic field data by extracting the accumulated phase and differentiating it to determine the local wave number k(s), providing a systematic reduction from full field descriptions to a reduced-order beam dynamics model. The model is implemented in the first order envelope code TRANSOPTR, with its results benchmarked against the particle tracking code ASTRA. Near perfect agreement is observed in the limit of negligible space charge, while good accuracy is maintained for higher-space charge applications. The TRANSOPTR model provides a practical framework for efficient tuning and optimization of systems incorporating traveling-wave linacs.

INTRODUCTION

Traveling-wave linear accelerators (TW linacs) accelerate charged particles using a forward-propagating radio-frequency (RF) electromagnetic wave whose phase velocity is matched to the velocity of the beam ($\beta_{\text{phase}} \approx \beta$). Consequently, they are mostly used for accelerating electrons, which quickly reach ultra-relativistic speeds where the particle velocity remains essentially constant along the structure.

Beyond the design stage, model-based operation of TW linacs requires control of transverse and longitudinal beam envelopes for matching and transport. While 3D particle-in-cell (PIC) tracking codes such as ASTRA [1] capture full phase-space dynamics, their computational overhead precludes real-time control, rapid parameter sweeps, and multi-objective optimisation.

Envelope codes bypass macroparticle tracking by integrating the second-moment equations of the beam matrix using infinitesimal transfer matrices [2]. The first-order envelope code TRANSOPTR [3] efficiently computes beam transport including space charge, relying on a canonical Hamiltonian formulation to define the element transport matrices.

In this work, we present a second-order Hamiltonian formulation for a beam in a traveling-wave RF structure with spatially varying wavenumber $k(s)$. From this Hamiltonian, we derive the full 6D F-matrix governing linear dynamics about the reference particle, convert the equations into TRANSOPTR's canonical variables, and benchmark the resulting envelope transport against ASTRA for a 9 cell slac-type TW cavity with input and output standing-wave couplers. Full details on the derivation are reported in Ref. [4].

Fields

The longitudinal electric field for a travelling wave cavity in the accelerating TM_{01} mode is often expressed as a superposition of spatial harmonics $E_z(r,z,t) = \sum_{n=-\infty}^{n=+\infty} a_n J_0(k_{rn} r) e^{j(\omega t - \beta_n z)}$ [5]. Here, n is the spatial harmonic index, $J_0(x)$ is the Bessel function of the first kind of order zero, a_n is the amplitude of the space harmonic of index n, $k_{rn}^2 = k^2 - \beta_n^2$ and $k = \omega/c$.

We evaluate this expression on axis ($r = 0$), take β_n to satisfy the Floquet condition, and introduce a phase function to re-express the physical electric field as:

$$E_z(0,z,t) = \mathscr{E}(z)\cos\psi; \quad \psi \equiv \omega t - \int_0^z k(u)\,du + \theta_0 \tag{1}$$

where $\mathscr{E}(z)$ is the spatial distribution of the longitudinal electric field. From Equation 1, we proceed to approximate the first-order transverse and longitudinal dynamics near the reference particle via the Hamiltonian and envelope equation.

HAMILTONIAN DERIVATION

Field Representation and Gauge Choice

With the distance along the reference trajectory s as the independent variable in the Frenet-Serret coordinate system, the general Hamiltonian for a charged particle in an electromagnetic field can be expressed in terms of the electromagnetic potentials as:

$$H(x,P_x,y,P_y,t,E;s) = -qA_s + \\ -\sqrt{\left(\frac{E-q\Phi}{c}\right)^2 - m^2c^2 - (P_x - qA_x)^2 - (P_y - qA_y)^2} \tag{2}$$

We first consider the electromagnetic potentials for a TW RF gap in a gauge with vanishing scalar potential in cylindrical coordinates (r,ϕ,z) as R. Ryne [6] does for the standing wave (SW) case. We then exploit the gauge invariance of electrodynamics to transform to a more convenient gauge, and similarly to R. Baartman's work for a SW linac [7], we choose a gauge such that $A_r = A_\phi = 0$:

$$\begin{aligned} &A_r = A_\phi = 0, \\ &A_s(r,s,t) = -\frac{1}{\omega}\mathscr{E}(s)\sin\psi(s,t)\left(1 - \frac{\omega^2 r^2}{4c^2}\right), \\ &\Phi(r,s,t) = \frac{r^2}{4}\left[\mathscr{E}(s)k(s)\sin\psi(s,t) + \mathscr{E}'(s)\cos\psi(s,t)\right] \end{aligned} \tag{3}$$

* eghelfi@triumf.ca

IFMIF-DONES ADVANCED MACHINE PROTECTION SYSTEM: INTERLOCK SIGNAL OPTIMIZATION

R. Lorenzo[1,†], C. Carvajal[1], I. Podadera[1,3], M.J. Gutiérrez[1], L. Maindive[1]
A. Moreno[1], P. Cara[2,3], M. Weber[1]
[1]IFMIF-DONES Spain Consortium, Granada, Spain
[2]Fusion For Energy (F4E), Barcelona, Spain
[3]DONES Programme Team, Granada, Spain

Abstract

The International Fusion Materials Irradiation Facility-DEMO-Oriented Neutron Source (IFMIF-DONES), a cutting-edge accelerator-based neutron source for fusion materials research. IFMIF-DONES Facility Project involves a particle accelerator that produces a deuterons beam of 40 MeV and 125 mA, impacting on a flowing liquid lithium target, generating the neutron source by nuclear stripping reaction, therefore a robust central control system for safe and efficient operation.

The current Machine Protection System (MPS) Interlock Signal List comprises more than 3,600 interlock signals distributed across 42 systems. This work presents an optimization approach where each Local MPS generates, as a general rule, only one Interlock Event upstream to the Satellite Units, while only a few systems may generate up to three different Interlock Function types. This reduces the upstream signals from over 3,600 to a range between 42 and approximately 52 signals, significantly simplifying cabling and system complexity while maintaining full flexibility for future expansions.

The resulting optimization design ensures that any new interlock signal arising within a system will not generate a new Interlock Function, as Interlock Functions are inherently bound to systems, not to individual signals, ensuring a stable and scalable MPS architecture while maintaining the required tight response time of 30 µs.

INTRODUCTION

The IFMIF-DONES facility [1] is currently under construction, producing a 125 mA deuteron beam accelerated up to 40 MeV, shaped to a cross section from 100×50 mm to 200×50 mm, striking a liquid lithium curtain 25 mm thick flowing at ~15 m/s. The resulting stripping reactions generate neutrons that irradiate material samples located behind the Lithium Target, on the Test Modules.

The plant systems are organized as follows (Fig. 1): the *Accelerator Systems (AS)* produce and deliver the beam; the *Lithium Systems (LS)* manage the lithium target; the *Test Systems (TS)* handle the irradiation test modules and Test Cell; the *Central Instrumentation and Control Systems (CICS)* perform global plant control; and the *Site, Building and Plant Systems (SBP)* provide buildings, power, cooling, ventilation, and remote handling services.

† ruben.lorenzo@ifmif-dones.es

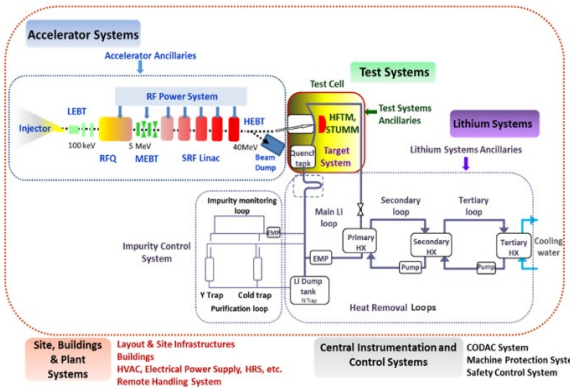


Figure 1: IFMIF-DONES schematic Plant Configuration.

Accelerator Systems

The main functions of Accelerator Systems are to generate and accelerate to an energy of 40 MeV an average current of 125 mA D^+ ions in continuous wave (CW) mode and direct them onto the lithium target to produce neutrons by nuclear stripping reactions.

Lithium Systems

The main functions of the Lithium Systems are to provide the liquid lithium jet whose interaction with the D^+ beam generates the neutron flux for the irradiation of the test modules; and to evacuate the heat power deposited in the lithium by the deuterons. The 125 mA, 40 MeV D^+ beam is injected into the lithium target, with a variable footprint of 200 mm nominal width and 50 mm nominal height.

Test Systems

The main function of Test Systems is to house the Target Assembly, and to allow controlled irradiation of the small steel specimens in the high neutron flux region, just behind the Target Assembly by means of the High Flux Test Module (HFTM) system. Also, to provide sufficient shielding to the surrounding rooms and areas against the intensive neutron and gamma radiation produced in the nuclear D-Li reaction.

Central Instrumentation and Control Systems

The IFMIF-DONES plant control is based on different systems with independent complex functions managed by a central coordination and management system called Central Instrumentation and Control System. It adopts a distributed control approach conferring autonomy to each of the systems to manage the single control loops

ISBN: 978-3-95450-275-2 ISSN: 2226-0366 doi: 10.18429/JACoW-LINAC2026-THPO052

DESIGN OF A SUPERCONDUCTING CAVITY FOR AN EUV ENERGY RECOVERY LINAC

M. Jung[1], M. Chung*,[1]
[1]Department of Physics, Pohang University of Science and Technology, Pohang, Korea

Content from this work may be used under the terms of the CC BY 4.0 licence (© 2026). Any distribution of this work must maintain attribution to the author(s), title of the work, publisher, and DOI.

Abstract

An energy recovery linac (ERL) is an accelerator in which electron bunches are decelerated in the linac after generating radiation to recover their energy. Through this process, the ERL can achieve high energy efficiency while maintaining a high beam current. Due to these advantages, the ERL is an attractive candidate for a next-generation extreme ultraviolet (EUV) light source in lithography. EUV lithography is a critical procedure in the semiconductor fabrication process. Since an EUV-ERL can produce higher power than other conventional methods, it is more cost-efficient in terms of both construction and operation. For efficient energy recovery, superconducting radio-frequency (SRF) cavities are used in the linac of the ERL. To design an SRF cavity, several factors and phenomena, such as the field flatness of the fundamental mode, peak electric and magnetic fields, higher-order mode (HOM) damping, and multipacting, should be considered simultaneously. In this paper, we designed and optimized an L-band SRF cavity for an EUV-ERL. For the optimization of the cavity, machine learning was employed, utilizing the cavity dimensions as input parameters and the impedances of HOMs as the objectives.

INTRODUCTION

The energy recovery linac (ERL) is a type of accelerator where electron bunches are decelerated inside the RF cavity for energy recovery after the radiation process. Through this process, most of the energy of the electron bunches can be reused to accelerate newly injected bunches. Due to this property, an ERL can deliver a high beam current while maintaining high beam quality.

Due to its high energy efficiency, an ERL can be applied in industrial use such as photolithography processes for the fabrication of semiconductor chips [1, 2]. The EUV photolithography process requires higher power to avoid defects in the circuit as the line width gets narrower. However, the conventional laser-produced plasma process is inefficient at producing high power EUV light. Hence, an ERL can be an attractive candidate for a higher power EUV light source for photolithography.

For the energy recovery process, a superconducting radio-frequency (SRF) cavity is used due to its high quality factor and its capability to store the extracted energy. The performance and stability of an SRF cavity depend mainly on its geometry. To ensure stable ERL operation, the peak electric and magnetic fields must be optimized to prevent field emission and quenching, respectively. Additionally, to produce EUV light at a power level of 10 kW, the operating beam current must be as high as 10 mA. Thus, higher order modes (HOMs) should be damped to suppress power dissipation or beam breakup (BBU) instability invoked by the HOMs.

In this paper, the current progress on the design and optimization of a 1.3 GHz 7-cell superconducting RF cavity for EUV-ERL is presented.

OPTIMIZATION OF CAVITY

Initial Setup

The number of cell is a factor that determines the performance of the cavity. Increasing the number of cell per single cavity can improve the acceleration efficiency, but it makes damping higher order modes more difficult. Thus, in this paper, we set the number of cells to 7 as a compromise between acceleration efficiency and HOM damping. Fig. 1 shows the initial 7-cell SRF cavity designed for EUV-ERL.

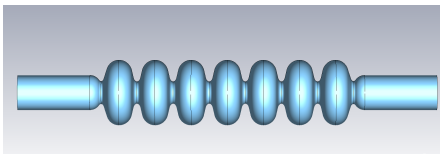


Figure 1: Image of 1.3 GHz 7-cell SRF cavity.

The dimensions of the center cell are based on the 1.3 GHz TESLA cavity design. In addition, the geometry of the end cell was optimized using CST Studio Suite simulation software. To achieve a uniform distribution of the electric field and fine-tune the fundamental frequency, the half-length of the end cell was reduced compared to that of the center cell.

Table 1 shows the initial RF parameters of the EUV-ERL SRF cavity at the fundamental frequency.

Table 1: RF Parameters of the 1.3 GHz SRF Cavity with Initial Design

RF parameter	Value
Frequency (f)	1.300 GHz
R/Q	789.8 Ω
E_{peak}/E_{acc}	2.056
B_{peak}/E_{acc}	4.256 mT/(MV/m)
Field flatness	98.51 %

Optimization for Fundamental Frequency

The most important parameter for the performance of an SRF cavity is the normalized shunt impedance R/Q at the fundamental frequency, which represents the efficiency for acceleration of charged particles. In addition, the normalized peak surface electric field E_{peak}/E_{acc} should be maintained below 2.1 to avoid field emission. Thirdly, to

* moses@postech.ac.kr

ISBN: 978-3-95450-275-2 ISSN: 2226-0366 doi: 10.18429/JACoW-LINAC2026-THPO053

DEVELOPMENT OF A RELATIVISTIC VORTEX ELECTRON SOURCE: CURRENT STATUS AND FIRST RESULTS

A.S. Dyatlov*[1,2], V.V. Kobets[2], M.V. Maksimov[1], M.A. Nozdrin[2],
K. Popov[2,3], K.E. Yunenko[2], D.V. Karlovets†[1]
[1]School of Physics and Engineering, ITMO University, Saint Petersburg, Russia
[2]Joint Institute for Nuclear Research, Dubna, Russia
[3]Institute of Nuclear Physics, Almaty, Kazakhstan

Abstract

Vortex electron beams – *quantum states carrying quantized orbital angular momentum (OAM)* – are of growing interest as novel probes for nucleon structure and spin-related phenomena. Extending these to relativistic energies remains challenging, currently restricted to the few-hundred keV regime in electron microscopes. We investigate MeV-scale vortex beam generation using a classical RF photoinjector. While we consider three OAM generation schemes, our primary focus is the direct transfer of OAM from structured laser radiation to photoelectrons during emission, followed by rapid RF acceleration. This minimizes space-charge degradation via controlled low-charge operation and is compatible with existing technologies. We report on generating twisted UV photons and calculate the evolution of a Laguerre–Gaussian electron wave packet in realistic RF and solenoidal fields.

CONCEPT OF OAM TRANSFER IN A PHOTOINJECTOR SETUP

The experiment utilizes the RF photoinjector test bench currently being developed at the Dzhelepov Laboratory of Nuclear Problems at the Joint Institute for Nuclear Research (JINR) for an electron linac upgrade. Previous vortex beam experiments were restricted to electron microscopes at 10–300 keV [1, 2]. The RF photoinjector enables MeV-scale, single-bunch operation with precise charge control via the drive laser. Low-charge operation suppresses collective space-charge-induced phase-space dilution and helps preserve conditions favorable for coherent single-electron dynamics. The detailed photoinjector layout is presented in in [3] and illustrated in Fig. 1.

We investigate three schemes for generating orbital angular momentum (OAM). The first method transfers OAM from structured laser radiation to electrons during photoemission. While theoretical models predict OAM projection conservation [4], the mode purity of the resulting vortex beam requires further investigation [5]. In our optical setup, the initial laser beam is focused directly onto a diffraction grating to generate the Laguerre–Gaussian modes [6].

The second approach utilizes electron emission in a strong longitudinal magnetic field, governed by the *quantum Busch theorem* [7]. The classical Busch theorem describes macroscopic (*extrinsic, non-quantized*) angular momentum acquisition, widely used in flat-to-round beam transformations [8]. Its quantum generalization implies a fundamentally different regime. By omitting the bucking coil and placing a 1 T solenoid peak field directly at the photocathode, we aim to produce beams with *intrinsic, quantized* OAM.

The third method employs electrostatic dipoles [9]. We propose an electrostatic spiral phase plate consisting of two 100 µm long silver nanoneedles with a tip radius of approximately 100 nm, mounted on a 1 µm thick silicon nitride membrane featuring a 5×5 mm window. Applying a voltage in the 1 V to 5 V range generates an OAM-carrying beam and allows for real-time tuning of the topological charge.

DRIVE LASER UPGRADE FOR UV VORTEX GENERATION

The photoinjector is driven by a custom IAP RAS laser system [10] with a fiber-based master oscillator and solid-state amplifiers, generating 10 ps (FWHM) infrared (IR) pulses at 1047 nm, which are subsequently frequency-quadrupled to the ultraviolet (UV) range for photoemission. Initially, the drive laser's master oscillator and solid-state amplifiers were upgraded [11]. To synchronize the laser with the 2856 MHz RF system, the original 10 MHz repetition rate was tuned to exactly 40.225 MHz (its 71st subharmonic) by reducing the fiber cavity length.

This exact subharmonic matching enabled the ongoing development of a phase-locked loop (PLL) system. This system is designed to precisely synchronize the laser pulse arrival at the photocathode with the 6 MW, 6 µs RF pulse filling the gun cavities. Further details on the synchronization system are provided in [12].

Implementing sequential, delayed pump-lamp triggering optimized the amplifiers. This boosted UV yield energy after the harmonic generation crystals from 1.8 µJ to a range of 3 µJ to 5 µJ. Notably, these enhancements were achieved using lower operating voltages on the pump lamps. Consequently, this upgraded energy output provides a significantly wider dynamic range for tuning the initial electron bunch charge during photoemission.

To generate and transport twisted modes to the photocathode, the laser line was equipped with periscopes to compensate for the height difference between the laser table and the beamline axis. The beam is conditioned by a spatial filter before passing through phase-modulating diffractive optical

* aleksandr.dyatlov@metalab.ifmo.ru
† d.karlovets@gmail.com

Content from this work may be used under the terms of the CC BY 4.0 licence (© 2026). Any distribution of this work must maintain attribution to the author(s), title of the work, publisher, and DOI.

ISBN: 978-3-95450-275-2 ISSN: 2226-0366 doi: 10.18429/JACoW-LINAC2026-THPO054

DEVELOPMENT OF CAPACITIVE BELLOWS TUNER FOR LOW-BETA SINGLE SPOKE CAVITY*

Jun Tamura†, Yasuhiro Kondo, Takatoshi Morishita
J-PARC, JAEA, Ibaraki, Japan

Abstract

We have been developing a capacitive bellows tuner to extend a frequency tuning range of low-β single-spoke cavities. By introducing a length-adjustable electrode close to the inner conductor electrode of a coaxial cavity resonator, it is expected to achieve a wider tuning range of the cavity frequency than is possible with conventional methods. To investigate the feasibility of the capacitive frequency tuner, we fabricated a bellows electrode from 1-mm-thick high-purity niobium sheets. The fabricated bellows electrode could be compressed by more than 45 mm from its natural length of approximately 700 mm. For the frequency measurement, it was incorporated into the 324 MHz single-spoke cavity currently under development at J-PARC. We confirmed that compressing the bellows electrode shifts the cavity frequency by more than +1 MHz.

INTRODUCTION

In superconducting (SC) cavities, adjusting their resonance frequency is a particularly important procedure. SC cavities are fabricated by press-forming high-purity niobium sheets and joining them together by electron beam welding (EBW). Therefore, compared with room temperature cavities which are typically fabricated through machining and brazing, SC cavities tend to have greater deviations from their design dimensions, and consequently, from their design frequencies.

We have been developing a capacitive tuner which may extend a frequency tuning range of low-β SC cavities. In coaxial-type cavity resonators such as half-wave resonators and single-spoke cavities, the electric field is concentrated at the center of the inner conductor electrode. By introducing an additional electrode, independent of beam acceleration electrodes, toward the center of the inner conductor electrode, the cavity frequency can be significantly shifted. To tune the frequency, it is necessary to control the distance between this externally-introduced electrode and the inner conductor electrode. Therefore, we conceived of designing an external electrode as a bellows structure resembling an elliptical SC cavity, so that the distance between those electrodes can be adjusted by its compression and extension. This paper describes the design and fabrication of the capacitive bellows tuner, as well as the frequency measurement of the 324 MHz single-spoke cavity combined with the bellows electrode.

* This work was supported by JSPS KAKENHI Grant Number JP24K15600.

† jtamura@post.j-parc.jp

DESIGN

In the development of the capacitive bellows tuner, we decided to design and fabricate a niobium bellows electrode capable of shifting the resonance frequency of our 324 MHz spoke cavity by more than 1 MHz. The single-spoke cavity currently under development at J-PARC was fabricated as a prototype of the low-β ($\approx$0.2) spoke cavity for the JAEA-ADS linac [1–3]. This spoke cavity, which is $\approx$300 mm long in the axial direction and $\approx$500 mm in diameter, has two RF ports with a diameter of 80 mm on the sidewall. These RF ports are arranged diametrically opposite each other and perpendicular to both the beam axis and the spoke electrode. The bellows electrode is inserted from the RF port toward the center of the spoke electrode. Figure 1 shows the simulation model [4] of the spoke cavity incorporated with the designed bellows electrode. Along its axial length of approximately 700 mm, the bellows electrode has 25 sets of peak (ϕ55 mm) and valley (ϕ22 mm). Examples of the electric and magnetic field distributions are also shown in Fig. 1.

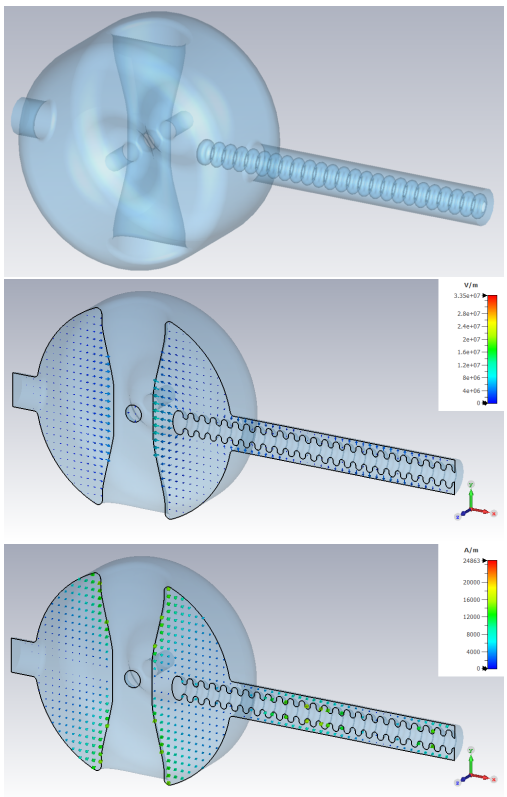


Figure 1: Simulation model (top) and cross-sectional views of the electric (middle) and magnetic (bottom) field distributions.

Content from this work may be used under the terms of the CC BY 4.0 licence (© 2026). Any distribution of this work must maintain attribution to the author(s), title of the work, publisher, and DOI.

ISBN: 978-3-95450-275-2 ISSN: 2226-0366 doi: 10.18429/JACoW-LINAC2026-THPO055

PHYSICS-INFORMED MULTI-OBJECTIVE GENETIC OPTIMIZATION FOR HIGH-CURRENT RFQ DESIGN*

Y. L. Ge, Z. Y. Zhang, W. Ma, L. Lu†
Sino-French Institute of Nuclear Engineering and Technology, Sun Yat-sen University, Zhuhai, Guangdong, China

Abstract

Radio-frequency quadrupole (RFQ) design involves multi-objective optimization in both beam-dynamics and electromagnetic design. This work presents a unified physics-informed genetic optimization framework for RFQ design. Physical and engineering knowledge is embedded into population generation and evolutionary operations to suppress non-physical candidates and reduce the effective search space. For beam dynamics, the framework is coupled with RFQGen and validated across four representative RFQ design scenarios, achieving transmission efficiencies of 97.4–99.8% with optimization costs of approximately 80–300 core-hours. For electromagnetic design, the framework is coupled with CST and validated on a C^{4+} RFQ, achieving a Q factor of 12,799, an 8.7% improvement over the original design, and a 16.7% reduction in RF power loss. The results demonstrate the applicability of physics-informed genetic optimization to automated RFQ design.

INTRODUCTION

The radio-frequency quadrupole (RFQ) is a key accelerating structure in the low-energy front end of modern ion accelerators. Increasing requirements on beam intensity, transmission efficiency, compactness, and operational stability have made RFQ design an increasingly complex optimization problem.

RFQ physical design comprises two coupled stages: beam-dynamics design, which defines vane modulation and focusing profiles, and electromagnetic design, which determines cavity geometry and RF performance. Both involve strongly coupled parameters subject to physical and engineering constraints, making conventional experience-based parameter scans inefficient for high-dimensional global optimization and limiting their ability to identify optimal designs.

Multi-objective genetic algorithms have been successfully applied to accelerator-related system optimization [1, 2]. However, direct application to RFQ design may remain computationally expensive because many generated candidates are physically invalid. We subsequently developed PIGArfq by incorporating physics-informed guidance and engineering constraints into RFQ beam-dynamics optimization [3]. This concept is further extended to electromagnetic design, establishing a unified physics-informed optimization strategy for RFQ design.

The framework embeds physics-informed guidance and engineering constraints into population generation and evolution, reducing infeasible solutions before numerical evaluation. RFQGen and CST are coupled for beam-dynamics and electromagnetic simulations, respectively, as illustrated in Fig. 1.

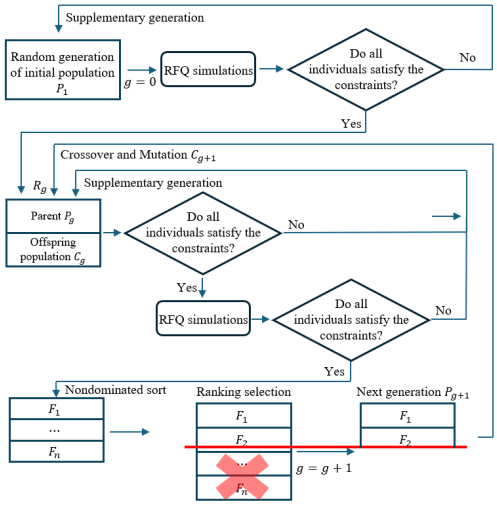


Figure 1: Unified physics-informed multi-objective optimization framework for RFQ beam-dynamics and electromagnetic design.

PHYSICS-INFORMED OPTIMIZATION FRAMEWORK

For beam-dynamics optimization, transmission efficiency η, transverse emittances ε_x and ε_y, longitudinal emittance ε_z, and RFQ length L are selected as objectives. The focusing strength $B(z)$, synchronous phase $\phi_s(z)$, modulation $m(z)$, and inter-vane voltage $V(z)$ are parameterized as design variables, with cell parameters generated by interpolation. The optimization can therefore be expressed conceptually as

$$X = [B(z), \phi_s(z), m(z), V(z)]$$
$$F(X) = [f_\eta(X) \uparrow, f_{\varepsilon_x}(X) \downarrow, f_{\varepsilon_y}(X) \downarrow, f_{\varepsilon_z}(X) \downarrow, f_L(X) \downarrow] \quad (1)$$

Physics-informed guidance for transverse and longitudinal stability, high-current beam transport, and peak surface electric field is combined with constraints on synchronous phase, modulation, and engineering feasibility. These constraints guide initialization and genetic evolution to suppress invalid candidates. RFQGen [3] evaluates the resulting designs, while NSGA handles the five optimization objectives.

For electromagnetic optimization, the resonant-frequency deviation from the target value $|f - f_0|$ and Q

* Work supported by the National Natural Science Foundation of China (Grant Nos. 12505173 and 12575170)
† luliang3@mail.sysu.edu.cn

Content from this work may be used under the terms of the CC BY 4.0 licence (© 2026). Any distribution of this work must maintain attribution to the author(s), title of the work, publisher, and DOI.

ISBN: 978-3-95450-275-2 ISSN: 2226-0366 doi: 10.18429/JACoW-LINAC2026-THPO056

DEVELOPMENT OF ACTINIUM-225 PRODUCTION USING THE 70 MeV CYCLOTRON AND ISOL SYSTEM AT IRIS*

B. S. Park†,1, Y. H. Yeon[1,2], D. H. Gil[1], H. W. Jung [1], I. Hong[1,2], H. Yim[1,2], J. H. Kim[1,2], J. Lee[1,2], T. Shin[1,2]
[1]Institute for Rare Isotope Science (IRIS), Institute for Basic Science (IBS), Daejeon, Korea
[2]TOPTIER Project, Institute for Rare Isotope Science (IRIS), Institute for Basic Science (IBS) Daejeon, Korea

Abstract

The Institute for Rare Isotope Science (IRIS) is developing accelerator-based production of actinium-225 (^{225}Ac) for targeted alpha therapy by combining a 70 MeV proton cyclotron, thorium dioxide (ThO_2) targetry, radiochemical processing, and isotope-separation capabilities. Inventory calculations for a 3-mm-thick ThO_2 production model irradiated at 70 MeV and 100 μA for 48 h predict approximately 100 mCi of in-target ^{225}Ac activity; this is a design estimate, not a demonstrated recovered yield. Separate engineering studies selected ThO_2 thicknesses of 4.0 and 2.5 mm for conduction-cooled and water-cooled targets, respectively. Steady-state finite-element analyses predicted peak temperatures of 82.6 °C at 10 μA and 105.1 °C at 100 μA. Low-current activation tests were also performed using aluminium and 5–6 g ThO_2 targets. Daughter-gamma measurements after approximately two days of cooling yielded measured-to-PHITS activity ratios of 0.34–0.50 for ^{221}Fr and ^{213}Bi, indicating that the absolute production model still requires validation. These results define a staged path toward higher-current irradiation, hot-cell separation, and product-quality assessment.

INTRODUCTION

Targeted alpha therapy couples an alpha-emitting radionuclide to a carrier that recognizes a molecular target. The high linear energy transfer and short tissue range of alpha particles can deliver highly localized damage, while ^{225}Ac offers a 9.9 d half-life and four alpha emissions through its decay chain [1]. Wider research and clinical use, however, remains constrained by supply and by the need to control radionuclidic impurities, particularly long-lived ^{227}Ac.

IRIS is therefore establishing an integrated development chain from proton irradiation to isotope recovery and evaluation. The present paper consolidates the 70 MeV cyclotron and ISOL platform, the preliminary ThO_2 target design, calculated production inventories, and initial low-current gamma-spectrometric tests. Calculated quantities, measured quantities, and planned capabilities are explicitly distinguished because the programme has not yet demonstrated routine high-current irradiation or chemically recovered product at the clinical scale.

* Work supported by an INNOPOLIS grant (RS-2026-25506728) and by the National Research Foundation of Korea under the TOPTIER project (RS-2024-00436392) and RS-2022-00165168, funded by the Ministry of Science and ICT, Republic of Korea.
† bspark@ibs.re.kr

IRIS ACCELERATOR AND ISOL PLATFORM

The IRIS cyclotron provides 30–70 MeV protons, with a design current up to 0.75 mA and a wobbled beam diameter of approximately 50 mm [2]. For ^{225}Ac development, the working energy interval is 40–70 MeV. The cyclotron also drives the isotope-separation-on-line (ISOL) system shown in Fig. 1, where reaction products are released, ionized, pre-separated, mass analysed, and directed either to low-energy users or to the superconducting linac. In August 2024, IRIS reported acceleration of the first ISOL beam, ^{25}Na, to 16.5 MeV/u [3]. This milestone demonstrates the transport and re-acceleration chain, but it is not yet a demonstration of mass-separated ^{225}Ac production.

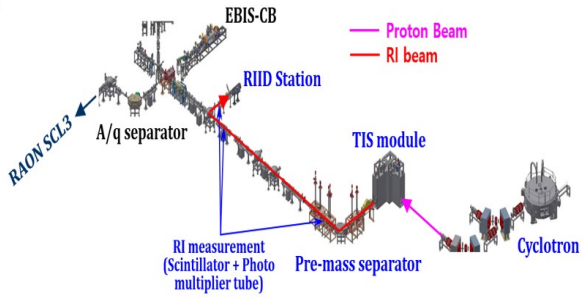


Figure 1: Proton-driven ISOL beamline at IRIS. The cyclotron, target-ion-source module, pre-mass separator, RI diagnostics, A/q separator, and re-acceleration path are shown.

AC-225 PRODUCTION CONCEPT

The baseline route irradiates natural ^{232}Th in oxide form and integrates the excitation functions over the proton slowing-down interval. Published measurements show that proton irradiation of thorium can produce ^{225}Ac [4]. IRIS calculations use 70 MeV incident protons and degrade the energy toward 40 MeV within the target to reduce higher-energy reaction channels and ^{227}Ac co-production. For a 3-mm-thick target model irradiated at 100 μA for 48 h, the estimated in-target ^{225}Ac activity is approximately 100 mCi. Figure 2 shows calculated activities during irradiation and subsequent cooling.

The activities of ^{225,226,227}Ac, ^{223,225}Ra, and ^{227,228}Th were calculated with the Radionuclide Yield Calculator (RYC) [5] for natural ThO_2 irradiated by 40–70 MeV protons.

Content from this work may be used under the terms of the CC BY 4.0 licence (© 2026). Any distribution of this work must maintain attribution to the author(s), title of the work, publisher, and DOI.

ISBN: 978-3-95450-275-2 ISSN: 2226-0366 doi: 10.18429/JACoW-LINAC2026-THPO057

EXPERIMENTAL VALIDATION OF AN X-BAND LLRF PROTOTYPE FOR HIGH-GRADIENT LINEAR ACCELERATORS*

P. D. Meruga[1,2,†], A. Mostacci[2], B. Serenellini[3], B. Baričevič[1], F. Cardelli[3], G. Latini[3]
L. Piersanti[3], M. Cargnelutti[1], M. Bellaveglia[3], S. Pioli[3], X. Fang[3]
[1]Instrumentation Technologies, Solkan, Slovenia
[2]Sapienza University of Rome, Rome, Italy
[3]Istituto Nazionale di Fisica Nucleare – Laboratori Nazionali di Frascati, Frascati, Italy

Abstract

Low-Level RF (LLRF) systems are essential for maintaining amplitude and phase stability in modern linear accelerators, directly affecting beam quality and operational reliability. The increasing use of X-band technology in compact, high-gradient linacs enables ultra-short RF pulses and higher accelerating fields, while also increasing sensitivity to phase noise, timing jitter, and thermal effects. To address these challenges, a dedicated X-band LLRF prototype has been developed within the framework of the EuPRAXIA Doctoral Network for application in next-generation X-band linear accelerators. The system combines a high-speed RF front-end with a FPGA-based digital back-end optimized for fast pulsed operation, low-latency processing, and precise amplitude and phase control. After extensive laboratory testing, the prototype was validated on a real accelerator test bench. This paper presents the system's concept and experimental results, including pulse-to-pulse stability and phase noise performance. The results confirm the feasibility of the proposed X-band LLRF approach for future high-gradient linac applications.

INTRODUCTION

Low-Level Radio Frequency (LLRF) systems control the amplitude and phase of the RF fields that determine beam energy, bunch timing, and longitudinal beam quality. Their stability requirements become especially demanding in compact high-gradient accelerators, where X-band structures not only provide high accelerating gradients and a reduced machine footprint, but also convert small RF phase perturbations into femtosecond-scale timing errors. The EuPRAXIA@SPARC_LAB concept combines an RF injector with plasma acceleration and includes an X-band booster operating at 11.9942 GHz [1, 2].

Therefore, a dedicated pulsed X-band LLRF prototype was developed within the EuPRAXIA Doctoral Network. Earlier contributions described the initial architecture and its laboratory evaluation [3, 4]. The present work concentrates on the subsequent installation and validation at the TEX (TEst stand for X-band) facility at INFN-LNF. In this campaign, the prototype drove a pulsed 1.3 kW X-band amplifier whose output was swept from approximately 400 W to the 1.1 kW saturation region. Individual noise contributions were compared up to 1.0 kW. This was an accelerator-relevant validation of the TEX driver/pre-amplifier section; the facility's full high-power klystron chain was not included in the measurements reported here.

PROTOTYPE DEVELOPMENT AND LABORATORY VALIDATION

The prototype uses a single-stage X-band down-conversion front-end and a double-stage up-conversion back-end. A common 11.9942 GHz master oscillator provides the phase reference. The local-oscillator module derives the X-band down-conversion signal, a 250 MHz ADC clock, a 9 GHz up-conversion signal, and the reference required by the IQ modulator. Two RF inputs are down-converted to intermediate frequency and digitized by 250 Msps ADCs. In the generation path, FPGA-defined in-phase and quadrature waveforms are converted by the DACs, applied to the IQ modulator, and up-converted to the final X-band drive frequency. The digital acquisition and generation hardware is based on the Libera LLRF platform [5]. The assembled X-band LLRF prototype and the laboratory measurement arrangement used for its initial validation are shown in Fig. 1.

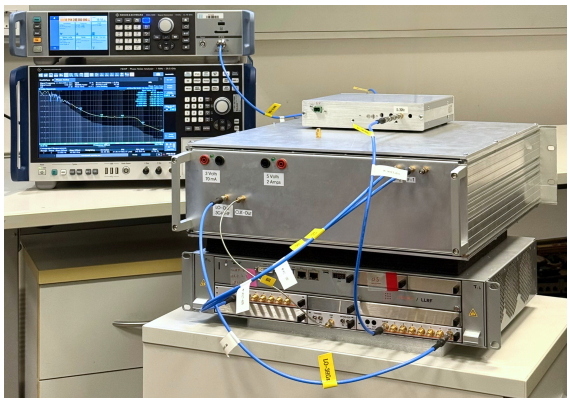


Figure 1: Assembled X-band LLRF prototype comprising analog and digital platforms.

The principal design and performance requirements used for the laboratory and TEX validation are summarized in Table 1. The prototype was evaluated in open-loop operation so that the measured fluctuations could be attributed directly to the acquisition and generation chains without feedback correction.

* This project has received funding from the European Union's Horizon Europe research and innovation programme under grant agreement no. 101073480 and the UKRI guarantee funds.
† phanideep.meruga@i-tech.si

Content from this work may be used under the terms of the CC BY 4.0 licence (© 2026). Any distribution of this work must maintain attribution to the author(s), title of the work, publisher, and DOI.

ISBN: 978-3-95450-275-2 ISSN: 2226-0366 doi: 10.18429/JACoW-LINAC2026-THPO059

GMM-BASED NEURAL SURROGATE FOR TRANSVERSE PHASE-SPACE RECONSTRUCTION AT RAON

Woo Hyeong Kim*,[1], Jang Won Kwon[2], Ji-Gwang Hwang[1]
[1]Kangwon National University, Gangneung, Republic of Korea
[2]Institute for Basic Science (IBS), Daejeon, Republic of Korea

Abstract

Accurate transverse phase-space characterization is important for assessing beam transport and matching in the Rare isotope Accelerator complex for ON-line experiments (RAON) injector low-energy beam transport (LEBT) section. Four wire scanners rapidly acquire one-dimensional transverse profiles, whereas an Allison scanner provides two-dimensional position–angle phase-space distributions but requires a comparatively long acquisition time. We propose a parametric machine-learning framework that maps wire-scanner profiles represented by Gaussian mixture model (GMM) to Allison-scanner phase-space parameters. Profiles generated at multiple electrostatic quadrupole settings provide additional constraints on this otherwise ambiguous inverse problem. A multi-beam database is generated using TRACK particle-in-cell simulation of $^{40}Ar^{8+}$ beams with varied initial beam conditions and electrostatic quadrupole voltages, and a neural surrogate is trained to learn the inverse mapping. Simulation tests evaluate the reconstruction accuracy for two to nine diagnostic settings.

INTRODUCTION

The Rare isotope Accelerator complex for ON-line experiments (RAON) injector consists of an electron cyclotron resonance ion source (ECR-IS), a low-energy beam transport (LEBT) line, radio-frequency quadrupole (RFQ) linac, and a medium-energy beam transport (MEBT) line. In the LEBT, the first bending magnet separates the extracted beam components by A/Q, and a slit selects the desired beams. The selected beam is transported at 10 keV/u and matched to the RFQ by electrostatic quadrupole (ESQ) [1]; the RFQ then accelerates it to approximately 500 keV/u [2]. The LEBT is instrumented with four wire scanners (WS), which measure the horizontal and vertical beam profiles, and one Allison scanner (AS), which measures the projected x–x' and y–y' phase-space distributions [3]. The beamline layout with beam diagnostics are shown in Fig. 1.

WS rapidly acquire transverse profiles, but these one-dimensional projections do not uniquely determine the underlying phase-space distribution. The AS directly measures the projected phase space by scanning its entrance slit and electrostatic deflection voltage; however, this sequential scan is substantially slower, making measurements at multiple machine settings burdensome [3]. Recent model-based tomography reproduced AS phase-space distributions from four WS profiles by accounting for space charge and nonlinear transport [4]. This result demonstrates that multiple profiles related through well-known beamline contain complementary information about the underlying phase space. The Particle-In-Cell (PIC) simulation code TRACK has previously been applied to beam commissioning which were consistent with observations [2, 5–7].

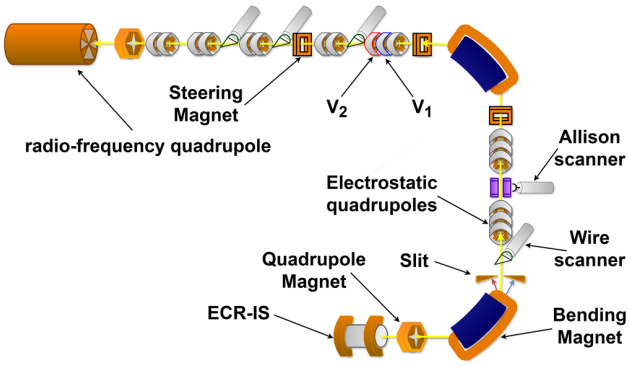


Figure 1: RAON LEBT layout. V_1 and V_2 denote the voltage parameters controlling the strengths of the selected horizontal- and vertical-focusing ESQ; these parameters were varied to generate the multi-setting simulation data.

In this work, a neural surrogate maps Gaussian-mixture-model (GMM) representations of the WS profiles, together with the corresponding ESQ voltages, to GMM representations of the projected AS phase spaces. TRACK particle-in-cell simulations are used in this work to generate an AS phase-space target and the corresponding WS profiles under nine voltage configurations of a selected ESQ pair. Combining profiles from multiple ESQ settings reduces the ambiguity of the inverse mapping, while Twiss parameters and emittance are obtained analytically from the predicted mixtures. Models using two to nine diagnostic settings are compared to quantify the trade-off between reconstruction accuracy and measurement requirements.

METHODS

Our previous single-shot framework represented the WS and AS measurements on fixed grids and performed the reconstruction using separately trained autoencoders and a latent-space mapper [8]. Grid discretization and the sequential–map–decode process introduced additional reconstruction errors, while measurements under a single focusing condition provided limited constraints on the inverse problem. The present method instead fits continuous GMM directly to particle coordinates and combines multiple ESQ-

* whkim1357@kangwon.ac.kr

Content from this work may be used under the terms of the CC BY 4.0 licence (© 2026). Any distribution of this work must maintain attribution to the author(s), title of the work, publisher, and DOI.

ISBN: 978-3-95450-275-2 ISSN: 2226-0366 doi: 10.18429/JACoW-LINAC2026-THPO060

RF DESIGN OF AN S-BAND HEM_{11} TRANSVERSE DEFLECTING CAVITY FOR THE eLABs AT PAL

Geunwoo Kim[1], Kwanghoon Kim[2], Yong-jung Park[2], Chang-Ki Min[2], Moses Chung[*,1]
[1]Pohang University of Science and Technology (POSTECH), Pohang, South Korea
[2]Pohang Accelerator Laboratory (PAL), Pohang, South Korea

Abstract

An 11-cell S-band HEM_{11} traveling-wave transverse deflecting cavity (TDC) was designed and fabricated at Pohang Accelerator Laboratory (PAL) using its in-house brazing facility. This work reports the RF design of the traveling-wave cavity using CST Studio Suite with a periodic-cell eigenmode model, a driven coupler model, and separate field and two-port models of the complete structure. The target $2\pi/3$ mode occurred at $f_{2\pi/3} = 2.856$ GHz and exhibited backward-wave propagation with $v_g = -0.0191c$. Over identical ±1.25 mm sweep ranges, the coupler-cell radius r_c produced the largest voltage standing-wave ratio (VSWR) excursion among the investigated dimensions. At $f_{2\pi/3}$, the integrated electric and magnetic terms added constructively to the vertical kick, yielding 0.503 MV under the CST field normalization. The copper-wall two-port response reached a minimum $S_{11} = -49.52$ dB at 2.8562 GHz. These simulation results provide a numerical baseline for subsequent low-power RF tuning.

INTRODUCTION

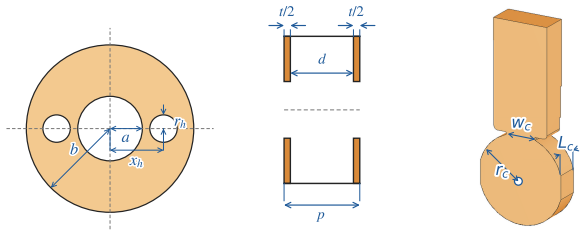
Time-resolved characterization of the longitudinal beam distribution requires a diagnostic that maps particle arrival time onto a measurable transverse coordinate. A transverse deflecting cavity (TDC) provides this mapping through a time-dependent transverse kick. The HEM_{11} deflecting mode used here is a hybrid of coupled TM_{11}-like and TE_{11}-like field components in an iris-loaded periodic structure [1]. An 11-cell S-band HEM_{11} TDC was designed and fabricated for the electron Linear Accelerator for Basic science (eLABs) at the Pohang Accelerator Laboratory (PAL). This paper follows the RF design from periodic-cell characterization through coupler selection to complete-structure two-port and integrated-field verification. Fabrication and preliminary low-power tests establish the present project status, while systematic tuning remains future work.

RF DESIGN

The RF design of the 11-cell cavity was evaluated for the $2\pi/3$ operating mode at $f_{2\pi/3} = 2.856$ GHz using CST Studio Suite 2026 [2]. The cavity comprises nine regular cells and two coupler cells. First, a periodic unit-cell eigenmode model was used to determine the dispersion and regular-cell quantities for the nine-cell body. Next, a coupler model excited through the waveguide port evaluated the matching sensitivity to the coupler dimensions. Finally, separate complete-structure field and two-port models, including both coupler cells, provided the integrated transverse voltage and two-port response, respectively.

Regular Cell

The regular cell geometry combines a 34.99 mm period with two lateral holes that lift the degeneracy of the orthogonal HEM_{11} polarizations. The main dimensions are summarized in Table 1 and Fig. 1. The cell gap length and disk thickness form the period. Each lateral hole has a radius of 9.525 mm and is centered 37.154 mm from the beam axis.



(a) (b) (c)

Figure 1: Geometry used in the CST models: (a) transverse and (b) longitudinal cross-sections of the regular cell, and (c) the coupler cell, showing the coupler-cell radius r_c, half-slot width w_c, and axial length L_c.

Table 1: Geometric Regular-Cell Design Parameters

Quantity	Value
Cells (regular + coupler)	11 (9 + 2)
Active RF length, L	0.379 m
Design frequency	2.856 GHz
Phase advance per cell	$2\pi/3$
Iris/cell radii, a/b	22.441/58.192 mm
Hole radius/offset, r_h/x_h	9.525/37.154 mm
Gap/disk thickness, d/t	29.148/5.842 mm
Cell period p	34.99 mm

Periodic eigenmode calculations with copper walls characterized the target polarization dispersion and group velocity. Figure 2 shows the target branch from the periodic cell eigenmode sweep. The phase advance was swept from 0° to 180°, and the target branch reached 2.856 GHz at 120°. The decreasing dispersion is consistent with the backward wave behavior attributed to magnetic coupling between adjacent cells in a similar T-cavity [3]. A five-point numerical derivative of the dispersion at this phase, using $v_g = 2\pi p\, df/d\theta$ with the 34.99 mm period p, gave $v_g = -0.0191c$.

The periodic-cell RF parameters follow from the dispersion result and loss calculation, and are summarized in Ta-

* moses@postech.ac.kr

Content from this work may be used under the terms of the CC BY 4.0 licence (© 2026). Any distribution of this work must maintain attribution to the author(s), title of the work, publisher, and DOI.

ISBN: 978-3-95450-275-2 ISSN: 2226-0366 doi: 10.18429/JACoW-LINAC2026-THPO064

TOWARD AN OPTIMIZATION FRAMEWORK FOR RFQ AND DTL CAVITIES: A STUDY OF BLACK-BOX METHODS

E. M. Ferrari*,[1], P. E. S. Silva[1], T. V. de Oliveira[1],
S. G. T. Brito[1], A. G. C. Pereira[1], A. B. da Costa[1], F. A. B. Neto[1]
[1]Brazilian Center for Research in Energy and Materials (CNPEM) - Brazil

Abstract

The design optimization of Radio Frequency Quadrupole (RFQ) and Drift Tube Linac (DTL) cavities involve time costly black-box simulations, hidden constraints coming from simulation failures and the absence of reliable derivative information. These characteristics make Derivative-Free Optimization (DFO) methods particularly interesting, yet their practical performance in a conjoint RFQ-DTL cavity design optimization has not yet been comprehensively studied. Our paper introduces a prototype optimization framework, Accelerating Cavity Optimization (rACCOon), connecting the execution of standard accelerator codes, automating post-processing and derivative-free optimization methods. This work discusses the performance of the derivative-free method MADS comparing it to a Bayesian approach in black-box optimization. We also validate the use of the framework for optimization of a composite problem RFQ+DTL.

INTRODUCTION AND MOTIVATION

Engineering design often come with underlying optimization challenges and the design of new accelerators is no exception [1–4]. Such optimizations are frequently performed in a somewhat manual way conducted by the specialist's judgment of fitness. The process consists of actively tuning the variables through empirical perturbation theory and trial and error, which is reported as a common issue in the field by [3, 4]. This can become a long and tedious process and some variable combinations can be completely disregarded. Building an algorithmic setting in which optimization methods are agnostic to the physics of the problem, data driven, can lead to previously unnoticed solutions.

When an optimization framework is put to work in an engineering setting, genetic algorithms such as NSGA-II [5] are primarily picked. However evolutionary algorithms typically need a few thousands of function evaluations. In the optimization problems discussed here, we operate under a tight evaluation budget, and due to time expensive simulations, we can afford one hundred, or at most a few hundred evaluations. This is because we are interested in studying design optimization where the project is still not yet fully mature, and the constraints and objectives are still somewhat unclear and under discussion. This is where low budget optimization comes in: it assists the project decision process by guiding discussions and possible alternatives by allowing the optimization problem to be iterated.

The main motivation for the development of a RFQ and DTL automation and optimization framework is connected to the purpose of the Brazilian Center for Research in Energy and Materials (CNPEM) in enriching its competence in accelerator modeling to allow applications in radioisotope production and proton therapy.

THE RACCOON FRAMEWORK

Our main contribution is the implementation of a framework capable of straightforwardly using optimization algorithms for the cavity accelerator design. Accelerating Cavity Optimization (rACCOon) is a prototype framework that connects derivative-free optimizers to traditional accelerator simulation codes. We automate the loop of proposing a design, evaluating it through simulation, and wrapping it around an optimization setup. Its central design principle is a strict separation between the optimization logic and the physics of each cavity. Both parts are mediated by an interface we refer to as the *contract*.

The contract is a minimal interface that every optimization problem must satisfy: it must provide the variable bounds and dimension, an evaluation function that maps a normalized point to an objective value, a set of constraint objects, and optional setup and teardown hooks that manage the simulation working directory tree. Any object constructed satisfying this contract can be optimized by any driver implemented. This is the key architectural decision of the framework, we wrote the optimizers once, respecting the contract, they know nothing about accelerator physics. The accelerator cavity code is written once, respecting the contract, and knows nothing about optimization. As a consequence, adding a new solver requires no changes to the physics code, and adding a new cavity or setup requires no changes to any solver.

The framework is driven by a single configuration file, see Fig. 1, which serves as the source of truth for a run. It declares which cavities are active, which variables are optimized, warm-started, or held fixed, their bounds, and the choice of optimization method. A dispatcher script reads this file, constructs the appropriate problem objects, and calls the selected optimization driver. This centralization means that changing what is optimized, or which method is used, requires editing only the configuration, never the source code.

Each cavity is implemented as an adapter that satisfies the contract while encapsulating the details of driving its simulation codes. The DTL adapter injects a candidate geometry into the SuperFish and Parmila codes and extracts

* eduardo.ferrari@cnpem.br

Content from this work may be used under the terms of the CC BY 4.0 licence (© 2026). Any distribution of this work must maintain attribution to the author(s), title of the work, publisher, and DOI.

ISBN: 978-3-95450-275-2 ISSN: 2226-0366 doi: 10.18429/JACoW-LINAC2026-THPO066

PHYSICS STUDIES FOR A MUON COLLIDER TARGET SYSTEM

W. Bishop*, University of Warwick, Coventry, UK
Rutherford Appleton Laboratory, Science and Technology Facilities Council, Didcot, UK,
endorsed by the International Muon Collider Collaboration

Abstract

The target system for a proposed Muon Collider must withstand multi-MW pulsed proton beams, at 5 GeV for 2 MW or 10 GeV for 4 MW, to produce muons through pion decay. It must also maintain long-term reliability while providing the required particle yield, with performance depending on its ability to sustain high thermal and radiation loads.

This study presents optimised pion-to-muon production yields and investigates radiation-induced heat loads for the tungsten powder target system across a 1 – 20 GeV kinetic energy scan range, using FLUKA, to determine the optimal target design for use within the colliders front-end target system. Idealised physics geometries are used throughout this work, with engineering feasibility estimated from the design constraints.

INTRODUCTION

The Muon Collider (MuCol) is a proposed future high-power accelerator (~10 TeV) aiming to be a possible successor to the Large Hadron Collider at CERN. It produces charged pions by directing the high-power proton beam onto the front-end target system, where the pions are then focused and decay to muons. These muons are then cooled by ionization and accelerated quickly until they collide. The MuCol is similar to other colliders but exploits the heavier muon's mass and fundamental-particle nature, producing higher energy-density collisions while minimising synchrotron radiation, enabling compact ring designs [1].

Several target concepts have been proposed, including graphite, liquid-metal jets, and tungsten (W) powder. The latter option is desirable for a pulsed 5 Hz 2 – 4 MW beam scenario, since tungsten's high thermal-shock resistance and melting point allow it to survive the intense beam environment. The incident proton beam test parameters used throughout this study are shown in Table 1. The beam spot rms radius was set so that the W powder material radius translates to 3σ of the transverse beam profile, allowing 98.9 % of the Gaussian beam to interact with the target. Its granular nature provides improved thermal dissipation, no cavitation, and enables self-replenishing behaviour. The particle yield is scored at the end of the target-taper region (z = 17.3 m) where the pions decay to muons, and a kinetic energy cut of 10 – 500 MeV is taken which matches the downstream capture channel [1]. Figure 1 shows the initial concept for the target design, where the tungsten powder and He cooling gas recirculates inside a pipe system, and secondary particles from the proton beam interactions are focused by the solenoid field.

* William.Bishop@warwick.ac.uk

Table 1: Incident Proton Beam Testing Parameters [2]

Parameter	Value
Beam Power	2 – 4 MW
Kinetic Energy	1 – 20 GeV
Repetition Rate	5 Hz
Pulse rms length	2.5 ms
Spot rms radius	1.67 – 8.33 mm
Tilt	0 – 200 mrad

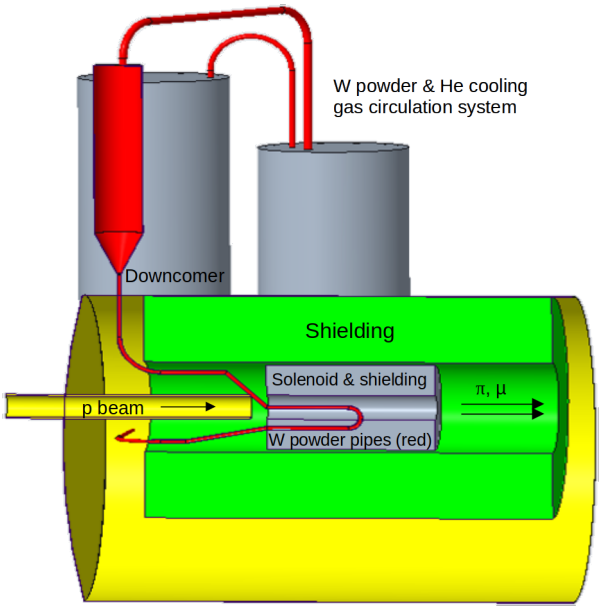


Figure 1: Concept of the W powder target design.

TARGET GEOMETRY

Maximising pion yields for downstream muon production creates challenges such as high heating, stress, strain and radiation load from the primary beam interacting with the target. The tungsten powder concept is being pursued as a possible target technology that could potentially address all of these issues. The density used throughout the paper is 5.8 g/cm^3, which is equivalent to ~30 % of the density of solid tungsten (19.3 g/cm^3). This defines the estimated engineering limit at which a constant flow rate within a circulating fluidised bed can be maintained [3]. A fraction of ~50 % would be more desirable in order to maximise production from the target, providing an aspirational goal.

Alongside the aforementioned benefits, the tungsten powder design is granular in nature, enhancing the target's resistance to shock wave damage and allowing for more efficient heat transfer. It could require less maintenance due to it

Content from this work may be used under the terms of the CC BY 4.0 licence (© 2026). Any distribution of this work must maintain attribution to the author(s), title of the work, publisher, and DOI.

ISBN: 978-3-95450-275-2 ISSN: 2226-0366 doi: 10.18429/JACoW-LINAC2026-THPO070

ENHANCING THE LIFETIME AND RELIABILITY OF THE ALBA LINAC

D. Lanaia, R. Muñoz Horta, F. Pérez
ALBA Synchrotron, Cerdanyola del Vallès, Spain

Content from this work may be used under the terms of the CC BY 4.0 licence (© 2026). Any distribution of this work must maintain attribution to the author(s), title of the work, publisher, and DOI.

Abstract

The future ALBA II facility, currently under design, will retain the existing ALBA injector, which has been in operation since 2012 and comprises a 100 MeV linac and a full-energy 3 GeV booster. Over the years, several modifications in the linac RF waveguide system have been implemented to increase redundancy and introduce alternative operating modes, thereby improving injector reliability and availability. In parallel, a comprehensive consolidation programme has been launched to extend the operational lifetime of the linac, to ensure reliable operation throughout the ALBA II operational period. This paper presents the reliability enhancements implemented in the injector together with the ongoing linac consolidation activities.

THE ALBA LINAC

The ALBA injector is based on a 100 MeV electron linac consisting of a 90 keV thermionic electron gun, two prebuncher cavities (PB1 at 500 MHz and PB2 at 3 GHz), a buncher structure (BU), and two identical accelerating structures (AS1 and AS2), all operating at 3 GHz [1]. The RF power system is based on two Thales TH2100 klystrons capable of delivering pulses of up to 37 MW peak power at a repetition rate of 3 Hz. RF power is transmitted through an SF6-filled waveguide network, with ceramic RF windows providing the vacuum interface to the RF cavities. ALBA operates in top-up mode, with beam reinjections performed every 20 minutes to maintain the storage ring current at 250 mA. A picture of the ALBA linac is shown in Fig. 1.

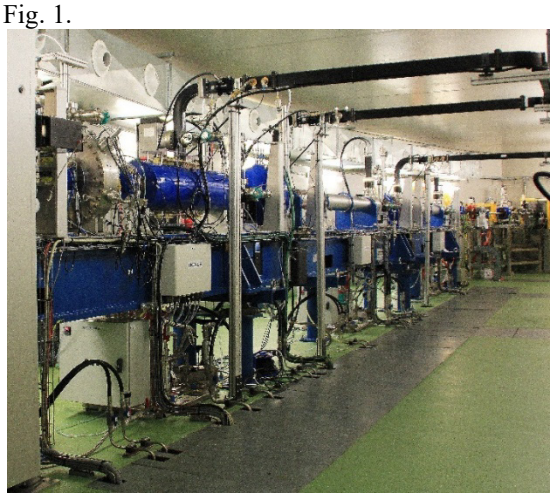


Figure 1: The ALBA linac.

RELIABILITY ENHANCEMENT

In the original as-designed linac configuration, the RF power distribution was such that klystron 1 (KA1) supplied RF power to PB2, BU, and AS1, while klystron 2 (KA2) powered exclusively AS2, as shown in Fig. 2. Under these operating conditions, the linac delivered a 108.5 MeV electron beam to the booster, with KA1 and KA2 providing 30 MW and 13 MW of RF power, respectively.

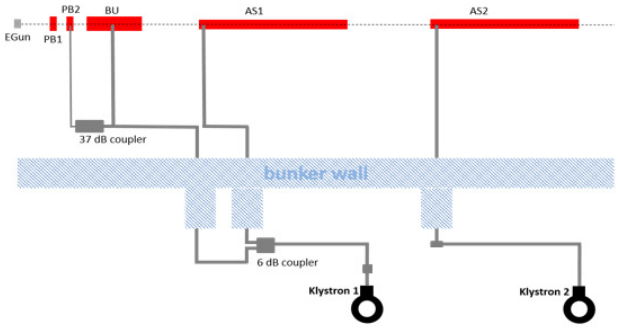


Figure 2: Original linac RF-distribution at 108.5 MeV.

Measures to anticipate and mitigate potential failures of the linac system relied on regular preventive maintenance and maintaining an adequate stock of spare parts, including two spare klystron tubes. Since linac commissioning in 2008, the two original TH2100 klystrons have accumulated well over 100,000 operating hours each. This remarkable operational lifetime is attributed to a combination of regular preventive maintenance and operation below the nominal power rating of the klystrons.

Nevertheless, major failures such as klystron failure, RF-window failure or cavity damage could result in several hours or even days of linac downtime.

67 MeV Rescue Mode

To mitigate the impact of a klystron failure and/or failure of one accelerating section, a reduced-energy injector mode at 67 MeV was commissioned in 2015 [2].

In this configuration, the linac is fed only up to the first accelerating structure using a single klystron. To enable operation with either klystron, an S-band RF switching system was implemented in 2014 in the waveguide network [3], as shown in Fig. 3. The 67 MeV rescue mode, together with the RF switching system, enables operation not only in the event of a klystron failure, but also in the event of a failure affecting either accelerating structure, thereby improving linac reliability and availability.

The booster was successfully commissioned at 67 MeV using either klystron delivering 26 MW of RF power. However, booster injection at 67 MeV proved to be less stable than at the nominal energy of 108.5 MeV. Consequently, the 67 MeV rescue mode was not adopted for routine operation. It was used twice in 2017 following problems with one of the two klystrons, and after the failure of an RF window in AS1, which required AS1 to be disconnected from the RF system.

ISBN: 978-3-95450-275-2 ISSN: 2226-0366 doi: 10.18429/JACoW-LINAC2026-THPO074

PERFORMANCE OF 2-STEP BAKED NIOBIUM CAVITIES FOR THE ITN CRYOMODULE

Eric Viklund*, Takafumi Hara, Sora Arai, Mathieu Omet, Ryo Katayama, Kensei Umemori
KEK, Tsukuba, Japan

Content from this work may be used under the terms of the CC BY 4.0 licence (© 2026). Any distribution of this work must maintain attribution to the author(s), title of the work, publisher, and DOI.

Abstract

To support the ILC Technology Network(ITN) Cryomodule project at KEK, we have constructed and assembled six single cell cavities and one 9-cell cavity for vertical testing (VT). A series of surface treatment were applied to the cavities using the proposed recipe for the construction of the International Linear Collider (ILC). This recipe consists of four steps: bulk electropolishing (EP), annealing, cold EP, and finally two step baking. Using this recipe, we can consistently exceed the ILC specifications. We analyze the performance and characteristics of these cavities using Q vs E and temperature mapping measurements. We also analyze the effect of cold EP and HPR on the maximum quench field and quality factor of the cavities.

INTRODUCTION

The ITN project aims to develop high-performance SRF technology suitable for future accelerator facilities [1]. As part of this effort, six single-cell cavities were fabricated and tested to prove our capability to achieve the ILC SRF cavity specification, quality factor of 10^{10} at 31.5 MV m^{-1} accelerating gradient. The ITN cavity processing recipe utilizes annealing, cold-EP, HPR, and 2-step baking to achieve high Q high gradient without field emission. The cavity batch includes both MG and FG niobium material types to investigate the performance of different niobium material types.

CAVITY OVERVIEW AND PROCESSING

Cavity Types

The six tested cavities are summarised as follows:

- **Medium Grain (MG):** 2 cavities
  R1MC01, R1MC02
- **Fine Grain (FG):** 4 cavities
  R1FC01, R1FC02, R1FC03, R1FC04

Processing Procedures

The cavity preparation procedure for the ITN cryomodule uses a combination of electropolishing (EP), high pressure water rinsing (HPR), 900 °C annealing, and 2-step baking to achieve high gradient and high quality factor. The steps are performed in the following order:

1. **Inspection:** Cavity inner surface is inspected and any defects are removed by manual grinding
2. **EP-1:** Bulk electropolishing to remove 5 µm by pre-EP and ~150 µm of material by EP-1
3. **HPR:** High-pressure ultrapure water rinse
4. **Annealing:** Heat treatment at 900 °C for 3 hours
5. **EP-2:** Cold electropolishing (~15 µm)
6. **HPR:** High-pressure ultrapure water rinse
7. **Assembly:** Power coupler, pumping port, and pick up antenna are attached and cavity is sealed
8. **2-Step Bake:** 75 °C for 4 hours followed by 120 °C for 48 hours
9. **Vertical Testing:** Cavity performance is measured

After cavities are received for processing the inside surface is inspected using a camera to look for defects. These inspection images are also used to compare with later inspections to see the effects of EP.

Electropolishing is performed in the STF EP facility using the horizontal cathode method. For EP-1 the cavities are polished using air cooling resulting in a cavity temperature of 26 °C. The polishing voltage for EP-1 is 41 V. For EP-2 the cavities are cooled by water from the outside, often referred to as cold-EP. The cavity temperature is maintained at 14 °C and a 16 V polishing voltage is used.

After each electropolishing the cavity is rinsed using ultrasonic cleaning for 30 min and then cleaned with HPR for 30 min. After EP-2 the cavity is thoroughly cleaned using HPR for 3 h and dried over night in a class 10 clean room before assembly. Assembly is performed in a class 10 cleanroom.

Annealing is performed in a high vacuum furnace at 900 °C for 3 h to outgas hydrogen from the cavity.

The ITN cavity preparation utilizes 2-step baking to be able to reach the high field required for the ILC specification. This process consists of two steps, a short 4 h heat treatment at 75 °C followed immediately by a 48 h heat treatment at 120 °C [2, 3]. A slow pumping system is used to minimize the turbulence in the cavity during pumping. This has been shown to reduce particulate contamination. Once the vacuum is below 1×10^{-3} Pa the temperature increase to 75 °C is started. The temperature of the cavity is measured using thermocouples placed at 0 °, 90 °, 180 °, and 270 ° to give a more accurate reading compared to the oven air temperature. After the 120 °C temperature ramp, an ion pump is used to bring the vacuum level down to 1×10^{-5} Pa.

One cavity, R1FC04, was processed with a simplified work flow that omitted EP-2 after annealing, to evaluate its necessity. Instead the cavity was rinsed right after annealing and then assembled.

* eric.viklund@kek.jp

ISBN: 978-3-95450-275-2 ISSN: 2226-0366 doi: 10.18429/JACoW-LINAC2026-THPO076

IMPLEMENTATION AND OPERATIONAL EXPERIENCE OF AN EtherNet/IP-BASED DEVICE INTERFACE IN RILAC TOWARD THE RIBF FACILITY UPGRADE PROJECT

A. Uchiyama*, M. Komiyama, K. Kumagai, H. Yamauchi, N. Fukunishi
RIKEN Nishina Center, Wako, Japan

Content from this work may be used under the terms of the CC BY 4.0 licence (© 2026). Any distribution of this work must maintain attribution to the author(s), title of the work, publisher, and DOI.

Abstract

A reliable device interface is essential in the long-term operation of an accelerator facility. In the RIKEN Radioactive Isotope Beam Factory (RIBF) control system, many devices are integrated with input/output controllers (IOCs) based on the Experimental Physics and Industrial Control System (EPICS) through TCP/IP-based socket communication. Although this approach is flexible and cost-effective, reconnecting after an unexpected power loss or the restart of a device or network switch is not always successful, and recovery may require restarting an IOC. To improve reliability and maintainability, Ethernet-based industrial field networks such as EtherCAT and EtherNet/IP were proposed for the future RIBF Facility Upgrade Project. Following a recommendation from the CSR1 Technical Advisory Committee to evaluate the proposed technologies in an existing accelerator facility, EtherNet/IP was implemented in the control system for the RIKEN linear accelerator (RILAC) as one of the candidate field networks. The system currently consists of a single scanner and 16 adapters with a requested packet interval of 10 ms and is used to control Faraday cup, beam attenuator, and vacuum systems. The existing EPICS process variable names and graphical user interfaces were retained without modification. The system was used during routine RILAC operation, including experiments using the superconducting RIKEN linear accelerator (SRILAC), from September 2025 through July 2026. During this period, no unscheduled reboot of the IOC was required, and no interruption of device control attributable to EtherNet/IP communication occurred.

INTRODUCTION

The RIKEN Radioactive Isotope Beam Factory (RIBF) is a heavy-ion accelerator facility consisting of several cyclotrons and linear accelerators [1]. The RIBF Facility Upgrade Project [2] includes the introduction of charge stripper rings (CSRs) to increase the intensity of heavy-ion beams [3]. The control system should use commercially available hardware and standard industrial technologies as much as possible to reduce maintenance and development efforts because many new accelerator components will be introduced such as electromagnet power supplies, beam diagnostic devices, and vacuum equipment. This approach is intended to reduce the overall cost of the control system accordingly.

The RIBF control system is based on the Experimental Physics and Industrial Control System (EPICS) [4]. Many commercial and in-house-developed devices are connected to EPICS input/output controllers (IOCs) through TCP/IP-based socket communication [4, 5]. This method is flexible and cost-effective. On the other hand, the socket connection is not always re-established successfully after an unexpected power interruption or restart of a device or network switch. In such cases, the IOC must be restarted to recover the connection, which results in an interruption of accelerator operations. To facilitate such recovery, an embedded EPICS IOC system that allows operators to monitor and restart IOC processes through a web interface was previously developed for RIBF [6]. However, restarting the IOC still results in an interruption of accelerator operations. Therefore, I/O signals provided through TCP/IP-based socket communication are not considered sufficiently reliable for applications requiring high communication reliability, such as interlock-related functions.

The installation of Ethernet-based industrial field networks such as EtherCAT [7] and EtherNet/IP [8] has been proposed for the future RIBF Facility Upgrade Project [9] to improve the reliability and maintainability of the device interface layer while retaining the convenience of Ethernet. At the CSR1 Technical Advisory Committee meeting held in 2023, it was recommended that the proposed technologies should first be implemented and evaluated in an existing accelerator facility before application to the CSR control system. At the RIBF, the RIKEN linear accelerator (RILAC) is used for standalone experiments in addition to its function as an injector for the cyclotrons [10]. Therefore, RILAC was selected as the first implementation site. As one of the candidate field networks, an EtherNet/IP-based controller was developed as a functional replacement for the existing TCP/IP-based device interfaces used for selected RILAC devices.

Ethernet-BASED FIELD NETWORKS

EtherNet/IP and EtherCAT use standard Ethernet technology in their physical layers. However, their network configurations and suitable applications differ. EtherCAT provides fast and deterministic cyclic communication and is suitable for applications that require response times less than 1 ms [9]. On the other hand, an EtherCAT system normally requires a dedicated network segment and additional cabling.

EtherNet/IP uses the Common Industrial Protocol (CIP) over standard Ethernet and can be connected through general-purpose Ethernet switches [7]. It can therefore coexist with conventional TCP/IP communication and other IP-based services such as file transfer protocol (FTP) on the same

* a-uchi@riken.jp

ISBN: 978-3-95450-275-2 ISSN: 2226-0366 doi: 10.18429/JACoW-LINAC2026-THPO077

OPERATIONAL ACHIEVEMENTS AND 2026 UPGRADES OF THE SC-RFQ LINAC AT KAHIF FOR HIGH-DOSE NUCLEAR MATERIAL IRRADIATION*

S. H. Lee†, D. W. Lee, D.-S. Chang, S. B. Lee, K. H. Lee, M. W. Kim, S.-R. Huh
Korea Atomic Energy Research Institute, Daejeon, Republic of Korea

Abstract

The KAERI Heavy-ion Irradiation Facility (KAHIF) is a linear-accelerator-based infrastructure designed to emulate neutron-induced displacement damage in next-generation nuclear and fusion structural materials. KAHIF consists of an 18 GHz electron cyclotron resonance (ECR) ion source, a 25.96 MHz split-coaxial radio-frequency quadrupole (SC-RFQ) operating at 178 keV/u, and a 51.92 MHz interdigital H-mode (IH) drift-tube linac accelerating heavy ions up to 1.09 MeV/u. In 2025, KAHIF established a high-flux solid-metal ion beam: by optimizing a Metal Ions from Volatile Compounds (MIVOC) system using ferrocene at room temperature, an Fe^{13+} beam was stably extracted and accelerated to 9.68 MeV, delivering 1.0 μA (1.3×10^{11} ions/cm^2·s) on target and enabling a 20 dpa self-ion irradiation of reduced-activation steel at 320 °C in only seven days. The facility recorded 239.5 h of beam irradiation with 80% equipment availability. This paper outlines the 2025 operational performance and the 2026 upgrades: a rebuilt medium-energy beam transport (MEBT) line with precise beam diagnostics, a 950°C ultra-high-temperature target chamber, and an He/Fe dual-beam irradiation architecture.

INTRODUCTION

Commercialization of next-generation nuclear systems such as small modular reactors (SMR), molten-salt reactors (MSR) and fusion reactors requires structural materials validated against harsh neutron environments [1, 2]. Fusion first-wall and blanket structures in particular face displacement damage of tens to hundreds of displacements per atom (dpa). Test reactors can reach only a few dpa per year, at high cost and with strongly activated specimens, so accelerator-based ion irradiation is now widely adopted as a fast, precisely controlled surrogate for neutron damage [3].

To meet this demand in Korea, the Korea Atomic Energy Research Institute (KAERI) built and operates the KAHIF, the country's only RF-linac-based ion irradiation test facility, in user service since 2022 [4–6]. Having long provided gas-ion beams (He and Ar), KAHIF commissioned a solid-metal Fe beam in 2025, enabling the most advanced dpa emulation in Korea. This paper summarizes the 2025 operation, during which the facility transitioned from a general-purpose service to a dedicated high-dose irradiation infrastructure, and details the accelerator-system upgrades under way in 2026.

FACILITY OVERVIEW

Figure 1 shows the KAHIF layout. Highly charged ions from an 18 GHz ECR source are mass-selected in the low-energy beam transport (LEBT) and injected at 2.07 keV/u into a 25.96 MHz split-coaxial RFQ, which accelerates species with $A/q \leq 28$ to 178.4 keV/u over 8.6 m. A 51.92 MHz IH drift-tube linac then brings ions with $A/q \leq 9$ to 1.09 MeV/u (e.g. 42.3 MeV Ar^{9+}). The machine runs at 8 ms/125 Hz with a 30–100% duty factor, i.e. up to CW-equivalent operation for irradiation service. Main linac parameters are listed in Table 1. The high-energy beam transport (HEBT) delivers the beam to a target station whose legacy chamber supports specimen heating to 450°C in high vacuum.

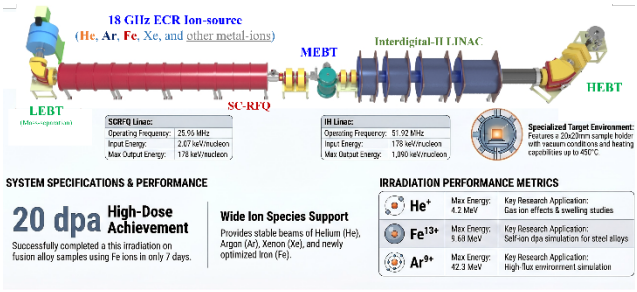


Figure 1: Layout of KAHIF: 18 GHz ECR ion source, LEBT (mass separation), 25.96 MHz SC-RFQ, MEBT, 51.92 MHz IH-DTL and HEBT to the irradiation target station.

Table 1: Main Parameters of the KAHIF Linac

Parameter	SC-RFQ	IH-DTL
Frequency [MHz]	25.96	51.92
Mass-to-charge A/q	≤ 28	≤ 9
Input energy [keV/u]	2.07	178.4
Output energy [keV/u]	178.4	1090
Length [m]	8.6	5.6
Eff. gradient [keV/(u·m)]	20.7	162.9
Norm. emitt. [π·mm·mrad]	0.6	0.6
Energy spread [%]	1.03	≤ 2.8

* Work supported by the National Research Foundation of Korea (NRF) grant funded by the Korea government (MSIT) (RS-2022-00156272) and by the National Research Council of Science & Technology (NST) grant funded by the Korea government (MSIT) (No. GTL25031-410).
† lsh0810@kaeri.re.kr

Content from this work may be used under the terms of the CC BY 4.0 licence (© 2026). Any distribution of this work must maintain attribution to the author(s), title of the work, publisher, and DOI.

ISBN: 978-3-95450-275-2 ISSN: 2226-0366 doi: 10.18429/JACoW-LINAC2026-THPO080

BEAM DYNAMICS STUDIES AND COMMISSIONING OF THE FIRST PROTON RFQ LINAC PROTOTYPE DEVELOPED BY CNPEM*

T. Ventorini[1,†], A. B. da Costa, W. F. D. Carvalho, P. E. S. Silva,
F. A. B. Neto, E. Figueiredo, J. P. C. da Costa, V. O. Freire, L. A. S. Tapia
Brazilian Center for Research in Energy and Materials, Campinas, Brazil
[1]also at Universidade Estadual de Campinas, Campinas, Brazil

Abstract

The Brazilian Center for Research in Energy and Materials (CNPEM) has initiated a proton linear accelerator development program aimed at broadening its expertise in accelerator technologies to enable future applications. As a first step in this initiative, a 1 MeV proton Radio Frequency Quadrupole (RFQ) operating at 476 MHz was designed, manufactured, and assembled in Brazil, and is currently under commissioning. This work discusses aspects of the beam dynamics, vane modulation design, and beam measurements of the prototype. Emphasis is given to comparisons between simulations and experimental measurements, including RFQ transmission, spectrometer-based characterization of the accelerated beam, and pre-RFQ emittance measurements. The comparisons provide insights to the team and increase overall confidence in engineering solutions adopted during the development, including the vacuum sealing strategy based on 3D O-rings. Finally, future developments planned for this initiative are outlined.

INTRODUCTION

CNPEM has initiated a proton linear accelerator development program to advance national capabilities in accelerator technology. Within this program, a prototype of a 1 MeV linear accelerator was developed and is now under commissioning.

BEAMLINE SETUP

The prototype consists of a Low Energy Beam Transport (LEBT) section, a 476 MHz RFQ, and a spectrometer. Figure 1 shows the complete experimental setup.

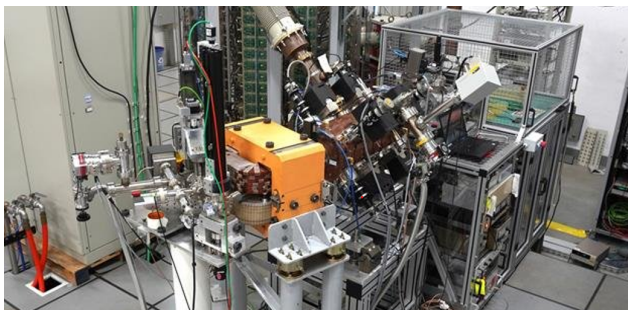


Figure 1: Picture of the prototype setup.

* Work supported by Brazilian Center for Research in Energy and Materials - CNPEM

† tarik.oliveira@cnpem.br

Low Energy Beam Transport

The LEBT section comprised a National Electrostatics Corp. (NEC) RF proton source [1] followed by a transport line equipped with beam diagnostics and focusing elements. The ion source consisted of a plasma chamber coupled to extraction and probe electrodes, providing an extraction voltage in the range of 20–25 kV. An Einzel lens located right after the extraction system provided the first transverse focusing of the beam. In the transport line, a Faraday cup was used for beam current measurements, while a second Einzel lens provided additional focusing. Figure 2 exemplifies the components of the LEBT and the electrodes of the ion source.

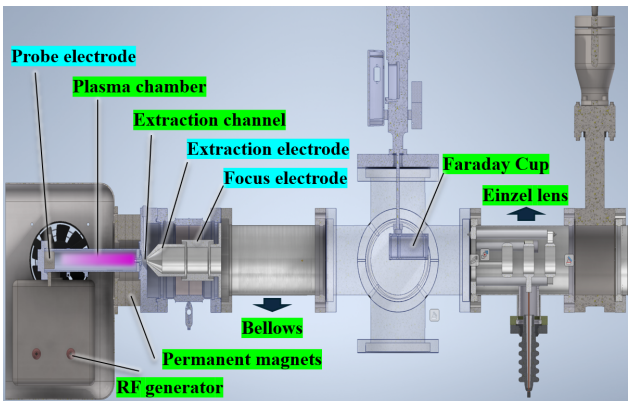


Figure 2: LEBT model. The electrodes highlighted in blue control the beam current and energy extracted from the ion source.

Radio Frequency Quadrupole

The RFQ was designed to operate at 476 MHz, matching the frequency of the solid-state Radio Frequency (RF) amplifiers from CNPEM's former synchrotron, UVX [2], which were also used in the prototype. The final energy of this cavity is 1 MeV, which was a value that respected the limits of RF power that the amplifiers could provide and still result in a compact structure, which enabled in-house manufacturing. The design aimed to have a bravery factor smaller than two, which is a common reference for pulsed RFQs [3], and, in order to minimize power and length, it was necessary to use a higher synchronous phase, which increases the energy gain per cell but reduces stable area of the longitudinal phase-space [4]. Table 1 summarizes the main design parameters of the prototype.

Content from this work may be used under the terms of the CC BY 4.0 licence (© 2026). Any distribution of this work must maintain attribution to the author(s), title of the work, publisher, and DOI.

ISBN: 978-3-95450-275-2 ISSN: 2226-0366 doi: 10.18429/JACoW-LINAC2026-THPO083

ICONE PROJECT – THE FRENCH SOLUTION FOR NEUTRON PRODUCTION

J. Dumas, B. Bolzon, D. Chirpaz-Cerbat, O. Delferrière, G. Ferrand, A. Gaget, E. Giner-Demange, P. Hamel, T. Hamelin, O. Tuske, D. Uriot
CEA Saclay, Gif-Sur-Yvette, France

Abstract

The HiCANS (High Current Accelerator-driven Neutron Source) concept offers a new technical solution for creating a neutron source suitable for neutron scattering techniques. It is based on a high-intensity (50-100 mA), pulsed (0.4-2 ms) and low-energy (10-70 MeV) proton beam accelerator.

The ICONE (Innovative COmpact NEutron facility) project is part of this approach. Led by the CEA and the CNRS, it aims to provide France with a source that is "accessible" on a national scale and does not require the construction of costly nuclear reactors (such as ILL) or very high-energy accelerators (such as ESS), to which it will be complementary.

CEA/Irfu, which is responsible for designing the accelerator, has drawn on its experience gained in major projects such as ESS, SARAF, SPIRAL2, LINAC4 and IPHI. During the two years of the detailed design phase (APD), its teams focused on designing an accelerator that meets the requirements of the ICONE project, while optimising development costs and significantly reducing the risks associated with such infrastructure. This presentation provides an overview of the ICONE project and its performance, and details the technical choices that were made.

INTRODUCTION

The development of compact accelerator-driven neutron sources offers an alternative to large-scale facilities. In this context, the ICONE project is developing a new neutron facility in France based on a high-current proton accelerator and dedicated neutron-production targets. The facility layout is shown in Fig. 1.

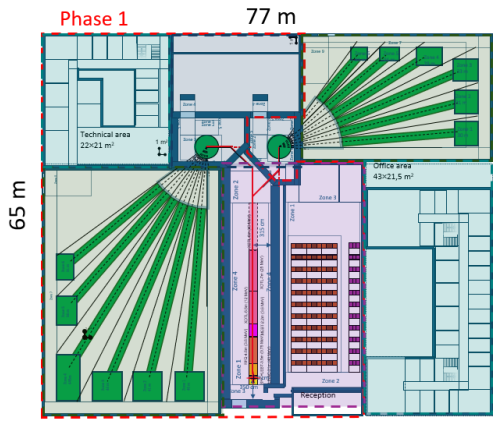


Figure 1: ICONE facility layout over 5000 m², proton accelerator (pink), two neutron production targets (green circles), experimental neutron lines (green), and technical areas (blue).

The accelerator is required to provide the beam conditions needed by the two target operating modes, while maintaining the beam quality and loss levels compatible with a high-power CW-capable linac. These requirements set the main constraints for the accelerator design, from beam production and RFQ injection to acceleration and transport to the targets.

The following sections therefore present the accelerator baseline established during the detailed design phase, focusing on the main accelerator systems, the associated beam-dynamics studies and the error analyses used to assess the robustness of the design.

LINAC ARCHITECTURE

The main function of the ICONE linear accelerator is to deliver a 25 MeV proton beam with a peak current of 80 mA to the neutron-production targets. The High-Flux (HF) target 1 requires beam pulses of 1.6–2 ms at repetition rates of 20–25 Hz, corresponding to an average beam power of up to 80 kW. The High-Resolution (HR) target 2 operates with pulses of 200–400 µs at repetition rates of 50–100 Hz, with an average beam power of up to 40 kW.

The accelerator consists of six main beamline sections and the overall accelerator architecture is shown in Fig. 2: the proton source, Low Energy Beam Transport (LEBT), Radio-Frequency Quadrupole (RFQ), Medium Energy Beam Transport (MEBT), X-DTL and High Energy Beam Transport (HEBT).

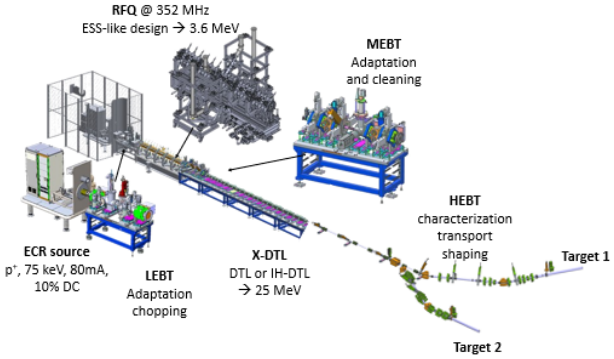


Figure 2: ICONE linac architecture and main components.

The design makes use of previously developed and validated solutions wherever appropriate, while dedicated developments are required to address the high peak current and associated space-charge, beam-loss and beam-quality constraints.

Content from this work may be used under the terms of the CC BY 4.0 licence (© 2026). Any distribution of this work must maintain attribution to the author(s), title of the work, publisher, and DOI.

ISBN: 978-3-95450-275-2 ISSN: 2226-0366 doi: 10.18429/JACoW-LINAC2026-THPO084

LOW-POWER RF MEASUREMENT AND TUNING OF THE LINAC4 RFQ2 AT CERN

W. L. Millar*, A. Grudiev, P. Martinez-Reviriego, S. Ramberger
CERN, Geneva, Switzerland

Abstract

The first RF accelerating structure in CERN's Linac4 is a 352.2 MHz radio-frequency quadrupole (RFQ), which focuses, bunches, and accelerates the 45 keV H^- beam from the ion source. As the RFQ constitutes a single point of failure in Linac4, a nearly identical spare cavity (RFQ2) has been manufactured at CERN. After fabrication and assembly, a combined field and frequency tuning procedure was employed to meet the target specifications for longitudinal field flatness, transverse field symmetry, and resonant frequency. After the initial low-power measurement and tuning campaign, the cavity was transported to the high-power test area, where a final in situ adjustment was performed. In this contribution, the procedures used to tune the frequency, electromagnetic field profile, and power coupler of RFQ2 are described, and the final results are presented.

INTRODUCTION

The 352.2 MHz radio-frequency quadrupole (RFQ) is the first RF accelerating structure in CERN's Linac4 [1–3]. As the RFQ constitutes a single point of failure for Linac4 operation, a spare (RFQ2) has been manufactured. The spare RFQ consists of three ∼1 m-long modules and is equipped with 32 cylindrical tuners. Of these, 16 house antennas that allow the field profile to be monitored during operation. In the central module, the power coupler occupies a rounded rectangular flange in one quadrant, while the corresponding flanges in the other three quadrants each house a full dummy element that was fixed prior to the tuning process reported herein. Figure 1 shows the RFQ in the tuning area.

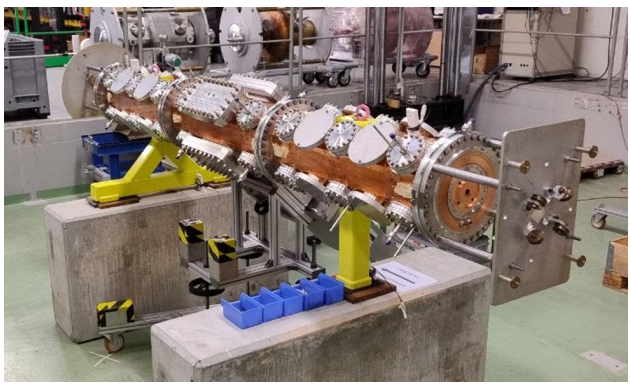


Figure 1: The spare RFQ assembly and bead-pull system. The tuning slugs and antennas are installed. The actuation systems used during the tuning procedure are not shown.

Following manufacture and assembly, the spare RFQ was tuned to bring the resonant frequency and longitudinal field distribution of the TE_{210} operating mode within the required tolerances. These objectives are often addressed separately in tuning procedures [4–7]. However, in this case a simultaneous frequency and field tuning was performed using a method that was previously demonstrated at CERN [8]. After tuning, the RFQ was transported and installed in a high-power RF test stand, where the resonant frequency and field distribution were found to have shifted outside the acceptable range. An algorithmic method for selecting practical tuner configurations was then employed, enabling recovery of the required RFQ performance using the existing tuners and a spare.

TUNING METHOD

The longitudinal field distribution was measured using the bead-pull technique, based on Slater's perturbation theorem [9, 10]. The bead-pull system for the RFQ is visible in Fig. 1. With this system, a titanium bead was moved longitudinally through each of the RFQ's four quadrants, while the phase of the reflected RF signal was recorded via a temporary, dummy power coupler. The results were then processed to obtain four longitudinal field amplitude profiles, a_1–a_4, each of which was signed according to the quadrupolar nature of the TE_{210} mode. The quadrupole and dipole field components were then calculated as

$$Q = \frac{a_1 + a_2 + a_3 + a_4}{4}, \tag{1}$$

$$D^S = \frac{a_1 - a_3}{2}, \tag{2}$$

$$D^T = \frac{a_2 - a_4}{2}, \tag{3}$$

where Q (the quadrupole component) is used to assess the longitudinal field flatness, while D^S and D^T (the dipole components) serve as a measure of transverse field symmetry.

Based on beam dynamics studies, acceptable field deviations were defined as ±1 % for Q and ±2 % for D^S and D^T. The target resonant frequency was 352.2 MHz at a cavity temperature of 25 °C in vacuum. However, given the available temperature tuning in Linac4, a frequency deviation of approximately ±29 kHz can be accommodated. The tuning technique employed has been previously reported in detail [8], and so only a summary is provided here. The tuners were initially positioned based on eigenmode simulation results to obtain an approximately correct resonant frequency. A bead-pull measurement was then performed and a column vector, $\boldsymbol{x}_{meas}$, containing the field components and resonant frequency was formed as

* lee.millar@cern.ch

Content from this work may be used under the terms of the CC BY 4.0 licence (© 2026). Any distribution of this work must maintain attribution to the author(s), title of the work, publisher, and DOI.

ISBN: 978-3-95450-275-2 ISSN: 2226-0366 doi: 10.18429/JACoW-LINAC2026-THPO085

A PROTON THERAPY LINAC WITH C-BAND TW ACCELERATOR

Yixing Lu, Cheng Wang, Yusen Guo, Zihe Gao, Xiaoxia Huang, Yifan Lan, Chaopeng Wang, Ping Wang†, Wencheng Fang‡, Zhentang Zhao
Shanghai Synchrotron Radiation Facility, Shanghai, China

Content from this work may be used under the terms of the CC BY 4.0 licence (© 2026). Any distribution of this work must maintain attribution to the author(s), title of the work, publisher, and DOI.

Abstract

A proton linac can take the advantages of FLASH therapy. C-band TW proton linacs have the superiorities of compactness and low cost which are essential factors of proton linac promotion, benefitting from the high gradient and less RF power source demand with the microwave pulse compressors. A new proposal of a proton therapy linac consisting of the 714 MHz injector, the S-band linac and the C-band TW linac is raised. With the microwave pulse compressors, less peak power is required for the C-band TW linac, thus the cost can be cut significantly. The preliminary beam dynamics simulation illustrates the transmission after the matching between the injector and the S-band linac is over 60%. Further study and comprehensive design of the whole proton therapy linac will be completed in the future.

INTRODUCTION

The proton linac has many advantages in proton therapy field, among which being suitable for FLASH (Ultra-high dose rate) therapy is a brilliant one. For a proton linac, when the proton beam has a very low energy, like from several tens of keV to several MeV, the RFQ (Radio Frequency Quadrupole) and DTL (Drifting Tube Linac) are commonly applied, whose operation frequencies usually range from several MHz to over 700 MHz; when the proton beam's energy reaches around ten MeV, higher-frequency accelerators should be adopted for the benefit of high gradient and high shunt impedance. Therefore, how to introduce the high frequency linacs reasonably to the proton linac is vital to compact proton linacs. Meanwhile, in order to reduce the cost of the proton therapy facility, small number of RF power sources is an effective solution as well, and the TW (Travelling Wave) linac can satisfy the requirements because microwave pulse compressors can be used in this case. Whatever which kind of accelerator employed, the matching between different frequency accelerators is definitely an important issue. The present solutions of proton therapy linacs usually combine the 750 MHz injector and the 3 GHz linac. Compared with S-band linacs, C-band linacs can have higher gradient and has the potential of making the proton therapy linac more compact.

Shanghai Synchrotron Radiation Facility (SSRF) has devoted to the researches on proton therapy facilities for more than ten years and technologies of the compact proton therapy accelerator [1], the proton computer tomography [2, 3] and FLASH therapy [4] are undergoing study. Recently, a 714 MHz injector is under construction. The injector consists of an electron cyclotron resonance ion source (ECRIS), a low-energy beam transport (LEBT), an RFQ, a matching section and an IH-DTL (Interdigital H-mode DTL) mainly. The injector accelerates the proton beam from 35 keV to 8 MeV within 3.5 m. The RMS energy spread at the exit of the IH-DTL is 93 keV, and the RMS beam length is 11 degrees. These parameters make the beam able to inject into the S-band linac. Further, the matching between S-band and C-band linacs can be easier. Based on these researches, our study on more compact proton therapy linac has been going on.

A new proposal of a proton linac with the C-band TW linac is raised to take advantages of its high gradient and low cost. The 714 MHz injector can produce the proton beam with energy of 8 MeV. The beam has a really short length with the RMS value of 11 degrees. Downstream the injector, there is a matching section consisting of three magnet quadrupoles. The basic choice for the S-band linac section is SC-DTL (Side Coupled DTL), and we are seeking for potential TW linacs. The proton beam will be accelerated with the phase from $-90°$ to $-20°$ in the S-band linac, aiming for high transmission. The S-band linac accelerates the proton beam to 30 MeV. In the C-band linac section, microwave pulse compressors are used, thus the cost of microwave power sources can be reduced significantly. The C-band linac accelerates the proton beam to the final energy of 250 MeV. Some beam dynamics simulation has been roughly conducted for the matching section after the injector, which contains the first part of the S-band linac. The results show the transmission is over 60%. More detailed design for the proton therapy linac will be made in the future.

OVERVIEW

The proton linac consists of the 714 MHz injector, the S-band linac and the C-band TW linac, as shown in Fig. 1.

The compact linac consists of an ECRIS, an LEBT, an RFQ, a matching section and an IH-DTL. A new beam dynamics design was introduced to the RFQ, which ensures the high transmission of the linac. The matching section includes three electromagnet quadrupoles and a buncher for beam focusing and rebunching respectively. The IH-DTL is designed with a synchronous phase of 0 degree, which becomes the Kombinierte Null Grad Struktur (KONUS) -like structure assembling with the matching section. The input beam of the linac is 35 keV,

† wangping@sari.ac.cn
‡ fangwc@sari.ac.cn

ISBN: 978-3-95450-275-2 ISSN: 2226-0366 doi: 10.18429/JACoW-LINAC2026-THPO087

CONCEPTUAL DESIGN OF A NOVEL 2.45 GHz ECR ION SOURCE USING AN RF ROTATOR

R.C. Qin[1,2], P. Wang[3], X.X. Huang[*,3], Z.H. Gao[3], C.P. Wang[3],
Y.S. Guo[3], Y.X. Lu[3], W.C. Fang[†,3], Z.T. Zhao[3]
[1]Shanghai Institute of Applied Physics, Shanghai, China
[2]University of Chinese Academy of Sciences, Beijing, China
[3]Shanghai Advanced Research Institute, Shanghai, China

Abstract

Ion therapy has attracted increasing attention because of its favorable dose distribution enabled by its Bragg-peak behavior. Motivated by the ion therapy facility project at Shanghai Synchrotron Radiation Facility (SSRF), a novel 2.45 GHz ECR ion source has been proposed in this paper. An RF rotator is employed for the first time in the field of ion sources to couple the microwave power into the plasma chamber and excite an intrinsically rotating electric field. The rotating direction of the electric field is designed to be consistent with the electron cyclotron motion in the magnetic field, which is expected to enhance the resonant absorption, boost the electron energy and consequently improve the production of low-to-medium charge-state ions.

INTRODUCTION

Ion therapy has received growing attention in recent years as an advanced radiotherapy modality. Owing to the Bragg-peak behavior, ion therapy enables highly conformal tumor irradiation while reducing the dose to surrounding healthy tissues [1]. Protons and carbon ions are the two most commonly used particles in ion therapy, while helium ions have recently attracted renewed interests as a promising intermediate option between protons and carbon ions [2]. At Shanghai Synchrotron Radiation Facility (SSRF), a full-linac proton therapy facility has been proposed as a compact and cost-effective solution for future FLASH treatment [3]. A compact synchrotron with a circumference of 28 m for a proton-and-helium therapy facility has also been designed [4]. So under the framework of the SSRF ion therapy facility project, a novel 2.45 GHz ECR ion source utilizing an RF rotator has been proposed. This paper presents the conceptual design of the ion source.

Electron cyclotron resonance ion source (ECRIS) is a type of cathode-free plasma source in which electrons are resonantly heated by microwaves under a suitable magnetic field configuration. The heated electrons subsequently ionize the working gas, producing a magnetically confined plasma from which ions could be extracted. ECR ion sources offer the advantages of long lifetime, high reliability and long-time stable operation. ECR ion sources are commonly identified by their microwave frequency. Among them, 2.45 GHz ECR ion sources have been widely used for the production of high-current low charge-state ion beams, especially single charged ions [5]. Benefiting from the mature technology, a simple structure, a low cost and high stability, 2.45 GHz ECR ion sources are well suited for the front ends of medical accelerator systems.

DESIGN CONSIDERATIONS AND DESIGN RESULTS

Design Considerations

Conventional 2.45 GHz ECR ion sources commonly adopt double-ridge waveguide or dielectric waveguide to couple the microwave power into the plasma chamber and to match the impedance. In such configurations, the electric field in the plasma chamber is linearly polarized. However, in the single-particle picture, only the component consistent with the electron cyclotron motion in the magnetic field directly contributes to ECR heating while the other component may be absorbed through mechanisms such as mode conversion.

Based on this consideration, a novel 2.45 GHz ECR ion source utilizing an RF rotator is proposed in this paper. Figure 1 shows the RF model of this 2.45 GHz ion source. The RF rotator excites two orthogonal modes with approximately equal amplitudes and a 90° phase difference, thereby generating a rotating electric field in the plasma chamber. The rotation direction of the electric field can be changed by changing the microwave injection port or the direction of the magnetic field current.

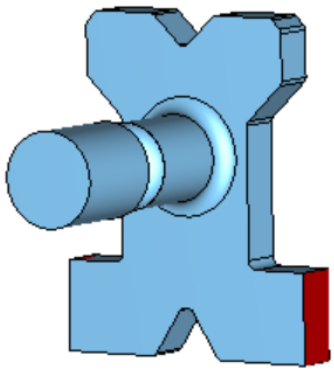


Figure 1: RF model of the novel 2.45 GHz ECR ion source

* huangxx@sari.ac.cn
† fangwc@sari.ac.cn

Content from this work may be used under the terms of the CC BY 4.0 licence (© 2026). Any distribution of this work must maintain attribution to the author(s), title of the work, publisher, and DOI.

ISBN: 978-3-95450-275-2 ISSN: 2226-0366 doi: 10.18429/JACoW-LINAC2026-THPO088

SYMMETRICAL HIGH OVERCOUPLED COUPLERS FOR STANDING WAVE NORMAL CONDUCTING LINACS: DEVELOPMENT AND OPERATIONAL EXPERIENCE

R. A. Zbruev†,1, A. A. Batov[1], T. V. Bondarenko[1], M. I. Demsky[2], M. A. Gusarova[1], K. V. Samarin[2], M. V. Lalayan[1], S. M. Polozov[1], M. V. Vladimirov[1]
[1]National Research Nuclear University MEPhI, Moscow, Russia
[2]CORAD LLC, Saint-Petersburg, Russia

Abstract

NRNU MEPhI and CORAD LLC has been developing and commissioning linear accelerators for industrial and scientific applications. The designed linacs are operate on a standing wave and S-band. Linacs are based on a biperiodic accelerating structures (BAS). Due to the sufficiently high values of the received beam currents (from several hundred mA and above) and, consequently, a significant beam loading, an overcoupled RF-power couplers (coupling coefficient more than 4) were developed and constructed for these accelerators. Symmetrical couplers allowed obtaining a coupling coefficient about 10. The work summarizes the experience gained over more than a decade of work and linacs commissioning and operation.

INTRODUCTION

Linear electron accelerators make up a significant part of the total number of accelerators for industrial and medical applications [1]. The article considers two linac projects, which were created by the teams of NRNU MEPhI and CORAD LLC. The first facility is based on an accelerating structure for average beam power of up to 15 kW and energy range from 7.5 to 10 MeV. The results obtained were used for a series of industrial accelerators (more than 10 units in total were put into operation), which are used for gamma activation analysis, sterilization of food and medical products, as well as irradiation of shrink wrap for the electronic industry. The second facility is a new two-section complex for radiation resistance test of electronic components, with beam energy about 8 MeV and beam current more than 1 A. The basic design principles were the following statements: the accelerating structure should have a high overcoupled RF-power coupler for maximal RF pulse power usage efficiency; the gentle buncher should be used to provide high capturing coefficient and narrow energy spectrum for all output energies.

MODELING, MANUFACTRUING AND EXPERIMENTS

For the described projects beam dynamics simulation is computed with using of developed at MEPhI codes: PIC code SUMA [2] for dynamics in electron gun, BEAMDULAC-BL [3] for dynamics in accelerating structures. BEAMDULAC-BL provides simulations taking into account the beam loading and the Coulomb field effects self-consistently. Additionally, CST MWS was used for electron gun dynamics in the two-section project.

Conventional three-electrode E-guns were used for injection in both projects. Parameters of the designed devices present in Table 1.

Table 1: E-guns Parameters

Linac	Emission current [A]	Transverse emittance [mm*rad]	Output beam diameter [mm]
Industrial series	0.5-0.7	2.5	2.0
Radiation resistance testing	1.8-2.0	31.4	8.0

For both E-guns some experiments were conducted to confirm the simulations result (see Fig. 1). For example, beam envelope was measured by collimated diaphragm current collector on different distance from gun anode and beam current was measured by Faraday cup; good experimental and calculated results agreement were obtained [4].

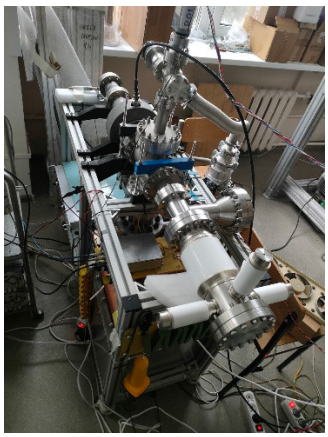


Figure 1: E-gun for radiation resistance testing linac during the experiments.

Beam dynamics optimization for accelerating structure was carried out to obtain the effective beam bunching and to achieve narrow energy spectrum. Industrial series linac is a one-section with 28 accelerating and 27 coupling cells, with six-period gentle buncher; radiation resistance testing linac is a two-section with six-period gentle buncher, 20 accelerating and 18 coupling cells in total. As a result of

† RAZbruev@mephi.ru

Content from this work may be used under the terms of the CC BY 4.0 licence (© 2026). Any distribution of this work must maintain attribution to the author(s), title of the work, publisher, and DOI.

ISBN: 978-3-95450-275-2 ISSN: 2226-0366 doi: 10.18429/JACoW-LINAC2026-THPO089

GREEN-FUNCTION BASED WAKEFIELD ANALYSIS IN THE SYLA LINEAR ACCELERATOR-INJECTOR

A. V. Makarov*, M. A. Gorbunov, V. I. Rashchikov
National Research Nuclear University MEPhI, Moscow, Russia

Abstract

Designing modern charged-particle accelerators requires a detailed analysis of beam dynamics that accounts for the collective effects limiting the achievable parameters of the facility. Accountability of the fields induced by a high-brightness beam in the linear accelerator-injector of a free-electron laser (FEL) is of particular importance, since these fields largely determine the final emittance and the energy spread, leading to beam instabilities. In the present work, based on numerical simulations when using a semi-analytical approach, the Green's function of the wake potential for the regular section of the SYLA linear accelerator-injector has been obtained; the given function is intended for subsequent calculations of the longitudinal and transverse beam dynamics.

INTRODUCTION

The design of linear accelerator-injectors for X-ray FELs requires a detailed analysis of the electron bunch dynamics with allowance for collective effects, since these are the effects that largely determine the ultimate parameters attainable by the facility. A special role is played by wake fields excited by short intense bunches passing through the accelerating structure: their action leads to the emittance growth and energy spread, as well as to bunch instabilities, which directly affects the parameters of the radiation generated in the FEL. The problem of calculating wake fields for travelling- and standing-wave structures has been studied in many high-current linac projects [1–4].

In terms of the fourth-generation synchrotron radiation SYLA source development, a linear electron accelerator with a total energy of 6 GeV is being designed, which serves as an injector both for the storage ring and for the FEL [5]. A preliminary analysis of the collective effects in the storage ring of the source has been carried out earlier [6,7]. A regular unit of the linear accelerator-injector comprises more than 100 standing-wave accelerating sections, so that a correct account of the beam-induced wake fields is required already at the first stage of the beam dynamics calculation.

In this paper, the Green's functions of the longitudinal and transverse dipole wake potentials for the regular section of the SYLA linear accelerator-injector have been obtained. The calculation has been carried out according to the following scheme: first, the wake potentials are computed numerically with the time-domain codes ECHO2D and ECHO3D [8]; then, using a semi-analytical approach, the Green's function for the longitudinal and transverse dipole wake potential is derived, which will subsequently be used for the calculations of the longitudinal and transverse beam dynamics in the accelerating structure of the SYLA injector.

* AVMakarov@mephi.ru

ACCELERATING SECTION GEOMETRY FOR THE NUMERICAL SIMULATION

The accelerating structure of the SYLA linear accelerator-injector is made as a chain of resonator cells, each of which contains internal coupling spaces. The aforementioned cavities make the structure geometry non-axisymmetric. Whilst, the ECHO2D code is applicable only to axisymmetric geometries, whereas the ECHO3D code is able to deal with an arbitrary three-dimensional shape, however, requiring considerably larger computational resources.

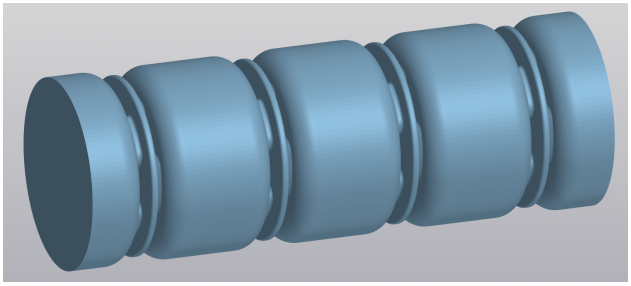


Figure 1: Geometry of a unit at the accelerating section period (4 cells, vacuum volume).

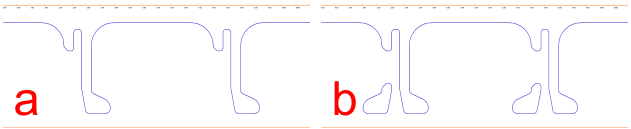


Figure 2: Axisymmetric models of the section for the calculation in ECHO2D: (a) without the coupling spaces; (b) with the coupling spaces.

To do so, three geometric models of the section have been prepared for the calculations. The first one is a full three-dimensional model of the vacuum volume (Fig. 1) reproducing the actual shape of the cells and coupling spaces; it is computed only with the ECHO3D code and serves as a reference. The other two are axisymmetric models suitable for calculations with the ECHO2D code: the first model does not consider any coupling cavities, while the second one includes these by projecting their profile onto the cross-section of the section (Fig. 2).

In order to estimate how far the axisymmetric simplification affects the result, the wake potential has been calculated for all three models with long bunches and the dependences compared.

Content from this work may be used under the terms of the CC BY 4.0 licence (© 2026). Any distribution of this work must maintain attribution to the author(s), title of the work, publisher, and DOI.

ISBN: 978-3-95450-275-2 ISSN: 2226-0366 doi: 10.18429/JACoW-LINAC2026-THPO091

MITIGATION OF LONGITUDINAL TRAPPING IN A 100 mA DUAL-BEAM RFQ VIA COUPLED OPTIMIZATION

T. Zhang*[1,2], Z. J. Wang[1,2], Y. Du[1,2], C. G. Su[1,2], Z. H. Liang[1,2], T. L. Wang[1,2], X. Zhang[1,2], T. Y. Ding[1,2], L. W. Liu[1,2], Y. M. Chu[1,2], M. Yi[3], D. Y. Jia[1,2]
[1]Institute of Modern Physics, Chinese Academy of Sciences, Lanzhou, China
[2]University of Chinese Academy of Sciences, Beijing, China
[3]Advanced Energy Science and Technology Guangdong Laboratory, Huizhou, China

Abstract

Simultaneous acceleration of positive and negative ions (H^+ and H^-) in a Multi-Beam RFQ is a promising approach for high-intensity linear accelerators. This study presents the design and beam dynamics analysis of a 100 mA dual-beam RFQ, building upon a robust single-beam periodic FODO lattice to ensure initial transverse matching and beam stability. Dual-beam simulations utilizing custom data processing pipelines reveal that longitudinal space-charge interactions degrade the longitudinal potential well. This degradation induces a "trapping" phenomenon, where ions escape their designated buckets, limiting the initial dual-beam transmission efficiency to 80 %. To mitigate this, a transverse-longitudinal coupled optimization was conducted. By increasing the modulation factor by 0.03 in the Shaper section, the longitudinal bunching force was enhanced to suppress trapping. Despite the intensified RF defocusing, the previously optimized transverse envelope maintained robust beam stability. This targeted optimization successfully improved the overall dual-beam transmission efficiency to 89.4 %, providing a practical reference for high-current Multi-Beam RFQ designs.

INTRODUCTION

The simultaneous acceleration of intense positive and negative ion beams within a single Radio Frequency Quadrupole (RFQ) is a highly attractive concept for modern high-intensity linear [1]. By mixing opposite charge states, the net transverse space-charge effect can be partially neutralized. While this neutralization is theoretically beneficial for transverse beam stability, the dual-beam operation introduces highly complex longitudinal dynamics [1, 2]. Specifically, the longitudinal interaction between adjacent oppositely charged bunches often disrupts the RF bucket, leading to severe longitudinal particle loss.

To systematically investigate this longitudinal bottleneck and optimize the overall transmission efficiency, it is essential to establish a robust single-beam baseline [3]. This paper presents the design of a 100 mA single-beam RFQ, followed by dual-beam dynamics simulations. By identifying the longitudinal "trapping" phenomenon caused by inter-bunch space-charge interactions, a transverse-longitudinal coupled optimization strategy is proposed and verified to significantly improve the overall dual-beam transmission efficiency [4].

* zhangtao@impcas.ac.cn

SINGLE-BEAM FOUNDATION AND TRANSVERSE MATCHING

In high-intensity multi-beam accelerators, the transverse stability of the beam is a prerequisite for achieving simultaneous acceleration. Before investigating the complex longitudinal space-charge interactions, the transverse structure of the baseline RFQ was rigorously matched.

Baseline RFQ Parameters

The baseline single-beam RFQ was designed to operate at 162.5 MHz, accelerating a 100 mA single-species beam from an initial energy of 0.08 MeV to a final extraction energy of 3.01 MeV. The intervane voltage is maintained at 0.08 MV. The total structure comprises 251 cells with a total length of 678.57 cm. To ensure a smooth beam exit and minimize emittance growth at the extraction region, the primary accelerating field is terminated at the 249th cell, utilizing the final two cells as a transition region. The final synchronous phase (ϕ_s) reaches $-35°$.

Transverse Envelope Stability

By simplifying the RFQ transverse structure into a FODO periodic lattice and utilizing the envelope equation, the transverse beam stability was systematically analyzed. The Radial Matching Section (RMS) consists of the first 5 cells, configured with an initial aperture of 0.3 cm to accept the injected DC beam and match its Twiss parameters to the time-varying acceptance of the RFQ. Comprehensive beam dynamics simulations were conducted utilizing PARMTEQ for the primary lattice design and Toutatis for high-resolution 3D PIC verification. As illustrated in Fig. 1, the transverse beam envelopes (x_{rms} and y_{rms}) are smoothly matched through the RMS and remain well-confined within the aperture limit along the entire structure. Even when the beam enters the Gentle Buncher (GB) section, where the synchronous energy reaches 0.64 MeV and longitudinal RF forces intensify, the transverse envelope is tightly maintained. Establishing this solid single-beam foundation ensures that any beam degradation observed in subsequent dual-beam simulations can be confidently attributed to longitudinal interactions.

DUAL-BEAM DYNAMICS AND TRAPPING EFFECT

Building upon the robust transverse single-beam foundation, dual-beam simulations were conducted using Toutatis

Content from this work may be used under the terms of the CC BY 4.0 licence (© 2026). Any distribution of this work must maintain attribution to the author(s), title of the work, publisher, and DOI.

ISBN: 978-3-95450-275-2 ISSN: 2226-0366 doi: 10.18429/JACoW-LINAC2026-FR1A001

A VERY COMPACT INVERSE COMPTON SCATTERING GAMMA-RAY SOURCE AT TSINGHUA UNIVERSITY*

Ch.X. Tang[†,1], W.H. Huang[1], Y.Ch. Du[#,1], H.B. Chen[1], J.R. Shi[1], L.X. Yan[1], Y.L. Li[1], Ch. Cheng[1], R. Qiu[1], Zh. Zhang[1], R.K. Li[1], H. Zha[1], L.M. Zheng[1], H. Zhang[1], Zh.J. Chi[2], H. Ding[1], H.Z. Zhang[1], Q.L. Tian[1], Y.Q. Jia[1], Y.J. Zhu[1], H. Wang[1], Ch. Hu[1], Y.Sh. Fan[1], H.Y. Jiang[1], T.K. Zhang[1], J.J. You[1], L.Y. Luo[1], W. Yue[1], Zh.K. Wang[1], R. Zou[1], F.J. Hu[1], H. Deng[1], X.L. Cao[1], J. Lin[1], Zh. Shen[1], J.Y. Sun[1], B.Y. Feng[1], H.P. Zhi[1], X.Q. Zhang[1], Sh.H. Zhang[1], J.Ch. Yuan[1], J. Gao[1], Q. Gao[1]
[1]Department of Engineering Physics, Tsinghua University, Beijing, China
[2]School of Physics, Beijing Normal University, Beijing, China

Abstract

The inverse Compton scattering (ICS) source based on the collision between high-quality electron beams and laser can generate high-brightness quasi-monoenergetic γ-rays. Our labs have developed a very compact ICS gamma ray source (VIGAS), which has been successfully commissioned. The VIGAS can generate gamma ray beam with energy from 0.2–4.8MeV, the spectrum is mono-chromatic and adjustable continuously. The photon flux at 1.5% spectrum is about 1.7×10^7 photons/second (0.2 ~ 2.4 MeV), and 4.1×10^6 phones/second (2.4 ~ 4.8 MeV). And the polarization of the gamma ray can be tunable continuously from linear to circular. The electron beam of VIGAS is generated from a high-quality compact electron linear accelerator, which integrated S-band (gun, buncher and pre-accelerator) and X-band (main accelerator) structures. The linac accelerates the electron beam energy to more than 320 MeV within 9.7 meters. There are two lasers at VIGAS, both Ti: Sapphire of 800 nm. One is working at its third harmonic, 266 nm to drive the photocathode RF gun, and another is the scattering laser working at 800nm or 400 nm. A low-level radio frequency (LLRF) system featuring high-precision synchronization has been successfully developed and has demonstrated stable operation. We have conducted some user experiments on VIGAS.

INTRODUCTION

Gamma ray is normally from the decay of radioactive nuclei, with photon energy higher or near MeV. The high energy photons from free or bounded electrons, such as bremsstrahlung, synchrotron radiation or free electron laser, and so on, normally are called x-ray. Here, the photon with energy of about MeV generated from ICS between a relativistic electron beam and a high power laser pulse, is called gamma ray. The ICS gamma ray sources have advantages compared to others, such as high Energy, mono-energetic, continuously tunable energy and polarization, micro focus spot size, ultra-short pulse length and the facility compactness.

Compton scattering is an inelastic scattering of a photon by a free charged particle, usually electron, and the photon transferring part of its energy to the particle, lengthening its wavelength, which was first discovered by Arthur H. Compton in 1923 [1]. And ICS is a charged particle transfers part of its kinetic energy to a photon, and shortening the photon wavelength. For a head-on collision between a relativistic ($\gamma \gg 1, \beta \sim 1$) electron and a photon of frequency ω, the scattering photon energy will be

$$\hbar\omega' \approx 4\gamma^2\hbar\omega. \quad (1)$$

For an 800 nm laser photon of energy about 1.55 eV scattering with an electron of 300 MeV, we can get a gamma ray photon of 2.15 MeV.

There are already several ICS gamma-ray sources such as Higs [2, 3], LEPS [4], SLEGS [5], in the world and they have played an important role in the area of nuclear physics, nuclear medicine and advanced gamma-ray imaging. VIGAS is a very compact facility compared to them. It is based on a high gradient X-band linear accelerator. This is why it can provide high to 5MeV gamma rays, is still very compact.

THE OVERALL DESIGN OF VIGAS

The layout of VIGAS is shown in Figure 1. It composes of an electron linac of 350 MeV, a high power 800 nm Ti:Sa laser of about 3 J, and a femto-second synchronization system. The linac consists of an S-band photocathode RF gun, an S-band buncher, an S-band pre-accelerator to 50 MeV, 6 high gradient X-band traveling wave waveguides with 80 MV/m gradient. VIGAS requires the linac provide electron bunches of the parameters shown in Table 1.

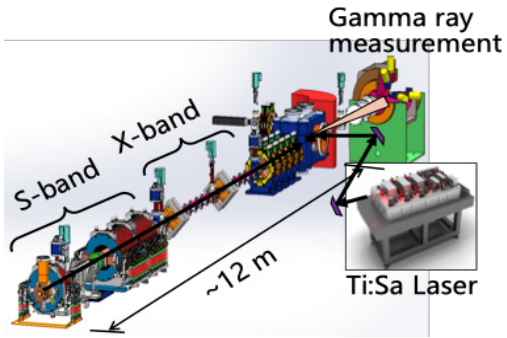


Figure 1: A sketch of VIGAS.

* Work supported by the National Natural Science Foundation of China (Grant No. 12027902)
† tang.xuh@tsinghua.edu.cn
dych@tsinghua.edu.cn

Content from this work may be used under the terms of the CC BY 4.0 licence (© 2026). Any distribution of this work must maintain attribution to the author(s), title of the work, publisher, and DOI.

ISBN: 978-3-95450-275-2 ISSN: 2226-0366 doi: 10.18429/JACoW-LINAC2026-FR1A002

LOW-EMITTANCE MUON BEAM ACCELERATION USING A RADIO FREQUENCY QUADRUPOLE FOR THE J-PARC MUON $g-2$/EDM EXPERIMENT

Y. Nakazawa* on behalf of the J-PARC muon $g-2$/EDM collaboration
High Energy Accelerator Research Organization (KEK), Tsukuba, Japan

Abstract

At Japan Proton Accelerator Research Complex (J-PARC), a low-emittance muon beam based on a linear accelerator is being developed for precision measurements of the muon anomalous magnetic moment ($g-2$) and electric dipole moment (EDM), as well as for non-destructive imaging applications. In the low-velocity section of the muon linac, a 324 MHz radio-frequency quadrupole linac (RFQ) is employed to bunch and accelerate muons from 5.7 keV to 340 keV. In this study, a muon-beam cooling and RFQ acceleration experiment was conducted at J-PARC. Thermal muons were produced via laser ionization of thermal muonium emitted from a room-temperature silica aerogel target, electrostatically extracted to 5.7 keV, and injected into the RFQ. The muons were accelerated to 340 keV, and their longitudinal and transverse beam profiles were measured at the RFQ exit. This work demonstrates an in-situ implementation of a full-scale RFQ for the world's first muon linac in the dedicated $g-2$/EDM experimental area at J-PARC. The experimental concept, beamline configuration, commissioning status, and outlook toward establishing a low-emittance muon linac are presented.

INTRODUCTION

At the Japan Proton Accelerator Research Complex (J-PARC), a linear accelerator dedicated to muons is being developed for a precision measurement of the muon anomalous magnetic moment $g-2$ and a search for the electric dipole moment (EDM) [1]. The muon linac consists of a radio-frequency quadrupole linac (RFQ) operating at 324 MHz, an interdigital H-mode drift tube linac (IH-DTL) at 324 MHz, a disk-and-washer coupled-cavity linac (DAW-CCL) at 1296 MHz, and a disk-loaded structure (DLS) at 2592 MHz [1]. The muons are accelerated to 212 MeV over a length of approximately 40 m and are injected into the storage magnet [1].

In 2024, cooling and acceleration of positive muons were demonstrated at J-PARC [2]. Thermal muons produced by laser ionization of muonium atoms were accelerated to 100 keV using a prototype RFQ, and the transverse emittance of the accelerated beam was measured. This demonstration was performed in a multipurpose user area, and the longitudinal time structure of the accelerated beam was not measured.

The dedicated experimental area for the $g-2$/EDM experiment, the H2 area of the Materials and Life Science Experimental Facility (MLF), has become available, and the full-scale RFQ was implemented in situ in the $g-2$/EDM beamline in 2026. The goal of the present experiment is to accelerate muons to 340 keV with this RFQ and to characterize the accelerated beam.

The longitudinal time structure of the accelerated beam is essential for the longitudinal matching to the subsequent IH-DTL [3]. In addition, the fraction of muons captured in the main bunch depends on the RF phase of the RFQ, and therefore an accurate measurement of the bunch structure and a phase adjustment are required. For this purpose, the beam monitors were upgraded from the 2024 configuration. This paper reports the experimental setup, the time-of-flight measurement of the accelerated muons, and the first results of the bunch-structure measurement downstream of the RFQ.

EXPERIMENTAL SETUP

The experimental setup in the H2 area is shown in Fig. 1, and a photograph of the apparatus installed in the H2 area is shown in Fig. 2. Surface muons are produced by the decay at rest of positive pions stopped near the surface of the graphite muon-production target irradiated by the 3-GeV proton beam [4, 5]. A surface muon beam with a kinetic energy of 4 MeV is delivered to the H2 area at a repetition rate of 25 Hz. The beam has a double-pulse structure, and the two pulses are separated by approximately 600 ns [2].

The surface muons are stopped in a room-temperature silica aerogel target, from which thermal muonium atoms with an energy of 30 meV are emitted into vacuum. Muonium is a hydrogen-like atom composed of a positive muon and an electron, and thermal positive muons are obtained by the laser ionization of thermal muonium [6]. In the present experiment, the muonium atoms are resonantly excited from the $1S$ state to the $2P$ state using 122-nm pulsed light and are subsequently photoionized by 355-nm light. The $1S$–$2P$ excitation scheme differs from the $1S$–$2S$ two-photon excitation used in the 2024 RF-acceleration demonstration [2].

The resulting thermal positive muons are extracted and accelerated to 5.7 keV by an electrostatic lens referred to as the Soa lens and are steered into the RFQ using four electrostatic deflectors, which adjust the beam trajectories in the horizontal and vertical directions. A photodiode monitors the laser shot timing, and a positron detector placed near the Soa chamber monitors the decay positrons, which determine the arrival timing of the surface muons.

A retractable electrostatic mirror upstream of the RFQ can direct the 5.7-keV muon beam to the ultraslow-muon diagnostic line (UDL). The UDL, consisting of an electrostatic-

* yuga.nakazawa@kek.jp

Content from this work may be used under the terms of the CC BY 4.0 licence (© 2026). Any distribution of this work must maintain attribution to the author(s), title of the work, publisher, and DOI.

ISBN: 978-3-95450-275-2 ISSN: 2226-0366 doi: 10.18429/JACoW-LINAC2026-FR1A005

STATUS AND OVERVIEW OF THE CLEAR FACILITY AT CERN

A. Gilardi*, R. Corsini, W. Farabolini, D. Gamba, J. P. Leygonie,
A. Malyzhenkov[1], C. M. Moore[2], S. J. Simonsson[3],
G. Tangari[4], S. Wang[5] CERN, Geneva, Switzerland
A. Aksoy PITZ-DESY, Zeuthen, Germany
[1]also at Swiss International Institute Lausanne (SIIL), Prilly, Switzerland
[2]also at University of Exeter, Exeter, United Kingdom
[3]also at Lund University, Lund, Sweden
[4]also at Sapienza University of Rome, Rome, Italy
[5]also at University of Oxford, Oxford, United Kingdom

Abstract

CLEAR (CERN Linear Electron Accelerator for Research) is a versatile electron beam user facility operating at CERN, providing beams with energies up to 200 MeV across a broad range of bunch charges, emittances, and timing configurations. The facility serves a diverse and growing internal and external user community, supporting a wide experimental program spanning multiple domains of accelerator research and applications. In this paper, we present an overview of the current status of CLEAR, summarizing the breadth of experiments conducted across recent operational runs and the key developments of the facility. We further report on the installation and commissioning of the second beam line, a new beamline branch featuring a dog-leg section, a set of slits in both dispersive and non-dispersive regions, and larger aperture focusing elements, which have the potential to significantly expand the facility's experimental capabilities and accessible beam parameter space. The continued development of CLEAR's infrastructure and the steady growth of its user base consolidate its role as a unique and flexible platform for accelerator research and technology demonstration at CERN.

INTRODUCTION

The CERN Linear Electron Accelerator for Research (CLEAR) [1] has been operating as a user facility at CERN since September 2017, built by converting and upgrading the CALIFES probe-beam injector of the CLIC Test Facility (CTF3) and installing a dedicated experimental beam line downstream of the LINAC.

Its mandate has been deliberately kept wide: development and validation of beam instrumentation and accelerator components, studies of novel acceleration and focusing concepts, irradiation of electronic components for space and accelerator applications, and, increasingly, medical applications of Very High Energy Electron (VHEE) beams.

Two features distinguish CLEAR within the CERN accelerator complex. It is at present the only user facility at CERN accelerating electrons, a role whose strategic value has grown given the consensus around an e^+e^- Higgs factory as the laboratory's next flagship project. It is also independent of the proton chain, and is therefore one of the few CERN accelerators expected to remain operational throughout Long Shutdown 3 (LS3).

An internal review held in 2024 commended both the operational efficiency of the facility and the quality of its support to user experiments, and concluded that continued exploitation beyond the originally foreseen end date of 2025 was scientifically justified. Operation has consequently been approved until at least 2030, and a consolidation programme launched to guarantee stable and reliable running over this extended time scale [2].

THE CLEAR FACILITY

CLEAR consists of a photoinjector followed by an S-band linac of approximately 20 m in length, and by an experimental beam line of comparable length hosting several test areas (Fig. 1). Electron bunches are produced by illuminating a Cs_2Te photocathode with deep-ultraviolet pulses generated by a picosecond Nd:YLF oscillator operating at 1.5 GHz, amplified and frequency-quadrupled [3]. Acceleration is provided by a 3 GHz RF gun and by S-band travelling-wave accelerating structures, and an RF deflecting cavity is available for longitudinal diagnostics.

The experimental areas are distributed over both beam lines. The original line hosts two in-air areas — VESPER, used mainly for radiation-hardness testing of electronics, and the more flexible In-Air Test Area, which has hosted the majority of the medical-application experiments — together with several in-vacuum areas, in particular the Beam Instrumentation test areas and the plasma lens region. The second beam line, described below, adds a further in-air area, better suited to large transverse beam sizes thanks to its larger aperture optics, and an additional in-vacuum stand giving permanent space for diagnostics prototypes.

Table 1 summarizes the beam parameters currently available to users. The parameter space has widened progressively since the beginning of operation: the lower energy bound has been reduced to serve dosimetry and radiobiology users, the bunch frequency can now be doubled from 1.5 to 3.0 GHz by means of a laser double-pulse scheme, and the maximum train charge has increased substantially following photocathode rejuvenation and improvements to beam transport.

* antonio.gilardi@cern.ch

Content from this work may be used under the terms of the CC BY 4.0 licence (© 2026). Any distribution of this work must maintain attribution to the author(s), title of the work, publisher, and DOI.

ISBN: 978-3-95450-275-2 ISSN: 2226-0366 doi: 10.18429/JACoW-LINAC2026-FR1A006

DEMONSTRATION OF CAVITY FIELD MAPPING BY FALLING DROPS OF LIQUID*

X. Du†, L. Groening
GSI Helmholtzzentrum für Schwerionenforschung GmbH, Darmstadt, Germany

Abstract

Radio-frequency cavity field mapping is conventionally performed by pulling a perturbing bead through the cavity on a dielectric wire. Although well established, this procedure requires cavity-specific mechanics and can introduce perturbations, vibration, and alignment errors. We demonstrate a compact wire-free alternative in which repeatable liquid drops fall through the cavity under gravity. A photoelectric gate provides a timing reference, a vector network analyzer records the transient phase perturbation, and a calibrated time-to-position relation converts each trace into a field profile. The method completes a longitudinal scan in less than 0.5 s and supports quasi-continuous monitoring at about 2 Hz. Repeated measurements can be combined by singular value decomposition to recover field distributions at low signal-to-noise ratio. Measurements on a 36.136 MHz three-gap buncher reproduce the simulated one- and two-dimensional field patterns. Tests on a scaled ten-gap Alvarez-type cavity resolve every accelerating gap despite a signal-to-noise ratio close to two. These results establish falling liquid drops as practical perturbators for rapid cavity diagnostics and tuning.

INTRODUCTION

Reliable radio-frequency (RF) field maps are required during the fabrication, acceptance testing, and tuning of accelerator cavities. The established bead-pull technique is based on small-perturbation theory: a bead moved through a resonant volume changes the stored electric and magnetic energies and therefore the resonant frequency or the transmission phase measured at a fixed frequency [1, 2]. For a sufficiently small perturbator and an electric-field-dominated trajectory, the relative field profile can be written as

$$E_{\mathrm{rel}}(z) = \sqrt{\frac{|\Delta\phi(z)|}{\max_z |\Delta\phi(z)|}}, \qquad (1)$$

where $\Delta\phi$ is the phase difference between the perturbed and unperturbed cavity responses. Absolute calibration requires the perturbator polarizability and the stored energy, but relative profiles are sufficient for field-flatness tuning.

In a conventional setup the perturbator is attached to a line driven by a motor and pulley system. The mechanics must be adapted to the cavity length and orientation, aligned at both ends, and operated without line slip or vibration. The line itself can perturb the cavity, particularly for transverse or higher-order modes. These constraints make repeated field measurements a significant part of a tuning campaign.

The falling-drop method removes the line and uses gravity for transport. A release unit, optical trigger, compact controller, and optional transverse stage form a portable device that is aligned once at the cavity entrance. A full technical account and additional analysis are given in Ref. [3]; the present contribution emphasizes the use of liquid drops, the calibration workflow, and experimental demonstrations relevant to rapid tuning.

FALLING-DROP METHOD

Measurement Principle

A blunt-tip medical needle produces repeatable water drops above the beam axis. The needle diameter and a flow-control valve set the drop size and repetition rate. The drop first crosses a laser-light-sensor gate and then traverses the cavity. Its dielectric volume perturbs the resonance while a vector network analyzer (VNA) records the complex transmission coefficient. Phase is used here because it is readily sampled at a fixed drive frequency and is sensitive to the short perturbation.

With the downward direction defined as positive, the longitudinal coordinate is obtained from

$$z(t) = z_{\mathrm{g}} + v_0\tau + \frac{1}{2}g\tau^2, \qquad \tau = t - t_{\mathrm{d}}, \qquad (2)$$

where z_{g} is the known gate position, v_0 is the drop velocity at the gate, and t_{d} is the combined trigger, communication, and VNA acquisition delay. Both unknowns are obtained experimentally from a cavity with known gap spacing. This calibration also absorbs small repeatable offsets in the release and trigger chain. Drag corrections can be introduced for longer trajectories, but the calibrated kinematic description was adequate for the cavities considered here.

Hardware and Acquisition

Figure 1 shows the device mounted on the buncher cavity. A 3D-printed housing supports the needle, optical gate, electronics, and a linear stage. A Raspberry Pi controller coordinates the stage, trigger, and VNA and streams the processed profile to a graphical interface. The compact assembly is about half the footprint of an A4 sheet, costs less than $300 excluding the VNA, and requires only a cavity-specific locating cap at the entrance.

The VNA intermediate-frequency bandwidth and number of samples must be high enough for a sub-second transit. The measurements reported here used 3000 samples over 0.4 s.

* Work supported by GSI Helmholtzzentrum für Schwerionenforschung GmbH

† x.du@gsi.de

Content from this work may be used under the terms of the CC BY 4.0 licence (© 2026). Any distribution of this work must maintain attribution to the author(s), title of the work, publisher, and DOI.